Physics of Collective Beam Instabilities in High Energy Accelerators

WILEY SERIES IN BEAM PHYSICS AND ACCELERATOR TECHNOLOGY

Series Editor MEL MONTH

BROWN –	FUNDAMENTALS OF ION SOURCES*
CHAO –	PHYSICS OF COLLECTIVE BEAM INSTABILITIES IN HIGH ENERGY ACCELERATORS
EDWARDS AND SYPHERS –	AN INTRODUCTION TO THE PHYSICS OF HIGH ENERGY ACCELERATORS
MICHELOTTI –	INTERMEDIATE CLASSICAL MECHANICS WITH APPLICATIONS TO PARTICLE ACCELERATOR PHYSICS*

*Forthcoming titles

Physics of Collective Beam Instabilities in High Energy Accelerators

ALEXANDER WU CHAO
Superconducting Super Collider Laboratory
Dallas, Texas

Wiley-Interscience Publication
JOHN WILEY & SONS, INC.
New York / Chichester / Brisbane / Toronto / Singapore

This text is printed on acid-free paper.

Library of Congress Cataloging in Publication Data:

Chao, Alex.
Physics of collective beam instabilities in high energy accelerators/Alexander Wu Chao.
p. cm.
Includes index.
ISBN 0-471-55184-8 (alk. paper)
1. Linear accelerators. 2. Particle beam instabilities.
I. Title.
QC787.L5C43 1993 92-39599
539.7'33–dc20

Printed in the United States of America

10 9 8 7 6 5 4 3 2 1

to Patricia, Clifford, and Laura

Contents

Preface

When I was a graduate student in Stony Brook, I wanted to become a high energy physicist. Then, in 1973, Professor Chen Ning Yang suggested that I learn a subject called accelerator physics. In the same year, Professor Ernest Courant started my learning process with an introductory course in accelerator theory. Later in 1974 as I was working on my thesis, Professor Yang advised me to consider accelerator physics as my career choice after my graduation. This advice I considered, debated, and eventually followed. For eighteen years since my graduation, I have thoroughly enjoyed this rich field of physics. One of the reasons for this enjoyment is what I will describe in this volume—the subject of collective beam instabilities in accelerators. Over the years, I have learned and been fascinated by this subject, and it is this fascination that I would like to share with the reader.

Beam physics is a branch of physics that studies the dynamics of charged particles, particularly in accelerators. This is a maturing field; much nurturing is needed, including a need of textbooks. The subject of collective beam instabilities is one of the main topics facing modern high performance accelerators. The knowledge is crucial for the successful design and understanding of these accelerators. This book is intended to provide the basics of this subject of beam physics.

I have assumed that the reader is knowledgeable in classical electrodynamics and mathematical physics at a lower graduate level. Previous knowledge of accelerators would be helpful but is not required. I have not pursued the more advanced research topics. Instead, my aim is to prepare the reader with a sufficiently broad basis of the subject for him/her to pursue his/her own research. References are restricted to those related to the discussions, and are not meant to be exhaustive.

Various collective instability effects for high energy accelerators are introduced and analyzed. The material is theory oriented, and the emphasis is on the underlying physical principles of these instabilities, typically using models and soluble examples as illustrations. Experimental observations are mentioned when appropriate.

I have tried to postpone formalism till a fairly solid intuitive picture has been established. Therefore, the conventional treatment of the subject using the Vlasov techniques is postponed to a later part of the book. This I regard as a humble achievement on my part.

The book is an outgrowth of several lecture series, delivered on various occasions since 1982. I wish to thank the students for their enthusiasm, their comments, and their difficult questions. In the preparation of the manuscript, I have enjoyed and benefited from innumerable discussions with my colleagues, among them Karl Bane, Dick Cooper, Miquel Furman, Tom Knight, Sam Kheifets, Phil Morton, Bob Siemann, and many others. Jacques Gareyte, Albert Hofmann, and John Seeman have kindly provided photos of their experimental observations. Special thanks must be given to Mel Month; the existence of this book is a result of his many encouragements.

ALEX CHAO

Highland Park, Texas

CHAPTER 1

Introduction

1.1 THE SUBJECT

Accelerators are devices that control and manipulate the motion of charged particles. To design an accelerator, one starts by considering the motion of a single particle. To describe the dynamics of a beam of particles, one then regards the beam as a collection of noninteracting single particles moving in the environment prescribed by the accelerator design. The environment is defined by the electric and magnetic fields of the various accelerator components specified in the design. Given these fields, intricate effects of linear and nonlinear dynamics of a single particle can be studied in detail.

Many accelerator applications, however, require beams of medium or high intensities. As the beam intensity is increased, the electromagnetic fields self-generated by the beam, particularly the fields generated by the beam interacting with its immediate surroundings, will perturb the external prescribed fields. When the perturbation becomes sufficiently strong, the beam becomes unstable. To describe this aspect of the beam dynamics, the single-particle picture does not suffice and a multiparticle picture is introduced. This multiparticle picture takes into consideration the important self-generated fields, but usually omits the detailed nonlinear aspects included in the single-particle picture.

To be more specific, consider an intense particle beam contained in a metallic vacuum chamber of an accelerator. The beam interacts electromagnetically with its surroundings to generate an electromagnetic field, known as the *wake field*. This field then acts back on the beam, perturbing its motion. Under unfavorable conditions, the perturbation on the beam further enhances the wake field; the beam-surroundings interaction then leads to an instability, known as a *collective instability*, and a subsequent beam loss. The beam and its surroundings form a self-consistent dynamical system, and it is this system that we will study. Thus,

$$\begin{aligned} \text{dynamical system} &= \text{beam} + \text{surroundings}, \\ \text{mediator of interaction} &= \text{wake field}. \end{aligned} \tag{1.1}$$

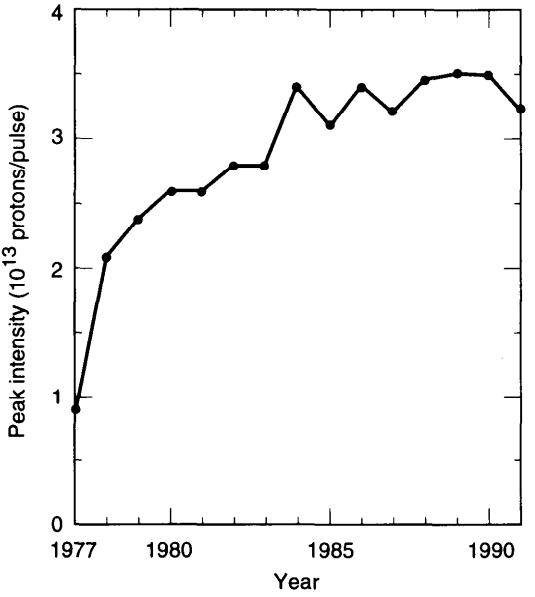

Figure 1.1. Peak beam intensity of the CERN Super Proton Synchrotron from 1977 to 1991. (Courtesy Jacques Gareyte, 1991.)

The subject of collective instabilities in high energy accelerators has been studied since the late 1950s and early 1960s. The importance of the subject lies in the fact that it is one of the main factors that determine the ultimate performance of the accelerator. The advancement of this subject over the years can be evidenced by the discovery and curing of several collective instability mechanisms. Each accelerator, when pushed for performance, will encounter some intensity limit. After this limit is analyzed, understood, and possibly cured, a new limit emerges. The process repeats, and the end result is the improved understanding and higher performance of the accelerator. One example is illustrated in Figure 1.1, the record of the peak beam intensity reached at the CERN Super Proton Synchrotron over the years. The confidence gained in turn provides a basis for ever more daring proposals for new accelerators.[1] Today, the subject has grown into a large collection of activities.[2] Each activity constitutes an important research area; each

[1]One can come up with an impressive list here: linear colliders, high luminosity circular colliders, free electron laser drivers, modern synchrotron light sources, inertial fusion drivers, etc.

[2]Another impressive list is in order: methods to measure the impedance, beam diagnostic techniques, beam cooling techniques, numerical simulation methods, calculation of wake fields and impedances of complex objects, impedance budgeting in accelerator design, feedback systems, and various theoretical studies.

needs to be understood or implemented on the accelerators of the future. In comparison, the present volume is merely one attempt to introduce the subject, and only some of the above-mentioned activities will be covered in detail.

In the rest of Chapter 1, we will first describe the simplified accelerator model upon which our investigations will be built. The *space charge effect*, the most basic collective phenomenon, will then be discussed in detail; these discussions provide a background for later developments.

In Chapter 2, the Maxwell equations are solved to obtain the wake field of a beam with a rigid particle distribution. The action of the wake field on the particle distribution is neglected here; thus the beam-surroundings system is not solved self-consistently. The concepts of *wake function* and *impedance* will be introduced and their properties investigated. As an illustration, the special case of a vacuum chamber pipe with a resistive wall will be presented explicitly. The equations needed in Chapters 1 and 2 are basically the Maxwell equations.

In Chapters 3 and 4, the influence of wake fields on the beam will be studied—Chapter 3 for linear accelerators (linacs), Chapter 4 for circular accelerators. In Chapter 4 and part of Chapter 3, the discussions are carried out with a simplified model for the beam distribution. In fact, the beam will be represented as a point charge without any internal structure. The beam-surroundings system is solved self-consistently with the restriction that the beam is allowed to have only a center-of-mass motion. This simplified view allows a few of the collective instability mechanisms to be studied. These *one-particle models* are sufficiently successful that the treatment is extended to include a few *two-particle models*, in which the beam is represented as two point-macroparticles interacting with each other through the wake forces. This picture gives an insight into the internal motions within the beam. The equation used in Chapters 3 and 4 is basically $F = ma$.

An important topic is treated in Chapter 5, namely, *Landau damping*. Since our preference is to postpone formal treatments until later, Chapter 5 attempts to describe the Landau damping mechanism using a direct treatment instead of the more conventional Vlasov technique.

A self-consistent treatment of the beam-surroundings system that permits a full evaluation of the internal beam motions will be given in Chapter 6. Here the equation of motion—the *Vlasov equation*—is established to describe the system. The formalism that allows the solution of this equation will then be presented. Results obtained in the previous chapters, as well as some additional results, will be derived or rederived.[3]

[3]Depending on choice of emphasis, some material may be skipped. One possible choice of emphasis would skip, for example, Sections 1.4, 1.5, 1.6, 2.4, 3.3, 4.4, 5.2, 6.8, and 6.9.

We will use cgs units. To convert to other unit systems, it is convenient to apply the following conversions:

$$\frac{4\pi}{c} = Z_0 = \text{impedance of free space} = 120\pi\ \Omega \approx 377\ \Omega, \quad (1.2)$$

$$\frac{e^2}{m_0 c^2} = r_0 = \text{classical radius of the particle}$$

$$= \begin{cases} 2.818 \times 10^{-13}\ \text{cm} & \text{for electrons,} \\ 1.535 \times 10^{-16}\ \text{cm} & \text{for protons,} \end{cases} \quad (1.3)$$

where c is the speed of light, and e and m_0 are the electric charge and rest mass of the particle under consideration. Equation (1.2) follows from the conversion $1\ \Omega = 1/30c \approx \frac{1}{9} \times 10^{-11}$ s/cm in the cgs system.

1.2 FREE SPACE AND A PERFECTLY CONDUCTING SMOOTH PIPE

The electromagnetic field carried by a relativistic point charge q in free space is a familiar subject treated in textbooks.[4] The field distribution, shown in Figure 1.2(a), is Lorentz contracted into a thin disk perpendicular to the particle's direction of motion with an angular spread on the order of $1/\gamma$, where γ is the Lorentz energy factor. In the ultrarelativistic limit of $v = c$, the disk shrinks into a δ-function thickness, as shown in Figure 1.2(b). The electric field $\vec{E}$ points strictly radially outward from the point charge. The magnitude of $\vec{E}$ is most easily obtained by drawing a pillbox with radius r and an infinitesimal height around the charge q, as shown in Figure 1.2(b), and then applying Gauss's law.[5] The result is

$$E_r = \frac{2q}{r}\delta(s - ct), \quad (1.4)$$

where we have adopted a cylindrical coordinate system (r, θ, s) with s pointing in the direction of motion of q.[6] Similarly, an application of

[4]See, for example, J. D. Jackson, *Classical Electrodynamics*, 2nd ed., Wiley, New York, 1975.

[5]The reader is reminded of the remarkable fact that Gauss's law is valid even if the charges under consideration are moving with relativistic speeds. The reader should also recall that Lorentz contraction does not cause bending of field lines; the field lines are straight lines pointing radially outward and get bent only when the charge is accelerated.

[6]We use s to designate the absolute longitudinal position in the laboratory frame. The more conventional symbol z is reserved to designate the *relative* longitudinal position of a particle relative to a comoving reference particle.

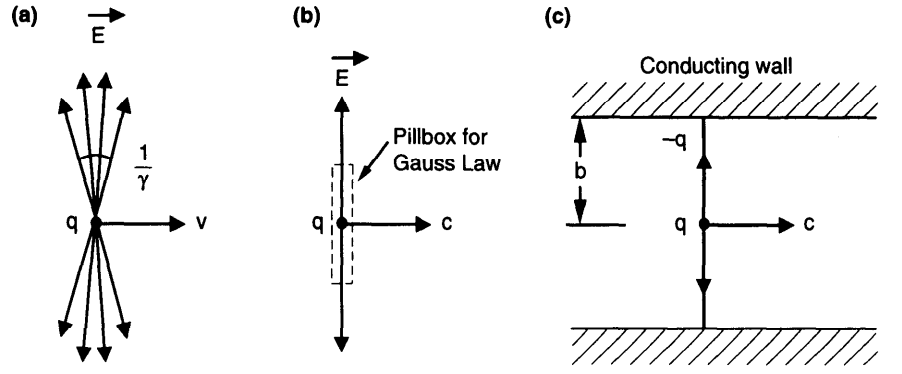

Figure 1.2. Electromagnetic field carried by an ultrarelativistic point charge: (a), (b) in free space; (c) in a perfectly conducting smooth pipe.

Ampere's law gives

$$B_\theta = \frac{2q}{r}\delta(s - ct), \tag{1.5}$$

which is equal to E_r. The shape of the field distribution resembles a pancake moving with the charge.

We now consider the case in which the point charge moves along the axis of an axially symmetric vacuum chamber pipe that is perfectly conducting, as shown in Figure 1.2(c). The same application of Gauss's and Ampere's laws again provides the results (1.4) and (1.5). The sole effect of the pipe wall is to truncate the field lines by terminating them onto the image charges and currents on the wall.

The above result that the pipe simply truncates the field lines without deformation applies only if the charge moves along the pipe axis. It is no longer correct for a point charge moving off-axis. One can consider, for instance, a particle that moves down the pipe with an offset a in the $\theta = 0$ direction. The charge and current density can be decomposed in terms of multipole moments,

$$\rho = \sum_{m=0}^{\infty} \rho_m \quad \text{and} \quad \vec{j} = \sum_{m=0}^{\infty} \vec{j}_m, \tag{1.6}$$

where the distribution with a pure mth moment is given by

$$\begin{aligned} \rho_m &= \frac{I_m}{\pi a^{m+1}(1 + \delta_{m0})}\delta(s - ct)\delta(r - a)\cos m\theta, \\ \vec{j}_m &= c\rho_m \hat{s}, \end{aligned} \tag{1.7}$$

where $\delta_{m0} = 1$ if $m = 0$, 0 if $m \neq 0$. In Eq. (1.7), the charge is distributed as an infinitesimally thin ring with radius a and with a $\cos m\theta$ angular dependence. The quantity I_m is the mth moment of the beam. The monopole moment I_0 is simply the net charge q of the beam. For an offset point charge, $I_m = qa^m$.

The reason that the pipe no longer simply truncates the free space field lines in this case is that if a simple truncation is made, the boundary conditions are no longer fulfilled, because the electric field is no longer perpendicular, and the magnetic field is no longer parallel, to the pipe wall. Indeed, the electromagnetic field carried by the $\cos m\theta$ ring beam (1.7) is obtained by solving the Maxwell equations together with proper boundary conditions. The result is

$$
\begin{aligned}
E_r &= \frac{2I_m}{1+\delta_{m0}}\delta(s-ct)\cos m\theta \begin{cases} \left(\frac{1}{b^{2m}} - \frac{1}{a^{2m}}\right) r^{m-1}, & r < a, \\ \frac{1}{r^{m+1}} + \frac{r^{m-1}}{b^{2m}}, & a < r < b, \end{cases} \\
E_\theta &= \frac{2I_m}{1+\delta_{m0}}\delta(s-ct)\sin m\theta \begin{cases} -\left(\frac{1}{b^{2m}} - \frac{1}{a^{2m}}\right) r^{m-1}, & r < a, \\ \frac{1}{r^{m+1}} - \frac{r^{m-1}}{b^{2m}}, & a < r < b, \end{cases} \\
B_r &= -E_\theta, \\
B_\theta &= E_r.
\end{aligned}
\tag{1.8}
$$

The derivation of Eq. (1.8) is omitted here. It can be reproduced as a special case of what we will derive in Section 2.1. [See discussion following Eq. (2.35).] The important facts here are that the particle has generated a field that has an angular dependence of $\sin m\theta$ and $\cos m\theta$, and that the field is Lorentz contracted into a δ-function in its longitudinal distribution. No wake field is left behind the particle as a result of this beam-environment interaction. The fact that a $\cos m\theta$ beam generates a field that has only the $\cos m\theta$ and $\sin m\theta$ angular dependences means different multipoles are decoupled, and is a consequence of the axial symmetry assumed.

Figure 1.3 shows the electric field pattern in the "pancake region" $s = ct$. Note that the electric field is perpendicular to the boundary $r = b$, but is not perpendicular to $r = a$ where the ring beam is located. Also, the field is not continuous across $r = a$.

There is no field inside the ring beam ($r < a$) for $m = 0$. The field pattern is uniform inside the beam for $m = 1$, and resembles the field inside a dipole magnet. Similarly, for $m = 2$ the field pattern resembles that of a quadrupole magnet, and for $m = 3$ a sextupole magnet.

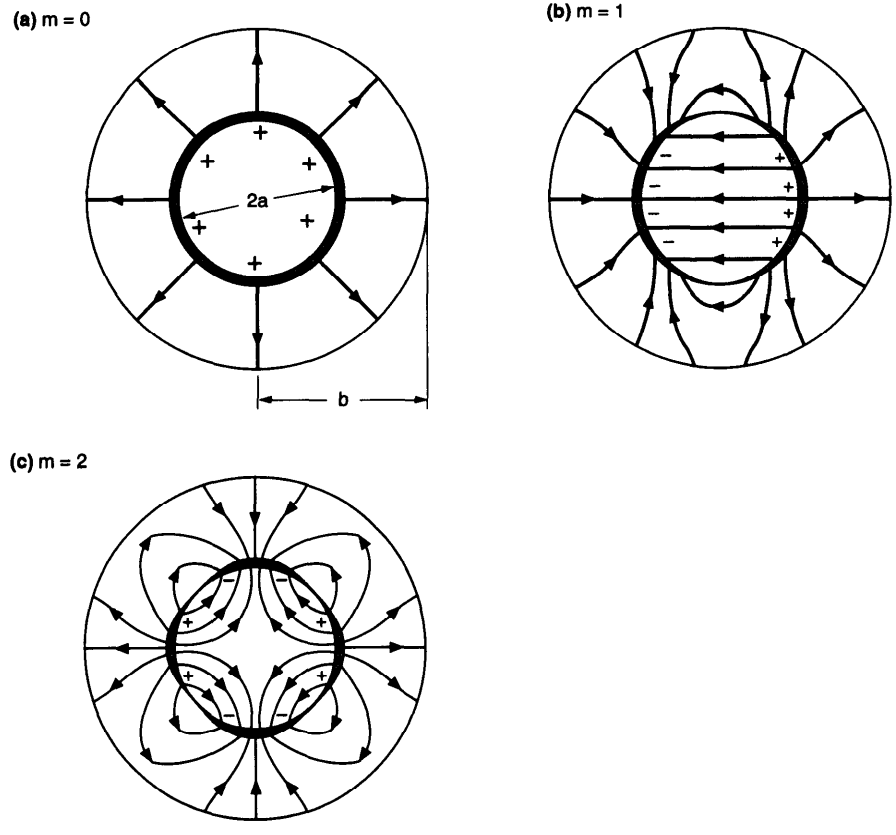

Figure 1.3. Electric field pattern associated with a $\cos m\theta$ ring beam. (a), (b), (c) are for $m = 0, 1, 2$, respectively. Shaded regions indicate the beam.

In free space or in a perfectly conducting pipe, because of the $\delta(s - ct)$ dependence in Eq. (1.8), an ultrarelativistic particle does not see the fields carried by other particles in the beam—unless the two particles move side by side with exactly the same longitudinal position, in which case they see each other's fields, but do not experience any Lorentz force because the electric force and the magnetic force cancel exactly.[7] Consequently, there can be no collective instability. Thus we arrive at one important conclusion, namely, for a collective instability to occur, the beam must not be ultrarelativistic, or its environment must not be a perfectly conducting smooth pipe.

[7]It is true that there is an electrostatic force in the rest frame of the beam, but when observed in the laboratory frame, motions are infinitely time dilated.

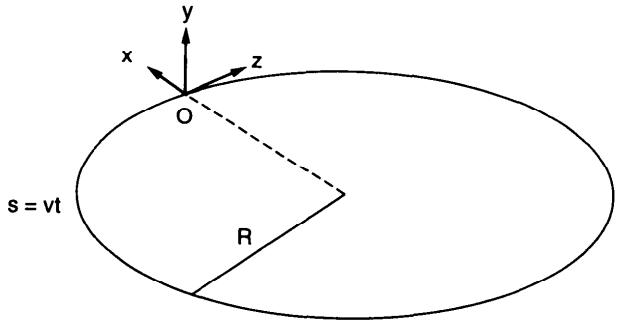

Figure 1.4. The accelerator model. The quantities x, y, and z are the horizontal, vertical and longitudinal coordinates of a particle relative to a reference particle O, which travels along the circumference with $s = vt$. The accelerator has a circumference $2\pi R$.

1.3 THE ACCELERATOR MODEL

We will model a circular accelerator so that its designed beam trajectory is a circle of circumference $2\pi R$. The beam circulates around the circumference inside a metallic vacuum chamber of a varying cross section. The unperturbed single-particle motion will be modeled as simple harmonic oscillators in the horizontal, vertical, and longitudinal coordinates x, y, and z with angular frequencies ω_{x0}, ω_{y0}, ω_{s0}, respectively.[8] We define the tunes $\nu_{x0,\,y0,\,s0}$ to be these frequencies divided by the particle's revolution frequency ω_0. See Figure 1.4. Typically we have $\nu_{x0} \gg 1$, $\nu_{y0} \gg 1$, and $\nu_{s0} \ll 1$.

The reference particle O has exactly the design energy and follows exactly the design orbit turn after turn in the accelerator. This fictitious particle is called the *synchronous* particle. Its trajectory will be designated by a coordinate s, which will have the meaning of the time variable in our description. The motions of all other particles are described relative to the synchronous particle. To completely describe the motion of a particle, we need six coordinates $(x, x', y, y', z, \delta)$ in the six-dimensional phase space, where $x' = dx/ds$ and $y' = dy/ds$ are the slopes of the horizontal and vertical coordinates of the particle relative to the designed direction of motion, and $\delta = \Delta P/P$ is the relative momentum error of the particle. The synchronous particle will have all six coordinates equal to zero. Under these assumptions our accelerator model can be summarized by the following unperturbed

[8]It is not possible to have *simultaneous* focusing in all three dimensions at a given time and space in an accelerator. The strong focusing accelerators, for example, do not provide simultaneous focusing in x and y. However, the job of an accelerator designer is to design an environment for the beam particles that resembles as much as possible a three-dimensional simple harmonic potential well which focuses in all three dimensions, although only in an *average* sense.

equations of motion for single particles:

$$\begin{aligned} x'' &+ \left(\frac{\nu_{x0}}{R}\right)^2 x = 0, \\ y'' &+ \left(\frac{\nu_{y0}}{R}\right)^2 y = 0, \\ z' &= -\eta\delta, \\ \delta' &= \begin{cases} 0, & \text{unbunched beams,} \\ \dfrac{1}{\eta}\left(\dfrac{\nu_{s0}}{R}\right)^2 z, & \text{bunched beams,} \end{cases} \end{aligned} \tag{1.9}$$

where a prime means taking the derivative with respect to s, and η is the *slippage factor* defined as

$$\eta = \alpha - \frac{1}{\gamma^2}, \tag{1.10}$$

with α an accelerator design constant called the *momentum compaction factor* and $\gamma = 1/\sqrt{1 - (v/c)^2}$. In a circular accelerator, α is typically positive and is approximately equal to $1/\nu_{x0}^2$. For high energy applications, $\delta = \Delta P/P$ is approximately equal to the relative energy error $\Delta E/E$.

The first two members in Eq. (1.9) describe the simple harmonic property of the *transverse betatron oscillation* of the particles. For the transverse motion, it is often useful to relate the tunes to the β-functions β_x and β_y of the accelerator design.[9] In the smooth accelerator model presently being considered, $2\pi\beta_{x,y}$ are just the betatron oscillation wavelengths, related to the tunes by

$$\nu_{x0} = \frac{R}{\beta_x} \quad \text{and} \quad \nu_{y0} = \frac{R}{\beta_y}. \tag{1.11}$$

Equation (1.9) also applies to linacs, provided one sets $\alpha = 0$ and replaces $\nu_{x0,y0}/R$ by $1/\beta_{x,y}$.

For ultrarelativistic cases, $\gamma \to \infty$, η is approximately equal to α and is most likely positive. For energies lower than a transition energy corresponding to $\gamma_{tr} \equiv 1/\sqrt{\alpha}$, η becomes negative. The accelerator operation is *below transition* if $\gamma < \gamma_{tr}$ and *above transition* if $\gamma > \gamma_{tr}$. When an accelerator is operated below transition, the longitudinal coordinate z of a particle, whose energy is slightly higher than the design energy ($\delta > 0$), will increase with

[9] E. D. Courant and H. S. Snyder, Ann. Phys. **3**, 1 (1958).

time s (i.e. $z' > 0$). On the other hand, if the accelerator is operated above transition, a higher energy particle will *slow down* ($z' < 0$) even though its actual velocity is higher than that of the synchronous particle. This unexpected sign is called the *negative mass* effect, and is due to the fact that higher energy particles will have to make larger orbits as they circulate around the accelerator. For linacs ($\alpha = 0$) the operation is always below transition.

Combining the two longitudinal equations for z and δ in Eq. (1.9), one obtains the *longitudinal synchrotron oscillation*

$$z'' + \left(\frac{\nu_{s0}}{R}\right)^2 z = 0. \tag{1.12}$$

For unbunched beams, the accelerator is operated with no longitudinal focusing; the equations of motion for z and δ can be described by Eq. (1.12) if we set $\nu_{s0} = 0$, and therefore can be considered a special case of bunched motion. However, we separate the bunched and unbunched cases explicitly because their beam dynamics are quite different.

At transition, $\eta = 0$, the flow of particles in the longitudinal phase space freezes. This is the moment when the beam is most vulnerable to perturbations and is a concern for accelerators (particularly proton synchrotrons) whose operation is such that the beam energy is accelerated to cross transition. Special care is often required to deal with transition crossing.

For an unbunched beam, δ does not change with time, and z' depends on δ. The unperturbed beam has a uniform longitudinal distribution with particles shearing against each other due to a spread in their energies. The particle motion in the three phase spaces (x, x'), (y, y'), and (z, δ) is shown in Figure 1.5. Unless otherwise noted, we ignore coupling among the three degrees of freedom.

Equation (1.9), together with Eqs. (1.10–1.12), describes our accelerator model.[10] They specify the unperturbed motions. Based on this model, one can study the various stability problems by introducing perturbations. Adding nonlinear terms on the right hand side of these equations, for example, leads to the study of single-particle nonlinear dynamics. We will study another type of perturbations, namely those due to collective electromagnetic fields.

[10]To explore the physics of accelerators further, read Henri Bruck, *Accélérateurs Circulaire de Particules*, Univ. France Press, 1966, English transl. LASL Report LA-TR-72-10(R); Matthew Sands, *The Physics of Electron Storage Rings, An Introduction*, SLAC Report 121 (1970); J. D. Lawson, *The Physics of Charged-Particle Beams*, Clarendon Press, Oxford, 1977; Stanley Humphries, Jr., *Principles of Charged Particle Acceleration*, Wiley, New York, 1986; N. S. Dikanski and D. V. Pestrikov, *Physics of Intense Beams in Storage Rings*, Nauka Publishers, Novosibirsk, 1989 (in Russian); Stanley Humphries, Jr., *Charged Particle Beams*, Wiley, New York, 1990; D. A. Edwards and M. J. Syphers, *An Introduction to the Physics of High Energy Accelerators*, Wiley, New York, 1993.

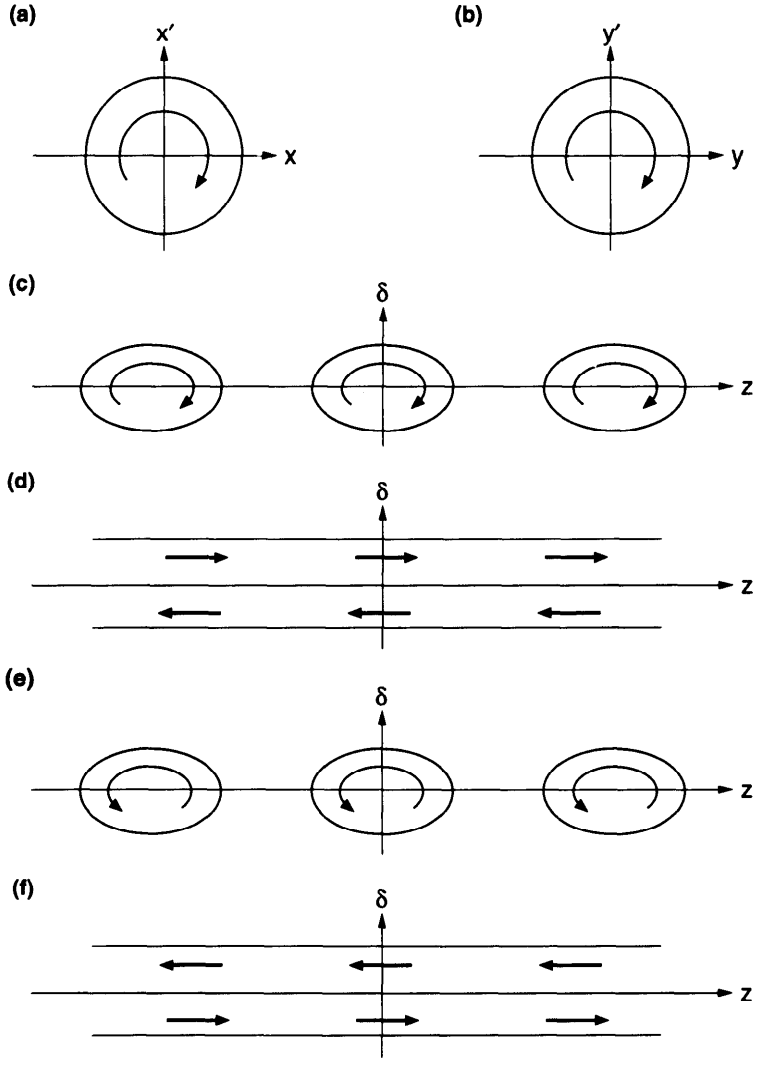

Figure 1.5. Motion of a distribution of particles in phase spaces. Arrows indicate the direction of motion of particle trajectories. (a) and (b) are transverse phase spaces. (c) and (d) are longitudinal phase spaces for bunched and unbunched beams below transition. (e) and (f) are the same as (c) and (d) but above transition. In (c) and (e), the two adjacent bunches are also shown. In the longitudinal phase space, there is a shearing of the particle flow pattern in the unbunched case. Note that the flow direction reverses as beam energy crosses transition. At transition, the flow pattern freezes. Above transition, the rotation is counterclockwise, which is opposite to the transverse cases and is a consequence of the negative mass effect.

Before leaving the subject of accelerator model, it is useful here to introduce the concept of a *tune shift*. Consider the case when the perturbation affects the focusing in y-motion, i.e., the perturbation is linear in y:

$$y'' + \left(\frac{\nu_{y0}}{R}\right)^2 y = Ky. \tag{1.13}$$

The perturbed motion can be described by a perturbed tune ν_y determined by

$$\nu_y^2 = \nu_{y0}^2 - KR^2. \tag{1.14}$$

For small perturbation $|KR^2| \ll \nu_{y0}^2$, the tune has shifted by an amount[11]

$$\Delta\nu_y = \nu_y - \nu_{y0} = -\frac{KR^2}{2\nu_{y0}}. \tag{1.16}$$

In case the linear perturbation (linear in y) occurs at a localized position around the accelerator, the right hand side of Eq. (1.13) reads $Ky\delta_p(s)2\pi R$, where δ_p is the periodic δ-function with period $2\pi R$. The tune shift to the first order in K is still given by Eq. (1.16). This means that, to the first order, the effect of a linear perturbation is the same whether it is spread out over the circumference of the accelerator or lumped at a discrete location. This approximation amounts to ignoring the resonance effects when ν_{y0} is close to half integers.

The concept of tune shift—the simplest manifestation of which is illustrated in Eqs. (1.13–1.16)—plays a crucial role in the study of collective effects. In later chapters, what we will often compute is $\Delta\nu$ when the perturbations are due to collective electromagnetic fields, and in general the tune shift is complex.[12] This point will become clear as the subject develops.

[11]For readers familiar with the formula

$$\Delta\nu = \frac{1}{4\pi}\oint ds\,\beta_y\,\Delta G = \frac{1}{2\pi}\oint ds\,\frac{\beta_y}{2}\,\Delta G, \tag{1.15}$$

the factor $\beta_y/2$ in the expression has the same physical meaning as the factor $1/2\nu_{y0}$ in Eq. (1.16) [see Eq. (1.11)], which in turn has the simple origin of Eq. (1.14), and is not something mysterious.

[12]Two particular aspects are worth mentioning here for later reference. (1) Just as the tune shift is independent of the detailed distribution of gradient errors around the accelerator (away from resonances), the detailed distribution of the impedance (which gives rise to the collective mode frequency shift and growth rate) does not matter and can often be regarded as being uniformly distributed around the accelerator for simplicity. (2) For the transverse collective effects, the mode frequency shifts and growth rates obtained using an uniformly distributed impedance can be modified to yield the result for a localized impedance by simply replacing $R/\nu \to \beta_Z$, where β_Z is the β-function at the location of the impedance.

1.4 TRANSVERSE SPACE CHARGE EFFECTS

The first collective effect to be considered is the space charge effect. It was previously mentioned that there are no collective effects in free space or in a perfectly conducting smooth pipe in the ultrarelativistic limit $\gamma \to \infty$. To study the space charge effect, we back off from this limit, although we will still consider a moderately relativistic beam with $\gamma \gg 1$. One difference between the ultra and moderate relativisticities was illustrated in Figure 1.2(a) and (b). In this and the next sections, we will study the transverse and longitudinal effects of the space charge forces on the motion of particles in the beam.

Consider an unbunched beam that has a longitudinal line charge density λe and moves with speed βc. Let N be the total number of particles in the beam; we have $\lambda = eN/2\pi R$. Let the beam have a round transverse distribution which is uniform up to a radius a. We consider the motion of a test particle in the beam at a radial distance r ($r < a$) away from the beam axis. Applying Gauss's law yields the electric field seen by the particle,

$$E_r = \frac{2\lambda e}{a^2} r. \tag{1.17}$$

Similarly, application of Ampere's law gives

$$B_\theta = \frac{2\lambda e\beta}{a^2} r = \beta E_r. \tag{1.18}$$

The Lorentz force experienced by the particle is in the radial direction,

$$F_r = e(E_r - \beta B_\theta) = \frac{2\lambda e^2}{a^2\gamma^2} r. \tag{1.19}$$

Note that the electric and magnetic forces almost cancel each other, yielding the factor of γ^2 in the denominator. The direct space charge effect is therefore nonrelativistic in nature.

Consider the vertical motion of the particle. The equation of motion is

$$y'' + \left(\frac{\nu_0}{R}\right)^2 y = \frac{F_y}{m\gamma\beta^2 c^2}, \tag{1.20}$$

where ν_0 is the unperturbed tune and the factor of $1/\gamma$ on the right-hand side represents the rigidity of the particle and F_y is given by Eq. (1.19). In terms of the classical radius of the particle r_0, we have the prescription of Eq. (1.13) with $K = 2\lambda r_0/a^2\beta^2\gamma^3$.

For small tune shifts $\Delta\nu = \nu - \nu_0$, we obtain, from Eq. (1.16), an expression for the *space charge tune shift*,

$$\Delta\nu = -\frac{\lambda r_0 R^2}{\nu_0 a^2 \beta^2 \gamma^3}. \tag{1.21}$$

The negative sign indicates that the direct space charge is defocusing. The same tune shift also occurs in the horizontal dimension provided ν_0 is interpreted as the horizontal unperturbed tune. In a strong focusing accelerator, one has the connection $\epsilon = a^2/2\beta_y$, where ϵ is the transverse emittance of the beam and in the smooth accelerator model is equal to $\nu_0 a^2/2R$. In the case of a proton beam, the emittance usually depends on beam energy in such a way that the normalized emittance $\epsilon_N \equiv \epsilon\beta\gamma$ is a constant even during acceleration when β and γ change. It would then be convenient to express Eq. (1.21) in terms of ϵ_N,

$$\Delta\nu = -\frac{\lambda r_0 R}{2\epsilon_N \beta\gamma^2}. \tag{1.22}$$

The tune shift $\Delta\nu$ specifies the limit of space charge effect on beam intensity. In a beam transport line, for example, defocusing due to space charge force must not be larger than the focusing provided by external focusing elements, i.e., $|\Delta\nu|$ must be less than ν_0. This leads to a stability limit on the beam current $I = e\lambda\beta c$ given by

$$I < \frac{2ec\beta^2\gamma^2\epsilon_N}{r_0\beta_y}. \tag{1.23}$$

In Eq. (1.23), $2\pi\beta_y$ is the average betatron wavelength in the transport line.

The stability condition imposed by space charge tune shift in circular accelerators is slightly different from that for transport lines. In a circular accelerator, the tune shift, Eq. (1.22), must not cause the tune value to cross a low order rational number where resonant effects cause the beam to become unstable. A typical value of this limit is approximately 0.5 to avoid major resonances; in other words, beam stability requires $|\Delta\nu| \lesssim 0.5$.[13] Note that $\Delta\nu$ is inversely proportional to $\beta\gamma^2$. The space charge effect decreases rapidly with increasing beam energy. Note also $\Delta\nu$ is proportional to the circumference of the accelerator, indicating a preference for a compact accelerator design.

[13]J. P. Delahaye et al., *Proc. 11th Int. Conf. on High Energy Accelerators*, Geneva, 1980, p. 299; E. Raka et al., IEEE Trans. Nucl. Sci. **NS-32**, 3110 (1985); C. Ankenbrandt and S. D. Holmes, *Proc. IEEE Conf. Part. Accel.*, Washington, 1987, p. 1066.

In the case of a bunched beam, Eq. (1.22) gives the maximum space charge tune shift if one takes λ to be $\hat{\lambda}$, the peak line charge density near the center of the beam bunch. For Gaussian beams, this means $\hat{\lambda} = N/\sqrt{2\pi}\sigma_z$. Take a proton synchrotron, for example, with $\epsilon_N = 1 \times 10^{-6}$ m, $R = 60$ m, $N = 10^{10}$, $\sigma_z = 0.3$ m, and $\nu_0 \approx 8$; one finds a beam size of $a = 3.8$ mm and a maximum tune shift of $\Delta\nu = -0.4$ at a beam momentum of 1 GeV/c. The electric field at the beam edge ($r = a$) is about 10 kV/m.

Exercise 1.1 Derive an expression of $\Delta\nu$ for a round Gaussian beam of rms transverse size σ. Consider small oscillation amplitudes. Show that the result is given by Eq. (1.22) if we replace a by $\sqrt{2}\sigma$ and define $\epsilon = \sigma^2/\beta_y$.

The cancellation between the electric and magnetic forces, and thus the nonrelativistic nature of the direct space charge effect, is a consequence of considering the beam in free space. When boundary conditions are included, this cancellation is destroyed, leading to a potentially much larger tune shift for relativistic beams.[14]

To illustrate this, consider the previous uniform unbunched beam in a vacuum chamber modeled as two parallel plates (made of perfectly conducting, nonmagnetic metal) located at vertical positions $y = h$ and $y = -h$. The boundary condition is such that the electric field is perpendicular to the plates. The electric field now contains, in addition to Eq. (1.17), a contribution from the image charges. Assuming $h \gg a$, the image charge contribution can be calculated as coming from a series of image line charges of density $-\lambda e$ at $y = \pm 2h, \pm 6h, \pm 10h, \ldots$, and density λe at $y = \pm 4h, \pm 8h, \ldots$, as shown in Figure 1.6(a). A particle at location y on the y-axis will experience an electric field, due to image charges, of

$$E_y = 2\lambda e\left(\frac{1}{2h - y} - \frac{1}{4h - y} + \frac{1}{6h - y} - \cdots - \frac{1}{2h + y} + \frac{1}{4h + y} - \frac{1}{6h + y} + \cdots\right). \tag{1.24}$$

For $|y| \ll h$, this gives, to first order in y,

$$E_y \approx -\frac{\lambda e}{h^2} y \sum_{n=1}^{\infty} \frac{(-1)^n}{n^2} = \frac{\pi^2}{12}\frac{\lambda e}{h^2} y. \tag{1.25}$$

The boundary condition for the static magnetic field is determined by the magnet pole faces (made of ferromagnetic material) instead of the vacuum chamber. Let the boundary be represented as two parallel plates located at

[14] L. J. Laslett, *Proc. Summer Study on Storage Rings, Accelerators, and Experimentation at Super-high Energies*, 1963, BNL Report 7534, p. 324.

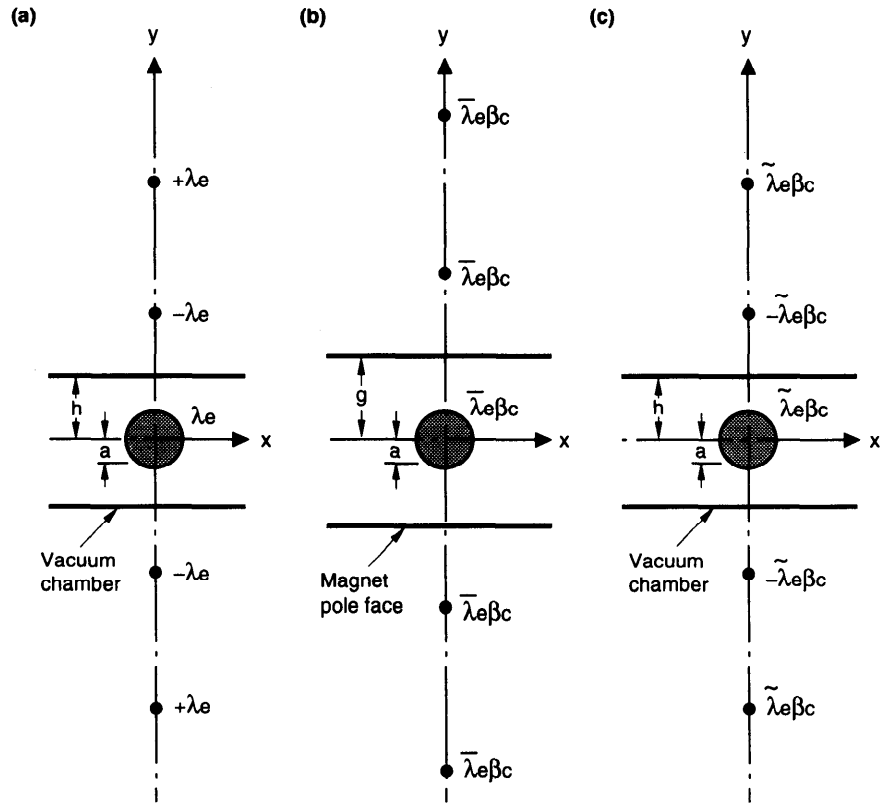

Figure 1.6. (a) Image charges due to a line charge density λe in a two-parallel-plate vacuum chamber. (b) Image currents due to a dc line current $\bar{\lambda} e\beta c$. (c) Image currents due to an ac line current $\tilde{\lambda} e\beta c$. The beam size a is assumed to be much smaller than the vacuum chamber pipe gap h and the magnet pole face spacing g ($g > h$, so that the vacuum chamber fits inside the magnet gap).

$y = g$ and $y = -g$. The boundary condition is that the magnetic field is perpendicular to the magnet pole faces. The image currents are $+\lambda e\beta c$ at $y = \pm 2g, \pm 4g, \pm 6g, \ldots$, yielding a magnetic field, seen by a particle at location y on the y-axis, equal to

$$B_x = 2\lambda e\beta\left(\frac{1}{2g-y} + \frac{1}{4g-y} + \frac{1}{6g-y} + \cdots - \frac{1}{2g+y} - \frac{1}{4g+y} - \frac{1}{6g+y} - \cdots\right)$$

$$\approx \frac{\lambda e\beta}{g^2} y \sum_{n=1}^{\infty} \frac{1}{n^2} = \frac{\pi^2}{6}\frac{\lambda e\beta}{g^2} y. \tag{1.26}$$

The successive image charges have alternating signs, but the image currents all have the same sign. Adding the image force $F_y = e(E_y + \beta B_x)$ to the direct space charge force, one obtains a vertical tune shift

$$\Delta\nu_y = -\frac{\lambda r_0 R^2}{\nu_{y0}\beta^2\gamma}\left(\frac{1}{a^2\gamma^2} + \frac{\pi^2}{24h^2} + \frac{\pi^2\beta^2}{12g^2}\right). \tag{1.27}$$

The first term comes from the direct space charge. The other two terms come from the image charges and currents, respectively. All these contributions are defocusing. The image contributions dominate if $\gamma > h/a$ or g/a. When h and g terms are removed, the expression reduces to the free space result, Eq. (1.21).[15]

Exercise 1.2 Equations (1.24–1.27) are for the y-motion. Repeat the analysis for the x-motion. Show that, for small amplitudes,

$$E_x = -\frac{\pi^2}{12}\frac{\lambda e}{h^2}x \quad \text{and} \quad B_y = \frac{\pi^2}{6}\frac{\lambda e\beta}{g^2}x. \tag{1.28}$$

Note that the fields due to the image charges and currents satisfy $\nabla \cdot \vec{E} = 0$ and $\nabla \times \vec{B} = 0$. Show that the horizontal tune shift is given by

$$\Delta\nu_x = -\frac{\lambda r_0 R^2}{\nu_{x0}\beta^2\gamma}\left(\frac{1}{a^2\gamma^2} - \frac{\pi^2}{24h^2} - \frac{\pi^2\beta^2}{12g^2}\right). \tag{1.29}$$

Equations (1.27) and (1.29) are applicable for an unbunched beam. As mentioned before, for a direct space charge effect, all we need to do for a bunched beam is to replace λ by $\hat{\lambda}$ to obtain the maximum tune shift. In case there is a boundary, the maximum electric field is still obtained by replacing λ by $\hat{\lambda}$, but the calculation of magnetic field is more involved. One has to decompose the current into a "dc" component $\bar{\lambda}$ and an "ac" component $\tilde{\lambda}$, where the dc component contains frequencies at which the skin depth is greater than the vacuum chamber pipe wall thickness, while the ac component has a skin depth that is small compared to the pipe thickness.[16] The boundary condition at $y = \pm g$ as was done to obtain the magnetic field (1.26) is to be applied to $\bar{\lambda}$. The boundary condition for $\tilde{\lambda}$ is that the magnetic field is parallel to the vacuum chamber walls at $y = \pm h$. The corresponding image currents are shown in Figure 1.6(c). Note that the successive images have alternating signs.

[15]For more general beam and vacuum chamber geometries, see B. W. Zotter, IEEE Trans. Nucl. Sci. **NS-22**, 1451 (1975).

[16]See Eq. (2.7) for a definition of the skin depth δ_{skin}. Strictly speaking, if the pipe is perfectly conducting, $\delta_{skin} = 0$, and all currents are ac.

If we identify $\bar{\lambda}$ as the average beam density and $\tilde{\lambda}$ as $\hat{\lambda} - \bar{\lambda}$, following Laslett,[17] and apply the proper boundary conditions, the vertical tune shift is found to be

$$\Delta\nu_y = -\frac{r_0 R^2}{\nu_{y0}\beta^2\gamma}\left[\frac{1}{\gamma^2}\left(\frac{1}{a^2} + \frac{\pi^2}{24h^2}\right)\hat{\lambda} + \beta^2\left(\frac{\pi^2}{24h^2} + \frac{\pi^2}{12g^2}\right)\bar{\lambda}\right] \quad (1.30)$$

The first term, containing $\hat{\lambda}/a^2$, is the direct space charge term, Eq. (1.21). Terms proportional to $\hat{\lambda}$ are suppressed by $1/\gamma^2$, but the $\bar{\lambda}$-terms are not similarly suppressed. For a beam of M Gaussian bunches, each containing N particles, we have $\bar{\lambda} = MN/2\pi R$ and $\hat{\lambda} = N/\sqrt{2\pi}\sigma_z$. For a highly bunched beam, the image effects dominate if γ is larger than $\sqrt{\hat{\lambda}/\bar{\lambda}}$ times g/a or h/a. For an unbunched beam with $\hat{\lambda} = \bar{\lambda}$, we recover Eq. (1.27). For perfectly conducting plates at $y = \pm h$, $\bar{\lambda} = 0$ because all currents are ac; the tune shift then acquires the relativistic suppression factor of $1/\gamma^2$.

The above analysis can be carried out similarly for the x-motion. The result is

$$\Delta\nu_x = -\frac{r_0 R^2}{\nu_{x0}\beta^2\gamma}\left[\frac{1}{\gamma^2}\left(\frac{1}{a^2} - \frac{\pi^2}{24h^2}\right)\hat{\lambda} - \beta^2\left(\frac{\pi^2}{24h^2} + \frac{\pi^2}{12g^2}\right)\bar{\lambda}\right]. \quad (1.31)$$

Continuing the numerical example that followed Eq. (1.23) and taking $M = 120$, $\nu_{x0} \approx \nu_{y0} \approx 8$, $g = 7$ cm, and $h = 5$ cm, we find that the image contributions to the tune shifts are $\Delta\nu_{x,y} = \pm 0.0014$, much smaller than the direct space charge contributions.

Equations (1.30–1.31) are known as the *Laslett tune shifts*. The focusing and defocusing properties of the various contributions are summarized in Table 1.1.

So far we have studied the motion of a single particle in an established beam distribution. This is an incoherent effect obtained by assuming the beam distribution is rigid, unperturbed by the motion of single particles. There are also collective effects that perturb the coherent motion of the beam distribution. Such effects will be discussed as we proceed.

For later use, we include here a calculation of the electromagnetic field generated by a perturbed beam distribution. The starting point of this calculation is Eq. (1.8). Consider a beam whose distribution contains a perturbation in the form of a $\cos m\theta$ ring multipole similar to Eq. (1.7) except that $\delta(s - ct)$ is replaced by a general distribution $\lambda(s - ct)$. Let the perturbed beam go down the axis of a perfectly conducting cylindrical pipe of radius b.

[17]This assumes δ_{skin}, evaluated at the revolution frequency, is much smaller than the wall thickness.

By superposition, the transverse fields are given by Eq. (1.8) in the ultrarelativistic limit with the same replacement $\delta(s - ct) \to \lambda(s - ct)$. If we back off from the ultrarelativistic limit but still keep $\gamma \gg 1$ and let the longitudinal distribution be given by $\lambda(s - \beta ct)$, the effect on the electric field is negligible. The magnetic field components become $B_\theta = \beta E_r$ and $B_r = -\beta E_\theta$. The transverse Lorentz force generated by the beam and seen by a test charge e located at (r, θ, s) that moves with the beam is given by

$$\vec{F}_\perp = e\left(\vec{E} + \beta\hat{s} \times \vec{B}\right)_\perp = \frac{e\vec{E}_\perp}{\gamma^2}$$

$$= \frac{2eI_m}{(1 + \delta_{m0})\gamma^2}\lambda(s - \beta ct)$$

$$\times \begin{cases} \left(\dfrac{1}{b^{2m}} - \dfrac{1}{a^{2m}}\right) r^{m-1}(\hat{r}\cos m\theta - \hat{\theta}\sin m\theta), \\ \dfrac{1}{r^{m+1}}(\hat{r}\cos m\theta + \hat{\theta}\sin m\theta) + \dfrac{r^{m-1}}{b^{2m}}(\hat{r}\cos m\theta - \hat{\theta}\sin m\theta), \end{cases} \tag{1.32}$$

where the two entries are for the $r < a$ and the $a < r < b$ regions respectively, and $\hat{r}$ and $\hat{\theta}$ are the directional unit vectors.

There is no transverse force in the beam region ($r < a$) for the case of $m = 0$, as shown already in Figure 1.3(a). For $m = 1$, the transverse force $\vec{F}_\perp$ is uniform across the transverse beam distribution. Implications of Eq. (1.32) on the collective beam instabilities will be studied in later chapters.

Table 1.1. Focusing and defocusing properties of the various space-charge contributions on the horizontal and vertical betatron oscillations. (F means focusing and D means defocusing)

	Horizontal	Vertical
Direct space charge:		
Electric	D	D
Magnetic	F	F
Net	D	D
Image charges and currents:		
Electric	F	D
Dc magnetic	F	D
Ac magnetic	D	F
Net	F	D

Exercise 1.3 Consider a transverse r-distribution that is not $\delta(r - a)$ but a general distribution $n(r)$:

$$\rho_m = \frac{2I_m}{1 + \delta_{m0}} \lambda(s - \beta ct) n(r) \cos m\theta \tag{1.33}$$

with the normalization $\int_0^\infty 2\pi r^{m+1}\, dr\, n(r) = 1$ and I_m the mth moment. Show that, by superposition,

$$\vec{F}_\perp = \frac{2eI_m}{(1 + \delta_{m0})\gamma^2} \lambda(s - \beta ct) \times \left\{ (\hat{r} \cos m\theta + \hat{\theta} \sin m\theta) \frac{1}{r^{m+1}} \int_0^r 2\pi r'^{m+1}\, dr'\, n(r') + (\hat{r} \cos m\theta - \hat{\theta} \sin m\theta) r^{m-1} \left[\frac{1}{b^{2m}} - \int_r^\infty 2\pi\, dr' \frac{n(r')}{r'^{m-1}} \right] \right\}. \tag{1.34}$$

In particular, for a uniform disk distribution with $n(r) =$ constant for $r < a$, the force inside the beam region ($r < a$) is

$$\vec{F}_\perp = \frac{2eI_m}{(1 + \delta_{m0})\gamma^2} \lambda(s - \beta ct) \times \left\{ (\hat{r} \cos m\theta + \hat{\theta} \sin m\theta) \frac{r}{a^{m+2}} + (\hat{r} \cos m\theta - \hat{\theta} \sin m\theta) \times \left[\frac{r^{m-1}}{b^{2m}} + \frac{m + 2}{m - 2} \left(\frac{r^{m-1}}{a^{2m}} - \frac{r}{a^{m+2}} \right) \right] \right\}. \tag{1.35}$$

For $m = 0$, this reduces to Eq. (1.19).

1.5 LONGITUDINAL SPACE CHARGE EFFECTS

The previous section deals with the transverse effects of the space charge force. For an unbunched beam with uniform longitudinal distribution, the electric and magnetic fields are purely transverse by symmetry. There are no longitudinal fields and no longitudinal forces. In case the longitudinal distribution is not uniform, but given by $e\lambda(s - \beta ct)$, longitudinal fields no longer vanish. Furthermore, we know that in free space or a perfectly conducting smooth pipe, there will be no longitudinal force in the ultrarelativistic limit.

This is an indication that the longitudinal force is proportional to $1/\gamma^2$. In this section, we will calculate this longitudinal force, which we will show is proportional to $\lambda'(s - \beta ct)/\gamma^2$, where a prime means taking the derivative with respect to s. The longitudinal force vanishes for a uniform beam because $\lambda' = 0$.

Consider a beam of radius a inside a cylindrical, perfectly conducting smooth pipe of radius b. Let the beam be ring-shaped similar to Eq. (1.7) with $m = 0$. The transverse electric and magnetic fields are approximately given by

$$E_r = \frac{B_\theta}{\beta} = 2e\lambda(s - \beta ct)\begin{cases} 0 & \text{if } r < a, \\ 1/r & \text{if } a < r < b. \end{cases} \tag{1.36}$$

Equation (1.36) is valid if the longitudinal spread of the field at the wall due to the $1/\gamma$ opening angle in Figure 1.2(a) is small compared with the distance over which the longitudinal distribution changes appreciably.[18] In this case, E_r and B_θ are determined by the *local* longitudinal beam density where the field is evaluated.

We next calculate the longitudinal electric field by applying Faraday's law

$$\oint d\vec{l} \cdot \vec{E} = -\frac{1}{c}\frac{\partial}{\partial t}\int d\vec{\mathscr{A}} \cdot \vec{B} \tag{1.37}$$

to the circuit shown in Figure 1.7(a). One of the sides of the circuit is on the pipe axis and the opposite side is just inside the perfectly conducting pipe wall where the longitudinal electric field component vanishes. The length of these two sides is Δs, which is considered infinitesimal. Application of Eq. (1.37) gives a condition for the longitudinal electric field E_s on the pipe axis:

$$E_s \Delta s + 2e[\lambda(s + \Delta s - \beta ct) - \lambda(s - \beta ct)]\int_a^b \frac{dr}{r}$$
$$= -\frac{2e\beta}{c}\frac{\partial \lambda(s - \beta ct)}{\partial t}\Delta s \int_a^b \frac{dr}{r}. \tag{1.38}$$

By connecting $\partial\lambda/\partial t = -\beta c\lambda'$, Eq. (1.38) gives

$$E_s = -\frac{2e}{\gamma^2}\lambda'(s - \beta ct)\ln\frac{b}{a}. \tag{1.39}$$

One can draw the circuit with the axis side off axis but still inside the beam, as shown in Figure 1.7(b). It follows that Eq. (1.39) applies to the region $r < a$, because E_r and B_θ vanish inside the beam. We thus conclude that E_s is constant, given by Eq. (1.39), inside the beam cross

[18] For a bunched beam with length l, this means $l \gg b/\gamma$. See Exercises 1.4 and 1.5 below.

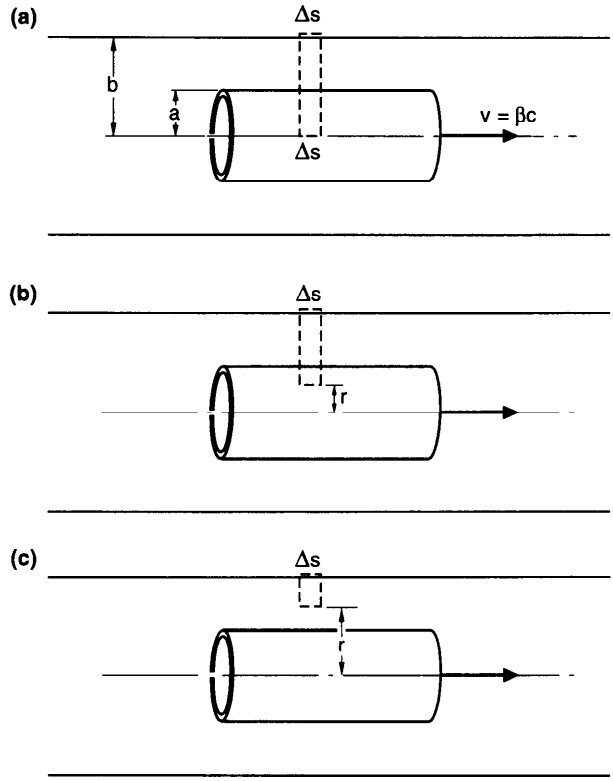

Figure 1.7. The longitudinal electric field can be calculated by drawing the various circuits as shown and applying Faraday's law. The cylinders represent the ring beam. These calculations are applied to both $m = 0$ and $m \neq 0$. The circuits are drawn in the $\theta = 0$ plane.

section. One can also place the axis side of the circuit outside the beam as shown in Figure 1.7(c), which yields, in the region $a < r < b$,

$$E_s = -\frac{2e}{\gamma^2}\lambda'(s - \beta ct)\ln\frac{b}{r}. \tag{1.40}$$

When $r = b$, this gives $E_s = 0$. Equations (1.36), (1.39), and (1.40) complete the field components; the rest of the field components E_θ, B_r, and B_s vanish.

As promised, the longitudinal force $F_s = eE_s$ is proportional to λ'/γ^2. Physically the force comes from an imbalance between the amounts of charge behind and in front of the test charge being considered. In case there are more charges in the front, λ' is positive, leading to a retarding force. In case there are more charges in back, the force is accelerating.

Exercise 1.4 Show that the approximate expressions (1.36), (1.39) and (1.40) satisfy the Maxwell equations if $\lambda \gg \lambda'' b^2/\gamma^2$. For a bunched beam, this requires the bunch length l to be much longer than b/γ. Show that the leading correction term to Eq. (1.36) is

$$\Delta E_r = \frac{\Delta B_\theta}{\beta} = \frac{e}{\gamma^2}\lambda''(s-\beta ct)\begin{cases} r\ln\dfrac{b}{a}, \\ r\ln\dfrac{b}{r} + \dfrac{r}{2} - \dfrac{a^2}{2r}, \end{cases} \tag{1.41}$$

where the two entries refer to the regions $r < a$ and the $a < r < b$, respectively.

Exercise 1.5 The above analysis was done in the presence of a beam pipe. Removing the beam pipe by setting $b \to \infty$ gives an apparent logarithmic divergence of E_s in free space. However, the analysis breaks down when b becomes comparable to γl. To illustrate this explicitly, consider the case of free space without a beam pipe. The longitudinal electric field at position z on the axis can be obtained by superposing contributions from infinitesimal rings. Show that

$$E_s(z) = -\frac{1}{\gamma^2}\int_{-\infty}^{\infty} e\lambda(z'-z)\,dz' \frac{z'}{\left(z'^2 + \dfrac{a^2}{\gamma^2}\right)^{3/2}}. \tag{1.42}$$

Consider the case with $\lambda(z) = (1/2l)(1 + z/l)$ for $|z| < l$, and 0 for $|z| > l$, which gives $\lambda' = 1/2l^2$. Assuming $\gamma l \gg a$, show that at the bunch center $E_s(0)$ is given by Eq. (1.39) with b replaced by γl.

In case the transverse distribution is not ring-shaped, but described by $n(r)$ [normalized by $\int_0^\infty 2\pi r\,dr\,n(r) = 1$], superposition gives

$$E_s = -\frac{2e}{\gamma^2}\lambda'(s-\beta ct)\left[\ln\frac{b}{r} - \int_r^b 2\pi r'\,dr'\,n(r')\ln\frac{r'}{r}\right]. \tag{1.43}$$

This E_s vanishes if $r = b$, as it should. In case the transverse beam distribution $n(r)$ is uniform in region $r < a$, the field is

$$E_s = -\frac{2e}{\gamma^2}\lambda'(s-\beta ct)\begin{cases} \ln\dfrac{b}{a} + \dfrac{1}{2} - \dfrac{r^2}{2a^2}, \\ \ln\dfrac{b}{r}. \end{cases} \tag{1.44}$$

This E_s gives a field on the pipe axis that differs from the ring beam case, Eq. (1.39), as the form factor $\ln(b/a)$ is replaced by $\ln(b/a) + \frac{1}{2}$.

Consider the longitudinal motion of a particle in a bunched beam that has a uniform transverse distribution. Let z be the longitudinal coordinate of the particle relative to the beam center. The longitudinal electric field, Eq. (1.44), will contribute to an energy gain gradient of $eE_s(z)$. From Eq. (1.9), the perturbed equations of motion for the particle is

$$\begin{aligned} z' &= -\eta\delta, \\ \delta' &= \frac{1}{\eta}\left(\frac{\nu_{s0}}{R}\right)^2 z + \frac{eE_s(z)}{\beta^2 E}, \end{aligned} \tag{1.45}$$

where E is the design energy of the accelerator. The factor $1/\beta^2$ comes from the conversion $\Delta P/P = \Delta E/\beta^2 E$. If the longitudinal distribution λ is parabolic in z with total length $2\hat{z}$, the perturbed synchrotron motion is described by

$$z'' + \left(\frac{\nu_{s0}}{R}\right)^2 z = -\frac{3Nr_0\eta}{\beta^2\gamma^3\hat{z}^3}\left(\ln\frac{b}{a} + \frac{1}{2}\right)z. \tag{1.46}$$

The perturbed motion (1.46) is of the type of Eq. (1.13). The synchrotron tune of single-particle motion in the presence of space charge perturbation is therefore given by

$$\nu_s^2 = \nu_{s0}^2 + \frac{3Nr_0\eta R^2}{\beta^2\gamma^3\hat{z}^3}\left(\ln\frac{b}{a} + \frac{1}{2}\right). \tag{1.47}$$

For a small tune shift, we obtain

$$\Delta\nu_s = \frac{3Nr_0\eta R^2}{2\beta^2\gamma^3\hat{z}^3\nu_{s0}}\left(\ln\frac{b}{a} + \frac{1}{2}\right). \tag{1.48}$$

This synchrotron tune shift has the same sign as η. The space charge force is focusing and defocusing according as the operation is above or below transition. This is to be compared with its transverse counterpart, Eq. (1.21), which always defocuses.

Continuing the numerical example that followed Eq. (1.23) and Eq. (1.31), and taking in addition $\eta = (1/\nu_{x0}^2) - (1/\gamma^2) = -0.45$, $\hat{z} = (9\pi/2)^{1/6}\sigma_z = 0.47$ m,[19] $\nu_{s0} = 0.04$, and $b = 5$ cm, the synchrotron tune is found from Eq. (1.47) to be significantly suppressed by the space charge force, from 0.04 to 0.016 in the present example.

[19]The factor $(9\pi/2)^{1/6}$ is chosen to give the same result for small oscillations when λ is Gaussian. See Exercise 3.4 also.

One can extend the analysis to higher multipole distributions with $m \neq 0$. To do so for the case of a ring-shaped beam, we first write down the transverse field components according to Eq. (1.8),

$$E_r = \frac{B_\theta}{\beta} = 2I_m\lambda(s - \beta ct)\cos m\theta \begin{cases} -\left(\frac{1}{a^{2m}} - \frac{1}{b^{2m}}\right) r^{m-1}, \\ \frac{1}{r^{m+1}} + \frac{r^{m-1}}{b^{2m}} \end{cases} \tag{1.49}$$

and

$$E_\theta = -\frac{B_r}{\beta} = 2I_m\lambda(s - \beta ct)\sin m\theta \begin{cases} \left(\frac{1}{a^{2m}} - \frac{1}{b^{2m}}\right) r^{m-1}, \\ \frac{1}{r^{m+1}} - \frac{r^{m-1}}{b^{2m}}. \end{cases} \tag{1.50}$$

If we draw circuits as shown in Figure 1.7(b) and (c) and apply Faraday's law, we obtain the longitudinal electric field

$$E_s = -\frac{2I_m}{m\gamma^2}\lambda'(s - \beta ct)\cos m\theta \begin{cases} \left(\frac{1}{a^{2m}} - \frac{1}{b^{2m}}\right) r^m, \\ \frac{1}{r^m} - \frac{r^m}{b^{2m}}. \end{cases} \tag{1.51}$$

Exercise 1.6

(a) The circuits in Figure 1.7 can also be used to calculate the longitudinal magnetic field by applying Ampere's law $\oint d\vec{l} \cdot \vec{B} = (1/c)(\partial/\partial t)\int d\vec{s} \cdot \vec{E}$, where we have used the fact that there is no contribution from the current source because $j_\theta = 0$. Following similar steps as before, show that B_s vanishes.

(b) Show explicitly that Eqs. (1.49–1.51) satisfy the Maxwell equations, ignoring terms involving λ''.

(c) It is amusing to show that fields for $m \neq 0$ reduce to those for $m = 0$ on setting $I_0 = e$ and taking the limit $m \to 0$, even though strictly m assumes only integral values. [Remember to include the factor $1/(1 + \delta_{m0})$.]

If the beam distribution is that of Eq. (1.33) with a general transverse distribution $n(r)$, the longitudinal electric field is obtained by superposition:

$$E_s = -\frac{2I_m}{m\gamma^2}\lambda'(s - \beta ct)\cos m\theta \times \left[\frac{1}{r^m}\int_0^r 2\pi r'^{m+1}\, dr'\, n(r') + r^m\int_r^b \frac{2\pi\, dr'\, n(r')}{r'^{m-1}} - \frac{r^m}{b^{2m}}\right]. \tag{1.52}$$

For uniform $n(r)$ up to radius $r = a$, the result is

$$E_s = -\frac{2I_m}{m\gamma^2}\lambda'(s-\beta ct)\cos m\theta \times \begin{cases} -r^m\left(\dfrac{1}{b^{2m}} + \dfrac{m+2}{m-2}\dfrac{1}{a^{2m}}\right) + \dfrac{2m}{m-2}\dfrac{r^2}{a^{m+2}}, \\ \dfrac{1}{r^m} - \dfrac{r^m}{b^{2m}}. \end{cases} \tag{1.53}$$

Comparing Eqs. (1.32) and (1.51), we find the ratio of longitudinal to transverse space charge forces is of the order of

$$F_{\parallel}/F_{\perp} \approx \frac{r}{m}\frac{\lambda'}{\gamma^2}\Big/\frac{\lambda}{\gamma^2}. \tag{1.54}$$

Both transverse and longitudinal space charge forces, being proportional to $1/\gamma^2$, are nonrelativistic effects. In the transverse case, it comes from the less than perfect cancellation between the electric and the magnetic forces. In the longitudinal case, it is due to Lorentz contraction. In case the bunch length is much longer than its transverse size, the longitudinal force is much weaker than the transverse force.

We have assumed in our treatment that all beam particles have the same energy. As an illustration of one mechanism which causes a spread of particle energies, consider the device sketched in Figure 1.8. Suppose all particles have the same energy when produced at the gun. Let the transverse focusing be provided by a longitudinal magnetic field $B_s = \infty$ so that all particles move strictly in the $\hat{s}$-direction. Sufficiently away from the gun, the beam reaches an equilibrium state. Let the transverse distribution in this equilibrium state be that of a uniform disk of radius a, and let the longitudinal density be λ. A transverse electric field E_r given by Eq. (1.17) is established, and the energy of a particle, $m_0c^2\gamma$, becomes dependent on its radial position r relative to

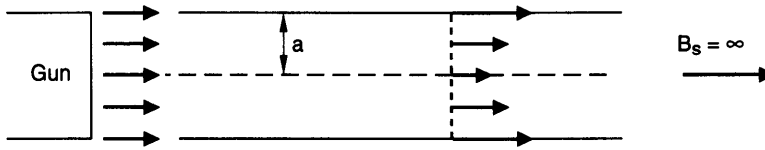

Figure 1.8. Illustration of an energy depression mechanism. All particles are produced with equal energies at the gun, which is maintained at a constant potential, but sufficiently downstream from the gun, particles at the beam center acquire an energy depression $\Delta\gamma = -\lambda r_0$ relative to particles at the beam edge.

the beam center. We have by energy conservation

$$m_0c^2\gamma(r) = m_0c^2\gamma(0) + e\int_0^r dr' E_r(r'). \tag{1.55}$$

A particle at the beam center has a lower energy than a particle at the beam edge. The energy of a particle at radius r is given by

$$\gamma(r) = \gamma(0) + \lambda r_0 \frac{r^2}{a^2}. \tag{1.56}$$

Equation (1.56) thus describes one mechanism for the beam to acquire an energy spread sufficiently downstream from the gun even when all particles are produced monoenergetic at the gun. Our treatment of space charge effects ignores the beam energy spread, and it applies if

$$\lambda r_0 \ll \gamma. \tag{1.57}$$

When $\lambda r_0 \gtrsim \gamma$, the center particles will come to a halt at some distance from the gun. This constitutes a limit on the beam intensity.[20]

1.6 ENVELOPE EQUATION

The previous two sections were developed in the context of circular accelerators. The space charge forces also have an effect on linacs or beam transport lines. The longitudinal space charge force causes an energy difference between the head and the tail of a beam bunch. The transverse space charge force perturbs the externally applied focusing force that confines the beam. The longitudinal effect on beam energy spread will be discussed later in Eq. (3.9). The transverse effect will be investigated in this section in terms of the envelope equation.[21]

Consider a transport line for a proton or heavy-ion beam which has a high intensity and a medium energy. The proton line may be one that is used to transport the proton beam from a linac to a synchrotron for further acceleration to higher energies. The heavy-ion line may be used as a driver for inertial confinement fusion. Let the beam particle have a charge Qe and a mass which is A times the proton mass. We suppose the beam is continuous, with a uniform longitudinal particle density λ. In case of a bunched beam, we

[20]See for example J. D. Lawson, *The Physics of Charged-Particle Beams*, Clarendon Press, Oxford, 1977.

[21]I. M. Kapchinskij and V. V. Vladimirskij, *Proc. 2nd Int. Conf. on High Energy Accel. and Instr.*, CERN, 1959, p. 274.

consider λ to be the maximum local density. We also suppose the externally applied forces are linear in the transverse displacements x and y, and we ignore the effects of vacuum chamber walls.

Consider a beam distribution in the four-dimensional transverse phase space (x, p_x, y, p_y) that lies on a δ-function shell as

$$\psi(x, p_x, y, p_y) = \frac{Qe\lambda}{\pi^2 \epsilon_x \epsilon_y} \delta\left(\frac{x^2}{a^2} + \frac{a^2 p_x^2}{\epsilon_x^2} + \frac{y^2}{b^2} + \frac{b^2 p_y^2}{\epsilon_y^2} - 1 \right), \quad (1.58)$$

which is normalized by

$$\int dx\, dp_x\, dy\, dp_y\, \psi = Qe\lambda. \quad (1.59)$$

The distribution (1.58) was introduced by Kapchinskij and Vladimirskij and is called the *KV distribution*. It has the property that when projected onto any two of the four phase space dimensions, one obtains a uniform elliptical distribution. For example, the projection onto the x-y plane is

$$\psi(x, y) = \frac{Qe\lambda}{\pi ab} H\left(1 - \frac{x^2}{a^2} - \frac{y^2}{b^2} \right), \quad (1.60)$$

where $H(u) = 1$ if $u > 0$ and 0 if $u < 0$ is the step function. Equation (1.60) gives a uniform elliptical distribution with horizontal and vertical extents a and b. The parameters $\epsilon_{x,y}$ in Eq. (1.58) are the horizontal and vertical beam emittances at the edge of the envelopes.

The electric field at position (x, y) produced by the beam charge is obtained by integrating over the beam distribution,

$$\vec{E}(x, y) = \frac{2Qe\lambda}{\pi ab} \iint_{1 > (x'/a)^2 + (y'/b)^2} dx'\, dy' \, \frac{(x - x')\hat{x} + (y - y')\hat{y}}{(x - x')^2 + (y - y')^2}. \quad (1.61)$$

The double integral in Eq. (1.61) can be evaluated—the algebra is lengthy but straightforward—to yield, for positions inside the beam distribution,

$$\vec{E}(x, y) = 4Qe\lambda \left[\frac{x}{a(a + b)} \hat{x} + \frac{y}{b(a + b)} \hat{y} \right]. \quad (1.62)$$

The space charge force must also include the magnetic force, which almost cancels the electric force for relativistic beams. When included, the net Lorentz force on a particle at position (x, y) is equal to the electric force

divided by γ^2, i.e.,

$$\vec{F}(x, y) = \frac{4Q^2e^2\lambda}{\gamma^2}\left[\frac{x}{a(a+b)}\hat{x} + \frac{y}{b(a+b)}\hat{y}\right]. \tag{1.63}$$

The KV model is notable because it offers a self-consistent picture. It gives a uniform elliptical beam distribution in the x-y plane; this distribution gives a linear space charge force in x and y inside the distribution; the linear forces in turn make it possible for the beam to maintain the four-dimensional ellipsoidal distribution it started out with. Therefore, the complex self-consistency problem is reduced to solving the dynamics of the two beam envelope parameters a and b.

In the presence of the space charge force (1.63), the single-particle equations of motion are

$$\begin{aligned} x'' + \left[K_x(s) - \frac{\xi}{a(a+b)}\right]x = 0, \\ y'' + \left[K_y(s) - \frac{\xi}{b(a+b)}\right]y = 0, \end{aligned} \tag{1.64}$$

where a prime means taking the derivative with respect to s, $K_{x,y}(s)$ specifies the external focusing, and

$$\xi = \frac{4Q^2r_0\lambda}{A\beta^2\gamma^2} \tag{1.65}$$

is a dimensionless space charge parameter.

We need to find a and b as functions of s by imposing conditions of self-consistency. To do so, consider a particle with the maximum allowed x-amplitude $a(s)$ at location s. This particle does not execute any y-motion, because $x = a$ necessarily means $y = 0$ and $p_y = 0$ in a KV distribution. We first write for this particle

$$x = a(s)\cos\phi_x(s) \tag{1.66}$$

where $\phi_x(s)$ is a certain phase yet to be found. Substituting into the left hand side of Eq. (1.64) results in two terms, one proportional to $\sin\phi_x(s)$ and the other proportional to $\cos\phi_x(s)$. In order for Eq. (1.64) to be valid for all s, both terms must vanish, yielding

$$\begin{aligned} a'' - a(\phi_x')^2 = -\left[K_x(s) - \frac{\xi}{a(a+b)}\right]a, \\ a\phi_x'' + 2a'\phi_x' = 0. \end{aligned} \tag{1.67}$$

The second equation of the pair (1.67) gives

$$\phi_x' \propto \frac{1}{a(s)^2}. \tag{1.68}$$

The proportionality constant is just the emittance ϵ_x, so far unspecified, i.e.,

$$\phi_x' = \frac{\epsilon_x}{a(s)^2}. \tag{1.69}$$

Substituting Eq. (1.69) into the first equation of (1.67) gives the self-consistency condition we are looking for. Similarly, if we start with a particle with the maximum allowed y-amplitude with $y = b\cos\phi_y$, we obtain the other self-consistency condition for $b(s)$. These two conditions constitute the *envelope equations*, as[22]

$$\begin{aligned} a'' + K_x a - \frac{\epsilon_x^2}{a^3} &= \frac{\xi}{a+b}, \\ b'' + K_y b - \frac{\epsilon_y^2}{b^3} &= \frac{\xi}{a+b}. \end{aligned} \tag{1.72}$$

Given the focusing strengths $K_{x,y}(s)$ and the space charge parameter ξ, the nonlinear coupled differential equations (1.72) determine the behavior of the beam envelopes $a(s)$ and $b(s)$.

Exercise 1.7 Show that in the absence of external focusing and space charge forces, the beam envelopes are hyperbolas,

$$a(s) = \sqrt{a_0^2 + \frac{\epsilon_x^2}{a_0^2}(s - s_0)^2}, \tag{1.73}$$

[22]For readers familiar with the β-function language of circular accelerators, Eqs. (1.69) and (1.72) are the transport equivalents of the Courant-Snyder relations

$$\begin{aligned} \phi_x' &= \frac{1}{\beta_x(s)}, \\ 2\beta_x\beta_x'' - (\beta_x')^2 + 4K_x\beta_x^2 &= 4, \end{aligned} \tag{1.70}$$

and their vertical counterparts. The equivalence can be established by the connections

$$a = \sqrt{\epsilon_x \beta_x} \quad \text{and} \quad b = \sqrt{\epsilon_y \beta_y}. \tag{1.71}$$

In this context, the space charge terms are modifications of the focusing strengths $K_{x,y}$, and the envelope equation is just a different form of the second number of Eq. (1.70).

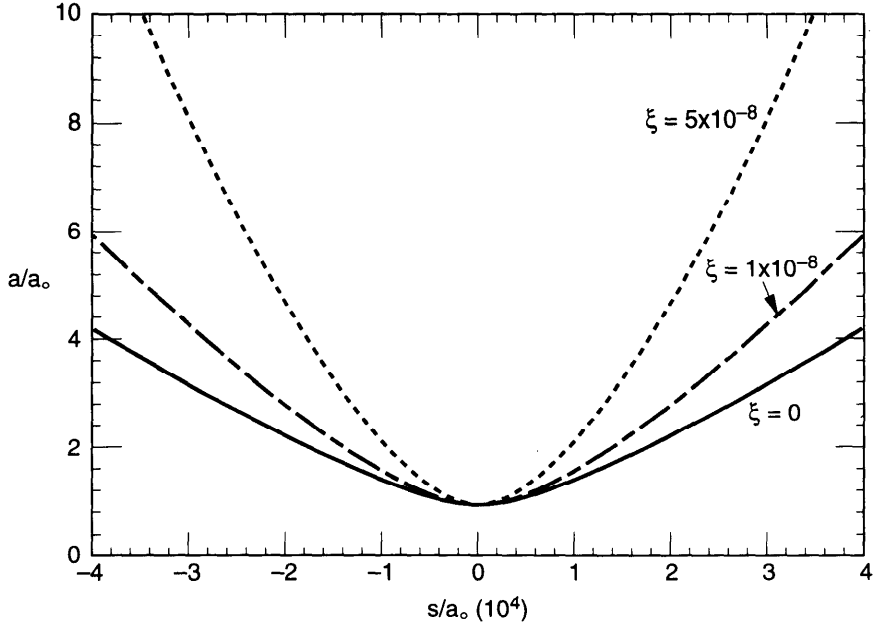

Figure 1.9. The effect of space charge on beam envelope near a beam waist in the absence of external focusing. The graph shows a / a_0 as a function of s / a_0, where a waist $a = a_0$ at $s = 0$ is assumed. The three curves are for $\xi = 0$, 1×10^{-8}, and 5×10^{-8}, and ϵ / a_0 is taken to be 10^{-4}. The case $\xi = 0$ is a hyperbola, Eq. (1.73).

where a_0 is the size of a beam "waist," and s_0 is the location of the waist. Note that a small waist size necessarily implies faster divergence away from the waist.

Exercise 1.8 Set up the envelope equation for a round beam with KV distribution under the influence of the space charge in free space. Solve the equation numerically to obtain $a(s)$ near a waist location. The result is shown in Figure 1.9.

Exercise 1.9 Show that for a round beam, if the focusing is provided by a solenoid magnet of strength B_s, the envelope equation reads

$$a'' + \left(\frac{eB_s}{2E}\right)^2 a - \frac{\epsilon^2}{a^3} = \frac{\xi}{2a}, \tag{1.74}$$

where E is the particle energy, and ϵ is the beam emittance.

Exercise 1.10 The envelope equation (1.72) is derived assuming no acceleration, and thus does not apply to linacs, but it can be modified to include acceleration.

(a) Show that if acceleration is adiabatic, i.e., if $\gamma'/\gamma \ll \beta^2 a'/a$, Eq. (1.69) still holds, and the modified envelope equation reads

$$a'' + \frac{\gamma'}{\beta^2\gamma}a' + K_x a - \frac{\epsilon_x^2}{a^3} = \frac{\xi}{a+b} \tag{1.75}$$

and similarly for b. Note that an extra term, proportional to a' and γ', is introduced, and that ξ, still defined by Eq. (1.65), depends on s through γ and β.

(b) Consider the case of a uniform acceleration, $(\beta\gamma)' = \alpha = \text{const}$. Make the transformation $a = A/\sqrt{\beta\gamma}$ and $b = B/\sqrt{\beta\gamma}$ to show that the envelope equation (1.72) is recovered if we make the replacements

$$\begin{gathered} A \to a, \qquad B \to b, \\ K_{x,y} + \frac{\alpha^2}{4\beta^2\gamma^2} \to K_{x,y}, \\ \beta\gamma\epsilon_{x,y} \to \epsilon_{x,y}, \quad \text{and} \quad \beta\gamma\xi \to \xi. \end{gathered} \tag{1.76}$$

The modification of $K_{x,y}$ is small, and can most likely be dropped for practical cases. The modification of $\epsilon_{x,y}$ is related to the definition of the normalized emittance introduced in Eq. (1.22).

To be more specific, consider a round beam with $a = b$ and $\epsilon_x = \epsilon_y = \epsilon$. Let the external focusing be smooth, $K_x = K_y = (\nu/R)^2$, where $2\pi R/\nu$ is the betatron oscillation wavelength along the transport line.[23] The envelope equation (1.72) gives an equation for the equilibrium beam size a_0,

$$\left(\frac{\nu}{R}\right)^2 a_0 - \frac{\epsilon^2}{a_0^3} - \frac{\xi}{2a_0} = 0. \tag{1.77}$$

In the absence of space charge force, the equilibrium beam size is given by

$$a_0^2 = \frac{\epsilon R}{\nu}, \tag{1.78}$$

which is just Eqs. (1.11) and (1.71) combined. Taking into account the space

[23]Symbols are chosen so results can be applied to a circular accelerator where ν is the betatron tune and $2\pi R$ is the accelerator circumference.

charge force, the equilibrium beam size is given by solving Eq. (1.77):

$$a_0^2 = \frac{\epsilon R}{\nu}\left[\sqrt{1 + \left(\frac{\xi R}{4\nu\epsilon}\right)^2} + \frac{\xi R}{4\nu\epsilon}\right]. \tag{1.79}$$

The beam size is significantly perturbed by the space charge force if

$$\frac{\xi R}{4\nu\epsilon} \gtrsim 1. \tag{1.80}$$

If the beam size becomes larger than the vacuum chamber aperture, there will be a beam loss. Even when the beam stays in the vacuum chamber, the beam distribution in phase space may be too distorted to meet the downstream requirements, whether those are for inertial confinement or for further acceleration in a synchrotron. The case of $\xi = 5 \times 10^{-8}$ in Figure 1.9 has $\xi R/4\nu\epsilon = 1.25$.

For weak beam intensities, when $\xi \ll \nu\epsilon/R$, the perturbation on the equilibrium beam size is

$$\Delta a_0^2 = \frac{\xi R^2}{4\nu^2}. \tag{1.81}$$

If this perturbation is interpreted as a perturbation on the single-particle tune ν according to $a_0^2 = \epsilon R/(\nu + \Delta\nu)$, we obtain an expression for the shift of the single-particle betatron wave number:

$$\frac{\Delta\nu}{R} = -\frac{\xi}{4\epsilon} = -\frac{Q^2\lambda r_0 R}{A\nu a_0^2\beta^2\gamma^3}. \tag{1.82}$$

Equations (1.81–1.82) have the interpretations of the β-function distortion and the betatron frequency shift caused by the space charge force. Equation (1.82) is consistent with Eq. (1.21) obtained earlier.

For an intense, low-energy beam, space charge defocusing may overcome external focusing, rendering the beam unstable. This occurs when

$$\left|\frac{\Delta\nu}{R}\right| \gtrsim \frac{\nu}{R}, \tag{1.83}$$

which is just Eq. (1.80) when Eq. (1.82) is substituted for $\Delta\nu/R$.

The instability (1.83) is most likely at low energies. Take a transport line for 50 MeV protons, for example, with $Q = 1$, $A = 1$, and a peak beam current $\hat{I} = \hat{\lambda}e\beta c = 2$ A, we find $\xi = 7 \times 10^{-6}$. If we further take an unperturbed beam size of $a_0 = 2$ cm, the space charge force is strong enough to overcome an external betatron focusing of focal length $R/\nu = 10$ m.

The beam may execute some collective motion on top of the equilibrium established by Eq. (1.79) or Eq. (1.81). Consider again a weak, round beam. Let the horizontal and vertical beam sizes be

$$a(s) = a_0 + \Delta a(s) \quad \text{and} \quad b(s) = a_0 + \Delta b(s), \tag{1.84}$$

where the perturbations Δa and Δb are considered infinitesimal. With a_0 obeying Eq. (1.77), we need to know how Δa and Δb depends on s.

Substitute Eq. (1.84) into the envelope equation (1.72) and linearize with respect to Δa and Δb. We obtain

$$\begin{aligned} \Delta a'' + \left(\frac{\nu}{R}\right)^2 \Delta a + \frac{3\epsilon^2}{a_0^4}\Delta a + \frac{\xi}{4a_0^2}(\Delta a + \Delta b) = 0, \\ \Delta b'' + \left(\frac{\nu}{R}\right)^2 \Delta b + \frac{3\epsilon^2}{a_0^4}\Delta b + \frac{\xi}{4a_0^2}(\Delta a + \Delta b) = 0. \end{aligned} \tag{1.85}$$

The two beam sizes execute coupled oscillations. These oscillations can be described by a superposition of two modes. Adding the two equations in (1.85) gives

$$(\Delta a + \Delta b)'' + \left[\left(\frac{\nu}{R}\right)^2 + \frac{3\epsilon^2}{a_0^4} + \frac{\xi}{2a_0^2}\right](\Delta a + \Delta b) = 0. \tag{1.86}$$

This equation states that one of the collective modes occurs when Δa and Δb oscillate in phase. Such a mode is designated as a + mode, or a 0-mode. Its oscillation frequency is given by

$$\left(\frac{\nu_+}{R}\right)^2 = \left(\frac{\nu}{R}\right)^2 + \frac{3\epsilon^2}{a_0^4} + \frac{\xi}{2a_0^2}. \tag{1.87}$$

The other mode is obtained by subtracting the two equations in (1.85):

$$(\Delta a - \Delta b)'' + \left[\left(\frac{\nu}{R}\right)^2 + \frac{3\epsilon^2}{a_0^4}\right](\Delta a - \Delta b) = 0. \tag{1.88}$$

This mode describes the beam motion in which Δa and Δb oscillate out of phase, and is designated as the − mode or the π-mode. Its mode frequency is given by

$$\left(\frac{\nu_-}{R}\right)^2 = \left(\frac{\nu}{R}\right)^2 + \frac{3\epsilon^2}{a_0^4}. \tag{1.89}$$

One observes the $-$ mode frequency is not directly affected by the space charge force, because it is independent of ξ. As the horizontal and the vertical beam sizes oscillate out of phase with equal amplitudes, the induced space charge force does not perturb the beam envelopes to first order of the oscillation amplitude. The $-$ mode oscillation of the beam sizes therefore does not respond to the space charge force. The opposite is true in the $+$ mode, where the in-phase oscillation of the beam sizes maximizes the effect of the space charge force.

However, the static, equilibrium space charge force is always present. The mode frequencies (1.87) and (1.89) contain the equilibrium beam size a_0, which depends on ξ according to Eq. (1.79) or (1.81). Both mode frequencies therefore shift with beam intensity. Substituting Eq. (1.81) into (1.87) and (1.89) gives, to first order in ξ,

$$\begin{aligned} \frac{\nu_+}{R} &= 2\frac{\nu}{R} - \frac{\xi}{4\epsilon}, \\ \frac{\nu_-}{R} &= 2\frac{\nu}{R} - \frac{3\xi}{8\epsilon}. \end{aligned} \tag{1.90}$$

Both mode frequencies then shift down with increasing beam intensity. In the unperturbed case, $\xi = 0$, the horizontal and vertical beam size oscillations are uncoupled, and the oscillation frequency is twice the natural betatron frequency.

Exercise 1.11 Consider a flat beam with $a \to \infty$, $\lambda \to \infty$, but $\lambda/a \to$ constant. Find the unperturbed vertical beam size b_0^2, and the first order perturbations of Δb_0^2 and $\Delta\nu_y/R$. Find the collective mode frequency by considering an infinitesimal perturbation on the beam size.

So far we have assumed a KV model (1.58). For more realistic distributions, one has to sacrifice the strict self-consistency and be content with approximate descriptions. This can be done by concentrating on the second moments of the beam[24] and ignoring the effects of higher moments.[25]

Consider a one-dimensional problem which has the single-particle equations of motion

$$x' = p \quad \text{and} \quad p' = -K_x x + f_x, \tag{1.91}$$

[24] F. Sacherer, IEEE Trans. Nucl. Sci. **NS-18**, 1105 (1971).

[25] For discussions of higher moments, see R. L. Gluckstern, R. Chasman, and K. Crandall, *Proc. Nat. Accel. Lab. Linear Accel. Conf.*, Vol. 2, Fermilab, 1970, p. 823; I. Hofmann, L. J. Laslett, L. Smith, and I. Haber, Part. Accel. **13**, 145 (1983). For an application of the envelope equation to circular accelerators, see P. Zhou, J. B. Rosenzweig, and S. Stahl, *Proc. IEEE Part. Accel. Conf.*, San Francisco, 1991, p. 1779.

where f_x is related to the force component F_x by $f_x = F_x/Amc^2\beta^2\gamma$. Let the second moments of the beam be designated as $\langle x^2\rangle$, $\langle xp\rangle$, and $\langle p^2\rangle$, where $\langle\ \rangle$ means taking an average over the beam distribution. The equations of motion of the second moments are

$$\begin{aligned}
\langle x^2\rangle' &= 2\langle xx'\rangle = 2\langle xp\rangle, \\
\langle xp\rangle' &= \langle x'p + xp'\rangle = \langle p^2\rangle - K_x\langle x^2\rangle + \langle xf_x\rangle, \\
\langle p^2\rangle' &= 2\langle pp'\rangle = -2K_x\langle xp\rangle + 2\langle pf_x\rangle.
\end{aligned} \tag{1.92}$$

The first two expressions in Eq. (1.92) can be combined to give

$$\langle x^2\rangle'' = 2\langle p^2\rangle - 2K_x\langle x^2\rangle + 2\langle xf_x\rangle. \tag{1.93}$$

Defining the rms beam emittance by [also see Eq. (4.76)]

$$\epsilon_{x,\text{rms}}^2 = \langle x^2\rangle\langle p^2\rangle - \langle xp\rangle^2, \tag{1.94}$$

we can express $\langle p^2\rangle$ in terms of the emittance as

$$\langle p^2\rangle = \frac{\epsilon_{x,\text{rms}}^2}{\langle x^2\rangle} + \frac{\langle xp\rangle^2}{\langle x^2\rangle} = \frac{\epsilon_{x,\text{rms}}^2}{\langle x^2\rangle} + \frac{\left(\langle x^2\rangle'\right)^2}{4\langle x^2\rangle}, \tag{1.95}$$

where use has been made of the first entry of Eq. (1.92). Substituting Eq. (1.95) into Eq. (1.93) and rewriting the result in terms of the rms beam size $\sigma_x = \sqrt{\langle x^2\rangle}$, we obtain

$$\sigma_x'' + K_x\sigma_x - \frac{\epsilon_{x,\text{rms}}^2}{\sigma_x^3} = \frac{\langle xf_x\rangle}{\sigma_x}. \tag{1.96}$$

Similarly, we have

$$\sigma_y'' + K_y\sigma_y - \frac{\epsilon_{y,\text{rms}}^2}{\sigma_y^3} = \frac{\langle yf_y\rangle}{\sigma_y}. \tag{1.97}$$

In the case of the KV model, the force components F_x and F_y are given by Eq. (1.63), and one obtains

$$\begin{aligned}
\sigma_x'' + K_x\sigma_x - \frac{\epsilon_{x,\text{rms}}^2}{\sigma_x^3} &= \frac{\xi}{4(\sigma_x + \sigma_y)}, \\
\sigma_y'' + K_y\sigma_y - \frac{\epsilon_{y,\text{rms}}^2}{\sigma_y^3} &= \frac{\xi}{4(\sigma_x + \sigma_y)},
\end{aligned} \tag{1.98}$$

which is the same as Eq. (1.72), since for the KV model, one has $\epsilon_{x,y} = 4(\epsilon_{x,y})_{\text{rms}}$, $a = 2\sigma_x$, and $b = 2\sigma_y$.

Equations (1.96–1.97) are valid for general beam distributions. In general, the forces F_x and F_y are nonlinear in x and y, and the quantities $\langle xf_x \rangle$ and $\langle yf_y \rangle$ involve moments higher than the second moments. The problem is therefore not closed. However, to the extent that the higher moments can be ignored, we keep only the linear terms (linear in x and y) in $f_{x,y}$; $\langle xf_x \rangle$ and $\langle yf_y \rangle$ can be expressed in terms of the second moments only, and we recover a closed system of equations as in the KV model.

Exercise 1.12 Apply Eqs. (1.96–1.97) to a Gaussian beam

$$\psi(x, p_x, y, p_y) = \frac{Qe\lambda\beta_x\beta_y}{4\pi^2\sigma_x^2\sigma_y^2} \exp\left(-\frac{x^2 + \beta_x^2 p_x^2}{2\sigma_x^2} - \frac{y^2 + \beta_y^2 p_y^2}{2\sigma_y^2} \right). \quad (1.99)$$

Linearize the space charge force for small $|x|$ and $|y|$ to obtain

$$\vec{F} \approx \frac{2Q^2e^2\lambda}{\gamma^2} \left[\frac{x}{\sigma_x(\sigma_x + \sigma_y)} \hat{x} + \frac{y}{\sigma_y(\sigma_x + \sigma_y)} \hat{y} \right]. \quad (1.100)$$

Show that the envelope equation reads

$$\begin{aligned} \sigma_x'' + K_x\sigma_x - \frac{\epsilon_{x,\text{rms}}^2}{\sigma_x^3} &= \frac{\xi}{2(\sigma_x + \sigma_y)}, \\ \sigma_y'' + K_y\sigma_y - \frac{\epsilon_{y,\text{rms}}^2}{\sigma_y^3} &= \frac{\xi}{2(\sigma_x + \sigma_y)}. \end{aligned} \quad (1.101)$$

The nonlinear space charge force associated with a Gaussian beam will cause the distribution to deviate from being Gaussian, but this fact is ignored when writing Eq. (1.101).

CHAPTER 2

Wake Fields and Impedances

A charged particle beam interacts electromagnetically with its vacuum chamber surroundings in an accelerator. As a first step in our treatment of the beam-surroundings system (1.1), we will study the properties of the wake electromagnetic fields generated by the beam in the vacuum chamber. For this purpose, the beam is considered to be rigid and unaffected by the wake field it generates (and therefore to show no collective instabilities). The beam is assumed to move with the speed of light. The wake field we are most interested in is that seen by a test charge that follows the beam at a fixed relative distance. In the relativistic limit, causality dictates that there will be no electromagnetic field in front of the beam; thus the term "wake."

The effect of the wake fields on the beam motion—the beam dynamics—will be treated in later chapters. The rigid beam picture adopted in this chapter is not self-consistent, but is an excellent approximation for relativistic beams as far as the calculation of the wake fields is concerned. Materials developed in this chapter serve as inputs to the later chapters.

In Section 1.2, we showed that a relativistic beam does not generate wake fields in a perfectly conducting smooth pipe. If the vacuum chamber is not a smooth pipe or if it is smooth but not perfectly conducting, a beam will generate behind it an electromagnetic wake. See Figure 2.1. We will first work out in some detail in Section 2.1 the wake field for the case of a smooth cylindrical pipe with a resistive wall. In the process, we will point out the general features of all wake fields. The general wake fields are then discussed in Section 2.2.

It is necessary that the concept of impedance also be introduced. This is done in Section 2.3. The wake field, a time domain quantity, and the

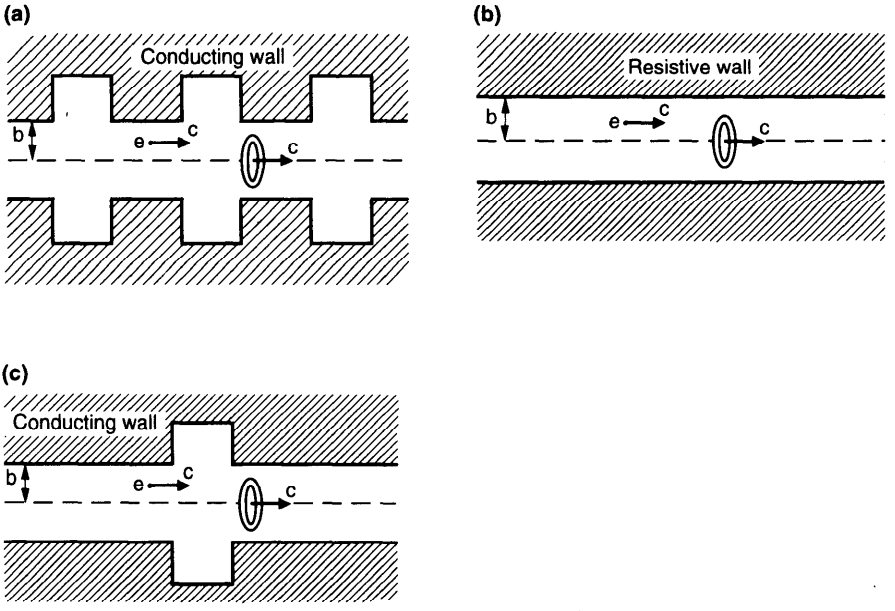

Figure 2.1. Examples of vacuum chamber pipe that generates wake fields. The beam is represented here as a ring possessing a multipole moment with $\cos m\theta$ distribution. A test charge e following the beam at a fixed distance is shown. (a) Periodic structure. (b) Resistive wall. (c) Single structure.

impedance, a frequency domain quantity, are related by Fourier transforms. We will investigate the properties of impedances. Calculation of wake fields and impedances is an important research activity. Two approaches—one in the time domain, one in the frequency domain—are mentioned in Section 2.4. Finally, in Section 2.5, we will discuss the parasitic energy loss—the energy source that feeds all collective instabilities—from the beam to the surroundings.

In the design stage of an accelerator, it is often necessary to budget a total impedance that is consistent with the beam intensity requirements. This total budget is then carefully allocated to individual vacuum chamber components.[1] The topic of how to measure the impedance or wake field of individual vacuum chamber components off-line before they are installed in an acceler-

[1]A possible list of these components: rf cavities, beam position monitors, bellows, flanges, special magnets, beam collimators, vacuum pump ports, vacuum valves, resistive wall, ceramic wall, synchrotron radiation shields, curvature of the pipe, and direct space charge. See the various accelerator design reports, and King Yuen Ng, *AIP Proc.* **184**, *Phys. Part. Accel.*, Fermilab 1987 and Cornell, 1988 p. 472.

ator is an important research and development area not treated in this volume.[2]

2.1 RESISTIVE WALL

In this section, the case of a resistive pipe wall [Figure 2.1(b)] will be worked out in detail. For simplicity, we assume the pipe wall has infinite thickness. We also assume the beam moves with the speed of light and has a distribution given by Eq. (1.7).[3] In this case, the wake field forms a fixed pattern behind the beam, and this pattern moves down the pipe with a phase velocity (not group velocity) c.

Let us first explicitly write down the Maxwell equations, component by component, in cylindrical coordinates:

$$
\begin{aligned}
\frac{1}{r}\frac{\partial(rE_r)}{\partial r} + \frac{1}{r}\frac{\partial E_\theta}{\partial \theta} + \frac{\partial E_s}{\partial s} &= 4\pi\rho, \\
\frac{1}{r}\frac{\partial B_s}{\partial \theta} - \frac{\partial B_\theta}{\partial s} - \frac{1}{c}\frac{\partial E_r}{\partial t} &= \frac{4\pi}{c} j_r, \\
\frac{\partial B_r}{\partial s} - \frac{\partial B_s}{\partial r} - \frac{1}{c}\frac{\partial E_\theta}{\partial t} &= \frac{4\pi}{c} j_\theta, \\
\frac{1}{r}\frac{\partial(rB_\theta)}{\partial r} - \frac{1}{r}\frac{\partial B_r}{\partial \theta} - \frac{1}{c}\frac{\partial E_s}{\partial t} &= \frac{4\pi}{c} j_s, \\
\frac{1}{r}\frac{\partial(rB_r)}{\partial r} + \frac{1}{r}\frac{\partial B_\theta}{\partial \theta} + \frac{\partial B_s}{\partial s} &= 0, \\
\frac{1}{r}\frac{\partial E_s}{\partial \theta} - \frac{\partial E_\theta}{\partial s} + \frac{1}{c}\frac{\partial B_r}{\partial t} &= 0, \\
\frac{\partial E_r}{\partial s} - \frac{\partial E_s}{\partial r} + \frac{1}{c}\frac{\partial B_\theta}{\partial t} &= 0, \\
\frac{1}{r}\frac{\partial(rE_\theta)}{\partial r} - \frac{1}{r}\frac{\partial E_r}{\partial \theta} + \frac{1}{c}\frac{\partial B_s}{\partial t} &= 0.
\end{aligned}
\tag{2.1}
$$

[2]A. Faltens et al., *Proc. 8th Int. Conf. High Energy Accel.*, Geneva, 1971, p. 338; P. B. Wilson, J. B. Styles, and K. L. F. Bane, IEEE Trans. Nucl. Sci. **NS-24**, 1496 (1977); G. Nassibian and F. Sacherer, CERN Report ISR-TH/77-61 (1977); H. Hahn and F. Pedersen, BNL Report 50870 (1978); G. Lambertson, LBL Report 29148 (1990); G. Jackson, *Proc. Workshop Fermilab III Instabilities*, Fermilab, 1990, p. 245; F. Caspers, *Frontiers of Particle Beams: Intensity Limitations*, Lecture Notes in Phys. **400**, Springer-Verlag, 1990, p. 80.

[3]Different treatments of the resistive wall problem can be found in P. L. Morton, V. K. Neil, and A. M. Sessler, J. Appl. Phys. **37**, 3875 (1966); K. W. Robinson, *Proc. Storage Ring Summer Study, 1965*, SLAC Report 49, p. 32; M. J. Lee, F. E. Mills, and P. L. Morton, SLAC Report 76 (1967); R. Briggs, SSC Laboratory Report 512 (1992); Robert L. Gluckstern, Johannes van Zeijts, and Bruno Zotter, Phys. Rev. E **47**, 656 (1993).

Given that ρ and j_s are proportional to $\cos m\theta$, the angular θ-dependence of the field components can be obtained by inspection: E_r, E_s, and B_θ are proportional to $\cos m\theta$, while E_θ, B_r, and B_s are proportional to $\sin m\theta$. One also expects the dependence on s and t to be such that all quantities depend on the combined variable $z \equiv s - ct$, which is the relative longitudinal displacement from the moving $\cos m\theta$ ring beam; $z > 0$ is ahead of the beam, and $z < 0$ is behind the beam. We then write the field components in terms of Fourier transformations[4]

$$\begin{aligned}(E_r, E_s, B_\theta) &= \cos m\theta \int_{-\infty}^{\infty} \frac{dk}{2\pi} e^{ikz}\left(\tilde{E}_r, \tilde{E}_s, \tilde{B}_\theta\right), \\ (E_\theta, B_r, B_s) &= \sin m\theta \int_{-\infty}^{\infty} \frac{dk}{2\pi} e^{ikz}\left(\tilde{E}_\theta, \tilde{B}_r, \tilde{B}_s\right),\end{aligned} \tag{2.2}$$

where $\tilde{E}_r$, etc. are complex quantities and are functions of k and r. Due to causality, our solution must satisfy the condition that no wake field is produced ahead of the beam, i.e., in the region $z > 0$. This requires that $\tilde{E}$ and $\tilde{B}$ components do not have singularities in the upper complex k-plane.

The $m = 0$ Wake

We will first work out the case $m = 0$. The beam considered is a thin ring with total charge q. The field components E_θ, B_r, and B_s vanish. Setting $m = 0$ in Eq. (2.2) and substituting the result, together with Eq. (1.7), into Eq. (2.1), we obtain three equations. [There are eight equations in (2.1), but five of them are redundant.] They are rather easy to solve, yielding

$$\begin{aligned}\tilde{E}_s &= A, \qquad r < b, \\ \tilde{E}_r = \tilde{B}_\theta &= \begin{cases} -ikA\dfrac{r}{2}, & r < a, \\ -ikA\dfrac{r}{2} + \dfrac{2q}{r}, & a < r < b, \end{cases}\end{aligned} \tag{2.3}$$

where A is a constant that depends only on k and is yet to be determined.

Note that there is a discontinuity in $\tilde{E}_r$ and $\tilde{B}_\theta$, but no discontinuity of $\tilde{E}_s$ at $r = a$. Note also that $\tilde{E}_s$, and therefore E_s, does not depend on r; the longitudinal component of the electric wake field at a given longitudinal position z relative to the ring beam is independent of the transverse position r and θ. This is a remarkable result, particularly since we have not yet imposed the boundary conditions. The $2q/r$ term in $\tilde{E}_r$ and $\tilde{B}_\theta$ is the pancake field due to direct space charge. The quantity A is closely related to something called the impedance, to be discussed in Section 2.3. [See Eq. (2.75).]

[4]There is a theorem stating when you have only a partial knowledge of the solution to a differential equation and do not know what to do next, make a Fourier transformation. This theorem is one reason why impedance is such a useful quantity.

For a perfectly conducting wall, $\tilde{E}_s$ vanishes at $r = b$; this means $A = 0$, and an inverse Fourier transform of Eq. (2.3) gives Eqs. (1.4) and (1.5). In case the wall is resistive, one needs to obtain A from the boundary conditions at $r = b$, and to do that, the fields inside the wall, $r > b$, need to be found.

To find the field in the metal wall, we first need a definition of metal. For our purposes, a metal is a material that obeys the conditions[5]

$$\rho = 0 \quad \text{and} \quad \vec{j} = \sigma \vec{E}, \tag{2.4}$$

where σ is the conductivity, assumed to be a constant, independent of k. Equation (2.4) says that a metal is charge free but not current free. Charges, if any, will have to stay on the metal surface. This property of metals leads to the fact (see Exercise 2.4) that the magnetic field tends to penetrate deeper into the metal than the electric field.

Substituting Eq. (2.2) into the Maxwell equation (2.1) and applying Eq. (2.4), we again obtain three nonredundant equations,

$$\begin{aligned} &\frac{1}{r}\frac{\partial}{\partial r}\left(r\frac{\partial \tilde{E}_s}{\partial r}\right) + \lambda^2 \tilde{E}_s = 0, \\ &\tilde{E}_r = \frac{ik}{\lambda^2}\frac{\partial \tilde{E}_s}{\partial r}, \\ &\tilde{B}_\theta = \left(1 + \frac{\lambda^2}{k^2}\right)\tilde{E}_r, \end{aligned} \tag{2.5}$$

where we have defined a parameter

$$\lambda = \sqrt{\frac{2\pi\sigma|k|}{c}}\,[i + \operatorname{sgn}(k)] \tag{2.6}$$

with $\lambda^2 = 4\pi i\sigma k/c$. The sign of λ is chosen so that its imaginary part $\operatorname{Im}\lambda > 0$. The parameter λ^{-1} has the dimensionality of length; it is related to the *skin depth* as a function of frequency $\omega = kc$ inside the metal wall:

$$\delta_{\text{skin}} = \frac{1}{\operatorname{Im}\lambda} = \frac{c}{\sqrt{2\pi\sigma|\omega|}}. \tag{2.7}$$

The procedure in solving Eq. (2.5) is to solve the first equation for $\tilde{E}_s$, then solve for the rest of the field components using the other two equations. This

[5]The definition (2.4) is not arbitrary. For example the equation of continuity must be satisfied, and is satisfied because $\nabla \cdot \vec{j} + \partial\rho/\partial t = \nabla \cdot \vec{j} = \sigma \nabla \cdot \vec{E} = 4\pi\sigma\rho = 0$.

procedure of solving for the longitudinal field components first is common in waveguide analysis. Typical values of σ at room temperature are

$$\sigma = \begin{cases} 3.2 \times 10^{17}\ \mathrm{s}^{-1} \\ 5.4 \times 10^{17} \\ 1.3 \times 10^{16} \end{cases} = \begin{cases} 3.5 \times 10^{7}\ \Omega^{-1}\ \mathrm{m}^{-1}, & \text{aluminum,} \\ 5.9 \times 10^{7}, & \text{copper,} \\ 1.4 \times 10^{6}, & \text{stainless steel.}^{6} \end{cases} \tag{2.8}$$

In what follows, we will assume $|\lambda|$ is much larger than $1/b$, i.e., the skin depth is much shorter than the pipe radius b. This assumption is good if wave number $|k|$ is much greater than $c/4\pi\sigma b^2$, or equivalently, if we are interested in the region

$$|z| \ll \frac{b}{\chi}, \tag{2.9}$$

where χ is a small dimensionless parameter defined by

$$\chi \equiv \frac{c}{4\pi\sigma b}. \tag{2.10}$$

For example, if $b = 5$ cm and the wall is made of aluminum, we have $\chi = 1.5 \times 10^{-9}$ and our approximation breaks down at a distance $\gtrsim 3 \times 10^7$ m behind the beam.

In case the vacuum chamber wall has a finite thickness t, our approximation also requires $|\lambda| \gg 1/t$. If $t = 3$ mm, the approximation breaks down at distance $\gtrsim 1 \times 10^5$ m. The corresponding low-frequency field components leak through the pipe wall, leading to the Laslett analysis of tune shifts (1.30–1.31).

Under the approximation $|\lambda| \gg 1/b$, the equation for $\tilde{E}_s$ in (2.5) becomes $\partial^2\tilde{E}_s/\partial r^2 + \lambda^2\tilde{E}_s = 0$, which has the solution[7]

$$\tilde{E}_s = A\, e^{i\lambda(r-b)}, \tag{2.11}$$

where the coefficient A is the same as that appearing in Eq. (2.3) to assure continuity of $\tilde{E}_z$. From Eq. (2.5), we then have

$$\begin{aligned} \tilde{E}_r &= -\frac{k}{\lambda} A\, e^{i\lambda(r-b)}, \\ \tilde{B}_\theta &= -\frac{k}{\lambda}\left(1 + \frac{\lambda^2}{k^2}\right) A\, e^{i\lambda(r-b)}. \end{aligned} \tag{2.12}$$

[6] We assume 18% chromium, 8% nickel.

[7] If we do not assume $|\lambda| \gg b^{-1}$, $\tilde{E}_s$ will be written in terms of Bessel functions. This complication is not required for our purposes. A slightly more accurate approximation would be to include an additional factor $\sqrt{b/r}$ in the field expressions (2.11–2.12).

The coefficient A is determined by the continuity of $\tilde{B}_\theta$ at $r = b$, yielding the result

$$A = \frac{2q/b}{\frac{ikb}{2} - \frac{\lambda}{k}}, \tag{2.13}$$

where a term $-k/\lambda$ in the denominator has been dropped because it is much smaller than the term $ikb/2$. Note that it would be incorrect to demand continuity of $\tilde{E}_r$ at $r = b$, because there is a surface charge on the wall pipe.

What we will have to do next is to make inverse Fourier transforms on $\tilde{E}_r$, $\tilde{E}_z$, and $\tilde{B}_\theta$ to obtain the fields. The exact expressions will be given later, but first, investigate the region where $|\lambda/k| \gg |kb|$. This condition on k in frequency space is equivalent to requiring in physical space the condition

$$|z| \gg \chi^{1/3} b. \tag{2.14}$$

Again taking an aluminum pipe with $b = 5$ cm, this condition excludes the study of wake fields within a distance $\lesssim 0.06$ mm behind the beam.

Under the assumptions (2.9) and (2.14), i.e., in the region $b/\chi \gg |z| \gg \chi^{1/3} b$, the quantity A becomes

$$A \approx -\frac{2qk}{b\lambda}. \tag{2.15}$$

The inverse Fourier transform can then be readily performed for the region $r < b$. The results for $z < 0$, i.e., behind the beam, are

$$\begin{aligned} E_s &= \frac{q}{2\pi b}\sqrt{\frac{c}{\sigma}}\,\frac{1}{|z|^{3/2}}, \\ B_\theta = E_r &= -\frac{3}{4}\frac{q}{2\pi b}\sqrt{\frac{c}{\sigma}}\,\frac{r}{|z|^{5/2}}. \end{aligned} \tag{2.16}$$

The fields vanish for $z > 0$ due to causality. In the region $a < r < b$, E_r and B_θ contain the additional pancake terms (1.4) and (1.5), but they are dropped because they are excluded by the condition (2.14). In deriving Eq. (2.16), we have used the formulas given in Table 2.1. Equation (2.16) shows that E_s decreases algebraically as $|z|^{-3/2}$ and is uniform in the transverse dimension (independent of r and θ), while the transverse field components decrease faster, with a $|z|^{-5/2}$ dependence, and are proportional to r.

Table 2.1. Fourier transform pairs $F(z) = \int_{-\infty}^{\infty}(dk/2\pi)e^{ikz}\tilde{F}(k)$. The quantity λ is given by Eq. (2.6). The function $F(z)$ vanishes for $z > 0$.

$\tilde{F}(k)$	$F(z)\,(z < 0)$
$1/k$	$-i$
$1/k^2$	z
$1/k^{n+1}$	$-(i/n!)(iz)^n$
λ/k^2	$-4i\sqrt{\sigma/c}\,\lvert z\rvert^{1/2}$
λ/k^3	$-(8/3)\sqrt{\sigma/c}\,\lvert z\rvert^{3/2}$
$1/\lambda$	$-(i/2\pi)\sqrt{c/\sigma}\,\lvert z\rvert^{-1/2}$
k/λ	$-(1/4\pi)\sqrt{c/\sigma}\,\lvert z\rvert^{-3/2}$
k^2/λ	$(3/8\pi)i\sqrt{c/\sigma}\,\lvert z\rvert^{-5/2}$
$e^{i\alpha\lambda}$ $(\alpha > 0)$	$\sqrt{\sigma/c}\,\alpha\lvert z\rvert^{-3/2}\exp(-\pi\sigma\alpha^2/c\lvert z\rvert)$

Exercise 2.1 The impedance per unit length, $Z_0^{\parallel}/L$, is related to A by $Z_0^{\parallel}/L = -A/qc$, as given by Eq. (2.75) below. Show that $\tilde{E}_s/\tilde{B}_\theta = -k/\lambda$ at $r = b^-$, and therefore, using Eq. (2.15),

$$\frac{Z_0^{\parallel}}{L} = \frac{Z_0}{2\pi b}\frac{\tilde{E}_s}{\tilde{B}_\theta}\bigg|_{r=b^-}, \tag{2.17}$$

where $Z_0 = 377\ \Omega$, as defined in Eq. (1.2). Equation (2.17) relates the impedance to the ratio of $\tilde{E}_s$ and $\tilde{B}_\theta$ at the pipe wall, as is often encountered in the analysis of waveguides.

Exercise 2.2 Consider a pipe with finite thickness t and conductivity σ. Follow the analysis of the text to show that, inside the pipe region, and for distances $b/\chi \gg |z| \gg \chi^{1/3}b$,

$$\tilde{E}_s = -\frac{2qk}{b\lambda}\frac{1 - e^{2i\lambda t}}{1 + e^{2i\lambda t}}. \tag{2.18}$$

Show that Eq. (2.17) is valid in this case also.

Exercise 2.3 Table 2.1, with the exception of the last entry, can be obtained by considering a general $F(z) = e^{\epsilon z}|z|^{p-1}$ for $z < 0$ and 0 for $z > 0$, where $\epsilon > 0$. Show that

$$\tilde{F}(k) = \Gamma(p)\left(\frac{i}{k + i\epsilon}\right)^p,$$

where $\Gamma(x)$ is the gamma function.[8] Show that this Fourier transform pair satisfies the Parseval theorem, Eq. (2.26).

Exercise 2.4 In the pipe wall ($r > b$) and in the region where $|z|$ is of the order of pipe radius b behind the beam, show that $B_\theta \gg E_s \gg E_r$ and that each is greater than the next by a factor of the order of $\chi^{-1/2}$. The magnetic field penetrates better into the metal than the electric field, and the component of the electric field perpendicular to the metal surface is stopped most effectively by the surface charge on the metal surface.

Exercise 2.5 Perform an inverse Fourier transformation on Eq. (2.11), using Table 2.1, to obtain E_s in the pipe wall:

$$E_s = \frac{q}{2\pi b}\sqrt{\frac{c}{\sigma}}\,|z|^{-3/2}\left[1 - \frac{2\pi\sigma(r-b)^2}{c|z|}\right]\exp\left[-\frac{\pi\sigma(r-b)^2}{c|z|}\right]. \quad (2.20)$$

The fields penetrate into the wall to a depth of the order of

$$\delta r = \sqrt{\frac{c|z|}{\pi\sigma}}\,. \quad (2.21)$$

This penetration depth, increasing as $\sqrt{|z|}$, is the time domain description of the skin depth effect.

Note that in the region of interest the field components are continuous across $r = a$ and, in fact, are even independent of a. By taking the limit $a \to 0$, we see that the results are also applicable to the case when the beam is represented as a point charge.

There is something disturbing about Eq. (2.16). Consider a test charge trailing the beam at a certain distance $|z|$. The sign of the longitudinal electric field E_s is such that the test charge gets *accelerated* if it has the same sign as q. If this were true for $|z| \to 0$, one would expect the point charge q to *gain* energy as it travels down the resistive pipe due to its own wake field. To make sure this unphysical phenomenon does not happen, we have to

[8]Gamma functions are generalized factorials. One is of course familiar with the factorials of integers; the gamma function defines how to take factorials of fractional numbers as well. Some properties of the gamma function that will be handy later are listed below:

$$\begin{aligned}
&\Gamma(n+1) = n!, \qquad \Gamma(x+1) = x\Gamma(x),\\
&\Gamma(x)\Gamma(1-x) = \frac{\pi}{\sin \pi x},\\
&\Gamma\left(\tfrac{1}{2}\right) = \sqrt{\pi}, \qquad \Gamma\left(\tfrac{1}{4}\right) = 3.626,\\
&\lim_{x\to\infty}\frac{\Gamma(x+a)}{\Gamma(x)} = x^a.
\end{aligned} \quad (2.19)$$

compute the field at very short distances behind the beam, which so far has been excluded by the condition (2.14).

To do this, we could perform the inverse Fourier transformations using the complete expression (2.13) for $A(k)$.[9] The derivation, which involves taking branch cuts in complex variables, is omitted here. The results in the pipe region are

$$E_s = -\frac{16q}{b^2}\left(\frac{1}{3}e^u\cos\sqrt{3}u - \frac{\sqrt{2}}{\pi}\int_0^\infty dx\frac{x^2 e^{ux^2}}{x^6+8}\right),$$

$$E_r = B_\theta = \frac{8qr}{(2\chi)^{1/3}b^3}\left(\frac{1}{3}e^u\cos\sqrt{3}u - \frac{1}{\sqrt{3}}e^u\sin\sqrt{3}u - \frac{\sqrt{2}}{\pi}\int_0^\infty dx\frac{x^4 e^{ux^2}}{x^6+8}\right), \tag{2.22}$$

where $u = z/(2\chi)^{1/3}b < 0$. The behavior of the fields at small $|z|$ can be obtained from Eq. (2.22).

Alternatively, we can take the opposite limit to Eq. (2.14), i.e., we can take the limit $|\lambda/k| \ll |kb|$, or equivalently $|z| \ll \chi^{1/3}b$. The parameter A then is approximately given by[10]

$$A \approx \frac{4q}{ikb^2}\left(1 - i\frac{2\lambda}{k^2 b} + \cdots\right). \tag{2.23}$$

Using Table 2.1, we perform inverse Fourier transformations to obtain, for a point charge with $a = 0$, in the pipe region $r < b$,

$$E_s \approx -\frac{4q}{b^2} + \frac{64}{3}\frac{q}{b^3}\sqrt{\frac{\sigma}{c}}|z|^{3/2},$$

$$E_r = B_\theta \approx \frac{2q}{b}\left(\frac{b}{r} - \frac{r}{b}\right)\delta(z) + 16\frac{q}{b^3}r\sqrt{\frac{\sigma}{c}}|z|^{1/2}. \tag{2.24}$$

Again these expressions are valid for $z < 0$; the fields vanish for $z > 0$. For very small $|z| \ll \chi^{1/3}b$, the first terms in Eq. (2.24) dominate. One finds that, immediately behind the charge q, E_s is indeed decelerating, that $E_s(0^-) = -4q/b^2$, and that E_r and B_θ contain only the "pancake" terms proportional to $\delta(z)$. The strength of E_s is uniform across the entire pancake plane, while $E_r = B_\theta$ decreases with increasing r and vanishes as r reaches the pipe radius b, as if the field is leaking out of the pancake region. This leakage, in fact, is what *becomes* the nonvanishing E_s.

[9]Karl L. F. Bane, SLAC Report AP-87 (1991); H. Henke and O. Napoly, *Proc. Euro. Part. Accel. Conf.*, Nice, 1990, p. 1046; O. Henry and O. Napoly, Part. Accel. **35**, 235 (1991).

[10]The short range behavior of the wake field depends on the assumption that the beam moves with the speed of light. The upper range of k in reality has a cutoff around γ/b. This introduces the condition that in order for Eq. (2.23) to be valid, the beam energy must be high enough so that $\gamma \gg \chi^{-1/3}$.

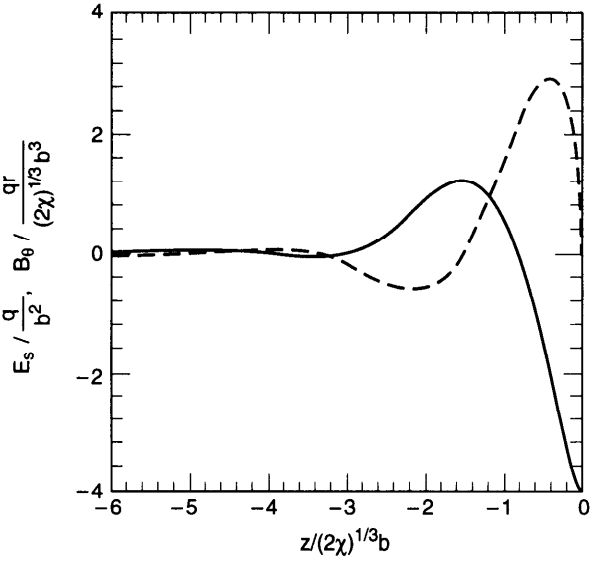

Figure 2.2. The short range wake field components due to a resistive wall are shown as functions of $u = z/(2\chi)^{1/3}b$. Solid and dashed curves are for E_s and $E_r = B_\theta$, normalized by q/b^2 and $qr/(2\chi)^{1/3}b^3$, respectively. The fields vanish for $z > 0$.

Note that although $E_s(0^-)$ is independent of the wall conductivity σ, the range of validity of Eq. (2.24) does depend on σ. In the limit $\sigma \to \infty$, a beam with finite length or a point charge with $v < c$, of course, does not lose energy to the vacuum chamber.

Figure 2.2 shows the fields immediately following the point charge calculated using the exact expressions (2.22). The transverse field components E_r and B_θ are much larger than the longitudinal component E_s, but decay faster with increasing $|z|$.[11] All field components switch signs three times following the point charge, and approach the power law behavior (2.16) asymptotically when $|z| \gg \chi^{1/3}b$. The fields $E_r = B_\theta = 0$ when E_s reaches its maxima, but $E_s \neq 0$ when $E_r = B_\theta$ reach their maxima. Figure 2.3 shows the electric field pattern in the pipe region.

Exercise 2.6 Derive the approximate expressions (2.16) and (2.24) in the proper limits using the exact formula (2.22). It is interesting to observe how fractional powers of u appear in the asymptotic forms starting from the innocent-looking Eq. (2.22).

[11] Be reminded of the fact that the transverse *force* vanishes even though the transverse *fields* are large.

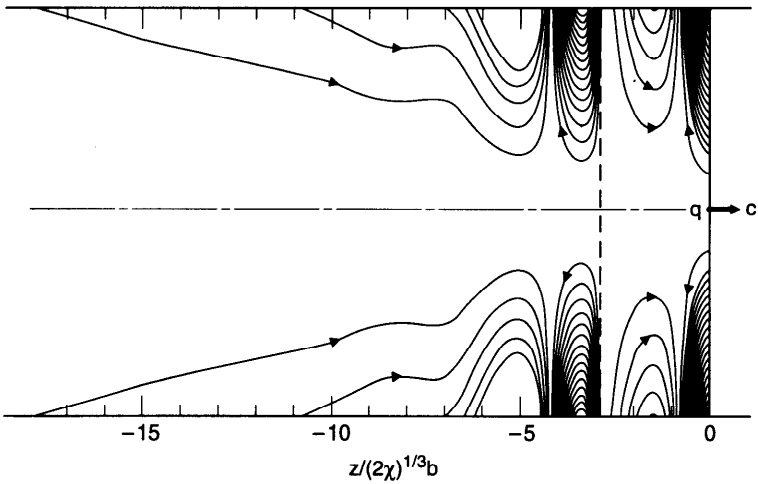

Figure 2.3. Wake electric field lines in a resistive wall pipe generated by a point charge q. The field pattern shows oscillatory behavior in the region $|z| \lesssim 5(2\chi)^{1/3}b$ (or $|z| \lesssim 0.35$ mm for an aluminum pipe with $b = 5$ cm). The field line density to the left of the dashed line has been magnified by a factor of 40. (Courtesy Karl Bane, 1991.)

One can obtain the rate of energy loss of the charge q by equating it to the heat generated in the resistive wall. This gives

$$\begin{aligned}\frac{d\mathscr{E}}{ds} &= -\frac{1}{c}\int_{\text{wall}} dV\vec{j}\cdot\vec{E} = -\frac{1}{c}\int_{\text{wall}} dV\,\sigma\vec{E}^2 \\ &= -\frac{\sigma}{c}\int_b^\infty 2\pi b\,dr\int_{-\infty}^\infty dz\left(E_s^2 + E_r^2\right) \\ &= -\frac{\sigma}{c}\int_b^\infty b\,dr\int_{-\infty}^\infty dk\left(|\tilde{E}_s|^2 + |\tilde{E}_r|^2\right),\end{aligned} \tag{2.25}$$

where we have used the Parseval theorem that

$$\int_{-\infty}^\infty dz\,F^2(z) = \int_{-\infty}^\infty \frac{dk}{2\pi}\left|\tilde{F}(k)\right|^2 \tag{2.26}$$

for Fourier transform pairs $F(z)$ and $\tilde{F}(k)$. Using the expressions (2.11) and (2.12) for $\tilde{E}_s$ and $\tilde{E}_r$ in the metal wall and Eq. (2.13) for A, and making the approximation that $\chi = c/4\pi\sigma b \ll 1$, we find[12]

$$\frac{d\mathscr{E}}{ds} = -\frac{2q^2}{b^2}. \tag{2.27}$$

[12]The algebra simplifies if one notes the contribution from $\tilde{E}_r$ is small.

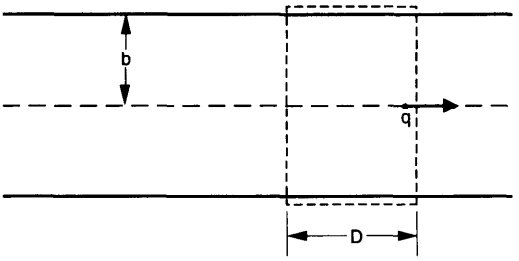

Figure 2.4. A box for computing the image charge using Gauss's law.

If we then associate this energy loss with an equivalent electric field as seen by the charge q, we find that it is exactly equal to half of the value of $E_s(z)$ in the limit $|z| \to 0$, given by Eq. (2.24). That is,

$$E_s\big|_{\text{seen by } q} = \tfrac{1}{2} E_s\big|_{z \to 0^-}. \tag{2.28}$$

Exercise 2.7 Equation (2.27), and thus Eq. (2.28), can be shown in different ways.

(a) Evaluate $E_s(0) = \int_{-\infty}^{\infty} (dk/2\pi) A(k)$ explicitly to show it is equal to $-2q/b^2$.

(b) Use the parasitic loss formula (2.103), combined with the resistive wall impedance (2.75) and $\tilde{\rho}(\omega) = q$ for a point charge.

(c) The energy flux into the wall is determined by the radial component of the Poynting vector $S_r = -cE_s B_\theta / 4\pi$. Calculate $d\mathscr{E}/ds$ by integrating S_r over the wall surface.

Exercise 2.8

(a) The surface charge density Σ on the pipe wall is related to the discontinuity of E_r at $r = b$. Show that the total charge on the wall surface is $-q$ by integrating Σ over the wall surface.

(b) Draw a box like Figure 2.4 and apply Gauss's law. Show that the total image charge contained between $|z| = 0$ and $|z| = D \gg \chi^{1/3} b$ behind the point charge q, to order $1/\sqrt{\sigma}$, is given by

$$-q\left(1 + \frac{b}{8\pi}\sqrt{\frac{c}{\sigma}}\, D^{-3/2}\right). \tag{2.29}$$

Note that the magnitude of this charge is larger than q.

Equation (2.28) actually is a general result, referred to as the *fundamental theorem of beam loading*.[13] The factor $\frac{1}{2}$ comes from the fact that charges in a beam see the wake produced only by those charges in front of it and as a result see on the average only half of the total beam charge.

[13] Perry B. Wilson, *AIP Proc.* **87**, *Phys. High Energy Accel.*, Fermilab, 1981, p. 450.

To prove Eq. (2.28) in general, consider a beam with short but finite length that has an otherwise arbitrary longitudinal charge density $\rho(z)$. The beam loses energy at a rate

$$\frac{d\mathscr{E}}{ds} = -\int_{-\infty}^{\infty} dz'\,\rho(z')\int_{z'}^{\infty} dz\,\rho(z)E_s(z'-z) \tag{2.30}$$

where $E_s(z'-z)$ is the wake produced by a unit point charge and seen by another point charge a distance $|z'-z|$ behind in an arbitrary vacuum chamber environment. If the bunch length is short enough that E_s behaves like a step function within the bunch distribution, Eq. (2.30) becomes

$$\frac{d\mathscr{E}}{ds} \approx -E_s(0^-)\int_{-\infty}^{\infty} dz'\,\rho(z')\int_{z'}^{\infty} dz\,\rho(z). \tag{2.31}$$

By a change of variable from z to $u = \int_z^{\infty} dz'\,\rho(z')$, Eq. (2.31) gives

$$\frac{d\mathscr{E}}{ds} \approx -E_s(0^-)\int_0^q u\,du = -\frac{q^2}{2}E_s(0^-), \tag{2.32}$$

which proves Eq. (2.28). The derivation assumed nothing but causality.

The $m \geq 1$ Wake

So far, electromagnetic wake fields have been obtained for the case $m = 0$. The fields are excited as the charge (i.e., the monopole moment) of the beam interacts with the resistive wall surroundings. If the beam possesses higher moments ($m = 1$ for dipole, $m = 2$ for quadrupole, etc.) in its transverse distribution, it will interact differently and generate different wake field patterns. In the following, we will work out the wake fields for cases $m \geq 1$.

Substituting Eqs. (1.7) and (2.2) into the Maxwell equation (2.1), we obtain the following results in the region $r < b$:

$$\begin{aligned}
\frac{\partial \tilde{E}_s}{\partial r} &= -\frac{m}{r}\tilde{B}_s,\\
\frac{\partial \tilde{B}_s}{\partial r} &= -\frac{m}{r}\tilde{E}_s,\\
\frac{1}{r}\frac{\partial}{\partial r}(r\tilde{E}_r) - \frac{m}{r}\tilde{B}_r &= \frac{4I_m}{a^{m+1}}\delta(r-a) - i\left(k + \frac{m^2}{kr^2}\right)\tilde{E}_s,\\
\frac{1}{r}\frac{\partial}{\partial r}(r\tilde{B}_r) - \frac{m}{r}\tilde{E}_r &= -i\left(k + \frac{m^2}{kr^2}\right)\tilde{B}_s,\\
\tilde{B}_\theta &= \tilde{E}_r - i\frac{m}{kr}\tilde{B}_s,\\
\tilde{E}_\theta &= -\tilde{B}_r + i\frac{m}{kr}\tilde{E}_s.
\end{aligned} \tag{2.33}$$

The first two of these equations are used to obtain $\tilde{E}_s$ and $\tilde{B}_s$; the second pair can then be solved for $\tilde{E}_r$ and $\tilde{B}_r$; then $\tilde{E}_\theta$ and $\tilde{B}_\theta$ are found from the last two expressions. The longitudinal components are easy to find,

$$\begin{aligned} \tilde{E}_s &= Ar^m, \qquad r < b, \\ \tilde{B}_s &= -Ar^m, \qquad r < b, \end{aligned} \tag{2.34}$$

where A is some coefficient that depends on k. Note that $\tilde{E}_s$ and $\tilde{B}_s$ are continuous across $r = a$.

Knowing $\tilde{E}_s$ and $\tilde{B}_s$, the solution for the other field components is not difficult to obtain. One needs only to observe that they generally can be written as polynomials in r, each containing three terms proportional to r^{m-1}, r^{m+1}, and r^{-m-1}, respectively. By properly choosing the coefficients for each of the terms for the two regions $r < a$ and $a < r < b$, the solution is found to be

$$\tilde{E}_r = \begin{cases} -\dfrac{ikA}{2(m+1)} r^{m+1} + \dfrac{1}{2}\left(-\dfrac{imA}{k} + B - \dfrac{4I_m}{a^{2m}} \right) r^{m-1}, \\ \dfrac{2I_m}{r^{m+1}} - \dfrac{ikA}{2(m+1)} r^{m+1} + \dfrac{1}{2}\left(-\dfrac{imA}{k} + B \right) r^{m-1}, \end{cases}$$

$$\tilde{E}_\theta = \begin{cases} -\dfrac{ikA}{2(m+1)} r^{m+1} + \dfrac{1}{2}\left(\dfrac{imA}{k} - B + \dfrac{4I_m}{a^{2m}} \right) r^{m-1}, \\ \dfrac{2I_m}{r^{m+1}} - \dfrac{ikA}{2(m+1)} r^{m+1} + \dfrac{1}{2}\left(\dfrac{imA}{k} - B \right) r^{m-1}, \end{cases} \tag{2.35}$$

$$\tilde{B}_r = \begin{cases} \dfrac{ikA}{2(m+1)} r^{m+1} + \dfrac{1}{2}\left(\dfrac{imA}{k} + B - \dfrac{4I_m}{a^{2m}} \right) r^{m-1}, \\ -\dfrac{2I_m}{r^{m+1}} + \dfrac{ikA}{2(m+1)} r^{m+1} + \dfrac{1}{2}\left(\dfrac{imA}{k} + B \right) r^{m-1}, \end{cases}$$

$$\tilde{B}_\theta = \begin{cases} -\dfrac{ikA}{2(m+1)} r^{m+1} + \dfrac{1}{2}\left(\dfrac{imA}{k} + B - \dfrac{4I_m}{a^{2m}} \right) r^{m-1}, \\ \dfrac{2I_m}{r^{m+1}} - \dfrac{ikA}{2(m+1)} r^{m+1} + \dfrac{1}{2}\left(\dfrac{imA}{k} + B \right) r^{m-1}, \end{cases}$$

where the upper and lower entries of each field component refer to the regions $r < a$ and $a < r < b$, respectively. The field components in the region $r < a$ do not contain r^{-m-1} terms, since they are unphysical at $r = 0$. The coefficient A appeared in Eq. (2.34), while B is a new coefficient. Both A and B are yet to be determined.

In the case of a perfectly conducting wall, $A = 0$ because $\tilde{E}_s$ must vanish at $r = b$. The condition that $\tilde{E}_\theta = 0$ at $r = b$ gives $B = 4I_m/b^{2m}$. An inverse Fourier transform then establishes Eq. (1.8).

To find A and B for the resistive-wall case, we need to solve for the fields in the metal wall. Inserting again Eq. (2.2) into the Maxwell equations and setting $\vec{j} = \sigma\vec{E}$ and $\rho = 0$, we obtain

$$
\begin{aligned}
&\frac{1}{r}\frac{\partial}{\partial r}\left(r\frac{\partial \tilde{E}_s}{\partial r}\right) + \left(\lambda^2 - \frac{m^2}{r^2}\right)\tilde{E}_s = 0,\\
&\frac{1}{r}\frac{\partial}{\partial r}\left(r\frac{\partial \tilde{B}_s}{\partial r}\right) + \left(\lambda^2 - \frac{m^2}{r^2}\right)\tilde{B}_s = 0,\\
&\tilde{E}_r = \frac{c}{4\pi\sigma}\left(\frac{m}{r}\tilde{B}_s + \frac{\partial \tilde{E}_s}{\partial r}\right),\\
&\tilde{E}_\theta = -\frac{c}{4\pi\sigma}\left(\frac{m}{r}\tilde{E}_s + \frac{\partial \tilde{B}_s}{\partial r}\right),\\
&\tilde{B}_r = \frac{c}{4\pi\sigma}\frac{\partial \tilde{B}_s}{\partial r} + \left(\frac{c}{4\pi\sigma} + \frac{i}{k}\right)\frac{m}{r}\tilde{E}_s,\\
&\tilde{B}_\theta = \frac{c}{4\pi\sigma}\frac{m}{r}\tilde{B}_s + \left(\frac{c}{4\pi\sigma} + \frac{i}{k}\right)\frac{\partial \tilde{E}_s}{\partial r}.
\end{aligned}
\tag{2.36}
$$

After the first pair of equations are solved for $\tilde{E}_s$ and $\tilde{B}_s$, the other field components are obtained from the remaining four equations. The quantity λ was defined in Eq. (2.6).

Following the analysis for the $m = 0$ case, we assume again that the skin depth is much smaller than b, i.e., we are interested in the region specified by Eq. (2.9). The first two equations in (2.36) then have the solution

$$
\tilde{E}_s = -\tilde{B}_s = Ab^m e^{i\lambda(r-b)}, \qquad r > b. \tag{2.37}
$$

Knowing $\tilde{E}_s$ and $\tilde{B}_s$, the rest of the field components are found to be

$$
\begin{aligned}
\tilde{E}_r = \tilde{E}_\theta &= -\frac{k}{\lambda}Ab^m e^{i\lambda(r-b)},\\
\tilde{B}_\theta &= -\left(\frac{k}{\lambda} + \frac{\lambda}{k}\right)Ab^m e^{i\lambda(r-b)},\\
\tilde{B}_r &= \left(\frac{k}{\lambda} + \frac{im}{kb}\right)Ab^m e^{i\lambda(r-b)}.
\end{aligned}
\tag{2.38}
$$

The requirement that $\tilde{E}_\theta$, $\tilde{B}_r$, and $\tilde{B}_\theta$ be continuous at $r = b$ (the component $\tilde{E}_r$ is not continuous across $r = b$, due to a surface charge on the wall) gives

$$A = \frac{4I_m}{b^{2m+1}\left(\dfrac{ikb}{m+1} - \dfrac{\lambda}{k} - \dfrac{im}{kb}\right)},$$
$$B = -\frac{\lambda}{k} bA. \tag{2.39}$$

If we further restrict our interest to the region specified by Eq. (2.14), the coefficients A and B become

$$A \approx -\frac{4I_m k}{b^{2m+1}\lambda},$$
$$B \approx \frac{4I_m}{b^{2m}}\left[1 + i\frac{k^2 b}{(m+1)\lambda} - \frac{im}{b\lambda}\right]. \tag{2.40}$$

Table 2.1 can then be used to find the field components, yielding

$$E_s = \frac{I_m}{\pi b^{2m+1}}\sqrt{\frac{c}{\sigma}}\, r^m \cos m\theta \frac{1}{|z|^{3/2}},$$
$$E_r = -\frac{3I_m}{4\pi b^{2m+1}}\sqrt{\frac{c}{\sigma}}\frac{1}{(m+1)} r^{m-1}\cos m\theta\,(r^2 + b^2)\frac{1}{|z|^{5/2}},$$
$$E_\theta = -\frac{3I_m}{4\pi b^{2m+1}}\sqrt{\frac{c}{\sigma}}\frac{1}{(m+1)} r^{m-1}\sin m\theta\,(r^2 - b^2)\frac{1}{|z|^{5/2}},$$
$$B_s = -\frac{I_m}{\pi b^{2m+1}}\sqrt{\frac{c}{\sigma}}\, r^m \sin m\theta \frac{1}{|z|^{3/2}}, \tag{2.41}$$
$$B_r = -E_\theta - \frac{2I_m}{\pi b^{2m+1}}\sqrt{\frac{c}{\sigma}}\, m r^{m-1}\sin m\theta \frac{1}{|z|^{1/2}},$$
$$B_\theta = E_r - \frac{2I_m}{\pi b^{2m+1}}\sqrt{\frac{c}{\sigma}}\, m r^{m-1}\cos m\theta \frac{1}{|z|^{1/2}}.$$

These expressions are valid for regions behind the beam and inside the pipe. Again, the field vanishes in front of the beam. Note that the beam dimension a does not appear explicitly in the fields, indicating that for a given mth moment of the beam, the wake field is independent of the detailed shape of the beam distribution. See Figure 2.5.

According to Eq. (2.41), the longitudinal electric field component E_s behaves like $|z|^{-3/2}$ and the transverse electric field components behave like

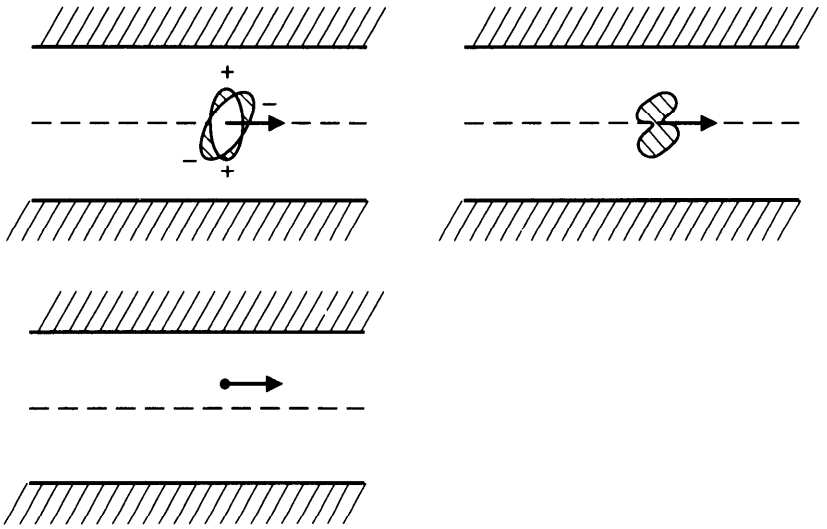

Figure 2.5. The wake field is independent of the detailed beam distribution. The same wake field is generated as long as the beam has the same mth moment. Cases shown are for $m = 2$.

$|z|^{-5/2}$, similarly to the $m = 0$ case, Eq. (2.16); but the magnetic field behaves very differently from the $m = 0$ case. First, B_s no longer vanishes. Second, the magnitude of the transverse magnetic field is comparable to the transverse electric field at distances $|z| \lesssim b$ behind the beam, but, having a long $|z|^{-1/2}$ tail, dominates at distances $|z| \gtrsim b$.

Equation (2.41) is obtained assuming I_m is a constant as it moves down the resistive pipe with $s = ct$. In case I_m changes with s, the wake field observed at a fixed location $s' < s$ in the accelerator is given by replacing I_m in Eq. (2.41) with its value $I_m(s')$ at the moment when it was passing by position s', and replacing z with $s' - s$.

Exercise 2.9 Verify that Eqs. (2.16), (2.22), (2.24), and (2.41) satisfy the Maxwell equations.

The electromagnetic field components can also be computed in the short range $|z| \ll \chi^{1/3}b$ for the case $m \geq 1$. The component E_s, for example, is determined by

$$A \approx -i\frac{4I_m(m+1)}{kb^{2m+2}}, \tag{2.42}$$

which gives

$$E_s(0^-) = -\frac{4I_m(m+1)}{b^{2m+2}}r^m \cos m\theta. \tag{2.43}$$

Compared with Eq. (2.41), E_s has to switch sign in the region $0 > z \gtrsim -\chi^{1/3}b$.

A point mth moment I_m, with charge density given by Eq. (1.7), going down the resistive wall pipe, thus loses energy at a rate

$$\frac{d\mathscr{E}}{ds} = \int dV \rho_m \frac{E_s(0^-)}{2}$$
$$= \int_0^{2\pi} d\theta \frac{I_m}{\pi a^m} \cos m\theta \frac{E_s(0^-)}{2} = -\frac{2I_m^2(m+1)}{b^{2m+2}}, \qquad (2.44)$$

where $E_s(0^-)$ is divided by 2 to take into account the fundamental theorem of beam loading.

Exercise 2.10 Consider an off-centered point charge described by superposition of moments, Eqs. (1.6–1.7). Show that this particle loses energy in the resistive pipe at a rate

$$\frac{d\mathscr{E}}{ds} = -\frac{2q^2b^2}{(b^2-a^2)^2}. \qquad (2.45)$$

Compared with a centered charge, the energy loss rate is faster by a factor of $b^4/(b^2-a^2)^2$, which diverges as a approaches b, i.e., as the point charge approaches the resistive wall.

2.2 WAKE FUNCTIONS

In Figure 2.1, we showed examples of environments in which a beam with a multipole moment can excite a wake electromagnetic field behind it. Consider now a test charge e trailing behind the $\cos m\theta$ ring beam in one such environment. The test charge experiences an electromagnetic wake force. The vacuum chamber pipe is considered to be axially symmetric, and both the beam and the trailing test charge travel with the speed of light c.

Consider first the case of resistive wall. The Lorentz force $\vec{F} = e(\vec{E} + \hat{s} \times \vec{B})$ experienced by the test charge has the components

$$F_\parallel = eE_s,$$
$$F_\theta = e(E_\theta + B_r), \qquad (2.46)$$
$$F_r = e(E_r - B_\theta).$$

Substituting from Eq. (2.41), Eq. (2.46) gives

$$F_\parallel = \frac{eI_m}{\pi b^{2m+1}(1+\delta_{m0})}\sqrt{\frac{c}{\sigma}}\, r^m \cos m\theta \frac{1}{|z|^{3/2}},$$
$$\vec{F}_\perp = \frac{2\,eI_m}{\pi b^{2m+1}}\sqrt{\frac{c}{\sigma}}\, mr^{m-1}\frac{1}{|z|^{1/2}}(\hat{r}\cos m\theta - \hat{\theta}\sin m\theta). \qquad (2.47)$$

These expressions also give the correct answer for $m = 0$ if we set $I_0 = q$. [See Eq. (2.16).] For $m = 0$, we have $\vec{F}_\perp = 0$, as one would also expect by symmetry.

It is interesting to observe that the $|z|^{-5/2}$ terms in the transverse fields (2.41) do not contribute to the transverse force, and that the transverse force comes solely from the $|z|^{-1/2}$ terms of the magnetic field. What happens is that the image current penetrates into the metal wall and, as it slowly resurfaces, drives the $|z|^{-1/2}$ tail of the magnetic field. The same thing does not happen to the electric field because the image charges stay on the wall surface without penetration into the metal.

Because of the translational symmetry in the case of resistive wall, the force seen by the test charge, Eq. (2.47), depends on s and t through the combination $s - ct = z$, which is the longitudinal separation of the test charge from the $\cos m\theta$ ring beam. The wake force pattern does not change as the beam and the test charge travel down the pipe. This is no longer true in the environments shown in Figure 2.1(a) and (c). In Figure 2.1(a), the force seen by the test charge varies periodically with the period of the structure. In Figure 2.1(c), the force occurs more or less as an impulse when the test charge passes by the wall structure. In these cases without translational symmetry, the wake force becomes much more complicated; it depends on s and t separately instead of the combined variable $z = s - ct$.

However, at high energies, the trajectory of the beam and the test charge is not perturbed much as they travel a distance over a wall structure. The net effect on the test charge can be obtained by integrating the force through a distance longer than the wall structure, and one considers quantities

$$\int_{-L/2}^{L/2} ds f \equiv \bar{f}, \tag{2.48}$$

where f represents the components of the force $\vec{F}$ (or the fields $\vec{E}$ and $\vec{B}$) seen by the test charge, and L is a distance of interest. For Figure 2.1(a), L is the structure period. For Figure 2.1(c), L is chosen to be a convenient distance much longer than the wall structure. For Figure 2.1(b), the wake force is independent of s and we have simply $\bar{f} = fL$.

The quantities $\bar{f}$, when properly integrated over s, are smoothed out so that the detailed s- and t-dependences combine into a z-dependence. As we will see next, the fact that we are interested only in the *integrated impulses* (2.48), rather than the detailed instantaneous forces, allows the problem at hand be drastically simplified. This simplification is possible because we are only interested in high energy beams.

There actually exists a general form of the wake force once it is integrated over the structure period; Eq. (2.47) is only a special case for the resistive wall. To obtain the general form, the Maxwell equations (2.1) are linearly combined into equations for the quantities $\bar{F}_\parallel$, $\bar{F}_r$, $\bar{F}_\theta$, and $e\bar{B}_s$, which are

functions of r, θ, and z. The result in the pipe region $r < b$ is surprisingly simple:

$$
\begin{aligned}
-\frac{e}{r}\frac{\partial}{\partial\theta}\bar{B}_s &= \frac{\partial}{\partial z}\bar{F}_r = \frac{\partial}{\partial r}\bar{F}_{\parallel}, \\
e\frac{\partial}{\partial r}\bar{B}_s &= \frac{\partial}{\partial z}\bar{F}_\theta = \frac{1}{r}\frac{\partial}{\partial\theta}\bar{F}_{\parallel}, \\
\frac{\partial}{\partial r}(r\bar{F}_r) &= -\frac{\partial}{\partial\theta}\bar{F}_\theta, \\
\frac{\partial}{\partial r}(r\bar{F}_\theta) &= \frac{\partial}{\partial\theta}\bar{F}_r.
\end{aligned}
\tag{2.49}
$$

In deriving Eq. (2.49), we have used the fact that in the region $r < b$ the source terms satisfy $j_r = j_\theta = 0$ and $j_s = c\rho$. Note that Eq. (2.49) does not contain source terms explicitly; neither does it depend on the boundary conditions.

Recalling that, for an axially symmetric environment, $F_{\parallel}$ and F_r are proportional to $\cos m\theta$ and B_s and F_θ are proportional to $\sin m\theta$, Eq. (2.49) can easily be solved to yield

$$
\begin{aligned}
\int_{-L/2}^{L/2} ds\,\vec{F}_\perp &= -eI_m W_m(z) m r^{m-1}(\hat{r}\cos m\theta - \hat{\theta}\sin m\theta), \\
\int_{-L/2}^{L/2} ds\,F_{\parallel} &= -eI_m W_m'(z) r^m \cos m\theta, \\
\int_{-L/2}^{L/2} ds\,eB_s &= eI_m W_m'(z) r^m \sin m\theta,
\end{aligned}
\tag{2.50}
$$

where W_m is a function of z yet to be determined, and W_m' is the derivative of W_m with respect to z. The case $m = 0$ is included provided we set $I_0 = q$. Causality dictates that the test charge does not experience a wake force if it is ahead of the ring beam. This requires $W_m(z) = 0$ if $z > 0$.

In the present ultrarelativistic approximation, the integrated wake force impulses (2.50) are applied to the test charge at the location where the wake fields are generated, i.e., at the location of the wall structure. Note that there is no transverse wake force when $m = 0$, because $\int ds\,\vec{F}_\perp = 0$. Note also that one can define a quantity V so that

$$
\begin{aligned}
\int_{-L/2}^{L/2} ds\,\vec{F} &= -\nabla V, \\
V &= eI_m W_m(z) r^m \cos m\theta.
\end{aligned}
\tag{2.51}
$$

The explicit form of W_m, of course, can only be determined after imposing the boundary conditions as was done for the resistive wall. It is interesting, however, that all the explicit r, θ, and z dependences in Eq. (2.50) are derived without referring to the boundary conditions at all, except that the boundary is axially symmetric.[14]

The function $W_m(z)$ in Eq. (2.50) is called the *wake function*; it describes the shock response of the vacuum chamber environment to a δ-function beam which carries an mth moment. Mathematically, W_m resembles a Green's function. Sometimes it may be more convenient to call $W_m(z)$ the transverse wake function and $W_m'(z)$ the longitudinal wake function, for reasons that should be obvious from Eq. (2.50). The dimensionality of W_m is L^{-2m} in cgs units. In analogy with the concept of the electric potential, the integrals on the left hand side of Eq. (2.50) are called the *wake potentials*.

In general, the wake functions are solely determined by the properties of the vacuum chamber environment; they are independent of the beam properties. The property (2.50) applies to the force components and not to the electromagnetic field components. Fortunately, it is the force components, not the field components, that we need.

The result (2.50) can be combined to say that the transverse gradient of the longitudinal wake potential is equal to the longitudinal gradient of the transverse wake potential,

$$\nabla_\perp \int_{-L/2}^{L/2} ds\, F_\parallel = \frac{\partial}{\partial z} \int_{-L/2}^{L/2} ds\, \vec{F}_\perp \,. \tag{2.52}$$

This expression is sometimes referred to as the *Panofsky-Wenzel theorem*.[15]

For the special case of a resistive wall, the wake function over a distance L is, for $z < 0$,

$$W_m(z) = -\frac{2}{\pi b^{2m+1}(1+\delta_{m0})} \sqrt{\frac{c}{\sigma}} \frac{1}{|z|^{1/2}} L. \tag{2.53}$$

The range of validity of Eq. (2.53) is $b/\chi \gg |z| \gg \chi^{1/3} b$, where χ is the small parameter defined in Eq. (2.10). In the range $|z| \ll \chi^{1/3} b$, we also have, from Eq. (2.24) for $m = 0$,

$$\frac{W_0(z)}{L} = \frac{4}{b^2} z + \frac{128}{15} \frac{1}{b^3} \sqrt{\frac{\sigma}{c}} |z|^{5/2}. \tag{2.54}$$

It was mentioned before that the wake functions are properties of the vacuum chamber environment, and are independent of the beam properties.

[14] In case the boundary is not axially symmetric, modes of different m's will couple. The $\cos m\theta$ and $\sin m\theta$ patterns no longer form an eigenmode. The analysis becomes more complicated.

[15] W. K. H. Panofsky and W. A. Wenzel, Rev. Sci. Instr. 27, 967 (1956).

Equation (2.50) was derived under the ultrarelativistic assumption $\gamma \to \infty$. The space charge forces, which are nonrelativistic in nature, are excluded from the treatment. It turns out, however, that the space charge forces can almost fit into the wake function framework, and when that is done, the wake functions will depend on beam properties such as the transverse beam size a and the beam energy γ. For a $\cos m\theta$ ring beam, the transverse and longitudinal space charge forces, Eqs. (1.32) and (1.51), in the region $r < a$ can be cast in the framework of (2.50) if we let

$$W_m(z) = \frac{2L}{\gamma^2}\delta(z)\begin{cases} \ln\dfrac{b}{a} & \text{if} \quad m = 0, \\ \dfrac{1}{m}\left(\dfrac{1}{a^{2m}} - \dfrac{1}{b^{2m}}\right) & \text{if} \quad m > 0, \end{cases} \tag{2.55}$$

although the third member of Eq. (2.50) is not satisfied.

For a uniform disk beam, the space charge forces (1.35), (1.44), and (1.53) cannot be cast in the wake function framework. However, it is often convenient to insist on it at least for the $m = 0$ longitudinal case. To do so, consider $r = 0$ and write

$$W_0(z) = \frac{2L}{\gamma^2}\delta(z)\left(\ln\frac{b}{a} + \frac{1}{2}\right). \tag{2.56}$$

As mentioned, Eqs. (2.55–2.56) depend on the beam properties a and γ.

If one considers a rigid uniform disk beam executing a small transverse dipole motion, the space charge force is a superposition of that of an $m = 0$ uniform disk beam force and an $m = 1$ ring-beam force. In this case, one can use Eq. (2.55) with $m = 1$ and Eq. (2.56) for $m = 0$ as the space charge wake functions. This model is the one used in most of our applications later.

Exercise 2.11 Equation (2.50) relates the *force* components to wake functions. For a general m, there are no simple a priori relations for the individual *field* components. However, Eq. (2.49) does not exhaust the information contained in the Maxwell equations without explicit knowledge of the boundary conditions. Show that, for $m = 0$ and in the free space behind the beam, the Maxwell equations give the additional relations

$$\bar{E}_r = \bar{B}_\theta = \frac{q}{2} r W_0''(z). \tag{2.57}$$

Confirm this with the resistive-wall case, Eqs. (2.16) and (2.24).

Immediately following the beam, we expect to see a longitudinal electric field that retards the beam, regardless of vacuum chamber properties. This

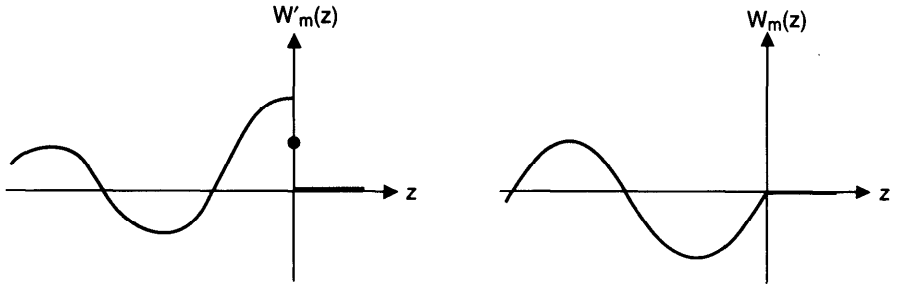

Figure 2.6. Sketches of the longitudinal wake function $W'_m(z)$ and the transverse wake function $W_m(z)$. Both W_m and W'_m vanish if $z > 0$. The value of $W'_m(z)$ at $z = 0$ is indicated by a solid dot and it sits exactly midway between the values of $W'_m(0^+) = 0$ and $W'_m(0^-) > 0$, according to the fundamental theorem of beam loading.

means the quantity $j_s F_{\|}$ must be negative definite, which implies

$$W'_m(z) > 0 \qquad \text{for} \quad z \to 0^-. \tag{2.58}$$

It follows that the longitudinal wake function $W'_m(z)$ of a resistive wall must switch sign in the range between $z = 0$ and $z \approx -\chi^{1/3} b$, since W'_m obtained from Eq. (2.53) is negative.

Another consequence of Eq. (2.58) is that the transverse wake function $W_m(z)$ is negative for $z < 0$, and its magnitude increases monotonically with $|z|$, at least initially, starting from $W_m = 0$ at $z = 0^+$. In other words, the longitudinal wake function is cosinelike and the transverse wake function is sinelike, as sketched in Figure 2.6. It follows that a point charge does not experience a deflecting force due to its own transverse wake. This is in contrast to the longitudinal dimension, in which a point charge does see its own retarding wake force. This property leads to a preference for short beams when the transverse wake effects dominate, while longer bunches are preferred when the main concern is the longitudinal wake effects.

There are several interesting properties of the wake functions. One has been listed in Eq. (2.58). Some of these properties for the longitudinal wake function $W'_m(z)$ are given in Exercise 2.12 below. Here let us demonstrate how property (c) can be shown; the other properties can be shown similarly. Consider a point charge q followed by another point charge q at a distance $|z|$ behind. After traveling a distance L, the first q loses an energy $\frac{1}{2}q^2 W'_0(0^-)$ due to the wake generated by itself, where the factor of $\frac{1}{2}$ is due to the fundamental theorem of beam loading. The trailing q loses an energy $\frac{1}{2}q^2 W'_0(0^-) + q^2 W'_0(z)$, where the second term is due to the wake left by the leading q. Physically, the two-charge system can never gain energy; this means $W'_0(z) \geq -W'_0(0^-)$ for any z. Similarly, if the second charge is $-q$ rather than q, one proves $W'_0(z) \leq W'_0(0^-)$. Property (c) is thus established for $m = 0$. From this property, it follows that $W'_m(0^-)$ is the maximum value

the function $W_m'(z)$ ever reaches, and $W_m'(0^-) = 0$ necessarily gives the trivial case when the entire wake potential vanishes.

Exercise 2.12 Show that the longitudinal wake function $W_m'(z)$ is unphysical unless the following properties are satisfied:

(a) $W_m'(z) = 0$ if $z > 0$.

(b) $W_m'(0^-) \geq 0$.

(c) $W_m'(0^-) \geq |W_m'(z)|$ for all z.

(d) If $W_m'(-D) = W_m'(0^-)$ for some D, then $W_m'(z)$ is periodic with period D, i.e., $W_m'(z - D) = W_m'(z)$ for any $z < 0$. [Hint: Consider three

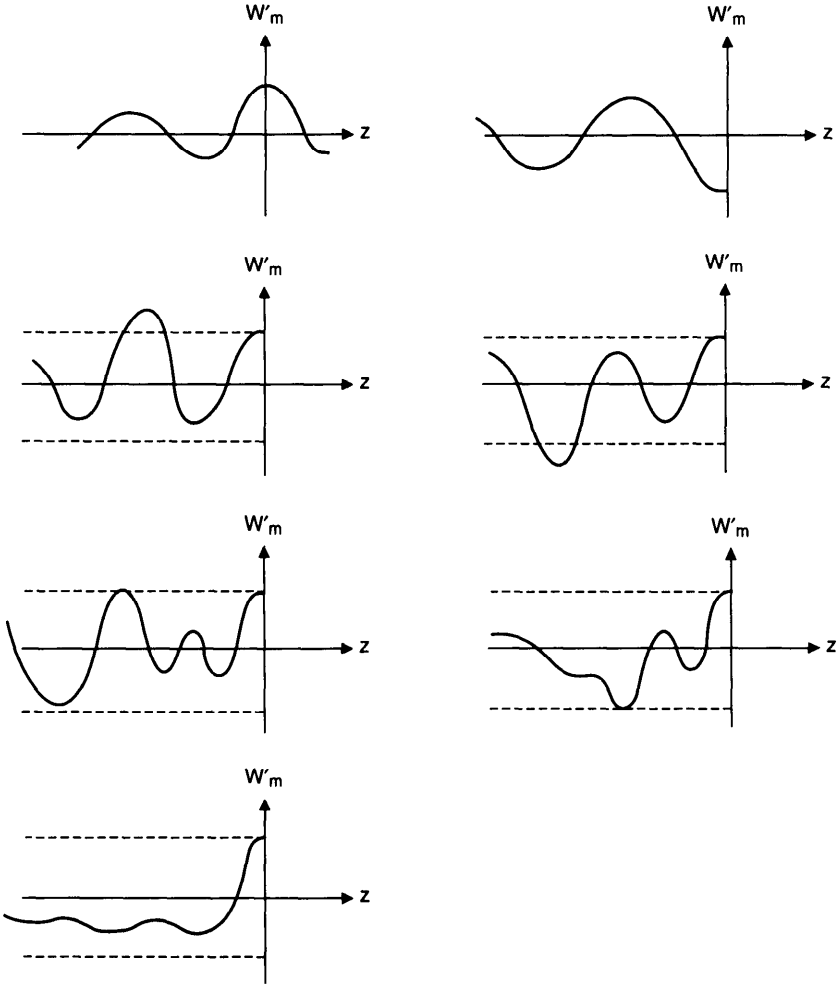

Figure 2.7. Sketches of some unphysical wake functions $W_m'(z)$.

charges q_1, q_2, and $-q_2$, with spacing z between q_1 and q_2, and spacing D between q_2 and $-q_2$.]

(e) If $W'_m(-D) = -W'_m(0^-)$ for some D, then $W'_m(z - D) = -W'_m(z)$.

(f) $\int_{-\infty}^{0} W'_m(z)\,dz \geq 0$, i.e., the area under $W'_m(z)$ is positive. [Hint: Consider a test charge in a continuous beam in steady state.]

(g) $1 \geq W'_m(z_1)W'_m(z_2)W'_m(z_1 + z_2)/[W'_m(0^-)]^3 \geq -\frac{1}{8}$ for any z_1, z_2.

Use these results to show that the wake functions sketched in Figure 2.7 are unphysical.

We now define a Cartesian coordinate system with $x = r\cos\theta$ and $y = r\sin\theta$, and orient the charge density in the x-y system at an angle θ_0 [i.e., in the expression (1.7) for ρ_m, $\cos m\theta$ is replaced by $\cos m(\theta - \theta_0)$]. In this Cartesian system, the beam now has two components of mth moments—one normal and another skewed. Table 2.2 lists the two moments (first the normal moment and then the skewed moment) and the associated wake potentials. A bracket $\langle\ \rangle$ means averaging over the transverse distribution of the beam; $\hat{x}$ and $\hat{y}$ are the unit vectors in the x- and y-directions. The wake potentials are those seen by a test charge e with transverse coordinates x, y that follows the beam at distance $|z|$ behind.

The transverse wake force experienced by the test charge for $m = 1$ listed in Table 2.2 behaves like the bending force seen in a horizontal or vertical dipole magnet. Similarly, the wakes act like quadrupole and skew quadrupole magnets for $m = 2$, sextupole and skew sextupole magnets for $m = 3$, etc. The $m = 0$ case does not have a transverse wake force, because the longitudinal wake potential does not have a transverse gradient.

Table 2.2. The longitudinal and transverse wake potentials $\int_{-L/2}^{L/2} ds\, F_{\parallel}$ and $\int_{-L/2}^{L/2} ds\, \vec{F}_{\perp}$ seen by a test charge e a distance $|z|$ behind a beam which possesses an mth moment.

m	Distribution Moments of Beam	Longitudinal Wake Potential	Transverse Wake Potential
0	q	$-eqW'_0(z)$	0
1	$q\langle x\rangle$	$-eq\langle x\rangle xW'_1(z)$	$-eq\langle x\rangle W_1(z)\hat{x}$
	$q\langle y\rangle$	$-eq\langle y\rangle yW'_1(z)$	$-eq\langle y\rangle W_1(z)\hat{y}$
2	$q\langle x^2 - y^2\rangle$	$-eq\langle x^2 - y^2\rangle(x^2 - y^2)W'_2(z)$	$-2eq\langle x^2 - y^2\rangle W_2(z)(x\hat{x} - y\hat{y})$
	$q\langle 2xy\rangle$	$-eq\langle 2xy\rangle 2xyW'_2(z)$	$-2eq\langle 2xy\rangle W_2(z)(y\hat{x} + x\hat{y})$
3	$q\langle x^3 - 3xy^2\rangle$	$-eq\langle x^3 - 3xy^2\rangle(x^3 - 3xy^2)W'_3(z)$	$-3eq\langle x^3 - 3xy^2\rangle W_3(z) \times[(x^2 - y^2)\hat{x} - 2xy\hat{y}]$
	$q\langle 3x^2y - y^3\rangle$	$-eq\langle 3x^2y - y^3\rangle(3x^2y - y^3)W'_3(z)$	$-3eq\langle 3x^2y - y^3\rangle W_3(z) \times[2xy\hat{x} + (x^2 - y^2)\hat{y}]$

If the wake forces come from cavity structures which are of a size similar to the pipe radius b, we will show later [see Eq. (2.114)] that W'_m/L scales as b^{-2m-2} and W_m/L scales as b^{-2m-1}. The longitudinal wake force, according to Table 2.2, scales as $a^{2m}W'_m/L \sim (a/b)^{2m}(1/b^2)$, and the transverse wake force scales as $a^{2m-1}W_m/L \sim (a/b)^{2m-1}(1/b^2)$, where a is the transverse beam size. Since typically $b \gg a$, the lower modes usually dominate, i.e., the $m = 0$ mode dominates the longitudinal wake effects, and the $m = 1$ mode dominates the transverse wake effects. The wake W'_0 therefore is often loosely referred to as *the* longitudinal wake function, although only the $m = 0$ member is being considered. Similarly, W_1 is sometimes referred to as *the* transverse wake function.

The longitudinal ($m = 0$) and transverse ($m = 1$) wake forces scale with b as b^{-2} and b^{-3}, respectively. In application to linear colliders, where there is a tendency to make the cavity structures small to save cost, the transverse wake effects tend to dominate. It then follows from the discussion following Eq. (2.58) that a short beam bunch is preferred in these applications.

One can also say something about the polarity of the transverse wake forces using Table 2.2. To do that, imagine a short beam traveling down the accelerator with a displacement in x. The head of the beam bunch will generate a wake force that kicks the particles that are in the tail further away from the accelerator axis, since $W_1(z) < 0$ if $|z|$ is short enough. Similarly, if the beam has an elliptical shape in its transverse distribution and thus possesses a quadrupole moment, the transverse wake force is such that it

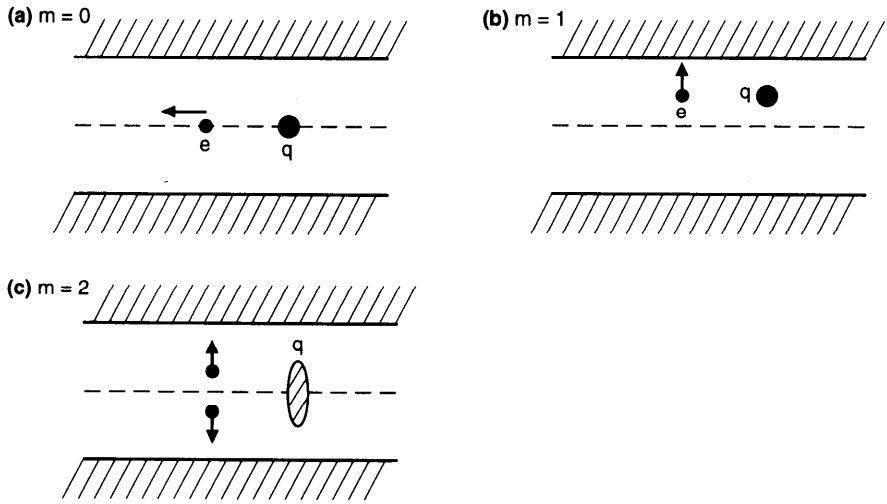

Figure 2.8. The polarity of the wake field always hurts a short beam. For $m = 0$, the longitudinal wake force is retarding. For $m = 1$, the transverse wake force further deflects the test charge e. For $m = 2$, the tail portion of an elliptical beam becomes further elongated. Arrows represent the wake force.

tends to elongate the ellipse further in the bunch tail. In general, one finds that the polarity of the transverse wake forces is such that it always hurts a short beam. See Figure 2.8.

As $|z|$ increases, W'_m and W_m may change signs and the wake forces become beneficial. In particular, W'_0 may become negative at some finite distance behind the head of the beam. Therefore, if one injects two beam bunches into the accelerator and if the separation of the two bunches is chosen strategically, the trailing bunch can be *accelerated* by the wake field of the leading bunch. This leads to the idea of *wake field accelerators*. We will not discuss such accelerators,[16] but as an illustration of the property of the wake functions, we will show below that a straightforward application of the wake field acceleration idea in which a short leading bunch is followed by a short trailing bunch traveling down the *same* path would not work very well.

To show this, consider a wake field accelerator consisting of a short leading bunch of charge $N_1 e$ and a short trailing bunch of charge $N_2 e$ a distance $|z|$ behind the leading bunch. After a distance L, the leading bunch loses an energy

$$\Delta \mathscr{E}_1 = -\tfrac{1}{2} N_1^2 e^2 W'_0(0^-). \tag{2.59}$$

To maximize the energy gain by the trailing bunch, we design the wake potential and choose the relative position of the two bunches in such a way that $W'_0(z) = -W'_0(0^-)$. The energy of the trailing bunch then changes by

$$\Delta \mathscr{E}_2 = \left(-\tfrac{1}{2} N_2^2 + N_1 N_2\right) e^2 W'_0(0^-), \tag{2.60}$$

where the first term is the energy loss due to self-field, and the second term comes from the accelerating wake field left behind by the leading bunch. For a given N_2, the acceleration rate of the trailing bunch can be made arbitrarily large by having a large N_1. However, a large N_1 also means the leading bunch is decelerated rapidly. In fact, let E_1 and E_2 be the energies of a single particle in the leading and trailing bunches; then the leading bunch will come to a full stop when it has exhausted all its energy, i.e., when $\Delta \mathscr{E}_1 = -N_1 E_1$. At this point, the energy of a particle in the trailing bunch has increased by an amount

$$\Delta E_2 = \frac{\Delta \mathscr{E}_2}{N_2} = \left(2 - \frac{N_2}{N_1}\right) E_1 < 2E_1. \tag{2.61}$$

[16]G.-A. Voss and T. Weiland, DESY Report 82-074 (1982); R. J. Briggs, T. J. Fessenden, and V. K. Neil, *Proc. 9th Int. Conf. High Energy Accel.*, SLAC, 1974, p. 278; M. Friedman, Phys. Rev. Lett. **31**, 1107 (1973); E. A. Perevedentsev and A. N. Skrinsky, *Proc. 6th All-Union Conf. Charged Part. Accel.*, Dubna, 1978, Vol. 2, p. 272; Andrew M. Sessler, *AIP Proc.* **91**, *Laser Accel. of Part.*, Los Alamos, 1982, p. 154; P. Chen, R. W. Huffad, and J. M. Dawson, Bull. Am. Phys. Soc. **29**, 1355 (1984); Yongho Chin, *Proc. Lin. Accel. Conf.*, Seeheim/Darmstadt, 1984, p. 159.

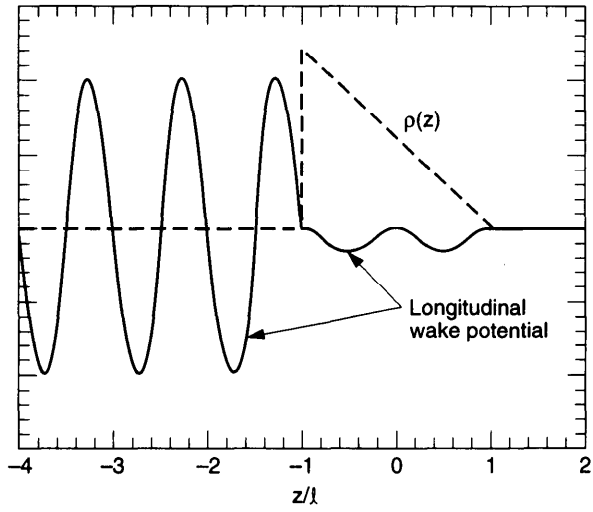

Figure 2.9. The longitudinal wake potential (solid curve) produced by the beam discussed in Exercise 2.13 as a function of z/l. The dashed curve gives $\rho(z)$. The vertical scales are unspecified.

An intense leading bunch indeed induces a large acceleration rate for the trailing bunch, but the total energy gained by each particle in the trailing bunch cannot exceed $2E_1$, no matter how intense the leading bunch is; most of the energy contained in the leading beam would be wasted. The *transformer ratio* $\Delta E_2/\Delta E_1$ cannot exceed 2.[17] To accelerate the trailing beam by 2 GeV, for instance, one has to prepare a 1 GeV leading beam first. Such a wake field accelerator is not very efficient. Note that this conclusion applies regardless of details of the wake field mechanism, whether it is provided by a resistive wall, cavity structures, or a plasma medium.

To improve the transformer ratio, one can consider two beams in *different* paths. This is the approach of klystrons, as well as many of the new generation of wake field accelerator concepts. In these devices, the wake field is generated in a special-purpose chamber, optimized, and sent by waveguides to accelerate another beam in a different vacuum chamber. The transformer ratio can then be made much larger than 2.

Exercise 2.13 The discussion leading to Eq. (2.61) assumes a short leading bunch. It is in fact possible, in principle at least, to defeat this limit on the transformer ratio by using a longer leading bunch. The wake potential of a long bunch can be obtained by superposition. As an illustration, consider a wake $W_0'(z < 0) = W_0 \cos kz$ and a leading bunch with a triangular-shaped

[17] J. Seeman, IEEE Trans. Nucl. Sci. **NS-30**, 3180 (1983); R. D. Ruth, A. W. Chao, P. L. Morton, and P. B. Wilson, Part. Accel. **17**, 171 (1985).

longitudinal charge density $\rho = (Ne/2l)(1 - z/l)$ if $|z| < l$ and 0 otherwise. Let the bunch length $2l$ be n times the wavelength of the wake field, i.e., $kl = \pi n$. Show that by locating a short trailing bunch optimally behind the leading bunch, one can achieve a transformer ratio of $2\pi n$.[18] Figure 2.9 shows the longitudinal wake potential as a function of z for the case of $n = 2$.

2.3 IMPEDANCES

So far the wake fields have been described as a function of time after the passage of a δ-function beam. It is often useful to examine the frequency content of the wake field by performing a Fourier transformation on it. One early indication of the usefulness of this procedure is the fact that we introduced the Fourier transformed quantities $\tilde{E}$ and $\tilde{B}$ when we worked out the case of the resistive wall in Section 2.1. Another indication is that the wake response often contains a number (say, 20) of sharply defined frequencies, which can be revealed by the proper Fourier transforms. Such a situation does not occur for a resistive wall wake, but does occur if the wake is generated by a cavity structure in an otherwise smooth vacuum chamber pipe as shown in Figure 2.1(a) and (c). The Fourier transform of the wake function is called the *impedance*. The idea of representing the accelerator environment by an impedance was introduced by Sessler and Vaccaro.[19]

Needless to say, the descriptions of the wake force in terms of wake functions in the time domain and in terms of impedances in the frequency domain are identical. In most practical applications, for example, the calculation of the wake functions at short distances poses a difficult technical problem. Exactly the same difficulty is encountered in calculating the impedance at high frequencies. It is a matter of taste which approach to take. For many later developments, we find a mixed approach convenient in which we use the time domain description to set up the equations of motion ($F = ma$) and then use the Fourier transform techniques to solve them.

So far we have considered δ-function beams. Wakes produced by other beam distributions can be constructed by superposition using the δ-function result. For example, consider a beam that has a current

$$J_0(s,t) = \hat{J}_0\, e^{i(ks-\omega t)}. \tag{2.62}$$

[18]K. L. F. Bane, P. B. Wilson, and T. Weiland, *AIP Proc.* **127**, *Phys. High Energy Part. Accel.*, BNL/SUNY, 1983, p. 875; K. L. F. Bane, Pisin Chen, and P. B. Wilson, IEEE Trans. Nucl. Sci. **NS-32**, 3524 (1985). Here we have defined the transformer ratio to be the ratio of the energy gain of a particle in the trailing bunch to the average—not the maximum—energy loss of a particle in the leading bunch. This definition is consistent with that used in deriving Eq. (2.61).

[19]A. Sessler and V. Vaccaro, CERN Report ISR-RF/67-2 (1967).

Only the real part of Eq. (2.62) is meaningful. The $m = 0$ wake potential at position s and time t is a superposition of the wakes produced by all charges in the beam that passed by the *same* position s at previous times, i.e.,

$$\begin{aligned}\bar{E}_s(s,t) &= -\frac{1}{c}\int_s^\infty ds' J_0\left(s, t - \frac{s'-s}{c}\right) W_0'(s-s') \\ &= -\frac{1}{c}\int_{-\infty}^0 dz J_0\left(s, t + \frac{z}{c}\right) W_0'(z) \\ &= -\frac{1}{c} J_0(s,t)\int_{-\infty}^\infty dz\, e^{-i\omega z/c} W_0'(z),\end{aligned} \tag{2.63}$$

where $\bar{E}_s(s,t)$ is the E_s integrated according to Eq. (2.48) over a cavity structure.[20] In the second step in Eq. (2.63), we changed variable from s' to $z = s - s'$. In the last step, the upper limit of integration has been extended to ∞, since $W_0' = 0$ for $z > 0$. We have used the fact that the $m = 0$ wake field is insensitive to the cross-sectional area of the beam so we can integrate the current density j_s over the cross section to obtain the beam current J_0.

Let the accelerator section that contains the wake field be of length L. One can define the wake potential across the section due to the wake field by $V(s,t) = \bar{E}_s(s,t)$; we then have the expression, for a sinusoidal current (2.62),

$$V(s,t) = -J_0(s,t) Z_0^{\parallel}(\omega), \tag{2.64}$$

where the quantity $Z_0^{\parallel}(\omega)$ is called the *longitudinal impedance* for the $m = 0$ mode at frequency ω. Comparing Eqs. (2.63) and (2.64) gives

$$Z_0^{\parallel}(\omega) = \int_{-\infty}^\infty \frac{dz}{c} e^{-i\omega z/c} W_0'(z). \tag{2.65}$$

Equation (2.65) says that the impedance $Z_0^{\parallel}$ is related to the wake function W_0' through a Fourier transformation, and so it describes the frequency content of W_0'. Instead of Eqs. (2.62) and (2.64), an alternative view is simply to take Eq. (2.65) as the definition of the impedance. What we have shown is that these two definitions are equivalent.

Note that in spite of the fact that the current (2.62) depends on both ω and k, the impedance is exclusively a function of ω, not k. This is due to the fact that the impedance is localized in space. It assembles the signal from the beam at a fixed location, and such a signal contains only the ω-information, not the k-information.

Exercise 2.14

(a) Consider a conducting material occupying the half space $s < 0$, with a surface current $\vec{K} = \hat{x} K_0 \cos \omega t$ established on its surface. Show that

[20] It is important to note that it is $J_0(s,t')$, not $J_0(s',t')$, where $t' = t - (s-s')/c$, that appears in the first step of Eq. (2.63). Physically, this comes from the fact that the wake field is generated by the current source as it passes by the location of the impedance.

this current source radiates a plane wave in the $s > 0$ region, given by

$$\vec{E} = -\frac{4\pi K_0}{c}\hat{x}\cos\left(\omega t - \omega\frac{s}{c}\right),$$
$$\vec{B} = -\frac{4\pi K_0}{c}\hat{y}\cos\left(\omega t - \omega\frac{s}{c}\right). \tag{2.66}$$

(b) Consider an upright square of side L on the surface $s = 0$. The power consumed to establish the surface current is carried away by the radiation. By identifying this power as $J^2 Z_0 = (KL)^2 Z_0$, show that, to this current source, the unbounded free space acts as a purely resistive impedance $Z_0 = 4\pi/c = 377\ \Omega$, independent of ω.[21]

Similarly, if the beam current possesses a multipole moment

$$J_m(s,t) = \hat{J}_m e^{i(ks-\omega t)}, \tag{2.67}$$

one can define the relationship

$$V = \bar{E}_s = -J_m Z_m^{\parallel} r^m \cos m\theta \tag{2.68}$$

through a longitudinal impedance

$$Z_m^{\parallel}(\omega) = \int_{-\infty}^{\infty}\frac{dz}{c}e^{-i\omega z/c}W_m'(z). \tag{2.69}$$

For the beam (2.67), one can further write the transverse wake force according to

$$\vec{F}_{\perp} = ieJ_m(s,t)mr^{m-1}(\hat{r}\cos m\theta - \hat{\theta}\sin m\theta)Z_m^{\perp}(\omega), \tag{2.70}$$

where $Z_m^{\perp}(\omega)$ is the transverse impedance given by

$$Z_m^{\perp}(\omega) = i\int_{-\infty}^{\infty}\frac{dz}{c}e^{-i\omega z/c}W_m(z). \tag{2.71}$$

In many applications, one is most interested in the $m = 0$ longitudinal effects and the $m = 1$ transverse effects. One then somewhat loosely calls $Z_0^{\parallel}$ the longitudinal impedance and $Z_1^{\perp}$ the transverse impedance. In cgs units, the dimensionality is TL^{-2m-1} for $Z_m^{\parallel}$ and TL^{-2m} for $Z_m^{\perp}$. Sometimes it is more convenient to express the impedances using the ohm as unit, in which case the dimensionality is ΩL^{-2m} for $Z_m^{\parallel}$ and ΩL^{-2m+1} for $Z_m^{\perp}$. For example, $Z_0^{\parallel}$ would be in ohms; $Z_1^{\perp}$ would be in ohms per meter.

[21] In a perfectly conducting smooth vacuum chamber pipe, the pancake fields are truncated by the pipe wall. The environment is not an unbounded free space into which the radiation continues to extract energy from the beam like a black hole, and thus does not present an impedance to the beam.

A minus sign is included in Eqs. (2.64) and (2.68) for the reason that the voltage seen by the beam tends to be retarding, i.e., 180° out of phase with the beam current. Similarly, we have included a factor i in Eq. (2.70) because the transverse force tends to be 90° out of phase with the beam current. These factors are included for convenience only. The impedances are complex quantities in general.

Inverting the Fourier transforms (2.69) and (2.71) allows us to construct the wake functions from the impedances:

$$\begin{aligned} W'_m(z) &= \frac{1}{2\pi}\int_{-\infty}^{\infty} d\omega\, e^{i\omega z/c} Z_m^{\parallel}(\omega), \\ W_m(z) &= \frac{-i}{2\pi}\int_{-\infty}^{\infty} d\omega\, e^{i\omega z/c} Z_m^{\perp}(\omega). \end{aligned} \tag{2.72}$$

The Panofsky-Wenzel theorem, Eq. (2.52), which relates the longitudinal wake function to the derivative of the transverse wake function, also gives a relationship between the longitudinal and transverse impedances for a given m,

$$Z_m^{\parallel}(\omega) = \frac{\omega}{c} Z_m^{\perp}(\omega). \tag{2.73}$$

Exercise 2.15 Equation (2.73) has its origin already imbedded in Eq. (2.33). Show first that the definitions of the impedances can be written in terms of

$$\tilde{E}_\theta + \tilde{B}_r = -icmI_m r^{m-1}\frac{Z_m^{\perp}}{L} \quad \text{and} \quad \tilde{E}_s = -cI_m r^m \frac{Z_m^{\parallel}}{L}. \tag{2.74}$$

Show then that Eq. (2.73) follows from Eq. (2.33).

For a resistive wall, the impedance per unit length is related to the quantity $A(k)$ of Eq. (2.13) for $m = 0$ and Eq. (2.39) for $m \neq 0$:

$$\begin{aligned} \frac{Z_m^{\parallel}(\omega)}{L} &= \frac{\omega}{c}\frac{Z_m^{\perp}(\omega)}{L} = -\frac{1}{cI_m} A\left(\frac{\omega}{c}\right) \\ &= \frac{4/b^{2m}}{(1+\delta_{m0})bc\sqrt{\dfrac{2\pi\sigma}{|\omega|}}\,[1+\operatorname{sgn}(\omega)i] - \dfrac{ib^2}{m+1}\omega + \dfrac{imc^2}{\omega}}. \end{aligned} \tag{2.75}$$

For frequencies $|\omega| \ll \chi^{-1/3}c/b$, Eq. (2.75) becomes

$$\frac{Z_m^{\parallel}(\omega)}{L} = \frac{\omega}{c}\frac{Z_m^{\perp}(\omega)}{L} \approx \sqrt{\frac{2}{\pi\sigma}}\frac{1}{(1+\delta_{m0})b^{2m+1}c}|\omega|^{1/2}[1-\mathrm{sgn}(\omega)i]. \quad (2.76)$$

Equation (2.76) is related to the Fourier transform of Eq. (2.53). In terms of the skin depth (2.7), we have, for the special cases of $m = 0$ and $m = 1$,

$$\frac{Z_0^{\parallel}(\omega)}{L} \approx \frac{1-\mathrm{sgn}(\omega)i}{2\pi b\,\delta_{\mathrm{skin}}\sigma}, \qquad \frac{Z_1^{\perp}(\omega)}{L} \approx \frac{c}{\omega}\frac{1-\mathrm{sgn}(\omega)i}{\pi b^3\,\delta_{\mathrm{skin}}\sigma}. \quad (2.77)$$

The $Z_0^{\parallel}/L$ expression can be understood physically from the fact that the resistivity per unit length is equal to $1/\sigma A$, where A is the cross-sectional area in which the image wall current flows. As sketched in Figure 2.10, $A \approx 2\pi b\delta_{\mathrm{skin}}$. Figure 2.11 shows the resistive-wall impedance for the case of an aluminum pipe. At very high frequencies, $|\omega| \gg \chi^{-1/3}c/b$, the impedance $Z_0^{\parallel}(\omega)/L \approx i4/b^2\omega$.

If the resistive-wall pipe has a finite thickness t,[22] it follows from Eq. (2.18) that

$$\frac{Z_0^{\parallel}(\omega>0)}{L} \approx \frac{1-i}{2\pi b\delta_{\mathrm{skin}}\sigma}\frac{1-\exp[-2(1-i)t/\delta_{\mathrm{skin}}]}{1+\exp[-2(1-i)t/\delta_{\mathrm{skin}}]}. \quad (2.78)$$

For $t \gg \delta_{\mathrm{skin}}$, this reduces to Eq. (2.77). For a thin pipe $t \ll \delta_{\mathrm{skin}}$, we obtain a purely imaginary impedance of $Z_0^{\parallel}/L \approx -i2t\omega/bc^2$. When the resistive-wall pipe is removed, $t = 0$, the impedance vanishes.

For the space charge effect, the wake function (2.55) gives the impedance for a $\cos m\theta$ ring beam. Setting $L = 2\pi R$ gives the total impedance of the circular accelerator,

$$Z_m^{\parallel}(\omega) = \frac{\omega}{c}Z_m^{\perp}(\omega) = iZ_0\frac{R\omega}{c\gamma^2}\begin{cases}\ln\dfrac{b}{a} & \text{if } m=0,\\ \dfrac{1}{m}\left(\dfrac{1}{a^{2m}}-\dfrac{1}{b^{2m}}\right) & \text{if } m>0,\end{cases} \quad (2.79)$$

where $Z_0 = 4\pi/c$. For a uniform disk beam, we have

$$Z_0^{\parallel}(\omega) = iZ_0\frac{R\omega}{c\gamma^2}\left(\ln\frac{b}{a}+\frac{1}{2}\right). \quad (2.80)$$

[22]The pipe is considered to be in an otherwise free space, or inside another larger perfectly conducting pipe.

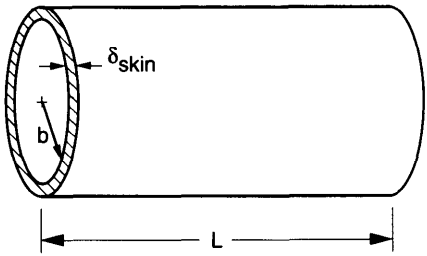

Figure 2.10. Geometry used to estimate the resistive-wall impedance $Z_0^{\parallel}$.

The space charge impedances are purely imaginary. As discussed following Eq. (2.56), a rigid uniform disk beam executing transverse dipole motion can be modeled by taking Eq. (2.80) for the longitudinal impedance and the $m = 1$ member of Eq. (2.79) for the transverse impedance.

The longitudinal impedance $Z_m^{\parallel}$ can often be modeled by an equivalent parallel LRC resonator circuit as shown in Figure 2.12(a).[23] The impedance of the circuit is given by

$$\frac{1}{Z_m^{\parallel}} = \frac{1}{R_S} + \frac{i}{\omega L} - i\omega C, \tag{2.81}$$

which gives

$$Z_m^{\parallel} = \frac{R_S}{1 + iQ\left(\dfrac{\omega_R}{\omega} - \dfrac{\omega}{\omega_R}\right)}, \tag{2.82}$$

where $Q = R_S\sqrt{C/L}$ is the quality factor and $\omega_R = 1/\sqrt{CL}$ is the resonant frequency. This impedance is drawn in Figure 2.12(b) and (c) for $Q = 1$ and 10. The quantity R_S has the dimension of Ω/L^{2m}. The area covered under $\text{Re}\, Z_m^{\parallel}(\omega)$ is

$$\int_0^{\infty} d\omega\, \text{Re}\, Z_m^{\parallel}(\omega) = \frac{\pi R_S \omega_R}{2Q}. \tag{2.83}$$

The width (half width at half maximum) of the resonance peak of $\text{Re}\, Z_m^{\parallel}(\omega)$ is about $\Delta\omega \approx \omega_R/2Q$ if $Q \gg 1$. A sharply peaked impedance has $Q \gg 1$, while a broad-band impedance has $Q \sim 1$.

[23]A. Hofmann, K. Hübner, and B. Zotter, IEEE Trans. Nucl. Sci. **NS-26**, 3514 (1979); P. B. Wilson et al., IEEE Trans. Nucl. Sci. **NS-24**, 1211 (1977); A. Hofmann, *Proc. 11th Int. Conf. High Energy Accel.*, Geneva, 1980, p. 540.

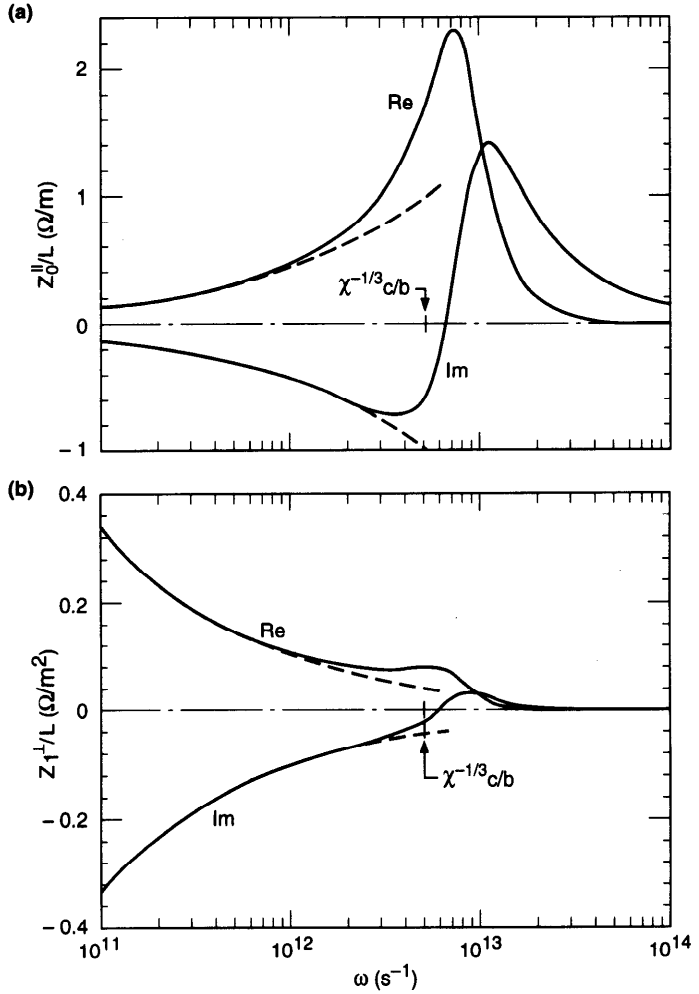

Figure 2.11. (a) Resistive-wall impedance per unit length $Z_0^{\parallel}/L$ as a function of frequency ω according to Eq. (2.75). (b) The same for $Z_1^{\perp}/L$. An aluminum pipe with $\sigma = 3 \times 10^{17}\ s^{-1}$ and $b = 5$ cm is assumed. The dashed curves give the low frequency approximation (2.77). The critical frequency $\chi^{-1/3}c/b$ is indicated.

The wake function $W_m'(z)$ can be obtained by performing a Fourier transformation on the impedance:

$$W_m'(z) = \begin{cases} 0 & \text{if} \quad z > 0, \\ \alpha R_S & \text{if} \quad z = 0, \\ 2\alpha R_S\, e^{\alpha z/c}\left(\cos\dfrac{\bar{\omega} z}{c} + \dfrac{\alpha}{\bar{\omega}}\sin\dfrac{\bar{\omega} z}{c}\right) & \text{if} \quad z < 0, \end{cases} \tag{2.84}$$

where $\alpha = \omega_R/2Q$ and $\bar{\omega} = \sqrt{\omega_R^2 - \alpha^2}$.

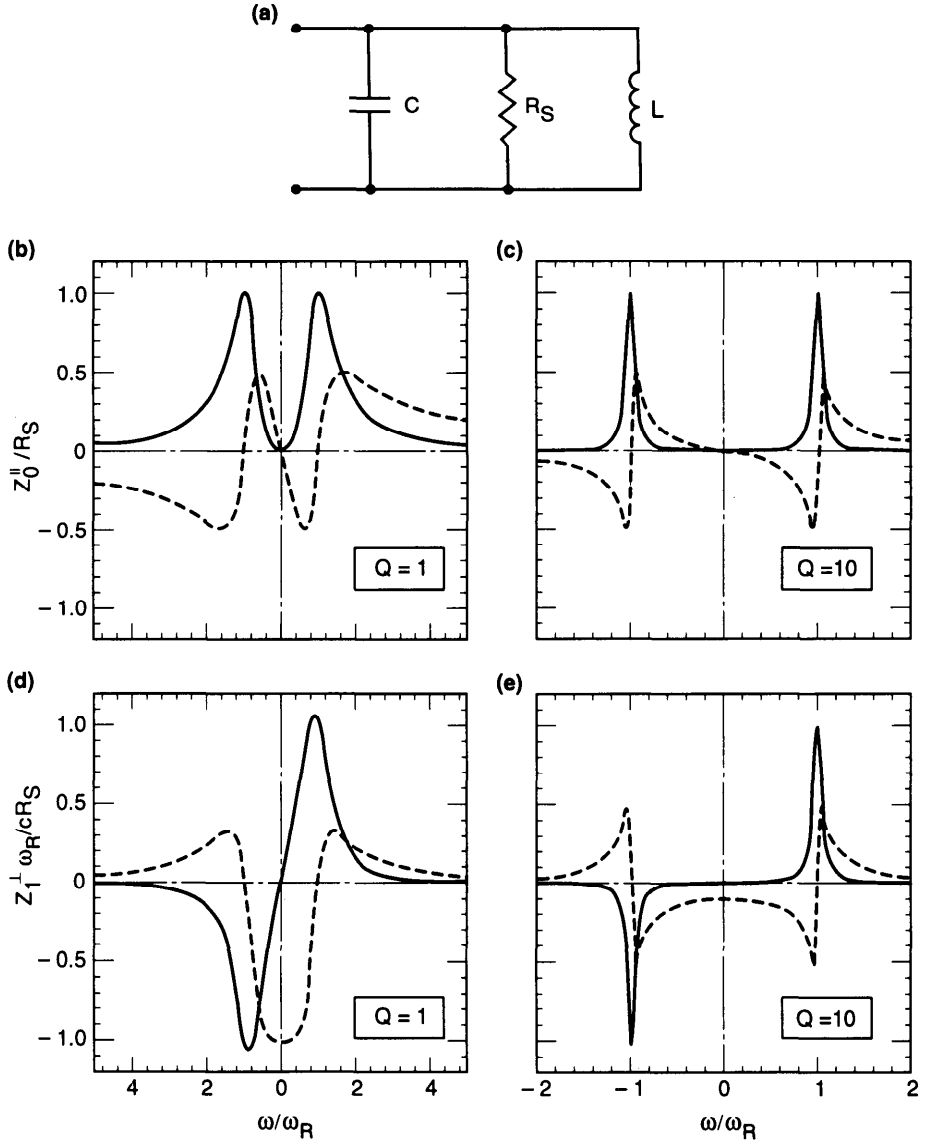

Figure 2.12. (a) An LRC resonator circuit. (b) and (c) are the longitudinal impedance of the circuit for $Q = 1$ and 10. (d) and (e) are the transverse impedance of the circuit for $Q = 1$ and 10. The solid curves give the real parts and the dashed curves give the imaginary parts of the impedances. The quality factor Q is typically ~ 1 for a broad-band resonator, or $\sim 10^4$ for a fine-tuned sharp resonator, or $\sim 10^9$ for a superconducting structure.

A sharply peaked impedance can sometimes be modeled by taking the limit $Q \to \infty$ and $R_S \to \infty$ but keeping R_S/Q fixed, i.e.,

$$\begin{aligned} \operatorname{Re} Z_m^{\parallel} &= \frac{\pi}{2}\frac{R_S\omega_R}{Q}\left[\delta(\omega-\omega_R)+\delta(\omega+\omega_R)\right], \\ \operatorname{Im} Z_m^{\parallel} &= \frac{R_S\omega_R}{2Q}\left(\frac{1}{\omega-\omega_R}+\frac{1}{\omega+\omega_R}\right). \end{aligned} \tag{2.85}$$

The corresponding wake function is

$$W_m'(z) = \frac{R_S\omega_R}{Q}\cos\frac{\omega_R z}{c} \qquad \text{for} \quad z<0. \tag{2.86}$$

Another particularly simple special case of resonator impedance occurs when $Q = 1/2$. See Eq. (2.99).

At low frequencies $|\omega| \ll \omega_R$, the *LRC* resonator impedance $Z_m^{\parallel}(\omega) \approx -i\omega L$ is inductive. For $|\omega| \gg \omega_R$, we have $Z_m^{\parallel}(\omega) \approx i/\omega C$, which is capacitive. Around the resonant frequency ω_R, the impedance $Z_m^{\parallel}(\omega) \approx R_S$ is mostly resistive. Sometimes, one calls an impedance *inductive* or *capacitive* according to the sign of $\operatorname{Im} Z_m^{\parallel}$ in the region $\omega > 0$; and inductive or capacitive impedance then means $\operatorname{Im} Z_m^{\parallel} < 0$ or > 0, respectively. Therefore, the resistive-wall impedance (2.77) is partly inductive and partly resistive, and the space charge impedance (2.80), in spite of the fact that it is proportional to ω like that of an inductance, is referred to as purely capacitive.

The Panofsky-Wenzel theorem requires that the same resonator (2.82) also give a transverse impedance,

$$Z_m^{\perp} = \frac{c}{\omega}\frac{R_S}{1+iQ\left(\dfrac{\omega_R}{\omega}-\dfrac{\omega}{\omega_R}\right)}. \tag{2.87}$$

This impedance is shown in Figure 2.12(d) and (e). The corresponding transverse wake function is (for $z < 0$)

$$W_m(z) = \frac{cR_S\omega_R}{Q\bar{\omega}}e^{\alpha z/c}\sin\frac{\bar{\omega}z}{c}. \tag{2.88}$$

For $Q \to \infty$, $R_S \to \infty$, and fixed R_S/Q, these expressions become

$$\begin{aligned} \operatorname{Re} Z_m^{\perp} &= \frac{\pi c R_S}{2Q}\left[\delta(\omega-\omega_R)-\delta(\omega+\omega_R)\right], \\ \operatorname{Im} Z_m^{\perp} &= \frac{cR_S\omega_R}{2Q\omega}\left(\frac{1}{\omega-\omega_R}+\frac{1}{\omega+\omega_R}\right), \end{aligned} \tag{2.89}$$

and

$$W_m(z) = \frac{cR_S}{Q}\sin\frac{\omega_R z}{c}. \tag{2.90}$$

Properties of Impedances

In addition to Eq. (2.73), there are a few other general properties of impedances which we describe below.

(i) Since the wake functions are real, Eqs. (2.69) and (2.71) imply

$$\begin{aligned} Z_m^{\parallel *}(\omega) &= Z_m^{\parallel}(-\omega), \\ Z_m^{\perp *}(\omega) &= -Z_m^{\perp}(-\omega), \end{aligned} \tag{2.91}$$

i.e., Re $Z_m^{\parallel}$ and Im $Z_m^{\perp}$ are even functions of ω, and Im $Z_m^{\parallel}$ and Re $Z_m^{\perp}$ are odd functions of ω. It follows from Eq. (2.91) and the causality of the wake functions that

$$\begin{aligned} W_m'(z<0) &= \frac{2}{\pi}\int_0^\infty d\omega\ \mathrm{Re}\ Z_m^{\parallel}(\omega)\cos\frac{\omega z}{c}, \\ W_m(z<0) &= \frac{2}{\pi}\int_0^\infty d\omega\ \mathrm{Re}\ Z_m^{\perp}(\omega)\sin\frac{\omega z}{c}. \end{aligned} \tag{2.92}$$

Equation (2.92) exhibits explicitly the cosinelike behavior of W_m' and the sinelike behavior of W_m, as sketched in Figure 2.6.

(ii) In most cases,[24] the transverse wake function satisfies $W_m(0) = 0$, which gives

$$\begin{aligned} \int_0^\infty d\omega\ \mathrm{Im}\ Z_m^{\perp}(\omega) &= 0, \\ \int_0^\infty d\omega \frac{\mathrm{Im}\ Z_m^{\parallel}(\omega)}{\omega} &= 0. \end{aligned} \tag{2.93}$$

It follows that in these cases, Im $Z_m^{\perp}(\omega)$ must not have only one sign in the region $\omega > 0$. Combined with Eq. (2.94) below, this also means Re $Z_m^{\parallel}(0) = 0$.

(iii) To guarantee causality of the wake functions, the impedances must not have singularities in the upper complex ω-plane. It follows from the

[24]One exception is the space charge effect. Another is mentioned later in Eq. (2.110). One also assumes the integrals in Eq. (2.93) converge properly.

Cauchy theorem (See Exercise 2.16 below) that the real and imaginary parts of $Z_m^{\parallel}(\omega)$ must be related by the Hilbert transforms,[25]

$$\begin{aligned} \text{Re } Z_m^{\parallel}(\omega) &= \frac{1}{\pi}\text{P.V.}\int_{-\infty}^{\infty} d\omega' \frac{\text{Im } Z_m^{\parallel}(\omega')}{\omega' - \omega}, \\ \text{Im } Z_m^{\parallel}(\omega) &= -\frac{1}{\pi}\text{P.V.}\int_{-\infty}^{\infty} d\omega' \frac{\text{Re } Z_m^{\parallel}(\omega')}{\omega' - \omega}, \end{aligned} \tag{2.94}$$

where P.V. means taking the principal value of the integral.[26] The same expressions apply to $Z_m^{\perp}$.

An inspection of Eq. (2.95) indicates that the integral (2.95) as a function of a resembles (although it does not equal) $f'(a)$. This is why, in view of Eq. (2.94), Re $Z(\omega)$ as a function of ω often resembles Im $Z'(\omega)$, and Im $Z(\omega)$ often resembles $-$Re $Z'(\omega)$.

The point of Eq. (2.94) is that, in principle, knowing either the real or the imaginary part of the impedance, one can construct the whole impedance and, in turn, the wake function. In practice, this may be a difficult operation and has to be applied with care.

Exercise 2.16 Perform a contour integral of $Z_m^{\parallel}(\omega')/(\omega' - \omega)$ in the complex ω'-plane over the upper half plane along the contour shown in Figure 2.13. Show that if $Z_m^{\parallel}(\omega')$ converges sufficiently fast at $|\omega'| \to \infty$,

$$\text{P.V.}\int_{-\infty}^{\infty} d\omega' \frac{Z_m^{\parallel}(\omega')}{\omega' - \omega} = \pi i Z_m^{\parallel}(\omega). \tag{2.96}$$

Show that Eq. (2.94) follows from Eq. (2.96). The P.V. occurs because the contour around the pole $\omega' = \omega$ is a semicircle.

[25]See for example, Philip M. Morse and Herman Feshbach, *Methods of Theoretical Physics*, McGraw-Hill, New York, 1953.

[26]The integrals (2.94) are undefined without specifying P.V. because of the divergence at $\omega' = \omega$. The trick of P.V. is to utilize the property that the divergences on the side $\omega' < \omega$ and the side $\omega' > \omega$ are of opposite signs and, if the integration is taken *symmetrically* about the singularity so that the divergences on the two sides cancel each other, the integral is actually well defined. Algebraically, this leads to

$$\text{P.V.}\int_{-\infty}^{\infty} dx \frac{f(x)}{x - a} = \int_0^{\infty} du \frac{f(a + u) - f(a - u)}{u}, \tag{2.95}$$

where the expression on the right is well behaved at $u = 0$.

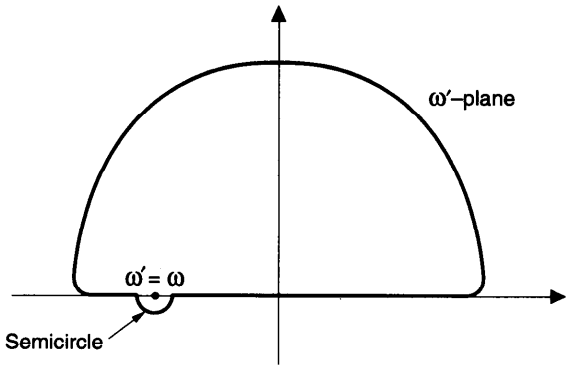

Figure 2.13. Contour in the complex ω'-plane to establish the Hilbert transform relation (2.94) for the impedance.

Exercise 2.17

(a) A simple model of Re $Z_m^{\parallel}$ could be Re $Z_m^{\parallel}(\omega) = R_0$ if $|\omega| < \omega_0$ and 0 if $|\omega| > \omega_0$. Show that the matching Im $Z_m^{\parallel}$ and $W_m'(z)$ are given by

$$\begin{aligned} \text{Im } Z_m^{\parallel}(\omega) &= \frac{R_0}{\pi} \ln \left| \frac{\omega + \omega_0}{\omega - \omega_0} \right|, \\ W_m'(z < 0) &= \frac{2R_0 c}{\pi z} \sin \frac{\omega_0 z}{c}. \end{aligned} \tag{2.97}$$

(b) Show that

$$\begin{aligned} W_m'(z < 0) &= W_0 J_0(\alpha z), \\ Z_m^{\parallel}(\omega) &= \begin{cases} -i \dfrac{W_0 \operatorname{sgn}(\omega)}{c\sqrt{\omega^2 - \alpha^2}} & \text{if} \quad |\omega| > \alpha, \\ \dfrac{W_0}{c\sqrt{\alpha^2 - \omega^2}} & \text{if} \quad |\omega| < \alpha, \end{cases} \end{aligned} \tag{2.98}$$

form a matching wake function and impedance pair.

(c) Show that

$$\begin{aligned} W_m(z < 0) &= W_0 z e^{\alpha z}, \\ Z_m^{\parallel}(\omega) &= \frac{i W_0 \omega}{(\omega + ic\alpha)^2}, \end{aligned} \tag{2.99}$$

form a matching pair. This is in fact a special case (the critically damped case) of the resonator impedance when $Q = 1/2$.

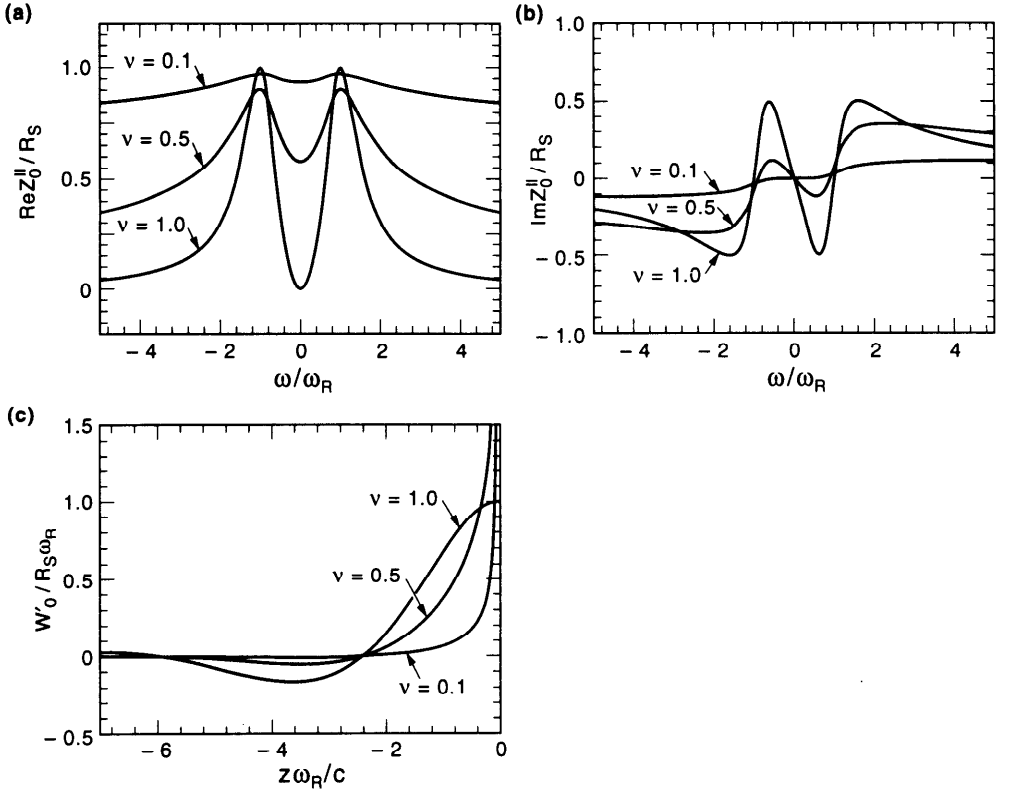

Figure 2.14. Generalized resonator impedance and wake function (2.100) for $\nu = 0.1$, 0.5, and 1. We have assumed $Q = 1$. The case of $\nu = 1$ has been shown in Figure 2.12.

(d) The resonator impedance (2.82) and wake function (2.84) can be generalized. Show that a possible model is given by[27]

$$Z_m^{\parallel}(\omega) = \frac{R_S}{2Q\bar{\omega}}\left[\omega_1\left(\frac{i\omega_R}{\omega-\omega_1}\right)^{\nu} - \omega_2\left(\frac{i\omega_R}{\omega-\omega_2}\right)^{\nu}\right],$$

$$W'_m(z<0) = \frac{R_S\omega_R}{Q\Gamma(\nu)}\left(-\frac{z\omega_R}{c}\right)^{\nu-1} e^{\alpha z/c} \times\left(\cos\frac{\bar{\omega}z}{c} + \frac{\alpha}{\bar{\omega}}\sin\frac{\bar{\omega}z}{c}\right), \tag{2.100}$$

where $\omega_1 = \bar{\omega} - i\alpha$, $\omega_2 = -\bar{\omega} - i\alpha$, $\bar{\omega} = \sqrt{\omega_R^2 - \alpha^2}$, $\alpha = \omega_R/2Q$,

[27]Toshio Suzuki, Yongho Chin, and Kohtaro Satoh, Part. Accel. **13**, 179 (1983). See also Exercise 2.3.

and $0 < \nu \leq 1$. The resonator model (2.82) corresponds to $\nu = 1$. The impedance and wake function (2.100) are shown in Figure 2.14. The impedance behaves as $\propto \omega^{-\nu}$ for large ω, and the wake function $\propto |z|^{\nu-1}$ for small $|z|$. Show that some physical properties are violated if $\nu > 1$.

Exercise 2.18

(a) Using the fact that $\text{P.V.}\int_{-\infty}^{\infty} d\omega'/(\omega' - \omega) = 0$, show from Eqs. (2.91) and (2.94) that

$$\begin{aligned}
\text{Re } Z_m^{\parallel}(\omega) &= \frac{2}{\pi}\text{P.V.}\int_0^{\infty} \frac{d\omega'}{\omega'^2 - \omega^2}\left[\omega' \text{ Im } Z_m^{\parallel}(\omega') - \omega \text{ Im } Z_m^{\parallel}(\omega)\right], \\
\text{Im } Z_m^{\parallel}(\omega) &= -\frac{2\omega}{\pi}\text{P.V.}\int_0^{\infty} \frac{d\omega'}{\omega'^2 - \omega^2}\left[\text{Re } Z_m^{\parallel}(\omega') - \text{Re } Z_m^{\parallel}(\omega)\right], \\
\text{Re } Z_m^{\perp}(\omega) &= \frac{2\omega}{\pi}\text{P.V.}\int_0^{\infty} \frac{d\omega'}{\omega'^2 - \omega^2}\left[\text{Im } Z_m^{\perp}(\omega') - \text{Im } Z_m^{\perp}(\omega)\right], \\
\text{Im } Z_m^{\perp}(\omega) &= -\frac{2}{\pi}\text{P.V.}\int_0^{\infty} \frac{d\omega'}{\omega'^2 - \omega^2}\left[\omega' \text{ Re } Z_m^{\perp}(\omega') - \omega \text{ Re } Z_m^{\perp}(\omega)\right].
\end{aligned} \tag{2.101}$$

(b) Verify that Eq. (2.101) satisfies the conditions (2.73) and (2.91).

(c) Verify that the resistive-wall impedance $Z_m^{\perp}$ of Eq. (2.76) satisfies Eq. (2.101).[28]

(iv) Energy loss consideration gives another general condition on impedance. Consider a beam whose mth moment has a longitudinal distribution $\rho(s - ct)$, normalized so that $\int dz\, \rho(z) = I_m$, the total mth moment of the beam. As this beam travels down the pipe for a distance L, its energy changes by [cf. Eq. (2.30)]

$$\Delta\mathscr{E} = -\int_{-\infty}^{\infty} dz'\, \rho(z') \int_{z'}^{\infty} dz\, \rho(z) W_m'(z' - z). \tag{2.102}$$

[28]The longitudinal impedance $Z_m^{\parallel}$ does not satisfy Eq. (2.94) or (2.101), because of the divergence at $|\omega'| \to \infty$.

This result can also be written in terms of the Fourier transformed quantities:

$$\Delta\mathscr{E} = -\frac{1}{2\pi}\int_{-\infty}^{\infty} d\omega |\tilde{\rho}(\omega)|^2 \operatorname{Re} Z_m^{\parallel}(\omega), \tag{2.103}$$

where

$$\begin{aligned} \tilde{\rho}(\omega) &= \int_{-\infty}^{\infty} dz\, e^{-i\omega z/c}\rho(z), \\ \rho(z) &= \frac{1}{2\pi c}\int_{-\infty}^{\infty} d\omega\, e^{i\omega z/c}\tilde{\rho}(\omega). \end{aligned} \tag{2.104}$$

Only the real part of the impedance contributions to the energy loss of the beam.

Since the beam as a whole cannot gain energy from the pipe structure, and this must be valid for arbitrary ρ and $\tilde{\rho}$, we conclude that[29]

$$\operatorname{Re} Z_m^{\parallel}(\omega) \geq 0 \qquad \text{for all } \omega. \tag{2.105}$$

This is the complete condition that is only partly studied in Figure 2.7. It then follows from Eq. (2.73) that

$$\operatorname{Re} Z_m^{\perp}(\omega)\begin{cases} \geq 0 & \text{if } \omega > 0, \\ \leq 0 & \text{if } \omega < 0. \end{cases} \tag{2.106}$$

(v) The relationship (2.73) holds for a given m. There is no a priori connection between the impedances of different m's. On the other hand, as mentioned before, the most important wake effects are the $m = 0$ longitudinal and the $m = 1$ transverse cases. A rough connection between the two leading impedances $Z_0^{\parallel}$ and $Z_1^{\perp}$ can be very useful if one knows one and wants to have some idea of the other. From a simple dimensionality argument, one expects $Z_1^{\parallel} \sim 2Z_0^{\parallel}/b^2$ and therefore[30]

$$Z_1^{\perp} \sim \frac{2c}{b^2\omega} Z_0^{\parallel}, \tag{2.107}$$

where b is a length characterizing the vacuum chamber structure and is taken to be the radius of the chamber pipe.[31] A factor of 2 is included so that this expression is strictly valid for the resistive-wall case. [See Eq. (2.77).]

[29]One may attempt to cast a feedback system in the impedance framework. In that case, Re $Z_m^{\parallel}$ may become negative.

[30]W. Schnell, CERN Report ISR-RF/70-7 (1970); B. Zotter and F. Sacherer, *Proc. Int. School of Part. Accel.*, Erice, 1976, CERN Report 77-13, p. 175.

[31]Another useful form of Eq. (2.107) in terms of the quantity $Z_0^{\parallel}/n$ is

$$Z_1^{\perp} \sim \frac{2R}{b^2}\frac{Z_0^{\parallel}}{n}, \tag{2.108}$$

where $n = \omega/\omega_0$, ω_0 is the revolution frequency, and $2\pi R$ is the accelerator circumference.

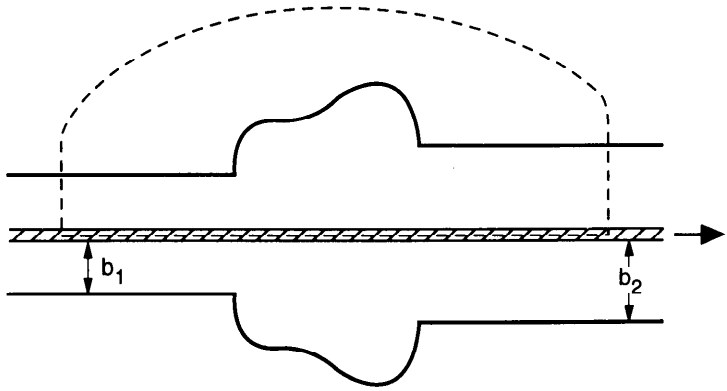

Figure 2.15. Demonstration of Eq. (2.110).

There is also a generalized form of Eq. (2.107),

$$Z_m^{\parallel} \sim \frac{2}{b^{2m}} Z_0^{\parallel} \quad \text{or} \quad Z_m^{\perp} \sim \frac{2c}{b^{2m}\omega} Z_0^{\parallel} . \tag{2.109}$$

The validity of Eqs. (2.107–2.109) rests on the fact that the electrodynamics are all occurring in the neighborhood of the pipe wall $r = b$. This will be the case for the resistive wall and the diffraction model impedance to be discussed later. It will also apply if the discontinuities of the structures on the beam pipe have dimensions $\ll b$. When electromagnetic wake fields penetrate into a cavity-like structure of depth $\gtrsim b$, Eqs. (2.107–2.109) will not be very accurate. In those cases, the relations (2.107–2.109) describe a gross averaged behavior; they apply more or less to frequencies near or above the cutoff frequency c/b and are not to be confused with the exact relationship (2.73).

Exercise 2.19 Consider a steady state continuous beam in a vacuum pipe that contains a transition section from radius b_1 to radius b_2 as illustrated in Figure 2.15. By drawing a circuit as shown by the dashed curve in Figure 2.15 and applying the steady state condition $\oint d\vec{l} \cdot \vec{E} = 0$, show that

$$\text{Re}\, Z_0^{\parallel}(0) = \frac{2}{c} \ln \frac{b_2}{b_1} = \frac{Z_0}{2\pi} \ln \frac{b_2}{b_1} . \tag{2.110}$$

This result apparently contradicts Eqs. (2.93), and (2.105) if $b_2 < b_1$. Explore how these apparent contradictions can be resolved.

Exercise 2.20 A stripline beam-position monitor consists of two striplines diametrically located across the beam pipe. It produces the impedances[32]

$$Z_m^{\parallel}(\omega) = -iR_{Sm} \sin\frac{\omega d}{c} e^{i\omega d/c}, \tag{2.111}$$

where R_{Sm} is the characteristic resistance of the monitor design for the mth mode, $R_{Sm} \approx R_{S0}/b^{2m}$, and d is the length of the monitor.

(a) Show that the longitudinal wake functions are

$$W'_m(z) = \frac{cR_{Sm}}{2}[\delta(z) - \delta(z + 2d)]. \tag{2.112}$$

Each of the striplines receives a signal proportional to

$$I_m W'_m(z) r^m \cos m\theta$$

according to Eq. (2.50), where I_m is the mth moment of the beam, (r, θ) is evaluated at the location of the stripline being considered.

(b) For a beam with longitudinal distribution $\rho(z)$ and a transverse offset of $a \ll b$, the signals received by the two striplines are approximately given by a superposition of the $m = 0$ and $m = 1$ signals. Show that the two signals are proportional to $(R_{S0} \pm abR_{S1})[\rho(z) - \rho(z + 2d)]$. The term $\rho(z)$ comes from a direct beam current; the term $\rho(z + 2d)$ comes from the reflection from the downstream end of the stripline. The sum of the two signals gives information on the beam intensity and the longitudinal beam distribution. The difference of the signals gives information on the transverse beam offset. Note that it is the longitudinal wakes (for both $m = 0$ and $m = 1$) that the monitor is measuring.

(c) Show that the $m = 1$ transverse wake function is given by

$$W_1(z) = -\frac{cR_{S1}}{b^2}\begin{cases} 1 & \text{if } 0 > z > -2d, \\ 0 & \text{otherwise.} \end{cases} \tag{2.113}$$

(d) Demonstrate how four striplines can provide a measurement of the ellipticity of the transverse beam profile. Generalize the result to obtain a device that measures the mth moment of the beam.

Having described the general properties of impedances, it may be instructive next to describe how one can estimate roughly the impedance of a cavity structure in the vacuum chamber. We will start by considering a cavity

[32] D. A. Goldberg and G. R. Lambertson, *AIP Proc.* **249**, *Phys. Part. Accel.*, 1992, Vol. 1, p. 539; Robert E. Shafer, ibid., p. 601.

structure whose dimension and length are of the order of the pipe radius b. In this case, since b is the only length parameter,[33] a simple dimensional analysis tells us that the wake functions per cavity (at distances $z \sim -b$) must be of the order of

$$W'_m(z) \approx \frac{1}{b^{2m+1}}, \qquad W_m(z) \approx \frac{1}{b^{2m}}, \tag{2.114}$$

and the impedances per cavity (at frequency $\omega \sim c/b$) are approximately given by

$$Z_m^{\parallel}(\omega) \approx \frac{b}{c} W'_m \approx \frac{1}{cb^{2m}}, \qquad Z_m^{\perp}(\omega) \approx \frac{b}{c} W_m \approx \frac{1}{cb^{2m-1}}. \tag{2.115}$$

To obtain the quantities per unit longitudinal length, divide the above expressions by $L \sim b$. Note that $1/c = Z_0/4\pi \approx 30\ \Omega$.

To gain more insight beyond the simple dimensional analysis, we will next illustrate Eq. (2.115) more explicitly by introducing two models—the *broad-band resonator model* and the *diffraction model*—which describe the gross features of the cavity impedance. The broad-band resonator model describes the impedance for low frequencies $\omega \lesssim c/b$, and the diffraction model for high frequencies $\omega \gtrsim c/b$.

Broad-Band Resonator Model

We first consider the $m = 0$ impedance $Z_0^{\parallel}$ at frequency $\omega \approx c/b$. To do so, consider a beam bunch of charge q and length b traveling down the pipe through the cavity. The electromagnetic field patterns of the beam are sketched in Figure 2.16. During the passage, wake fields are generated. After the passage, some fields are "scraped off" by the edge of the exit step of the cavity. The energy contained in the wake field scraped off by the cavity is related to the energy lost by the beam. A rough estimate of this energy can be obtained by calculating the field energy contained in the shaded region of

[33]This does not apply for the space charge and resistive-wall cases. In the resistive-wall case, we have another length scale δ_{skin}. This leads to an extra factor of δ_{skin}/b in Eqs. (2.114–2.115) where δ_{skin} is evaluated at $\omega \sim c/b$. Since typically $\delta_{\text{skin}} \ll b$, the resistive-wall wake fields are usually smaller than those due to pipe discontinuities.

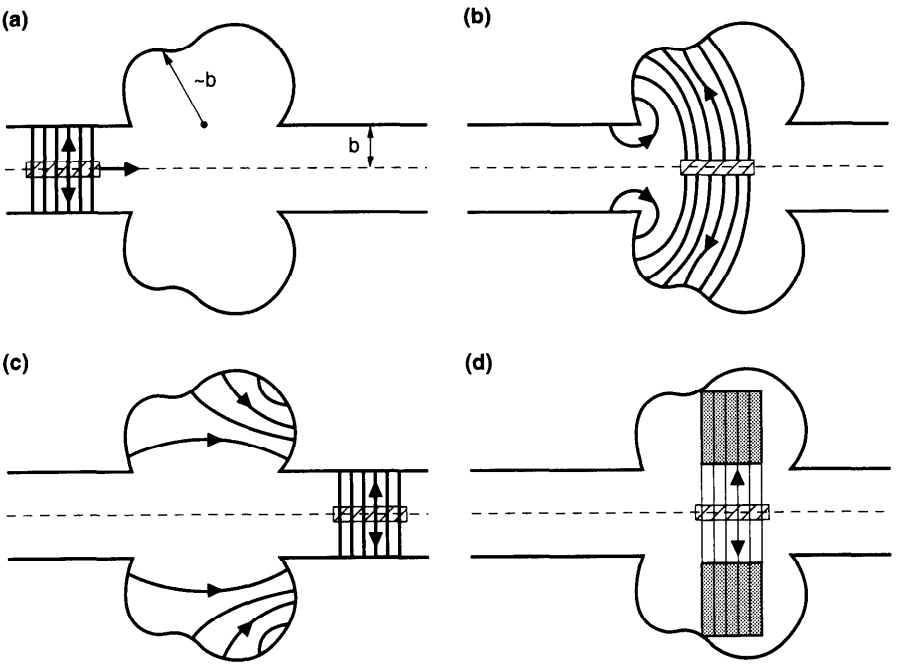

Figure 2.16. (a), (b), and (c), Field patterns as a beam bunch is traversing a cavity structure. (d) The energy loss of the beam can be estimated by calculating the field energy contained in the shaded region. The bunch length and the size of the cavity are both taken to be comparable to the pipe radius b.

Figure 2.16(d), which gives

$$\Delta\mathscr{E} \approx -\frac{1}{8\pi}\int dV\left(E_r^2 + B_\theta^2\right) = -\frac{2q^2}{b}\ln 2, \tag{2.116}$$

where we have used $E_r = B_\theta = 2q/rb$ and the integral over r is from b to $2b$.

Equation (2.116) gives the field energy trapped in the cavity. At high frequencies $\omega \gtrsim c/b$, an equal amount of energy is diffracted into the pipe region by the cavity edges to create the wake fields in the pipe, as sketched later in Figure 2.20.[34] The energy loss of the beam is therefore *twice* that of Eq. (2.116). By equating this energy loss with $-(b/c)J^2Z_0^{\parallel}$, where b/c is the time duration of beam passage, $J^2Z_0^{\parallel}$ is the power of beam energy loss, and

[34]At frequency $\omega \sim c/b$, part of this energy is reabsorbed by the beam. The 80 Ω estimate of Eq. (2.117) for $\omega \sim c/b$ is therefore likely to be a slight over-estimate. This leads to the choice of 60 Ω value in Eq. (2.121), which follows more from Eq. (2.120) than from Eq. (2.117).

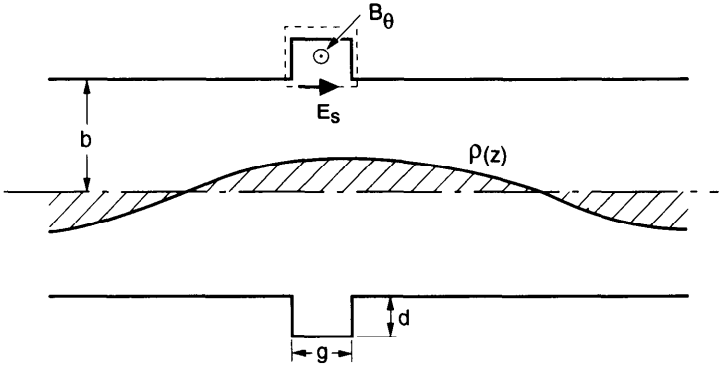

Figure 2.17. The impedance of a small cavity ($g \lesssim d \lesssim b$) is predominantly inductive at low frequencies ($\omega \ll c/b$). The voltage across the cavity gap can be obtained by applying Faraday's law to the dashed circuit.

$J = qc/b$ is the beam current, one obtains, at $\omega \sim c/b$,

$$Z_0^{\parallel} \approx \frac{4}{c} \ln 2 \approx 80\ \Omega. \tag{2.117}$$

We thus conclude that a cavity of the size of the beam pipe radius contributes approximately 80 Ω of impedance $Z_0^{\parallel}$, regardless of its actual size. This gives another proof of Eq. (2.115) for $m = 0$. Fourier transform properties then establish Eq. (2.114).

In deriving Eq. (2.116), the depth of the cavity is taken to be $\sim b$. The result (2.116), however, still applies if the cavity depth is larger than b. This is because the field will not penetrate more than a distance b into the cavity during the beam passage and the cavity region beyond $r = 2b$ is irrelevant to our consideration here.

We have just shown that for a cavity structure of size $\sim$ pipe radius b, the impedance $Z_0^{\parallel} \approx 80\ \Omega$ at $\omega \sim c/b$. At this frequency, the main effect on the beam is an energy loss and the impedance is mostly resistive. To complete the broad-band resonator model, we have yet to consider the regime $\omega \ll c/b$, which can be done by considering a beam with charge density $\rho(z) \propto e^{i\omega z/c}$ where the wavelength $2\pi c/\omega \gg b$.[35] Let the cavity have length g and depth d ($g \lesssim d \lesssim b$) as sketched in Figure 2.17. As the beam passes by, a magnetic field $B_\theta \approx 2\rho/b$ is established in the cavity region. The magnetic flux $\Phi \approx gdB_\theta$ in the cavity region varies slowly with the beam density

[35]Karl L. Bane, *Proc. Euro. Part. Accel. Conf.*, Rome, 1988, p. 637.

$\rho \propto e^{-i\omega t}$, generating a voltage across the cavity gap,

$$V = \int_{\text{gap}} ds\, E_s = -\frac{1}{c}\dot{\Phi} = i\omega \frac{2gd\rho}{cb} \tag{2.118}$$

Relating Eq. (2.118) to $V = -Z_0^{\parallel} J$ with the beam current $J = \rho c$, we obtain for $\omega \ll c/b$

$$Z_0^{\parallel} \approx -i\omega Z_0 \frac{gd}{2\pi bc}. \tag{2.119}$$

The small cavity thus behaves as an inductance $L = Z_0 gd/2\pi bc$ at low frequencies. The inductance is proportional to the cavity cross-sectional area gd. When $g \sim b$ and $d \sim b$, we find

$$Z_0^{\parallel} \approx -i\omega Z_0 \frac{b}{2\pi c} \approx -i\frac{\omega}{c/b} \times 60\ \Omega. \tag{2.120}$$

Combining Eq. (2.117) near $\omega \sim c/b$ and Eq. (2.120) for $\omega \ll c/b$, we recognize that the cavity impedance resembles an LRC resonator [Eq. (2.82) with $m = 0$] with

$$R_S \approx 60\ \Omega, \qquad Q \approx 1, \qquad \omega_R \approx \frac{c}{b}. \tag{2.121}$$

Equation (2.121) is the broad-band resonator model for the $m = 0$ impedance $Z_0^{\parallel}$ of the cavity of size $\sim b$.

The broad-band resonator model does not give an accurate description of the impedance at high frequencies $\omega \gg c/b$; it predicts a purely capacitive impedance, while, as we will show later, a more accurate model—the diffraction model—predicts an impedance which is half capacitive and half resistive. For this reason, the model does not give accurate wake functions at very short ranges $|z| \ll b$.

The broad-band resonator model ignores the possibility of the cavity responding resonantly to sharply defined frequencies, i.e., it ignores the possible existence of cavity modes. These cavity modes occur at frequencies below the cutoff frequency $\sim c/b$, and they give rise to wake functions which ring for long periods of time. Neglecting these long-range contributions, the model also does not give accurate wake functions at very long ranges $|z| \gg b$.

In spite of its limitations, however, the broad-band resonator model gives a good estimate of the impedance near $\omega \sim c/b$ and wake functions near $|z| \sim b$. For applications where the beam bunch length is comparable to the cavity size, it provides a very simple and handy tool.

If one imagines a carelessly built circular accelerator in which the vacuum chamber is filled with all sorts of cavities and discontinuities of approximately the same size as the pipe radius, the total impedance around the circumference is $Z_0^{\parallel} \approx n_{\text{cav}} \times 60\ \Omega$, where $n_{\text{cav}} \approx 2\pi R/2b = \pi R/b$ is the total number of cavities, assuming each cavity occupies a distance $2b$, and ignoring any interference effects of adjacent cavities. As we will show in later chapters, one quantity that characterizes the magnitude of the collective effects in a circular accelerator is $Z_0^{\parallel}/n$, where $n = \omega/\omega_0$ with $\omega_0 = c/R$ the revolution frequency. Setting $\omega \approx c/b$, we find that each cavity of size $\sim b$ contributes

$$\frac{Z_0^{\parallel}}{n}\ (\text{per cavity}) \approx 60\ \Omega \times \frac{b}{R}, \tag{2.122}$$

and that this carelessly designed accelerator has a total $Z_0^{\parallel}/n$ of

$$\frac{Z_0^{\parallel}}{n}\ (\text{total}) \approx 60\ \Omega \times \frac{b}{R} n_{\text{cav}} \approx 60\pi\ \Omega = \frac{1}{2} Z_0. \tag{2.123}$$

This *careless limit* (2.123) is independent of the accelerator size R and the pipe size b.

The impedance $Z_0^{\parallel}$ is a quantity integrated over the accelerator circumference, and tends to be proportional to R. The quantity $Z_0^{\parallel}/n$ has the significance of the impedance per unit length along the circumference, because it contains a factor of $n \propto R$ in the denominator. In addition, since the impedance is likely to be inductive and linear in ω at low frequencies, and since $n \propto \omega$, $Z_0^{\parallel}/n$ has also the significance that it gives the inductance at low frequencies. In other words, the beam dynamics respond more to the inductance than the resistance of the impedance, and the quantity $Z_0^{\parallel}/n$ has the significance of the *inductance per unit length* in the circular accelerator.[36] In particular, for a vacuum chamber structure much smaller than the bunch length, the impedance may be peaked at a frequency much higher than the frequency corresponding to the bunch length, but the effect on the beam may still be significant because of its inductive contribution at lower frequencies.

In case a fraction f of the accelerator is filled with cavities, one has

$$\frac{Z_0^{\parallel}}{n} \approx \frac{f}{2} Z_0. \tag{2.124}$$

In a typical modern accelerator, attempts are made to make $Z_0^{\parallel}/n$ less than $1\ \Omega$ or so. This means the vacuum chamber has to be sufficiently smooth to suppress the impedance by a factor of a few hundred compared with the careless limit.

[36] Put in another, somewhat exaggerated, way: what affects the beam dynamics is not measured in ohms; it is not even ohms per meter; it is henries per meter.

The rough estimate (2.117) can be extended to $m \neq 0$ cases. Consider a beam of length b with an mth moment I_m. The energy loss in the cavity can be estimated by the field energy contained in the same shaded region as in Figure 2.16(d), where the fields are given by Eq. (1.8) with the outer boundary located at $r \sim 2b$. This gives

$$\begin{aligned}\Delta\mathscr{E} &\approx -\frac{1}{8\pi}\int dV\left(E_r^2 + E_\theta^2 + B_r^2 + B_\theta^2\right) \\ &= -\frac{I_m^2}{mb^{2m+1}}\left(1 - \frac{1}{2^{4m}}\right) \approx -\frac{I_m^2}{mb^{2m+1}}.\end{aligned} \tag{2.125}$$

As before, the energy lost by the beam is approximately twice Eq. (2.125). By equating this energy loss to $-(b/c)J_m^2 Z_m^{\parallel}$ with $J_m = I_m c/b$, we obtain

$$Z_m^{\parallel} \approx \frac{2}{mcb^{2m}}. \tag{2.126}$$

This establishes Eq. (2.115) for $m \neq 0$.

The transverse impedance can then be obtained by relating it to the longitudinal impedance using Eq. (2.73). For example, for $m = 1$, we have for $\omega \lesssim c/b$

$$Z_1^{\perp} \approx \frac{2}{cb} \approx 60\ \Omega \times \frac{1}{b}. \tag{2.127}$$

A deep cavity in a $b = 5$ cm pipe, therefore, contributes approximately $Z_1^{\perp} \approx 1.2\ \text{k}\Omega/\text{m}$ in the neighborhood of $\omega/2\pi \lesssim 1$ GHz. In the same spirit as Eq. (2.121), a transverse broad-band resonator impedance [Eq. (2.87) with $m = 1$] that represents this cavity would have

$$R_S \approx 60\ \Omega \times \frac{1}{b^2}, \qquad Q \approx 1, \qquad \omega_R \approx \frac{c}{b} \tag{2.128}$$

Comparing Eqs. (2.121) and (2.128) with Eq. (2.107), we find that Eq. (2.107) is off by a factor of 2. This is not unreasonable in view of the approximate nature of the three equations involved.

Figure 2.18 shows the longitudinal and transverse wake functions corresponding to the broad-band impedances, (2.121) and (2.128). One should keep in mind that these wake functions do not apply to very short ($|z| \ll b$) or very long ($|z| \gg b$) ranges.

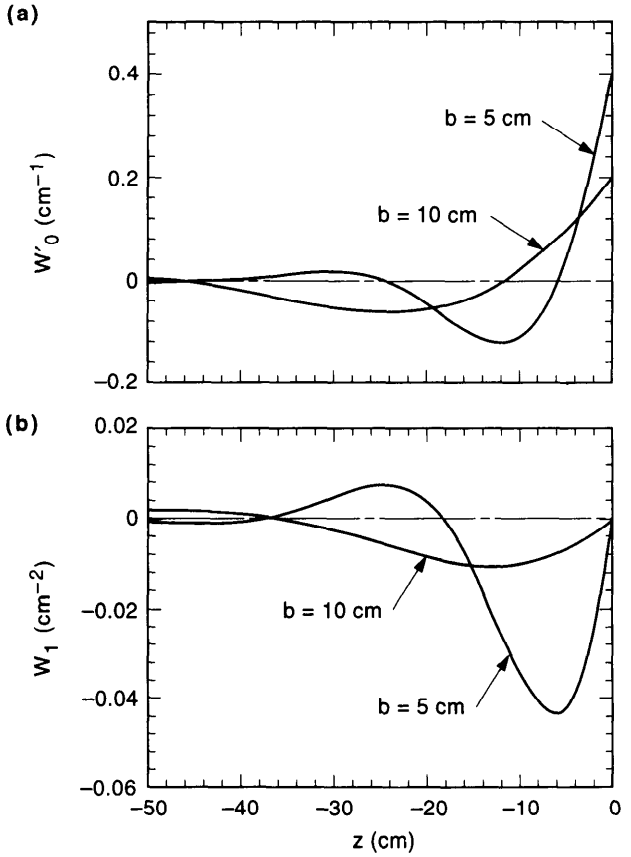

Figure 2.18. Wake functions of the broad-band impedances (2.121) and (2.128). (a) is longitudinal; (b) is transverse. Two values of b, 5 and 10 cm, are presented to indicate the scaling of the wake functions with respect to b.

Exercise 2.21 Consider a shallow cavity and the arrangement of Figure 2.17 except that $\rho(z)$ is the distribution of the dipole moment (instead of the charge) of the beam. Follow the argument (2.118–2.120) of the text to show that the transverse impedance $Z_1^{\perp}(\omega)$ at low frequencies $|\omega| \ll c/b$ is approximately given by

$$Z_1^{\perp}(\omega) \approx -iZ_0 \frac{gd}{\pi b^3} \tag{2.129}$$

Show that, aside from a numerical factor, this result is consistent with the broad-band resonator model (2.128). As can be expected, Eqs. (2.119) and (2.129) satisfy the condition (2.107).

Exercise 2.22

(a) Consider a cavity structure of length and depth g, where $g \ll b$, and consider a beam of length g. Follow the reasoning in the text to show

that this cavity has an impedance, at frequency $\omega \approx c/g$, given by

$$Z_0^{\parallel} \approx \frac{Z_0}{2\pi}\frac{g}{b}. \tag{2.130}$$

If the accelerator pipe is covered with these cavities, one has

$$\frac{Z_0^{\parallel}}{n} \approx \frac{Z_0}{2}\frac{g}{b}. \tag{2.131}$$

(b) Take g to be the skin depth δ_{skin}, and show that the result is consistent with the resistive-wall impedance (2.77). This means the resistive wall behaves almost like a continuum of small cavities of size $\sim \delta_{\text{skin}}$.

(c) Use Eq. (2.131) to estimate $Z_0^{\parallel}/n$ due to the roughness of the pipe wall. Show that

$$\frac{Z_0^{\parallel}}{n} \approx \frac{Z_0 g}{4b},$$

where g is the size of the granularities on the wall surface.

Exercise 2.23 The reasoning leading to the conclusion that the impedance of a cavity is mainly inductive at low frequencies and is given by Eq. (2.119) can also be applied to estimate the impedance of a perfectly smooth beam pipe of radius b with a small circular hole of radius $r \ll b$ on the pipe wall. Provide the reasoning that the low-frequency impedance can be roughly estimated by setting $g \sim d \sim r$ in Eq. (2.119) and multiplying the result by the factor $r/\pi b$, the fraction of the azimuthal extent of the hole. Compare the result with that obtained by an exact consideration,[37] which gives an inductance

$$L = \frac{Z_0}{6\pi^2 c}\frac{r^3}{b^2}. \tag{2.132}$$

Note the cubic dependence of the impedance on the hole size.

Exercise 2.24 Estimate $Z_0^{\parallel}/n$ and $Z_1^{\perp}$ for the accelerator sketched in Figure 2.19. Give a broad-band resonator representation of your estimates. Assume a resistive-wall aluminum pipe of radius $b = 5$ cm. Let there be 10 bellows (with depth $\Delta = 1$ cm), 10 stripline monitors (with characteristic resistance $R_{S0} = 3\ \Omega$ and length $d = 20$ cm), and 2 rf cavities. Consider an accelerator circumference of 200 m.

[37] H. A. Bethe, Phys. Rev. **66**, 163 (1944); M. Sands, SLAC Report PEP-253 (1977); S. S. Kurennoy, Part. Accel. **39**, 1 (1992); R. L. Gluckstern, Phys. Rev. A **46**, 1106 (1992) and Phys. Rev. A **46**, 1110 (1992).

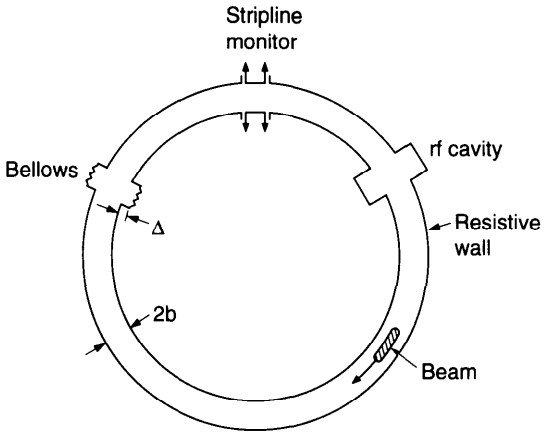

Figure 2.19. An accelerator with objects that contribute to impedances.

Exercise 2.25 Consider a circular accelerator with $b = 5$ cm and $|Z_0^{\parallel}/n| = 1\ \Omega$. Model the impedance as a number of cavities, each represented by the broad-band resonator (2.121). Show that the accelerator has one such cavity approximately every 25 m.

Diffraction Model

The broad-band resonator model addresses the impedance for frequencies $\omega \lesssim c/b$. It turns out that it is also possible to estimate the impedance at high frequencies $\omega \gg c/b$. The method used is called the diffraction model, and was first introduced by Lawson.[38]

To illustrate this method, we follow Bane and Sands to consider a single cavity in an infinitely long beam pipe as sketched in Figure 2.20. Since in this calculation we are interested in the frequency dependence of the impedance, we consider a sinusoidal beam current J_0 which is given by the real part of $\hat{J}_0 \exp[-i\omega(t - s/c)]$. In the region sufficiently upstream from the cavity, the electromagnetic field is given by a plane wave with the same sinusoidal t and s dependences as the beam current. At the pipe radius, we have $E_r = B_\theta = 2J_0/cb$. As the beam enters the cavity, this plane wave is diffracted by the entrance edge of the cavity as sketched in Figure 2.20. We let g be the longitudinal extent of the cavity.

At high frequencies $\omega \gg c/b$, according to the diffraction model, the electromagnetic field in the cavity region is the same as that produced by a plane wave impinging on an obscuring screen. Furthermore, at high frequen-

[38] J. D. Lawson, Rutherford Lab. Report RHEL/M 144 (1968), and Part. Accel. **25**, 107 (1990). See also G. Dome, IEEE Tran. Nucl. Sci. **NS-32**, 2531 (1985); S. A. Heifets and S. A. Kheifets, Part. Accel. **25**, 61 (1990); Karl Bane and Matthew Sands, Part. Accel. **25**, 73 (1990); R. B. Palmer, Part. Accel. **25**, 97 (1990); R. L. Gluckstern, *AIP Proc.* **249**, *Phys. Part. Accel.*, 1992, Vol. 1, p. 237.

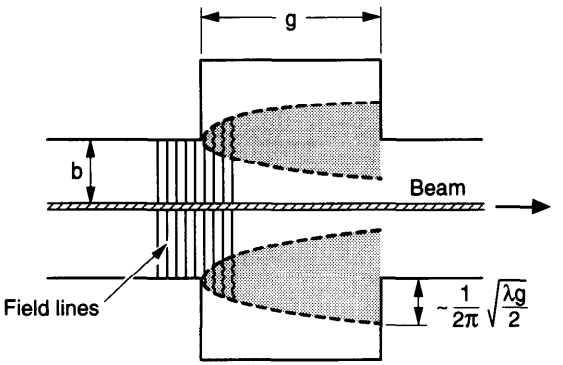

Figure 2.20. The diffraction model of high frequency impedance for a single cavity structure. The beam and the field lines are sketched. The shaded region between the dashed curves indicates the region where the fields are perturbed by diffraction. The depth of the cavity is assumed to be larger than $(1/2\pi)\sqrt{\lambda g/2}$. Approximately half the diffracted field energy is trapped in the cavity; the other half propagates down the vacuum chamber pipe.

cies the screen can be approximated as a semi-infinite plane with a straight edge, and the polar plane electromagnetic wave can be approximated as a Cartesian plane wave with $E_y = -B_x = -2J_0/cb$ and wavelength $\lambda = 2\pi c/\omega$. The beam-cavity system of Figure 2.20 is therefore modeled as shown in Figure 2.21. The incident wave carries an energy flux (energy flowing by per unit area per unit time)

$$F_0 = \frac{c}{8\pi}\left(E_y^2 + B_x^2\right) = \frac{J_0^2}{\pi c b^2}. \tag{2.133}$$

As it enters the cavity, the plane wave is diffracted at the edge of the obscuring screen (the entrance edge of the cavity) into the shadow region. By

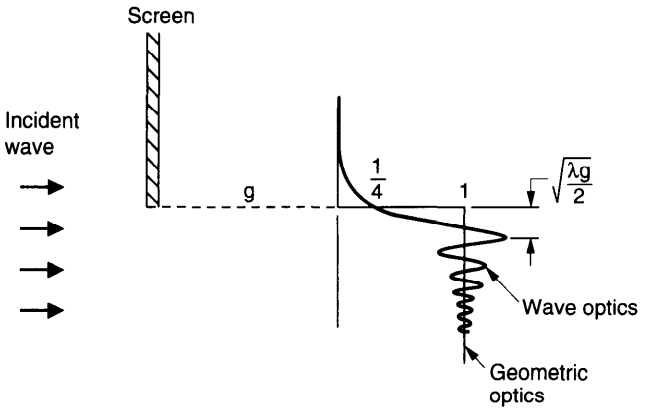

Figure 2.21. Geometry of the diffraction model. Energy flux behind the screen is shown on the right. Two curves are shown; one indicates what would happen with geometric optics without diffraction, the other is the result of wave optics.

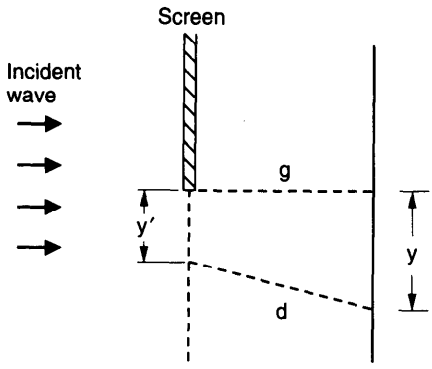

Figure 2.22. Geometry used to calculate the diffraction pattern.

the time the field reaches the exit edge of the cavity, the diffracted field has acquired a spread in the y-direction (the direction that lies in the plane of the screen and is perpendicular to the screen edge). The energy flux, as a function of y, is given by (see Exercise 2.26)

$$F(y) = F_0 \tfrac{1}{2}\left\{\left[C(u) + \tfrac{1}{2}\right]^2 + \left[S(u) + \tfrac{1}{2}\right]^2\right\} \equiv F_0\Phi(u), \quad (2.134)$$

where $u = y\sqrt{2/\lambda g}$, and $C(u)$ and $S(u)$ are the Fresnel integrals defined by

$$C(u) + iS(u) = \int_0^u dt\, e^{i(\pi/2)t^2}, \quad (2.135)$$

which are odd functions of u and have the properties $C(\pm\infty) = S(\pm\infty) = \pm\frac{1}{2}$.

Exercise 2.26 Consider the geometry shown in Figure 2.22. The diffracted field is proportional to $|a(y)|^2$, where

$$a(y) \propto \int_0^\infty dy'\, e^{i\omega d/c}, \quad (2.136)$$

where d, shown in Figure 2.22, is approximately given by $g + (y - y')^2/2g$. Derive Eq. (2.134) using Eqs. (2.135–2.136).

The energy loss from the beam is given by the energy contained in the diffracted fields. The power of this energy loss into the shadow region $y < 0$ is given by integrating Eq. (2.134) over the appropriate area:

$$\mathscr{P} = 2\pi b \int_{-\infty}^{0} dy\, F(y). \quad (2.137)$$

The integral can be evaluated to yield

$$\mathscr{P} = \frac{J_0^2}{\pi cb}\sqrt{\frac{\pi cg}{\omega}}, \quad (2.138)$$

where we have used $\int_{-\infty}^{0}\Phi(u)\,du = 1/2\pi$. As the wave is diffracted, half of the diffracted field energy goes into the shadow region, and represents the part of energy to be scraped off by the exit edge of the cavity. The other half is diffracted toward the pipe region and propagates down the pipe with the beam. The total loss of field energy by the beam is thus twice that given by Eq. (2.138). The effective depth that the field is diffracted into the shadow region is $\mathscr{P}/2\pi bF_0 = (1/2\pi)\sqrt{\lambda g/2}$.

Exercise 2.27 Show that:

(a) The wave energy flux at the shadow edge $y = 0$ is $\frac{1}{4}$ of the incident flux, i.e., $\Phi(0) = \frac{1}{4}$.

(b) The wave energy flux deep in the shadow region is given by $F(y) \approx \lambda g F_0/4\pi^2 y^2$.

(c) The total field energy contained in the diffracted wave pattern is the same as that contained in the geometrical optics pattern, i.e., total wave energy is conserved. [Hint: Show $\int_{-\infty}^{0} du\,\Phi(u) + \int_{0}^{\infty} du[\Phi(u) - 1] = 0$.]

(d) The energy lost by the plane wave in the shadow region $y < 0$ is equal to that in the region $y > 0$. [Hint: Show $\int_{-\infty}^{0} dy|a(y) - a(-\infty)|^2 = \int_{0}^{\infty} dy|a(y) - a(\infty)|^2$.]

The power loss (2.138), multiplied by 2, is then equated with $\operatorname{Re} Z_0^{\parallel} J_0^2$ to give the real part of the impedance at high frequencies,

$$\operatorname{Re} Z_0^{\parallel}(\omega) = \frac{Z_0}{2\pi^{3/2}}\frac{1}{b}\sqrt{\frac{cg}{\omega}}, \tag{2.139}$$

where $Z_0 = 4\pi/c = 377\ \Omega$. Causality requires a matching imaginary part of the impedance. The total impedance is

$$Z_0^{\parallel}(\omega) = [1 + \operatorname{sgn}(\omega)i]\frac{Z_0}{2\pi^{3/2}}\frac{1}{b}\sqrt{\frac{cg}{|\omega|}}. \tag{2.140}$$

The corresponding wake function is

$$W_0'(z < 0) = \frac{2\sqrt{2g}}{\pi b}|z|^{-1/2}. \tag{2.141}$$

Exercise 2.28 For a short Gaussian bunch with $\sigma_z \ll b$, use Eq. (2.139) to calculate the parasitic loss

$$\Delta\mathscr{E} = -\frac{1}{\pi}\Gamma\left(\frac{1}{4}\right)\frac{q^2}{b}\sqrt{\frac{g}{\pi\sigma_z}}. \tag{2.142}$$

Note that $\Delta\mathscr{E} \to \infty$ as $\sigma_z \to 0$. Setting $\sigma_z \sim g \sim b$ gives essentially Eq. (2.116) other than a numerical factor.

For $m \neq 0$, consider an mth moment current $J_m = \hat{J}_m \exp[-i\omega(t - s/c)]$. The electromagnetic field at the entrance edge of the cavity is $E_y = -B_x = -(4J_m \cos m\theta)/(cb^{m+1})$. The energy flux of the diffracted wave is given by

$$F(y,\theta) = \frac{4}{\pi}\frac{J_m^2}{cb^{2m+2}}\cos^2 m\theta\,\Phi(u), \tag{2.143}$$

where $\Phi(u)$ is defined in Eq. (2.134). The power lost by the beam in the shadow region is then

$$\mathscr{P} = b\int_{-\infty}^{0} dy \int_0^{2\pi} d\theta\, F(y,\theta) = \frac{Z_0}{2\pi^{3/2}}\frac{J_m^2}{b^{2m+1}}\sqrt{\frac{cg}{\omega}}\,. \tag{2.144}$$

Equating twice this amount to $\mathrm{Re}\, Z_m^{\parallel} J_m^2$ and matching an imaginary part to it, we obtain the impedance, for $m \neq 0$,

$$Z_m^{\parallel}(\omega) = \frac{\omega}{c}Z_m^{\perp}(\omega) = [1 + \mathrm{sgn}(\omega)i]\frac{Z_0}{\pi^{3/2}}\frac{1}{b^{2m+1}}\sqrt{\frac{cg}{|\omega|}}\,. \tag{2.145}$$

The corresponding wake functions are

$$\begin{aligned} W_m(z<0) &= -\frac{8\sqrt{2g}}{\pi b^{2m+1}}|z|^{1/2}, \\ W_m'(z<0) &= \frac{4\sqrt{2g}}{\pi b^{2m+1}}|z|^{-1/2}. \end{aligned} \tag{2.146}$$

Equation (2.140) and the $m = 1$ member of Eq. (2.145) satisfy Eq. (2.107) exactly. This is not surprising because the electrodynamics of the diffraction model are all happening near the pipe radius $r = b$. Furthermore, the generalized form (2.109) is also valid for the diffraction model.

According to the diffraction model, therefore, the longitudinal impedance $Z_m^{\parallel} \propto \omega^{-1/2}$ and the transverse impedance $Z_m^{\perp} \propto \omega^{-3/2}$ at high frequencies. At these high frequencies, we also find that the impedances are proportional to $\sqrt{g}$. By taking the lower end of the range of applicability, $\omega \approx c/b$, and setting $g = b$, we find the impedances are consistent with Eqs. (2.117) and (2.127), aside from a numerical factor of the order of unity. The diffraction impedance for $\omega \gg c/b$ therefore matches reasonably smoothly the broad-band resonator impedance for $\omega \lesssim c/b$. The wake function W_m' diverges as $z \to 0^-$. A point charge or a point multipole, therefore, loses an infinite

amount of energy to the cavity structure. At distance $|z| \approx b$, and $g = b$, we obtain Eq. (2.114).

The diffraction model applies to the case of a single cavity structure in an infinitely long smooth beam pipe. A beam pipe with a periodic array of cavities has an impedance whose high frequency behavior is very different from the diffraction model result. See Eq. (2.175) below.

2.4 CALCULATION OF WAKE FIELDS AND IMPEDANCES

In Section 2.1, we worked out in detail the wake fields of a resistive-wall pipe. The reason for using the resistive wall as an example is that it can be handled analytically and yet contains most of the important features of a general case. In most practical cases, the resistive-wall contribution is small compared with other wake fields found in an accelerator, such as those associated with discontinuities in the vacuum chamber pipe.

The computation of wake functions and impedances for practical accelerator applications is a rather demanding task. One encounters vacuum chamber components that require special attention of one kind or another (lack of axial symmetry, nonmetal material, vacuum pipe thinner than the skin depth, etc.). Practicality dictates the calculation to be performed, and sophisticated techniques have been developed to deal with these problems. Below we will describe two methods, one due to Condon[39] (the frequency domain approach), another by direct numerical solution of the Maxwell equations (the time domain approach). Not covered is for example a perturbation technique valid for smoothly varying wall boundaries.[40]

Frequency Domain

Consider a point charge q passing through a cavity with perfectly conducting walls. We suppose first the cavity is closed and the point charge traverses the cavity through infinitesimal holes. In the frequency domain, the cavity wake fields generated by the passage of the point charge are described in terms of a superposition of modes. Each mode can be specified by an equivalent LRC resonator impedance (2.85) and wake function (2.86) with its own mode frequency ω_R and R_S/Q.[41] The energy deposited by the point charge into a

[39] E. U. Condon, J. Appl. Phys. **12**, 129 (1941).

[40] M. Chatard-Moulin and A. Papiernik, Nucl. Instr. Meth. **205**, 37 (1983); R. K. Cooper, S. Krinsky, and P. L. Morton, Part. Accel. **12**, 1 (1982); S. Krinsky and R. L. Gluckstern, IEEE Trans. Nucl. Sci. **NS-28**, 2621 (1981).

[41] A resonator impedance is specified by three parameters: ω_R, R_S, and Q. But for a closed cavity with perfectly conducting walls assumed here, the analogy to an LRC circuit is meaningful only on setting $R_S \to \infty$, $Q \to \infty$ with R_S/Q fixed.

given mode after its passage through the cavity is given by

$$q^2\frac{W_0'(0^-)}{2} = q^2\frac{R_S\omega_R}{2Q} \equiv q^2k, \tag{2.147}$$

where the factor of $\frac{1}{2}$ is due to the fundamental theorem of beam loading. The quantity $k = R_S\omega_R/2Q$ is called the *loss factor*;[42] it is a property of the cavity and not of the beam.

The total longitudinal and transverse wake functions of the cavity are superpositions of (2.86) and (2.90) from all cavity modes. The λth mode is characterized by a mode frequency ω_λ and loss factor k_λ. Thus, for $z < 0$, we have

$$\begin{aligned} W_0'(z) &= 2\sum_\lambda k_\lambda \cos\frac{\omega_\lambda z}{c}, \\ W_0(z) &= 2\sum_\lambda \frac{k_\lambda c}{\omega_\lambda}\sin\frac{\omega_\lambda z}{c}. \end{aligned} \tag{2.148}$$

The corresponding impedances are given by Eqs. (2.85) and (2.89) with $R_S\omega_R/2Q$ replaced by k_λ. Computation of the wake functions and impedances is therefore reduced to computation of ω_λ and k_λ for all cavity modes. The total energy change of a point charge q is obtained by summing Eq. (2.147) over all modes:

$$\Delta\mathscr{E} = -q^2\sum_\lambda k_\lambda. \tag{2.149}$$

To proceed, we write the wake field generated by the beam as

$$\begin{aligned} \vec{E} &= -\nabla\Phi - \frac{1}{c}\frac{\partial\vec{A}}{\partial t}, \\ \vec{B} &= \nabla\times\vec{A}, \end{aligned} \tag{2.150}$$

where the scalar and vector potentials satisfy the Maxwell equations in Coulomb gauge,[43]

$$\begin{aligned} \nabla^2\Phi &= -4\pi\rho, \\ \nabla^2\vec{A} - \frac{1}{c^2}\frac{\partial^2\vec{A}}{\partial t^2} &= -\frac{4\pi}{c}\vec{j} + \frac{1}{c}\nabla\frac{\partial\Phi}{\partial t}. \end{aligned} \tag{2.151}$$

[42]R. F. Koontz, G. A. Loew, R. H. Miller, and P. B. Wilson, IEEE Trans. Nucl. Sci. **NS-24**, 1493 (1977); Perry B. Wilson, *AIP Proc.* **87**, *Phys. High Energy Accel.*, Fermilab, 1981, p. 450.
[43]J. D. Jackson, *Classical Electrodynamics*, 2nd ed., Wiley, New York, 1975.

To apply the *Condon method*, we expand the scalar and vector potentials in terms of the eigenmodes of the empty cavity according to

$$\begin{aligned} \vec{A}(\vec{x},t) &= \sum_{\lambda} q_\lambda(t)\vec{a}_\lambda(\vec{x}), \\ \Phi(\vec{x},t) &= \sum_{\lambda} r_\lambda(t)\phi_\lambda(\vec{x}), \end{aligned} \tag{2.152}$$

where the eigenmodes satisfy

$$\begin{aligned} \nabla^2\vec{a}_\lambda + \left(\frac{\omega_\lambda}{c}\right)^2 \vec{a}_\lambda &= 0, \\ \nabla^2\phi_\lambda + \left(\frac{\omega_\lambda}{c}\right)^2 \phi_\lambda &= 0, \end{aligned} \tag{2.153}$$

as well as the boundary conditions that $\vec{a}_\lambda$ is perpendicular to the conducting walls and that $\phi_\lambda = 0$ on the walls. We have adopted the Coulomb gauge $\nabla \cdot \vec{a}_\lambda = 0$ and the normalization conditions

$$\int_{\text{cavity}} dV \vec{a}_\lambda \cdot \vec{a}^*_{\lambda'} = \int_{\text{cavity}} dV \phi_\lambda \phi^*_{\lambda'} = \delta_{\lambda\lambda'}, \tag{2.154}$$

where $\delta_{\lambda\lambda'} = 1$ if $\lambda = \lambda'$ and 0 otherwise.

By a proper choice of a distance L, one can consider that the beam enters the cavity at location $s = 0$ at time $t = 0$, and exits the cavity at location $s = L$ at time $t = L/c$. By substituting Eq. (2.152) into Eq. (2.151) and applying the orthonormality condition (2.154), $r_\lambda(t)$ can be found readily:

$$r_\lambda(t) = \frac{4\pi c^2}{\omega_\lambda^2} \int_{\text{cavity}} dV \rho(\vec{x},t)\phi^*_\lambda(\vec{x}). \tag{2.155}$$

One also finds that $q_\lambda(t)$ satisfies

$$\ddot{q}_\lambda + \omega_\lambda^2 q_\lambda = 4\pi c \int_{\text{cavity}} dV \vec{j}(\vec{x},t) \cdot \vec{a}^*_\lambda(\vec{x}), \tag{2.156}$$

which has the explicit solution

$$q_\lambda(t) = \begin{cases} 0 & \text{if} \quad t < 0, \\ \dfrac{4\pi c}{\omega_\lambda} \displaystyle\int_0^{\min(t,\,L/c)} dt' \sin \omega_\lambda(t - t') & \\ \qquad \times \displaystyle\int_{\text{cavity}} dV \vec{j}(\vec{x},t') \cdot \vec{a}^*_\lambda(\vec{x}) & \text{if} \quad t > 0. \end{cases} \tag{2.157}$$

Knowing $\rho(\vec{x}, t)$ and $\vec{j}(\vec{x}, t)$, Eqs. (2.155) and (2.157) give directly the expansion coefficients $r_\lambda(t)$ and $q_\lambda(t)$. Note that r_λ (and therefore the scalar potential Φ) vanishes at times when the beam is absent, i.e., when $t < 0$ or $t > L/c$. The same is not true for the vector potential $\vec{A}$. Its expansion coefficients q_λ vanish before the beam enters the cavity ($t < 0$), but continue to "ring" after the beam has left the cavity.

We now consider the special case of a point charge,

$$\begin{aligned} \rho &= q\delta(x)\delta(y)\delta(s - ct), \\ \vec{j} &= c\rho\hat{s}. \end{aligned} \tag{2.158}$$

Substituting into Eqs. (2.155) and (2.157) gives

$$r_\lambda(t) = \begin{cases} \dfrac{4\pi c^2}{\omega_\lambda^2} q\phi_\lambda^*(0,0,ct) & \text{if } \dfrac{L}{c} > t > 0, \\ 0 & \text{otherwise,} \end{cases}$$

$$q_\lambda(t) = \begin{cases} 0 & \text{if } t < 0, \\ \dfrac{4\pi c^2 q}{\omega_\lambda} \displaystyle\int_0^{\min(t,\, L/c)} dt' \sin \omega_\lambda(t - t')\, a_{\lambda s}^*(0,0,ct') & \text{if } t > 0. \end{cases} \tag{2.159}$$

The energy loss of the point charge can be obtained by integrating the longitudinal electric field across the cavity:

$$\begin{aligned} \Delta\mathscr{E} &= qc\int_0^{L/c} dt\, E_s(0,0,ct) \\ &= -qc\sum_\lambda \int_0^{L/c} dt \left[r_\lambda(t) \frac{\partial\phi_\lambda(0,0,ct)}{c\partial t} + \frac{1}{c}\dot{q}_\lambda(t) a_{\lambda s}(0,0,ct) \right]. \end{aligned} \tag{2.160}$$

The loss factor k_λ is related to the energy deposited into the λth mode. On substituting (2.159) into (2.160), the first term on the right hand side vanishes after integrating over t due to the boundary condition of ϕ_λ. After some algebraic manipulations, the second term gives what we are looking for,[44]

$$k_\lambda = 2\pi \left| \int_0^{L/c} c\, dt\, e^{-i\omega_\lambda t}\, a_{\lambda s}(0,0,ct) \right|^2. \tag{2.161}$$

[44] For a guide to this derivation, see K. L. F. Bane, P. B. Wilson, and T. Weiland, *AIP Proc.* **127**, *Phys. of High Energy Accel.*, BNL/SUNY, 1983, p. 875.

Given the eigenmodes $a_\lambda(\vec{x})$ of the empty cavity, Eq. (2.161) gives the loss factors k_λ on integrating a_λ over the trajectory of the point charge along its path through the cavity. Knowing the mode frequencies and loss factors, the wake functions can be calculated using Eq. (2.148).

Exercise 2.29

(a) The loss factor (2.161) can also be obtained by calculating the field energy deposited in the cavity after the point charge has departed. Show that this derivation gives the same result, Eq. (2.161).

(b) By considering a test charge e a distance $|z|$ behind the point charge q, calculate the longitudinal wake function $W_0'(z)$ by using Eq. (2.50):

$$-eqW_0'(z) = \int_{-z/c}^{(L-z)/c} c\,dt\,eE_s(0,0,ct+z), \qquad z<0. \quad (2.162)$$

Verify explicitly that the wake function is given by Eq. (2.148).

So far we have been considering a closed cavity. In case of a periodic cavity array like that shown in Figure 2.1(a), the analysis can be applied if L is chosen to be the structure period and the modes are taken to be those with phase velocity equal to that of the beam, i.e., $v_{\text{ph}} = c$.

To calculate the wake functions for modes with $m \neq 0$, we consider a $\cos m\theta$ ring beam, Eq. (1.7), traversing the cavity. We assume the vacuum chamber pipe is axially symmetric, and switch to polar coordinates (r, θ, s). This gives, for $t > 0$,

$$r_\lambda(t) = \begin{cases} \dfrac{4c^2 I_m}{\omega_\lambda^2 a^m} \displaystyle\int_0^{2\pi} d\theta \cos m\theta\, \phi_\lambda^*(a,\theta,ct) & \text{if } \dfrac{L}{c} > t > 0, \\ 0 & \text{if } t > \dfrac{L}{c}, \end{cases} \quad (2.163)$$

$$q_\lambda(t) = \frac{4c^2 I_m}{\omega_\lambda a^m} \int_0^{\min(t,\,L/c)} dt' \sin\omega_\lambda(t-t') \times \int_0^{2\pi} d\theta \cos m\theta\, a_{\lambda s}^*(a,\theta,ct').$$

Note that it is the mth Fourier harmonic of the normal modes that drives the wake fields when the beam has a pure mth multipole moment.

Following similar steps to those for the point charge, Eqs. (2.160–2.161), we obtain the energy loss of the mth moment I_m,

$$\Delta\mathscr{E} = -I_m^2 \sum_\lambda k_\lambda^{(m)}, \quad (2.164)$$

where the loss factor is

$$k_\lambda^{(m)} = \frac{2\pi}{b^{2m}} \left| \int_0^{L/c} c\,dt\, e^{-i\omega_\lambda t} \frac{1}{(1+\delta_{m0})\pi} \int_0^{2\pi} d\theta \cos m\theta\, a_{\lambda s}(b,\theta,ct) \right|^2 . \tag{2.165}$$

Note that it is $a_{\lambda s}$ evaluated at the pipe radius $r = b$ that appears in the integral. The wake functions are then given, for $z < 0$, by

$$\begin{aligned} W'_m(z) &= 2\sum_\lambda k_\lambda^{(m)} \cos\frac{\omega_\lambda z}{c}, \\ W_m(z) &= 2\sum_\lambda \frac{k_\lambda^{(m)} c}{\omega_\lambda} \sin\frac{\omega_\lambda z}{c}. \end{aligned} \tag{2.166}$$

The dimensionalities of the loss factors k_λ and $k_\lambda^{(m)}$ are L^{-1} and L^{-2m-1}. To convert k_λ to other units, one can use

$$1\ \text{V/pC} = 1\ \text{k}\Omega\text{-GHz} = 1.11\ \text{cm}^{-1}. \tag{2.167}$$

As one application of the Condon method, below we calculate the electromagnetic fields generated by a point charge, Eq. (2.158), between two infinite, perfectly conducting plates located at $s = 0$ and $s = L$, as shown in Figure 2.23.[45] To do so, we first calculate the normal mode potentials for an empty cavity. These are found to be

$$\begin{aligned} \omega_\lambda &= c\sqrt{k_x^2 + k_y^2 + \left(\frac{p\pi}{L}\right)^2}, \\ \phi_\lambda &= \frac{1}{\pi\sqrt{2L}} e^{i(k_x x + k_y y)} \sin\frac{p\pi s}{L}, \\ \vec{a}_\lambda &= \frac{ce^{i(k_x x + k_y y)}}{\omega_\lambda \sqrt{2L\left(k_x^2 + k_y^2\right)(1+\delta_{p0})}} \\ &\quad \times \left[\hat{x}\left(\frac{-ipk_x}{L}\sin\frac{p\pi s}{L}\right) + \hat{y}\left(\frac{-ipk_y}{L}\sin\frac{p\pi s}{L}\right) + \hat{s}\left(\frac{k_x^2 + k_y^2}{\pi}\cos\frac{p\pi s}{L}\right)\right], \end{aligned} \tag{2.168}$$

where the mode index λ stands for the three mode numbers k_x, k_y, and p,

[45] This model ignores the effects of the outer boundary of the cavity walls which would be there if the cavity had the geometry of a pillbox. However, this simplification is strictly correct when the bunch length or distance of interest is sufficiently short so that causality precludes any effect of the wake fields reflected from the outer cavity walls.

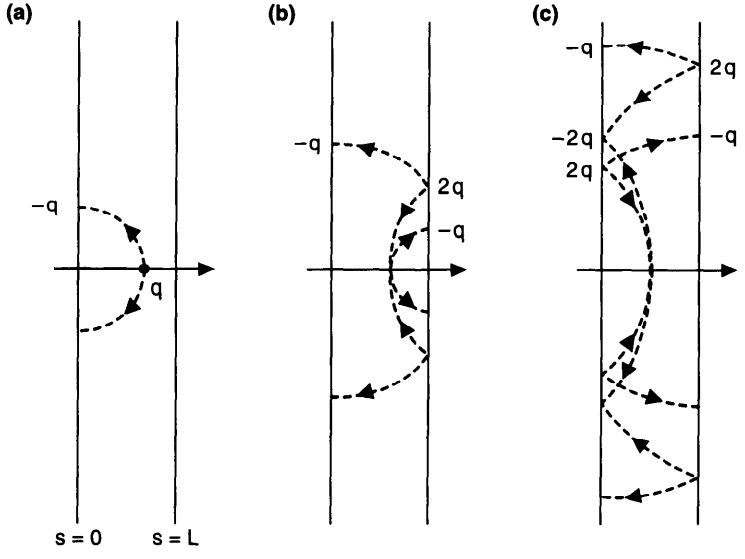

Figure 2.23. Wake field generated by a point charge passing through two perfectly conducting, infinite parallel plates. Dashed curves are the wake fields. Arrows indicate directions of the electric fields. (a) When the charge is between the plates; (b), (c) after the charge has left the cavity.

and

$$\sum_{\lambda} \to \int_{-\infty}^{\infty} dk_x \int_{-\infty}^{\infty} dk_y \sum_{p=0}^{\infty} . \tag{2.169}$$

It follows from Eqs. (2.155) and (2.157) that

$$r_\lambda(t) = \frac{4c^2 q}{\omega_\lambda^2 \sqrt{2L}} \begin{cases} \sin \dfrac{p\pi ct}{L}, \\ 0, \end{cases} \tag{2.170}$$

$$q_\lambda(t) = \frac{4cq}{\omega_\lambda \sqrt{2L\left(k_x^2 + k_y^2\right)(1 + \delta_{p0})}} \begin{cases} -\cos \omega_\lambda t + \cos \dfrac{p\pi ct}{L}, \\ -\cos \omega_\lambda t + (-1)^p \cos \omega_\lambda \left(t - \dfrac{L}{c}\right), \end{cases}$$

where the first entry refers to $L/c > t > 0$, the second to $t > L/c$.

After some algebraic manipulations, the field components are found using Eqs. (2.150) and (2.152):[46]

$$E_r = \begin{cases} \dfrac{2q}{r}A, \\ \dfrac{2q}{r}B_- - \dfrac{2q}{r}C_-, \end{cases}$$

$$E_s = \begin{cases} -\dfrac{2q}{\sqrt{c^2t^2 - r^2}}A, \\ -\dfrac{2q}{\sqrt{c^2t^2 - r^2}}B_+ + \dfrac{2q}{\sqrt{(ct - L)^2 - r^2}}C_+, \end{cases} \tag{2.171}$$

$$B_\theta = \begin{cases} \dfrac{2qct}{r\sqrt{c^2t^2 - r^2}}A, \\ \dfrac{2qct}{r\sqrt{c^2t^2 - r^2}}B_+ - \dfrac{2q(ct - L)}{r\sqrt{(ct - L)^2 - r^2}}C_+, \end{cases}$$

where $r^2 = x^2 + y^2$ and we have introduced the symbols

$$\begin{aligned} A &= H(ct - r)\delta\left(s - \sqrt{c^2t^2 - r^2}\right), \\ B_\pm &= H(ct - r)\sum_{n=-\infty}^{\infty}\Big[\delta\left(s - \sqrt{c^2t^2 - r^2} + 2nL\right) \\ &\qquad \pm\delta\left(s + \sqrt{c^2t^2 - r^2} - 2nL\right)\Big], \\ C_\pm &= H(ct - L - r)\sum_{n=-\infty}^{\infty}\left\{\delta\left[s - \sqrt{(ct - L)^2 - r^2} + (2n + 1)L\right]\right. \\ &\qquad \left.\pm\delta\left[s + \sqrt{(ct - L)^2 - r^2} - (2n + 1)L\right]\right\} \end{aligned} \tag{2.172}$$

with $H(x) = 1$ if $x > 0$, and 0 if $x < 0$.

As the point charge q enters the cavity, charges and currents are induced on the first conducting plate. These charges move out radially at the speed of light and stay on a circle of radius $r = ct$. The total charge on the plate is $-q$. The field due to these induced charges and currents plus the field due to

[46]For a guide to the derivation, see A. W. Chao and P. L. Morton, SLAC Report PEP-105/SPEAR-182 (1975).

the point charge and current is a δ-function wake field on the surface of the spherical shell $c^2t^2 = r^2 + s^2$. See Figure 2.23(a). The electric field is tangential to the shell surface, while the Poynting vector is perpendicular to the shell surface. The magnetic field is along the θ-direction and satisfies $|\vec{B}| = |\vec{E}|$. No field exists inside or outside the spherical shell surface.

At time $t = L/c$, both the point charge and the spherical wavefront of the field arrive at the second plate. At this time, drastic changes occur at the second plate. The net result is two sets of induced charges and currents. One set, with total charge $2q$, travels out radially on a circle $r^2 = c^2t^2 - L^2$ (with an apparent speed greater than the speed of light) and produces a reflection of the wave which reverses the sign of E_r but preserves the signs of E_s and B_θ. The second set of induced charges and currents, with a total charge of $-q$, travels out on a circle $r = ct - L$ at the speed of light. The field due to this second set is a δ-function signal on a new spherical shell $(ct - L)^2 = r^2 + (s - L)^2$. See Figure 2.23(b).

At time $t = 2L/c$, both of these wavefronts return to the first plate and are reflected by it, as shown in Figure 2.23(c). The wake fields then reflect between the two plates and are trapped by the cavity. Note that a test charge traveling behind the source charge along the axis will not experience any wake force until after the source charge q has passed through the second plate.

A moment's reflection indicates that we have also solved the case for a point charge penetrating a single perfectly conducting plate through an infinitesimal hole. The results are shown in Figure 2.24.

The loss factors for the case of two parallel plates are obtained from Eq. (2.161):

$$k_\lambda = \frac{2}{\pi L(1 + \delta_{p0})\left(k_x^2 + k_y^2\right)}\left[1 - (-1)^p \cos\frac{\omega_\lambda L}{c}\right]. \qquad (2.173)$$

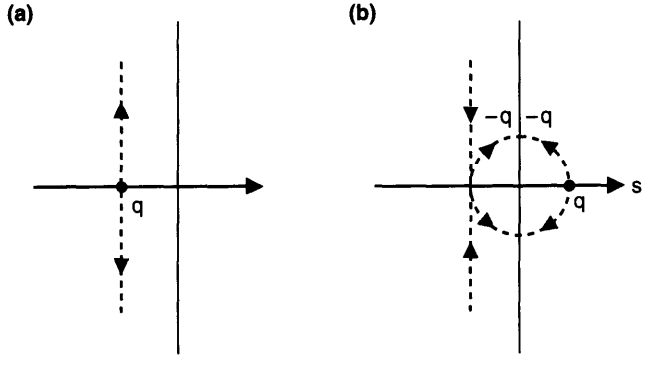

Figure 2.24. Wake field generated by a point charge penetrating through an infinitesimal hole on a perfectly conducting plate: (a) before penetration, (b) after penetration.

Similarly, from Eq. (2.165) we obtain

$$k_\lambda^{(m)} = \frac{8}{\pi L(1+\delta_{p0})(1+\delta_{m0})^2} \frac{k^{2m-2}}{(m!)^2 2^{2m}} \times \cos^2 m\phi \left[1 - (-1)^p \cos\frac{\omega_\lambda L}{c}\right], \tag{2.174}$$

where we have defined $k_x = k\cos\phi$ and $k_y = k\sin\phi$. In obtaining (2.174), we have let $b \to 0$ for the infinitesimal size of the entrance and exit holes of the cavity. For $m = 0$, Eq. (2.174) becomes (2.173).

As mentioned before, the wake functions can be obtained once we know the frequencies and loss factors of all normal modes of the empty cavity. For an idealized cavity geometry, such as two parallel plates, this can be done analytically. In general, however, no analytic solution is available and one has to resort to numerical calculations. If the vacuum chamber pipe is perfectly conducting, a commonly used approach is as follows. The region inside the pipe is first divided into subregions; in each subregion, the normal mode is expressed as an expansion in terms of functions that satisfy the wave equation and the boundary condition of that subregion. The expansion coefficients, as well as the mode frequency, are then determined by matching the fields across the junctions between subregions. The efficient implementation of the technique is a difficult research topic, and only becomes somewhat simplified if there is a symmetry (such as an axial symmetry) in the pipe geometry.

In Figure 2.25 we show the numerical results[47] for the SLAC linac structure, which is modeled as an infinite cavity array shown in Figure 2.25(a). A computer program KN7C[48] was used to obtain the loss factors of the $m = 0$ modes up to 150 GHz, and another program, TRANSVERS,[49] was used to calculate the loss factors of the $m = 1$ modes up to 75 GHz. In Figure 2.25(b) and (c), those loss factors are shown versus frequency.

Figure 2.25(b) and (c) can also be regarded as plots of the real parts of the impedances by recalling Eqs. (2.85) and (2.147). Note that it is only the real part of the impedance that contains the δ-function spikes shown in Figure 2.25(b) and (c). The imaginary part is a continuum; for each δ-function peak of $\mathrm{Re}\, Z_m^{\parallel}$ located at ω_λ, there is an imaginary part $\mathrm{Im}\, Z_m^{\parallel}$ that has a long $(\omega - \omega_\lambda)^{-1}$ tail around it.

The wake functions W_0' and W_1, obtained by Eqs. (2.148) and (2.166), are shown in Figure 2.26. They oscillate as functions of z, indicating the electromagnetic wake field "rings" in the cavity after being excited. The ringing wavelength is comparable to the cavity structure dimensions. The order of

[47] K. Bane and P. B. Wilson, *Proc. 11th Int. Conf. High Energy Accel.*, Geneva, 1980, p. 592.
[48] E. Keil, Nucl. Instr. Meth. **100**, 419 (1972).
[49] K. Bane and B. Zotter, *Proc. 11th Int. Conf. High Energy Accel.*, CERN, 1980, p. 581.

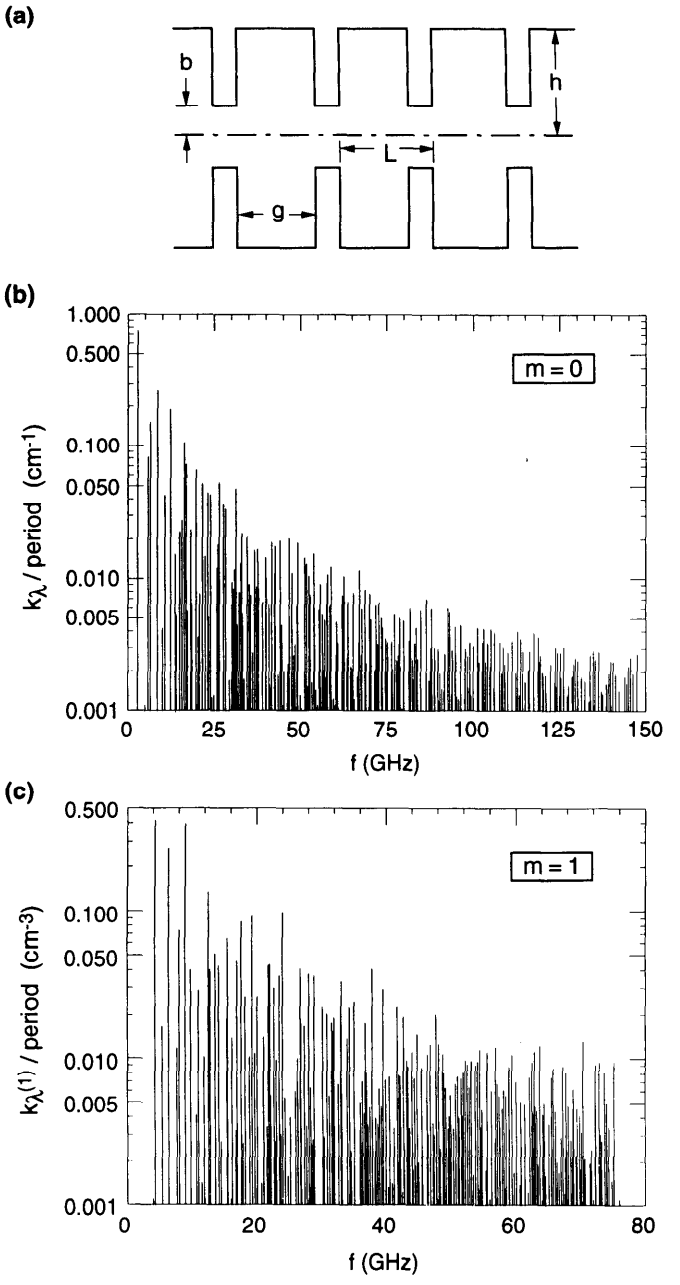

Figure 2.25. (a) The cavity model for the SLAC linac, $L = 3.499$ cm, $b = 1.163$ cm, $h = 4.134$ cm, $g = 2.915$ cm. (b) Loss factor k_λ per cavity period for the $m = 0$ modes versus frequency $f_\lambda = \omega_\lambda / 2\pi$, up to $f = 150$ GHz, for the SLAC linac. (c) Loss factor $k_\lambda^{(1)}$ per cavity period for the $m = 1$ modes up to $f = 75$ GHz.

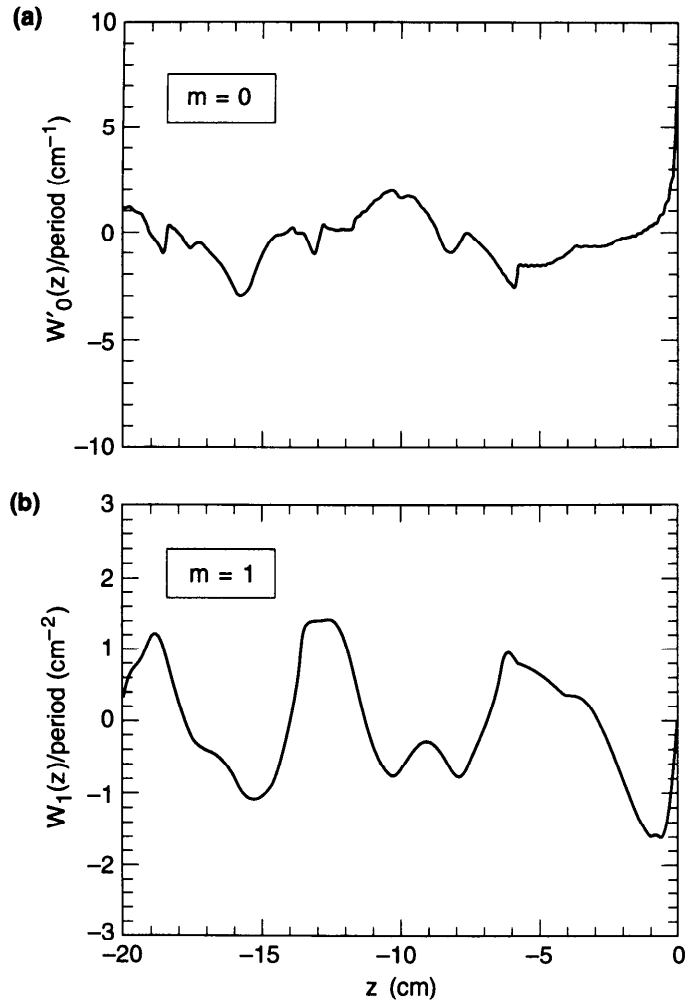

Figure 2.26. Wake functions per cavity period for the SLAC linac. (a) is for W'_0 and (b) is for W_1.

magnitude of these wakes agrees with the rough estimates (2.114) if we take b to be the disk hole radius, 1.163 cm.

The wake functions shown in Figure 2.26 are not accurate for short ranges ($|z| \lesssim 0.3$ mm). To calculate the short range behavior of the wake functions accurately, it is necessary to find modes whose frequencies are higher than 150 GHz. The behavior of the impedance at high frequencies much beyond the cutoff frequency $\omega \gg c/b$, or equivalently of wake fields at short distances $|z| \ll b$, is a difficult technical problem which we will not elaborate. It is particularly an important problem in the study of the dynamics of very short beam bunches. In addition to the calculational difficulty of requiring

more higher order modes, the crosstalk between adjacent cavity structures—which we have ignored—becomes relevant at high frequencies.

In the previous section, we introduced a diffraction model which predicted an impedance $Z_0^{\parallel} \propto \omega^{-1/2}$ at high frequencies for a single cavity structure in an infinitely long beam pipe. This $\omega^{-1/2}$ dependence of $Z_0^{\parallel}$ led to the conclusion that an ultrarelativistic point charge loses an infinite amount of energy due to the passage through the cavity structure. For an infinite cavity array—in contrast to a single standalone cavity—of Figure 2.25(a), however, the dependence of the impedance on ω is qualitatively different. In the steady state, a point charge traveling in the pipe cannot lose an infinite amount of energy per cavity, because the field that is available for the cavity to scrape was established only since the passage of the previous cavity. Calculation of the impedance at high frequencies for an infinite cavity array will not be given here.[50] The high-frequency impedance is found to be

$$Z_0^{\parallel}(\omega) \propto \omega^{-3/2}. \tag{2.175}$$

The ω-dependence (2.175) is confirmed numerically by the fact that the loss factor per unit frequency interval, $dk/d\omega$, in Figure 2.25(b) scales like $\omega^{-3/2}$ at high frequencies.[47]

One way to include the short-range behavior of the wake functions is to make an analytic extrapolation assuming $dk/d\omega$ is strictly proportional to $\omega^{-3/2}$ at high frequencies. This extension, if included, would change Figures 2.26(a) and (b) at short distances by about 10%.

The fact that the real parts of the impedances in Figure 2.25 consist of δ-function peaks is due to the assumptions that the vacuum chamber wall is infinitely conducting and that the cavity structure is infinitely periodic. When there are only a small number of cavity structures in the entire pipe or when the cavity walls are not perfectly conducting, the impedance actually looks like that sketched in Figure 2.27.

For modes whose frequencies are below the cutoff frequency $\sim c/b$, the wake fields are trapped by the cavity and ring in the cavity after the beam has departed. The widths of these modes are determined by the resistivity on the cavity wall and are described by the quality factor Q.

[50]Interested readers should read L. A. Veinshtein, Sov. Phys. JETP **17**, 709 (1963); A. M. Sessler, unpublished communication cited in E. Keil, Nucl. Instr. Meth. **100**, 419 (1972); D. Brandt and B. Zotter, CERN-ISR/TH/82-13 (1982). This approach is referred to in the literature as the *optical resonator model*. More discussions, including the transition from a single cavity to an infinite cavity array, can be found in R. L. Gluckstern, Phys. Rev. D **39**, 2733 (1989); H. Henke, Part. Accel. **25**, 183 (1990); P. B. Palmer, Part. Accel. **25**, 97 (1990); S. A. Heifets and S. A. Kheifets, Rev. Mod. Phys. **63**, 631 (1991); R. L. Gluckstern, *Proc. IEEE Part. Accel. Conf.*, Chicago, 1989, p. 1157.

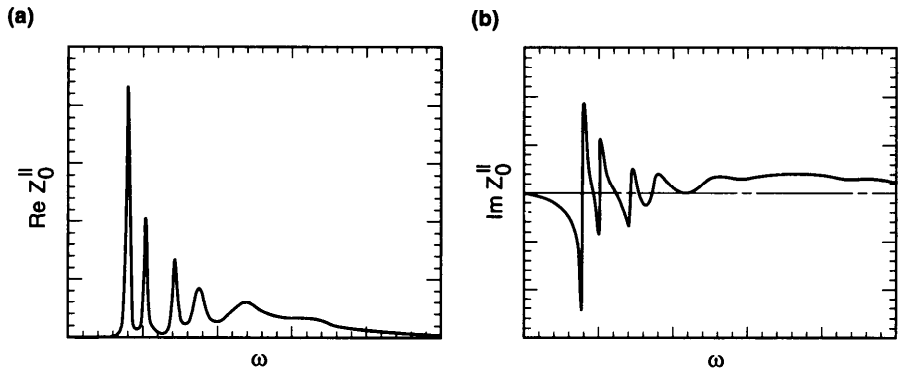

Figure 2.27. Sketch of the real and imaginary parts of a typical-looking impedance for a small number of cavities in series.

A rough estimate of Q for a cavity mode can be obtained by[43]

$$Q \approx \frac{V}{S\,\delta_{\text{skin}}}, \tag{2.176}$$

where V and S are the volume and the total surface area of the cavity, and δ_{skin} is the skin depth evaluated at the mode frequency. For the SLAC linac cavity, we have $V/S \approx 1$ cm and $f \approx 2.8$ GHz for the fundamental cavity mode. Taking $\sigma = 5 \times 10^{17}\ \text{s}^{-1}$ for copper, we find $\delta_{\text{skin}} \approx 1.3\ \mu\text{m}$ and $Q \approx 6 \times 10^3$. Larger cavities tend to have higher Q-values because of the larger value V/S (even though the lower mode frequency makes δ_{skin} larger). For superconducting cavities, Q can be as high as 10^9 or more.

Below the cutoff frequency c/b, the impedance consists more or less of discrete modes. Above cutoff, the wake field leaks out of the cavity and propagates in the pipe. The impedance in this region forms a continuum. Roughly, one can obtain this part of the impedance from that of Figure 2.25 by spreading each impedance peak over a width of $\Delta\omega/\omega \sim 1/N$, where N is the number of cavities in series. For this reason, the impedances are often either sharply peaked (below cutoff) or broad-banded (above cutoff) and not often in between. The corresponding wakes either ring for a long time or decohere quickly after being excited.

Time Domain

As mentioned at the beginning of this section, wake fields and impedances can also be calculated in the time domain by integrating the Maxwell equations. Below we will illustrate this technique by considering the $m = 0$ wake generated by an ultrarelativistic beam in an axially symmetric, perfectly conducting, vacuum chamber pipe. We will follow the illustration by

Weiland.[51] The beam is considered to be a ring charge moving along the pipe axis in the $\hat{s}$-direction with the speed of light c, i.e.,

$$\rho = \frac{1}{2\pi a}\delta(r-a)\lambda(s-ct) \quad \text{and} \quad \vec{j} = c\rho\hat{s}. \tag{2.177}$$

To proceed, we first write down the integral form of the Maxwell equations,

$$\begin{aligned}
&\oint d\vec{\mathscr{A}} \cdot \vec{E} = 4\pi \int dV \rho, \\
&\oint d\vec{\mathscr{A}} \cdot \vec{B} = 0, \\
&\oint d\vec{l} \cdot \vec{E} = -\frac{1}{c}\int d\vec{\mathscr{A}} \cdot \frac{\partial \vec{B}}{\partial t}, \\
&\oint d\vec{l} \cdot \vec{B} = \frac{1}{c}\int d\vec{\mathscr{A}} \cdot \frac{\partial \vec{E}}{\partial t} + \frac{4\pi}{c}\int d\vec{\mathscr{A}} \cdot \vec{j}.
\end{aligned} \tag{2.178}$$

The space inside the pipe is then divided into a grid of meshes. Because of the axial symmetry, each mesh accounts for a toroidal region axially symmetric around the axis. For simplicity, we assume the grids are divided evenly along the r- and the s-dimensions with grid sizes Δr and Δs. The ring beam size a in Eq. (2.177) is supposed smaller than the mesh size Δr.

The time t is also divided into discrete steps; the lth step occurs at time $t = l\,\Delta t$. The electromagnetic field components $E_r^{m,n,l}$, $E_s^{m,n,l}$, and $B_\theta^{m,n,l}$ (other field components vanish for $m = 0$) of the (m, n)th mesh, at the lth time step, are shown in Figure 2.28. The electric and magnetic field components are defined at interleaving, discrete locations as shown. Having defined the fields on the mesh grid, we are now ready to apply the Maxwell equations (2.178).

Take the third member of Eq. (2.178) first. Integrating around the rectangle of the (m, n)th mesh gives

$$\Delta s E_s^{m,n,l} + \Delta r E_r^{m+1,n,l} - \Delta s E_s^{m,n+1,l} - \Delta r E_r^{m,n,l} = -\frac{1}{c}\Delta s\,\Delta r\left(\frac{\partial B_\theta}{\partial t}\right)^{m,n,l}. \tag{2.179}$$

On the right hand side of Eq. (2.179) appears the time derivative of the

[51] T. Weiland, CERN/ISR-TH/80-07 (1980); Thomas Weiland, Part. Accel. **15**, 245 (1984).

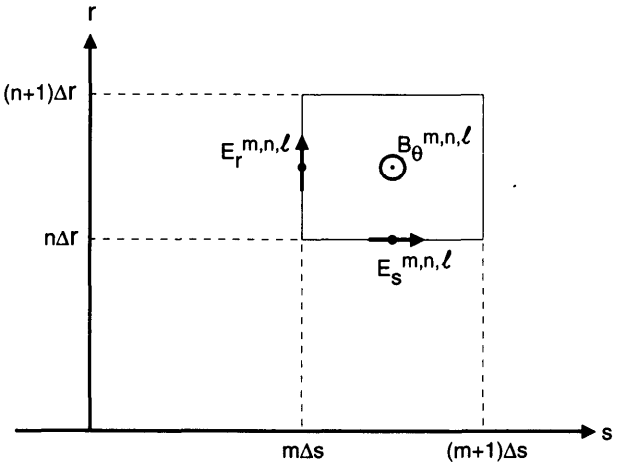

Figure 2.28. The (m, n)th mesh in the calculation of the axially symmetric time-domain wake field. The meshes are generated in the half plane defined by $\theta = 0$. For simplicity, we assume uniform mesh sizes Δr and Δs. The electromagnetic field components E_r, E_s, and B_θ at the lth time step $t = l\Delta t$ are defined at positions indicated.

magnetic field. To evaluate this time derivative, the magnetic field is evaluated at times $\Delta t/2$ away from the electric fields, and the time derivative can be written as

$$\left(\frac{\partial B_\theta}{\partial t}\right)^{m,n,l} = \frac{1}{\Delta t}\left(B_\theta^{m,n,l+1/2} - B_\theta^{m,n,l-1/2}\right). \tag{2.180}$$

This method of alternating the time steps between electric and magnetic fields is referred to in the literature as the *alternating explicit time scheme*, and was suggested by Yee.[52] Substituting Eq. (2.180) into (2.179) gives an expression for B_θ in terms of field components at earlier times according to

$$B_\theta^{m,n,l+1/2} = B_\theta^{m,n,l-1/2} - c\,\Delta t\left(\frac{E_s^{m,n,l} - E_s^{m,n+1,l}}{\Delta r} + \frac{E_r^{m+1,n,l} - E_r^{m,n,l}}{\Delta s}\right). \tag{2.181}$$

We now turn to the fourth member of Eq. (2.178). This equation gives two equations according to the choice of the integration surface. If we choose the integration surface to be the one generated by rotating the line segment between the centers of the (m, n)th mesh and the $(m + 1, n)$th mesh around

[52] Kane S. Yee, IEEE Trans. Antennas & Propagation **SP-14**, 302 (1966).

the axis, we obtain, at time $(l + \frac{1}{2})\Delta t$,

$$B_\theta^{m,n,l+1/2} 2\pi\left(n + \frac{1}{2}\right)\Delta r - B_\theta^{m+1,n,l+1/2} 2\pi\left(n + \frac{1}{2}\right)\Delta r = \frac{1}{c}\Delta s\, 2\pi\left(n + \frac{1}{2}\right)\Delta r\left(\frac{\partial E_r}{\partial t}\right)^{m+1,n,l+1/2}. \tag{2.182}$$

The time derivative of the electric field component is written as

$$\left(\frac{\partial E_r}{\partial t}\right)^{m+1,n,l+1/2} = \frac{1}{\Delta t}\left(E_r^{m+1,n,l+1} - E_r^{m+1,n,l}\right). \tag{2.183}$$

Combining Eqs. (2.182–2.183) gives an expression of E_r in terms of the field components at earlier times

$$E_r^{m+1,n,l+1} = E_r^{m+1,n,l} + \frac{c\,\Delta t}{\Delta s}\left(B_\theta^{m,n,l+1/2} - B_\theta^{m+1,n,l+1/2}\right). \tag{2.184}$$

If we choose the surface generated by rotating the line segment between the centers of the (m, n)th mesh and the $(m, n + 1)$th mesh around the axis, we obtain at time $t = (l + \frac{1}{2})\Delta t$ (except for the case $n = -1$, which contains the beam)

$$-B_\theta^{m,n,l+1/2} 2\pi\left(n + \frac{1}{2}\right)\Delta r + B_\theta^{m,n+1,l+1/2} 2\pi\left(n + \frac{3}{2}\right)\Delta r = \frac{1}{c}\left[\pi\left(n + \frac{3}{2}\right)^2 \Delta r^2 - \pi\left(n + \frac{1}{2}\right)^2 \Delta r^2\right]\left(\frac{\partial E_s}{\partial t}\right)^{m,n+1,l+1/2}. \tag{2.185}$$

Expressing the time derivative as in Eqs. (2.180) and (2.183), we arrive at an expression for E_s $(n \neq -1)$:

$$E_s^{m,n+1,l+1} = E_s^{m,n+1,l} + \frac{c\,\Delta t}{\Delta r}\left(-\frac{n + \frac{1}{2}}{n+1} B_\theta^{m,n,l+1/2} + \frac{n + \frac{3}{2}}{n+1} B_\theta^{m,n+1,l+1/2}\right). \tag{2.186}$$

For the meshes with $n = -1$, which contain the beam, the surface is the circular disk of radius $\Delta r/2$ oriented perpendicularly to the axis. Let the beam current be defined at the discrete locations $s = (m + \frac{1}{2})\Delta s$ along the axis. Let $\lambda^{m,l+1/2}\Delta s$ be the beam charge between $s = m\,\Delta s$ and $(m + 1)\Delta s$

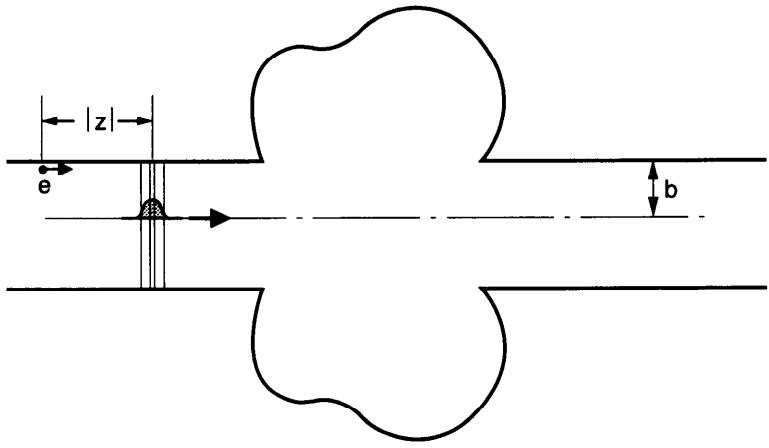

Figure 2.29. Configuration of the beam, the cavity, and the electromagnetic fields when the numerical integration of the Maxwell equations is launched. A test charge e is included in order to calculate the wake function $W_0'(z)$.

at time $(l + \frac{1}{2})\,\Delta t$. An application of the fourth member of Eq. (2.178) gives

$$B_\theta^{m,0,l+1/2} 2\pi \frac{\Delta r}{2} = \frac{\pi}{c}\left(\frac{\Delta r}{2}\right)^2 \left(\frac{\partial E_s}{\partial t}\right)^{m,0,l+1/2} + 4\pi\lambda^{m,l+1/2}, \quad (2.187)$$

which in turn gives

$$E_s^{m,0,l+1} = E_s^{m,0,l} + \frac{4c\,\Delta t}{\Delta r} B_\theta^{m,0,l+1/2} - \frac{16c\,\Delta t}{\Delta r^2}\lambda^{m,l+1/2}. \quad (2.188)$$

Equations (2.181), (2.184), (2.186), and (2.188) are our time domain numerical representation of the Maxwell equations. The remaining members of Eq. (2.178) are automatically satisfied. The meshes have to be distorted near the pipe wall to match the wall geometry. The boundary conditions that the electric field must be perpendicular to the wall surface and that the magnetic field must be tangential to the surface are straightforward to incorporate.

To start the numerical integration, at times $t = 0$ and $t = \Delta t/2$, the field configuration in the beam pipe is prepared as shown in Figure 2.29. The electromagnetic fields are just the pancake fields, and the cavity is empty. The Maxwell equations are then integrated in subsequent time steps to obtain the fields at all times and locations.

To account for the beam charges properly, Δs is chosen to be an integral multiple of $c\,\Delta t$, i.e.,

$$\Delta s = Nc\,\Delta t. \quad (2.189)$$

To assure numerical convergence,[53] we need to have

$$c\,\Delta t \leq \frac{1}{\sqrt{\frac{1}{\Delta r^2} + \frac{1}{\Delta s^2}}}. \tag{2.190}$$

Combining Eqs. (2.189–2.190), we obtain a limit on the number of time steps per longitudinal step,

$$N \geq \sqrt{\left(\frac{\Delta s}{\Delta r}\right)^2 + 1}\,. \tag{2.191}$$

For example, one may choose $\Delta r = \Delta s = 2c\,\Delta t$.

Calculation of wake functions is most difficult at short distances. To calculate the wake functions down to a small distance d, the mesh sizes must be chosen smaller than or equal to d. The total number of meshes, and therefore the computer memory required, is proportional to d^{-2} (d^{-3} without axial symmetry). Since the total number of time steps is proportional to d^{-1}, the computer CPU time to perform the field calculation is then proportional to d^{-3} (d^{-4} without axial symmetry). The computational expense escalates very rapidly if short range wake information is needed.

To calculate the wake functions, a beam bunch (say a Gaussian bunch) of length σ_z in the configuration shown in Figure 2.29 is launched to drive the wake fields. The bunch length is chosen to be comparable to d. The wake fields are calculated at all grid points and all time steps as prescribed above. Also shown in Figure 2.29 is a test charge e that trails the driving bunch by a fixed longitudinal distance $|z|$. The longitudinal force experienced by this test charge is integrated as it traverses the vacuum chamber structure. As we proved in Eq. (2.50), the integrated longitudinal force on the test charge depends on z, but not on the radial position r of the test charge for the $m = 0$ mode. This powerful property gives us the freedom of locating the test charge at any r and obtaining the same result. In Figure 2.29, the test charge is located immediately inside the vacuum chamber pipe boundary $r = b$. This has the advantage that, because the longitudinal electric field vanishes on the pipe wall, the integration of the wake force needs to be performed only in the cavity region. The wake function $W_0'(z)$ is then obtained by integrating the force on the test charges at varying distances $|z|$ behind the driving beam. The impedance $Z_0^{\parallel}(\omega)$ follows by performing a Fourier transformation on $W_0'(z)$.

The above calculation was implemented, for example, in the program BCI of Weiland.[54] It can be generalized to the $m \neq 0$ modes. In those cases, all

[53]Allen Taflove and Morris E. Brodwin, IEEE Trans. Microwave Theory & Techniques **MTT-23**, 623 (1975).

[54]T. Weiland, *Proc. 11th Int. Conf. High Energy Accel.*, CERN, 1980, p. 570.

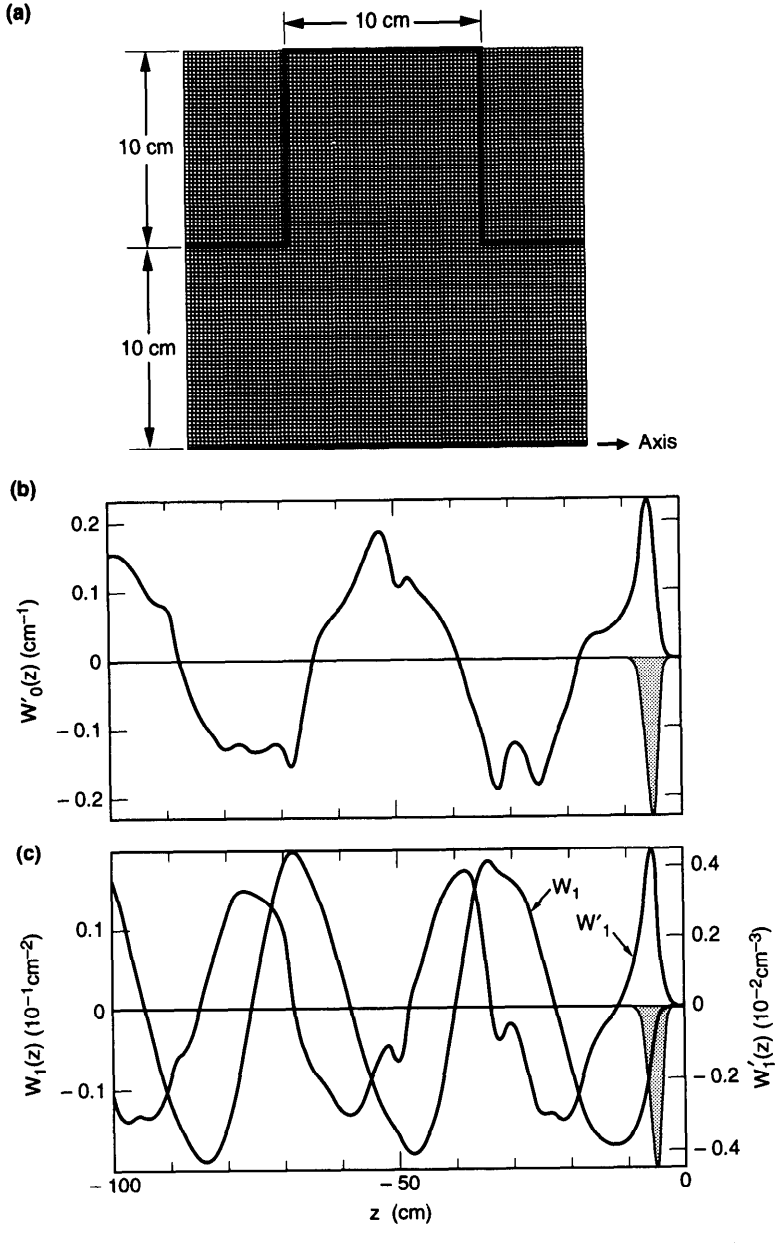

Figure 2.30. A time domain calculation of wake functions for a single cavity using the program TBCI. (a) The cavity geometry and the mesh used for the calculation. (b) The wake function $W_0'(z)$ calculated using a Gaussian driving beam (shaded curve) with $\sigma_z = 1$ cm. The peak of the driving beam is located at $z = -5$ cm. (c) Wake function $W_1(z)$ and $W_1'(z)$. (Courtesy Tom Weiland, Weiren Chou, and Bo Chen, 1991.)

six field components have to be included. This has been implemented for example in the program TBCI.[55] Although in the $m \neq 0$ cases one is most likely interested in the transverse wake functions, the integration being performed is the longitudinal wake on the test charge e. The transverse wake is obtained by integrating the longitudinal wake over z.

Shown in Figure 2.30 are some results of a wake function calculation using TBCI for a single cavity. These results are to be compared with the $b = 10$ cm case shown in Figure 2.18 using the broad-band resonator model. The agreement at short distance $|z| \lesssim b$ is reasonable. In the range between b and a few times b, the broad-band model somewhat underestimates the wakes. At long ranges, the model of course misrepresents the ringing part of the wakes, as seen in Figure 2.30.

Exercise 2.30 There is an error associated with using a bunch of finite length to derive the wake functions numerically. Suppose $\overline{W}(z)$ is the wake function found numerically by using a Gaussian beam of rms length σ_z, and $\overline{Z}(\omega)$ is the impedance obtained by Fourier transforming $\overline{W}(z)$. Show that the actual impedance is given by

$$Z(\omega) = \overline{Z}(\omega)\, e^{\omega^2\sigma_z^2/2c^2}. \tag{2.192}$$

Although Eq. (2.192) means in principle one can obtain $Z(\omega)$ by using a Gaussian beam of arbitrary length, the numerical accuracy becomes doubtful when $\omega \gtrsim c/\sigma_z$.

2.5 PARASITIC LOSS

As a beam traverses an impedance, it loses a certain amount of energy to the impedance. This energy loss, given by Eqs. (2.102–2.103), is referred to as the *parasitic loss* of the beam. For example, the space charge force does not cause any net parasitic loss on a beam, because its impedance is purely imaginary. Physically this is because particles exert forces on each other; energy gain of one particle necessarily means energy loss of an equal amount by another particle. The total energy loss of the beam, the parasitic loss, is therefore zero. A resistive wall, on the other hand, does induce parasitic losses. For a Gaussian bunch with

$$\rho(z) = \frac{q}{\sqrt{2\pi}\,\sigma_z} e^{-z^2/2\sigma_z^2} \quad \text{and} \quad \tilde{\rho}(\omega) = q\, e^{-\omega^2\sigma_z^2/2c^2}, \tag{2.193}$$

the parasitic loss rate is obtained by substituting the impedance (2.75) into

[55] T. Weiland, Nucl. Instr. Meth. **212**, 13 (1983).

Eq. (2.103). The result is

$$\frac{\Delta \mathscr{E}}{L} = \begin{cases} -\dfrac{2q^2}{b^2} & \text{if} \quad \sigma_z \ll \chi^{1/3} b, \\ -\dfrac{1}{2\pi}\Gamma\left(\dfrac{3}{4}\right)\dfrac{q^2}{b\sigma_z^{3/2}}\sqrt{\dfrac{c}{2\pi\sigma}} & \text{if} \quad \sigma_z \gg \chi^{1/3} b, \end{cases} \tag{2.194}$$

where χ is the small parameter defined by Eq. (2.10) and $\Gamma(x)$ is the gamma function. Take for example $q = 10^{11}\, e$, $\sigma_z = 10$ cm, $b = 5$ cm, $\Gamma(\frac{3}{4}) = 1.23$, and an aluminum pipe with $\sigma = 3 \times 10^{17}\ \text{s}^{-1}$; the long bunch limit of Eq. (2.194) applies, and the average energy loss rate per particle in the bunch is about 0.2 eV/m. Although this is a small energy loss, the heating of the vacuum chamber walls may not be negligible for superconducting accelerators if this heat is to be removed at liquid helium temperature. This is one reason why it is sometimes desirable to coat the inside of the vacuum chamber with copper for these accelerators.[56]

The short bunch result for $\sigma_z \ll \chi^{1/3} b$ in Eq. (2.194) is just Eq. (2.27) reproduced. Aside from a numerical factor, the long bunch ($\sigma_z \gg \chi^{1/3} b$) result, which is more relevant in practice, can be understood from

$$\frac{\Delta \mathscr{E}}{L} \sim \frac{1}{\sigma A} J^2 \Delta t, \tag{2.195}$$

where the heating is generated by a current $J \sim qc/\sigma_z$ that flows in a cross-sectional area of $A \sim 2\pi b\, \delta_{\text{skin}}$ (where δ_{skin} is the skin depth evaluated at frequency $\omega \sim c/\sigma_z$) and lasts for a time $\Delta t \sim \sigma_z/c$. See Figure 2.10. The long bunch loss is smaller than the point bunch limit by a factor of $\sim (\chi^{1/3} b/\sigma_z)^{3/2}$.

Exercise 2.31 Consider a beam (not necessarily Gaussian) which travels with a transverse offset a from the pipe axis. By summing over all multipole moments of order m, show that, in the long bunch limit, the resistive wall heating is increased from that of a centered beam by a factor of $(b^2 + a^2)/(b^2 - a^2)$. The loss becomes infinite as a approaches the pipe radius b. The short bunch limit was obtained before in Eq. (2.45).

In case the vacuum chamber pipe contains a structure which is modeled by the resonator impedance (2.82) with the corresponding wake function (2.84),

[56] Particularly if the vacuum chamber pipe is made of stainless steel.

the energy loss of a Gaussian bunch as it traverses the structure is

$$\Delta\mathscr{E} = -\frac{q^2 R_S c}{\pi\sigma_z} f\left(\frac{\omega_R \sigma_z}{c}, Q\right), \tag{2.196}$$

where we have defined a dimensionless function[57]

$$f(u, Q) = \int_0^\infty dx \frac{e^{-x^2}}{1 + Q^2\left(\frac{u}{x} - \frac{x}{u}\right)^2}. \tag{2.197}$$

If the bunch length is much longer than the resonant wavelength of the impedance, i.e., $\sigma_z \gg c/\omega_R$, the energy loss becomes

$$\Delta\mathscr{E} \approx -\frac{q^2 R_S c^3}{4\sqrt{\pi} Q^2 \omega_R^2 \sigma_z^3}. \tag{2.198}$$

The parasitic loss is proportional to σ_z^{-3} for long bunches. For short bunches, $\sigma_z \ll c/\omega_R$, one finds the point charge limit [Cf. Eq. (2.149)]

$$\Delta\mathscr{E} \approx -\frac{q^2 R_S \omega_R}{2Q}. \tag{2.199}$$

which is independent of σ_z, because $\Delta\mathscr{E}$ is simply related to the area under Re $Z_0^\parallel$ [Eq. (2.83)].

Figure 2.31 shows the function $f(u, Q)$. The dashed curves are the long bunch and short bunch limits (2.198–2.199). One observes that for the $Q = 1$ case the long bunch approximation is already reasonably accurate when $u = \omega_R \sigma_z / c \approx 1$. With a broad-band resonator (2.121) for a cavity size ~ 5 cm, and a beam bunch with $q = 10^{11}\, e$ and $\sigma_z = 20$ cm, the average energy loss of a particle in the bunch is 60 eV per traversal of the cavity. The total energy loss from the beam bunch is 10 erg, and, recalling the discussion leading from Eq. (2.116) to (2.117), about half of that energy is deposited in the cavity proper.

In a circular accelerator, one could also express Eqs. (2.198–2.199) in terms of $Z_0^\parallel/n$ of the resonator. To do this, one might identify $|Z_0^\parallel/n|$ as the slope of Im $Z_0^\parallel$ with respect to $n = \omega/\omega_0$ for small ω,

$$\left|\frac{Z_0^\parallel}{n}\right| \approx \frac{R_S \omega_0}{Q\omega_R}, \tag{2.200}$$

[57] $f(u, Q)$ can also be expressed in terms of the complex error function. See M. Furman, H. Lee, and B. Zotter, *Proc. IEEE Part. Accel. Conf.*, Washington, 1987, p. 1049.

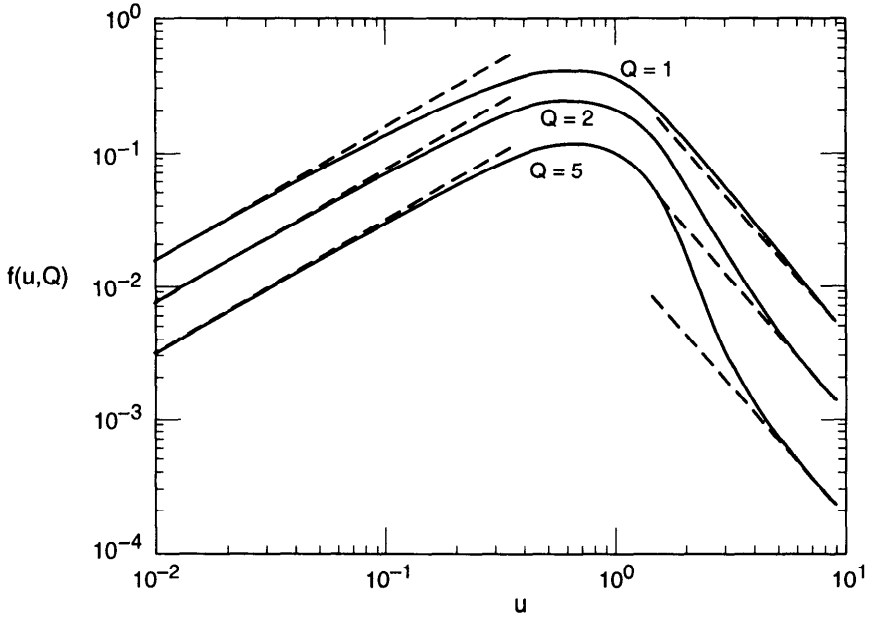

Figure 2.31. The function $f(\upsilon, Q)$ of Eq. (2.197) versus $\upsilon = \omega_R \sigma_z / c$ for $Q = 1, 2, 5$. Dashed curves are the approximations $f(\upsilon, Q) \approx \sqrt{\pi} / (4Q^2\upsilon^2)$ for $\upsilon \gg 1$ (the long bunch limit) and $f \approx \pi\upsilon / 2Q$ for $\upsilon \ll 1$ (the short bunch limit).

which in turn gives the parasitic loss power

$$P_{\text{parasitic}} = -\frac{\Delta\mathscr{E}}{T_0} \approx \begin{cases} -\dfrac{q^2c^3}{8\pi^{3/2}Q\omega_R\sigma_z^3}\left|\dfrac{Z_0^{\parallel}}{n}\right|, & \text{long bunch,} \\ -\dfrac{q^2\omega_R^2}{4\pi}\left|\dfrac{Z_0^{\parallel}}{n}\right|, & \text{short bunch,} \end{cases} \tag{2.201}$$

where $T_0 = 2\pi/\omega_0 = 2\pi R/c$ is the period of revolution of the beam around the accelerator. Taking $\omega_R = 3$ GHz, $q = 10^{11}\,e$, $\sigma_z = 20$ cm, and $Z_0^{\parallel}/n = 1\ \Omega$ (one 60 Ω broad-band resonator impedance every 38 m), we have $P_{\text{parasitic}} = 8$ W.

Conversely, Eq. (2.201) can be used to estimate the impedance $|Z_0^{\parallel}/n|$ of an accelerator by measuring the parasitic loss of a stored beam. (See also footnote 16 of Chapter 6.) Take the electron storage ring SPEAR II, for example; the loss factor $k = \Delta\mathscr{E}/q^2$ was measured to be 8 V/pC when $\sigma_z = 4.5$ cm.[58] Taking $2\pi R = 240$ m, $\omega_R = 8$ GHz, and $Q = 1$, and using the

[58] P. B. Wilson et al., IEEE Trans. Nucl. Sci. **NS-24**, 1211 (1977).

long bunch formula, one obtains $|Z_0^{\parallel}/n| = 12\ \Omega$. (SPEAR II had a relatively large impedance because it has an early vacuum chamber design.) An equivalent of 6% of the circumference is occupied by cavity-like objects according to Eq. (2.124).

When the wake function is expressed in mode expansion [Eq. (2.148)], the parasitic loss is given by

$$\Delta\mathscr{E} = -\sum_{\lambda} k_{\lambda} |\tilde{\rho}(\omega_{\lambda})|^2. \tag{2.202}$$

For a Gaussian bunch,

$$\Delta\mathscr{E} \equiv -q^2 k_{\text{Gauss}} = -q^2 \sum_{\lambda} k_{\lambda}\, e^{-\omega_{\lambda}^2 \sigma_z^2/c^2}. \tag{2.203}$$

For a point charge ($\sigma_z = 0$), we recover Eq. (2.149). When the cavity structure and the bunch length are both comparable to the vacuum chamber pipe radius b, the parasitic loss of the beam is roughly $\sim q^2/b$.

Using the loss factor k_{λ} in Eq. (2.173), we can calculate the parasitic loss of a Gaussian bunch traversing a closed cavity modeled as two parallel plates. This gives

$$\Delta\mathscr{E} = -q^2 \sum_{p=0}^{\infty} \int_{-\infty}^{\infty} dk_x \int_{-\infty}^{\infty} dk_y\, k_{\lambda}\, e^{-\omega_{\lambda}^2 \sigma_z^2/c^2} = -\frac{q^2}{L} f\left(\frac{\sigma_z}{L}\right), \tag{2.204}$$

where

$$f(u) = 2\int_0^{\infty} \frac{d\alpha}{\alpha} e^{-\alpha^2 u^2}(1 - \cos\alpha) + 4\sum_{p=1}^{\infty} \int_0^{\infty} \frac{d\alpha}{\alpha} e^{-p^2\pi^2 u^2(1+\alpha^2)}\left[1 - (-1)^p \cos\left(p\pi\sqrt{1+\alpha^2}\right)\right]. \tag{2.205}$$

The first term in $f(u)$ comes from the lowest longitudinal $p = 0$ mode in the cavity. Figure 2.32 shows the behavior of $f(u)$. For $u \gtrsim 0.5$, almost all energy deposited in the cavity is in the $p = 0$ mode. For a point bunch, $u \to 0$, the parasitic loss is infinite. In case $u \gtrsim 1$, the first term in $f(u)$ is approximately

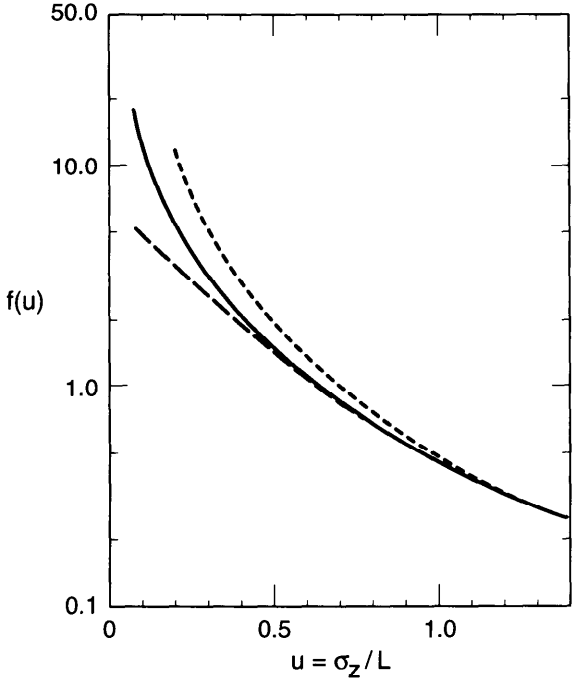

Figure 2.32. The function $f(u)$ of Eq. (2.205) versus $u = \sigma_z / L$. The dashed curve is the first term on the right hand side of Eq. (2.205), representing the energy deposited into the $p = 0$ mode only. The dotted curve is the approximation $f(u) \approx 1 / 2u^2$ for $u \gg 1$.

equal to $1/2u^2$. Therefore, when $\sigma_z \gtrsim L$, the parasitic loss is approximately

$$\Delta\mathscr{E} \approx -\frac{q^2 L}{2\sigma_z^2}. \tag{2.206}$$

Taking $q = 10^{11}\, e$, $L = 10$ cm, $\sigma_z = 20$ cm, the average energy loss per particle going through this cavity is 170 eV.

Let us examine the structure of Eqs. (2.198) and (2.206), both applicable for long bunches. Consider a broad-band resonator with $Q \sim 1$, and write $\Delta\mathscr{E}$ of Eq. (2.198) as $\sim J^2 Z_0^{\parallel} \Delta t$, where $J \sim qc/\sigma_z$ and $\Delta t \sim \sigma_z/c$. We obtain $Z_0^{\parallel} \sim R_S (L/\sigma_z)^2$, where $L = c/\omega_R$ is the characteristic dimension of the cavity. This means the long bunch has introduced a suppression form factor $(L/\sigma_z)^2$ on the effective impedance. Similar analysis of Eq. (2.206) leads to a suppression factor of L/σ_z. Closed cavities suppress less and tend to overestimate the parasitic loss for long bunches.

Exercise 2.32

(a) Use Eqs. (2.164) and (2.174) to show that the parasitic loss deposited in the two-parallel-plate cavity by a Gaussian bunch with a net mth

moment I_m is given by

$$\Delta\mathscr{E} = -\frac{I_m^2}{L}\frac{4}{(1+\delta_{m0})(m!)^2 2^{2m}} \times\left\{\int_0^\infty \frac{d\alpha}{\alpha}\left(\frac{\alpha}{L}\right)^{2m} e^{-\sigma_z^2\alpha^2/L^2}(1-\cos\alpha) +2\sum_{p=1}^{\infty}\int_0^\infty \frac{d\alpha}{\alpha}\left(\frac{\alpha p\pi}{L}\right)^{2m} e^{-\sigma_z^2 x^2/L^2}\left[1-(-1)^p\cos x\right]\right\}, \tag{2.207}$$

where $x = p\pi\sqrt{1+\alpha^2}$.

(b) Consider a Gaussian bunch with total charge q traversing the two-parallel-plate cavity with a transverse displacement a. Represent this bunch going through the infinitesimal openings as a superposition of multipole modes m and show that the parasitic loss of the off-centered bunch is

$$\Delta\mathscr{E} = -\frac{2q^2}{L}\left\{\int_0^\infty \frac{d\alpha}{\alpha}\left[2I_0\left(\frac{a\alpha}{L}\right)-1\right]e^{-\sigma_z^2\alpha^2/L^2}(1-\cos\alpha) +2\sum_{p-1}^{\infty}\int_0^\infty \frac{d\alpha}{\alpha}\left[2I_0\left(\frac{a\alpha p\pi}{L}\right)-1\right] \times e^{-\sigma_z^2 x^2/L^2}\left[1-(-1)^p\cos x\right]\right\}, \tag{2.208}$$

where $x = p\pi\sqrt{1+\alpha^2}$ and $I_0(x)$ is the Bessel function.

(c) Show that, in the long bunch limit $\sigma_z \gtrsim L$, if $L \gg a$, the parasitic loss of the offset bunch is larger than that of the centered bunch, Eq. (2.206), by a factor of $1 + a^2/2\sigma_z^2$.

Figure 2.33 shows the net loss factor k_{Gauss} per cavity as a function of bunch length σ_z for the SLAC linac using the loss factors k_λ in Figure 2.25(b) and Eq. (2.203). The parasitic loss is sensitive to the bunch length, especially for short bunches. For bunches longer than the wavelength of the fundamental cavity mode, the parasitic loss is small because the bunch tail recovers part of the energy lost by the bunch head.

Figure 2.33 is based on the calculated cavity modes up to 150 GHz. Results shown for bunch lengths $\sigma_z \lesssim 0.03$ cm or so assume the contribution from higher order modes is negligible, which will be true if the high

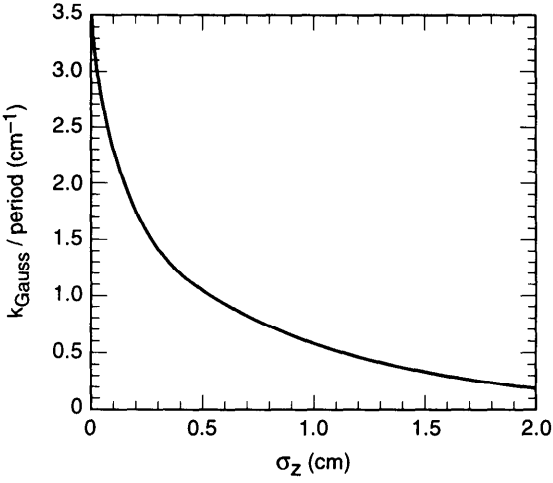

Figure 2.33. Loss factor k_{Gauss} per cavity as a function of bunch length σ_z for the SLAC linac. Shorter bunches suffer larger parasitic losses.

frequency impedance behaves according to Eq. (2.175). If so, $k_{\text{Gauss}}(\sigma_z = 0) = \frac{1}{2}W_0'(0^-) \approx 3.5\ \text{cm}^{-1}$, as shown in Figures 2.26(a) and 2.33. Taking for example $\sigma_z = 1$ mm, $q = 5 \times 10^{10}e$, and cavity length $L = 3.5$ cm, the average parasitic loss per particle of the bunch propagating down the length of the SLAC linac of 3000 m is about 1.5 GeV.

Exercise 2.33 Consider a 10 km linac with a fundamental accelerating mode frequency of $\omega_R = 2\pi \times 20$ GHz. Estimate the parasitic loss per particle in a beam bunch with $q = 10^{10}e$. [Hint: Take cavity structure dimension ~ pipe radius $b \sim c/\omega_R$, W_0' per cavity $\sim 1/b$, and $\Delta\mathscr{E}$ per cavity $\sim -q^2W_0'/2$.]

Equations (2.102–2.103) are valid for a beam traversing the impedance once. In a circular accelerator, the situation is somewhat different. As the beam traverses an impedance, it sees not only the wake field generated during this traversal, but also all traversals made in previous revolutions. The energy loss can then be written as (take $m = 0$)

$$\Delta\mathscr{E} = -\int_{-\infty}^{\infty} dz'\,\rho(z')\int_{-\infty}^{\infty} dz\,\rho(z)\sum_{k=-\infty}^{\infty} W_0'(kC + z' - z), \quad (2.209)$$

where C is the circumference of the accelerator, k sums over revolutions, and we have used the fact that $W_0'(z) = 0$ if $z > 0$.

It is more convenient to express Eq. (2.209) in terms of impedance. To do so, we will use the following identity (the Poisson sum formula):

$$\sum_{k=-\infty}^{\infty} F(kC) = \frac{1}{C} \sum_{p=-\infty}^{\infty} \tilde{F}\left(\frac{2\pi p}{C}\right), \tag{2.210}$$

where $F(z), \tilde{F}(k)$ are arbitrary Fourier transform pairs. In other words, summing a function at a regular interval C is equal to summing over its Fourier transform at the regular intervals $2\pi/C$. A particularly useful special case of Eq. (2.210) is

$$\sum_{k=-\infty}^{\infty} e^{ikx} = 2\pi \sum_{p=-\infty}^{\infty} \delta(x - 2\pi p). \tag{2.211}$$

Using Eq. (2.210), the summation over W_0' in Eq. (2.209) becomes a summation over the total impedance $Z_0^{\parallel}$ in a circular accelerator. The energy loss of a beam per revolution then becomes

$$\Delta\mathscr{E} = -\frac{\omega_0}{2\pi} \sum_{p=-\infty}^{\infty} |\tilde{\rho}(p\omega_0)|^2 \operatorname{Re} Z_0^{\parallel}(p\omega_0), \tag{2.212}$$

where $\omega_0 = 2\pi c/C$ is the revolution frequency and $\tilde{\rho}(\omega)$ is the Fourier transform of $\rho(z)$ according to Eq. (2.104). Here we see one manifestation of the usefulness of the impedance concept; Eq. (2.212) contains a single summation, but Eq. (2.209) involves a summation and a double integral.

In case the range of the wake field is shorter than the accelerator circumference, one would expect the difference between the multiturn and single-pass results to disappear. To demonstrate this, note that in this case the impedance $Z_0^{\parallel}(\omega)$ cannot have sharp structures in any frequency interval $\Delta\omega \lesssim \omega_0$. This means the summation over p in Eq. (2.212) can be replaced by an integration over p. Equation (2.212) then reduces to Eq. (2.103), as it should. In case the wake field lasts for distances $\gtrsim C$, Eq. (2.212) must be used instead of Eq. (2.103).

Exercise 2.34 Consider a narrow-band resonator impedance with $\omega_R/Q \ll \omega_0$. Let h be the closest integer such that $\omega_R \approx h\omega_0$, and define $\Delta = (h\omega_0 - \omega_R)/\omega_R$. Show that, for a Gaussian bunch with $\sigma_z \ll c/\omega_R|\Delta|$,

$$\Delta\mathscr{E} \approx -\frac{\omega_0 q^2 R_S}{2\pi} \frac{e^{-\omega_R^2\sigma_z^2/c^2}}{1 + 4Q^2\Delta^2}. \tag{2.213}$$

Most of the parasitic loss occurs as the beam traverses a discontinuous structure in the vacuum chamber pipe. Part of the wake field gets trapped by the structure if the structure is cavity-like and if the wake field frequency is

below the cutoff frequency of the pipe. This trapped field energy is eventually deposited as heat on the cavity walls. The rest of the wake field, with frequency higher than the cutoff frequency, propagates down the pipe and eventually deposits its energy on lossy material elsewhere in the vacuum chamber, much like heating a potato in a microwave oven.[59]

The parasitic energy lost by the beam goes into the wake fields. Typically, only a small fraction of the particle energy is depleted to produce the wake fields, and most of the energy stored in the wake fields ends up as heat on the vacuum chamber walls; but under unfavorable conditions, the wake field energy can be transferred systematically back to beam motion, causing beam instabilities. The parasitic loss, therefore, is ultimately responsible for the various collective beam instabilities. How the wake fields affect the beam dynamics and what are the mechanisms of the various collective beam instabilities are subjects to which we will devote the following chapters. The parasitic energy loss, of course, will have to be supplied back to the beam by an rf accelerating voltage.

[59]Next time you put a potato into a microwave oven, think of it as the impedance.

CHAPTER 3

Instabilities in Linear Accelerators

The wake fields discussed in the previous chapter impose an important limitation on the maximum beam intensity that can be accelerated in a linear accelerator (linac). The limitation is manifested through various collective instabilities when the beam intensity is increased. In Chapter 1, we explained how the direct space charge force imposes intensity limits for proton or heavy ion transport lines. In this chapter, we will investigate the effects of wake fields in general on beam dynamics in a linac. The various linac instabilities mentioned in this chapter are also the basic mechanisms underlying many of the instabilities in circular accelerators to be treated in later chapters.

Compared with their circular counterparts, the wake field effects in a high energy linac do not have the complication of synchrotron motion. The relative longitudinal position of a particle in a beam bunch can be considered to be "frozen." This feature considerably simplifies the linac instability mechanism.

Exercise 3.1

(a) Estimate the relative longitudinal position variations of a particle due to its transverse betatron oscillations. Use $dz/ds \approx -y'(s)^2/2$, where $y(s)$ is the betatron displacement. In the presence of acceleration, $y(s)$ is given by Eq. (3.35). Show that the total change in z due to betatron oscillation is

$$\Delta z \approx -\frac{\hat{y}^2 k_\beta^2 L_0 \gamma_i}{4\gamma_f} \ln \frac{\gamma_f}{\gamma_i}, \tag{3.1}$$

where the symbols are defined in connection with Eq. (3.35).

(b) Estimate the longitudinal position change due to a constant relative energy error $\Delta E/E$. Use

$$\frac{dz}{ds} \approx \frac{1}{\gamma(s)^2} \frac{\Delta E}{E}$$

to show that

$$\Delta z \approx \frac{L_0}{\gamma_i \gamma_f} \frac{\Delta E}{E}. \tag{3.2}$$

(c) Estimate Δz for the SLAC linac, assuming $\gamma_i m_0 c^2 = 1$ GeV, $\gamma_f m_0 c^2 = 50$ GeV, $L_0 = 3$ km, $\hat{y} = 3$ mm, $k_\beta = 0.06$ m^{-1}, and $\Delta E/E = 1\%$. Compare the results with the bunch length, which is of the order of 1 mm.

For some applications, modern linacs are required to perform with increasingly high intensities while maintaining the quality of the beam. One example of such applications is linear colliders for high energy physics experiments. To accelerate particles to TeV energies (1 TeV = 1000 GeV) in a linac requires an extensive length of linac structures, which serve as rf accelerating cavities. To minimize the linac cost and the rf power required, it is desirable to reduce the size of these structures, which generally means strong wake fields. For linear collider applications, one has the challenge that at the end of acceleration, the beam must maintain a small energy spread and a small transverse beam size in spite of these strong wake fields.

In this chapter, the instability mechanisms are often illustrated using a model in which the beam is represented as one or two macroparticles. These macroparticle models give a simple description of the beam dynamics involved. In a *one-particle model*, the beam bunch is a single rigid point charge Ne. The only motion allowed is its center-of-charge motion. In a *two-particle model*, the bunch is represented as two macroparticles separated by a distance $|z|$, which is of the order of the bunch length. Each of the two macroparticles is considered to be a rigid point charge $Ne/2$, whose center of charge is free to move. The two macroparticles interact with the accelerator environment and with each other through the wake fields. These one- and two-particle models will be extended to circular accelerators in Chapter 4.

Three types of linac instabilities are investigated in this chapter, corresponding to the $m = 0$, 1, and 2 components of the wake field, respectively. The $m = 0$ wake causes the parasitic energy loss and an energy spread across the length of the bunch. The parasitic loss effect was discussed in Section 2.5. The energy spread effect is the subject of Section 3.1. Section 3.2 treats the $m = 1$ wake, which causes a dipole mode instability called the *beam breakup* effect in the literature. The $m = 2$ wake, which causes beam breakup in the

quadrupole mode, is the subject of Section 3.3. In all cases, when the beam intensity is sufficiently high, the beam bunch tail will be damaged and perhaps the tail particles will be lost.

3.1 BEAM ENERGY SPREAD

Consider a bunch of charged particles traveling down the accelerator along the axis of the vacuum chamber pipe. The $m = 0$ wake field excited by the beam produces a longitudinal force[1] on particles in the beam. The main effect of this longitudinal force is a retarding voltage, causing energy changes of individual particles. Equations (2.102–2.103) and Section 2.5 address the *total* energy loss of a beam bunch as it traverses an impedance. However, not all particles in the bunch lose the same amount of energy. The wake field thus causes the beam to acquire an energy *spread*, which is the subject of this section.

Consider first a one-particle model in which the beam bunch is a macroparticle of charge Ne that consists of N particles of charge e. As this macroparticle beam travels down the linac, it experiences the self-generated retarding longitudinal field and loses energy accordingly. The parasitic loss per particle is

$$\Delta E = -\tfrac{1}{2}Ne^2W_0'(0^-). \tag{3.3}$$

Take the SLAC linac for example. We have from Figure 2.26(a) that $W_0'(0^-) = 7\ \text{cm}^{-1} \times L_0/L$, where $L_0 = 3$ km is the total length of the linac, and $L = 3.5$ cm is the length of the cavity period. Equation (3.3) then gives an estimate of the parasitic loss of 2.2. GeV for $N = 5 \times 10^{10}$.

This estimate can be improved by using a two-particle model. The beam bunch is then represented by two macroparticles, one leading and another trailing at a distance $|z|$ behind (we have the sign convention $z < 0$). The parasitic loss per particle in the leading macroparticle is half of that for a one-particle model, i.e., 1.1 GeV, because the leading macroparticle contains only half the beam population. The trailing macroparticle loses, in addition to the 1.1 GeV due to self-field, an energy of

$$\Delta E = -\tfrac{1}{2}Ne^2W_0'(z) \tag{3.4}$$

due to the wake field left behind by the leading macroparticle. If we take $z = -\sigma_z = -1$ mm, $N = 5 \times 10^{10}$, and $W_0'(-1\ \text{mm}) = 4.5\ \text{cm}^{-1} \times L_0/L$, each particle in the trailing macroparticle loses an additional 1.4 GeV. The net loss of a trailing particle is therefore 2.5 GeV.

[1] Be reminded that there is no transverse wake force for $m = 0$.

Comparing the one- and the two-particle model results, the one-particle model estimates a parasitic loss per particle of 2.2 GeV; the two-particle model estimates an average loss of $(1.1 + 2.5)/2 = 1.8$ GeV. The results agree reasonably well, but the two-particle model offers the additional information that the wake field has introduced an energy split between the bunch head and the bunch tail, and its magnitude is approximately 1.4 GeV by the time the bunch reaches the end of the linac. If the beam energy at the end of the linac is 50 GeV, this energy spread across the bunch is approximately 3%.

For linear collider applications, this energy spread makes it difficult to focus the beam to a small spot at the collision point in a final focus system, and is to be avoided. Most of this spread can be removed by properly phasing the accelerating rf voltage relative to the beam, as will be discussed in more detail later in this section.

One concern for a high-intensity linear collider can be described as follows. The energy spread at the end of the linac scales as

$$\frac{\Delta E}{E} \approx \frac{\frac{1}{2}Ne^2W_0'}{GL_0} \approx \frac{\frac{1}{2}Ne^2}{Gb^2}, \tag{3.5}$$

where G is the acceleration gradient, and $W_0' \approx L_0/b^2$ is the longitudinal wake function, where b is the vacuum chamber radius characterizing the size of the accelerating cavities. On the other hand, the efficiency of energy extraction by the beam from the field energy U stored in the accelerating cavities $[U \approx (1/8\pi)(G/e)^2 \times \pi b^2 L_0]$ is given by

$$\text{extraction efficiency} \approx \frac{NE}{U} \approx \frac{8Ne^2}{Gb^2}, \tag{3.6}$$

which is equal to 16 times the energy spread (3.5). In other words, to improve the energy spread of the beam at the end of the linac necessarily requires sacrificing the energy extraction efficiency. One way to ameliorate this problem is to compensate $\Delta E/E$ by phasing the rf voltage. Another way is to send a *train* of M bunches per filling of the rf cavities. This will increase the energy extraction efficiency by a factor of M, although at the cost of having to deal with the multibunch interactions due to the long range wake fields.

Exercise 3.2 Even though the transverse wake *force* is zero for $m = 0$, the transverse wake *fields* are not zero. Use Eq. (2.57) to estimate the strengths of E_r and B_θ at the pipe radius $r = b$ for the SLAC linac. Compare the results with the accelerating rf voltage of 600 kV/period.

We now depart from the simplified models and consider a bunch with a general longitudinal distribution $\rho(z)$. The energy change for a test charge e

at longitudinal position z can be written as $eV(z)$, where

$$V(z) = -\int_z^\infty dz'\, \rho(z') W_0'(z - z'). \tag{3.7}$$

A negative $V(z)$ means the test charge loses energy from the wake field. An additional integration of $V(z)$ over the bunch then gives the parasitic loss,

$$\Delta\mathscr{E} = \int_{-\infty}^{\infty} \rho(z) V(z)\, dz. \tag{3.8}$$

For the case of space charge, $V(z)$ can be obtained from Eq. (1.44) [or Eq. (2.80) if one applies Eq. (3.10) below]. For a bunch with Gaussian longitudinal distribution and uniform disk transverse distribution, for example,

$$\frac{V(z)}{L} = \sqrt{\frac{2}{\pi}} \frac{q}{\gamma^2 \sigma_z^2} \left(\ln \frac{b}{a} + \frac{1}{2} \right) f\left(\frac{z}{\sigma_z} \right), \tag{3.9}$$

$$f(u) = u e^{-u^2/2}.$$

Figure 3.1(a) shows the function $f(u)$.

Generally, particles in the front of the bunch ($z > 0$) lose energy due to wake fields, while particles in the back of the bunch ($z < 0$) may gain or lose energy, depending on the length of the bunch. This is not true for the special case of the space charge effect, for which particles in the front of the bunch gain energy, and particles in the back of the bunch lose energy. For the space charge effect, the energy gained by the bunch head is necessarily given up by the bunch tail so that the net energy of the bunch is unchanged.

Consider the numerical example of a 50 MeV proton transport line mentioned following Eq. (1.83). If we take $q = 10^{10}e$, $\sigma_z = 3$ cm, $a = 2$ cm, and $b = 5$ cm, we obtain a longitudinal space charge force of ± 6 V/m for particles located at $z = \pm\sigma_z$. The net energy change of these particles after traveling 100 m of this transport line is $eV/\beta = \pm 2$ keV. The space charge induced beam energy spread is therefore $\pm 4 \times 10^{-5}$.

To calculate $V(z)$ for the resistive wall, it is more convenient to use the frequency domain counterpart of Eq. (3.7), which reads

$$V(z) = -\frac{1}{2\pi} \int_{-\infty}^{\infty} d\omega\, e^{i\omega z/c} Z_0^{\parallel}(\omega) \tilde{\rho}(\omega). \tag{3.10}$$

For a long Gaussian bunch with $\sigma_z \gg \chi^{1/3} b$, we can use the impedance

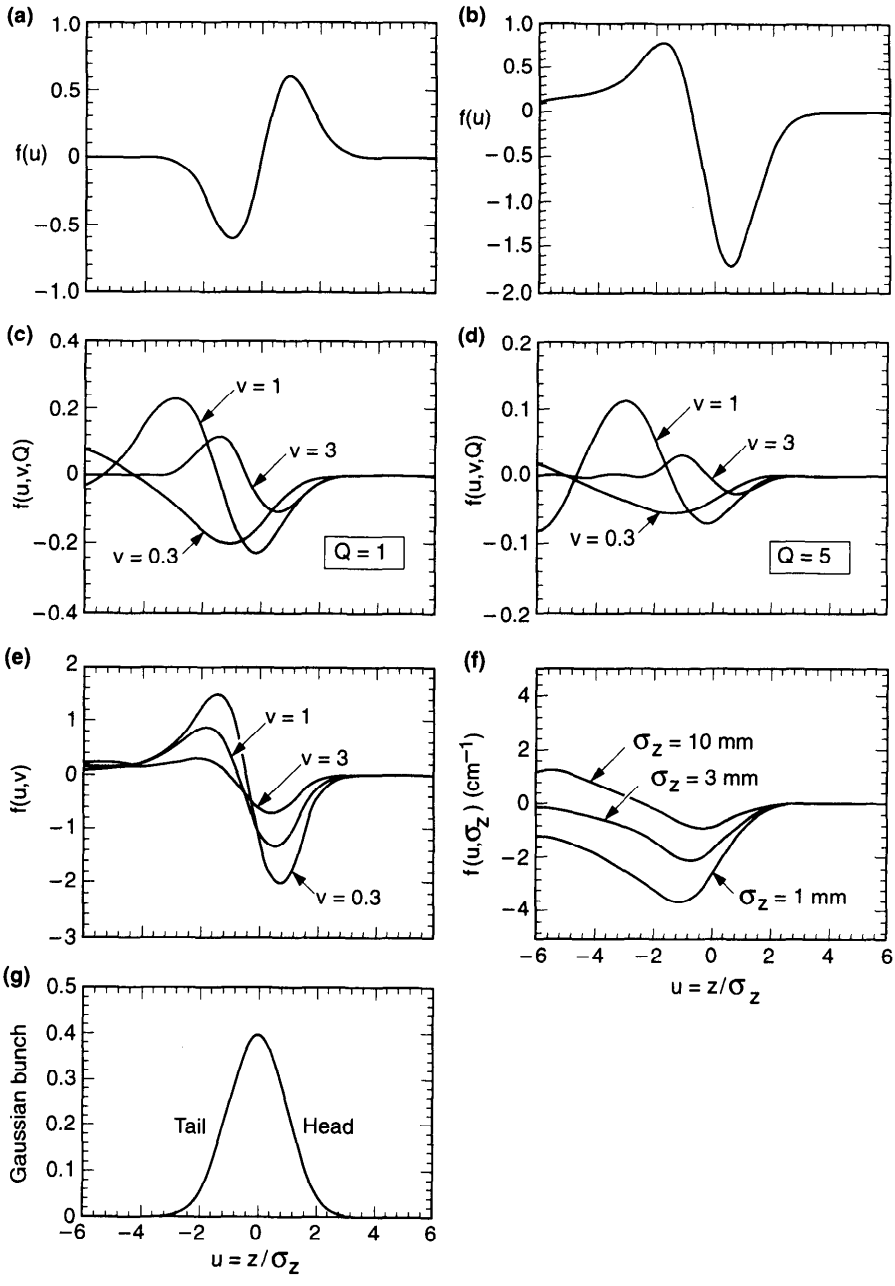

Figure 3.1. (a) The function $f(\upsilon)$ of Eq. (3.9) for the space charge wake effect. (b) The function $f(\upsilon)$ of Eq. (3.11) for the resistive-wall wake. (c) The function $f(\upsilon, v, Q)$ of Eq. (3.14) for a resonator impedance with $Q = 1$ and $v = \omega_R \sigma_z / c = 0.3$, 1, and 3. (d) Same as (c), but for $Q = 5$. (e) The function $f(\upsilon, v)$ of Eq. (3.19) for two parallel plates for $v = L / \sigma_z = 0.3$, 1, and 3. (f) The function $f(\upsilon, \sigma_z)$ of Eq. (3.20) for the SLAC linac for $\sigma_z = 1$, 3, and 10 mm. In all cases, $\upsilon = z / \sigma_z$ and $\upsilon > 0$ is the bunch head. The Gaussian bunch is shown in (g) for reference. All functions f are dimensionless except for part (f).

equation (2.76) to obtain,[2]

$$\frac{V(z)}{L} = \frac{q}{4b\sigma_z^{3/2}}\sqrt{\frac{c}{2\pi\sigma}}\, f\left(\frac{z}{\sigma_z}\right),$$
$$f(u) = -|u|^{3/2}e^{-u^2/4}\left[(I_{-1/4} - I_{3/4})\mathrm{sgn}(u) - I_{1/4} + I_{-3/4}\right] \tag{3.11}$$

with the Bessel functions $I_{\pm 1/4}$ and $I_{\pm 3/4}$ evaluated at $u^2/4$. The function $f(u)$ is shown in Figure 3.1(b).

We continue the above numerical example. Assuming an aluminum pipe and using Figure 3.1(b), a particle located at $0.5\sigma_z$ ahead of bunch center loses an energy of 0.1 eV after traveling 100 m, and a particle located at $1.8\sigma_z$ behind the bunch center gains 0.04 eV.

Exercise 3.3

(a) Integrate Eq. (3.11) over the bunch to recover Eq. (2.194) for the long bunch case.

(b) For a test charge that follows the bunch at a distance $\gg \sigma_z$, i.e., $u \to -\infty$, show that $f(u) \approx \sqrt{8/\pi}|u|^{-3/2}$, and the resulting $V(z)/L$ becomes Eq. (2.16).

(c) Show that, for the resistive-wall wake, a particle at the bunch center loses energy at a rate $2^{3/4}$ times faster than the average in the bunch.

(d) Show that

$$\frac{V'(0)}{L} = -\frac{\Gamma(\frac{1}{4})}{2^{7/4}\pi}\frac{q}{b\sigma_z^{5/2}}\sqrt{\frac{c}{2\pi\sigma}}\,. \tag{3.12}$$

(e) Relate the quantity $V'(0)$ to the synchrotron tune shift in a circular accelerator as discussed following Eq. (1.45) to obtain

$$\Delta\nu_s \approx \frac{\eta R^2}{2\nu_{s0}E}\frac{eV'(0)}{L} = -\frac{\Gamma(\frac{1}{4})}{2^{11/4}\pi}\frac{Nr_0\eta R^2}{\nu_{s0}\gamma b\sigma_z^{5/2}}\sqrt{\frac{c}{2\pi\sigma}}\,. \tag{3.13}$$

For the case of a resonator impedance, we have, using Eq. (3.7),

$$V(z) = \sqrt{\frac{2}{\pi}}\frac{qR_S c}{\sigma_z} f\left(\frac{z}{\sigma_z}, \frac{\omega_R\sigma_z}{c}, Q\right),$$
$$f(u,v,Q) = -\int_0^\infty dx \exp\left[-\frac{1}{2}\left(u + \frac{2Q}{v}x\right)^2 - x\right] \tag{3.14}$$
$$\times\left[\cos\left(x\sqrt{4Q^2-1}\right) - \frac{\sin\left(x\sqrt{4Q^2-1}\right)}{\sqrt{4Q^2-1}}\right].$$

[2]A. Piwinski, DESY Report HERA 92-11 (1992).

The function $f(u, v, Q)$ is shown in Figure 3.1(c) and (d) versus u for various values of v and Q. In the long-bunch limit with $v = \omega_R \sigma_z / c \gg Q$, i.e., when fields decay in a distance $\ll \sigma_z$, we have

$$V(z) \approx -\frac{qR_S c}{\sqrt{2\pi} Q v \sigma_z} \exp\left(-\frac{z^2}{2\sigma_z^2}\right)\left[\frac{1}{Qv}\left(1 - \frac{z^2}{\sigma_z^2}\right) + \frac{z}{\sigma_z}\right]. \quad (3.15)$$

The first term in the square brackets is the resistive contribution; its integration according to Eq. (3.8) gives the parasitic loss (2.198). The second term is a reactive term whose function is to transfer energy from bunch head to bunch tail with no net change of energy for the bunch as a whole. In the long bunch limit, the magnitude of the reactive contribution is larger than the resistive contribution.

If the wake function is written in terms of loss factors according to Eq. (2.148), the retarding voltage of a Gaussian bunch becomes

$$V(z) = -\sqrt{\frac{2}{\pi}} \frac{q}{\sigma_z} \sum_\lambda k_\lambda \int_0^\infty dx \exp\left[-\frac{(z+x)^2}{2\sigma_z^2}\right] \cos\frac{\omega_\lambda x}{c}. \quad (3.16)$$

A test particle at the center of the Gaussian bunch sees a voltage

$$V(0) = -q \sum_\lambda k_\lambda \exp\left(-\frac{\omega_\lambda^2 \sigma_z^2}{2c^2}\right). \quad (3.17)$$

Comparing with the parasitic loss of the entire bunch, Eq. (2.203), we see that the particle at the center of the bunch loses energy faster than average, and that this is true *differentially*, i.e., it holds for each of the individual cavity modes.

For the case of two parallel plates, Eq. (3.16) can be used to obtain $V(z)$ for a Gaussian bunch. The same result can be obtained more readily by using expressions for the wake fields, Eq. (2.171). The result is[3]

$$V(z) = 2 \sum_{n=0}^{\infty} \int_{2nL}^{2(n+1)L} dx\, \rho'(z+x) \ln\left(1 + \frac{2L}{x + 2nL}\right), \quad (3.18)$$

where $\rho'(z)$ is the derivative of ρ. For a Gaussian bunch, we have

$$V(z) = \sqrt{\frac{2}{\pi}} \frac{qL}{\sigma_z^2} f\left(\frac{z}{\sigma_z}, \frac{L}{\sigma_z}\right),$$
$$f(u, v) = \sum_{n=0}^{\infty} \int_{2n}^{2(n+1)} dx (u + xv) e^{-\frac{1}{2}(u+xv)^2} \ln\left(1 + \frac{2}{x + 2n}\right). \quad (3.19)$$

[3]A. Papiernik, M. Chartard-Moulin, and B. Jecko, *Proc. 9th Int. Conf. High Energy Accel.*, SLAC, 1974, p. 375.

Figure 3.1(e) shows the behavior of $f(u, v)$. Integrating Eq. (3.19) over the bunch gives the parasitic loss (2.204–2.205).

For the case of the SLAC linac with loss factors and wake functions shown in Figures 2.25–2.26, we have

$$V(z) = qf\left(\frac{z}{\sigma_z}, \sigma_z\right),$$
$$f(u, \sigma_z) = -\frac{1}{\sqrt{2\pi}} \int_0^\infty dx\, e^{-(x+u)^2/2} W_0'(-x\sigma_z). \tag{3.20}$$

The function $f(u, \sigma_z)$ per cavity period is shown in Figure 3.1(f). Integrating $V(z)$ over the bunch gives Figure 2.33. Note that the sign of the longitudinal wake forces in Figure 3.1, with the exception of the space charge case, is always retarding at the bunch head.

According to Figure 3.1(f), for a bunch with $N = 5 \times 10^{10}$ and $\sigma_z = 1$ mm, a particle located ahead or behind the bunch center by $\sigma_z/2$ loses an energy of 1.2 or 2.1 GeV, respectively. This compares well with the two-particle estimate made at the beginning of this section.

Exercise 3.4 Give expressions for $V(0)$ and $V'(0)$ for the cases of the space charge, the resonator impedance, and the two-parallel-plate cavity. Show that a particle at the bunch center loses more energy than the bunch average by a factor of $2\sqrt{2}$ and 2, respectively, for the resonator and the two-parallel-plate cases in the proper long bunch limits. Given $V'(0)$, compute the incoherent synchrotron tune shift for the various cases. The space charge case gives the same result as Eq. (1.48) for a parabolic bunch if one identifies $\hat{z} = (9\pi/2)^{1/6}\sigma_z$, which is obtained by matching the curvatures of the Gaussian and the parabolic distributions for small z.

In addition to the wake fields, particles in a linac also experience the accelerating rf voltage $V_{\rm rf}(z) = \hat{V}\cos(\omega_{\rm rf} z/c + \phi)$, where $\omega_{\rm rf}$ is the rf angular frequency and ϕ is the phase offset between the bunch center and the rf voltage. (A positive ϕ means the bunch tail gains more energy from the accelerating rf than the bunch head.) The total voltage seen by the beam is $V_{\rm tot}(z) = V_{\rm rf}(z) + V(z)$, where $V(z)$ is the wake field contribution (3.7). To compensate for the wake-induced energy spread, one can adjust the phase offset ϕ at the cost of a slight reduction in the acceleration rate. In particular, one may choose ϕ so that the total voltage in the neighborhood of the bunch center is independent of particle position z, i.e., $V_{\rm tot}'(0) = 0$. This is achieved by choosing ϕ so that

$$\sin\phi = \frac{cV'(0)}{\omega_{\rm rf}\hat{V}}. \tag{3.21}$$

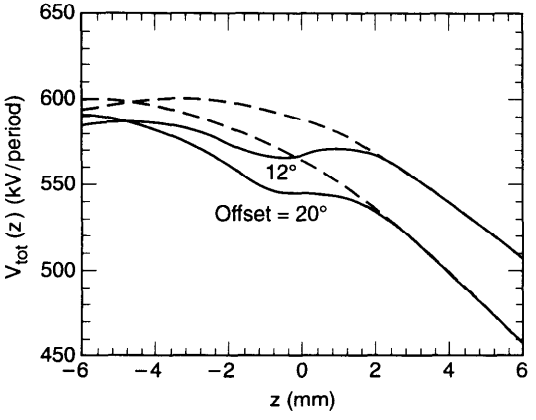

Figure 3.2. Solid curves are the total voltage V_{tot} seen by particles in a SLAC beam with $N = 5 \times 10^{10}$ and $\sigma_z = 1$ mm. Dashed curves are the externally applied rf accelerating voltage with $\hat{V} = 600$ kV / period. Two phase offsets, $\phi = 12°$ and 20°, are shown. The bunch center is at $z = 0$.

Take the SLAC linac with $\sigma_z = 1$ mm, $N = 5 \times 10^{10}$, $\omega_{rf} = 2\pi \times 2.8$ GHz, and $\hat{V} = 600$ kV per cavity period. Using the result from Figure 3.1(f), we find from Eq. (3.21) that $\phi = 20°$. With this choice of phase offset, the acceleration rate at the bunch center is $\hat{V}\cos\phi + V(0) = 545$ kV/period. About $\frac{1}{3}$ of the reduction from 600 kV/period is due to the direct wake field; the remaining $\frac{2}{3}$ is due to the phase offset. By sacrificing beam energy (3 GeV out of 50 GeV), the energy spread between the bunch head and tail is reduced substantially by the phase offset. A compromise between the loss of acceleration rate and reduction of energy spread can be made by choosing a somewhat smaller offset, e.g., 12° instead of 20°. Figure 3.2 shows V_{tot} as a function of z for these two phase offsets.

3.2 BEAM BREAKUP

In the previous section, the beam was considered to be centered in the vacuum chamber pipe. There were no transverse wake forces. In case the beam is off center, for example due to its executing a betatron oscillation,[4] an $m = 1$ dipole wake field will be excited by the head of the bunch, which causes transverse deflection of the tail of the bunch. For a high-intensity beam, the betatron motion of the bunch tail can be seriously perturbed, leading to a transverse breakup of the beam, as will be discussed in this

[4]Dipole wake fields are also excited if the beam is off center for other reasons, such as a misaligned beam trajectory relative to the cavities.

section. The first observation of this beam breakup effect was made on the SLAC linac.[5]

To proceed with a simplified macroparticle model, we first note that a one-particle model is not very useful here, because, unlike the longitudinal $m = 0$ case, a point charge does not exert a transverse wake force on itself. In the two-particle model, the leading macroparticle, unperturbed by its own transverse wake field, executes a free betatron oscillation

$$y_1(s) = \hat{y} \cos k_\beta s, \tag{3.22}$$

where s is the distance coordinate along the linac and k_β is the betatron wave number. The trailing macroparticle, at a distance $|z|$ behind, sees a deflecting wake field left behind by its leading partner. According to Table 2.2, we have

$$\begin{aligned} y_2'' + k_\beta^2 y_2 &= -\frac{Ne^2 W_1(z)}{2EL} y_1 \\ &= -\frac{Nr_0 W_1(z)}{2\gamma L} \hat{y} \cos k_\beta s \end{aligned} \tag{3.23}$$

where $E = \gamma m_0 c^2$ is the beam particle energy, r_0 is the classical radius of the particle [Eq. (1.3)], $W_1(z)$ is the transverse wake function for one cavity period, and L is the cavity period. In writing down Eqs. (3.22–3.23), we have assumed smooth betatron focusing (i.e., k_β is independent of s) and $k_\beta L \ll 1$, so that the wake field can be averaged over cavity periods when describing the particle motion. We have also ignored acceleration of the beam energy in Eq. (3.23). For the SLAC linac, $k_\beta \approx 0.06\ \text{m}^{-1}$ and $k_\beta L \approx 0.002$.

Equation (3.23) shows that the mechanism of beam breakup is that particles in the tail of the beam are driven exactly on resonance by the oscillating wake left by the head of the beam. The solution to Eq. (3.23) is

$$y_2(s) = \hat{y}\left[\cos k_\beta s - \frac{Nr_0 W_1(z)}{4k_\beta \gamma L} s \sin k_\beta s\right], \tag{3.24}$$

in which the first term describes the free oscillation and the second term is the resonant response to the driving wake force. The amplitude of the second term grows linearly with s.

At the end of the linac, the oscillation amplitude of the bunch tail relative to the bunch head is characterized by the dimensionless growth parameter

$$\Upsilon = -\frac{Nr_0 W_1(z) L_0}{4k_\beta \gamma L}, \tag{3.25}$$

[5] R. B. Neal and W. K. H. Panofsky, Science **152**, 1353 (1966); W. K. H. Panofsky and M. Bander, Rev. Sci. Instr. **39**, 206 (1968).

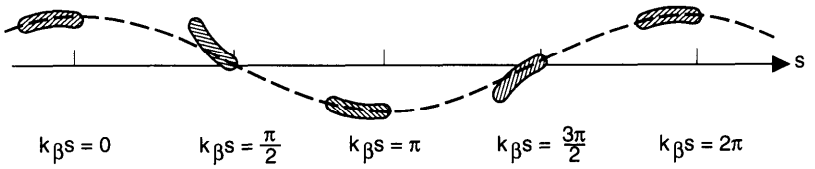

Figure 3.3. Sequence of snapshots of a beam undergoing dipole beam breakup instability in a linac. Values of $k_\beta s$ indicated are modulo 2π. The dashed curves indicate the trajectory of the bunch head.

where L_0 is the total linac length. For short bunches, $W_1(z) < 0$, the parameter Υ is positive.

For a beam bunch with realistic distribution, the wake field due to the off-axis motion of the bunch head deflects the bunch tail so that the bunch is distorted into a banana shape, as sketched in Figure 3.3. The sequence of snapshots shown in Figure 3.3 reflects the fact that the motion of the bunch head is described by $\cos k_\beta s$, while the deviation of the bunch tail relative to the bunch head is described by $s \sin k_\beta s$. In particular, when the bunch head is at a maximum displacement ($k_\beta s = n\pi$), the tail lines up with the bunch head, but when the bunch head displacement is zero [$k_\beta s = (n + \frac{1}{2})\pi$], the tail swing is maximum. As the beam propagates down the linac, the swing amplitude of the flapping tail increases with s until the tail breaks up and particles are lost. Note that the sign of the tail swing shown in Figure 3.3 is not arbitrary, because $\Upsilon > 0$.

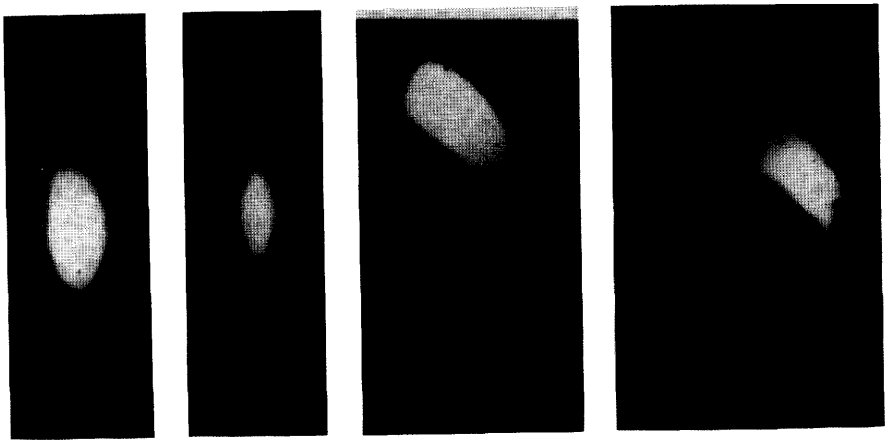

Figure 3.4. Four transverse beam profiles observed at the end of the SLAC linac are shown when the beam was carefully injected and injected with 0.2, 0.5, and 1 mm offsets. The beam sizes σ_x and σ_y are about 120 μm. (Courtesy John Seeman, 1991.)

Figure 3.4 shows four transverse beam profiles observed at the end of the SLAC linac with a beam intensity of $N = 2 \times 10^{10}$.[6] The leftmost profile was observed when the beam was carefully steered so that its trajectory was well centered in the beam pipe. When the beam was injected off center by 0.2, 0.5, and 1 mm, the beam profiles are as shown successively to the right. One observes that a tail develops as the injection offset is increased. The curling of the tail indicates the offset has both horizontal and vertical components.

Consider a beam coasting down the SLAC linac at 1 GeV without acceleration. The tail swing is magnified by a factor of $\Upsilon \approx 180$ compared to the bunch head if we take $N = 5 \times 10^{10}$, $W_1(-1 \text{ mm}) = -0.7 \text{ cm}^{-2}$, $L_0 = 3$ km, $L = 3.5$ cm, and $k_\beta = 0.06 \text{ m}^{-1}$.[7] To preserve the beam emittance, it is necessary to have $|\Upsilon \hat{y}| \ll$ transverse beam size. This means the beam must be injected onto the linac axis with an accuracy better than a fraction of a per cent of the beam size, which is difficult to achieve.

Exercise 3.5 Consider a circular accelerator that has an isochronous design so that it is operated at transition where the slippage factor $\eta = 0$.[8] The longitudinal z-positions of particles are frozen, as in the linac case. Let the accelerator have a broad-band resonator impedance characterized by $\omega_R = c/b$, $Q = 1$, and $Z_0^{\parallel}/n = R_S b/R$, where b is the vacuum pipe radius and $2\pi R$ is the accelerator circumference. Assume the accelerator has a transverse impedance that is related to the longitudinal impedance by Eq. (2.107). Use a two-particle model and Eq. (3.25) to show that if the beam starts with a transverse center-of-charge displacement, the displacement of the bunch tail will double in a time

$$\tau \approx \frac{\gamma b^4 Z_0}{N r_0 c \beta_Z \hat{z} \left(Z_0^{\parallel}/n\right)}, \tag{3.26}$$

where $Z_0 = 377\ \Omega$, $\beta_Z = 1/k_\beta$ is the β-function at the location of the impedance, $\hat{z}$ is the separation of the two macroparticles characterizing the bunch length, and we have assumed a short bunch $\hat{z} \ll b$.

So far we have ignored beam acceleration, which has an important stabilizing effect because, as its energy increases, the beam becomes more rigid and less vulnerable to the wake fields. We will now repeat the two-particle analysis taking account of acceleration. The equation of the free betatron motion for the leading macroparticle is

$$\frac{d}{ds}\left[\gamma(s)\frac{dy_1}{ds}\right] + k_\beta^2 \gamma(s) y_1 = 0, \tag{3.27}$$

where we have assumed that the focusing strength has been increased

[6] J. T. Seeman, K. L. F. Bane, T. Himel, and W. L. Spense, Part. Accel., **30**, 97 (1990).
[7] Strictly speaking, the two-particle model is no longer applicable for a beam broken up so badly.
[8] Claudio Pellegrini and David Robin, Nucl. Instr. Meth. Phys. Res. **A301**, 27 (1991).

proportionally to the beam energy. We further assume a uniform acceleration rate, so that the beam energy increases linearly with s,

$$\gamma(s) = \gamma_i(1 + \alpha s), \tag{3.28}$$

where $\gamma_i m_0 c^2$ is the beam energy at injection. By a change of variable from s to $u = 1 + \alpha s$, Eq. (3.28) becomes

$$\frac{d^2 y_1}{du^2} + \frac{1}{u}\frac{dy_1}{du} + \left(\frac{k_\beta}{\alpha}\right)^2 y_1 = 0. \tag{3.29}$$

The solution with the initial conditions $y_1(0) = \hat{y}$ and $y_1'(0) = 0$ is

$$y_1(u) = \hat{y}\frac{\pi k_\beta}{2\alpha}\left[J_1\left(\frac{k_\beta}{\alpha}\right)N_0\left(\frac{k_\beta}{\alpha}u\right) - N_1\left(\frac{k_\beta}{\alpha}\right)J_0\left(\frac{k_\beta}{\alpha}u\right)\right], \tag{3.30}$$

where $J_n(x)$ and $N_n(x)$ are Bessel and Neumann functions.[9]

The equation of motion for the trailing macroparticle is

$$\frac{d^2 y_2}{du^2} + \frac{1}{u}\frac{dy_2}{du} + \left(\frac{k_\beta}{\alpha}\right)^2 y_2 = -\frac{Nr_0 W_1(z)}{2\gamma_i \alpha^2 L u} y_1(u). \tag{3.31}$$

The solution of Eq. (3.31) can be written as

$$y_2(u) = y_1(u) - \frac{Nr_0 W_1(z)}{2\gamma_i \alpha^2 L}\int_1^u du'\, G(u,u')\, y_1(u'), \tag{3.32}$$

where the first term gives the unperturbed contribution, the second term is the response to the wake force, and $G(u,u')$ is the Green's function

$$G(u,u') = \frac{\pi}{2}\left[N_0\left(\frac{k_\beta}{\alpha}u\right)J_0\left(\frac{k_\beta}{\alpha}u'\right) - J_0\left(\frac{k_\beta}{\alpha}u\right)N_0\left(\frac{k_\beta}{\alpha}u'\right)\right]. \tag{3.33}$$

In most practical cases, the acceleration gradient is much smaller than the betatron focusing, i.e., $\alpha \ll k_\beta$. In this case, the arguments of $J_{0,1}$ and $N_{0,1}$ are much greater than unity, and we can use the asymptotic expressions, for $x \gg 1$,

$$\begin{aligned} J_0(x) &\approx -N_1(x) \approx \sqrt{\frac{2}{\pi x}}\cos\left(x - \frac{\pi}{4}\right), \\ J_1(x) &\approx N_0(x) \approx \sqrt{\frac{2}{\pi x}}\sin\left(x - \frac{\pi}{4}\right). \end{aligned} \tag{3.34}$$

[9]The Bessel functions are complicated in appearance, but not in essence. One could imagine the functions J_n and N_n as the cosine and sine functions expressed in polar coordinates. Similarly, I_n and K_n are like exponential functions expressed in polar coordinates.

This means the motion of the leading macroparticle, Eq. (3.30), is approximately given by

$$y_1(s) \approx \frac{\hat{y}}{\sqrt{1+\alpha s}} \cos k_\beta s, \tag{3.35}$$

and the Green's function (3.33) becomes

$$G(s,s') \approx \frac{\alpha}{k_\beta} \frac{\sin[k_\beta(s-s')]}{\sqrt{(1+\alpha s)(1+\alpha s')}}. \tag{3.36}$$

Compared with the case without acceleration [Eq. (3.22)], Eq. (3.35) contains an extra factor of $1/\sqrt{1+\alpha s}$. This factor can be written as $\sqrt{\gamma_i/\gamma(s)}$, and is the factor responsible for the adiabatic damping of betatron oscillations as particles are accelerated.

Substituting Eqs. (3.35–3.36) into Eq. (3.32) and performing the integration with the approximation $\alpha \ll k_\beta$ gives

$$y_2(s) \approx \frac{\hat{y}}{\sqrt{1+\alpha s}} \left[\cos k_\beta s - \frac{N r_0 W_1(z)}{4 k_\beta \gamma_i \alpha L} \ln(1+\alpha s) \sin k_\beta s \right]. \tag{3.37}$$

At the end of the linac, $s = L_0$, the oscillation amplitude of the bunch tail relative to the bunch head is characterized by the growth parameter

$$\Upsilon = -\frac{N r_0 W_1(z) L_0}{4 k_\beta \gamma_f L} \ln \frac{\gamma_f}{\gamma_i}, \tag{3.38}$$

where $\gamma_f = \gamma_i(1+\alpha L_0) \gg \gamma_i$ gives the final particle energy.

It is interesting to note that the tail growth parameter (3.38) can be obtained from the coasting beam result (3.25) by simply replacing the factor L_0/γ by its integral counterpart $\int_0^{L_0} ds/\gamma(s)$. Due to acceleration, the tail amplitude thus grows logarithmically rather than linearly with s, and the growth parameter is much reduced. If the beam is accelerated in the SLAC linac from 1 to 50 GeV, the factor Υ becomes 14, instead of 180, which was calculated earlier for a beam coasting at 1 GeV.

The beam breakup instability described above is quite severe even with acceleration. To control it, the beam has to be tightly focused, rapidly accelerated, and carefully injected, and its trajectory carefully steered down the linac.[10] It turns out, however, that there is another interesting and

[10] Interestingly, the contribution from trajectory missteering can in principle be largely compensated by an intentional misinjection. See the SLC Linear Collider Conceptual Design Report, SLAC-229 (1980).

effective method to ameliorate the situation. This method, known as the *BNS damping* after Balakin, Novokhatsky, and Smirnov,[11] is described next.

Consider first the case without acceleration, where the leading macroparticle executes a betatron oscillation (3.22). The idea of BNS damping requires introducing a slightly stronger betatron focusing of the bunch tail than the bunch head. The equation of motion of the tail particles can be written as

$$y_2'' + (k_\beta + \Delta k_\beta)^2 y_2 = -\frac{Nr_0 W_1(z)}{2\gamma L}\hat{y}\cos k_\beta s. \tag{3.39}$$

The solution, assuming $|\Delta k_\beta / k_\beta| \ll 1$, is

$$y_2(s) = \hat{y}\cos(k_\beta + \Delta k_\beta)s + \frac{Nr_0 W_1(z)}{4k_\beta \Delta k_\beta \gamma L}\hat{y}\left[\cos(k_\beta s + \Delta k_\beta s) - \cos k_\beta s\right]. \tag{3.40}$$

Compared with Eq. (3.24), one observes that, by introducing a slightly different focusing strength for the bunch tail, the beam breakup mechanism of the bunch head resonantly driving the bunch tail is removed. A further inspection of Eq. (3.40) shows that there exists an interesting condition for the bunch tail to follow the bunch head exactly for all s, namely,

$$\frac{Nr_0 W_1(z)}{4k_\beta \Delta k_\beta \gamma L} = -1, \tag{3.41}$$

or equivalently,

$$\frac{\Delta k_\beta}{k_\beta} = -\frac{Nr_0 W_1(z)}{4k_\beta^2 \gamma L} = \frac{\Upsilon}{k_\beta L_0}, \tag{3.42}$$

where Υ is defined by Eq. (3.25), and $k_\beta L_0$ is the total betatron phase advance of the linac. For short bunches, Υ and Δk_β are positive; the betatron focusing required to fulfill Eq. (3.42) is therefore stronger at the bunch tail than at the bunch head.

Under the BNS condition (3.42), $y_2(s) = y_1(s) = \hat{y}\cos k_\beta s$, and the beam no longer breaks up.[12] Physically, this happens because the additional external focusing force introduced for the bunch tail has compensated for the defocusing dipole deflection force due to the wake field left behind by the

[11] V. Balakin, A. Novokhatsky, and V. Smirnov, *Proc. 12th Int. Conf. High Energy Accel.*, Fermilab, 1983, p. 119.

[12] The mechanism of BNS damping is not to be confused with that of Landau damping, to be discussed in Chapter 5. They have little in common other than the fact that both involve a frequency spread in the bunch population.

bunch head. Note that the BNS focusing has to be adjusted according to the beam intensity.

There are different ways to provide the BNS focusing. One is to introduce a radio frequency quadrupole whose strength changes as the bunch passes by, so that the head and tail of the bunch see different quadrupole strengths. Another is to choose the location of the bunch relative to the acceleration rf voltage in such a way that the bunch tail acquires a lower energy than the bunch head. The energy spread across the bunch then causes a spread in betatron focusing according to

$$\frac{\Delta k_\beta}{k_\beta} = \xi \frac{\Delta E}{E}, \tag{3.43}$$

where ξ is a quantity called the *chromaticity*, which is determined by the linac design. For a FODO lattice design, for example,

$$\xi = -\frac{2}{\mu} \tan \frac{\mu}{2}, \tag{3.44}$$

where μ is the betatron phase advance per FODO cell. By properly choosing the phase of the rf voltage relative to the beam bunch, the betatron focusing required by the BNS condition can be obtained, provided the required $\Delta k_\beta / k_\beta$ is not excessive.

In case of an accelerated beam, the BNS condition is still given by Eq. (3.42), except that the parameter Υ is now that given by Eq. (3.38) instead of Eq. (3.25). Take the SLAC linac, for example, and assume $\mu = 90°$; then the energy deviation of the bunch tail from the bunch head required by the BNS condition is about -5.5%. BNS damping has been routinely employed to control the beam breakup instability in the SLAC linac operations.

Exercise 3.6 The two-particle model analysis can be extended to M particles, and the results can be applied to the case of a train of M equally spaced bunches, each represented as a macroparticle of charge Ne. Let D be the bunch spacing.

(a) In the absence of BNS damping, the kth bunch ($k = 1, 2, \ldots, M$) would have a leading contribution from the wake field that is proportional to N^{k-1}. Show that the betatron displacement of the kth bunch, $y^{(k)}$, is given by the real part of

$$y^{(k)}(s) \approx \frac{\hat{y}}{(k-1)!} \left[\frac{iNr_0 W_1(-D)}{2k_\beta \gamma L} s \right]^{k-1} e^{ik_\beta s}. \tag{3.45}$$

The fact that $y^{(k)} \propto s^{k-1}$ is a consequence of resonant driving of the

kth bunch by the wake field left behind by the $(k-1)$th bunch. For a long train of bunches, the later bunches could therefore be severely perturbed.

(b) One way to control the multibunch beam breakup is to minimize the long range wake fields by a proper design of the accelerating cavities. Show that another way is to apply BNS damping by choosing the focusing strengths for the individual bunches according to[13]

$$\frac{\Delta k_\beta^{(k)}}{k_\beta} = -\frac{Nr_0}{2k_\beta^2 \gamma L} \sum_{j=1}^{k-1} W_1(-jD). \tag{3.46}$$

Does the BNS condition (3.46) apply when different bunches are injected with different initial conditions?

So far we have considered a two-particle model. The beam breakup analysis becomes more involved for a bunch with general distribution $\rho(z)$. Consider first a coasting beam without acceleration. Let $y(s, z)$ be the betatron displacement of a slice of the bunch at longitudinal position z (relative to the bunch center) as it passes the linac coordinate s. The equation of motion of this bunch slice is [assume normalization $\int_{-\infty}^{\infty} dz\, \rho(z) = 1$]

$$y''(s,z) + \left[k_\beta + \Delta k_\beta(z)\right]^2 y(s,z) = -\frac{Nr_0}{\gamma L} \int_z^\infty dz'\, \rho(z') W_1(z - z') y(s, z'). \tag{3.47}$$

In the absence of BNS damping, $\Delta k_\beta(z) = 0$ and the betatron focusing is independent of z. To achieve BNS damping, we would like to have $y(s, z) = \hat{y} \cos k_\beta s$ be the solution of Eq. (3.47) for all values of z. Substituting into Eq. (3.47) yields the condition[14]

$$\frac{\Delta k_\beta(z)}{k_\beta} = -\frac{Nr_0}{2k_\beta^2 \gamma L} \int_z^\infty dz'\, \rho(z') W_1(z - z'). \tag{3.48}$$

Under this condition, there will be no transverse emittance growth due to wake fields. Equation (3.48) is the generalization of the two-particle model result (3.42).

The integral on the right hand side of Eq. (3.48) is also related to the transverse kick received by the beam particles as the beam traverses an impedance with a transverse offset y_0. More specifically, the transverse kick

[13] K. A. Thompson and R. D. Ruth, Phys. Rev. D. **41**, 964 (1990).

[14] V. E. Balakin, *Proc. Workshop on Linear Colliders*, SLAC, 1988, p. 55.

received by a test charge e at position z is

$$\Delta y'(z) = -\frac{Nr_0 y_0}{\gamma}\int_z^\infty dz'\,\rho(z')W_1(z-z'). \tag{3.49}$$

Combining Eqs. (3.48–3.49), the BNS focusing is related to the single-pass wake kick by

$$\Delta k_\beta(z) = \frac{\Delta y'(z)}{2k_\beta y_0 L}. \tag{3.50}$$

Equation (3.49) can also be expressed in terms of the impedance $Z_1^\perp$:

$$\Delta y'(z) = \frac{Nr_0 y_0}{\gamma}\frac{i}{2\pi}\int_{-\infty}^\infty d\omega\, e^{i\omega z/c}Z_1^\perp(\omega)\tilde{\rho}(\omega). \tag{3.51}$$

The kick to the center of charge of the bunch is obtained by integrating $\Delta y'(z)$ over the bunch, yielding

$$\begin{aligned}\langle \Delta y'\rangle &= \int_{-\infty}^\infty dz\,\rho(z)\,\Delta y'(z)\\ &= -\frac{Nr_0 y_0}{\pi\gamma}\int_0^\infty d\omega\,\mathrm{Im}\,Z_1^\perp(\omega)|\tilde{\rho}(\omega)|^2.\end{aligned} \tag{3.52}$$

Note that it is the imaginary part of $Z_1^\perp$ that describes the net kick to the beam. This is in contrast to the net parasitic loss $\Delta\mathscr{E}$, which involves only the real part of $Z_0^\parallel$.

For a Gaussian bunch, we have

$$\begin{aligned}\Delta y'(z) &= \frac{Nr_0 y_0}{\gamma}f\left(\frac{z}{\sigma_z},\sigma_z\right),\\ f(u,\sigma_z) &= -\frac{1}{\sqrt{2\pi}}\int_0^\infty dx\,e^{-(u+x)^2/2}W_1(-x\sigma_z).\end{aligned} \tag{3.53}$$

For the SLAC linac, for example, $W_1(z)$ is that shown in Figure 2.26(b).

When the wake function is expressed in terms of the loss factors as in Eq. (2.166), we have

$$\Delta y'(z) = \sqrt{\frac{2}{\pi}}\frac{Nr_0 y_0 c}{\gamma\sigma_z}\sum_\lambda \frac{k_\lambda^{(1)}}{\omega_\lambda}\int_0^\infty dx\,\exp\left[-\frac{(z+x)^2}{2\sigma_z^2}\right]\sin\frac{\omega_\lambda x}{c}. \tag{3.54}$$

Exercise 3.7 For the space charge wake field (2.55) and a Gaussian bunch, show that

$$\Delta y'(z) = -\sqrt{\frac{2}{\pi}}\frac{NLr_0y_0}{\sigma_z\gamma^3}\left(\frac{1}{a^2}-\frac{1}{b^2}\right)e^{-z^2/2\sigma_z^2}, \tag{3.55}$$

and that $\langle \Delta y' \rangle = \Delta y'(0)/\sqrt{2}$.

Exercise 3.8 For the case of resistive wall, show that[15]

$$\Delta y'(z) = -\frac{NLr_0y_0}{2\gamma b^3}\sqrt{\frac{c}{\pi\sigma\sigma_z}}f\left(\frac{z}{\sigma_z}\right),$$
$$f(u) = |u|^{1/2}e^{-u^2/4}\left[\operatorname{sgn}(u)I_{1/4}\left(\frac{u^2}{4}\right)-I_{-1/4}\left(\frac{u^2}{4}\right)\right]. \tag{3.56}$$

and that

$$\langle \Delta y' \rangle = \frac{\Delta y'(0)}{2^{1/4}} = \frac{NLr_0y_0}{2\pi\gamma b^3}\sqrt{\frac{c}{\pi\sigma\sigma_z}}\Gamma\left(\frac{1}{4}\right). \tag{3.57}$$

Exercise 3.9 For a resonator wake function (2.88), show that

$$\Delta y'(z) = \sqrt{\frac{2}{\pi}}\frac{Nr_0y_0cR_S}{\gamma}f\left(\frac{z}{\sigma_z},\frac{\omega_R\sigma_z}{c},Q\right),$$
$$f(u,v,Q) = \frac{2Q}{v}\int_0^\infty dx\exp\left[-\frac{1}{2}\left(u+\frac{2Q}{v}x\right)^2-x\right] \tag{3.58}$$
$$\times\frac{\sin\left(x\sqrt{4Q^2-1}\right)}{\sqrt{4Q^2-1}}$$

and that, for long bunches with $v = \omega_R\sigma_z/c \gg Q$,

$$\Delta y'(z) \approx \frac{Nr_0y_0cR_S}{\sqrt{2\pi}Qv\gamma}\left(1-\frac{1}{vQ}\frac{z}{\sigma_z}\right)e^{-z^2/2\sigma_z^2}. \tag{3.59}$$

Equations (3.49–3.59) for $\Delta y'(z)$ have their longitudinal counterparts $V(z)$ discussed in the previous section. The various functions defined in those

[15] A. Piwinski, DESY Report 84-097 (1984).

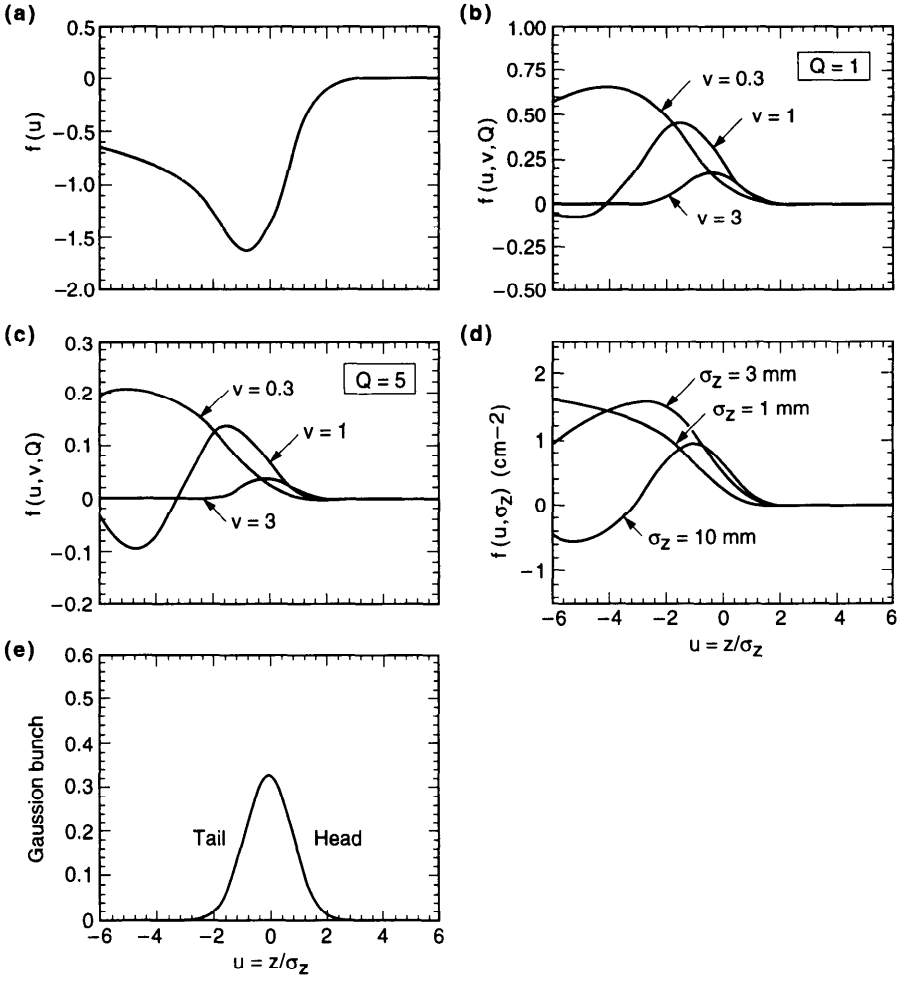

Figure 3.5. (a) The function $f(u)$ of Eq. (3.56) for the resistive-wall impedance. (b) The function $f(u,v,Q)$ of Eq. (3.58) for a resonator impedance with $Q = 1$ and $v = \omega_R \sigma_z / c = 0.3$, 1, and 3. (c) Same as (b), but with $Q = 5$. (d) The function $f(u,\sigma_z)$ of Eq. (3.53) for the SLAC linac, for $\sigma_z = 1$, 3, and 10 mm. In all cases, $u = z / \sigma_z$ and $u > 0$ is the head of the bunch. A Gaussian bunch is shown in (e) for reference.

equations are shown in Figure 3.5. Note that, aside from the space charge case, the sign of $\Delta y'$ tends to be the same as that of y_0 over the bunch population, which reflects the fact that, for an offset beam, the dipole wake field tends to deflect its tail further away from the pipe axis.

As mentioned, with the condition (3.48), the BNS focusing exactly cancels the defocusing effect due to wake fields. In the absence of BNS damping, however, an intense beam can be broken up by the wake fields it generates.

To examine this,[16] let us consider a perturbation expansion

$$y(s, z) = \sum_{n-0}^{\infty} y^{(n)}(s, z), \tag{3.60}$$

where the leading term

$$y^{(0)}(s, z) = \hat{y} \cos k_\beta s \qquad \text{for all } z \tag{3.61}$$

is the unperturbed particle trajectory. The nth term $y^{(n)}$ is $(n-1)$th order in the wake field strength [and therefore $(n-1)$th order in the beam intensity], and is determined by the iteration condition

$$\frac{d^2}{ds^2} y^{(n)}(s, z) + k_\beta^2 y^{(n)}(s, z) = -\frac{Nr_0}{\gamma L} \int_z^\infty dz'\, \rho(z') W_1(z - z') y^{(n-1)}(s, z'). \tag{3.62}$$

The solution to Eq. (3.62) can be expressed in terms of a Green's function $G(s, s') = (1/k_\beta) \sin k_\beta (s - s')$ as

$$y^{(n)}(s, z) = -\frac{Nr_0}{\gamma L} \int_0^s ds'\, G(s, s') \int_z^\infty dz'\, \rho(z') W_1(z - z') y^{(n-1)}(s', z'). \tag{3.63}$$

Equations (3.60), (3.61), and (3.63) give the complete solution to the beam breakup problem in the absence of BNS damping or acceleration. For relatively weak beams, it suffices to keep to the first order term in beam intensity, i.e.,

$$\begin{aligned} y(s, z) &\approx y^{(0)}(s, z) + y^{(1)}(s, z) \\ &= \hat{y}\left[\cos k_\beta s - \frac{Nr_0}{2k_\beta \gamma L} s \sin k_\beta s \int_z^\infty dz'\, \rho(z') W_1(z - z')\right]. \end{aligned} \tag{3.64}$$

This behavior was sketched in Figure 3.3. Note the appearance of the same integral mentioned in conjunction with Eqs. (3.48–3.49). The first order

[16]Analysis of the beam breakup instability under various linac operation and design conditions is a topic much studied in the literature. See R. Helm and G. Loew, *Linear Accelerators*, North Holland, Amsterdam, 1970, Chapter B.1.4; R. F. Koontz, G. A. Loew, R. H. Miller, and P. B Wilson, IEEE Trans. Nucl. Sci. **NS-24**, 1493 (1977); V. K. Neil, L. S. Hall, and R. K. Cooper, Part. Accel. **9**, 213 (1979); Alexander W. Chao, Burton Richter, and Chi-Yuan Yao, *Nucl. Instr. Meth.* **178**, 1 (1980); K. Yokoya, DESY Report 86-084 (1986); T. Suzuki, *AIP Proc.* **156**, *Workshop on Advanced Accel. Concepts*, Madison, 1987, p. 480; Glenn Decker and Jiunn-Ming Wang, Phys. Rev. D **38**, 980 (1988); R. L. Gluckstern, F. Neri, and R. K. Cooper, Part. Accel. **23**, 37 (1988), **23**, 53 (1988); Y. Y. Lau, Phys. Rev. Lett. **63**, 1141 (1989); Yujiro Ogawa, Tetsuo Shidara, and Akira Asami, Phys. Rev. D **43**, 258 (1991).

approximation (3.64) holds if

$$\left| \frac{L_0}{k_\beta} \frac{\Delta y'(z)}{2y_0 L} \right| \ll 1. \tag{3.65}$$

For high intensity beams, the betatron displacement of the beam tail exponentiates with respect to the beam intensity, and we need to include higher order terms in the perturbation expansion. For most practical cases of high energy linacs, the beam executes many betatron oscillations over the length L_0 of the linac, i.e., $k_\beta L_0 \gg 1$. In this case, Eqs. (3.61) and (3.63) can be used to find $y^{(n)}$ at the end of the linac $s = L_0$:

$$y^{(n)}(L_0, z) \approx \frac{\hat{y}}{n!} \left(\frac{iNr_0 L_0}{2k_\beta \gamma L} \right)^n R_n(z) e^{ik_\beta L_0}, \tag{3.66}$$

where taking the real part of the right hand side is understood, and

$$R_n(z) = \int_z^\infty dz_1 \, \rho(z_1) W_1(z - z_1) \int_{z_1}^\infty dz_2 \, \rho(z_2) W_1(z_1 - z_2)$$
$$\cdots \int_{z_{n-1}}^\infty dz_n \, \rho(z_n) W_1(z_{n-1} - z_n) \tag{3.67}$$

with $R_0(z) = 1$.

Exercise 3.10 Consider a beam going through a linac section without betatron focusing. In the absence of wake fields, the beam trajectory is $y(s) = y_0 + y_0' s$. Let the transverse wake function be that given in Eq. (3.70) below.

(a) Use a two-particle model to find the trajectory of the trailing macroparticle.

(b) Solve the general problem following a procedure similar to Eqs. (3.60) and (3.62).

Exercise 3.11 The analysis from Eq. (3.60) to Eq. (3.67) applies also to the case when the external focusing is provided by a solenoid with strength $K = eB_S/E$. The equations of motion are

$$\begin{aligned} x''(s, z) - Ky'(s, z) &= -\frac{Nr_0}{\gamma L} \int_z^\infty dz' \, \rho(z') W_1(z - z') x(s, z'), \\ y''(s, z) + Kx'(s, z) &= -\frac{Nr_0}{\gamma L} \int_z^\infty dz' \, \rho(z') W_1(z - z') y(s, z'). \end{aligned} \tag{3.68}$$

Observe the beam motion in a rotating frame by defining

$$u = e^{iKs/2}(x + iy).$$

Show that

$$u''(s,z) + \frac{K^2}{4}u(s,z) = -\frac{Nr_0}{\gamma L}\int_z^\infty dz'\,\rho(z')W_1(z-z')u(s,z'). \quad (3.69)$$

The analysis in the text then applies straightforwardly.

To proceed, let us consider the special case in which the bunch distribution is uniform with total length l and the wake function is linear in z, i.e.,

$$\begin{aligned} \rho(z) &= \begin{cases} 1/l & \text{if} \quad |z| < l/2, \\ 0 & \text{otherwise}, \end{cases} \\ W_1(z) &= \frac{W_0 z}{l} \qquad \text{if} \quad 0 > z > -l. \end{aligned} \quad (3.70)$$

In this parametrization, W_0 is necessarily positive. We find from Eq. (3.67),

$$R_n(z) = \frac{1}{(2n)!}\left[-NW_0\left(\frac{1}{2} - \frac{z}{l}\right)^2\right]^n, \qquad |z| < \frac{l}{2}. \quad (3.71)$$

Equations (3.60) and (3.66) then give

$$y(L_0,z) = \hat{y}e^{ik_\beta L_0}\sum_{n=0}^{\infty}\frac{1}{n!(2n)!}\left(\frac{\Upsilon}{2i}\right)^n, \quad (3.72)$$

where we have defined a dimensionless wake strength parameter

$$\Upsilon = \frac{Nr_0L_0W_0}{k_\beta\gamma L}\left(\frac{1}{2} - \frac{z}{l}\right)^2. \quad (3.73)$$

The parameter Υ depends on the location z within the beam bunch. At the bunch head $z = l/2$, we have $\Upsilon = 0$. At the bunch tail $z = -l/2$, Υ has its maximum value. For $\Upsilon \ll 1$, we have the condition (3.65), and Eq. (3.64) is recovered from Eq. (3.72). In the limit $\Upsilon \gg 1$, Eq. (3.72) has the following

asymptotic expression:[17]

$$y(L_0, z) \approx \frac{\hat{y}}{\sqrt{6\pi}} \Upsilon^{-1/6} \exp\left(\frac{3^{3/2}}{4}\Upsilon^{1/3}\right)\cos\left(k_\beta L_0 - \frac{3}{4}\Upsilon^{1/3} + \frac{\pi}{12}\right). \tag{3.74}$$

The bunch tail thus breaks up exponentially with an exponent proportional to $\Upsilon^{1/3}$.

In case the beam is being accelerated in the linac, the result (3.74) still applies provided we replace $\hat{y}$ by the adiabatically damped value $\hat{y}\sqrt{\gamma_i/\gamma_f}$, where $\gamma_{i,f}m_0c^2$ are the initial and final particle energies, and the factor L_0/γ in the expression (3.73) by its average value $(L_0/\gamma_f)\ln(\gamma_f/\gamma_i)$. These substitution rules have been discussed following Eq. (3.38) in connection with the two-particle model.

For the SLAC linac, we may take $W_0 = 1.4$ cm^{-2}, $L = 3.5$ cm, $L_0 = 3000$ m, $N = 5 \times 10^{10}$, $\gamma_i = 2 \times 10^3$, $\gamma_f = 10^5$, $k_\beta = 0.06$ m^{-1}, and $\alpha = 0.016$ m^{-1}, and obtain $\Upsilon = 115$ at the very tail of the uniform bunch for the accelerated beam. For the case of a beam coasting at 1 GeV, we have $\Upsilon = 1400$ at the bunch tail. Figure 3.6(a) shows the snapshots of an accelerated beam as it approaches the end of the linac. The coasting beam snapshots are shown in Figure 3.6(b). For relatively weak beams, the corresponding beam behavior was illustrated in Figure 3.3.

Exercise 3.12 Consider a uniform bunch as in Eq. (3.70) but a constant wake $W_1(z) = -W_0$ ($W_0 > 0$). Show that

$$y(L_0, z) \approx \hat{y}e^{ik_\beta L_0} I_0\left(\sqrt{-2i\Upsilon}\right),$$
$$\Upsilon = \frac{Nr_0 L_0 W_0}{k_\beta \gamma L}\left(\frac{1}{2} - \frac{z}{l}\right), \tag{3.75}$$

where $I_0(x)$ is the Bessel function. For $\Upsilon \gg 1$, show that

$$y(L_0, z) \approx \frac{\hat{y}}{2^{3/4}\pi^{1/2}} \Upsilon^{-1/4} e^{\sqrt{\Upsilon}} \cos\left(k_\beta L_0 - \sqrt{\Upsilon} + \frac{\pi}{8}\right). \tag{3.76}$$

[17]The derivation of Eq. (3.74), omitted here, can be obtained by the method of steepest descents. This mathematical technique follows from the observation that the summation in Eq. (3.72) involves terms that are products of a rapidly rising function of n, namely Υ^n, and a rapidly diminishing function of n, namely $1/n!(2n)!$. The summation is therefore over a sharply peaked function of n. The method of steepest descents, which basically means fitting this sharply peaked function with a Gaussian and approximating the summation by the area under the Gaussian, can be applied to yield Eq. (3.74).

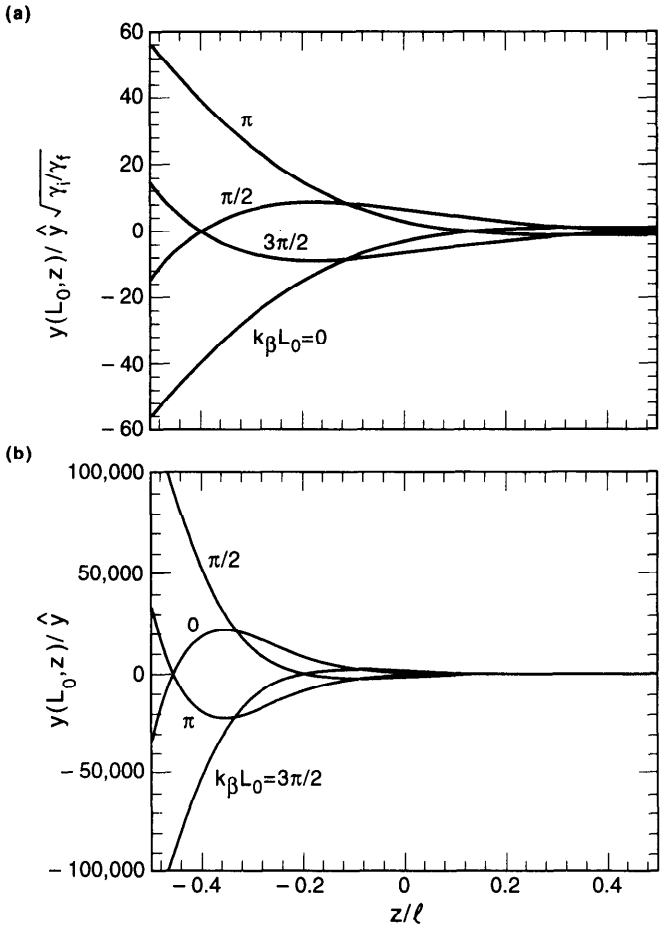

Figure 3.6. Bunch distortion due to dipole beam breakup for the case when the beam distribution and the wake function are described by Eq. (3.70). Four snapshots are shown with $k_\beta s$ (modulo 2π) $= 0, \pi/2, \pi$, and $3\pi/2$ towards the end of the linac. The wake strength parameter at the bunch tail is (a) $\Upsilon = 115$ for an accelerated beam, and (b) $\Upsilon = 1400$ for a coasting beam.

Exercise 3.13 Consider a uniform bunch and a resistive-wall wake $W_1(z) = -W_0\sqrt{-l/z}$. Show that

$$y(L_0, z) \approx \hat{y} e^{ik_\beta L_0} \sum_{m=0}^{\infty} \left(-\frac{\pi\Upsilon^2}{4}\right)^m \times \left[\frac{1}{m!(2m)!} - i\frac{2^m\Upsilon}{(2m+1)!!(2m+1)!}\right], \quad (3.77)$$

$$\Upsilon = \frac{Nr_0L_0W_0}{k_\beta\gamma L}\sqrt{\frac{1}{2} - \frac{z}{l}}\,.$$

So far we have been considering the transverse effects of the $m = 1$ wake fields. It should be remembered that this same transverse dipole wake force also has a longitudinal partner that affects the beam energy spread. If the beam is injected off center into a linac, in addition to a transverse deflecting wake force connected with $W_1(z)$, it also generates a dipole longitudinal wake force connected with $W_1'(z)$. To illustrate this, let us again consider a two-particle model with a leading macroparticle of charge $Ne/2$ with displacement y_1 and a trailing macroparticle, which is a distance $|z|$ behind and has a displacement y_2. A particle in the trailing macroparticle sees, in addition to a transverse wake potential $-Ne^2W_1(z)y_1/2$, a longitudinal wake potential

$$\Delta E = -\tfrac{1}{2}Ne^2W_1'(z)y_1y_2. \tag{3.78}$$

A consequence of this longitudinal wake is to cause an energy spread in the beam that depends on both the longitudinal and transverse positions of the particle. In contrast, the $m = 0$ wake force produces an energy spread that depends only on the longitudinal position of the particle under consideration.

If the beam displacement comes from an injection error, and if the transverse wake fields are ignored, we have $y_1 = y_2 = (\hat{y}\cos k_\beta s)/\sqrt{1 + \alpha s}$. It follows by integrating Eq. (3.78) over the linac that

$$\Delta E \approx -\frac{1}{4}Ne^2\hat{y}^2W_1'(z)\frac{\gamma_i}{\gamma_f}\ln\frac{\gamma_f}{\gamma_i}. \tag{3.79}$$

Equation (3.79) can be compared with the energy spread caused by the $m = 0$ wake, Eq. (3.4). Since W_0'/W_1' is of the order of b^2, where b is the vacuum chamber pipe radius, the energy loss due to the $m = 0$ wake is typically much larger than that due to the $m = 1$ wake if the transverse beam displacement $|y| \ll b$. For the SLAC linac, if we take $W_1'(-1\text{ mm}) = 6\text{ cm}^{-3} \times L_0/L$, cavity period $L = 3.5$ cm, $\hat{y} = 1$ mm, $N = 5 \times 10^{10}$, $\gamma_f/\gamma_i = 50$, and a total linac length of $L_0 = 3$ km, the energy loss of a particle in the trailing macroparticle due to this effect is 0.7 MeV.

3.3 QUADRUPOLE BEAM BREAKUP

The next topic to be discussed is the transverse *quadrupole beam breakup instability* ($m = 2$) in a linac. This instability becomes significant when the transverse beam size is comparable to the beam pipe radius b. What happens then is that the quadrupole wake field generated by the bunch head perturbs the focusing force on the bunch tail, leading to an instability if the beam is sufficiently intense. Unlike the dipole beam breakup instability, this $m = 2$ effect does not have to originate from injection or alignment errors. As we will soon see, a well-steered beam can be broken up by the $m = 2$ wake forces.

Consider a beam bunch whose trajectory in a linac is centered in the vacuum chamber pipe so that no dipole wake fields are generated. Quadrupole wake fields, however, can be generated if the transverse beam shape is not round, in which case the beam possesses two types of quadrupole moments, one normal and one skewed:

$$Q_n = \langle x^2 \rangle - \langle y^2 \rangle \quad \text{and} \quad Q_s = 2\langle xy \rangle, \tag{3.80}$$

where the brackets indicate averaging over the transverse bunch distribution.

Consider a beam represented as an elliptically shaped slice of charge q and quadrupole moments Q_n and Q_s. Quadrupole wake fields are generated behind this beam slice. A test charge e that trails the beam slice at a distance $|z|$ $(z < 0)$ would see a transverse wake force

$$\vec{F}_\perp = -2eq\frac{W_2(z)}{L}\left[Q_n(x\hat{x} - y\hat{y}) + Q_s(y\hat{x} + x\hat{y})\right], \tag{3.81}$$

where $W_2(z)$ is the quadrupole wake function of the linac for one cavity period and L is the cavity period length. The wake force due to Q_n resembles the force seen by a particle as it traverses a quadrupole magnet, and the wake force due to Q_s resembles that of a skew quadrupole magnet.

For a beam bunch with total charge Ne and longitudinal distribution $\rho(z)$, a particle located at a position z relative to the bunch center sees the quadrupole wake fields left behind by all charge slices in front of it. These wake fields are equivalent to that of a quadrupole magnet of strength

$$\frac{1}{B\rho}\frac{\partial B_y}{\partial x} = \frac{1}{B\rho}\frac{\partial B_x}{\partial y} = \frac{2Nr_0}{\gamma L}\int_z^\infty dz'\,\rho(z')W_2(z - z')Q_n(z'), \tag{3.82}$$

and a skew quadrupole magnet of strength

$$\frac{1}{B\rho}\frac{\partial B_y}{\partial y} = -\frac{1}{B\rho}\frac{\partial B_x}{\partial x} = \frac{2Nr_0}{\gamma L}\int_z^\infty dz'\,\rho(z')W_2(z - z')Q_s(z'), \tag{3.83}$$

where $1/B\rho = e/E$ is the beam rigidity. In the following, we assume the transverse beam distribution is upright in the x-y plane, so that the skew moment $Q_s = 0$.

There are two main sources of the normal quadrupole moments of the beam distribution. The first comes from the fact that the beam sizes $\langle x^2 \rangle$ and $\langle y^2 \rangle$ scale with the β-functions β_x and β_y, respectively. In a FODO lattice, for example, β_x and β_y alternate their maximum and minimum values along the accelerator, giving rise to a nonvanishing Q_n that oscillates with a period equal to the FODO cell length. The second source of

quadrupole moment results from injecting a beam whose beam size at the injection point does not match that prescribed by the linac lattice.

The first source is there even in an ideal operation. Instability occurs when the phase advance per FODO cell, μ, is close to 180°. However, even if μ is away from 180° so that the motion of the bunch tail is stable, the quadrupole wake fields can distort the tail distribution and cause an effective increase of the beam emittance. The second source is a result of operation errors. Its corresponding quadrupole moment, and thus the wake force, oscillates with twice the betatron oscillation frequency. Such an oscillation resonantly drives the particles in the bunch tail, leading to a beam breakup instability just like the dipole beam breakup mechanism. Effects of both sources of quadrupole moments are discussed below.

Consider a FODO lattice, and a beam with equal horizontal and vertical emittances $\epsilon_x = \epsilon_y = \epsilon(s)$. Identifying $\langle x^2 \rangle = \epsilon_x \beta_x$ and $\langle y^2 \rangle = \epsilon_y \beta_y$, the quadrupole moment at position s is given by

$$Q_n(s) = \epsilon(s)\big[\beta_x(s) - \beta_y(s)\big]. \tag{3.84}$$

With acceleration, the beam energy and emittance are given by

$$\gamma(s) = \gamma_i(1 + \alpha s) \quad \text{and} \quad \epsilon(s) = \frac{\epsilon_i}{1 + \alpha s}, \tag{3.85}$$

where γ_i and ϵ_i are the quantities at the injection point of the linac.

The quadrupole wake force induces a perturbation of the betatron phase advances, ψ_x and ψ_y, on particles in the bunch tail. When μ is sufficiently away from 180°, these phase advance perturbations, accumulated over the length L_0 of the linac, are given by

$$\begin{aligned}\Delta\psi_{x,y} &= \pm\frac{1}{2}\int_0^{L_0} ds\, \beta_{x,y}\left(\frac{1}{B\rho}\frac{\partial B_y}{\partial x}\right) \\ &= \pm\frac{Nr_0\epsilon_i}{\gamma_i L}\int_z^{\infty} dz'\,\rho(z')W_2(z - z')\int_0^{L_0} ds\,\frac{\beta_{x,y}(s)\big[\beta_x(s) - \beta_y(s)\big]}{(1 + \alpha s)^2},\end{aligned} \tag{3.86}$$

where the upper and lower signs are for $\Delta\psi_x$ and $\Delta\psi_y$, respectively.

If acceleration is slow, so that the particle energy does not vary significantly over a FODO cell, we can approximate the quantity $\beta_{x,y}(\beta_x - \beta_y)$ in the integrand of Eq. (3.86) by their average values over a FODO cell,

$$\big\langle \beta_{x,y}(s)\big[\beta_x(s) - \beta_y(s)\big]\big\rangle = \pm\frac{L_c^2}{6\cos^2(\mu/2)}, \tag{3.87}$$

where L_c is the FODO cell length. The divergence at $\mu = 180°$ is evident.

Substituting Eq. (3.87) into Eq. (3.86) gives

$$\Delta\psi_x \approx \Delta\psi_y \approx \frac{Nr_0\epsilon_i L_c^2}{6\gamma_i \alpha L \cos^2(\mu/2)} \int_z^\infty dz'\, \rho(z') W_2(z - z'). \quad (3.88)$$

For short bunches, the integral in Eq. (3.88) and thus the betatron phase perturbation $\Delta\psi_{x,y}$ are negative. This reflects the fact that the quadrupole wake force tends to *defocus* on bunch tail.

In some applications, such as for a free electron laser or a linear collider, it is important to avoid emittance growths. Since the betatron phase advances at the bunch head and tail are different, there is a significant growth of the effective emittance if $|\Delta\psi_{x,y}| \gtrsim 1$.

With a two-particle model (actually a two-slice model), the tail slice has a phase advance perturbation

$$\Delta\psi_{x,y} \approx \frac{Nr_0\epsilon_i L_c^2 W_2(z)}{12\gamma_i \alpha L \cos^2(\mu/2)}. \quad (3.89)$$

If $N = 5 \times 10^{10}$, $\epsilon_i = 1.5 \times 10^{-8}$ m, $L_c = 25$ m, $W_2(-1\text{ mm}) = -0.4\text{ cm}^{-4}$, $\mu = 90°$, $\alpha = 0.016\text{ m}^{-1}$, and $L = 3.5$ cm, we obtain $\psi_{x,y} \approx -8$ mrad.

This type of quadrupole beam breakup can be avoided if solenoids are used instead of quadrupole magnets for focusing, in which case the transverse beam shape can be made round. It is also possible to avoid it by the equivalent of a BNS damping. This can be achieved by adjusting the betatron focusing along the length of the bunch according to

$$\Delta k_\beta(s, z) \approx -\frac{Nr_0\epsilon(s) L_c^2}{6\gamma(s) L \cos^2(\mu/2)} \int_z^\infty dz'\, \rho(z') W_2(z - z') \quad (3.90)$$

to compensate for the wake induced perturbation (3.88).

To illustrate the second quadrupole beam breakup mechanism, we consider a two-slice model consisting of two elliptically shaped thin slices of charge $Ne/2$ each.[18] Consider for simplicity a coasting beam which by design has a round transverse beam distribution with $\langle x^2\rangle = \langle x'^2\rangle/k_\beta^2 = \langle y^2\rangle = \langle y'^2\rangle/k_\beta^2 = a^2$, where k_β is the betatron wave number, assumed uniform along the linac and equal in the x and y planes. Assume the beam is injected with an error in the horizontal beam size with $\langle x^2\rangle = a^2(1 + \Delta)$ and $\langle x'^2\rangle/k_\beta^2 = a^2(1 - \Delta)$, where $|\Delta| \ll 1$ is an error parameter.

The beam sizes of the leading particle slice behave according to

$$\langle x^2\rangle = a^2 + a^2\Delta \cos 2k_\beta s \quad \text{and} \quad \langle y^2\rangle = a^2. \quad (3.91)$$

[18]A one-slice model would not be very useful, because the slice would not see its own transverse wake force.

The vertical beam size is unperturbed, and the horizontal beam size oscillates with twice the betatron frequency. The quadrupole moment of the leading slice is given by $Q_n = \langle x^2 \rangle - \langle y^2 \rangle = a^2\Delta \cos 2k_\beta s$.

In the absence of BNS damping, a test charge e in the trailing particle slice is driven resonantly by the quadrupole wake field left behind by the leading slice according to[19]

$$\begin{aligned} x'' + k_\beta^2 x &= -\frac{Nr_0 W_2(z) a^2 \Delta}{\gamma L} x \cos 2k_\beta s, \\ y'' + k_\beta^2 y &= \frac{Nr_0 W_2(z) a^2 \Delta}{\gamma L} y \cos 2k_\beta s. \end{aligned} \tag{3.92}$$

For a modestly strong beam, Eq. (3.92) can be solved by iteration, keeping only the resonant contributions, to yield

$$\begin{aligned} x &\approx x_0 \cos k_\beta s + \frac{x_0'}{k_\beta} \sin k_\beta s \\ &\quad - \frac{Nr_0 W_2(z) a^2 \Delta}{4k_\beta \gamma L} s \left[x_0 \sin k_\beta s + \frac{x_0'}{k_\beta} \cos k_\beta s \right], \\ y &\approx y_0 \cos k_\beta s + \frac{y_0'}{k_\beta} \sin k_\beta s \\ &\quad + \frac{Nr_0 W_2(z) a^2 \Delta}{4k_\beta \gamma L} s \left[y_0 \sin k_\beta s + \frac{y_0'}{k_\beta} \cos k_\beta s \right]. \end{aligned} \tag{3.93}$$

The wake field term is proportional to s, indicating the bunch tail is resonantly driven.

We are interested in the rms beam size of the trailing slice, which is given by

$$\begin{aligned} \langle x^2 \rangle &\approx a^2 + a^2 \Delta \cos 2k_\beta s - \frac{Nr_0 W_2(z) a^4 \Delta}{2k_\beta \gamma L} s \sin 2k_\beta s, \\ \langle y^2 \rangle &\approx a^2 + \frac{Nr_0 W_2(z) a^4 \Delta}{2k_\beta \gamma L} s \sin 2k_\beta s. \end{aligned} \tag{3.94}$$

The behavior of these two particle slices is sketched in Figure 3.7. The

[19]These are special cases of Mathieu's equation.

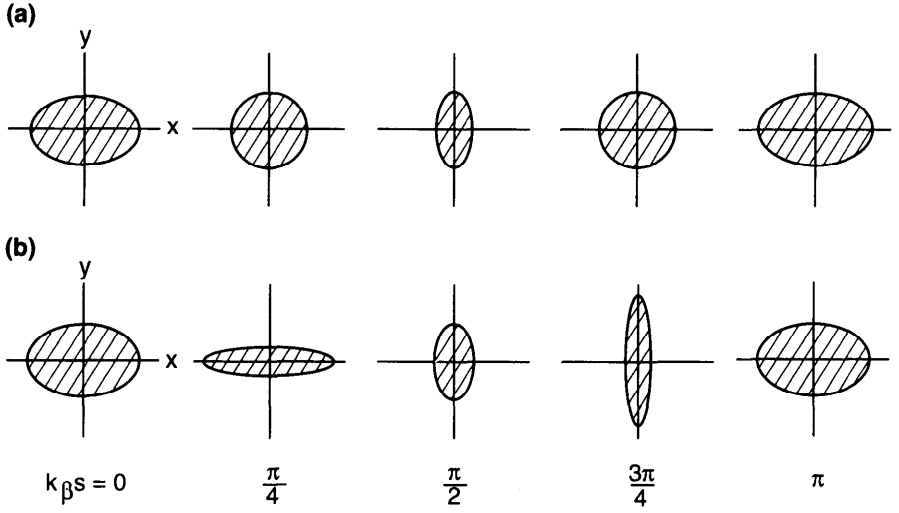

Figure 3.7. Snapshots of the beam shape when the bunch is injected with a mismatch in the horizontal beam size. The transverse *x-y* profiles are shown for a slice of the beam in (a) the bunch head and (b) the bunch tail. The values of $k_\beta s$ indicated are modulo π.

trailing slice has the same *x-y* profile as the leading slice when $k_\beta s$ (modulo π) = 0 or $\pi/2$, but looks very different at intermediate times. In particular, the vertical size of the leading slice is unperturbed by the wake field, but that of the trailing slice is perturbed. The polarity of the bunch tail deformation is not arbitrary. Exchanging the profiles at $k_\beta s = \pi/4$ and $k_\beta s = 3\pi/4$ in Figure 3.7(b), for example, would be incorrect.

Equation (3.94) says that if the beam is injected with a mismatched beam size, then at the end of the linac the bunch-tail size mismatch will grow by an extra factor of Υ compared with the bunch-head mismatch, where Υ is the growth parameter

$$\Upsilon = -\frac{Nr_0 W_2(z) L_0 a^2}{2k_\beta \gamma L}. \tag{3.95}$$

To control this type of quadrupole beam breakup instability, it is necessary to have $\Upsilon \ll 1$. For an accelerated beam, we have

$$\Upsilon = -\frac{Nr_0 W_2(z) a_i^2}{2k_\beta \gamma_i \alpha L}, \tag{3.96}$$

where a_i and γ_i are quantities taken at the injection point.

Exercise 3.14 One could BNS damp the wake induced beam size oscillation (3.94) by introducing extra focusing in the bunch tail. For a coasting beam, show that this requires

$$\Delta k_\beta = -\frac{Nr_0 W_2(z)a^2}{4k_\beta \gamma L}. \tag{3.97}$$

Figure 3.8 gives the results of a numerical simulation of the beam size of a Gaussian beam with intensity $N = 5 \times 10^{10}$ being accelerated from 42 MeV to 1.2 GeV in the first section of the SLAC linac of length 112 m. Eleven slices, evenly spaced longitudinally over a span of $4\sigma_z = 4$ mm, are used to model the bunch. In the simulation, the beam is assumed to be injected on axis, so that no dipole ($m = 1$) wake fields are generated. The longitudinal ($m = 0$) wake is included, although most of its effect has been compensated by phasing the bunch center 15° ahead of the accelerating rf voltage. The

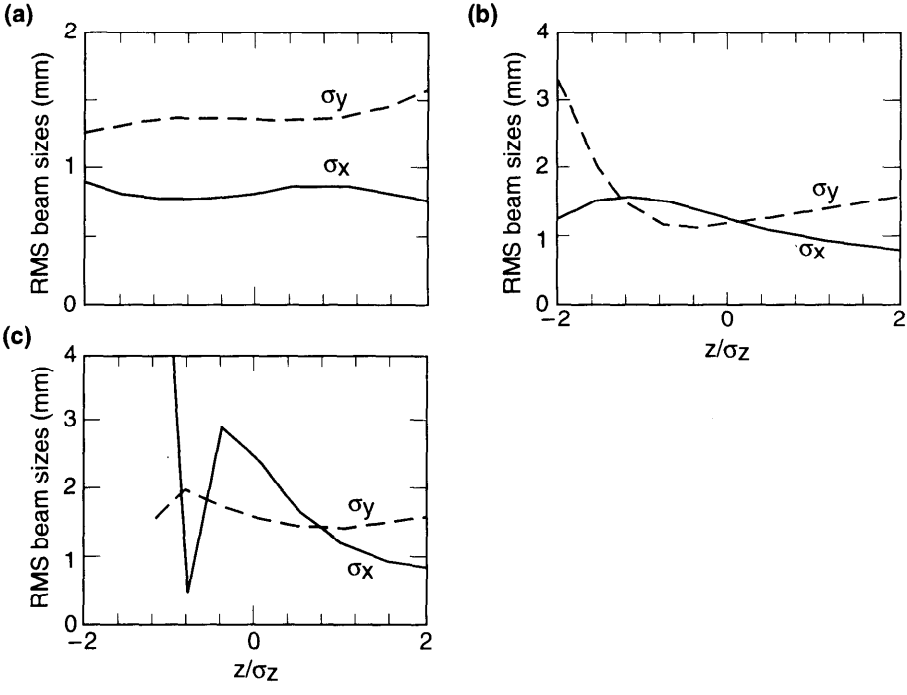

Figure 3.8. Results of a numerical simulation that demonstrates the effect of a quadrupole beam breakup in a linac. (a) The rms horizontal and vertical beam sizes along the bunch at the end of the linac section when only the $m = 0$ wake is included. (b) Same as (a), but including the $m = 2$ wake due to the FODO structure of the linac lattice. (c) The beam contains an additional quadrupole moment due to a 20% injection mismatch. In all cases, $z > 0$ is toward the head of the bunch.

slight variation of the beam sizes along the bunch in Figure 3.8(a) results from the slight energy variation along the bunch due to the $m = 0$ wake. When the quadrupole wake due to the FODO nature of the linac lattice is included, Figure 3.8(b) shows clearly that the bunch tail is perturbed. When the beam is further assumed to be injected with a 20% mismatch in σ_x and -20% in σ_x', the quadrupole beam breakup is much enhanced, as seen in Figure 3.8(c).[20]

Analysis similar to the above can be extended to higher multipole wake fields ($m > 2$). For instance, the $m = 3$ case requires the consideration of triangularly shaped charge slices. We then obtain a growth parameter Υ that resembles Eqs. (3.25) and (3.38) for $m = 1$, and Eqs. (3.95–3.96) for $m = 2$:

$$\Upsilon = -\frac{Nr_0 W_m(z)}{4k_\beta L}\begin{cases} mL_0 a^{2(m-1)}/\gamma & \text{coasting beam,} \\ ma_i^{2(m-1)}/(m-1)\alpha\gamma_i & \text{accelerated beam.} \end{cases} \tag{3.98}$$

As m increases, the growth parameter decreases roughly as $a^{2(m-1)}/b^{2m}$, where a is the transverse beam size and b is the pipe radius.

[20]Alexander W. Chao and Richard K. Cooper, Part. Accel. **13**, 1 (1983).

CHAPTER 4

Macroparticle Models

In Chapter 2, we studied the wake fields generated by a beam in the vacuum chamber of an accelerator. In that study, we assumed that the particle distribution within the beam is rigid and that the beam motion is unperturbed by the wake fields other than the parasitic energy losses. In Chapter 3, these results were applied to study the effect of wake fields acting back upon the beam in linacs. In particular, we have considered a few one- and two-particle models in which the beam is represented simply as one or two macroparticles interacting with the vacuum chamber surroundings and, in the case of two-particle models, among themselves.

A one-particle model, in which a rigid, structureless beam interacts with its own wake fields, is the simplest model that describes the beam-environment interaction. A two-particle model offers the opportunity of looking into the instability mechanisms associated with the internal degrees of freedom in the beam distribution.

In linacs, the macroparticles are considered frozen in their relative longitudinal positions. For circular accelerators this is no longer true, because particles execute longitudinal synchrotron oscillations, and the instability analysis becomes more involved. In this chapter, a few one- and two-particle models will be developed to illustrate the various longitudinal and transverse instabilities encountered by bunched beams in circular accelerators.

The advantage of the simplified one- and two-particle models is that they provide an intuitive picture of the instability mechanisms. In fact, we find these models sufficiently useful that we are dedicating the present chapter to them. A full account of the internal beam motions will be postponed until

Chapter 6, where most of the results obtained in this chapter will be rederived systematically using the Vlasov formalism.[1]

4.1 ROBINSON INSTABILITY

The mechanism of the Robinson instability is one of the most basic instability mechanisms encountered in circular accelerators. The radio frequency (rf) accelerating cavities in a circular accelerator are tuned so that the resonant frequency ω_R of the fundamental mode[2] is very close to an integral multiple of the revolution frequency ω_0 of the beam. This necessarily means that the wake field excited by the beam in the cavities contains a major frequency component near $\omega_R \approx h\omega_0$, or equivalently, the impedance $Z_0^{\parallel}$ has a sharp peak at $\omega_R \approx h\omega_0$, where h is an integer called the *harmonic number*.

As we will soon show, the exact value of ω_R relative to $h\omega_0$ is of critical importance for the stability of the beam. Above the transition energy, the beam will be unstable if ω_R is slightly above $h\omega_0$ and stable if slightly below. This instability mechanism was first analyzed by Robinson.[3] Since then, different approaches have been developed to describe it.[4]

We will begin with the longitudinal motion of a one-particle beam, i.e., a point charge Ne. Let z_n be the longitudinal displacement of the beam at the accelerating rf cavity in the nth revolution, measured relative to the synchronous particle. The rate of change of z_n is related to the relative energy error $\delta_n = \Delta E/E$ of the beam in the same nth revolution by Eq. (1.9), i.e.,

$$\frac{d}{dn} z_n = -\eta C \delta_n, \tag{4.1}$$

where η is the slippage factor defined in Eq. (1.10); C is the accelerator circumference. A positive z_n means the beam arrives at the rf cavity earlier than the synchronous particle. Again from Eq. (1.9), we have

$$\frac{d}{dn} \delta_n = \frac{(2\pi\nu_s)^2}{\eta C} z_n, \tag{4.2}$$

[1]Historically, the Vlasov equation technique was actually introduced earlier than the simplified models.

[2]That is, the lowest $m = 0$ cavity mode. In Figure 2.27, it corresponds to the tallest peak in Re $Z_0^{\parallel}$, which has the lowest resonant frequency.

[3]K. W. Robinson, Cambridge Electron Accel. Report CEAL-1010 (1964).

[4]M. Lee, SLAC Report SPEAR-31 (1970); Matthew Sands, Orsay LAL Reports 2-76, 3-76, 4-76 (1976); A. Hofmann, *Proc. Int. School Part. Accel.*, Erice, 1976, CERN Report 77-13, p. 139; P. B. Wilson, *AIP Proc.* **87**, *Phys. High Energy Accel.*, Fermilab, 1981, p. 450. One approach, adopted by Robinson but not in the present text, is to apply an equivalent circuit analysis. This is especially useful if one is interested not only in the beam dynamics but also the response of the rf system, the beam loading effect, and its feedback control.

where ν_s is the synchrotron tune. Typically, $\nu_s \ll 1$, i.e., the beam does not execute much synchrotron motion during the time it completes one revolution.

Equation (4.2) is valid when the beam has a vanishing intensity. For an intense beam, the energy variation also depends on the wake field generated by the beam. The $d\delta_n/dn$ equation then acquires an additional term,

$$\frac{d}{dn}\delta_n = \frac{(2\pi\nu_s)^2}{\eta C} z_n + \frac{eV(z_n)}{E}$$

$$= \frac{(2\pi\nu_s)^2}{\eta C} z_n - \frac{Nr_0}{\gamma} \sum_{k=-\infty}^{n} W_0'(kC - nC + z_n - z_k), \quad (4.3)$$

where W_0' is the longitudinal wake function accumulated over one turn of the accelerator. The summation over k is over the wake fields left behind by the beam from all revolutions previous to the nth. The argument of the wake function is the longitudinal separation of beam positions between the nth and the kth revolution. Combining Eqs. (4.1) and (4.3) yields the equation of motion

$$\frac{d^2 z_n}{dn^2} + (2\pi\nu_s)^2 z_n = \frac{Nr_0\eta C}{\gamma} \sum_{k=-\infty}^{n} W_0'(kC - nC + z_n - z_k). \quad (4.4)$$

In case the beam bunch has an oscillation amplitude much shorter than the wavelength of the fundamental cavity mode, one can expand the wake function:

$$W_0'(kC - nC + z_n - z_k) \approx W_0'(kC - nC) + (z_n - z_k) W_0''(kC - nC). \quad (4.5)$$

The first term on the right hand side of Eq. (4.5) is a static term independent of the motion of the beam. It describes the parasitic loss effect already discussed in Section 2.5 and can be taken care of by a constant shift in z_n. We will drop this term altogether. The second term, on the other hand, does involve the dynamics of the beam. The quantity $z_n - z_k$ is the difference of z's and—although we will not make such an approximation—resembles a time derivative dz/dn. An inspection of Eq. (4.4) then suggests an instability, since a dz/dn term in a d^2z/dn^2 equation indicates a possible exponential growth of z.

Substituting Eq. (4.5) into Eq. (4.4) gives a linear equation for z_n, which one can try to solve staying in the time domain. However, transforming to the

frequency domain at this point simplifies the mathematics considerably. In the frequency domain, z_n as a function of n is written as

$$z_n \propto e^{-in\Omega T_0}, \tag{4.6}$$

where $T_0 = C/c = 2\pi/\omega_0$ is the beam revolution period, and Ω is the mode frequency of the beam oscillation and is a key quantity yet to be determined. An ansatz of the form (4.6) is applicable only if the equation of motion is linear in z. By writing down Eq. (4.6), the problem of solving the differential equation of motion becomes the problem of solving an algebraic equation for Ω,

$$\Omega^2 - \omega_s^2 = -\frac{Nr_0\eta c}{\gamma T_0} \sum_{k=-\infty}^{\infty} (1 - e^{-ik\Omega T_0}) W_0''(kC), \tag{4.7}$$

where $\omega_s = \nu_s \omega_0$ is the synchrotron oscillation frequency and we have extended the summation over k to ∞ taking advantage of the causality property of the wake function.

The wake function can be expressed in terms of the longitudinal impedance using Eq. (2.72). An application of the identity from Eq. (2.210) then gives

$$\Omega^2 - \omega_s^2 = -i\frac{Nr_0\eta}{\gamma T_0^2} \sum_{p=-\infty}^{\infty} \left[p\omega_0 Z_0^{\parallel}(p\omega_0) - (p\omega_0 + \Omega) Z_0^{\parallel}(p\omega_0 + \Omega) \right]. \tag{4.8}$$

The factors $p\omega_0$ and $p\omega_0 + \Omega$ in front of $Z_0^{\parallel}$ come from taking the derivative of the induced voltage $V(z)$ with respect to z when we made the approximation (4.5). Given the impedance, Eq. (4.8) can in principle be solved for Ω. Here we will take a perturbative approach and assume Ω does not deviate much from ω_s for modest beam intensities. We thus replace Ω by ω_s on the right hand side of Eq. (4.8).

In general, Ω is complex. The real part of Ω is the perturbed synchrotron oscillation frequency of the collective beam motion, and the imaginary part gives the growth rate (or damping rate if negative) of the motion. Equation (4.8) then gives a *mode frequency shift*

$$\begin{aligned} \Delta\Omega &= \mathrm{Re}(\Omega - \omega_s) \\ &= \frac{Nr_0\eta}{2\gamma T_0^2 \omega_s} \sum_{p=-\infty}^{\infty} \left[p\omega_0 \,\mathrm{Im}\, Z_0^{\parallel}(p\omega_0) - (p\omega_0 + \omega_s) \mathrm{Im}\, Z_0^{\parallel}(p\omega_0 + \omega_s) \right] \end{aligned} \tag{4.9}$$

and an *instability growth rate*

$$\tau^{-1} = \mathrm{Im}(\Omega - \omega_s) = \frac{Nr_0\eta}{2\gamma T_0^2 \omega_s} \sum_{p=-\infty}^{\infty} (p\omega_0 + \omega_s)\mathrm{Re}\, Z_0^{\parallel}(p\omega_0 + \omega_s). \quad (4.10)$$

It is the imaginary part of the impedance that contributes to the collective frequency shift, and the real part that contributes to the instability growth rate.

There are two terms under the summation for $\Delta\Omega$ in Eq. (4.9). As we will show later in Eq. (6.59), the first term comes from a static phenomenon called *potential-well distortion*, while the origin of the second term is dynamical. Note that the growth rate τ^{-1} has a contribution only from the dynamical term. The static potential-well distortion does not contribute to τ^{-1}; mathematically, this term vanishes because $\mathrm{Re}\, Z_0^{\parallel}$ is an even function of ω.

It may be instructive at this point to make a detour to investigate why the impedance is sampled at the frequencies $p\omega_0$ and $p\omega_0 + \omega_s$ in Eqs. (4.9–4.10).[5] Consider first a point bunch circulating in the accelerator without synchrotron oscillation. The impedance will see the beam signal at times $t = kT_0$, i.e.,

$$\text{beam signal} \propto \sum_{k=-\infty}^{\infty} \delta(t - kT_0), \quad (4.11)$$

where the summation is over all revolutions; larger k means later revolutions. The frequency spectrum of the signal, obtained by a Fourier transformation, is

$$\begin{aligned} \text{spectrum} &\propto \int dt\, e^{i\omega t} \sum_{k=-\infty}^{\infty} \delta(t - kT_0) \\ &= \sum_{k=-\infty}^{\infty} e^{i\omega k T_0} = \omega_0 \sum_{p=-\infty}^{\infty} \delta(\omega - p\omega_0), \end{aligned} \quad (4.12)$$

where use has been made of Eq. (2.211). The frequency content of the beam signal is therefore a series of δ-functions at $\omega = p\omega_0$. This beam signal and spectrum are shown in Figure 4.1. For the static potential-well effect, the relevant signal seen by the impedance is therefore sampled at multiples of the revolution frequency $\omega = p\omega_0$.

[5] R. Littauer, *AIP Proc.* **105**, *Phys. High Energy Accel.*, SLAC, 1982, p. 869; S. Chattopadhyay, *AIP Proc.* **127**, *Phys. High Energy Accel.*, BNL/SUNY, 1983, p. 460; R. H. Siemann, *AIP Proc.* **184**, *Phys. Part. Accel.*, Fermilab 1987 and Cornell 1988, p. 430; J. Gareyte, *ibid.*, p. 343.

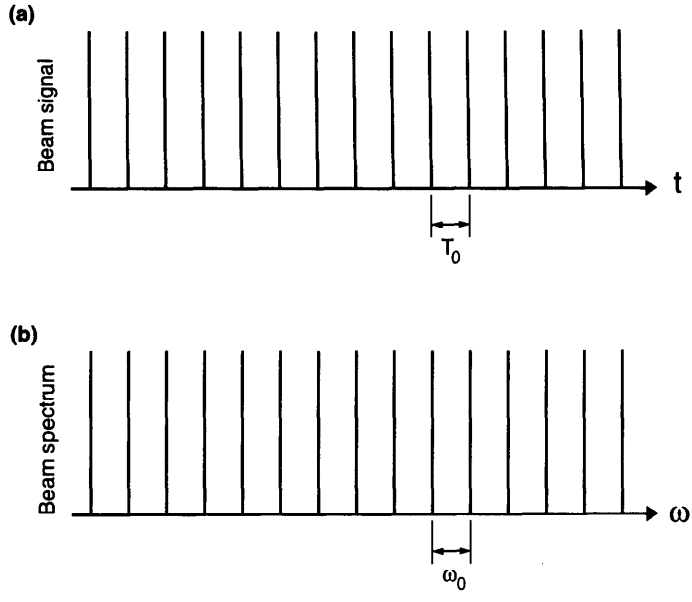

Figure 4.1. (a) Signal of a point-charge beam received by a pickup electrode or an impedance. (b) Spectrum of the signal in (a).

Exercise 4.1 The signal (4.11) is for a point-charge beam. For a beam with finite length, we have

$$\text{beam signal} \propto \sum_{k=-\infty}^{\infty} \rho(-ct + ckT_0), \tag{4.13}$$

where $\rho(z)$ is the bunch distribution ($z > 0$ is the bunch head). Show that the beam spectrum still consists of a series of δ-functions at frequencies $\omega = p\omega_0$, but the strengths of those δ-functions now contain an extra form factor of $\tilde{\rho}(\omega)$, given by Eq. (2.104), i.e.,

$$\text{spectrum} \propto \sum_{p=-\infty}^{\infty} \tilde{\rho}(p\omega_0)\delta(\omega - p\omega_0). \tag{4.14}$$

This beam signal and spectrum are shown in Figure 4.2 for a Gaussian beam. This additional form factor is the reason why the parasitic loss has the form of Eq. (2.212). It also says in order to obtain information on the

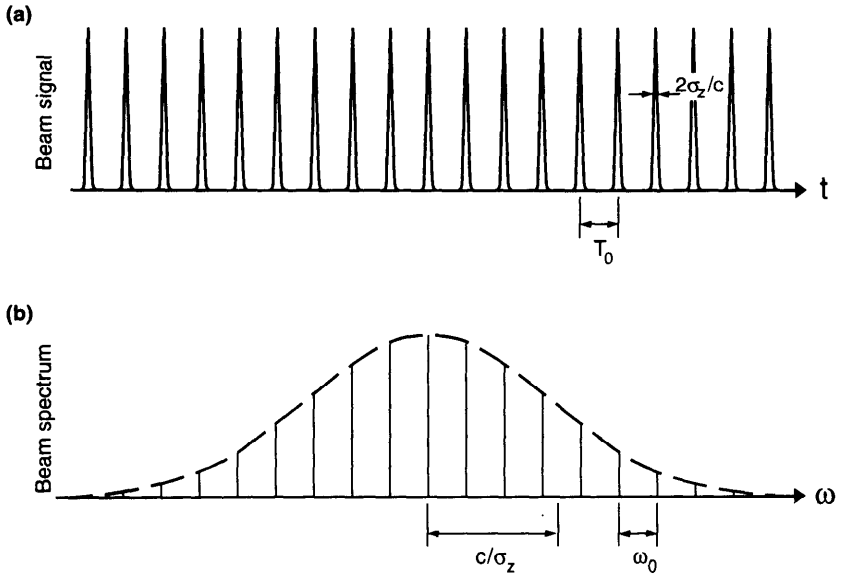

Figure 4.2. (a) Signal of a Gaussian beam, $\sigma_z / c = 0.05T_0$. (b) The spectrum of the Gaussian beam consists of a series of δ-functions like Figure 4.1(b), but also an additional Gaussian form factor whose rms width is $\sigma_\omega = c / \sigma_z$.

bunch length, a pickup must be sensitive to frequencies $p\omega_0 \gtrsim c/\sigma_z$, i.e., it must have a bandwidth $\gtrsim c/\sigma_z$.

We now let the point bunch execute a synchrotron oscillation, in which case we have

$$\text{beam signal} \propto \sum_{k=-\infty}^{\infty} \delta\left[t - kT_0 + \hat{\tau}\cos(\omega_s kT_0)\right], \tag{4.15}$$

where $\hat{\tau}$ is some small synchrotron oscillation amplitude. The frequency content of this signal is

$$\text{spectrum} \propto \sum_k e^{i\omega[kT_0 - \hat{\tau}\cos(\omega_s kT_0)]}. \tag{4.16}$$

For small oscillation amplitudes, this becomes

$$\text{spectrum} \propto \sum_k e^{i\omega kT_0}\left[1 - i\omega\hat{\tau}\cos(\omega_s kT_0)\right]. \tag{4.17}$$

Compared with Eq. (4.12), the spectrum contains a new term

$$
\begin{aligned}
&-i\omega\hat{\tau}\sum_k e^{i\omega kT_0}\cos(\omega_s kT_0) \\
&\quad = -\frac{i}{2}\omega\hat{\tau}\sum_k\left[e^{ikT_0(\omega+\omega_s)} + e^{ikT_0(\omega-\omega_s)}\right] \\
&\quad = -\frac{i}{2}\hat{\tau}\omega_0\sum_{p=-\infty}^{\infty}\left[(p\omega_0-\omega_s)\delta(\omega-p\omega_0+\omega_s)\right. \\
&\qquad\qquad \left.+(p\omega_0+\omega_s)\delta(\omega-p\omega_0-\omega_s)\right]. \qquad (4.18)
\end{aligned}
$$

The impedance responding to the synchrotron oscillation is therefore to be evaluated at $p\omega_0 \pm \omega_s$, i.e., the synchrotron sidebands of multiples of the revolution frequency. Equation (4.18) explains the form of the second terms of Eqs. (4.8–4.9), and Eq. (4.10).

Exercise 4.2 Consider the point-charge beam executing synchrotron oscillation and generating the signal of Eq. (4.15). In case the oscillation amplitude is not small, show that[5]

$$
\text{spectrum} \propto \sum_{l=-\infty}^{\infty}\sum_{p=-\infty}^{\infty} i^{-l}J_l\left[(p\omega_0+l\omega_s)\hat{\tau}\right]\delta(\omega-p\omega_0-l\omega_s). \qquad (4.19)
$$

Use Table 6.1 if necessary. The spectrum still consists of δ-functions. There is a set of δ-functions located at $\omega = p\omega_0$, whose amplitudes are proportional to $J_0(\omega\hat{\tau})$. For each p, there is a set of sidebands around $p\omega_0$, the lth sideband ($l = \pm$integers) occurs at $p\omega_0 + l\omega_s$, and their spectral strengths are proportional to $J_l(\omega\hat{\tau})$. This behavior is shown in Figure 4.3. For small $\hat{\tau}$, Eq. (4.19) becomes Eq. (4.18). What happens to the beam spectrum if the bunch has a finite length?

The Bessel function form factors mentioned in Exercise 4.2 come from the beam executing synchrotron oscillation. They are not to be confused with the form factor coming from the finite bunch length as discussed in Exercise 4.1. As we will see in Chapter 6, Bessel functions play an important role in the kinematics of collective modes, and the reason for their repeated appearance is embedded in the discussion in Exercise 4.2. The same Bessel form factors also appear in the frequency modulated (fm) signals for radios.

We now return to Eq. (4.10). Consider the resonator impedance of the form of Eq. (2.82) for the fundamental cavity mode. The only significant contributions to the growth rate (4.10) come from two terms in the summation, namely $p = \pm h$, assuming the width of the impedance peak $\omega_R/2Q$

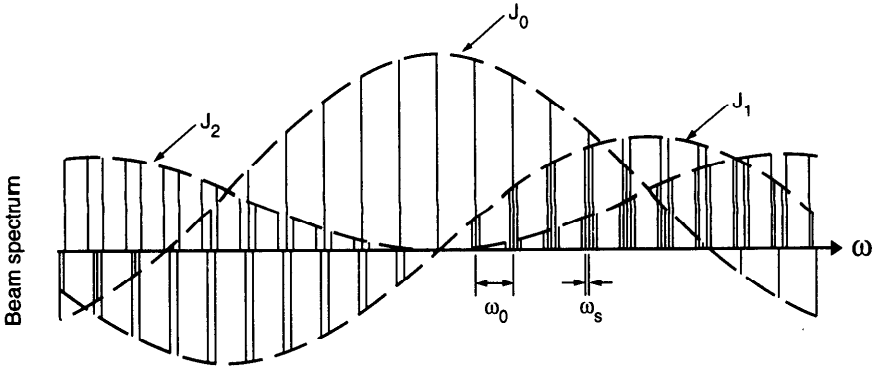

Figure 4.3. Spectrum of a point-charge beam which is synchrotron oscillating with frequency $\omega_s = \omega_0 / 10$ and an exaggerated amplitude of $\hat{\tau} = 1 / 3\,\omega_0$. Around each $p\omega_0$, there is a cluster of sidebands spaced by ω_s. Each sideband is specified by one index l, and the lth sideband has a strength proportional to $J_l[(p\omega_0 + l\omega_s)\hat{\tau}]$. Sidebands up to $l = \pm 2$ are shown.

and the synchrotron frequency ω_s are both much less than ω_0. This gives

$$\tau^{-1} \approx \frac{Nr_0\eta h\omega_0}{2\gamma T_0^2\omega_s}\left[\mathrm{Re}\, Z_0^{\parallel}(h\omega_0 + \omega_s) - \mathrm{Re}\, Z_0^{\parallel}(h\omega_0 - \omega_s)\right]. \quad (4.20)$$

Beam stability requires $\tau^{-1} \leq 0$. That is, the real part of the impedance must be lower at frequency $h\omega_0 + \omega_s$ than at frequency $h\omega_0 - \omega_s$ if $\eta > 0$ (above transition), and the other way around if $\eta < 0$ (below transition). This condition implies the *Robinson criterion* that, above transition, the resonant frequency ω_R of the fundamental cavity mode should be slightly detuned downwards from an exact integral multiple of ω_0. Below transition, stability requires ω_R be slightly higher than $h\omega_0$. The situation is illustrated in Figure 4.4. When the Robinson criterion is met, the synchrotron oscillation of the beam is "Robinson damped," and this damping will help in stabilizing the beam against similar instabilities due to other impedance sources.

Substituting Eq. (2.82) into Eq. (4.20) and assuming that both ω_s and $\Delta\omega = \omega_R - h\omega_0$ are much less than the resonator width $\omega_R/2Q$ which, in turn, is much less than ω_0, we obtain

$$\tau^{-1} \approx \frac{4Nr_0\eta R_S Q^2\,\Delta\omega}{\pi\gamma T_0 h}. \quad (4.21)$$

Similarly we have

$$\Delta\Omega \approx -\frac{12Nr_0\eta R_S Q^3\nu_s\,\Delta\omega}{\pi\gamma T_0 h^2}. \quad (4.22)$$

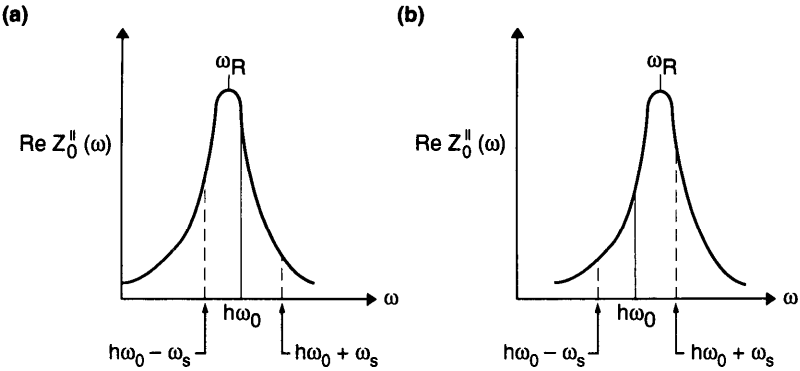

Figure 4.4. Illustration of the Robinson stability criterion. The rf fundamental mode is detuned so that ω_R is (a) slightly below $h\omega_0$ and (b) slightly above $h\omega_0$. (a) is Robinson damped above transition and antidamped below transition. (b) is antidamped above transition and damped below transition.

Taking for example $\eta = 0.03$ (above transition), $N = 10^{11}$, $E = 1$ GeV,[6] $\omega_0 = 9.4 \times 10^6\ \mathrm{s}^{-1}$, $\nu_s = 0.01$, $h\omega_0/2\pi = 360$ MHz, $R_S = 1\ \mathrm{M}\Omega$, $Q = 2000$, $\Delta\omega/2\pi = -10$ kHz (rf detuned lower for stability), $h = 240$, we find $\tau = -1.2$ ms and $\Delta\Omega = 0.2 \times 10^3\ \mathrm{s}^{-1}$. Robinson damping (or antidamping) can be rather strong. Figure 4.5 gives the numerical results obtained by inserting the resonator impedance (2.82) into Eqs. (4.9) and (4.10) and their comparison with the approximate expressions (4.21) and (4.22).

Physically, Robinson instability comes from the fact that the revolution frequency of an off-momentum beam is not given by ω_0 but by $\omega_0(1 - \eta\delta)$. To illustrate the Robinson instability mechanism, consider a beam executing synchrotron oscillation above transition. Due to the energy error of the beam, the impedance samples the beam signal at a frequency slightly below $h\omega_0$ if $\delta > 0$, and slightly above $h\omega_0$ if $\delta < 0$. In order to damp this synchrotron oscillation of the beam, we need to let the beam lose energy when $\delta > 0$ and gain energy when $\delta < 0$ (at least relative to the case when $\delta = 0$). This can be achieved by having an impedance that decreases with increasing frequency in the neighborhood of $h\omega_0$. The Robinson criterion then follows.

Although the Robinson instability was originally considered for the fundamental mode of the rf cavities, it is obvious that the same analysis applies to the higher rf modes, in which case we would pay attention to accidentally landing the frequencies $p\omega_0$ for some integer p on the wrong side of some higher order impedance peak. Since there are typically many higher order modes for a given rf cavity design, it is sometimes necessary to damp them by

[6]This is meant to be the particle energy at injection. In a circular accelerator, it is usually during the low energy operation that the beam is least stable. The beam usually becomes more stable when accelerated to higher energies.

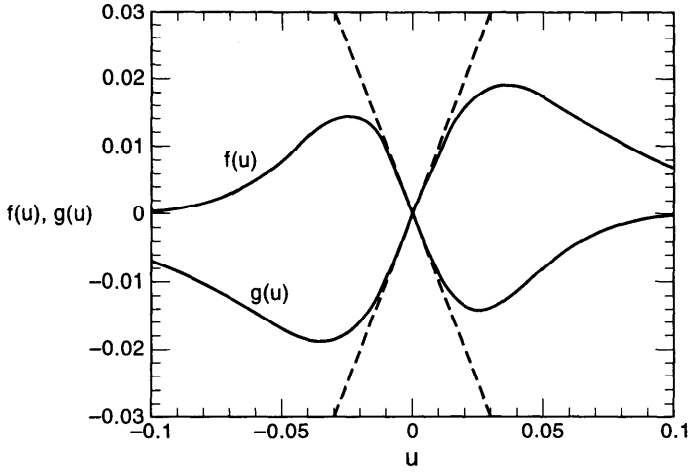

Figure 4.5. The collective mode frequency shift $\Delta\Omega = (3Q\nu_s\xi / h)f(\upsilon)$ and growth rate $\tau^{-1} = \xi g(\upsilon)$ due to a resonator impedance are shown as functions of the detuning $\upsilon = (\omega_R - h\omega_0) / \omega_0$. We have defined $\xi = 8Nr_0\eta R_S Q^2 / \gamma T_0^2 h$. For small $\omega_s \ll \omega_R / 2Q$, the maximum Robinson damping and antidamping occur when $\upsilon = \pm h / 2\sqrt{3}Q$. The dashed curves are the approximate expressions (4.21 – 4.22), or $f(\upsilon) \approx -\upsilon$ and $g(\upsilon) \approx \upsilon$. We have taken $h = 240$, $Q = 2000$, and $\nu_s = 0.01$.

a careful design in order to assure beam stability.[7] As a rough estimate of the maximum growth rate due to a higher order cavity mode, one may substitute $\Delta\omega \approx \pm\omega_R / 2\sqrt{3}Q$ (the worst case) into Eq. (4.21). Often in practice a proper detuning of the fundamental mode frequency will overcome the contributions from the accidental higher order modes.

Note that Eqs. (4.9) and (4.10) apply also to impedances other than the rf impedance. The space charge impedance (2.80), for example, being purely imaginary, causes a collective frequency shift but not an instability. However, substituting Eq. (2.80) into Eq. (4.9) or substituting the resistive-wall impedance (2.76) into Eqs. (4.9–4.10) leads to divergent results. These are consequences of the point-charge assumption. When a more realistic bunch distribution is used, the bunch spectrum will cut off the high-frequency divergences, yielding physically meaningful results. These will be elaborated further in Section 6.3.

To generalize the context further, it should be mentioned that the Robinson analysis does not have to be restricted to longitudinal effects. A similar analysis, given in the next section, for the transverse $m = 1$ wake fields leads to a "transverse Robinson" effect. Furthermore, as will be discussed in Chapter 6, by allowing internal degrees of freedom in the beam, higher bunch modes—so far excluded from the analysis because we assumed

[7]This involves the *de-Q*-ing of those higher order rf cavity modes. See further discussions following Eq. (4.32).

a one-particle model—also have their own versions of longitudinal and transverse Robinson instability and their corresponding stability criteria.

In case the longitudinal impedance is broad-banded in such a way that there are no fine structures of frequency width $\lesssim \omega_0$, the summation Σ_p in Eq. (4.10) can be approximated by $\int dp$. The fact that $\mathrm{Re}\, Z_0^{\parallel}$ is an even function of ω leads to the important conclusion that broad-band impedances (or equivalently, short range wake fields) do not cause instabilities of the Robinson type characterized by Eq. (4.10). This point will be elaborated further in Section 6.5.

Exercise 4.3 So far we have been considering a circulating beam with a single bunch.

(a) Follow steps similar to those in the text to set up the problem for a beam with two bunches, each with charge Ne and located diametrically opposite on the circumference. Show that there are two modes of collective motions, whose complex mode frequencies are

$$\Omega_{\pm} - \omega_s \approx -i\frac{Nr_0\eta}{2\gamma T_0^2\omega_s}\sum_{p=\infty}^{\infty}\Big\{\big[1+(-1)^p\big]p\omega_0 Z_0^{\parallel}(p\omega_0) - \big[1\pm(-1)^p\big](p\omega_0+\omega_s)Z_0^{\parallel}(p\omega_0+\omega_s)\Big\}. \quad (4.23)$$

Use Eq. (4.23) to show that the Robinson stability criterion remains the same as in the single-bunch case for a sharp rf fundamental mode. What happens if the two bunches have slightly different ω_s? How about slightly different intensities? [Hint: Refer to Section 4.6 if necessary. For the case with two bunches, the harmonic number h must be an even number].

(b) How, if at all, is the Robinson criterion modified if the two bunches have charges Ne and $-Ne$ and circulate in opposite directions around the accelerator?

4.2 RIGID BEAM TRANSVERSE INSTABILITY

We now consider a one-particle beam executing a transverse betatron oscillation, say in the vertical y-direction. The beam possesses an instantaneous dipole moment $Ney(s)$. A particle that follows the beam at a distance d behind sees, according to Table 2.2, a vertical wake force

$$-Ne^2y(s)W_1(-d)/C.$$

The equation of motion of the one-particle beam is

$$y''(s) + \left(\frac{\omega_\beta}{c}\right)^2 y(s) = -\frac{Nr_0}{\gamma C}\sum_{k=1}^{\infty} y(s-kC)W_1(-kC), \quad (4.24)$$

where a prime on $y(s)$ means taking derivative with respect to s, W_1 is the wake function integrated around the accelerator circumference C,[8] and the summation over k sums the wake fields over all previous revolutions. This model was first suggested by Courant and Sessler,[9] and also by Ferlenghi, Pellegrini, and Touschek.[10]

Of course, an off-axis beam also possesses distribution moments other than the dipole moment. For instance, it possesses a monopole moment (i.e., the total beam charge) and higher moments such as the quadrupole moment. The monopole moment has been considered in Section 4.1 and in any case does not give rise to a transverse wake force. Effects due to the higher moments can be ignored as compared with the dipole wake effects if we assume the beam displacement y is much smaller than the vacuum chamber pipe radius.

One may still object that a dipole moment also generates a longitudinal wake, which is not considered in Eq. (4.24). Indeed, strictly speaking, a rigorous treatment of the problem must also include the longitudinal motion of the beam. Thus, the transverse wake force in the betatron equation of motion (4.24) should be modulated by the arrival time of the beam, while the synchrotron motion should be perturbed by the betatron motion through the longitudinal wake W_1'. Only when this coupled synchro-betatron motion is considered does the system strictly satisfy the Maxwell equations and become fully Hamiltonian. However, for practical purposes, as long as the synchrotron and betatron frequencies are not close to a resonance condition $\omega_\beta \pm \omega_s = n\omega_0$ (where $\omega_0 = 2\pi c/C = 2\pi/T_0$) and the transverse displacements are small, Eq. (4.24) still accurately describes the transverse motion of the beam. We will return to this point following Eq. (6.162).

We again solve Eq. (4.24) in the frequency domain. Letting $y \propto \exp(-i\Omega s/c)$ and transforming the wake function into the transverse impedance, we obtain the following equation for the complex mode frequency Ω,

$$\Omega^2 - \omega_\beta^2 = \frac{Nr_0 c}{\gamma T_0} \sum_{k=1}^{\infty} e^{ik\Omega T_0} W_1(-kC)$$

$$= -i\frac{Nr_0 c}{\gamma T_0^2} \sum_{p=-\infty}^{\infty} Z_1^{\perp}(p\omega_0 + \Omega), \tag{4.25}$$

where $Z_1^{\perp}$ is the total impedance around the accelerator circumference.

[8] In the present approximation, it does not matter if the impedance is localized or distributed around the circumference. See discussion following Eq. (1.16).

[9] Ernest D. Courant and Andrew M. Sessler, *Rev. Sci. Instr.* **37**, 1579 (1966).

[10] E. Ferlenghi, C. Pellegrini, and B. Touschek, *Nuovo Cimento* **44B**, 253 (1966); C. Pellegrini, *Physics with Intersecting Storage Rings*, Enrico Fermi Int. School of Phys., Academic Press, New York, 1971, p. 221.

The structure of Eq. (4.25) can be understood by observing that

$$\Delta\nu_y \sim \frac{\beta_y}{4\pi}\left(\frac{-ieIZ_1^{\perp}}{E}\right), \tag{4.26}$$

where $\Delta\nu_y = (\Omega - \omega_\beta)/\omega_0$ is the mode tune shift, $\beta_y = R/\nu_y$ is the β-function, and $-iIZ_1^{\perp}$ is the transverse voltage per unit vertical displacement. At a fundamental level, the quantity $\Delta\nu_y$ is just the tune shift as described in Eqs. (1.13–1.16), except that the perturbation now comes from the collective wake forces instead of errors in the external focusing force, and that the resultant frequency shift is complex in general.

In contrast with Eqs. (4.8–4.10), the transverse case does not contain a potential-well distortion term. This is a consequence of the fact that, given the wake field established in previous revolutions, the transverse force on the macroparticle beam does not depend on the instantaneous transverse displacement of the beam. In other words, the transverse $m = 1$ wake field does not form a potential well.

Assuming Ω does not deviate much from ω_β so that Ω on the right hand side of Eq. (4.25) can be replaced by ω_β, we have a mode frequency shift

$$\Delta\Omega = \mathrm{Re}(\Omega - \omega_\beta) \approx \frac{Nr_0c}{2\gamma T_0^2\omega_\beta}\sum_{p=-\infty}^{\infty} \mathrm{Im}\, Z_1^{\perp}(p\omega_0 + \omega_\beta) \tag{4.27}$$

and growth rate

$$\tau^{-1} = \mathrm{Im}(\Omega - \omega_\beta) \approx -\frac{Nr_0c}{2\gamma T_0^2\omega_\beta}\sum_{p=-\infty}^{\infty} \mathrm{Re}\, Z_1^{\perp}(p\omega_0 + \omega_\beta). \tag{4.28}$$

The reason the impedance is sampling the frequencies $p\omega_0 + \omega_\beta$ follows from a consideration similar to that following Eq. (4.11). In the present case,

$$\text{beam signal} \propto \sum_{k=-\infty}^{\infty} \delta(t - kT_0)\,\hat{y}e^{-i\omega_\beta t}, \tag{4.29}$$

where $\hat{y}$ is some betatron oscillation amplitude. The spectrum seen by the impedance is the Fourier transformation of Eq. (4.29),

$$\text{spectrum} \propto \hat{y}\omega_0 \sum_{p=-\infty}^{\infty} \delta(\omega - p\omega_0 - \omega_\beta). \tag{4.30}$$

The impedance therefore responds to frequencies $\omega = p\omega_0 + \omega_\beta$, i.e., the betatron sidebands of multiples of the revolution frequency.

Given the transverse impedance, Eqs. (4.27–4.28) are our main results. They are the transverse counterparts of the longitudinal Robinson instability effect. The real and the imaginary parts of the impedance contribute to the instability growth rate and the collective frequency shift, respectively, just as in the longitudinal Robinson case. In particular, for the case of space charge, the purely imaginary impedance gives rise to only a mode frequency shift and not an instability growth.

If the real part of $Z_1^{\perp}(\omega)$ contains sharp resonant peaks, there can be a *transverse Robinson instability*. More explicitly, if a resonant frequency ω_R is close to $h\omega_0$, an integral multiple of ω_0, then

$$\tau^{-1} \approx -\frac{Nr_0c}{2\gamma T_0^2\omega_\beta}\left[\operatorname{Re} Z_1^{\perp}(h\omega_0 + \Delta_\beta\omega_0) - \operatorname{Re} Z_1^{\perp}(h\omega_0 - \Delta_\beta\omega_0)\right], \quad (4.31)$$

where Δ_β is the noninteger part of the betatron tune $\nu_\beta = \omega_\beta/\omega_0$ and we have chosen $-\frac{1}{2} < \Delta_\beta < \frac{1}{2}$. A positive Δ_β means ν_β is above an integer; a negative Δ_β means ν_β is below an integer. For stability, ω_R should be slightly above $h\omega_0$ if $\Delta_\beta > 0$ and below $h\omega_0$ if $\Delta_\beta < 0$. The stability criterion of the transverse Robinson instability does not depend on whether the accelerator is operated above or below transition. Instead, it depends on whether the betatron tune is above or below an integer.

For a sharp resonator impedance whose resonant frequency ω_R happens to be close to $h\omega_0$, and assuming that both $|\omega_R - h\omega_0|$ and $|\Delta_\beta\omega_0|$ are much less than $\omega_R/2Q$, which is in turn much less than ω_0, we have

$$\begin{aligned} \Delta\Omega &\approx -\frac{Nr_0c^2R_SQ}{2\pi^2\gamma\omega_\beta h^2}(\omega_R - h\omega_0), \\ \tau^{-1} &\approx -\frac{2Nr_0c^2R_SQ^2}{\pi^2\gamma\omega_\beta h^3}(\omega_R - h\omega_0)\Delta_\beta. \end{aligned} \quad (4.32)$$

As a numerical example, let $N = 10^{11}$, $R_S = 40\ \mathrm{M\Omega/m^2}$, $Q = 2000$, $E = 1$ GeV (electron beam), $\omega_0 = 9.4 \times 10^6\ \mathrm{s^{-1}}$, $\nu_\beta = 6.05$, $h = 518$, and $(\omega_R - h\omega_0)/\omega_0 = \pm h/2\sqrt{3}Q$ (the worst case). We find $\tau = \mp 5$ ms and $\Delta\Omega = \mp 260\ \mathrm{s^{-1}}$. Figure 4.6 shows the mode frequency shift and the growth rate as functions of $\omega_R - h\omega_0$.

Since the exact values of all the transverse cavity mode frequencies are not easy to control, the value of ω_R of a transverse cavity mode is equally likely to be above or below $h\omega_0$ for some integer h; this collective beam motion is equally likely to be damped or antidamped.[11] In designing an accelerator for

[11]A statistical analysis can be found in C. Pellegrini and M. Sands, SLAC Report PEP-258 (1977); R. Siemann, *IEEE Trans. Nucl. Sci.* **NS-28**, 2437 (1981).

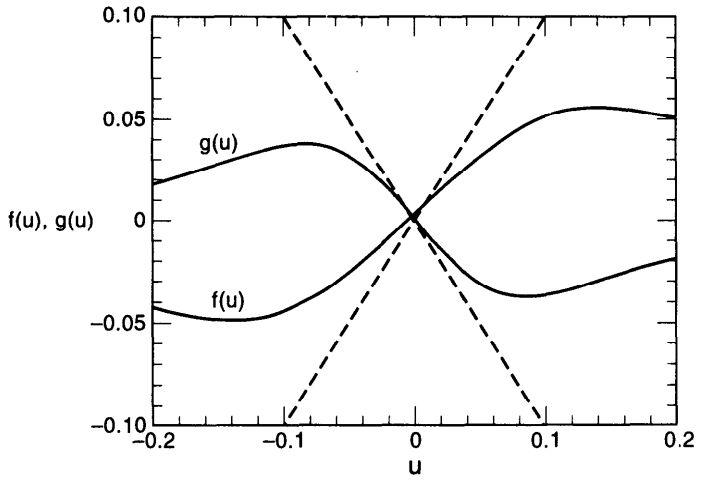

Figure 4.6. Mode frequency shift $-\xi f(\upsilon)$ and growth rate $(4Q\Delta_\beta \xi / h)g(\upsilon)$ as functions of $\upsilon = (\omega_R - h\omega_0)/\omega_0$, where $\xi = Nr_0c^2R_SQ / 2\pi^2\gamma\nu_\beta h^2$. For small $\Delta_\beta \ll h / 2Q$, maximum damping and antidamping occur when $\upsilon = \pm h / 2\sqrt{3}Q$. The dashed curves are the approximate expressions (4.32), which correspond to $f(\upsilon) \approx \upsilon$ and $g(\upsilon) \approx -\upsilon$. The parameters chosen are $\Delta_\beta = 0.05$, $Q = 2000$, $h = 518$. The dependence on Δ_β is weak as long as it is much less than $h / 2Q$.

high intensity beams, therefore, it is often necessary to *de-Q* the higher order modes by either passively or actively removing their field energies from the rf cavities. The higher order mode field energy often needs to be reduced by one or two orders of magnitude before the next beam bunch comes along. This is a demanding technology[12] because, among other considerations, the higher order modes must be de-*Q*ed without significantly affecting the operation of the cavity fundamental mode. By reducing the *Q*-value of the higher order modes sufficiently, the growth rates are reduced and the remaining collective instability can be handled by a conventional feedback system.

Unlike its longitudinal counterpart, the transverse Robinson instability does not have the strong damping provided by the fundamental rf cavity mode (assumed properly tuned), which makes it more of a serious concern. In principle, one could obtain a transverse Robinson damping by intentionally introducing an rf cavity whose resonator impedance is near $\omega_R \approx h\omega_0$ and tuning it favorably to counteract the accidental modes.

In case of a broad-band impedance (short range wake field), the summation over p can be approximated by an integral over p. It then follows from Eq. (4.28) and the fact that $\mathrm{Re}\, Z_1^\perp$ is an odd function of frequency

[12]R. Klatt and T. Weiland, DESY Report M-84-06 (1984); R. Palmer, SLAC-PUB-4542 (1989); H. Padamsee et al., *AIP Proc.* **214**, *Beam Dynamics Issues of High-Luminosity Asymmetric Collider Rings*, Berkeley, 1990, p. 235.

that $\tau^{-1} = 0$.[13] Broad-band impedances therefore do not cause transverse Robinson instability, a situation similar to the longitudinal case. However, as will be explained later in Sections 4.5 and 6.7, a broad-band impedance does cause an instability when the betatron frequency of a particle is not a constant, as assumed so far, but depends on its relative energy deviation δ.

Exercise 4.4 Using Eq. (4.28), show that the instability growth rate $\tau^{-1} = 0$ if ν_β = integer or if ν_β = integer + $\frac{1}{2}$. This is true for an arbitrary impedance.

As another application of the analysis of this section, let us find the instability growth rate and mode frequency shift for an accelerator with a resistive vacuum chamber. Substituting the transverse wake function (2.53) into Eq. (4.25), we obtain the result[14]

$$\tau^{-1} \approx -\frac{Nr_0c^2}{b^3\gamma\omega_\beta T_0\sqrt{\pi\sigma\omega_0}} f(\Delta_\beta),$$
$$f(\Delta_\beta) = \sum_{k=1}^{\infty} \sqrt{\frac{2}{k}} \sin(2\pi k\Delta_\beta), \tag{4.34}$$

and

$$\Delta\Omega \approx -\frac{Nr_0c^2}{b^3\gamma\omega_\beta T_0\sqrt{\pi\sigma\omega_0}} g(\Delta_\beta),$$
$$g(\Delta_\beta) = \sum_{k=1}^{\infty} \sqrt{\frac{2}{k}} \cos(2\pi k\Delta_\beta). \tag{4.35}$$

The functions $f(\Delta_\beta)$ and $g(\Delta_\beta)$ are depicted in Figure 4.7. We see that $f(\Delta_\beta)$ is positive (so that $\tau^{-1} < 0$ and the beam is stable) if $0 < \Delta_\beta < \frac{1}{2}$, and negative if $-\frac{1}{2} < \Delta_\beta < 0$. This means one should choose the betatron tune above an integer to assure stability against the resistive-wall wake fields. This is to be compared with the case of the resonator impedance, Eq. (4.31), for which the stability condition on Δ_β depends on the sign of $\omega_R - h\omega_0$.

[13]Incidentally, one would also expect $\Delta\Omega = 0$ for a broad-band impedance because $W_1(0) = 0$, i.e., the one-particle beam does not see its own wake force. This is indeed true by replacing $\Sigma_p \to \int dp$ in Eq. (4.27) and observing Eq. (2.93).

[14]One could also obtain Eq. (4.34) by inserting the impedance (2.76) into Eq. (4.28). This leads to another expression for $f(\Delta_\beta)$, i.e.,

$$f(\Delta_\beta) = \frac{1}{\sqrt{2}} \sum_{p=-\infty}^{\infty} \frac{\operatorname{sgn}(p + \Delta_\beta)}{|p + \Delta_\beta|^{1/2}}. \tag{4.33}$$

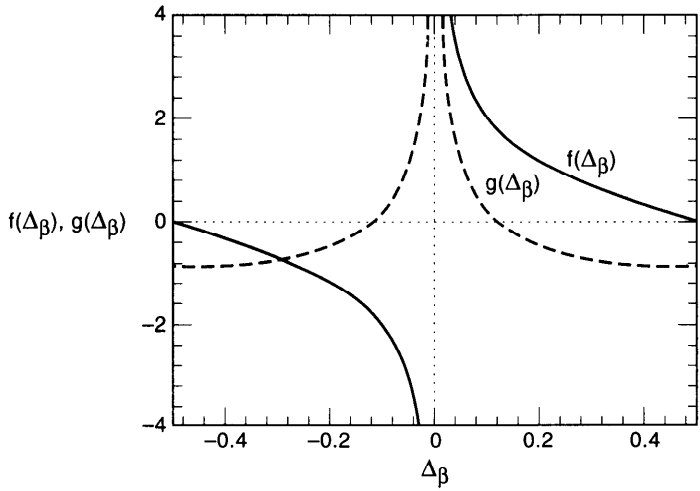

Figure 4.7. The functions $f(\Delta_\beta)$ and $g(\Delta_\beta)$ of Eqs. (4.34 – 4.35) are given as solid and dashed curves, respectively.

Take for example, $N = 10^{11}$, $b = 5$ cm, $E = 1$ GeV (electron beam), $\nu_\beta = 5.9$ (below an integer; therefore the beam is unstable), $\omega_0 = 9.4 \times 10^6$ s^{-1}, and $\sigma = 3 \times 10^{17}$ s^{-1}. We find $f(\Delta_\beta) = -2.0$ and an instability growth time of $\tau = 0.5$ s.

It will be shown later by Eq. (5.90) that, because the resistive-wall instability is rather weak, a small spread of betatron tune of the particles in the beam will stabilize the beam even if the betatron tune is below an integer. In practice, therefore, the choice of betatron tune is most likely not seriously restricted by the resistive-wall effect.

The stability criterion invariably involves the sign of Δ_β. This is because the beam oscillation is damped or antidamped depending on the relative phase between the beam oscillation and the wake force induced by the beam oscillation (damped if the wake force lags the beam oscillation and antidamped if the wake force leads the beam oscillation, much like what a child does when playing a swing set), and the relative phase is determined by Δ_β in the multiturn stability being considered.

4.3 STRONG HEAD-TAIL INSTABILITY

In Section 3.2, we treated the dipole beam breakup effect in linacs. There is also a dipole beam breakup mechanism in a circular accelerator; it will be called the *strong head-tail instability* here.[15] It is sometimes also called the

[15]The modifier "strong" is to distinguish this instability mechanism from that to be mentioned in Section 4.5.

transverse mode coupling instability, the transverse turbulent instability, or the transverse microwave instability in the literature.[16] The difference from the linac case is that now the beam particles are no longer frozen in their relative longitudinal positions. Instead, they execute synchrotron oscillations, thus constantly changing their relative longitudinal positions, with a low frequency ω_s.

To illustrate the mechanism of the strong head-tail instability, consider a two-particle beam that is made of two macroparticles, each with charge of $Ne/2$ and each executing synchrotron oscillation. We assume their synchrotron oscillations have equal amplitude but opposite phases. During time $0 < s/c < T_s/2$, where $T_s = 2\pi/\omega_s$ is the synchrotron oscillation period, particle 1 leads particle 2; the equations of motion for the two macroparticles are

$$\begin{aligned} y_1'' + \left(\frac{\omega_\beta}{c}\right)^2 y_1 &= 0, \\ y_2'' + \left(\frac{\omega_\beta}{c}\right)^2 y_2 &= \frac{Nr_0 W_0}{2\gamma C} y_1. \end{aligned} \tag{4.36}$$

Similarly, during $T_s/2 < s/c < T_s$, we have the same equations with indices 1 and 2 exchanged. Then during $T_s < s/c < 3T_s/2$, Eq. (4.36) applies again, etc. The quantities y_1 and y_2 are considered to be infinitesimal initially. Whether the beam is stable depends on their behavior in time. If the beam is stable, they will remain infinitesimal. If the beam is unstable, they will grow exponentially with time. This model was first suggested by Kohaupt[17] and Talman.[18]

In writing down Eq. (4.36), we have assumed for simplicity that the wake function (integrated over the accelerator circumference C), $W_1(z)$, is a constant, and yet it vanishes before the beam completes one revolution, i.e.,

$$W_1(z) = \begin{cases} -W_0 & \text{if } 0 > z > -(\text{bunch length}), \\ 0 & \text{otherwise.} \end{cases} \tag{4.37}$$

The property of wake functions requires that $W_0 > 0$. The short range wake function of (4.37) corresponds to an impedance which is broad-banded. In contrast with the Robinson-type instabilities, the strong head-tail instability is essentially a single-turn phenomenon.

[16]The latter two terms tend to imply instabilities involving higher order collective modes not properly represented by a two-particle model, but this subtlety is not important for our purpose here.

[17]R. D. Kohaupt, DESY Report M-80/19 (1980).

[18]R. Talman, CERN Report ISR-TH/81-17 (1981); R. Talman, *Nucl. Instr. Meth.* **193**, 423 (1982).

We now analyze the stability condition of the two-particle beam system. From Eq. (4.36), the solution for y_1 is simply a free betatron oscillation,

$$\tilde{y}_1(s) = \tilde{y}_1(0)e^{-i\omega_\beta s/c}, \tag{4.38}$$

where

$$\tilde{y}_1 = y_1 + i\frac{c}{\omega_\beta}y_1'. \tag{4.39}$$

Both the real and imaginary parts are meaningful in the representation (4.38–4.39).

Substituting Eq. (4.38) into the equation for y_2 yields the solution

$$\tilde{y}_2(s) = \tilde{y}_2(0)e^{-i\omega_\beta s/c} + i\frac{Nr_0W_0c}{4\gamma C\omega_\beta}\left[\frac{c}{\omega_\beta}\tilde{y}_1^*(0)\sin\frac{\omega_\beta s}{c} + \tilde{y}_1(0)se^{-i\omega_\beta s/c}\right]. \tag{4.40}$$

There are three terms in Eq. (4.40). The first two terms describe the free betatron oscillation; the third term, proportional to s, is the resonantly driven response. Equation (4.40) has its linac counterpart given by Eq. (3.24).

Equation (4.40) can be simplified if $\omega_\beta T_s/2 \gg 1$, or equivalently, $\omega_\beta \gg \omega_s$. In that case, the second term on the right hand side of Eq. (4.40) can be dropped because it is much smaller than the third term, and we can write the solution for the equations of motion during the period $0 < s/c < T_s/2$ in a matrix form,

$$\begin{bmatrix}\tilde{y}_1\\ \tilde{y}_2\end{bmatrix}_{s=cT_s/2} = e^{-i\omega_\beta T_s/2}\begin{bmatrix}1 & 0\\ i\Upsilon & 1\end{bmatrix}\begin{bmatrix}\tilde{y}_1\\ \tilde{y}_2\end{bmatrix}_{s=0}, \tag{4.41}$$

where [cf. Eq. (3.25)] we have defined a positive, dimensionless parameter

$$\Upsilon = \frac{\pi Nr_0W_0c^2}{4\gamma C\omega_\beta\omega_s}. \tag{4.42}$$

The time evolution during $T_s/2 < s/c < T_s$ can be obtained by exchanging indices 1 and 2 in the above analysis. The total transformation for one full synchrotron period is therefore

$$\begin{aligned}\begin{bmatrix}\tilde{y}_1\\ \tilde{y}_2\end{bmatrix}_{cT_s} &= e^{-i\omega_\beta T_s}\begin{bmatrix}1 & i\Upsilon\\ 0 & 1\end{bmatrix}\begin{bmatrix}1 & 0\\ i\Upsilon & 1\end{bmatrix}\begin{bmatrix}\tilde{y}_1\\ \tilde{y}_2\end{bmatrix}_0\\ &= e^{-i\omega_\beta T_s}\begin{bmatrix}1-\Upsilon^2 & i\Upsilon\\ i\Upsilon & 1\end{bmatrix}\begin{bmatrix}\tilde{y}_1\\ \tilde{y}_2\end{bmatrix}_0.\end{aligned} \tag{4.43}$$

As time evolves, the vector formed by the phasors $\tilde{y}_1$ and $\tilde{y}_2$ is repeatedly transformed by the 2×2 matrix in Eq. (4.43). Stability of the system is thus determined by the eigenvalues of this matrix. The two eigenvalues for the two modes (a + mode and a − mode) are

$$\lambda_{\pm} = e^{\pm i\phi}, \qquad \sin\frac{\phi}{2} = \frac{\Upsilon}{2}, \tag{4.44}$$

and the eigenvectors are

$$V_{\pm} = \begin{bmatrix} \pm e^{\pm i\phi/2} \\ 1 \end{bmatrix}. \tag{4.45}$$

Stability requires ϕ real, which is fulfilled if $|\sin(\phi/2)| \leq 1$, or

$$\Upsilon \leq 2. \tag{4.46}$$

For weak beams, $\Upsilon \ll 1$, we have $\phi \approx \Upsilon$. Near the instability, ϕ approaches π as Υ approaches 2.

An inspection of Eq. (4.41) indicates that the instability that occurs when $\Upsilon > 2$ causes a rather severe disruption of the beam, as seen by the fact that, during half a synchrotron period, the motion of the trailing particle has grown by an amount more than twice the amplitude of the free-oscillating leading particle. For $\Upsilon \leq 2$, the growths made during the half synchrotron periods when the particle is trailing do not accumulate and the beam is stable. As the beam intensity increases so that $\Upsilon > 2$, the growths of the particles then do accumulate and bootstrap into an instability. This *threshold* behavior is very different from the linac case, in which the beam—at least its tail—is always unstable. One can imagine that, by periodically exchanging the roles of leading and trailing particles, the two-particle beam is made more stable. The more frequently they are exchanged, the more stable is the beam. This shows up in the fact that Υ is inversely proportional to ω_s. Synchrotron oscillation is thus an effective stabilizing mechanism in circular accelerators. Strong betatron focusing and a high beam energy also help stabilize the beam, as indicated by the fact that Υ is inversely proportional to γ and ω_β. The factor $1/\omega_\beta$ in Υ is related to the β-function. If the β-function β_Z at the location of the impedance is known, a better expression for Υ would be obtained by replacing c/ω_β by β_Z.

In an accelerator, the most readily available beam signal comes from the beam position monitors that measure the center of charge of the beam. In the two-particle model, the center-of-charge signal is given by $y_1 + y_2$. In particular, it will be useful to examine its frequency spectrum. To do that, consider a two-particle beam that is in a pure eigenstate $V_{\pm}$ at time $s/c = 0$. In the stable region, it is straightforward to show that the subsequent motion

of the beam center of charge is given by

$$(\tilde{y}_1 + \tilde{y}_2)(s) = \exp\left[-i\left(\omega_\beta \mp \frac{\phi\omega_s}{2\pi}\right)\frac{s}{c}\right]\sum_{l=-\infty}^{\infty} C_l e^{-il\omega_s s/c},$$
$$C_l = 2i\Upsilon\frac{1 \pm (-1)^l}{(2\pi l \mp \phi)^2}(1 \mp e^{\pm i\phi/2}). \tag{4.47}$$

The $\pm$ modes as observed by a beam position monitor therefore contain the following frequencies:

$$\begin{aligned} &+ \text{ mode:} && \omega_\beta + l\omega_s - \frac{\phi}{2\pi}\omega_s, && l \text{ even} \\ &- \text{ mode:} && \omega_\beta + l\omega_s + \frac{\phi}{2\pi}\omega_s, && l \text{ odd.} \end{aligned} \tag{4.48}$$

Note that each mode contains a multiplicity of frequencies when observed continuously in time.

For weak beams, the two macroparticles move up and down in phase in the + mode and out of phase in the − mode. As Υ increases, the mode frequencies shift and the particle motions become more complicated; each mode then contains a combination of in-phase and out-of-phase motions. At the stability limit $\Upsilon = 2$, the frequencies of the two modes merge into each other and become imaginary, which means the beam is unstable. Figure 4.8 shows the spectrum as a function of Υ. In Figure 4.8, the index l is that appearing in Eqs. (4.47–4.48). It will also become a mode index when we consider realistic bunch distributions in Chapter 6.

If the beam receives a sudden kick at time $s/c = 0$, we have

$$\begin{bmatrix} \tilde{y}_1 \\ \tilde{y}_2 \end{bmatrix}_{s=0} = \begin{bmatrix} 1 \\ 1 \end{bmatrix}. \tag{4.49}$$

The subsequent center-of-charge motion is described as a superposition of the two eigenmodes. We find

$$(\tilde{y}_1 + \tilde{y}_2)(s) = \frac{2\Upsilon^2}{\cos(\phi/2)} e^{-i\omega_\beta s/c}\left[\exp\left(i\frac{\phi}{2\pi}\frac{\omega_s s}{c}\right)\sum_{l\,\text{even}}\frac{e^{-il\omega_s s/c}}{(2\pi l - \phi)^2}\right.$$
$$\left. - \exp\left(-i\frac{\phi}{2\pi}\frac{\omega_s s}{c}\right)\sum_{l\,\text{odd}}\frac{e^{-il\omega_s s/c}}{(2\pi l + \phi)^2}\right]. \tag{4.50}$$

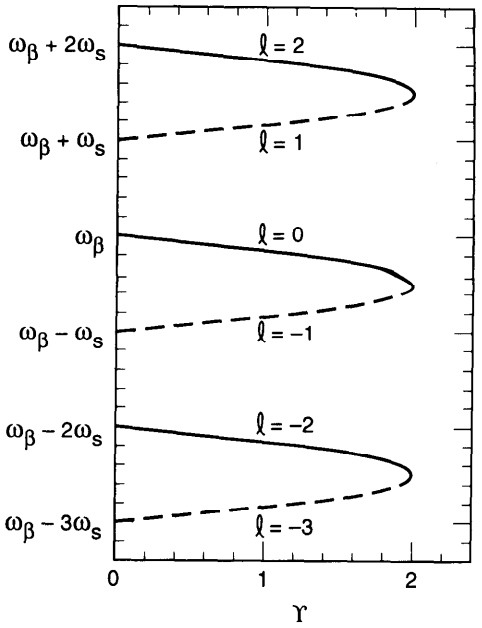

Figure 4.8. Frequency spectrum of the center-of-charge signal of the beam in the stable region $\Upsilon < 2$ in a two-particle model. The solid curves are the spectrum of the + mode, and the dashed curves are that of the − mode. Instability occurs at the point where the mode frequencies merge.

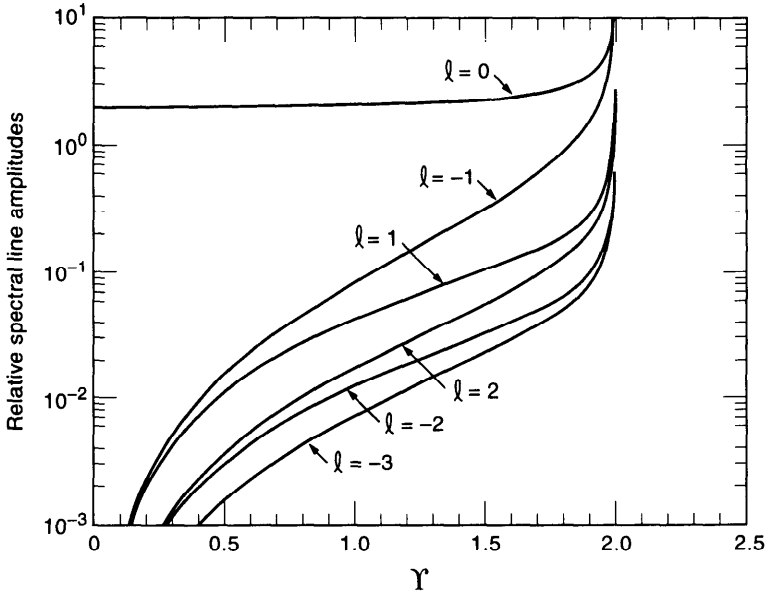

Figure 4.9. The relative amplitude of the spectral lines as observed at a beam position monitor after a two-particle beam is kicked. The spectral lines occur at frequencies given by Eq. (4.48). The normalization is arbitrarily chosen such that the $l = 0$ spectral strength at $\Upsilon = 0$ is equal to 2.

The relative amplitudes of the spectrum observed at the beam position monitor are shown in Figure 4.9 as a function of Υ. For $\Upsilon = 0$, the observed beam signal has only the unperturbed frequency ω_β. As the beam intensity increases, the amplitudes in the other spectral lines increase relative to the $l = 0$ line. Close to the instability threshold, the relative amplitudes of the $l = 0$ and the $l = -1$ lines become equal. At the threshold, all spectral line amplitudes diverge. Note that in the interest of having a high beam intensity, the accelerator is most likely operated not too far from the instability threshold.

Exercise 4.5 For modest beam intensities, one may keep only the $l = 0$ and $l = -1$ terms in Eq. (4.50). Show that the beam-position-monitor signal amplitude as a function of time exhibits a beating behavior with

$$\begin{aligned} \text{beat period} &= \frac{\pi T_s}{\pi - \phi}, \\ \text{relative depth of beat} &= \frac{2\phi^2(2\pi - \phi)^2}{\phi^4 + (2\pi - \phi)^4}. \end{aligned} \tag{4.51}$$

For weak beams, the beat frequency is the synchrotron frequency, and the depth of the beat is zero. Near the instability threshold, the beat frequency is low, while the depth for the beat approaches 100%. These expressions for the beat period and the depth of the beat can be used to extract information about the accelerator impedance from experimental measurements such as those shown in Figure 4.11 on page 186.

As mentioned, the most readily available signal from the beam is that of its center-of-charge motion observed by a beam position monitor. Using special instruments such as a streak camera, however, it is possible to observe the motion of the beam across the length of the beam. One such observation, made on the electron storage ring LEP at CERN, is shown in Figure 4.10.[19]

The strong head-tail instability is one of the cleanest instabilities to observe in electron storage rings.[20] In particular, one may measure the threshold beam intensity when the beam becomes unstable transversely and associate the observation with $\Upsilon = 2$. Another approach is to measure the "betatron frequency" (what is measured is, in fact, the frequency of the $l = 0$ spectral line of Figures 4.8 and 4.9) as the beam intensity is varied. From Eq.

[19]E. Rossa et al., *Proc. Euro. Part. Accel. Conf.*, Berlin, 1992, p. 144.

[20]R. Kohaupt, IEEE Trans. Nucl. Sci. **NS-26**, 3480 (1979); D. Rice et al., IEEE Trans. Nucl. Sci. **NS-28**, 2446 (1981); PEP Group, *Proc. 12th Int. Conf. High Energy Accel.*, Fermilab, 1983, p. 209.

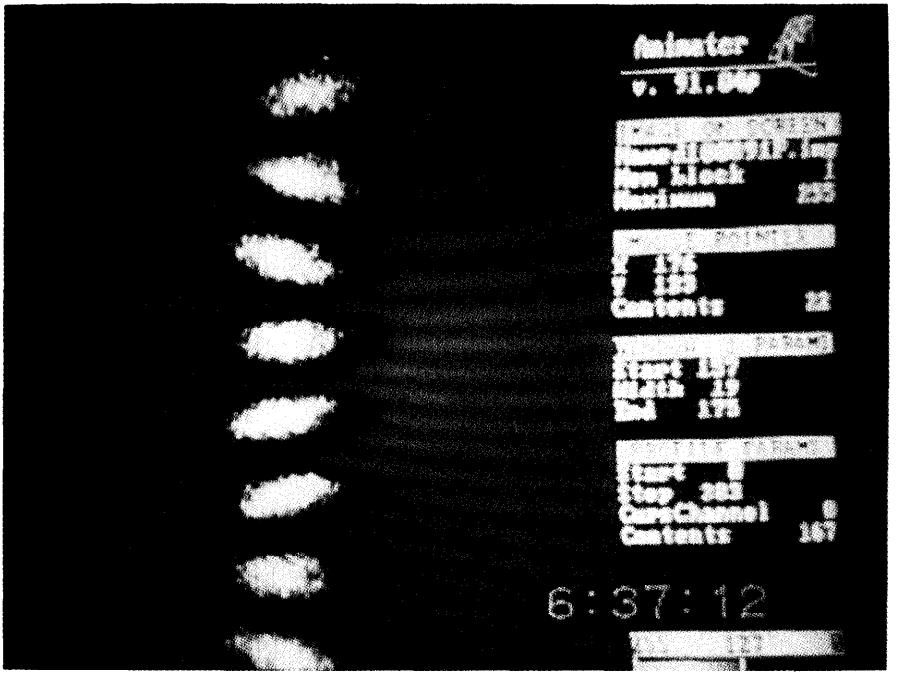

Figure 4.10. The turn-by-turn pictures, taken by a streak camera, of a beam executing a transverse head-tail oscillation in the electron storage ring LEP. The bunch is seen from the side and one observes a vertical head-tail oscillation (with mode $l = 1$). The horizontal scale is 500 ps for the total image while the vertical scale is not calibrated. The figure shows the same bunch each turn going from top to bottom. (Courtesy Albert Hofmann and Edouard Rossa, 1992.)

(4.48), the initial slope of this frequency with respect to the beam intensity is

$$\left(\frac{d\omega_\beta}{dN}\right)_{N=0} = -\frac{\omega_s}{2\pi}\left(\frac{d\phi}{dN}\right)_{N=0} = -\frac{r_0 W_0 c^2}{8\gamma C \omega_\beta}. \tag{4.52}$$

By measuring the instability threshold or by measuring the initial slope of the betatron frequency, information on the wake field or impedance can be obtained.

At the instability threshold, the measured betatron frequency has shifted by $\omega_s/2$, according to the two-particle model. The measured value of $(d\omega_\beta/dN)_{N=0}$ can be used to predict the instability threshold N_{th} by

$$N_{\text{th}} = -\frac{\omega_s}{\pi}\frac{1}{(d\omega_\beta/dN)_{N=0}}. \tag{4.53}$$

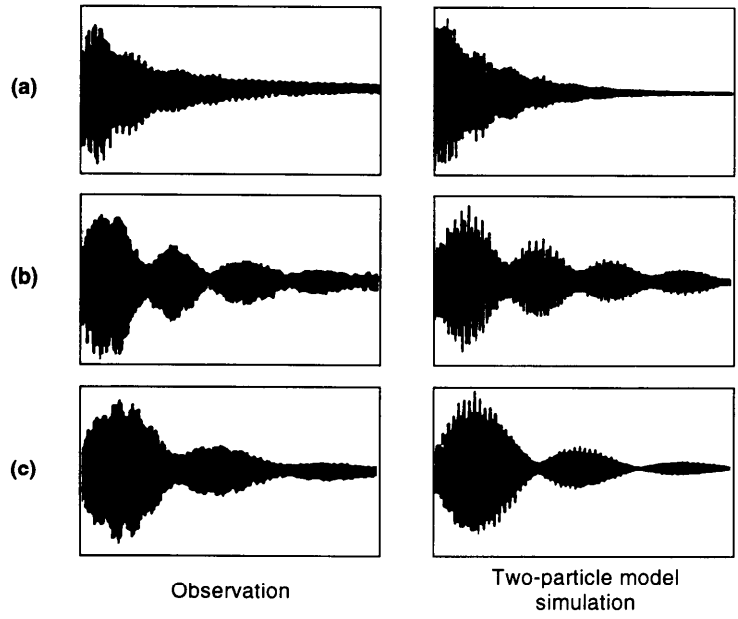

Figure 4.11. The beam-position-monitor signal as a function of time after the beam is kicked. On the left are the signals observed at the PEP storage ring: (a) is when the beam intensity N is 0.86 times the threshold intensity N_{th}, (b) $N / N_{th} = 0.93$, and (c) $N / N_{th} = 0.988$. On the right are the results of simulation using a two-particle model with (a) $\Upsilon / 2 = 0.77$, (b) $\Upsilon / 2 = 0.96$, and (c) $\Upsilon / 2 = 0.99$.

This is useful when the beam intensity is limited for reasons other than the strong head-tail instability. By measuring ω_β at low beam intensities, the eventual instability threshold can be estimated using Eq. (4.53).

Equation (4.52) indicates that the $l = 0$ frequency always shifts *down* as the beam intensity is increased. Physically, this is because, for short bunches, the sign of the wake force is such that the bunch tail is always deflected further away from the vacuum chamber axis if the beam is transversely displaced. With the head and the tail moving together in the $l = 0$ mode, the wake force acts as a defocusing effect and the mode frequency shifts down.

The center-of-charge signal of the beam as a function of time after the beam receives an initial transverse kick was analyzed in Eq. (4.50) for a two-particle model. One can also do a numerical simulation of the process. In Figure 4.11, results of the numerical simulation are compared with the experimental observation at the electron storage ring PEP.[21] Although the exact values of Υ used in the simulation have been slightly adjusted to make the comparison (see caption of Figure 4.11), the agreement is quite reasonable, indicating that the two-particle model describes this instability mecha-

[21] PEP Group, *Proc. 12th Int. Conf. High Energy Accel.*, Fermilab, 1983, p. 209.

nism remarkably well. The fact that the signal exhibits damping is due to the radiation damping effect in electron storage rings, which is not essential to the discussion here, but was included in the simulation.

The instability threshold observed at PEP occurred when the beam intensity was $N_{\text{th}} = 6.4 \times 10^{11}$ with betatron tune $\omega_\beta/\omega_0 = 18.19$, synchrotron tune $\omega_s/\omega_0 = 0.044$, $E = 14.5$ GeV, and $\omega_0 = 0.86 \times 10^6$ s^{-1}. By relating these parameters to $\Upsilon = 2$, one obtains an estimate of the wake function for PEP of $W_0 = 58$ cm^{-2}. This translates into an effective angular kick at the bunch tail of 18 μrad per millimeter of bunch head displacement per revolution. As mentioned, information on W_0 can also be obtained by measuring the betatron frequency as a function of beam intensity and applying Eq. (4.52).

These data can be used to estimate the impedances. Using Eq. (2.115), we have $Z_1^\perp \approx (R/\beta_Z \nu_\beta) b W_0/c$, where $R/\beta_Z \nu_\beta$ is the weighting factor due to β_Z, the β-function at the location of the impedance. Taking a beam pipe radius $b = 5$ cm and $R/\beta_Z \nu_\beta = 0.5$ for PEP, we find $Z_1^\perp = 0.44$ MΩ/m. Equation (2.108) then gives $Z_0^\parallel/n \approx 1.6$ Ω. This value of $Z_0^\parallel/n$ indicates that, according to Eq. (2.124), about 0.8% of the accelerator circumference is effectively occupied by cavities or their equivalents.

We have obtained the results using a two-particle beam, assuming the wake of Eq. (4.37). We will show later (see Exercise 6.25) the result of a more sophisticated calculation assuming the same wake, but taking fully into account the internal motions of the beam. We will then find that Figure 4.8 does offer a qualitative description of the beam spectrum for the $l = 0$ and $l = -1$ modes, while it is not surprising that the two-particle model fails to describe the behavior of the higher modes. It will also be shown that the instability threshold occurs when the $l = 0$ mode frequency shifts by an amount somewhat larger than, but remaining comparable to, $\omega_s/2$, the value predicted by the two-particle model.

One might want to have an idea of what happens in the unstable region. Suppose we are slightly above the instability threshold, so that $\Upsilon = 2 + \epsilon$ with $\epsilon \ll 1$. Equation (4.44) can be used to find the instability growth rate: $\tau^{-1} = 2\sqrt{\epsilon}\,/T_s$. Note the square root dependence of τ^{-1} on ϵ. This means a small ϵ can give rise to a sharp growth rate; for instance, an intensity 10% above threshold gives $\tau \approx T_s$. One consequence is that the radiation damping effect and the use of conventional feedback systems are not very effective in bringing the beam intensity substantially beyond the threshold unless the feedback damping rate is significantly larger than ω_s.

Exercise 4.6 A conventional feedback system functions by damping the center-of-charge motion of the beam. An inspection of Figure 4.8, however, suggests an alternative.[22] The instability comes about when the frequencies of modes $l = 0$ and $l = -1$ merge and become complex. By

[22] S. Myers, *Proc. IEEE Part. Accel. Conf.*, Washington, 1987, p. 503.

introducing a *reactive* feedback system—rather than the conventional system, which is resistive—that shifts the $l = 0$ mode frequency so as to delay the merging, the instability threshold may be raised. In the presence of a reactive feedback system, the equation of motion in the first half of the synchrotron period is

$$\begin{aligned} y_1'' + \left(\frac{\omega_\beta}{c}\right)^2 y_1 &= \sigma(y_1 + y_2), \\ y_2'' + \left(\frac{\omega_\beta}{c}\right)^2 y_2 &= \alpha y_1 + \sigma(y_1 + y_2), \end{aligned} \tag{4.54}$$

where $\alpha = Nr_0W_0/2\gamma C$ and σ specifies the strength of the reactive feedback, which acts on the center of charge $y_1 + y_2$ of the beam. Assuming $\omega_\beta \gg \omega_s$, show that the eigenvalues are determined by[23]

$$\lambda + \frac{1}{\lambda} = (2 - qr)\cos\mu \pm \sin\mu\sqrt{4qr - q^2r^2} \tag{4.55}$$

and stability requires $qr < 4$, where $\mu = 2\pi\omega/\omega_s$, $q = \sin^2(\pi\sigma c^2/2a\omega\omega_s)$, $\omega = \sqrt{\omega_\beta^2 - \sigma c^2}$, $r = (a + 1/a)^2$, and $a = \sqrt{\sigma/(\sigma + \alpha)}$. The instability threshold can be raised by properly choosing the feedback strength σ.

It would in principle be possible to damp the strong head-tail instability by the BNS damping introduced to prevent dipole beam breakup in linacs. The BNS condition of Eq. (3.42) for a two-particle model in a linac [or Eq. (3.48) for a general beam distribution] also gives the damping condition for a circular accelerator if $\omega_\beta \gg \omega_s$. According to Eq. (3.42), the bunch tail must be focused more strongly than the bunch head by an amount

$$\frac{\Delta\omega_\beta}{\omega_\beta} = \frac{Nr_0W_0c^2}{4\gamma C\omega_\beta^2} = \frac{\Upsilon\omega_s}{\pi\omega_\beta}, \tag{4.56}$$

where Υ is the parameter of Eq. (4.42). Near the instability threshold, $\Upsilon \approx 2$, we find $\Delta\omega_\beta/\omega_\beta = 1.5 \times 10^{-3}$ is needed to BNS damp the PEP instability mentioned above. To provide the variation of betatron focusing across the bunch, one could consider tilting the longitudinal phase space distribution of

[23]R. Ruth, CERN Report LEP-TH/83-22 (1983). In case there is an interplay among the various effects of reactive feedback, localized impedance, and synchro-betatron resonances, the picture becomes more complicated. See B. Zotter, IEEE Trans. Nucl. Sci. **NS-32**, 2191 (1985); S. Myers, CERN Report LEP-523 (1984).

the bunch so that the bunch tail has a lower energy relative to the bunch head by an amount $\Delta\delta = \Upsilon\omega_s/\pi\omega_\beta\xi$, where ξ is the chromaticity defined in Eq. (3.43). One could also consider introducing a radio frequency quadrupole magnet system.

There are some interesting effects that were inadvertently dropped when we made the approximation $\omega_\beta \gg \omega_s$ following Eq. (4.40). To recover these effects, we have to be more careful in keeping all the terms.[24] We will deal with four-dimensional vectors

$$\begin{bmatrix} y_1 \\ \dfrac{c}{\omega_\beta} y_1' \\ y_2 \\ \dfrac{c}{\omega_\beta} y_2' \end{bmatrix} \tag{4.57}$$

instead of the complex two-dimensional ones used in Eq. (4.41). The transformation for the first half of synchrotron period for this vector is found to be

$$\begin{bmatrix} A & 0 \\ B & A \end{bmatrix}, \tag{4.58}$$

where A and B are the 2×2 matrices

$$\begin{aligned} A &= \begin{bmatrix} \cos\dfrac{\mu}{2} & \sin\dfrac{\mu}{2} \\ -\sin\dfrac{\mu}{2} & \cos\dfrac{\mu}{2} \end{bmatrix}, \\ B &= \Upsilon \begin{bmatrix} \sin\dfrac{\mu}{2} & \dfrac{2}{\mu}\sin\dfrac{\mu}{2} - \cos\dfrac{\mu}{2} \\ \dfrac{2}{\mu}\sin\dfrac{\mu}{2} + \cos\dfrac{\mu}{2} & \sin\dfrac{\mu}{2} \end{bmatrix} \end{aligned} \tag{4.59}$$

with $\mu = 2\pi\omega_\beta/\omega_s$ and Υ defined in Eq. (4.42). The results obtained previously correspond to dropping terms in B that contain the factor $2/\mu$. In the second half of synchrotron period, the transformation is

$$\begin{bmatrix} A & B \\ 0 & A \end{bmatrix}. \tag{4.60}$$

[24] J. M. Jowett, CERN Report LEP-474 (1983).

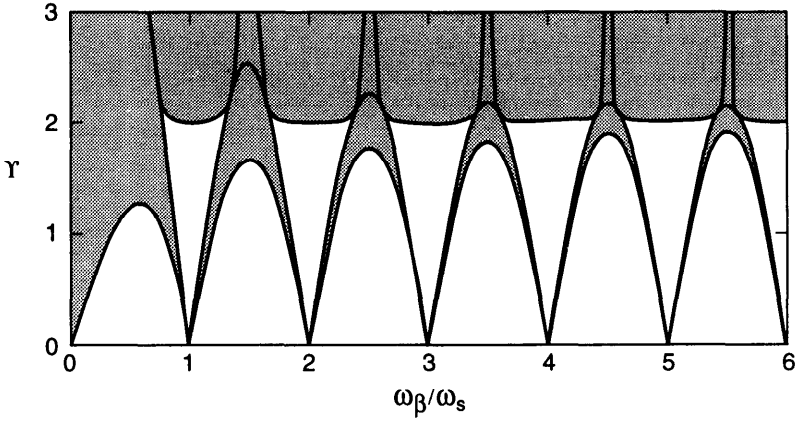

Figure 4.12. Stability region in the $(\omega_\beta / \omega_s, \Upsilon)$ plane for a two-particle beam against the strong head-tail instability. Synchro-betatron structure of the instability is pronounced near the synchro-betatron resonance conditions $\omega_\beta / \omega_s =$ integer. Unstable regions are shown shaded.

The total transformation is given by the product of the two half synchrotron periods. The resulting 4×4 matrix is then eigenanalyzed to see if the system is stable. The four eigenvalues λ are given by the roots of the characteristic function,

$$\left(\lambda + \frac{1}{\lambda}\right)^2 + 2\left(\lambda + \frac{1}{\lambda}\right)\left[\frac{2\Upsilon^2}{\mu^2}(\cos\mu - 1) + \Upsilon^2 \cos\mu - 2\cos\mu\right] + \left\{4\Upsilon^2(\cos\mu - 1) + \left[\Upsilon^2 + \frac{2\Upsilon^2}{\mu^2}(\cos\mu - 1) - 2\cos\mu\right]^2\right\} = 0. \tag{4.61}$$

Stability requires that all solutions for $\lambda + 1/\lambda$ be real and that their values be between -2 and 2.

The information we lost by assuming $\omega_\beta \gg \omega_s$ is a detailed synchro-betatron coupling effect.[25] Exercise 4.7 below shows that $\Upsilon = 2$ is the threshold condition when ω_β/ω_s is an integer or when $\omega_\beta/\omega_s \gg 1$. Away from these values of ω_β/ω_s, however, a pattern of synchro-betatron coupling emerges. The threshold value of Υ as a function of ω_β/ω_s is plotted in Figure 4.12. The synchro-betatron structure is apparent around each synchro-betatron resonance $\omega_\beta/\omega_s =$ integer, even for large values of ω_β/ω_s.

[25]Another synchro-betatron coupling mechanism, not treated here, is due to the beam having a closed-orbit distortion and a momentum dispersion at the location of the impedance. See R. Kohaupt, DESY Report 85-59 (1985); Yongho Chin, DESY Report 86-081 (1986).

Note that although the stability limit occurs at $\Upsilon = 2$ exactly on resonances $\omega_\beta = n\omega_s$, there are instability stopbands in the immediate neighborhood at low values of Υ. The regions close to the resonances are therefore to be avoided. In Figure 4.12, the stability region boundaries (the solid curves) are determined by

$$\Upsilon = \frac{2}{\sqrt{1 - \frac{4}{\mu^2}\tan^2\frac{\mu}{2}}} \quad \text{and} \quad \Upsilon = \frac{2\left|\sin\frac{\mu}{2}\right|}{1 \pm \frac{2}{\mu}\sin\frac{\mu}{2}}. \tag{4.62}$$

In case the impedance is localized at a certain position in the storage ring, the betatron frequency relevant for the resonance conditions is ω_β modulo the revolution frequency ω_0. The effective betatron frequency is then much less than ω_β itself, making the synchro-betatron structure more pronounced.

Exercise 4.7

(a) Right on a synchro-betatron resonance $\omega_\beta = n\omega_s$, use Eq. (4.61) to show that

$$\lambda + \frac{1}{\lambda} = -\Upsilon^2 + 2. \tag{4.63}$$

This gives the stability condition $\Upsilon \leq 2$.

(b) When $\omega_\beta \gg \omega_s$, show that

$$\lambda + \frac{1}{\lambda} = -(\Upsilon^2 - 2)\cos\mu \pm \Upsilon \sin\mu\sqrt{4 - \Upsilon^2}. \tag{4.64}$$

Writing $\lambda = \exp(i\mu + i\phi)$ gives Eq. (4.44). Show that the stability condition is $\Upsilon \leq 2$.

(c) When $\omega_\beta = (n + \frac{1}{2})\omega_s$, show that

$$\lambda + \frac{1}{\lambda} = -2 + \Upsilon^2\left(1 \pm \frac{2}{\mu}\right)^2 \tag{4.65}$$

and the stability condition is

$$\Upsilon \leq \frac{2\pi\left(n + \frac{1}{2}\right)}{\pi\left(n + \frac{1}{2}\right) + 1}. \tag{4.66}$$

4.4 TRANSVERSE QUADRUPOLE INSTABILITY

In Chapter 3, we observed the similarity between the dipole and quadrupole beam breakup effects in linacs. In particular, we found that the perturbations at the bunch tail by the wake fields are characterized by the growth parameters from Eqs. (3.25) and (3.95) [or (3.38) and (3.96) for accelerated beams] for the dipole and quadrupole cases, respectively. For circular accelerators, we expect to find a *quadrupole strong head-tail instability* similar to the dipole strong head-tail instability discussed in the previous section. By drawing an analogy to the analysis for linacs, one is led to expect a stability condition that assumes the form

$$\Upsilon = \frac{\pi N r_0 W_0 c^2 a^2}{2\gamma C \omega_\beta \omega_s} \leq 2, \tag{4.67}$$

where a is the rms radius of the unperturbed beam cross section, and W_0 is a constant parametrizing the quadrupole wake function integrated over the accelerator circumference C, i.e.,

$$W_2(z) = -W_0 \qquad \text{for} \quad 0 > z > -(\text{bunch length}). \tag{4.68}$$

What happens here is that the throbbing motions of the bunch head and bunch tail couple through the quadrupole wake force, leading to an instability. To derive Eq. (4.67), we adopt a *two-slice* model in which the beam consists of two elliptically-shaped slices of charge $Ne/2$, each described by a symmetric 4×4 Σ-matrix whose elements are the second moments of the slice,

$$\Sigma_i = \begin{bmatrix} \langle x^2 \rangle_i & \langle xx' \rangle_i & 0 & 0 \\ \langle xx' \rangle_i & \langle x'^2 \rangle_i & 0 & 0 \\ 0 & 0 & \langle y^2 \rangle_i & \langle yy' \rangle_i \\ 0 & 0 & \langle yy' \rangle_i & \langle y'^2 \rangle_i \end{bmatrix}, \qquad i = 1, 2. \tag{4.69}$$

We have assumed the ellipses are upright in the x-y plane. The slices are assumed to execute synchrotron oscillations, and therefore exchange their leading and trailing roles every half synchrotron period $T_s/2$.

We first concentrate on the leading slice ($i = 1$). The second moments of the slice execute free betatron oscillations. The equation of motion is[26]

$$c\Sigma_1' = \Omega\Sigma_1 + \Sigma_1\tilde{\Omega}, \tag{4.70}$$

[26] Karl L. Brown, SLAC Report 75, Rev. 3 (1972).

where a tilde means taking the transpose of a matrix, and

$$\frac{\Omega}{c} = \begin{bmatrix} 0 & 1 & 0 & 0 \\ -k_x^2 & 0 & 0 & 0 \\ 0 & 0 & 0 & 1 \\ 0 & 0 & -k_y^2 & 0 \end{bmatrix} \tag{4.71}$$

with $k_{x,y}$ the betatron wave numbers. Equation (4.70) has the solution

$$\Sigma_1(s) = T\Sigma_1(0)\tilde{T}, \tag{4.72}$$

where

$$T = \begin{bmatrix} \cos k_x s & \frac{1}{k_x}\sin k_x s & 0 & 0 \\ -k_x \sin k_x s & \cos k_x s & 0 & 0 \\ 0 & 0 & \cos k_y s & \frac{1}{k_y}\sin k_y s \\ 0 & 0 & -k_y \sin k_y s & \cos k_y s \end{bmatrix}. \tag{4.73}$$

Exercise 4.8 Verify Eqs. (4.70) and (4.72) by back substitution as follows. Consider the x-dimension only. We know the single-particle motion has the solution

$$\begin{aligned} x(s) &= x_0 \cos k_x s + \frac{x_0'}{k_x}\sin k_x s \\ x'(s) &= -k_x x_0 \sin k_x s + x_0' \cos k_x s. \end{aligned} \tag{4.74}$$

It follows that

$$\begin{aligned} \langle x^2\rangle(s) &= \langle x^2\rangle_0 \cos^2 k_x s + \frac{\langle xx'\rangle_0}{k_x}\sin 2k_x s + \frac{\langle x'^2\rangle_0}{k_x^2}\sin^2 k_x s, \\ \langle xx'\rangle(s) &= -\frac{k_x\langle x^2\rangle_0}{2}\sin 2k_x s + \langle xx'\rangle_0 \cos 2k_x s + \frac{\langle x'^2\rangle_0}{2k_x}\sin 2k_x s, \\ \langle x'^2\rangle(s) &= k_x^2\langle x^2\rangle_0 \sin^2 k_x s - k_x\langle xx'\rangle_0 \sin 2k_x s + \langle x'^2\rangle_0 \cos^2 k_x s, \end{aligned} \tag{4.75}$$

which can be shown to satisfy Eqs. (4.70) and (4.72). Also show that the quantity

$$\det(\Sigma_x) = \langle x^2\rangle\langle x'^2\rangle - \langle xx'\rangle^2 \tag{4.76}$$

is a constant of the motion. This quantity is related to the beam emittance according to Eq. (1.94).

In the following we will do a perturbation calculation. Let

$$\begin{aligned}
\langle x^2\rangle_i &= a^2 + A_{xi},\\
\langle xx'\rangle_i &= 0 + B_{xi},\\
\langle x'^2\rangle_i &= k_x^2 a^2 + C_{xi},\\
\langle y^2\rangle_i &= a^2 + A_{yi},\\
\langle yy'\rangle_i &= 0 + B_{yi},\\
\langle y'^2\rangle_i &= k_y^2 a^2 + C_{yi}, \qquad i = 1,2
\end{aligned} \tag{4.77}$$

The first terms on the right hand sides are the unperturbed values, and the second terms are small, time dependent perturbations. We have assumed that the unperturbed beam is round with rms radius a. The index i refers to the two slices.

Since the beam emittances

$$\sqrt{\langle x^2\rangle_i\langle x'^2\rangle_i - \langle xx'\rangle_i^2} \quad \text{and} \quad \sqrt{\langle y^2\rangle_i\langle y'^2\rangle_i - \langle yy'\rangle_i^2}$$

are constants of the motion, it follows that $k_x^2 A_{xi} + C_{xi}$ and $k_y^2 A_{yi} + C_{yi}$ are invariants. Without losing any beam stability information, we are therefore free to choose the constraints

$$\begin{aligned}
C_{xi} &= -k_x^2 A_{xi},\\
C_{yi} &= -k_y^2 A_{yi}, \qquad i = 1,2.
\end{aligned} \tag{4.78}$$

In terms of the perturbation moments, Eq. (4.72) or (4.75) can be written explicitly as

$$\begin{aligned} A_{x1}(s) &= A_{x1}(0)\cos 2k_x s + \frac{1}{k_x}B_{x1}(0)\sin 2k_x s, \\ B_{x1}(s) &= -k_x A_{x1}(0)\sin 2k_x s + B_{x1}(0)\cos 2k_x s, \end{aligned} \tag{4.79}$$

and another set of expressions with x replaced by y. Equation (4.79) describes the free quadrupole oscillation of the first slice. The oscillation frequency of its second moments is twice the free betatron oscillation.

Bunch slice 1 leaves behind a quadrupole wake force that, according to Eq. (3.82), is equivalent to the force due to a quadrupole magnet with a gradient $\partial B_y/\partial x = -NeW_0(\langle x^2\rangle_1 - \langle y^2\rangle_1)/C = -NeW_0(A_{x1} - A_{y1})/C$. The equation of motion of the trailing slice can be obtained by modifying the betatron focusing according to

$$\begin{aligned} k_x^2 &\to k_x^2 - \frac{Nr_0W_0}{\gamma C}(A_{x1} - A_{y1}), \\ k_y^2 &\to k_y^2 + \frac{Nr_0W_0}{\gamma C}(A_{x1} - A_{y1}). \end{aligned} \tag{4.80}$$

To first order in the perturbations A_{xi}, B_{xi}, A_{yi}, and B_{yi}, we then have

$$c\Sigma_2' = \Omega\Sigma_2 + \Sigma_2\tilde{\Omega} + \frac{Nr_0W_0ca^2}{\gamma C}(A_{x1} - A_{y1})\begin{bmatrix} 0 & 1 & 0 & 0 \\ 1 & 0 & 0 & 0 \\ 0 & 0 & 0 & -1 \\ 0 & 0 & -1 & 0 \end{bmatrix}, \tag{4.81}$$

where the matrix Ω is that defined in Eq. (4.71). Equation (4.81) can be integrated exactly, but we will keep only the resonant terms. We assume k_x and k_y are different, so that there is no resonant coupling between the two dimensions, and we need only to consider one of the two dimensions, say the x-dimension. Substituting Eq. (4.79) into Eq. (4.81) then yields, after some algebraic manipulations,

$$\Sigma_2(s) = TS\tilde{T}, \tag{4.82}$$

where T is the 2×2 block of Eq. (4.73) and

$$S = \Sigma_2(0) + \frac{Nr_0W_0a^2s}{2\gamma C}\begin{bmatrix} -\frac{1}{k_x^2}B_1(0) & A_1(0) \\ A_1(0) & B_1(0) \end{bmatrix}. \tag{4.83}$$

We have dropped the subscript x from all the A's and B's. Note that the second term in S is proportional to s.

The solution (4.82–4.83), written in terms of the perturbation moments, gives

$$\begin{aligned} A_2(s) &= A_2(0)\cos 2k_x s + \frac{B_2(0)}{k_x}\sin 2k_x s \\ &\quad + \frac{Nr_0W_0a^2s}{2\gamma Ck_x}\left[-\frac{B_1(0)}{k_x}\cos 2k_x s + A_1(0)\sin 2k_x s\right], \\ B_2(s) &= -k_x A_2(0)\sin 2k_x s + B_2(0)\cos 2k_x s \\ &\quad + \frac{Nr_0W_0a^2s}{2\gamma C}\left[\frac{B_1(0)}{k_x}\sin 2k_x s + A_1(0)\cos 2k_x s\right]. \end{aligned} \tag{4.84}$$

Equation (4.84) is the solution during the time $0 < s/c < T_s/2$. If we now form two phasors

$$\begin{aligned} \tilde{Q}_1 &= A_1 + i\frac{B_1}{k_x}, \\ \tilde{Q}_2 &= A_2 + i\frac{B_2}{k_x}, \end{aligned} \tag{4.85}$$

the transformation from $s = 0$ to $s = cT_s/2$ is found to be

$$\begin{bmatrix} \tilde{Q}_1 \\ \tilde{Q}_2 \end{bmatrix}_{s=cT_s/2} = e^{-ik_x cT_s}\begin{bmatrix} 1 & 0 \\ i\Upsilon & 1 \end{bmatrix}\begin{bmatrix} \tilde{Q}_1 \\ \tilde{Q}_2 \end{bmatrix}_0, \tag{4.86}$$

where Υ is the parameter defined in Eq. (4.67).

Equation (4.86) appears almost identical to its dipole counterpart, Eq. (4.41). The same analysis of the previous section then leads to the expected stability criterion (4.67). The frequency spectrum of the two-slice beam under the influence of a quadrupole wake therefore looks the same as Figure 4.8, except that the mode frequencies cluster around $2\omega_\beta$ instead of ω_β.

The ratio of the quadrupole strength parameter (4.67) to the dipole parameter (4.42) is of the order of $2a^2/b^2$, where a is the rms transverse beam size, and b is the size of the vacuum chamber where the impedance is

located. Quadrupole instability is relatively unimportant unless the beam virtually fills the vacuum chamber.

4.5 HEAD-TAIL INSTABILITY

In our analysis of the strong head-tail instability in Section 4.3, we assumed that the betatron and the synchrotron motions are decoupled from each other. In doing so, we ignored an important source of instability known as the *head-tail instability*, to which we now turn.

The head-tail instability is one of the cleanest to be observed experimentally.[27] Although it involves a mechanism more subtle than that of the strong head-tail instability, this instability can occur at much lower beam intensities. This may explain the fact that it was actually observed and explained[28] earlier than the strong head-tail instability.[29]

The betatron oscillation frequency of a particle in a circular accelerator depends on the energy error $\delta = \Delta E/E$ of the particle. If we denote that betatron frequency of an on-momentum particle as ω_β, the betatron frequency for an off-momentum particle can be written as

$$\omega_\beta(\delta) = \omega_\beta(1 + \xi\delta), \tag{4.87}$$

where ξ is the chromaticity parameter determined by the accelerator design and was introduced already in Eq. (3.43).[30] To assure that the beam has a small betatron frequency spread due to a spread in δ, the absolute value of ξ must not be too large. A consequence of the head-tail consideration, as we will soon see, is that in addition to this requirement, ξ must also have a definite sign. The main reason for introducing sextupoles in circular accelerators is, in fact, to control ξ.

In Section 4.3, we have used s, the longitudinal coordinate along the accelerator, as the independent variable, and the time t is related to s simply by $s = ct$. It is no longer so simple here, because now we have to consider synchrotron motions, and the varying time of arrival confounds the connection between s and t. It turns out to be simpler to use s as the independent variable, as will be done below.

[27]The SPEAR Group, *Proc. 9th Int. Conf. High Energy Accel.*, SLAC, 1974, p. 338; J. Gareyte and F. Sacherer, *Proc. 9th Int. Conf. High Energy Accel.*, SLAC, 1974, p. 341; Y. Miyahara and K. Takata, Part. Accel. **10**, 125 (1980).

[28]C. Pellegrini, Nuovo Cimento **64A**, 447 (1969); M. Sands, SLAC Reports TN-69-8 and TN-69-10 (1969). See also F. Sacherer, CERN Report SI-BR/72-5 (1972); F. Sacherer, *Proc. 9th Int. Conf. High Energy Accel.*, SLAC, 1974, p. 347.

[29]It may also explain the fact that this instability has preempted the name of "head-tail instability" although almost any other collective instability could justify the same name.

[30]Sometimes in the literature the chromaticity is defined differently, as $\omega_\beta(\delta) = \omega_\beta + \xi\delta\omega_0$.

Let us first examine the free betatron oscillation in the absence of wake fields. The accumulated betatron phase is given by an integration of Eq. (4.87), i.e.,

$$\phi_\beta(s) = \int \omega_\beta(\delta)\frac{ds}{c} = \omega_\beta\left(\frac{s}{c} + \xi\int\delta\frac{ds}{c}\right)$$
$$= \omega_\beta\left[\frac{s}{c} - \frac{\xi}{c\eta}z(s)\right], \tag{4.88}$$

where η is the slippage factor, and we have used Eq. (1.9), $z' = -\eta\delta$.

Equation (4.88) is already a remarkable result. It says that the deviation of the betatron phase of a particle from the nominal value $\omega_\beta s/c$ is determined by its longitudinal position. In other words, the chromatic modulation of the betatron phase depends only on z and not on other dynamic variables, such as δ.[31] The modulation, of course, is slow and weak.

We now consider two macroparticles whose synchrotron oscillations are given by

$$z_1 = \hat{z}\sin\frac{\omega_s s}{c} \quad \text{and} \quad z_2 = -z_1, \tag{4.89}$$

where ω_s is the synchrotron oscillation frequency. Particle 1 leads particle 2 during $0 < s/c < \pi/\omega_s$ and trails it during $\pi/\omega_s < s/c < 2\pi/\omega_s$. The free betatron oscillations of the two particles are described by

$$y_1(s) = \tilde{y}_1 e^{-i\phi_{\beta 1}(s)} = \tilde{y}_1 \exp\left(-i\omega_\beta\frac{s}{c} + i\frac{\xi\omega_\beta}{c\eta}\hat{z}\sin\frac{\omega_s s}{c}\right),$$
$$y_2(s) = \tilde{y}_2 e^{-i\phi_{\beta 2}(s)} = \tilde{y}_2 \exp\left(-i\omega_\beta\frac{s}{c} - i\frac{\xi\omega_\beta}{c\eta}\hat{z}\sin\frac{\omega_s s}{c}\right). \tag{4.90}$$

As the particles exchange the roles of leading particle and trailing particle, the betatron phases are such that the leading particle always lags in phase relative to the trailing particle if $\xi/\eta > 0$ and the situation reverses if $\xi/\eta < 0$, as illustrated in Figure 4.13.

The factor $\xi\omega_\beta\hat{z}/c\eta$ is called the *head-tail phase*. It is the physical origin of the head-tail instability. As a numerical example, one may have an electron accelerator with $\eta = 0.003$, $\xi = 0.2$, $\hat{z} = 3$ cm, and $\omega_\beta = 1.4 \times 10^7\ \text{s}^{-1}$, which gives a head-tail phase of $2\pi \times 0.016$.

Recalling the strong head-tail instability studied previously, the trailing particle is always unstable due to the resonant driving by the wake field of

[31] Modulation of the betatron phase by z or the betatron frequency by δ leads to an instability. Modulation of the betatron phase by δ or the betatron frequency by z does not lead to an instability.

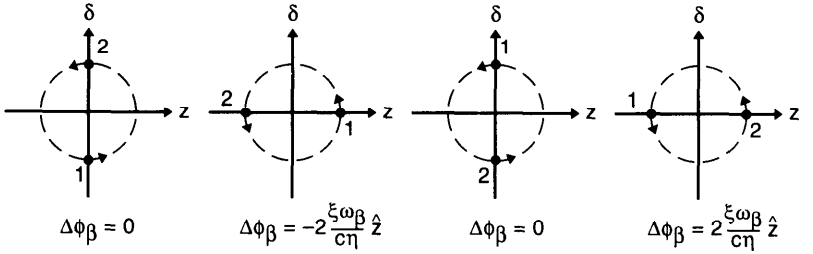

Figure 4.13. The synchrotron oscillation of a two-particle beam observed in the longitudinal phase space. The quantity $\Delta\phi_\beta = \phi_{\beta 1} - \phi_{\beta 2}$ is the difference of the betatron phases of the two particles; it is modulated by the synchrotron motion as shown. The sense of rotation of particle motion in the phase space is for the case above transition, i.e., $\eta > 0$.

the leading particle; the growths of the trailing particle during the half synchrotron periods are strong, but below a certain threshold the synchrotron oscillation washes away the growths and the net result is that the beam becomes stable. The additional chromatic term that we are considering now does not have this fortunate property. As we will see, the weak growths associated with chromaticity do accumulate persistently from one half synchrotron period to the next, and thus slowly build up an instability without a threshold.

Let us look at the motion of particle 2 during $0 < s/c < \pi/\omega_s$ in the presence of the wake field. The wake function, we assume, is that given by Eq. (4.37). The equation of motion is

$$y_2'' + \left[\frac{\omega_\beta(\delta_2)}{c}\right]^2 y_2 = \frac{Nr_0W_0}{2\gamma C} y_1,$$
$$\omega_\beta(\delta_2) = \omega_\beta\left(1 + \frac{\xi\hat{z}\omega_s}{c\eta}\cos\frac{\omega_s s}{c}\right). \tag{4.91}$$

The y_1 on the right hand side is given by the free oscillation result from Eq. (4.90). If we let y_2 also be given by Eq. (4.90), but allow $\tilde{y}_2$ to be slowly varying in time, Eq. (4.91) leads to an equation for $\tilde{y}_2$,

$$\tilde{y}_2'(s) \approx \frac{iNr_0W_0c}{4\gamma C\omega_\beta}\tilde{y}_1(0)\exp\left(2i\frac{\xi\omega_\beta\hat{z}}{c\eta}\sin\frac{\omega_s s}{c}\right). \tag{4.92}$$

For most practical cases, the head-tail phase $\xi\omega_\beta\hat{z}/c\eta$ is much less than unity, the exponential factor in Eq. (4.92) can be Taylor expanded, and y_2

can be integrated to yield

$$\tilde{y}_2(s) = \tilde{y}_2(0) + \frac{iNr_0W_0c}{4\gamma C\omega_\beta}\tilde{y}_1(0)\left[s + i\frac{2\xi\omega_\beta\hat{z}}{\eta\omega_s}\left(1 - \cos\frac{\omega_s s}{c}\right)\right]. \quad (4.93)$$

The first term in the brackets is the resonant response already studied in Section 4.3 and is responsible for the strong head-tail instability. The second, chromatic term is small, because it is proportional to the head-tail phase and also because it is not a resonant response. On the other hand, the important fact here is that the chromatic term is 90° out of phase from the resonant term.

The transformation from $s = 0$ to $s = \pi c/\omega_s$ is thus described by

$$\begin{bmatrix}\tilde{y}_1\\ \tilde{y}_2\end{bmatrix}_{\pi c/\omega_s} = \begin{bmatrix}1 & 0\\ i\Upsilon & 1\end{bmatrix}\begin{bmatrix}\tilde{y}_1\\ \tilde{y}_2\end{bmatrix}_0, \quad (4.94)$$

where

$$\Upsilon = \frac{\pi Nr_0W_0c^2}{4\gamma C\omega_\beta\omega_s}\left(1 + i\frac{4\xi\omega_\beta\hat{z}}{\pi c\eta}\right). \quad (4.95)$$

This Υ, of course, reduces to Eq. (4.42) if $\xi = 0$, but now it has acquired an imaginary part if $\xi \neq 0$. A similar procedure applied to the period $\pi c/\omega_s < s < 2\pi c/\omega_s$ leads to the transformation

$$\begin{bmatrix}\tilde{y}_1\\ \tilde{y}_2\end{bmatrix}_{2\pi c/\omega_s} = \begin{bmatrix}1 & i\Upsilon\\ 0 & 1\end{bmatrix}\begin{bmatrix}\tilde{y}_1\\ \tilde{y}_2\end{bmatrix}_{\pi c/\omega_s}. \quad (4.96)$$

As we did before, the stability of the system is determined by the total transformation matrix

$$\begin{bmatrix}1 & i\Upsilon\\ 0 & 1\end{bmatrix}\begin{bmatrix}1 & 0\\ i\Upsilon & 1\end{bmatrix} = \begin{bmatrix}1 - \Upsilon^2 & i\Upsilon\\ i\Upsilon & 1\end{bmatrix}. \quad (4.97)$$

The eigenvalues of this matrix have been obtained before in Eq. (4.44). For a weak beam intensity, $|\Upsilon| \ll 1$, the two eigenvalues are

$$\lambda_\pm \approx e^{\pm i\Upsilon}. \quad (4.98)$$

The + mode (− mode) is the mode when the two macroparticles oscillate in phase (out of phase) in the limit of weak beam intensity. The imaginary part

of Υ thus gives a growth rate of the betatron oscillations,

$$\tau_{\pm}^{-1} = \mp \frac{Nr_0 W_0 c\xi\hat{z}}{2\pi\gamma C\eta}. \tag{4.99}$$

When the + mode is unstable, the − mode is stable; the transverse displacement of the beam center of charge grows with time, but the transverse size of the beam essentially remains constant. When the − mode is unstable, the + mode becomes stable; the beam center of charge does not oscillate, but the beam size grows exponentially.

The + mode is damped if $\xi/\eta > 0$ and antidamped if $\xi/\eta < 0$. The − mode is damped if $\xi/\eta < 0$ and antidamped if $\xi/\eta > 0$. We conclude from this that the only value of ξ that assures a stable beam is $\xi = 0$. However, as we will see later in Chapter 6 using a Vlasov equation technique, the two-particle model has overestimated the growth rate of the − mode. This consideration, together with the presence of some stabilizing mechanisms (such as Landau damping, or radiation damping in the case of circular electron accelerators) leads us to choose slightly positive values for ξ for operation above transition, and slightly negative ξ below transition.

The growth rate is proportional to N and ξ, and inversely proportional to γ as one would expect. The linear dependence on the bunch length $\hat{z}$ as given in Eq. (4.99), however, is a consequence of the constant wake model. Had we assumed a different wake model, the dependence of τ^{-1} on $\hat{z}$ would change. Another examination of the structure of Eq. (4.99) will be given later in Eqs. (6.219–6.220).

Note that the same transverse wake field is responsible for the strong head-tail instability and the head-tail instability. Continuing the PEP example mentioned after Eq. (4.53), and further taking $\hat{z} = 3$ cm and $\xi = 0.2$, we find the head-tail growth rate ∓ 0.6 ms at the threshold for strong head-tail instability, $N = 6.4 \times 10^{11}$.[32] The head-tail damping or antidamping can be rather fast.

In addition to the methods mentioned after Eq. (4.53), the head-tail growth rate provides another way to measure the transverse wake function and the impedance of an accelerator. To do so, ξ is made slightly positive (above transition), a beam center-of-charge motion (in a + mode) is excited by a kicker, and its subsequent damped motion is observed. The linear dependence of the damping rate on ξ allows the extraction of the wake function information. The various methods of measuring the wake function are not expected to give identical values for the transverse impedance $Z_1^{\perp}$, but the results should at least be comparable.

[32]Strictly speaking, Eq. (4.99) applies only when $|\Upsilon| \ll 1$. We apply it here, even though $\mathrm{Re}\,\Upsilon = 2$, to obtain an order of magnitude estimate.

Once $Z_1^\perp$ is established, Eq. (2.108) gives an estimate of $Z_0^\parallel/n$. One may compare the value of $Z_0^\parallel/n$ obtained this way with that obtained by measuring the parasitic loss, which was discussed following Eq. (2.201).

Exercise 4.9 In case the head-tail phase is not much less than unity, show that the parameter Υ is given by

$$\Upsilon = \frac{Nr_0W_0c^2}{4\gamma C\omega_\beta\omega_s} f\left(\frac{2\xi\omega_\beta\hat{z}}{c\eta}\right), \qquad f(u) = \int_0^\pi dx\, e^{iu\sin x}. \tag{4.100}$$

The function $f(u)$ is plotted in Figure 4.14. The real part of $f(u)$ is equal to π times the Bessel function $J_0(u)$. Since the real part of Υ is responsible for the strong head-tail instability, and the imaginary part of Υ is responsible for the head-tail instability, Eq. (4.100) indicates that it is in principle possible to increase the strong head-tail threshold by having a head-tail phase so that $u \approx 2.405$, the root of $J_0(u)$. The imaginary part of f can be used to obtain the head-tail growth rates

$$\tau_\pm^{-1} = \mp \frac{Nr_0W_0c^2}{8\pi\gamma C\omega_\beta} \operatorname{Im} f\left(\frac{2\xi\omega_\beta\hat{z}}{c\eta}\right). \tag{4.101}$$

In particular, $\tau_\pm^{-1} = 0$ if $u = 0$ or $u = 4.33$.

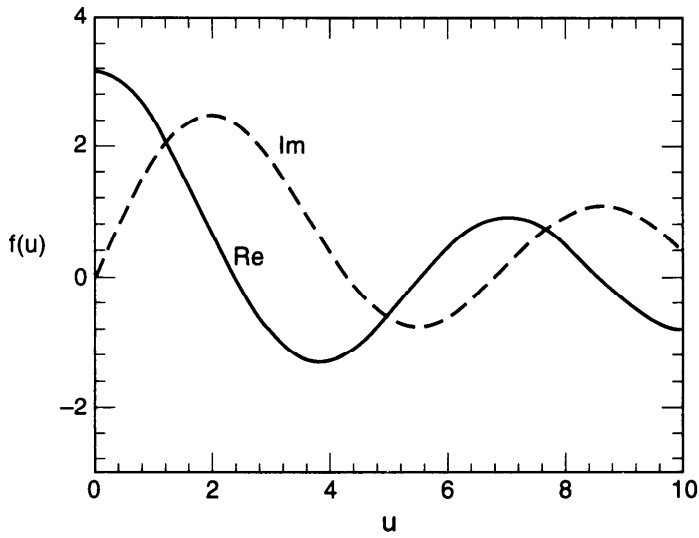

Figure 4.14. The function $f(u)$ in Eq. (4.100).

Exercise 4.10 It was observed in the electron storage ring SPEAR I that the head-tail damping time is 1 ms under the conditions $I = 20$ mA, $E = 1.5$ GeV, $\xi = 0.67$, $\hat{z} = 13$ cm, $\eta = 0.037$, $C = 240$ m, $b = 5$ cm.[33] Estimate the magnitudes of the transverse wake function and the impedances $Z_1^{\perp}$ and $Z_0^{\parallel}/n$.

Exercise 4.11 Suppose the linear chromaticity ξ has been accurately made to vanish, the leading chromatic term is therefore quadratic in δ, i.e., $\omega_\beta(\delta) = \omega_\beta(1 + \xi_2\delta^2)$. Does such an accelerator have a head-tail instability? First consider a constant wake, then a general wake.

4.6 MULTIPLE BUNCHES

So far we have treated a beam that has only one bunch of particles. In this section, we will consider a beam with multiple bunches. To be specific, consider first a beam that has two bunches circulating in the same direction in the accelerator. Let each bunch be a point charge Ne, and let the two bunches be separated by half the accelerator circumference. We will specify the two bunches by indices 0 and 1.

We assume that a transverse $m = 1$ wake force is functioning. The equations of motion for the two point macroparticles are

$$\ddot{y}_0(t) + \omega_\beta^2 y_0(t) = -\frac{Nr_0c}{\gamma T_0}\sum_{k=0}^{\infty}\left[W_1\left(-kC - \frac{C}{2}\right)y_1\left(t - kT_0 - \frac{T_0}{2}\right) + W_1(-kC)\,y_0(t - kT_0)\right], \tag{4.102}$$

and another equation with y_0 and y_1 exchanged, where $C = cT_0$ is the accelerator circumference. The index k sums over all previous revolutions. We have used time t as the independent variable.

Let the two bunches be executing transverse motion in a mode with frequency Ω, i.e.,

$$y_{0,1}(t) = \tilde{y}_{0,1}e^{-i\Omega t}. \tag{4.103}$$

The complex quantities $\tilde{y}_{0,1}$ give the amplitudes and phases at a fixed time t, i.e., they are the "snapshot" quantities rather than quantities observed at a fixed location.

[33]The SPEAR Group, *9th Int. Conf. on High Energy Accel.*, Stanford, 1974, p. 338.

Substituting Eq. (4.103) into Eq. (4.102) and assuming Ω is close to ω_β, we obtain

$$\begin{aligned}(\Omega - \omega_\beta + \omega_\beta \Upsilon_A)\tilde{y}_0 + \omega_\beta \Upsilon_B \tilde{y}_1 &= 0,\\ \omega_\beta \Upsilon_B \tilde{y}_0 + (\Omega - \omega_\beta + \omega_\beta \Upsilon_A)\tilde{y}_1 &= 0,\end{aligned} \tag{4.104}$$

where we have introduced two dimensionless quantities

$$\begin{aligned}\Upsilon_A &= -\frac{Nr_0 c}{2\gamma T_0 \omega_\beta^2} \sum_{k=0}^{\infty} W_1(-kC) e^{i\omega_\beta k T_0},\\ \Upsilon_B &= -\frac{Nr_0 c}{2\gamma T_0 \omega_\beta^2} \sum_{k=0}^{\infty} W_1\left(-kC - \frac{C}{2}\right) e^{i\omega_\beta (k+1/2) T_0}.\end{aligned} \tag{4.105}$$

In terms of the impedance, Eq. (4.105) reads

$$\begin{aligned}\Upsilon_A &= i\frac{Nr_0 c}{2\gamma T_0^2 \omega_\beta^2} \sum_{p=-\infty}^{\infty} Z_1^{\perp}(p\omega_0 + \omega_\beta),\\ \Upsilon_B &= i\frac{Nr_0 c}{2\gamma T_0^2 \omega_\beta^2} \sum_{p=-\infty}^{\infty} (-1)^p Z_1^{\perp}(p\omega_0 + \omega_\beta),\end{aligned} \tag{4.106}$$

where $\omega_0 = 2\pi/T_0$.

The only solution to the pair of equations (4.104) is the trivial solution $\tilde{y}_0 = \tilde{y}_1 = 0$, unless

$$\det\begin{bmatrix} \Omega - \omega_\beta + \omega_\beta \Upsilon_A & \omega_\beta \Upsilon_B \\ \omega_\beta \Upsilon_B & \Omega - \omega_\beta + \omega_\beta \Upsilon_A \end{bmatrix} = 0. \tag{4.107}$$

In other words, in order for a mode to exist, Ω must satisfy Eq. (4.107). Solving it gives two values for Ω,

$$\begin{aligned}\Omega_{\pm} - \omega_\beta &= -\omega_\beta(\Upsilon_A \pm \Upsilon_B)\\ &= -i\frac{Nr_0 c}{2\gamma T_0^2 \omega_\beta} \sum_{p=-\infty}^{\infty} \left[1 \pm (-1)^p\right] Z_1^{\perp}(p\omega_0 + \omega_\beta).\end{aligned} \tag{4.108}$$

It follows that the + mode is affected only by the impedance sampled at $p\omega_0 + \omega_\beta$ with even p's, while the − mode is affected only by odd p's. Compared with Eqs. (4.27–4.28) for the single-bunch case, the right hand side of Eq. (4.108) contains an extra factor of two, but the summation over p is twice as sparse. Note that N is the number of particles per bunch, not the total number of particles in the beam.

Substituting Eq. (4.108) into Eq. (4.104), we find that the snapshot displacements of the two bunches oscillate in phase for the + mode and out of phase for the − mode, i.e.,

$$\begin{aligned} \tilde{y}_0 &= \tilde{y}_1 \qquad \text{for + mode,} \\ \tilde{y}_0 &= -\tilde{y}_1 \qquad \text{for − mode.} \end{aligned} \tag{4.109}$$

For this reason, the + mode is also called the 0-mode and the − mode is called the π-mode. The fact that the two eigenmodes of the two bunches have the simple pattern (4.109) is independent of the strength of the coupling (i.e., the beam intensity and the impedance) between them.

The above analysis can be generalized to the case of M equally spaced, equally populated bunches. Let $y_n(t)$ $(n = 0, 1, \ldots, M-1)$ be the snapshot displacements of the individual bunches. The indexing is such that the $n = 1$ bunch is ahead of the $n = 0$ bunch, the $n = 2$ bunch is ahead of the $n = 1$ bunch, etc. The equations of motion are

$$\begin{aligned} \ddot{y}_n(t) + \omega_\beta^2 y_n(t) = &-\frac{Nr_0 c}{\gamma T_0} \sum_k \sum_{m=0}^{M-1} W_1\left(-kC - \frac{m-n}{M}C\right) \\ &\times y_m\left(t - kT_0 - \frac{m-n}{M}T_0\right). \end{aligned} \tag{4.110}$$

Letting

$$y_n(t) = \tilde{y}_n e^{-i\Omega t}, \tag{4.111}$$

we obtain

$$\begin{aligned} (\Omega - \omega_\beta)\tilde{y}_n &= \frac{Nr_0 c}{2\gamma T_0 \omega_\beta} \sum_{m=0}^{M-1} \tilde{y}_m \sum_k \exp\left[i\omega_\beta T_0\left(k + \frac{m-n}{M}\right)\right] \\ &\quad \times W_1\left(-kC - \frac{m-n}{M}C\right) \\ &= -i\frac{Nr_0 c}{2\gamma T_0^2 \omega_\beta} \sum_{m=0}^{M-1} \tilde{y}_m \sum_p Z_1^\perp(p\omega_0 + \omega_\beta)\exp\left(-i2\pi p\frac{m-n}{M}\right). \end{aligned} \tag{4.112}$$

There will be a total of M modes of the multibunch motion, each specified by an index μ which assumes the values $0, 1, \ldots, M-1$. The amplitudes of the M bunches, as the whole beam is executing the μth multibunch mode, are given by

$$\tilde{y}_n^{(\mu)} \propto e^{2\pi i \mu n/M}. \tag{4.113}$$

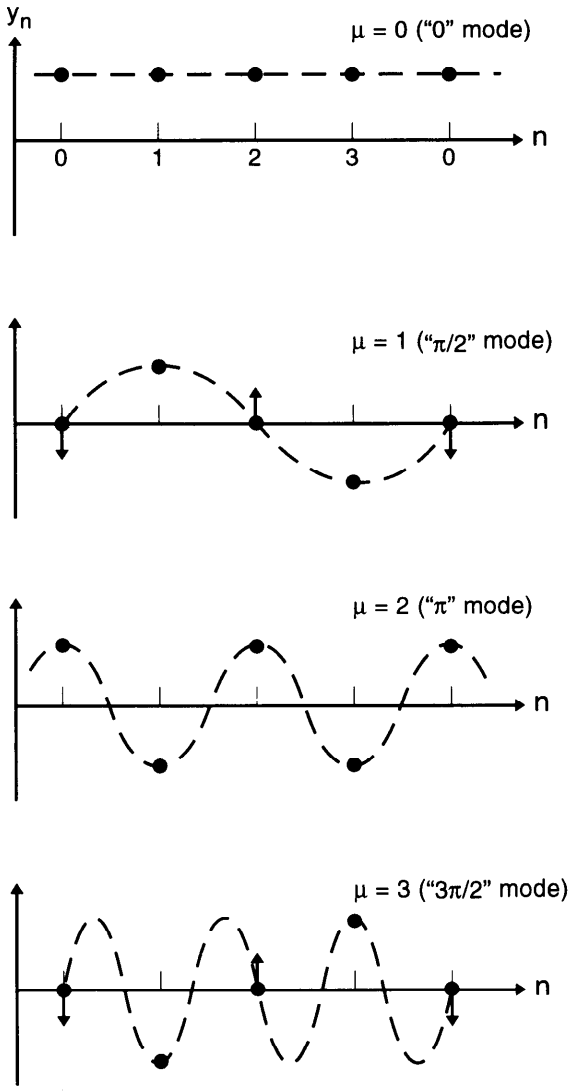

Figure 4.15. Snapshot patterns of the multibunch modes for a beam with four bunches. Arrows indicate the instantaneous directions of motion of a bunch.

The oscillation amplitudes y_n in various modes are shown in Figure 4.15 for the case of $M = 4$. The mode frequencies, obtained by substituting Eq. (4.113) into Eq. (4.112), are given by

$$\Omega^{(\mu)} - \omega_\beta = -i\frac{MNr_0c}{2\gamma T_0^2\omega_\beta}\sum_{p=-\infty}^{\infty} Z_1^\perp\left[\omega_\beta + (pM + \mu)\omega_0\right]. \quad (4.114)$$

For $M = 2$, Eq. (4.114) reduces to Eq. (4.108) if we identify $\mu = 0$ with the + mode and $\mu = 1$ with the − mode.

Compared with Eq. (4.25), these complex mode frequency shifts contain an extra factor of M in front, but the summation is M times as sparse. For an impedance broader than $M\omega_0$, Eq. (4.114) gives the same result as Eq. (4.25). This is expected, because in this case the wake field is shorter than the spacing between bunches and the beam behaves as M individual bunches which do not interact with one another. For sharp impedances, however, the difference between Eq. (4.114) and Eq. (4.25) can be substantial.

The reason the impedance is evaluated at $\omega = \omega_\beta + pM\omega_0 + \mu\omega_0$ can be understood similarly as Eq. (4.30). Observed at a fixed location where the impedance is located, the signal from a beam executing the μth multibunch mode is

$$\text{beam signal} \propto \sum_{k=-\infty}^{\infty} \sum_{n=0}^{M-1} y_n^{(\mu)}(t)\,\delta\left(t - kT_0 + \frac{nT_0}{M}\right)$$

$$\propto \sum_k \sum_n e^{-i\omega_\beta t} e^{i2\pi\mu n/M} \delta\left(t - kT_0 + \frac{nT_0}{M}\right). \qquad (4.115)$$

The spectrum of this signal is

$$\text{spectrum} \propto \int dt\, e^{i\omega t}(\text{beam signal})$$

$$\propto \sum_k \sum_n e^{i2\pi\mu n/M} \exp\left[i(\omega - \omega_\beta)\left(kT_0 - \frac{nT_0}{M}\right)\right]$$

$$= M\omega_0 \sum_{p=-\infty}^{\infty} \delta(\omega - \omega_\beta - pM\omega_0 - \mu\omega_0). \qquad (4.116)$$

The μth multibunch mode therefore samples the betatron sidebands of the frequencies $(pM + \mu)\omega_0$ where $p = \pm$ integers, as Eq. (4.114) indicates.

As an application of Eq. (4.114), consider a resistive wall. Recall that, with a $\omega^{-1/2}$ dependence, the transverse resistive-wall impedance is large at low frequencies. The mode that is most affected by the wake field is the one whose mode index μ is such that $-PM - \mu$ is closest to the betatron tune $\nu_\beta = \omega_\beta/\omega_0$ for some integer P, and the leading term in the summation of Eq. (4.114) comes from the term $p = P$. Letting $\nu_\beta = N_\beta + \Delta_\beta$, where N_β is the closest integer to ν_β and Δ_β is between $-\frac{1}{2}$ and $\frac{1}{2}$, we have $\mu = -N_\beta$ (modulo M).[34] Keeping only the leading term in the summation, the growth

[34] For example, if $\nu_\beta = 7.2$ and $M = 3$, we have $N_\beta = 7$, $\Delta_\beta = 0.2$, $P = -3$, $\mu = 2$, and the impedance is to be evaluated at $\omega = 0.2\omega_0$.

rate for this mode is found to be

$$\frac{1}{\tau^{(\mu)}} \approx -\frac{MNr_0c^2}{b^3\gamma\omega_\beta T_0\sqrt{2\pi\sigma\omega_0}}\frac{\text{sgn}(\Delta_\beta)}{\sqrt{|\Delta_\beta|}}, \tag{4.117}$$

which is about M times the growth rate of Eq. (4.34) for a single bunch. It is the *total* beam current that drives the leading mode of transverse resistive-wall instability. This is expected in view of the low frequency nature of the impedance. The mode is damped or antidamped according to whether Δ_β is positive or negative, respectively. Modes with other values of μ are not as affected by the resistive-wall impedance.

When observed in a snapshot at a given time, the bunches executing the above resistive-wall mode have a pattern with $N_\beta \approx \nu_\beta$ oscillations around the accelerator. When observed at a fixed location, however, such as a beam position monitor or a feedback system, the signal has a low frequency $\Delta_\beta\omega_0$ —the same low frequency observed by the resistive-wall impedance. To damp this instability, the bandwidth required by a feedback system is $\Delta f = \Delta_\beta\omega_0/2\pi$, which is typically quite narrow and is easy to provide. In comparison, a feedback system to damp a multibunch instability in general would require a much wider bandwidth, $\Delta f = M\omega_0/2\pi$.

The resistive-wall instability is a more important consideration for large accelerators when there are many bunches. For a given bunch spacing, this shows up as the factor $1/\sqrt{\omega_0}$ in Eq. (4.117), and is a consequence of the impedance sampling at the low frequency $\Delta_\beta\omega_0$. For this reason, the vacuum chamber walls of large circular accelerators are often copper coated.[35]

Exercise 4.12

(a) Consider a beam with 100 equally-spaced bunches, each affecting only the next bunch through the wake function $W_1(-D)$, where D is the bunch spacing. Show that the mode frequencies are given by

$$\Omega^{(\mu)} - \omega_\beta = \frac{Nr_0c^2}{2\gamma C\omega_\beta}W_1(-D)e^{i2\pi(\mu+\nu_\beta)/M},$$

$$\mu = 0, 1, \ldots, 99, \tag{4.118}$$

where $\nu_\beta = \omega_\beta/\omega_0$. Show that 50 modes are damped and 50 are antidamped. What happens if one bunch is removed from the beam so that the "loop" is broken? (Hint: Eigenanalysis does not apply. This accelerator acts like a linac.)

[35]Another reason was mentioned after Eq. (2.194).

(b) Suppose a bunch also weakly affects the second next bunch with $W_1(-2D)$. Show that the mode frequencies are

$$\Omega^{(\mu)} - \omega_\beta = \frac{Nr_0c^2}{2\gamma C\omega_\beta}\left[W_1(-D)e^{i2\pi(\mu+\nu_\beta)/M} + W_1(-2D)e^{i4\pi(\mu+\nu_\beta)/M}\right]. \quad (4.119)$$

What happens if one bunch is removed from the bunch train?[36]

(c) Show that

$$\sum_{\mu=0}^{M-1}\left(\Omega^{(\mu)} - \omega_\beta\right) = 0 \quad (4.120)$$

for both cases (a) and (b). The sum of the growth and damping rates of all modes is zero. The existence of damped modes implies the existence of at least one antidamped mode, and vice versa.

So far we have been considering the transverse multibunch motion. A similar analysis can be applied to the longitudinal case. Again consider M equally spaced bunches, each containing a point charge Ne. The equation of motion for the nth bunch is

$$z_n''(s) + \left(\frac{\omega_{s0}}{c}\right)^2 z_n(s) = \frac{Nr_0\eta}{\gamma C}\sum_k\sum_{m=0}^{M-1} W_0'\left[-kC - \frac{m-n}{M}C + z_n(s) - z_m\left(s - kC - \frac{m-n}{M}C\right)\right], \quad n = 0, 1, 2, \ldots, M-1, \quad (4.121)$$

where ω_{s0} is the unperturbed synchrotron frequency. Let

$$z_n(s) = \tilde{z}_n e^{-i\Omega s/c}, \quad (4.122)$$

and drop the parasitic loss term, as was done following Eq. (4.5). We obtain

$$\left(\Omega^2 - \omega_{s0}^2\right)\tilde{z}_n = -\frac{Nr_0\eta c}{\gamma T_0}\sum_k\sum_{m=0}^{M-1} W_0''\left(-kC - \frac{m-n}{M}C\right) \times\left\{\tilde{z}_n - \tilde{z}_m\exp\left[i\Omega T_0\left(k + \frac{m-n}{M}\right)\right]\right\}. \quad (4.123)$$

[36] F. J. Sacherer, *Proc. Spring Study on Accel. Theory*, Geneva, 1972, p. 175.

The first term in the curly braces is the potential-well term. It can be absorbed into a redefinition of the synchrotron frequency as

$$\omega_s^2 = \omega_{s0}^2 - \frac{Nr_0\eta c}{\gamma T_0}\sum_k \sum_{m=0}^{M-1} W_0''\left(-kC - \frac{M-n}{M}C\right). \tag{4.124}$$

Assuming this incoherent synchrotron frequency shift is small, we may express it in terms of impedance as

$$\Delta\omega_s \approx \frac{MNr_0\eta}{2\gamma T_0^2\omega_s}\sum_{p=-\infty}^{\infty} pM\omega_0 \operatorname{Im} Z_0^{\parallel}(pM\omega_0). \tag{4.125}$$

When $M = 1$, this becomes the first term in Eq. (4.9). Compared with the single-bunch result, the beam intensity is M times larger, but the impedance is sampled M times less frequently.

With a redefinition of synchrotron frequency and written in terms of the impedance, Eq. (4.123) reads

$$(\Omega - \omega_s)\tilde{z}_n = i\frac{Nr_0\eta}{2\gamma T_0^2\omega_s}\sum_{m=0}^{M-1}\tilde{z}_m\sum_p (p\omega_0 + \omega_s)Z_0^{\parallel}(p\omega_0 + \omega_s) \times \exp\left(-i2\pi p\frac{m-n}{M}\right). \tag{4.126}$$

As before, the μth multibunch mode has

$$\tilde{z}_n \propto e^{i2\pi\mu n/M}, \tag{4.127}$$

which, when substituted in Eq. (4.126), gives the mode frequency

$$\Omega^{(\mu)} - \omega_s = i\frac{MNr_0\eta}{2\gamma T_0^2\omega_s}\sum_{p=-\infty}^{\infty}(pM\omega_0 + \mu\omega_0 + \omega_s)Z_0^{\parallel}(pM\omega_0 + \mu\omega_0 + \omega_s). \tag{4.128}$$

This expression is to be compared with Eq. (4.10) and the second term in Eq. (4.9).

Unlike the transverse case, the resistive-wall impedance at low frequencies does not play an important role here. A more instructive application of Eq. (4.128) is for the Robinson instability. Let the fundamental rf cavity mode be sharply peaked around $\omega_R = h\omega_0 + \Delta\omega$, where the harmonic number h is necessarily a multiple of M for a multibunch operation, and $\Delta\omega$ is the amount of frequency detuning. The most unstable mode is the $\mu = 0$ mode,

in which all bunches oscillate in phase. The Robinson growth rate is found from Eq. (4.128) to be a factor of M larger than that predicted by the single-bunch result, Eq. (4.20). The dominant $\mu = 0$ mode for Robinson instability is driven by the total beam current of all bunches. For other modes with $\mu \neq 0$, the Robinson growth rates are small.

4.7 SIMULATION TECHNIQUES

The models introduced in the previous sections of this chapter are limited to a small number of macroparticles. As the number of macroparticles is increased, the analysis rapidly becomes cumbersome. To proceed, one may resort to computers for numerical simulations. With the advent of increasingly powerful computers, numerical simulations have become one of the most effective tools in the study of accelerator beam dynamics in general and the study of collective effects in particular.

By employing a computer, macroparticle models can easily be extended to 10^3 or 10^4 macroparticles, and many more detailed internal modes of the bunch motion can be studied. In addition, simulations also serve the critical function of connecting analyses and experiments.[37] On the one hand, it extends the analysis in the sense that effects not easily studied analytically can be simulated. On the other hand, it modelizes the accelerator in such a way that accelerator operation conditions can be varied at will and free of the obscurities of a real accelerator. We have already mentioned the simulation study of a quadrupole beam breakup effect in a linac in Section 3.3, and the simulation of a two-particle strong head-tail effect in a circular accelerator in Section 4.3. In this section, we will mention a few more examples of simulation studies.[38]

To perform a simulation, one first sets up the problem to be simulated, i.e., one has to know what one intends to learn. This includes determining whether the problem at hand is longitudinal or transverse or both, and whether the wake field is short-ranged or long-ranged. One chooses a short range wake field (for a broad-band impedance) to study single-bunch effects, and long range one (for a sharply peaked impedance) to study multibunch or multiturn effects. One may also choose to emphasize the interplay between two separate effects, which is where analyses typically have the most difficulties. In a simulation, one usually stays in the time domain, which means it is more convenient to use the wake functions than the impedances. The impedance is often considered to be lumped at some fixed location(s) in the accelerator.

[37]As one might say, simulation is the geometric mean between analysis and experiment.

[38]Examples are chosen for illustration only. The reader is encouraged to explore these topics in the literature. See for example, R. H. Siemann, Nucl. Instr. Meth. **203**, 57 (1982); D. Brandt and B. Zotter, *Proc. 12th Int. Conf. High Energy Accel.*, Fermilab, 1983, p. 309.

Consider a circular accelerator and a single-bunch beam modeled as M macroparticles. Let the jth macroparticle have charge $N_j e$, where $\sum_{j=1}^{M} N_j = N$ is the total number of particles in the bunch. The beam bunch passes by a lumped impedance, which we assume is where the rf cavity sits, once per revolution. Consider a particular revolution. Let z_j be the longitudinal position of the jth macroparticle ($z > 0$ is the bunch head), so that it arrives at the impedance at time $-z_j/c$ relative to the synchronous particle, which is considered to be located at the bunch center and unperturbed by the wake fields. Let δ_j, y_j, and y_j' be the relative energy error, the transverse displacement, and the transverse slope of the jth macroparticle as it passes by the impedance. Let the transverse and longitudinal wake functions due to the impedance be $W_1(z)$ and $W_0'(z)$.[39]

We are now in a position to write down the transverse and longitudinal wake forces experienced by a test charge e in the jth macroparticle. First consider the case when the wakes are short-ranged. A test charge in the leading macroparticle (the one with the largest value of z_j in the particular passage under consideration) will experience

$$\int ds\, F_{\parallel} = -\tfrac{1}{2} N_j e^2 W_0'(0^-) \quad \text{and} \quad \int ds\, F_{\perp} = 0. \tag{4.129}$$

For a test charge in a later macroparticle, say the jth, we have

$$\begin{aligned} \left(\int ds\, F_{\parallel}\right)_j &= -\tfrac{1}{2} N_j e^2 W_0'(0^-) \\ &\quad - \sum_{k \neq j} N_k e^2 \left[W_0'(z_j - z_k) + y_k y_j W_1'(z_j - z_k) \right], \\ \left(\int ds\, F_{\perp}\right)_j &= -\sum_{k \neq j} N_k e^2 y_k W_1(z_j - z_k), \end{aligned} \tag{4.130}$$

where the summation over $k \neq j$ is over the macroparticles, except that macroparticles behind the jth do not contribute to the sums, because $W_0(z)$ and $W_1(z)$ vanish if $z > 0$. The quantities $\int ds\, F_{\parallel}$ and $\int ds\, F_{\perp}$ couple the dynamic variables of a macroparticle to those of the other macroparticles. The W_1' term in Eq. (4.130) gives the longitudinal effect of the $m = 1$ wake field.

In case the wakes are long-ranged so that they are longer than the accelerator circumference C, we have to take into account contributions from

[39] Here we consider simultaneously the $m = 0$ and the $m = 1$ wake fields, but ignore the $m = 2$ wake fields. To include the $m = 2$ wake effects would be more involved; in particular, the dynamic variables of the macroparticles will have to include, in addition to z_j, δ_j, y_j, and y_j', also the other transverse coordinate x_j, its slope x_j', and the normal and skew second moments Q_{nj} and Q_{sj}.

residual wake fields from previous revolutions. Equation (4.130) then acquires the following additional terms:

$$\left(\int ds\, F_{\parallel}\right)_j = -\sum_{m=1}^{\infty}\sum_{k=1}^{M} N_k e^2 \left[W_0'\left(z_j - z_k^{(m)} - mC\right) + y_k^{(m)} y_j W_1'\left(z_j - z_k^{(m)} - mC\right)\right], \quad (4.131)$$

$$\left(\int ds\, F_{\perp}\right)_j = -\sum_{m=1}^{\infty}\sum_{k=1}^{M} N_k e^2 y_k^{(m)} W_1\left(z_j - z_k^{(m)} - mC\right),$$

where $z_k^{(m)}$ and $y_k^{(m)}$ are the coordinates of the kth macroparticle m revolutions before.

The changes of the dynamic variables of the jth macroparticle as the bunch passes by the impedance can be written in a matrix form,

$$\begin{bmatrix} \Delta z_j \\ \Delta \delta_j \\ \Delta y_j \\ \Delta y_j' \end{bmatrix} = \frac{1}{E} \begin{bmatrix} 0 \\ \left(\int ds\, F_{\parallel}\right)_j - eV_{\mathrm{rf}} \sin \dfrac{\omega_{\mathrm{rf}} z_j}{c} \\ 0 \\ \left(\int ds\, F_{\perp}\right)_j \end{bmatrix}. \quad (4.132)$$

An extra term proportional to the rf voltage V_{rf} has been added to δ_j because we have assumed the impedance is located at the rf cavity. If nonlinearities of the rf focusing are not important in the study, one may replace $\sin(\omega_{\mathrm{rf}} z_j/c)$ by $\omega_{\mathrm{rf}} z_j/c$.

The transformation of the dynamic variables between impedances is given by the unperturbed betatron and synchrotron motions prescribed by the accelerator design.[40] For example, if the betatron motion is that of a simple harmonic motion, we have

$$\begin{bmatrix} z_j \\ \delta_j \\ y_j \\ y_j' \end{bmatrix}_s = \begin{bmatrix} 1 & -\eta & 0 & 0 \\ 0 & 1 & 0 & 0 \\ 0 & 0 & \cos \dfrac{\omega_\beta s}{c} & \dfrac{c}{\omega_\beta} \sin \dfrac{\omega_\beta s}{c} \\ 0 & 0 & -\dfrac{\omega_\beta}{c} \sin \dfrac{\omega_\beta s}{c} & \cos \dfrac{\omega_\beta s}{c} \end{bmatrix} \begin{bmatrix} z_j \\ \delta_j \\ y_j \\ y_j' \end{bmatrix}_0. \quad (4.133)$$

If the only impedance is located at the rf cavity, one has $s = C$.

The simulation procedure is then to apply Eqs. (4.132–4.133) alternately between the impedance and the accelerator section. The beam bunch is

[40] E. D. Courant and H. S. Snyder, Ann. Phys. **3**, 1 (1958).

launched with a certain set of initial values of the dynamic variables of all of its macroparticles, and the evolution of these variables is observed as the simulation proceeds.

Calculation of the multiturn wake forces using Eq. (4.131) involves double summations—one over the macroparticles, the other over the previous revolutions—which consume much computer time. For resonator impedances, however, this can be avoided by noting that the wake function can be written as a phasor[41] according to

$$W_0'(z) \equiv \operatorname{Re} \tilde{W}_0'(z), \qquad z < 0. \tag{4.134}$$

It follows from Eq. (2.84) that $\tilde{W}_0'$ satisfies the phasor condition

$$\tilde{W}_0'(z + D) = \tilde{W}_0'(z) e^{(i\bar{\omega}+\alpha)D/c}, \qquad D < 0, \tag{4.135}$$

where the parameters α and $\bar{\omega}$ were defined in Eq. (2.84). The same expressions hold for the $m = 1$ wake functions W_1 and W_1', provided the parameters α and $\bar{\omega}$ are taken from the $m = 1$ impedance.

The double summations in Eq. (4.131) can now be simplified. For example, one of the terms on the right hand side can be written as

$$\begin{aligned} -\sum_{m=1}^{\infty}\sum_{k=1}^{M} N_k e^2 \tilde{W}_0'\left(z_j - z_k^{(m)} - mC\right) &= -\sum_{k=1}^{M} N_k e^2 \tilde{W}_0'\left(z_j - z_k^{(1)} - C\right) \\ &\quad -\sum_{m=2}^{\infty}\sum_{k=1}^{M} N_k e^2 \tilde{W}_0'\left(z_j - z_k^{(m)} - mC\right). \end{aligned} \tag{4.136}$$

The second term on the right hand side of Eq. (4.136) can be written as

$$\begin{aligned} -\sum_{m=1}^{\infty}\sum_{k=1}^{M} N_k e^2 \tilde{W}_0'\left[z_j - z_k^{(m+1)} - (m+1)C\right] \\ = -\sum_{m=1}^{\infty}\sum_{k=1}^{M} N_k e^2 \tilde{W}_0'\left(z_j^{(1)} - z_k^{(m+1)} - mC\right) e^{-(i\bar{\omega}+\alpha)(C+z_j^{(1)}-z_j)}. \end{aligned} \tag{4.137}$$

The term in front of the phase factor on the right hand side of Eq. (4.137) is the same quantity already calculated for the jth macroparticle in the previous revolution. If this information has been stored in the computer, the double summation reduces to a single summation over the macroparticles. A similar reduction occurs in the other two double summations in Eq. (4.131). The first term in Eq. (4.136) gives the wake field excited by the beam in the last revolution. The second term gives the ringing wake fields accumulated over all previous revolutions.

[41] Perry B. Wilson, *AIP Proc.* **87**, *Phys. High Energy Part. Accel.*, Fermilab, 1981, p. 450.

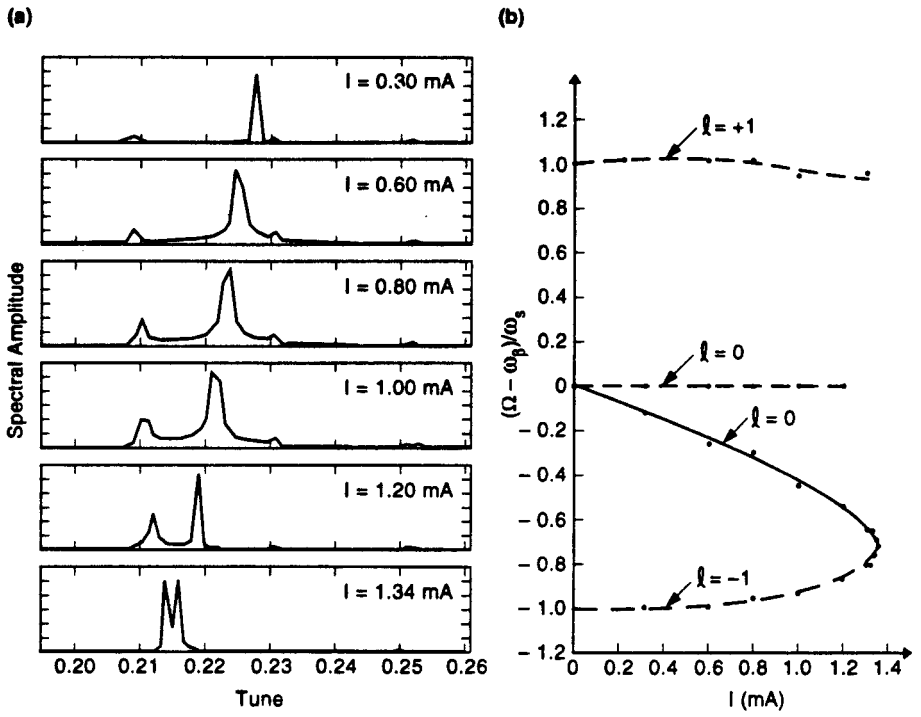

Figure 4.16. Simulation of the strong head-tail instability for the PEP storage ring. (a) Spectrum of the beam center of charge showing the collective modes for several beam intensities. (b) Mode frequencies $(\Omega - \omega_\beta)/\omega_s$ versus the average beam current $I = Ne/T_0$. (Courtesy Steve Myers, 1992.)

Figure 4.16 is a simulation result performed for the PEP storage ring at 4.5 GeV.[42] What is being studied is the strong head-tail instability. The impedance is assumed to come from the rf cavities. Figure 4.16(a) shows the Fourier spectrum of the beam center of charge for various beam intensities. We observe four mode frequency peaks of varying strengths; one corresponds to mode index $l = -1$, one to $l = 1$, and two to $l = 0$.[43] The most prominent feature is the gradual convergence of the frequencies of the $l = -1$ and one of the $l = 0$ modes as the beam intensity is increased. When they merge, at a beam current of $I = 1.4$ mA, the beam becomes unstable. Figure 4.16(b) is a plot of the mode frequencies versus I. The behavior is in good agreement with the two-particle model for the lowest modes.

Another simulation for PEP of the head-tail instability is shown in Figure 4.17.[44] When the chromaticity $\xi < 0$, one observes from Figure 4.17(a) that

[42]Stephen Myers, *Proc. IEEE Part. Accel. Conf.*, Washington, 1987, p. 503.

[43]Discussion of these various modes, beyond those of the two-particle model, is the subject of Sections 6.6 and 6.7.

[44]R. H. Siemann, Nucl. Instr. Meth. **221**, 293 (1984); R. H. Siemann, *AIP Proc.* **127**, Phys. High Energy Part. Accel., BNL/SUNY, 1983, p. 368.

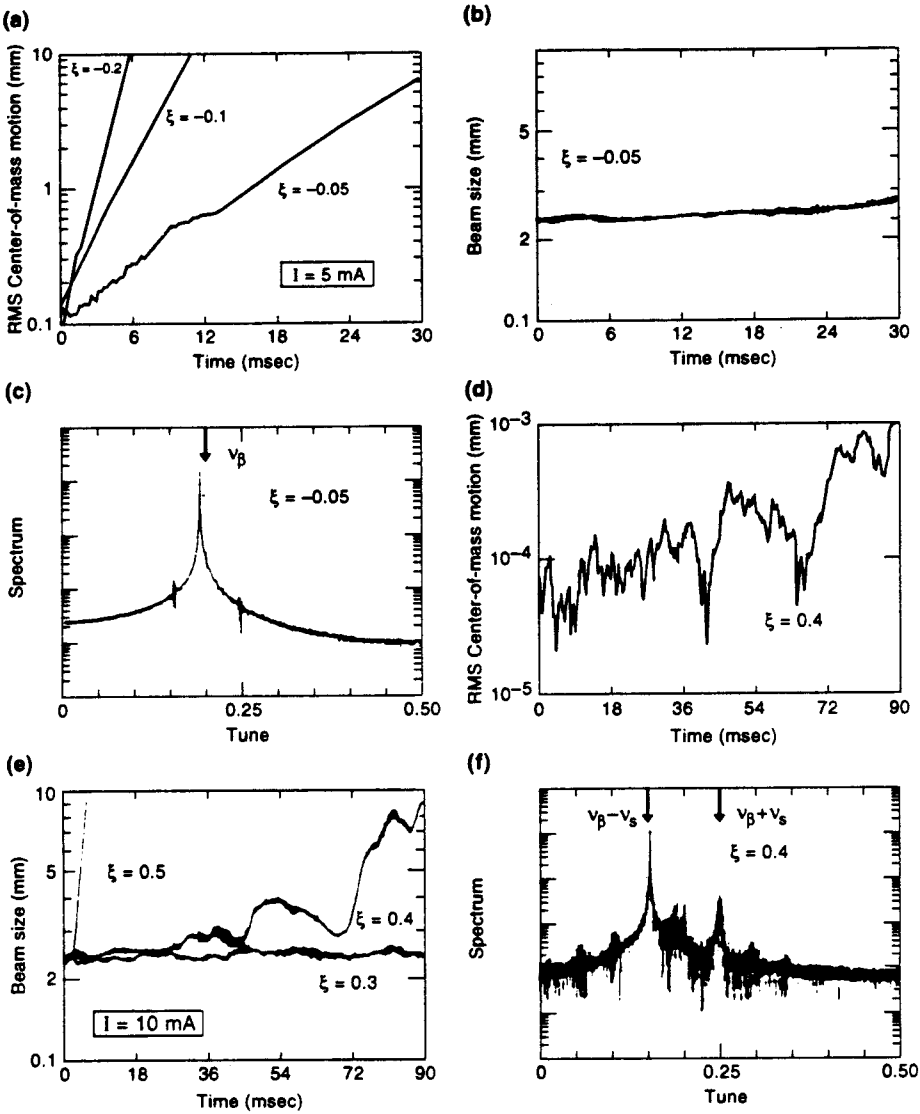

Figure 4.17. Simulation of the head-tail instability for the PEP storage ring. (a) The amplitude of the beam center-of-charge motion grows with the beam storage time for three values of $\xi < 0$ and a fixed beam current $I = 5$ mA. (b) The beam size stays basically constant when $\xi < 0$. (c) Spectrum of the beam center-of-charge motion for a negative ξ. (d), (e), and (f) are the same as (a), (b), and (c), but for $\xi > 0$. Arrows in (c) and (f) indicate the unperturbed betatron tune $\nu_\beta = \omega_\beta / \omega_0$ and its synchrotron sidebands $\nu_\beta \pm \nu_s$. (Courtesy Robert Siemann, 1992.)

the amplitude of the beam center-of-charge motion (reflecting the + mode) becomes unstable and grows exponentially with a growth rate more or less proportional to ξ. Figure 4.17(b) shows that when $\xi < 0$, the rms beam size (reflecting the − mode) stays basically constant. The center-of-charge motion is Fourier analyzed to yield the spectrum shown in Figure 4.17(c). When $\xi > 0$, the behavior is reversed as shown in Figures 4.17(d) and (e), i.e., the beam center of charge stays basically constant, whereas the beam size grows exponentially. Since PEP is operated above transition, this behavior is consistent with the results from Eq. (4.99) of the two-particle model. The beam spectra in Figures 4.17(c) and (f) are also consistent with this picture: when $\xi < 0$, the beam is mainly executing a center-of-charge motion near the betatron frequency; when $\xi > 0$, the beam motion is mainly in the $l \neq 0$ modes, particularly the $l = \pm 1$ modes with mode frequencies near $\omega_\beta \pm \omega_s$.

The flexibility of simulation studies allows them to include effects in addition to the wake field effects to be studied simultaneously. For example, one may include radiation damping and quantum excitation, which play a role in circular electron accelerators. The interplay between collective phenomena and nonlinearities in single-particle motion can be simulated by including nonlinear terms in the transformation (4.133). Landau damping effects (see Chapter 5) can be simulated by including spreads in the unperturbed synchrotron or betatron frequencies of the macroparticles. Inclusions of synchro-betatron coupling, more realistic wake functions, localized impedances, and feedback systems are straightforward in a simulation.

The choice of the number of macroparticles, M, depends on the problem at hand. In practice, one varies M until the result stabilizes, and makes the choice after judging against the computer time consumed. Two considerations affect the choice of M: one is dynamics, and the other is statistics. The dynamical consideration is that the number of macroparticles must be larger (if possible, much larger) than the highest order of the modes of interest. A simulation of the longitudinal bunch lengthening phenomenon (see Section 6.5), for example, tends to require a large M because higher modes are involved in the dynamics. The statistical consideration is more pronounced in the studies of longitudinal instabilities. It comes from the fact that the wake function is discontinuous at $z = 0$. One close encounter between two macroparticles can lead to very different subsequent results, depending on which particle happens to be slightly ahead. One way to improve the statistics is to increase M. Another, adopted in obtaining Figure 4.17, is to write the instantaneous beam distribution as a superposition of orthogonal polynomials, the expansion coefficients of which are fitted every time the beam passes by the impedance. The expansion is truncated at some order, and the truncation order then plays a role equivalent to the number of macroparticles, except that the noise problem is much eased.

CHAPTER 5

Landau Damping

As the previous chapters demonstrated, there are a large number of collective instability mechanisms acting on a high intensity beam in an accelerator, demanding a wide range of (sometimes conflicting) stability conditions. Yet the beam as a whole seems basically stable, as evidenced by the existence of a wide variety of working accelerators, many of them with demanding beam intensities. One of the reasons for this fortunate outcome is *Landau damping*,[1] which provides a natural stabilizing mechanism against collective instabilities if particles in the beam have a small spread in their natural (synchrotron or betatron) frequencies. The purpose of the present chapter is to introduce this important topic. Section 5.1 describes the physical origin of Landau damping. The results are applied in Section 5.2 to demonstrate Landau damping of bunched beams in circular accelerators, using a macroparticle model. Sections 5.3 and 5.4 then describe the Landau damping of unbunched beams. Finally, in Section 5.5 we briefly discuss a quantity called the beam transfer function.

The theory of Landau damping of unbunched beams was first formulated using the Vlasov technique by Neil and Sessler[2] for the longitudinal case and by Lasslet, Neil, and Sessler[3] for the transverse case. In this chapter, we will proceed with a somewhat different treatment, postponing the Vlasov treatment until Chapter 6. For bunched beams, we consider only a macroparticle model. Landau damping of bunched beams in general (not just for macroparticle models) using the Vlasov technique is beyond the scope of this book.[4]

[1] L. D. Landau, J. Phys. USSR **10**, 25 (1946).
[2] V. Kelvin Neil and Andrew M. Sessler, Rev. Sci. Instr. **6**, 429 (1965).
[3] L. Jackson Laslett, V. Kelvin Neil, and Andrew M. Sessler, Rev. Sci. Instr. **6**, 46 (1965).
[4] G. Besnier, Nucl. Instr. Meth. **164**, 235 (1979); B. Zotter, CERN Report SPS/81-19 (DI) (1981); Yongho Chin, Kohtaro Satoh, and Kaoru Yokoya, Part. Accel. **13**, 45 (1983).

In an accelerator, the spread in natural frequency of the beam comes from several sources. A dependence of the betatron frequency ω_β on the energy of the particle, together with an energy spread in the beam, leads to a spread in ω_β. Nonlinearities in the focusing system cause a dependence of ω_β on the particle's betatron amplitude. A spread in betatron amplitudes then leads also to a spread in ω_β.[5] In the longitudinal case the source of frequency spread depends on whether the beam is bunched or unbunched. For bunched beams, a spread in the synchrotron frequency ω_s can result from nonlinearity in the rf focusing voltage. For unbunched beams, dependence of the revolution frequency on the particle energy plays a similar role. In the following, for all cases studied, we will simply assume a frequency spread specified by an externally given beam frequency spectrum.

5.1 PHYSICAL ORIGIN

Consider a simple harmonic oscillator which has a natural frequency ω. Let this oscillator be driven, starting at time $t = 0$, by a sinusoidal force of frequency Ω. The equation of motion is

$$\ddot{x} + \omega^2 x = A \cos \Omega t \tag{5.2}$$

with the initial conditions $x(0) = 0$ and $\dot{x}(0) = 0$. The solution is

$$x(t > 0) = -\frac{A}{\Omega^2 - \omega^2}(\cos \Omega t - \cos \omega t). \tag{5.3}$$

In Eq. (5.3), the $\cos \Omega t$ term gives the main term responding to the driving force; the $\cos \omega t$ term comes from matching the initial conditions.

Following a treatment by Hereward,[6] Eq. (5.3) is our starting point for the Landau damping analysis. In particular, we will see that the explicit inclusion of the initial conditions plays an important role. Otherwise, one could have

[5]In the following, we assume the spread in ω_β is independent of the amplitude of excitation due to the instability. This will not be true if the ω_β spread is caused by nonlinearities. This subtlety, however, will not be pursued. Interested reader may refer to H. G. Hereward, CERN Report MPS/DL 69-11 (1969), where it is shown that the equivalent of Eq. (5.7) reads

$$\langle x \rangle = -\frac{\pi}{2} A e^{-i\Omega t} \int_0^\infty dJ \frac{J\rho'(J)}{\omega(J) - \Omega}, \tag{5.1}$$

where $J = x^2 + (\dot{x}/\omega)^2$ is the betatron action, and $\rho(J)$ is the unperturbed phase space density normalized by $\int_0^\infty \pi\, dJ[\omega(J) + J\omega'(J)]\rho(J) = 1$. Nonlinearity is characterized by $\omega'(J) \neq 0$.

[6]H. G. Hereward, CERN Report 65-20 (1965). See also A. Hoffmann, CERN Accel. School, Advanced Accel. Phys., CERN Report 89-01 (1989), p. 40; A. Hofmann, *Frontiers of Part. Beams: Intensity Limitations*, Hilton Head Island, Lectures in Phys. **400**, Springer-Verlag, 1990, p. 110.

hastily written down the solution

$$x(t) = -\frac{A}{\Omega^2 - \omega^2}\cos \Omega t \quad \text{or} \quad x(t) = -\frac{A}{\Omega^2 - \omega^2}e^{-i\Omega t}. \tag{5.4}$$

The main difference between Eqs. (5.4) and (5.3) is that Eq. (5.4) contains a singularity at $\Omega = \omega$ while Eq. (5.3) is well behaved there. This singularity is the source of many subtleties and at this point is to be avoided. As we will see later, by applying some mathematical tricks, it is possible to bypass the explicit inclusion of the initial conditions and go straight to Eq. (5.4), but at this point, it is more appropriate to use the well-behaved expression (5.3).

Consider now an ensemble of oscillators (each oscillator represents a single particle in the beam) which do not interact with each other and have a spectrum of natural frequency ω with a distribution $\rho(\omega)$ satisfying $\int_{-\infty}^{\infty} d\omega\, \rho(\omega) = 1$. Now starting at time $t = 0$, subject this ensemble of particles to the driving force $A \cos \Omega t$ with all particles starting with initial conditions $x(0) = 0$ and $\dot{x}(0) = 0$. We are interested in the ensemble average of the response, which is given by superposition,

$$\langle x \rangle (t > 0) = -\int_{-\infty}^{\infty} d\omega\, \rho(\omega) \frac{A}{\Omega^2 - \omega^2}(\cos \Omega t - \cos \omega t). \tag{5.5}$$

In a single-particle response (5.3), the main $\cos \Omega t$ term is in phase (i.e., no $\sin \Omega t$ term) and in frequency relative to the driving force, but the initial condition $\cos \omega t$ term is out of frequency. It seems as if the main ensemble response to the driving force were

$$-\cos \Omega t \int_{-\infty}^{\infty} d\omega\, \rho(\omega) \frac{A}{\Omega^2 - \omega^2}, \tag{5.6}$$

which is in phase and in frequency with the driving force. Equation (5.6) is in fact what we would obtain if we used Eq. (5.4) instead of Eq. (5.3) for the response of single particles. But this observation is incorrect. When the beam spectrum covers the driving frequency Ω, there is a singularity at $\Omega = \omega$. This singularity, when treated properly, contributes to a $\sin \Omega t$ term that is out of phase with the driving force. What is more, this mysterious $\sin \Omega t$ component has a definite sign, which in turn has important consequences.

To observe the $\sin \Omega t$ component, it is necessary to use the complete expression (5.3). For simplicity, let us consider a narrow beam spectrum around a frequency ω_x and a driving frequency near the spectrum, i.e., $\Omega \approx \omega_x$.[7] The beam response is then

$$\langle x \rangle (t) = -\frac{A}{2\omega_x} \int d\omega\, \rho(\omega) \frac{1}{\Omega - \omega}(\cos \Omega t - \cos \omega t). \tag{5.7}$$

[7]Depending on whether the betatron or synchrotron dimension is of interest, ω_x will be taken to be ω_β or ω_s. The coordinate x will be chosen similarly.

Changing variable from ω to $u = \omega - \Omega$ leads to

$$\begin{aligned}\langle x\rangle(t) &= \frac{A}{2\omega_x}\int_{-\infty}^{\infty} du\,\frac{\rho(u+\Omega)}{u}\left[\cos\Omega t - \cos(\Omega t + ut)\right] \\ &= \frac{A}{2\omega_x}\left[\cos\Omega t\int_{-\infty}^{\infty} du\,\rho(u+\Omega)\frac{1-\cos ut}{u}\right. \\ &\qquad \left. +\sin\Omega t\int_{-\infty}^{\infty} du\,\rho(u+\Omega)\frac{\sin ut}{u}\right]. \end{aligned} \tag{5.8}$$

In the above manipulations, we have made sure that all integrals are well behaved at $u = 0$.

Equation (5.8) contains a $\cos\Omega t$ term and a $\sin\Omega t$ term, but their coefficients are time dependent. The next step is to show that those coefficients approach well-behaved limits, and particularly that the $\sin\Omega t$ coefficient does not approach zero. To do so, one first observes

$$\begin{aligned}\lim_{t\to\infty}\frac{\sin ut}{u} &= \pi\delta(u), \\ \lim_{t\to\infty}\frac{1-\cos ut}{u} &= \text{P.V.}\left(\frac{1}{u}\right).\end{aligned} \tag{5.9}$$

The proof of Eq. (5.9) is illustrated in Figure 5.1. As t increases, one notes that $(\sin ut)/u$ peaks around $u = 0$ with increasing height and decreasing width. The area under the function is a constant, given by π, for all t. A moment's reflection verifies the first member of Eq. (5.9). Similarly, as t increases, the function $(1 - \cos ut)/u$ approaches $1/u$ to increasing accuracy around $u = 0$, as shown in Figure 5.1(b). The sole function of the $\cos ut$ term, which oscillates rapidly as $t \to \infty$, is to avoid the singularity at $u = 0$. Recalling the definition of principal values (see Footnote 26 of Chapter 2) proves the second member of Eq. (5.9). Note that Eq. (5.9) is applied only when an integral over u is to be taken next.

If we are not interested in the transient effects immediately following the onset of the driving force, we may substitute Eq. (5.9) into Eq. (5.8) and obtain

$$\langle x\rangle(t) = \frac{A}{2\omega_x}\left[\cos\Omega t\ \text{P.V.}\int d\omega\,\frac{\rho(\omega)}{\omega-\Omega} + \pi\rho(\Omega)\sin\Omega t\right]. \tag{5.10}$$

This expression now contains explicitly a $\cos\Omega t$ term and, as promised, also a $\sin\Omega t$ term.

The sign of the $\cos\Omega t$ term relative to the driving force depends on the sign of $\text{P.V.}\int d\omega\,\rho(\omega)/(\omega - \Omega)$. Generally, this term is approximately given

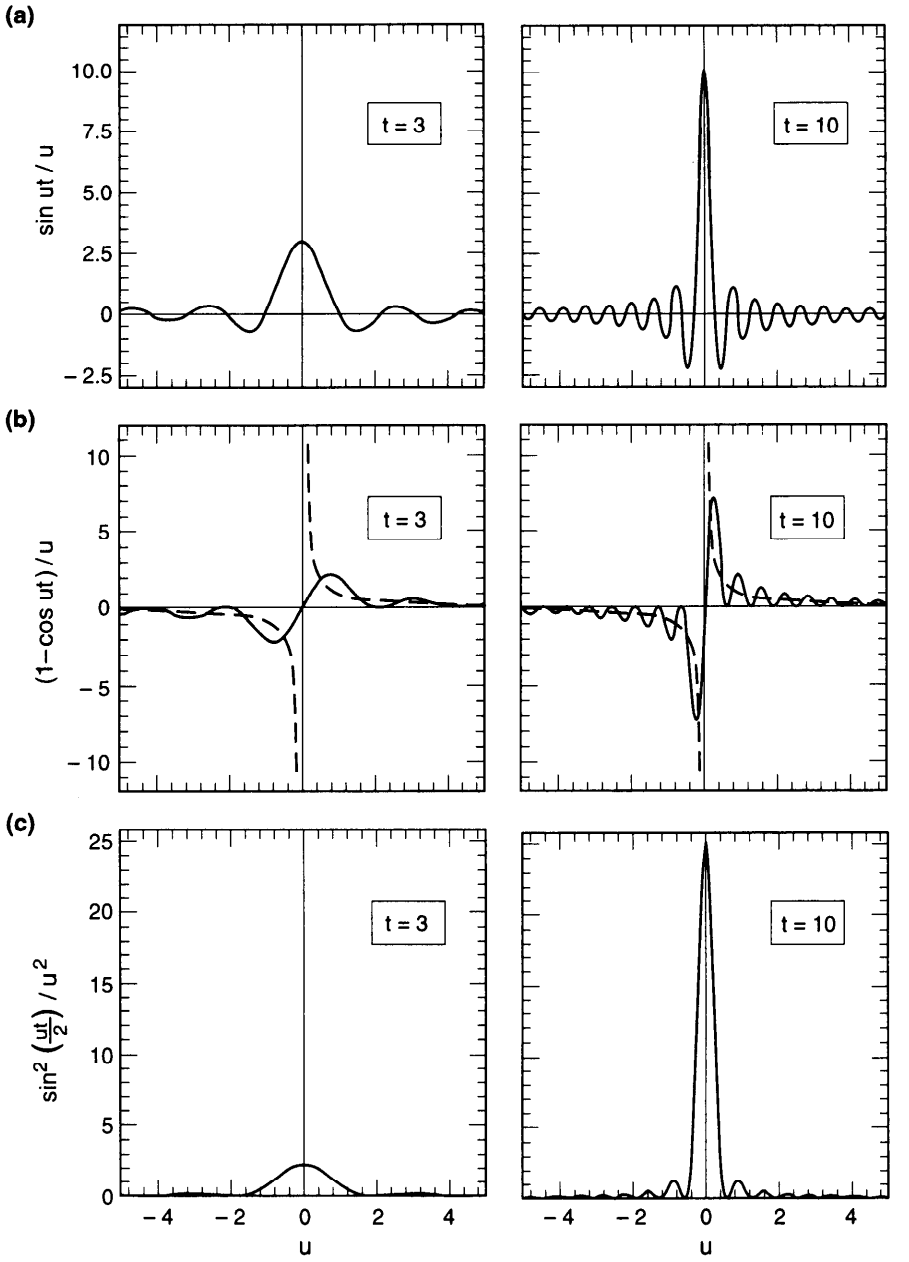

Figure 5.1. The functions $\sin(ut)/u$, $(1-\cos ut)/u$, and $\sin^2(ut/2)/u^2$ are shown in (a), (b), and (c) for two values $t = 3$ and 10. The dashed curves in (b) are for the function $1/u$.

by $1/(\omega_x - \Omega)$ outside the spectrum and crosses through zero somewhere inside the spectrum. (See Figure 5.3 below for examples). A system is referred to as "capacitive" or "inductive" based on whether its sign is positive or negative.

The $\sin \Omega t$ term has a definite sign relative to the driving force, because $\rho(\Omega)$ is always positive. In particular, $d\langle x\rangle/dt$ is always in phase with the force, indicating work is being done on the system. The system always reacts to the force "resistively."

Exercise 5.1 In case the driving force is $A\cos(\Omega t + \phi)$, follow the steps leading to Eq. (5.10) to show that the asymptotic beam response is

$$\langle x\rangle(t) = \frac{A}{2\omega_x}\left[\cos(\Omega t + \phi)\text{P.V.}\int d\omega\,\frac{\rho(\omega)}{\omega - \Omega} + \pi\rho(\Omega)\sin(\Omega t + \phi)\right]. \tag{5.11}$$

Other than replacing Ωt by $\Omega t + \phi$, the only difference in beam response from the case when $\phi = 0$ is in the transients.

The Landau damping effect is to be distinguished from a *decoherence* (also called phase-mixing, or filamentation) effect that occurs when the beam has nonzero initial conditions. Had we included an initial condition $x(0) = x_0$ and $\dot{x}(0) = \dot{x}_0$, we would have introduced two additional terms into the ensemble response:

$$x_0\int d\omega\,\rho(\omega)\cos\omega t + \dot{x}_0\int d\omega\,\rho(\omega)\frac{\sin\omega t}{\omega}. \tag{5.12}$$

These terms do not participate in the dynamic interaction of the beam particles and are not very interesting for our purposes here. In this decoherence effect, individual particles continue to execute oscillations of constant amplitude, but the total beam response $\langle x\rangle$ decreases with time.[8]

As mentioned, work is continuously being done on the system. However, the amplitude of $\langle x\rangle$, as given in Eq. (5.10), does not increase with time. Where did the energy go? To investigate this, let us first identify the energy of a particle as the square of its oscillation amplitude. From Eq. (5.3), the amplitude of a particle is given by the slowly varying envelope

$$\text{amplitude} = \frac{A}{\omega_x(\Omega - \omega)}\sin\frac{(\Omega - \omega)t}{2}. \tag{5.13}$$

[8]Provided $\rho(\omega) = 0$ at $\omega = 0$. See Exercise 5.2(b).

This leads to a total oscillation energy of

$$\mathscr{E} = N\int d\omega\, \rho(\omega)\left[\frac{A}{\omega_x(\Omega-\omega)}\sin\frac{(\Omega-\omega)t}{2}\right]^2$$

$$= \frac{NA^2}{\omega_x^2}\int du\, \rho(u+\Omega)\frac{\sin^2(ut/2)}{u^2}, \tag{5.14}$$

where N is the total number of particles in the beam. Figure 5.1(c) shows the behavior of $\sin^2(ut/2)/u^2$. As t increases, the region where this function assumes significant values narrows around $u = 0$. The range of the region decreases as $1/t$, but the height of the function increases quadratically as t^2, leading to an area under the function that increases linearly with t. In fact,

$$\lim_{t\to\infty}\frac{\sin^2(ut/2)}{u^2} = \frac{\pi t}{2}\delta(u). \tag{5.15}$$

Equation (5.14) then reads

$$\mathscr{E} = \frac{\pi}{2}\frac{NA^2}{\omega_x^2}\rho(\Omega)t, \tag{5.16}$$

which increases linearly with time. The system therefore absorbs energy from the driving force indefinitely while holding the ensemble beam response within bounds.

An analogy occurs in the decoherence behavior described by Eq. (5.12). In that case, the single-particle energies and thus the total beam energy are constant in time, but the ensemble signal $\langle x\rangle$ decreases with time.

The stored energy (5.16) is incoherent in the sense that the energy is contained in the individual particles, but it is not to be regarded as heat in the system. This is because the stored energy is not distributed more or less uniformly in all particles, but is selectively stored in particles with continuously narrowing range of frequencies around the driving frequency. Figure 5.2 shows the driving force and the single-particle responses (5.3) for different particle frequencies. One sees that a particle with $\omega = \Omega$, being resonantly driven, continues to increase in amplitude as t increases. A particle with ω away from Ω gets out of resonance after a time approximately $\pi/|\omega - \Omega|$, and at time $t = 2\pi/|\omega - \Omega|$, the particle returns all its energy back to the driving force in a beating process.

It is mainly those particles with $|\omega - \Omega| < 1/t$ that contribute to the $\sin\Omega t$ response, and those particles with $|\omega - \Omega| > 1/t$ that contribute to the $\cos\Omega t$ response. Since the number of particles with $|\omega - \Omega| < 1/t$ decreases with time as $1/t$ while their amplitude increases as t, the net $\sin\Omega t$ contribution to $\langle x\rangle$ is constant in time.

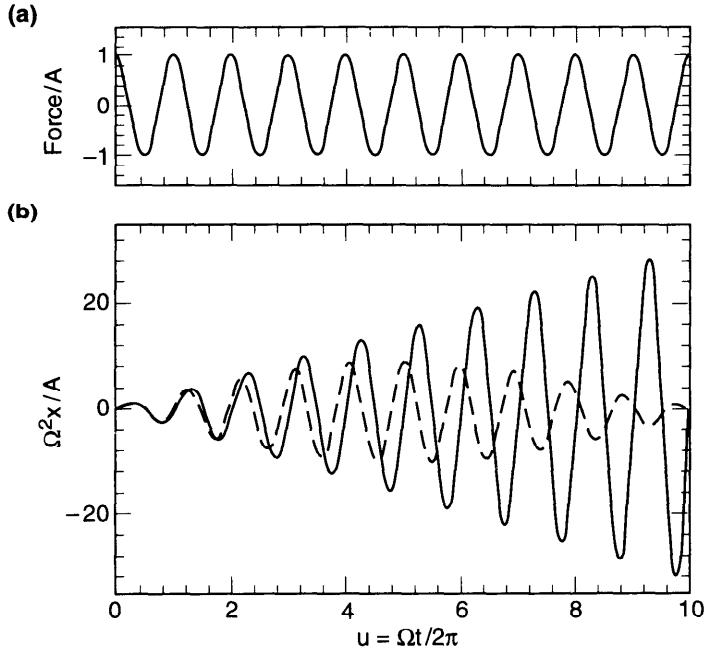

Figure 5.2. Single-particle response $x(t)$ to a sinusoidal driving force $f(t) = A\cos\Omega t$. (a) $f(t)/A$ versus $\upsilon = \Omega t/2\pi$; (b) $\Omega^2 x(t)/A$ versus υ. The solid curve is for a particle on resonance with $\omega = \Omega$. The dashed curve is for a particle with $\omega = 1.1\Omega$.

The asymptotic behavior (5.10) applies if one waits for a time longer than $1/\Delta\omega$, where $\Delta\omega$ is the frequency spread of the beam spectrum. For $t < 1/\Delta\omega$, the beam response is confounded by transient terms. Furthermore, the $\sin\Omega t$ term is proportional to $\rho(\Omega)$. If the spectrum is such that there are no particles near frequency Ω to continuously absorb energy, Landau damping will cease and a beating phenomenon takes over. Since a beam consists of a finite number of particles, Landau damping will cease when t is larger than $1/\delta\omega$, where $\delta\omega$ is the frequency spacing between two nearest particles. The range of time for Eq. (5.10) to be applicable is therefore

$$\frac{1}{\delta\omega} \gg t \gg \frac{1}{\Delta\omega}. \tag{5.17}$$

With N particles in the beam, one might have $\delta\omega \approx \Delta\omega/N$. Taking $N = 10^{11}$ and $\Delta\omega = 10^3\ \mathrm{s}^{-1}$ for example, the time is limited to the range between 1 ms and 10^8 s.

Of course the upper limit can be exceeded long before 10^8 s if the resonant particles are lost when their amplitudes exceed b, the radius of the vacuum chamber. Using Eq. (5.13), this occurs when $At/2\omega_x > b$. The

applicable time for Landau damping then becomes

$$\frac{2b\omega_x}{A} > t \gg \frac{1}{\Delta\omega}. \tag{5.18}$$

An alternative way to consider the beam response that avoids the consideration of transient effects (and therefore removes the limit $t \gg 1/\Delta\omega$) is to pretend that the driving force has been in existence since $t \to -\infty$, except that the force contains an extra exponential factor $e^{\epsilon t}$ which goes to 0 as $t \to -\infty$, i.e., the force has been turned on adiabatically. This extra exponential factor effectively takes into account the initial conditions while removing the transient effects. The price to pay is that the force then grows indefinitely as $t \to \infty$. Fortunately it is just the slightly growing solutions that most interest us, because they correspond to the situation when the beam is at the edge of instability. These considerations will be elaborated upon as the subject of Landau damping is developed.

In the following, we give several explicit examples, the first of which is when all particles in the beam have the same natural frequency, i.e.,

$$\rho(\omega) = \delta(\omega - \omega_x). \tag{5.19}$$

In this trivial case, we have the following asymptotic beam response to a driving force $A \cos \Omega t$:

$$\langle x \rangle = \frac{A}{2\omega_x}\left[\frac{\cos \Omega t}{\omega_x - \Omega} + \pi\delta(\Omega - \omega_x)\sin \Omega t\right]. \tag{5.20}$$

The first nontrivial case to be considered is for a Lorentz spectrum

$$\rho(\omega) = \frac{\Delta\omega}{\pi}\frac{1}{(\omega - \omega_x)^2 + \Delta\omega^2}. \tag{5.21}$$

We have[9]

$$\text{P.V.}\int d\omega \frac{\rho(\omega)}{\omega - \Omega} = \frac{\omega_x - \Omega}{(\omega_x - \Omega)^2 + \Delta\omega^2}. \tag{5.22}$$

Substituting into Eq. (5.10) yields the beam response

$$\langle x \rangle = \frac{A}{2\omega_x}\frac{(\omega_x - \Omega)\cos \Omega t + \Delta\omega \sin \Omega t}{(\omega_x - \Omega)^2 + \Delta\omega^2}. \tag{5.23}$$

[9]Derivation of Eq. (5.22) is omitted here. It can be obtained by a complex variable technique or by applying Eq. (2.95).

The system is purely resistive if driven on resonance with $\Omega = \omega_x$, capacitive if $\Omega < \omega_x$, and inductive if $\Omega > \omega_x$.

Exercise 5.2

(a) Equation (5.23) gives the asymptotic behavior when $t \gg 1/\Delta\omega$. Show that, for the Lorentz spectrum, the exact expression including the transient effect is

$$\begin{aligned}\langle x\rangle(t) = {} & \frac{A}{2\omega_x\left[(\omega_x - \Omega)^2 + \Delta\omega^2\right]} \\ & \times\Big\{\cos\Omega t\left[\omega_x - \Omega - \Delta\omega\, e^{-\Delta\omega t}\sin(\omega_x t - \Omega t)\right. \\ & \qquad \left. + (\omega_x - \Omega)e^{-\Delta\omega t}\cos(\omega_x t - \Omega t)\right] \\ & + \sin\Omega t\left[\Delta\omega - \Delta\omega\, e^{-\Delta\omega t}\cos(\omega_x t - \Omega t)\right. \\ & \qquad \left. - (\omega_x - \Omega)e^{-\Delta\omega t}\sin(\omega_x t - \Omega t)\right]\Big\}, \quad (5.24)\end{aligned}$$

which reduces to Eq. (5.23) when $t \gg 1/\Delta\omega$. The fact that the transient terms decay exponentially is specific to the Lorentz spectrum. A different spectrum would give a different time dependence of the transients, but the general conclusion is still valid that they decay when $t \gg 1/\Delta\omega$ for a distribution with frequency spread $\Delta\omega$.

(b) Show that the decoherence term (5.12) for a Lorentz spectrum is

$$\begin{aligned}\langle x\rangle(t) = {} & e^{-\Delta\omega t}\left(x_0\cos\omega_x t - \dot{x}_0\frac{\Delta\omega\cos\omega_x t - \omega_x\sin\omega_x t}{\omega_x^2 + \Delta\omega^2}\right) \\ & + \frac{\Delta\omega\,\dot{x}_0}{\omega_x^2 + \Delta\omega^2}. \quad (5.25)\end{aligned}$$

Note that $\langle x\rangle$ does not approach zero as $t \to \infty$. This comes from particles with $\omega \to 0$; with $\dot{x}_0 \neq 0$, their amplitudes increase indefinitely. The decoherence signal decays only when $\rho(0) = 0$.

For a general beam frequency spectrum, we parametrize the asymptotic beam response as

$$\langle x\rangle = \frac{A}{2\omega_x\,\Delta\omega}\left[f(u)\cos\Omega t + g(u)\sin\Omega t\right], \quad (5.26)$$

where we have introduced

$$f(u) = \Delta\omega \,\text{P.V.} \int d\omega \, \frac{\rho(\omega)}{\omega - \Omega},$$
$$g(u) = \pi \Delta\omega \, \rho(\omega_x - u \, \Delta\omega), \tag{5.27}$$
$$u = \frac{\omega_x - \Omega}{\Delta\omega}.$$

In this notation, we have for the δ-function spectrum

$$f(u) = \frac{1}{u} \quad \text{and} \quad g(u) = \pi\delta(u), \tag{5.28}$$

and for the Lorentz spectrum

$$f(u) = \frac{u}{1 + u^2} \quad \text{and} \quad g(u) = \frac{1}{1 + u^2}. \tag{5.29}$$

A few more examples of different frequency spectra are given below. For a rectangular spectrum

$$\rho(v) = \frac{1}{2\,\Delta\omega} H(1 - |v|), \qquad v = \frac{\omega_x - \omega}{\Delta\omega}, \tag{5.30}$$

where $H(x)$ is the step function $H(x) = 1$ if $x > 0$ and 0 if $x < 0$, the asymptotic beam response is described by

$$f(u) = \frac{1}{2} \ln\left|\frac{u + 1}{u - 1}\right| \quad \text{and} \quad g(u) = \frac{\pi}{2} H(1 - |u|). \tag{5.31}$$

For a parabolic spectrum, we have

$$\rho(v) = \frac{3}{4\,\Delta\omega}(1 - v^2) H(1 - |v|),$$
$$f(u) = \frac{3}{4}\left[(1 - u^2)\ln\left|\frac{u + 1}{u - 1}\right| + 2u\right], \tag{5.32}$$
$$g(u) = \frac{3\pi}{4}(1 - u^2) H(1 - |u|).$$

For an elliptical spectrum, we have

$$\begin{aligned} \rho(v) &= \frac{2}{\pi \Delta\omega} H(1 - |v|)\sqrt{1 - v^2}, \\ f(u) &= 2\left[u - \operatorname{sgn}(u) H(|u| - 1)\sqrt{u^2 - 1}\right], \\ g(u) &= 2H(1 - |u|)\sqrt{1 - u^2}. \end{aligned} \tag{5.33}$$

For a bi-Lorentz spectrum, we have

$$\begin{aligned} \rho(v) &= \frac{2}{\pi \Delta\omega(v^2 + 1)^2}, \\ f(u) &= \frac{u(u^2 + 3)}{(u^2 + 1)^2}, \\ g(u) &= \frac{2}{(u^2 + 1)^2}. \end{aligned} \tag{5.34}$$

And, finally, for a Gaussian spectrum, we have

$$\begin{aligned} \rho(v) &= \frac{1}{\sqrt{2\pi}\,\Delta\omega} e^{-v^2/2}, \\ f(u) &= \sqrt{\frac{2}{\pi}}\, e^{-u^2/2} \int_0^\infty \frac{dy}{y} e^{-y^2/2} \sinh(uy), \\ g(u) &= \sqrt{\frac{\pi}{2}}\, e^{-u^2/2}. \end{aligned} \tag{5.35}$$

The function $f(u)$ for the Gaussian spectrum is approximately equal to u for small u and to $1/u$ for large u.

Figure 5.3 shows the functions f and g for the various spectra. The function g is simply related to the spectrum by $\rho = g/(\pi \Delta\omega)$, and the function f is related to the principle value integral over the spectra. An inspection of Figure 5.3 indicates that $f(u)$ resembles $-g'(u)$. The reason for this behavior should become clear on inspecting the principle value integral expression for $f(u)$.

Exercise 5.3 Although $f(u)$ resembles $-g'(u)$, show that no realistic spectrum gives $f(u) \propto -g'(u)$ exactly.

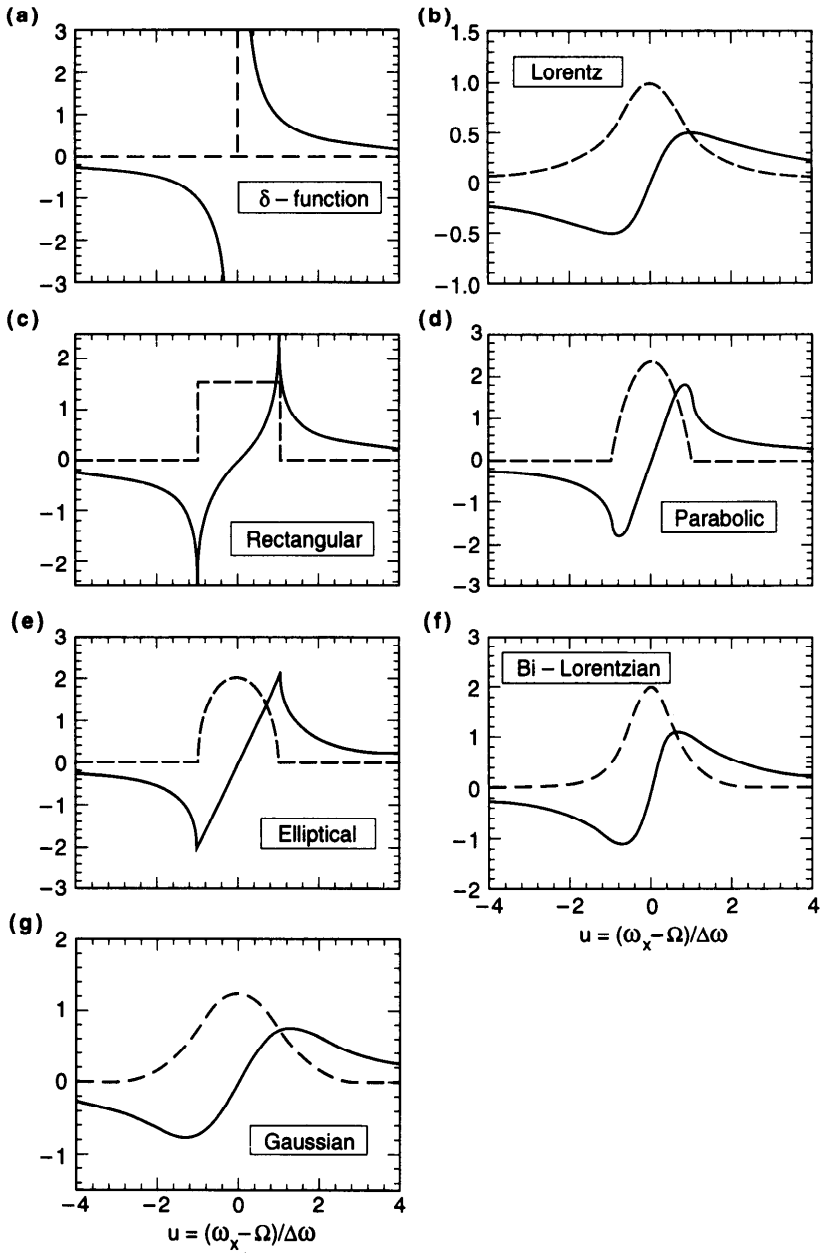

Figure 5.3. The functions $f(\upsilon)$ (solid curves) and $g(\upsilon)$ (dashed curves) versus $\upsilon = (\omega_x - \Omega)/\Delta\omega$ for various beam frequency spectra. The shape of the spectra is the same as the dashed curves.

Exercise 5.4 Show for the above examples that when $|\Omega - \omega_x| \gg \Delta\omega$, the entire beam responds to the driving force as a single particle, with $\langle x \rangle$ given by Eq. (5.4).

To proceed, let us write the beam response (5.10) in a complex notation, which we have tried to avoid so far, keeping in mind that only the real parts are meaningful:

$$\text{driving force} = Ae^{-i\Omega t},$$

$$\langle x \rangle = \frac{A}{2\omega_x} e^{-i\Omega t}\left[\text{P.V.}\int d\omega \, \frac{\rho(\omega)}{\omega - \Omega} + i\pi\rho(\Omega)\right] \tag{5.36}$$

$$= \frac{A}{2\omega_x \, \Delta\omega} e^{-i\Omega t}[f(u) + ig(u)],$$

where $u = (\omega_x - \Omega)/\Delta\omega$. In this expression, one could include a phase in the driving force by considering a complex A. (See Exercise 5.1.) We will refer to the dimensionless complex quantity $f + ig$ as the *beam transfer function* (BTF), which is the subject of Section 5.5 below.

Having demonstrated the detailed treatment of the initial conditions, the apparent singularities, and the out-of-phase beam responses, we are now ready to introduce a mathematical trick which bypasses most of these subtleties and makes the analysis much more concise. It turns out that one can "derive" the same result by venturing with the response (5.4). In complex notation, the single-particle motion (5.4) gives a total beam response

$$\langle x \rangle = \frac{A}{2\omega_x} e^{-i\Omega t} \int d\omega \, \frac{\rho(\omega)}{\omega - \Omega}. \tag{5.37}$$

The detailed examinations so far now provide a well-defined way to deal with the otherwise undefined integral in Eq. (5.37), namely, we are supposed to make the connection

$$\int d\omega \, \frac{\rho(\omega)}{\omega - \Omega} \to \text{P.V.}\int d\omega \, \frac{\rho(\omega)}{\omega - \Omega} + i\pi\rho(\Omega), \tag{5.38}$$

or more symbolically

$$\frac{1}{\omega - \Omega} \to \text{P.V.}\left(\frac{1}{\omega - \Omega}\right) + i\pi\delta(\omega - \Omega). \tag{5.39}$$

Again, it is necessary to include an out-of-phase term—with a definite sign—as evidenced by the imaginary term $i\pi\rho(\Omega)$ in Eq. (5.38), even though the expression on the left hand side seems to be for a real quantity.

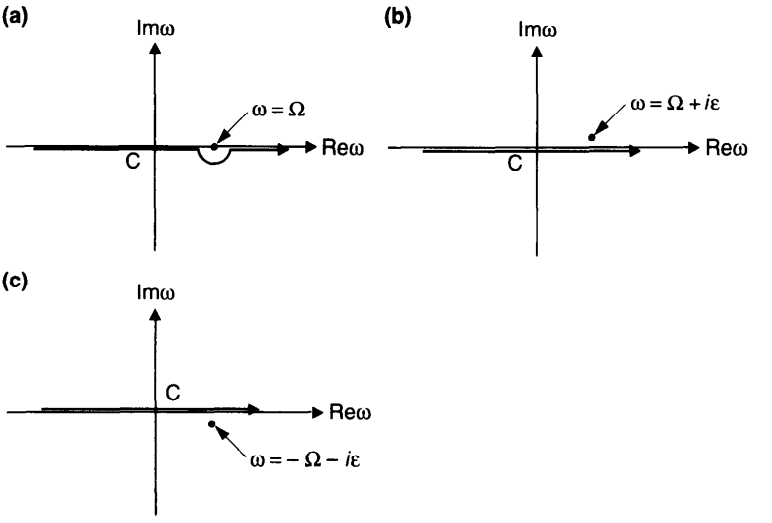

Figure 5.4. Contours in the complex ω-plane: (a) for Eq. (5.40); (b) for Eq. (5.41); (c) for Eq. (5.45) when $\Omega < 0$. The contours can be closed either in the upper half plane or the lower half plane provided $\rho(\omega)$ converges sufficiently rapidly as $|\omega| \to \infty$.

The right hand side of Eq. (5.38) in fact is equal to the left hand side provided one takes the integration to be executed in the complex ω-plane and the contour of integration, C, is as illustrated in Figure 5.4(a). The connection (5.38) now reads

$$\int d\omega \frac{\rho(\omega)}{\omega - \Omega} \to \int_C d\omega \frac{\rho(\omega)}{\omega - \Omega}. \tag{5.40}$$

The straight line portion of C gives the principal value term in $\langle x \rangle$, and the semicircular portion gives the pole contribution $i\pi\rho(\Omega)$.

Equivalently one could consider the integration along the real axis of the ω-plane, but move the pole at $\omega = \Omega$ up by an infinitesimal amount. This leads to an alternative expression

$$\int d\omega \frac{\rho(\omega)}{\omega - \Omega} \to \int_{-\infty}^{\infty} d\omega \frac{\rho(\omega)}{\omega - \Omega - i\epsilon}, \tag{5.41}$$

or

$$\frac{1}{\omega - \Omega} \to \frac{1}{\omega - \Omega - i\epsilon}, \tag{5.42}$$

or simply

$$\Omega \to \Omega + i\epsilon. \tag{5.43}$$

The connection (5.43) has the physical meaning of considering a force that has a time dependence of $\exp(-i\Omega t + \epsilon t)$, i.e., a force that grows with time at an infinitesimal rate. This means the driving force has not been in existence since $t = -\infty$, which has the same effect as introducing explicit initial conditions as far as removing the singularity is concerned.

Exercise 5.5 Establish the equivalence between Eq. (5.42) and Eq. (5.39) by explicitly showing that the real part of $(\omega - \Omega - i\epsilon)^{-1}$ gives P.V.$(\omega - \Omega)^{-1}$, and the imaginary part is equal to $\pi\delta(\omega - \Omega)$.

Exercise 5.6 In case one has to consider a driving force $Ae^{-i\Omega t}$ with a negative frequency $\Omega < 0$ and a spectrum that peaks around $\omega_x > 0$, the singularity will be located at $\omega = -\Omega = |\Omega|$. Follow the steps leading to Eq. (5.38) to show that

$$\langle x \rangle = \frac{A}{2\omega_x}\left[\cos \Omega t \ \text{P.V.}\int \frac{\rho(\omega)}{\omega + \Omega} - \pi\rho(|\Omega|)\sin \Omega t\right], \tag{5.44}$$

or

$$\int d\omega \frac{\rho(\omega)}{\omega + \Omega} \to \text{P.V.}\int d\omega \frac{\rho(\omega)}{\omega - |\Omega|} - i\pi\rho(|\Omega|). \tag{5.45}$$

The imaginary part has switched sign from Eq. (5.38). The contour C will now make an excursion above the pole at $\omega = -\Omega$ as shown in Figure 5.4(c), which means the connection (5.43) is maintained. Show that the $\sin \Omega t$ component gives rise to a $d\langle x \rangle/dt$ term which is in phase with the driving force, indicating the system is absorbing energy from the driving force.

It is now a matter of taste whether to regard our main conclusion (5.38) as a result of a simple derivation starting with Eq. (5.4) and then make an educated connection (5.40) or (5.43), or to regard it as a result of a detailed calculation which takes account of initial conditions.

We proceed in the remainder of this chapter to demonstrate Landau damping of collective instabilities in circular accelerators.

5.2 ONE-PARTICLE MODEL FOR BUNCHED BEAMS

Results obtained in the previous section, when applied to circular accelerators, lead to Landau damping of collective instabilities. To demonstrate this for a bunched beam, consider a one-particle model in which the bunched beam is a single macroparticle of charge Ne, as we did in Section 4.2, except

now the N individual particles have a spread in their natural frequencies. The fact that they form one macroparticle even though they have different frequencies is a result of the bunch executing a collective motion.

The driving force on the individual particles comes from the center-of-charge displacement of the beam as a whole, $\langle y \rangle$. Equation (4.24) is therefore slightly modified to give, for a single particle whose betatron frequency is ω,

$$y''(s) + \left(\frac{\omega}{c}\right)^2 y(s) = -\frac{Nr_0}{\gamma C} \sum_{k=1}^{\infty} \langle y \rangle (s - kC) W_1(-kC). \quad (5.46)$$

Consider the situation when the vertical betatron y-motion of the macroparticle is just at the edge of exponential growth due to a collective instability. We have

$$\langle y \rangle (s) = Be^{-i\Omega s/c}. \quad (5.47)$$

Because we are considering the case when the beam is at the edge of instability, we let Ω to carry an imaginary part $i\epsilon$, where ϵ is infinitesimally positive, as prescribed by Eq. (5.43).

It is not very interesting to search for damped, stable solutions. Instability occurs when there are antidamped solutions, irrespective of how many damped solutions there may be. Finding stable solutions does not assure beam stability, but finding one unstable solution reveals the beam to be unstable.

Substituting Eq. (5.47) into Eq. (5.46) gives

$$y''(s) + \left(\frac{\omega}{c}\right)^2 y(s) = -\frac{BNr_0}{\gamma C} \mathscr{W} e^{-i\Omega s/c}, \quad (5.48)$$

where we have defined a complex quantity

$$\mathscr{W} = \sum_{k=1}^{\infty} W_1(-kC) e^{i\omega_\beta k T_0}, \quad (5.49)$$

or in terms of impedance,

$$\mathscr{W} = -\frac{i}{T_0} \sum_{p=-\infty}^{\infty} Z_1^{\perp}(p\omega_0 + \omega_\beta). \quad (5.50)$$

In writing down Eqs. (5.49–5.50), we have used the notation $C/c = T_0 = 2\pi/\omega_0$. We have also assumed the mode frequency shift is small, so that $\Omega \approx \omega_\beta$, where ω_β is the center of the beam frequency spectrum. To assure

the validity of a one-particle model, the mode frequency shift must be much less than the synchrotron frequency ω_s.

Equation (5.48) says that the beam is driven by a force of the form $Ae^{-i\Omega s/c}$ as prescribed in the previous section. Equation (5.36) gives the response of the beam to the driving force, and it reads

$$\langle y \rangle = -\frac{BNr_0 \mathscr{W} c}{2\omega_\beta \gamma T_0} e^{-i\Omega s/c} \left[\text{P.V.} \int d\omega \, \frac{\rho(\omega)}{\omega - \Omega} + i\pi\rho(\Omega) \right]. \quad (5.51)$$

But we have already assumed that the collective beam motion is given by Eq. (5.47). This means the mode frequency Ω is not arbitrary. In order for the beam motion to be nontrivial,[10] Ω must satisfy a self-consistency condition, known as the *dispersion relation*,

$$1 = -\frac{Nr_0 \mathscr{W} c}{2\omega_\beta \gamma T_0} \left[\text{P.V.} \int d\omega \, \frac{\rho(\omega)}{\omega - \Omega} + i\pi\rho(\Omega) \right] \quad (5.52)$$

or, in terms of the function $f(u)$ and $g(u)$ defined in Eq. (5.27),

$$-\frac{Nr_0 \mathscr{W} c}{2\omega_\beta \gamma T_0 \, \Delta\omega} = \frac{1}{f(u) + ig(u)}. \quad (5.53)$$

Exercise 5.7 Find the dispersion relation for a system in which the driving force on individual particles comes from $\langle y \rangle$ according to

$$\ddot{y} + \omega^2 y = W_1 \langle y \rangle + \frac{W_2}{\omega_\beta} \frac{d\langle y \rangle}{dt}, \quad (5.54)$$

where ω_β is the center of the beam frequency spectrum. Compare with Eq. (5.53) to establish a connection between W_1, W_2, and the impedance. Note the sign of W_2 defines the stability of the beam in the absence of Landau damping.

Exercise 5.8 A feedback system can be modeled as

$$\ddot{y}(t) + \omega^2 y(t) = g\langle y \rangle (t - \tau), \quad (5.55)$$

where g is the gain of the feedback system. A resistive feedback system is given by $\tau = \pi/2\omega$. A reactive feedback system has $\tau = 0$ or π/ω. (a) Find the equivalent impedance of the feedback system (5.55). (b) Find the dispersion relation.

[10] A trivial solution means $B = 0$, i.e., the beam does not oscillate.

In Section 4.2, we obtained an expression (4.25) for the complex mode frequency shift in the *absence* of Landau damping, which, denoted as ξ_1, is given by

$$\xi_1 \equiv (\Omega - \omega_\beta)_{\text{no Landau damping}} = \frac{Nr_0 c\mathscr{W}}{2\omega_\beta \gamma T_0}. \tag{5.56}$$

Equation (5.56) contains essentially the beam intensity, multiplied by the impedance, divided by the focusing strength and the particle rigidity. Combining Eqs. (5.53) and (5.56) leads to the dispersion relation

$$-\frac{\xi_1}{\Delta\omega} = \frac{1}{f(u) + ig(u)}. \tag{5.57}$$

The left hand side of Eq. (5.57) contains the information about the beam intensity and the impedance. The right hand side contains information about the beam frequency spectrum. Calculation of the left hand side is straightforward. For a given impedance, one only needs to calculate the complex mode frequency shift ξ_1 in the absence of Landau damping as was done in Section 4.2. Without Landau damping, the condition for the beam to be stable is simply Im $\xi_1 < 0$.

Once its left hand side is obtained, Eq. (5.57) can in principle be used to determine the mode frequency Ω in the presence of Landau damping when the beam is at the edge of instability. However, the exact value of Ω is not a very useful piece of information. The more useful question to ask is under what conditions the beam becomes unstable regardless of the exact value of Ω under these conditions, and Eq. (5.57) can be used in a reversed manner to address this question. To do so, one considers the real parameter $u = (\omega_\beta - \Omega)/\Delta\omega$ and observes the lotus traced out in the complex $\mathscr{D}_1$-plane as u is scanned from ∞ to $-\infty$, where $\mathscr{D}_1$ is the right hand side of Eq. (5.57),

$$\mathscr{D}_1 = \frac{1}{f(u) + ig(u)}. \tag{5.58}$$

This lotus defines a *stability boundary diagram*. The left hand side of Eq. (5.57), a complex quantity, is then plotted in the complex $\mathscr{D}_1$-plane as a single point. If this point lies on the lotus, it means the solution of Ω for Eq. (5.57) is real, and this ξ_1 value is such that the beam is just at the edge of instability. If it lies on the inside of the lotus (the side which contains the origin of the $\mathscr{D}_1$-plane), the beam is stable. If it lies on the outside of the lotus, the beam is unstable.

Figure 5.5 depicts the stability boundary diagrams for various beam frequency spectra. The beam is unstable if $-\xi_1/\Delta\omega$ lies in the shaded regions. In case of the δ-function spectrum, which is the case without Landau

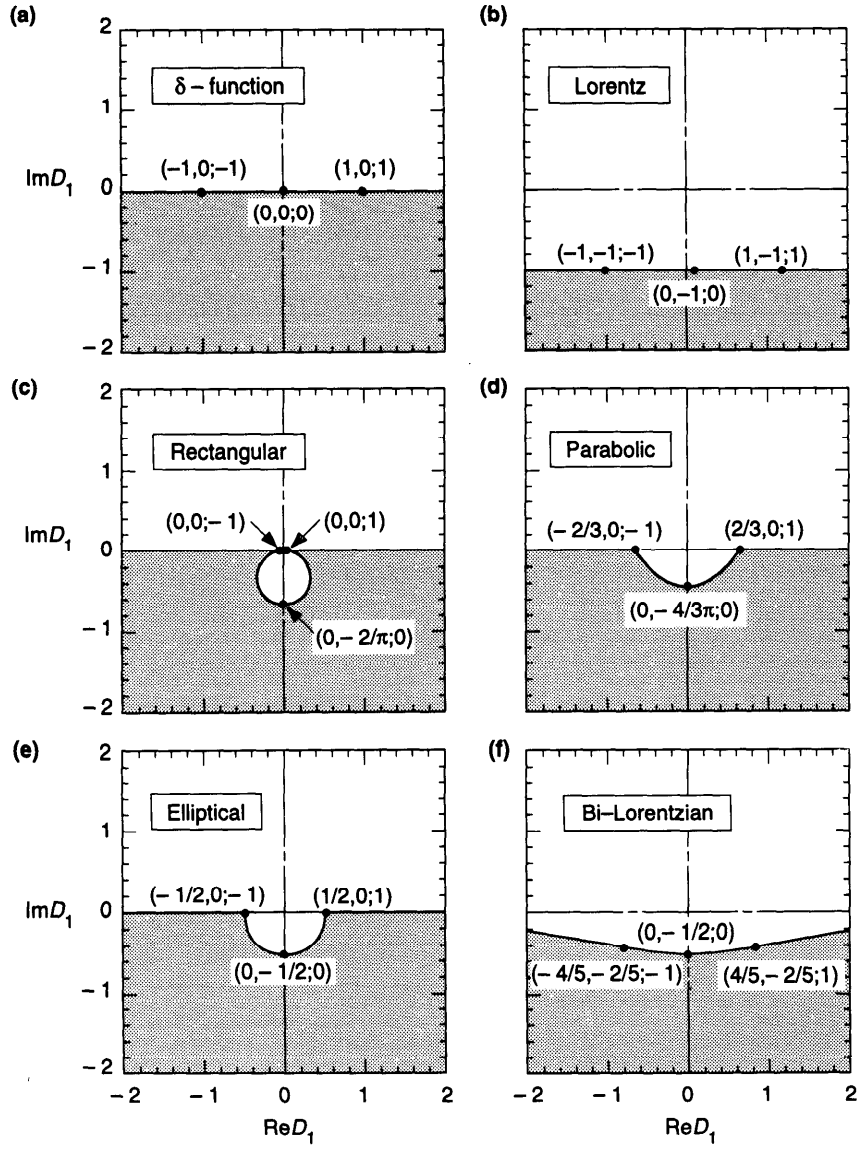

Figure 5.5. The stability boundary diagrams for various spectra in the complex $\mathscr{D}_1$-plane. (a) δ-function spectrum, no Landau damping. (b) Lorentz spectrum. (c) Rectangular spectrum. (d) Parabolic spectrum. (e) Elliptical spectrum. (f) Bi-Lorentzian spectrum. (g) Gaussian spectrum. The boundary for (b) is $\operatorname{Im} \mathscr{D}_1 = -1$. The boundary for (c) contains a displaced circle of radius $1 / \pi$. The boundary for (e) contains a semicircle of radius $\frac{1}{2}$. If the complex quantity $-\xi_1 / \Delta\omega$ lies in a shaded region, the beam is unstable. Three values are assigned to a chosen set of points on the boundaries; they refer to $(\operatorname{Re} \mathscr{D}_1, \operatorname{Im} \mathscr{D}_1; v)$. The value of v can be used to obtain the mode frequency Ω. Case (h) is the simplified criterion (5.62) assuming $\Delta\omega_{1/2} = \sqrt{3}\, \Delta\omega / 2$.

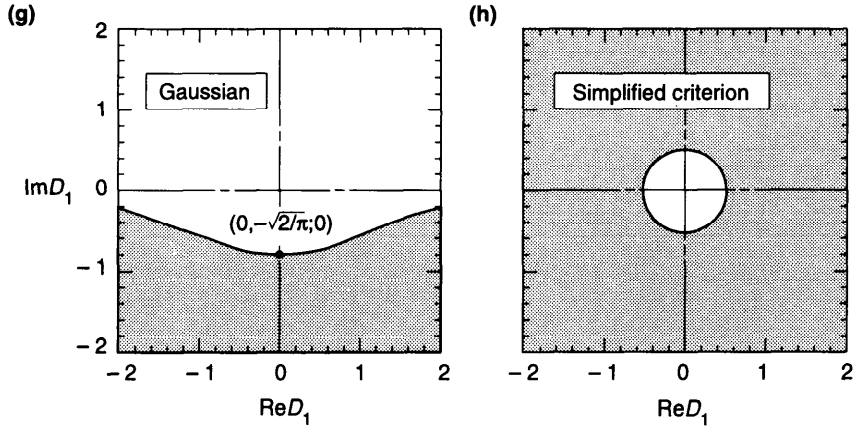

Figure 5.5. *(Continued)*

damping, the stability region reduces to the condition $\text{Im}\,\xi_1 < 0$. All the other cases have larger regions of stability. A finite spread in the natural frequencies thus helps stabilize the beam against collective instabilities, demonstrating the Landau damping mechanism.

Exercise 5.9 It will be instructive to go through the details of how a stability diagram is established.

(a) Either derive one of the examples in the text, or work out a new example such as $\rho(v) \propto (1 - v^2)^2 H(1 - |v|)$, where v and $H(x)$ are defined in Eq. (5.30).

(b) All the spectra so far are symmetric with respect to the spectral center (i.e., even functions of v). Study a case with asymmetric spectrum such as $\rho(v) \propto (1 + v)H(1 - |v|)$ and observe the effect of asymmetry on the stability boundary diagram.

The dispersion relation is particularly simple for the Lorentz spectrum. From Eqs. (5.57) and (5.29), we find

$$\Omega = \omega_\beta + \xi_1 - i\,\Delta\omega. \tag{5.59}$$

The stability condition $\text{Im}\,\Omega < 0$ therefore becomes

$$\text{Im}\,\xi_1 < \Delta\omega, \tag{5.60}$$

which is what appears in the stability diagram, Figure 5.5(b).

The fact that the stable region is always enlarged by the frequency spread can be traced back to the fact that $g(u)$ is always positive. As pointed out in

Section 5.1, this in turn comes from the fact that the beam continues to absorb energy from the driving force without having to let $\langle y \rangle$ grow.

For a given spectral shape, the tolerable ξ_1 is proportional to $\Delta\omega$. The larger the frequency spread, the stronger the Landau damping. Also, for a given $\Delta\omega$, the effectiveness of Landau damping is different for different spectral shapes. Among the spectra shown in Figure 5.5, the Lorentz spectrum, having a long distribution tail, is the most effective; spectra with cutoff tails tend to be less effective, while the δ-function spectrum, of course, is not effective at all. Sharp edges in a spectral shape are reflected in sharp edges in the stability boundary.

To facilitate a more quantitative comparison among different spectra, it may be useful to relate $\Delta\omega$ to the half width at half maximum, $\Delta\omega_{1/2}$, of the various spectra. This is given by

$$\Delta\omega_{1/2} = \Delta\omega \times \begin{cases} 1, & \text{Lorentz,} \\ 1, & \text{rectangular,} \\ \dfrac{1}{\sqrt{2}}, & \text{parabolic,} \\ \dfrac{\sqrt{3}}{2}, & \text{elliptical,} \\ \sqrt{\sqrt{2}-1}, & \text{bi-Lorentzian,} \\ \sqrt{2\ln 2}, & \text{Gaussian.} \end{cases} \tag{5.61}$$

A fair comparison of two spectral shapes is made when they have the same $\Delta\omega_{1/2}$, not the same $\Delta\omega$.

For practical accelerator operations, there may be approximate information on the value of $\Delta\omega_{1/2}$, but not enough detailed information on the shape of the frequency spectrum; or there may be only a need of a rough estimate of whether the collective instability is Landau damped. For those purposes, we introduce a simplified stability criterion as[11]

$$|\xi_1| = \frac{Nr_0 c}{2\omega_\beta \gamma T_0^2} \left| \sum_{p=-\infty}^{\infty} Z_1^{\perp}(p\omega_0 + \omega_\beta) \right| < \frac{1}{\sqrt{3}} \Delta\omega_{1/2}, \tag{5.62}$$

where the factor $1/\sqrt{3}$ is chosen so that it coincides with the semicircular portion of the boundary for the elliptical spectrum. Figure 5.5(h) shows the stability region corresponding to Eq. (5.62). It is to be compared with the stability boundaries for the more realistic spectra shown in Figure 5.5(b) to (g).

[11] This is done in the same spirit as Eq. (5.130) to be discussed later.

Although the exact stability condition depends on details of the spectrum, Eq. (5.62) is an important qualitative result. It says that if the mode frequency shift or growth rate, calculated without Landau damping, is comparable to or larger than the frequency spread of the beam, Landau damping most likely will not rescue the beam from instability.

Consider the numerical example following Eq. (4.32) for the case of transverse rigid-beam instability due to the higher order rf cavity modes. The growth time without Landau damping was estimated to be 5 ms. To Landau damp this instability, the required frequency spread is roughly $\Delta\omega_\beta \approx \sqrt{3}/(5\text{ ms})$. This gives a required betatron tune spread of $\Delta\nu_\beta = 4 \times 10^{-5}$, which is rater small and is likely to be readily available. It is not too difficult to Landau damp this instability.

Exercise 5.10 Right on the stability boundary, the growth rate $\operatorname{Im}\Omega = 0$, but the mode frequency shift $\Delta\Omega = \operatorname{Re}\Omega - \omega_\beta \neq 0$. Show that

$$\frac{\Delta\Omega}{\Delta\omega} = \begin{cases} \dfrac{\operatorname{Re}\xi_1}{\Delta\omega}, & \text{Lorentz,} \\ \tanh\left(\dfrac{\Delta\omega}{|\xi_1|^2}\operatorname{Re}\xi_1\right), & \text{rectangular,} \\ \operatorname{sgn}(\operatorname{Re}\xi_1)\sqrt{1 - \dfrac{4}{3\pi}\dfrac{\Delta\omega}{|\xi_1|^2}\operatorname{Im}\xi_1}, & \text{parabolic,} \\ \dfrac{\Delta\omega}{2|\xi_1|^2}\operatorname{Re}\xi_1, & \text{elliptical,} \\ \operatorname{sgn}(\operatorname{Re}\xi_1)\sqrt{\sqrt{\dfrac{2|\xi_1|^2}{\Delta\omega\operatorname{Im}\xi_1}} - 1}, & \text{bi-Lorentzian,} \\ \operatorname{sgn}(\operatorname{Re}\xi_1)\sqrt{-2\ln\left(\sqrt{\dfrac{2}{\pi}}\dfrac{\Delta\omega}{|\xi_1|^2}\operatorname{Im}\xi_1\right)}, & \text{Gaussian.} \end{cases} \tag{5.63}$$

Observe that Landau damping does not affect the mode frequency shift for the Lorentz spectrum, as evidence also by the real part of Eq. (5.59).

A similar analysis can also be performed for the longitudinal Robinson instability using a one-particle model. In pace of Eqs. (4.4–4.5), we have

$$z''(s) + \left(\frac{\omega_s}{c}\right)^2 z(s) = \frac{Nr_0\eta}{\gamma C}\sum_{k=1}^{\infty}[\langle z\rangle(s) - \langle z\rangle(s - kC)]W_0''(-kC)$$
$$= \frac{Nr_0\eta}{\gamma C}Be^{-i\Omega s/c}\mathscr{W}, \tag{5.64}$$

where we have introduced

$$\langle z\rangle(s) = Be^{-i\Omega s/c} \tag{5.65}$$

and

$$\begin{aligned}\mathscr{W} &= \sum_{k=1}^{\infty} (1 - e^{i\omega_s kT_0}) W_0''(-kC) \\ &= \frac{i}{C} \sum_{p=-\infty}^{\infty} \left[p\omega_0 Z_0^{\parallel}(p\omega_0) - (p\omega_0 + \omega_s) Z_0^{\parallel}(p\omega_0 + \omega_s) \right].\end{aligned} \tag{5.66}$$

Self-consistency then gives rise to a dispersion relation

$$\frac{Nr_0\eta\mathscr{W}c^2}{2\omega_s\gamma C\Delta\omega} = \frac{1}{f(u) + ig(u)}, \tag{5.67}$$

which can be written in a form identical to Eq. (5.57), except that the complex mode frequency shift in the absence of Landau damping is now given by Eqs. (4.9–4.10), i.e.,

$$\xi_1 = -\frac{Nr_0\eta\mathscr{W}c^2}{2\omega_s\gamma C}. \tag{5.68}$$

The analysis for the transverse case therefore carries over straightforwardly to the longitudinal case. In particular, the simplified stability criterion (5.62) reads, in the longitudinal case,

$$\begin{aligned}|\xi_1| &= \frac{Nr_0\eta c^2}{2\omega_s\gamma C^2} \left| \sum_{p=-\infty}^{\infty} \left[p\omega_0 Z_0^{\parallel}(p\omega_0) - (p\omega_0 + \omega_s) Z_0^{\parallel}(p\omega_0 + \omega_s) \right] \right| \\ &< \frac{1}{\sqrt{3}} \Delta\omega_{1/2},\end{aligned} \tag{5.69}$$

where $\Delta\omega_{1/2}$ refers to the spread of synchrotron frequency of the beam particles.

The conclusion that the longitudinal Landau damping behaves analogously to the transverse case, however, is valid only for *bunched* beams for which $\omega_s \neq 0$, and under the assumption that the mode frequency shift is smaller than ω_s. In case of unbunched beams, $\omega_s = 0$, the longitudinal analysis gives results very different from its transverse counterpart. This point will be explained in more detail in Section 5.4.

Taking the numerical example following Eqs. (4.21–4.22), but assuming the rf frequency is tuned to the unstable side, the Robinson instability growth time is 1.2 ms. To Landau damp this instability requires a synchrotron frequency spread of $\Delta\omega_s \approx \sqrt{3}/(1.2\text{ ms})$, which corresponds to a relative spread of $\Delta\omega_s/\omega_s \approx 1.5\%$.

Although the above analyses assume a one-particle beam, one may venture to apply the result to a two-particle instability. For example, one may conclude that, to substantially raise the strong head-tail instability threshold by Landau damping, it is necessary to have a betatron frequency spread that is comparable to the synchrotron frequency. This is not easy to do in practice, and the conclusion discourages an attempt to Landau damp the strong head-tail instability.

5.3 TRANSVERSE INSTABILITY OF UNBUNCHED BEAMS

The previous section addressed the Landau damping of bunched beams. In this and the next section, we will address the Landau damping of unbunched beams. Consider an unbunched beam circulating in an accelerator as sketched in Figure 5.6(a). Let the beam have a rigid uniform round cross section with radius a. Consider an infinitesimal transverse displacement of the beam that behaves in time as $\exp(-i\Omega t)$ and in angular coordinate as $\exp(ins/R)$, where the integer n is a mode index and $2\pi R$ is the accelerator circumference. Observed at a fixed location s, the beam oscillates with a frequency Ω. Observed at a fixed time t as a snapshot, the beam makes n oscillations around the accelerator circumference. As will be analyzed in this section, this perturbation induces a perturbing electromagnetic wake field; the field acts back on the beam, leading to a reduction of an enhancement of the initial beam perturbation, and the beam is stable or unstable accordingly.

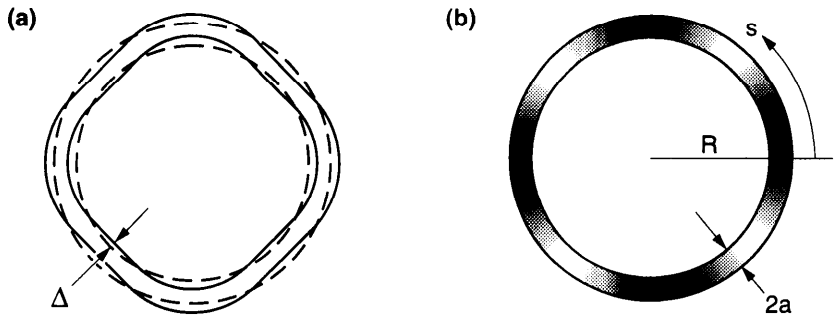

Figure 5.6. Snapshots of an unbunched beam executing a collective mode with mode index $n = 4$. (a) Transverse mode; dashed curves indicate the unperturbed beam. (b) Longitudinal mode; heavy and light shadings indicate the variation of the particle density distribution.

Now consider the beam in a vacuum chamber with a wake function $W_1(z)$ and a corresponding impedance $Z_1^{\perp}(\omega)$. The perturbing part of the oscillating beam has a ring-beam distribution

$$\rho = \frac{D}{\pi a^2}\delta(r - a)\cos\theta, \tag{5.70}$$

where D is the dipole moment per unit length; it is related to the maximum beam displacement Δ, shown in Figure 5.6(a), according to

$$D(s,t) = \frac{Ne\Delta}{2\pi R}\exp\left(in\frac{s}{R} - i\Omega t\right), \tag{5.71}$$

where N is the total number of particles in the beam.

The suggested dependence on t and s in Eq. (5.71) is an ansatz. It remains to be shown that this ansatz allows a self-consistent solution of the problem. Once established, Eq. (5.71) is remarkable in that it holds for an arbitrary impedance. An indication of its validity can be obtained by reviewing the multibunch analysis of Section 4.6. In particular, it is consistent with Eq. (4.127) on considering the limit $M \to \infty$ and identifying $\mu \to n$ and $n/M \to s/2\pi R$. Equation (4.127) is valid independent of the impedance, and so is Eq. (5.71).

The transverse force F_y on a test charge, at location s and time t, is determined by the dipole moment of the ring beam at the same location s as it past by at an earlier time t'. By superposition, the wake force is obtained by integrating the wake field over t'.[12] This gives

$$F_y(s,t) = -\frac{e}{2\pi R}\int_{-\infty}^{t} c\,dt'\,W_1(ct' - ct)\,D(s,t'). \tag{5.72}$$

Substituting Eq. (5.71) for D and expressing the result in terms of the impedance $Z_1^{\perp}$ yields

$$F_y(s,t) = ecD(s,t)i\frac{Z_1^{\perp}(\Omega)}{2\pi R}, \tag{5.73}$$

which is to be recognized as a rederivation of Eq. (2.70), since cD is just the dipole moment current. Note that the impedance is evaluated at frequency Ω. This is a consequence of the fact that it is responding to the beam signal observed at a fixed location. In particular, the impedance does not have any information on, and therefore does not respond to, the mode index n.

[12]Strictly speaking, a $\cos\theta$ ring beam generates a transverse wake force in the x-direction, but we will call it the y-direction.

Consider now a specific particle in the beam that passes position S at time 0. It is located at position $s = S + ct$ at time t, and experiences a transverse force $F_y(S + ct, t)$ at any time t. Modeling the impedance as evenly distributed around the accelerator circumference, the equation of motion of the particle is

$$\ddot{y} + \omega_\beta^2 y = \frac{F_y(S + ct, t)}{m_0 \gamma}$$
$$= \frac{N r_0 c^2}{\gamma T_0} i \frac{Z_1^\perp(\Omega)}{2\pi R} \Delta \exp\left[in \frac{S}{R} - i(\Omega - n\omega_0)t \right], \quad (5.74)$$

where we have defined the revolution frequency $\omega_0 = c/R = 2\pi/T_0$, and ω_β is the betatron frequency of the particle under consideration.

Although the impedance responds only to Ω, the moving particle sees a force with a driving frequency $\omega_d = \Omega - n\omega_0$. The solution of Eq. (5.74) with $s = S + ct$ for the particle under consideration, is

$$y(s, t) = \frac{N r_0 c^2}{\gamma T_0} i \frac{Z_1^\perp(\Omega)}{2\pi R} \frac{\Delta \exp[in(s/R) - i\Omega t]}{\omega_\beta^2 - (\Omega - n\omega_0)^2}. \quad (5.75)$$

Self-consistency requires that the beam at (s, t) have a displacement of $y(s, t) = \Delta \exp[in(s/R) - i\Omega t]$. This yields the dispersion relation

$$1 = \frac{N r_0 c^2}{\gamma T_0} i \frac{Z_1^\perp(\Omega)}{2\pi R} \frac{1}{\omega_\beta^2 - (\Omega - n\omega_0)^2}. \quad (5.76)$$

The mode frequency Ω is to be found from Eq. (5.76). The fact that the s and t dependences nicely cancel in obtaining Eq. (5.76) is a consequence of the correct choice of the ansatz (5.71).

There are two solutions of Eq. (5.76) for Ω, one close to $n\omega_0 - \omega_\beta$, the other close to $n\omega_0 + \omega_\beta$. In the following, we consider the solution close to $n\omega_0 + \omega_\beta$. The other solution would lead to an identical instability criterion. The solution to Eq. (5.76) can be written as

$$\Omega = n\omega_0 + \omega_\beta + \xi_1, \quad (5.77)$$

where

$$\xi_1 = -\frac{N r_0 c^2}{2\omega_\beta \gamma T_0} i \frac{Z_1^\perp(\Omega)}{2\pi R} \quad (5.78)$$

is the complex mode frequency shift in the absence of Landau damping.

In the unperturbd case, the mode frequency is given by $n\omega_0 + \omega_\beta$, and the beam displacement behaves according to $\exp[in(s - ct)/R - i\omega_\beta t]$. The beam displacement pattern rotates around the accelerator with an angular frequency $\omega_0 + (\omega_\beta/n)$. Waves with $n > 0$ are called *fast waves*; those with $n < 0$ are *slow waves*. The beam displacement observed at a fixed location s oscillates with frequency $n\omega_0 + \omega_\beta$. The displacement observed relative to the moving beam oscillates at frequency ω_β, as it should.

The quantity ξ_1 in Eq. (5.78) involves the impedance evaluated at frequency Ω, but to first order in beam intensity, it can be evaluated at the unperturbed frequency $n\omega_0 + \omega_\beta$. The instability growth rate is given by the imaginary part of Ω. According to Eq. (5.77), we have

$$\tau^{-1} = \operatorname{Im} \xi_1 = -\frac{Nr_0c^2}{2\omega_\beta\gamma T_0} \frac{\operatorname{Re} Z_1^\perp(n\omega_0 + \omega_\beta)}{2\pi R}. \tag{5.79}$$

Similarly, the mode frequency shift is given by

$$\Delta\Omega = \operatorname{Re} \xi_1 = \frac{Nr_0c^2}{2\omega_\beta\gamma T_0} \frac{\operatorname{Im} Z_1^\perp(n\omega_0 + \omega_\beta)}{2\pi R}. \tag{5.80}$$

Only the real part of the impedance appears in the growth rate, and only the imaginary part appears in the mode frequency shift.

It is interesting to note that Eq. (5.79) gives the same growth rate (4.28) obtained for a one-particle model of bunched beams if we add a summation over n in the expression. A similar summation of Eq. (5.80) over n gives Eq. (4.27) if the shift is interpreted as a shift in ω_β.

As an example, the resistive-wall impedance, Eq. (2.76), gives

$$\xi_1 = -\frac{Nr_0c^2}{\omega_\beta\gamma T_0 b^3} \frac{1}{\sqrt{2\pi\sigma|n\omega_0 + \omega_\beta|}} \left[1 + i \operatorname{sgn}(n\omega_0 + \omega_\beta)\right]. \tag{5.81}$$

The dominating mode occurs when n is equal to the nearest integer to $-\omega_\beta/\omega_0$. Let the betatron tune $\nu_\beta = \omega_\beta/\omega_0$ be written as $N_\beta + \Delta_\beta$, where Δ_β is the fractional part of ν_β, which can be positive or negative depending on whether ν_β is above or below its nearest integer N_β. The dominating mode is then a slow wave with $n = -N_\beta$. The instability growth rate and mode frequency shift are given by the imaginary and real parts of

$$\Omega - \Delta_\beta\omega_0 = -\frac{Nr_0c^2}{\omega_\beta\gamma T_0 b^3} \frac{1 + i \operatorname{sgn}(\Delta_\beta)}{\sqrt{2\pi\sigma\omega_0|\Delta_\beta|}}. \tag{5.82}$$

The growth rate agrees with Eqs. (4.33–4.34) if we keep the leading term $p = 0$ in the function $f(\Delta_\beta)$. The beam is stable if the tune is above an integer and unstable below an integer. Note that the frequency of this dominating mode is approximately $\Delta_\beta \omega_0$, which is usually much less than the betatron frequency ω_β. In obtaining Eq. (5.82) we have assumed the resistive wall is much thicker than the skin depth evaluated at frequency $\Delta_\beta \omega_0$.

So far we have not included Landau damping. In case not all particles have the same natural betatron frequency, and the beam has a spectrum $\rho(\omega)$ [normalized by $\int d\omega\, \rho(\omega) = 1$], the dispersion relation (5.76) reads

$$1 = \frac{Nr_0c^2}{\gamma T_0} i \frac{Z_1^\perp(\Omega)}{2\pi R} \int d\omega \frac{\rho(\omega)}{\omega^2 - (\Omega - n\omega_0)^2}. \tag{5.83}$$

There are two poles located at $\omega = \pm(n\omega_0 - \Omega)$. For a given mode n, usually only one of the pole terms dominates. Consider the $\omega = -n\omega_0 + \Omega$ pole. The dispersion relation can be written as

$$1 = -\xi_1 \int d\omega \frac{\rho(\omega)}{\omega - \omega_d}, \tag{5.84}$$

where $\omega_d = \Omega - n\omega_0$ is the frequency of the driving wake force and ξ_1 is given by Eq. (5.78).

Equation (5.84) assumes the dominance of a single pole, which follows if the mode frequency shift and growth rate are small compared with the natural focusing frequency ω_β (modulus ω_0) > 0. A similar assumption cannot be made in the case of longitudinal instability of unbunched beams because there is no natural focusing. As we will see in Section 5.4, this leads to a qualitatively different behavior of the longitudinal instability of unbunched beams.

To determine the instability threshold conditions, we have seen that Eq. (5.84) is to be interpreted as [see Eqs. (5.38) and (5.45)]

$$1 = -\xi_1 \left[\text{P.V.} \int d\omega \frac{\rho(\omega)}{\omega - |\omega_d|} + i\pi \operatorname{sgn}(\omega_d) \rho(|\omega_d|) \right] \tag{5.85}$$

or, using Eq. (5.27),

$$1 = -\frac{\xi_1}{\Delta\omega} [f(u) + ig(u)]. \tag{5.86}$$

The spectrum width $\Delta\omega$ and the functions $f(u)$ and $g(u)$ in Eq. (5.86) are as defined in the previous section, but ξ_1 is to be inserted from Eq. (5.78), and $u = (\omega_\beta - |\omega_d|)/\Delta\omega$. We have used in Eq. (5.86) the fact that $\omega_d > 0$ for the pole chosen because $\omega_d = \Omega - n\omega_0 \approx \omega_\beta > 0$. Had we chosen the other

pole with $\omega_d \approx -\omega_\beta$, we have to take the sign properly according to Eq. (5.85).

For a given spectrum, Eq. (5.86) gives the stability threshold condition. Beam stability is determined by whether the quantity $-\xi_1/\Delta\omega$ lies in the stable region in the complex $\mathscr{D}_1 = (f + ig)^{-1}$ plane, as shown in Figure 5.5. When unstable, the beam is said to have a *transverse microwave instability*, since the frequency $n\omega_0 + \omega_\beta$ of the beam signal observed by a pickup electrode is often in the microwave range.

The transverse instabilities of unbunched beams in the presence of Landau damping therefore follow closely those of the bunched beams. For example, a Lorentz spectrum gives the complex mode frequency

$$\Omega = n\omega_0 + \omega_\beta + \xi_1 - i\,\Delta\omega. \tag{5.87}$$

The beam stability condition is then

$$\text{Im}\,\xi_1 = -\frac{Nr_0c^2}{2\omega_\beta\gamma T_0}\frac{\text{Re}\,Z_1^\perp(n\omega_0 + \omega_\beta)}{2\pi R} < \Delta\omega. \tag{5.88}$$

One concludes from Eq. (5.88) the expected result that the frequency spread helps stabilize the beam.

The condition (5.88) is always satisfied if $\text{Re}\,Z_1^\perp(n\omega_0 + \omega_\beta) > 0$. It follows from Eq. (2.106) that fast waves are always stable. It is the stability of the slow waves that requires Landau damping.

In the case of a resistive wall, Eq. (5.88) gives the stability condition, for a beam with Lorentz spectrum,

$$-\frac{Nr_0c^2}{\omega_\beta\gamma T_0 b^3}\frac{\text{sgn}(\Delta_\beta)}{\sqrt{2\pi\sigma\omega_0|\Delta_\beta|}} < \Delta\omega, \tag{5.89}$$

where the left hand side is the growth rate without Landau damping and is given by the imaginary part of Eq. (5.82). For the beam to be stable against resistive-wall instability, we must choose the betatron tune to be either above an integer, i.e., $\Delta_\beta > 0$, or below an integer with

$$\Delta_\beta < -\left(\frac{Nr_0c^2}{\omega_\beta\gamma T_0 b^3\,\Delta\omega}\right)^2\frac{1}{2\pi\sigma\omega_0}. \tag{5.90}$$

Continuing the numerical example following Eqs. (4.34–4.35), we find the beam is unstable only in a very small tune region $0 > \Delta_\beta > -0.00013$ if there is a small betatron tune spread of $\Delta\omega/\omega_\beta = 10^{-6}$. Resistive-wall instability therefore does not noticeably affect the choice of betatron tunes in this example.

In case the detailed spectral distribution is not available, one could apply the simplified criterion (5.62), which now reads

$$|\xi_1| = \frac{Nr_0 c}{2\omega_\beta \gamma T_0^2} \left| Z_1^\perp (n\omega_0 + \omega_\beta) \right| < \frac{1}{\sqrt{3}} \Delta\omega_{1/2}. \tag{5.91}$$

It is interesting to note that Eq. (5.91) for the transverse stability of an unbunched beam gives, up to a numerical factor of the order of unity, the stability condition (4.46) for a bunched beam against the strong head-tail instability when one makes the replacement $\Delta\omega_{1/2} \to \omega_s$, identifies $|iZ_1^\perp/T_0|$ with W_0, and lets N be the number of particles in the bunch. This again supports the observation that synchrotron oscillation has a stabilizing effect against collective instabilities, and ω_s plays for bunched beams a role similar to the one the frequency spread $\Delta\omega_{1/2}$ plays for unbunched beams.

Landau damping results from a finite $\Delta\omega_{1/2}$, which is a spread of $n\omega_0 + \omega_\beta$. One source of this spread is an energy spread of the particles in the beam, which in fact gives two contributions: one due to the dependence of ω_β on δ through the chromaticity ξ, and the other due to a dependence of the revolution frequency ω_0 on δ through the slippage factor η. This leads to

$$\Delta\omega_{1/2} = | - n\omega_0 \eta + \xi\omega_\beta | \, \Delta\delta_{1/2}. \tag{5.92}$$

Inserting Eq. (5.92) into Eq. (5.91) gives a stability condition

$$\left| Z_1^\perp (n\omega_0 + \omega_\beta) \right| < Z_0 \frac{2\pi R\gamma | - n\eta + \xi\nu_\beta |}{\sqrt{3}\, Nr_0 \beta_Z} \Delta\delta_{1/2}, \tag{5.93}$$

where $Z_0 = 4\pi/c = 377\ \Omega$, and we have written ω_β/ω_0 as ν_β, the betatron tune, and c/ω_β as β_Z, the β-function at the location of the impedance.

In case $\xi = 0$, Landau damping comes from a spread in the revolution frequency due to energy spread. In case $\eta = 0$ (the beam is operated at transition), Landau damping comes from the chromaticity effect. For the particular mode which has $-n\eta + \xi\nu_\beta \approx 0$, Landau damping has to be provided by nonchromatic sources such as a spread in ω_β introduced by octupole magnets. To avoid this requirement, it would be desirable to arrange the parameters so that the condition $-n\eta + \xi\nu_\beta = 0$ occurs in the fast wave regime, where, as mentioned before, the mode is naturally damped.[13] This means $n > 0$, and ξ must have the same sign as η. In other words, it would be desirable to have $\xi > 0$ above transition and $\xi < 0$ below transition. This criterion is the same as that for a bunched beam against the

[13] J. Gareyte, *Frontiers of Particle Beams: Intensity Limitations*, Hilton Head Island, Lectures in Phys. **400**, Spring-Verlag, 1990, p. 14.

head-tail instability. There will be more discussion of this point when we come to Eqs. (6.264–6.265). Below we consider the case $\xi = 0$.

The stability criterion (5.93) has a few useful variations which are given below.

(i) For a broad band impedance, one may take $n\omega_0 + \omega_\beta$ to be approximately given by a certain cutoff frequency ω_c (most likely, $\omega_c \approx c/b$, where b is the vacuum chamber pipe radius), and $n \approx \omega_c/\omega_0$. Equation (5.93) becomes

$$|Z_1^\perp(\omega_c)| < Z_0 \frac{2\pi R\gamma|\eta|\omega_c}{\sqrt{3}\, N r_0 \beta_Z \omega_0} \Delta\delta_{1/2}. \tag{5.94}$$

(ii) In case the instability growth rate is much faster than the synchrotron oscillation, one may obtain a stability criterion against transverse microwave instability for *bunched* beams.[14] This is done by simply replacing the unperturbed beam density of an unbunched beam by the peak beam density of a bunched beam because, in the fast growing regime, the instability occurs locally and it would be the peak beam density that determines the instability threshold. For an elliptical distribution, this means replacing $N/2\pi R$ by $\sqrt{3}\, N_B/\pi\, \Delta z_{1/2}$, where N_B is the number of particles in the beam bunch. One then obtains from Eq. (5.94),

$$|Z_1^\perp(\omega_c)| < Z_0 \frac{\pi\gamma|\eta|\omega_c}{3N_B r_0 \beta_Z \omega_0} \Delta\delta_{1/2}\, \Delta z_{1/2}. \tag{5.95}$$

Equation (5.95) can also take another form if we note that

$$\Delta\delta_{1/2} = \frac{\omega_s}{|\eta|c} \Delta z_{1/2}. \tag{5.96}$$

We then have

$$|Z_1^\perp(\omega_c)| < Z_0 \frac{\pi\gamma\omega_s\omega_c}{3N_B r_0 \beta_Z \omega_0 c} \Delta z_{1/2}^2. \tag{5.97}$$

(iii) For a long bunch, the cutoff is not due to the pipe radius b, but due to the bunch length $\Delta z_{1/2}$. The cutoff frequency is given by $\omega_c \approx c/\Delta z_{1/2}$. Equation (5.97) then reads

$$|Z_1^\perp| < Z_0 \frac{\pi\gamma\omega_s}{3N_\beta r_0 \beta_Z \omega_0} \Delta z_{1/2}. \tag{5.98}$$

[14] D. Boussard, CERN Lab II/RF/Int 75-2 (1975); R. D. Ruth and J. M. Wang, IEEE Trans. Nucl. Sci. **NS-28**, 2405 (1981). This is called the *Boussard criterion* in the literature.

It may be instructive to consider another view of Eq. (5.98) as follows. Consider a bunch executing a transverse betatron oscillation. Its transverse wake force perturbs the betatron focusing force that is equivalent to a quadrupole magnet with field gradient $K \approx e\hat{I}Z_1^{\perp}/2\pi RE$, where E is the particle energy and $\hat{I} \approx N_B ec/\Delta z_{1/2}$ is the peak beam current. Beam stability requires that the wake induced betatron tune shift to be less than the synchrotron tune ω_s/ω_0 (recall the mechanism of the strong head-tail effect), i.e.,

$$\left|\frac{1}{2}\beta_Z RK\right| < \frac{\omega_s}{\omega_0}. \tag{5.99}$$

Equation (5.98) then follows.

Equations (5.94–5.98) apply to the transverse microwave instability. It is derived for unbunched beams, but has been extended heuristically to bunched beams. What Eq. (5.99) demonstrates is that the mechanism of the microwave instability is basically the same as that of the strong head-tail instability, which is also called the mode coupling instability in the literature.

We now have two simplified stability criteria for the transverse instability of bunched beams. One of them is Eq. (5.98), which applies when the instability growth rate $\gg \omega_s$. The other is Eq. (5.62), which holds when the growth rate $\ll \omega_s$. On the other hand, observing $\Sigma_p |Z_1^{\perp}(p\omega_0 + \omega_\beta)| \approx (\omega_c/\omega_0)|Z_1^{\perp}(\omega_c)|$ with $\omega_c \approx c/\Delta z_{1/2}$, it is interesting to note that Eq. (5.62) becomes Eq. (5.98)—up to a numerical factor of the order of unity—if we replace the betatron frequency spread $\Delta\omega_{1/2}$ by ω_s.

(iv) It is sometimes useful to relate the transverse impedance $|Z_1^{\perp}|$ to the longitudinal impedance $|Z_0^{\parallel}/n|$ by the approximate relation (2.108) even though the case being considered is for the transverse instability. For an unbunched beam, Eq. (5.94) gives

$$\left|\frac{Z_0^{\parallel}}{n}\right| < Z_0 \frac{\pi R\gamma|\eta|b}{\sqrt{3}\, Nr_0\beta_Z}\, \Delta\delta_{1/2}, \tag{5.100}$$

where we have assumed $\omega_c \approx c/b$. For a bunched beam, if the bunch length $\Delta z_{1/2}$ is shorter than the pipe radius b, Eqs. (5.95) and (5.97) give

$$\begin{aligned}\left|\frac{Z_0^{\parallel}}{n}\right| &< Z_0 \frac{\pi\gamma|\eta|b}{6N_B r_0\beta_Z}\, \Delta\delta_{1/2}\, \Delta z_{1/2} \\ &= Z_0 \frac{\pi\gamma\omega_s b}{6N_B r_0\beta_Z c}\, \Delta z_{1/2}^2.\end{aligned} \tag{5.101}$$

For a long bunch with $\Delta z_{1/2} > b$, the cutoff frequency is taken to be $\omega_c \approx c/\Delta z_{1/2}$, we have

$$\left|\frac{Z_0^{\parallel}}{n}\right| < Z_0 \frac{\pi\gamma|\eta|b^2}{6N_B r_0 \beta_Z} \Delta\delta_{1/2}$$

$$= Z_0 \frac{\pi\gamma\omega_s b^2}{6N_B r_0 \beta_Z c} \Delta z_{1/2}. \tag{5.102}$$

5.4 LONGITUDINAL INSTABILITY OF UNBUNCHED BEAMS

We have investigated the Landau damping effect for bunched beams—both the transverse and longitudinal cases—in Section 5.2. We have also investigated the transverse case for unbunched beams in Section 5.3. The analyses of these cases are all rather similar. In this section, the remaining case, the longitudinal case for unbunched beams, is treated. We will see that the analysis becomes quite different because there is no external focusing, i.e., $\omega_s = 0$. In particular, Landau damping in this case does not come directly from a spread in the natural focusing frequencies, but indirectly from a spread in the revolution frequencies.

Consider a relativistic unbunched beam executing a longitudinal collective motion as sketched in Figure 5.6(b). Let the unperturbed beam have a uniform distribution with the longitudinal line density

$$\lambda_0 = \frac{N}{2\pi R}. \tag{5.103}$$

Let the perturbation be an infinitesimal longitudinal density wave given by

$$\Delta\lambda(s,t) = \Delta\hat{\lambda} \exp\left(in\frac{s}{R} - i\Omega t\right). \tag{5.104}$$

The mode $n = 0$ is excluded because it violates charge conservation. The beam interacts with the vacuum chamber environment characterized by a longitudinal wake function $W_0'(z)$ and a corresponding impedance $Z_0^{\parallel}(\omega)$.

Consider a test charge at position s and time t. The longitudinal wake force F_s on the test charge is determined by the beam density as it passes by position s at an earlier time $t' < t$. By superposition, we have

$$F_s(s,t) = -\frac{e^2}{2\pi R}\int_{-\infty}^{t} c\,dt'\, W_0'(ct' - ct)\,\Delta\lambda(s,t'). \tag{5.105}$$

Substituting Eq. (5.104) for $\Delta\lambda$ and Eq. (2.72) for W_0' gives

$$F_s(s,t) = -e^2 c\,\Delta\lambda(s,t)\,\frac{Z_0^{\parallel}(\Omega)}{2\pi R}. \tag{5.106}$$

The last expression is to be compared with Eq. (2.64), identifying $ec\,\Delta\lambda$ as the instantaneous beam current.

Consider now a specific particle that passes position S at time $t = 0$. It experiences a longitudinal force $F_s(S + ct, t)$ at time t. Let the energy deviation and longitudinal coordinate of this particle be designated at δ_S and z_S; the equations of motion are

$$\begin{aligned} \dot{z}_S &= -\eta c \delta_S, \\ \dot{\delta}_S &= -\frac{r_0 c}{\gamma T_0}\,\Delta\hat{\lambda}\exp\left[in\frac{S}{R} - i(\Omega - n\omega_0)t\right] Z_0^{\parallel}(\Omega). \end{aligned} \tag{5.107}$$

We first ignore Landau damping. The solution to Eq. (5.107) is

$$\begin{aligned} \delta_S(t) &= -i\frac{r_0 c}{\gamma T_0}\frac{\Delta\hat{\lambda}}{\Omega - n\omega_0}\exp\left[in\frac{S}{R} - i(\Omega - n\omega_0)t\right] Z_0^{\parallel}(\Omega), \\ z_S(t) &= -\frac{nr_0 c^2}{\gamma T_0}\frac{\Delta\hat{\lambda}}{(\Omega - n\omega_0)^2}\exp\left[in\frac{S}{R} - i(\Omega - n\omega_0)t\right] Z_0^{\parallel}(\Omega). \end{aligned} \tag{5.108}$$

The density perturbation $\Delta\lambda$ is related to $z_S(t)$ by the equation of continuity. The particles in the space between s and $s + \Delta s$ in the unperturbed beam at time t are the same ones occupying the space between $s + z_{s-ct}(t)$ and $s + \Delta s + z_{s+\Delta s-ct}(t)$ at time t in the perturbed beam, so that their number is

$$\lambda_0\,\Delta s = [\lambda_0 + \Delta\lambda(s,t)]\{[s + \Delta s + z_{s+\Delta s-ct}(t)] - [s + z_{s-ct}(t)]\}, \tag{5.109}$$

which gives, for small Δs,

$$\begin{aligned} \Delta\lambda(s,t) &= -\lambda_0\frac{\partial z_{s-ct}}{\partial s} \\ &= \frac{2\pi N r_0 \eta}{\gamma T_0^3}\frac{in}{(\Omega - n\omega_0)^2}\,\Delta\hat{\lambda}\exp\left(in\frac{s}{R} - i\Omega t\right) Z_0^{\parallel}(\Omega). \end{aligned} \tag{5.110}$$

Self-consistency requires that the beam at (s, t) have a density perturbation of $\Delta\hat{\lambda}\exp(ins/R - i\Omega t)$. This yields the dispersion relation

$$1 = \frac{\xi_2}{(\Omega - n\omega_0)^2}, \tag{5.111}$$

where we have introduced a parameter

$$\xi_2 = i\frac{2\pi N r_0 n\eta}{\gamma T_0^3} Z_0^{\parallel}(n\omega_0). \tag{5.112}$$

To first order of perturbation, the impedance in Eq. (5.112) has been evaluated at the unperturbed frequency $n\omega_0$.

The real and imaginary parts of $\Omega - n\omega_0$ obtained from Eq. (5.111) give

$$\begin{aligned}\Delta\Omega = \mathrm{Re}(\Omega - n\omega_0) &= \mp \mathrm{sgn}(\mathrm{Im}\,\xi_2)\sqrt{\frac{|\xi_2| + \mathrm{Re}\,\xi_2}{2}} \\ &= \mp \mathrm{sgn}(n\eta)\sqrt{\frac{\pi N r_0}{\gamma T_0^3}\left(|n\eta Z_0^{\parallel}| - n\eta\,\mathrm{Im}\,Z_0^{\parallel}\right)}\end{aligned} \tag{5.113}$$

and

$$\begin{aligned}\tau^{-1} = \mathrm{Im}(\Omega - n\omega_0) &= \mp\sqrt{\frac{|\xi_2| - \mathrm{Re}\,\xi_2}{2}} \\ &= \mp\sqrt{\frac{\pi N r_0}{\gamma T_0^3}\left(|n\eta Z_0^{\parallel}| + n\eta\,\mathrm{Im}\,Z_0^{\parallel}\right)},\end{aligned} \tag{5.114}$$

where the impedance $Z_0^{\parallel}$ is evaluated at $n\omega_0$, and the $\pm$ signs refer to two solutions for the mode.

Recall that, in the transverse case, only the real part of the impedance appears in the growth rate and only the imaginary part appears in the mode frequency shift; this is no longer true here. For stability, τ^{-1} must not be positive for both solutions in Eq. (5.114). This is possible only when ξ_2 is real and positive, in which case the instability growth rate is zero. Away from the positive real axis, the + mode grows and the − mode damps.

The dispersion relation (5.111) has an important difference from the previous dispersion relations, namely, it is the *square* of the complex mode frequency shift $\Omega - n\omega_0$ that is related to the impedance here, whereas in all previous cases, the mode frequency shift is linearly related to the impedance.

This feature can be traced back to the fact that there is no external focusing in the longitudinal motion of an unbunched beam. This quadratic dependence has an important consequence. In all previous cases, half of the complex ξ_1-plane is stable even without Landau damping [see Figure 5.5(a)], whereas in the present case, as just mentioned [also see Figure 5.8(a) below], the corresponding stable region is restricted to the positive real ξ_2-axis. Landau damping is absolutely required against the longitudinal collective instabilities for unbunched beams. Once more one observes that synchrotron oscillation is one effective way to counteract collective instabilities.

Comparing Figure 5.8 with Figure 5.5, the quadratic nature of Eq. (5.111) is reflected in that the unstable (shaded) region of Figure 5.8 can be obtained from Figure 5.5 by a process of "folding over" its upper half plane. To illustrate this, consider Figure 5.5 and imagine rotating the negative real axis clockwise around the origin toward the positive real axis, stretching elastically the unstable region behind it; the process would result in a figure that resembles Figure 5.8. In the case without Landau damping, the only stable region after folding is the positive real axis. This folding operation—the equivalent of squaring a quantity in the complex plane—is applicable even in the presence of Landau damping for the various spectra illustrated.

Equation (5.111) can be compared with Eq. (4.8) obtained from a one-particle bunched beam. By dropping the potential-well distortion term and setting $\omega_s = 0$, Eq. (4.8) can be obtained by summing Eq. (5.111) over n from $-\infty$ to ∞.

As mentioned, the only chance of stability at this point is when Im $\xi_2 = 0$, i.e., when the impedance is purely imaginary. Furthermore, the impedance must be purely inductive above transition, and purely capacitance below transition.[15] Consider the case of the space charge effect, which is purely capacitive. Substituting the impedance Eq. (2.80) into Eqs. (5.113–5.114) gives

$$\Delta\Omega = \begin{cases} 0 & \text{if} \quad \eta > 0, \\ \pm \operatorname{sgn}(n) \sqrt{-\dfrac{Nr_0 n^2 c^2 \eta}{2\pi\gamma^3 R^3}\left(2\ln\dfrac{b}{a}+1\right)} & \text{if} \quad \eta < 0, \end{cases}$$

$$\tau^{-1} = \begin{cases} \mp \sqrt{\dfrac{Nr_0 n^2 c^2 \eta}{2\pi\gamma^3 R^3}\left(2\ln\dfrac{b}{a}+1\right)} & \text{if} \quad \eta > 0, \\ 0 & \text{if} \quad \eta < 0. \end{cases} \tag{5.115}$$

The beam is therefore longitudinally unstable above transition. This is in contrast with the bunched beam case, where the space charge force causes

[15]Recall that we call an impedance inductive or capacitive according to whether Im $Z_0^{\|}(\omega) < 0$ or > 0, respectively, in the region $\omega > 0$.

only a mode frequency shift and not an instability. This instability is called the *negative mass instability*.[16]

The physical origin of the negative mass instability can be illustrated as follows. Consider an unbunched beam, and let there be a small accidental density clustering at a certain position along the beam. The head and the tail of the cluster will experience space charge forces that push them apart in such a way that the head will be accelerated while the tail will be decelerated. The head therefore gains energy and the tail loses energy due to the space charge force. Above transition, one has the peculiar feature that a particle slows down if it gains energy because of the larger circumference it has to make—the longitudinal mass is negative. Therefore, the head of the cluster will move backward toward the center, and similarly, the tail of the cluster will move forward, also toward the center. The result is that the cluster becomes more clustered, creating a spontaneous lumping of the beam, leading to the negative mass instability above transition.

The fact that the unbunched beam is intrinsically unstable longitudinally in the absence of Landau damping is also reflected in the fact that $\tau^{-1} \propto |n|$ in Eq. (5.115). Physically, this is because the space charge force is proportional to the derivative $\lambda'(s)$ of the longitudinal beam density, which is in turn proportional to n. As a consequence, the beam becomes infinitely unstable with increasing mode number n. It is not meaningful to discuss longitudinal instability of unbunched beams without Landau damping.

Landau damping for the longitudinal instabilities of an unbunched beam comes from a spread in the revolution frequency ω_0 (which could result from an energy spread of the beam). Let $\rho(\omega_0)$ be the spectrum centered around $\bar{\omega}_0$ and satisfying $\int d\omega_0\, \rho(\omega_0) = 1$; then we have the dispersion relation

$$1 = \xi_2 \int d\omega_0 \frac{\rho(\omega_0)}{(n\omega_0 - \Omega - i\epsilon)^2} \tag{5.116}$$

where the impedance in the expression for ξ_2, Eq. (5.112), is to be evaluated at $n\bar{\omega}_0$. We have also attached an infinitesimal imaginary part to Ω according to the prescription (5.43). Given $\rho(\omega_0)$ and the impedance, Eq. (5.116) can be solved for the mode frequency Ω.

Exercise 5.11 Equation (5.115) shows that the beam is stable against the space charge effect below transition ($\eta < 0$) even if $\rho(\omega_0) = \delta(\omega_0 - \bar{\omega}_0)$, i.e., without Landau damping. What happens if $\rho(\omega_0)$ contains two δ-function peaks, $\rho(\omega_0) = \frac{1}{2}\delta(\omega_0 - \omega_a) + \frac{1}{2}\delta(\omega_0 - \omega_b)$ where $\omega_a \approx \omega_b \approx \bar{\omega}_0$?

[16]C. E. Nielson and A. M. Sessler, Rev. Sci. Instr. **30**, 80 (1959); C. E. Nielson, A. M. Sessler, and K. R. Symon, *Proc. Int. Conf. High Energy Accel. and Instru.*, CERN, 1959, p. 239; L. J. Laslett, V. K. Neil, and A. M. Sessler, Rev. Sci., Instr. **32**, 276 (1961); M. Q. Barton and C. E. Nielson, *Proc. Int. Conf. High Energy Accel.*, BNL, 1961, p. 16; H Bruck et al., *Proc. Int. Conf. High Energy Accel.*, BNL, 1961, p. 175.

Naively, one would expect the two-peak beam is more stable than a one-peak beam because it has a better chance of being Landau damped, but this is not so.

(a) Show that the beam becomes unstable due to space charge effect even below transition if ω_a and ω_b are sufficiently close to each other,

$$|\omega_a - \omega_b| < \sqrt{-\frac{4Nr_0\eta c^2}{\pi\gamma^3 R^3}\left(\ln\frac{b}{a} + \frac{1}{2}\right)}. \tag{5.117}$$

This instability is related to the *two-stream instability* in plasma physics.[17] Its mechanism involves the interplay and exchange of energies in the two beam streams.

(b) Establish the stability boundary diagram for the two-peak spectrum as will be done in Figure 5.8 for other spectra.

An integration by parts gives an alternative expression of Eq. (5.116),

$$\begin{aligned} 1 &= \frac{\xi_2}{n}\int d\omega_0 \frac{\rho'(\omega_0)}{n\omega_0 - \Omega - i\epsilon} \\ &= \frac{\xi_2}{n}\left[\text{P.V.}\int d\omega_0 \frac{\rho'(\omega_0)}{n\omega_0 - \Omega} + \frac{i\pi}{|n|}\rho'\left(\frac{\Omega}{n}\right)\right]. \end{aligned} \tag{5.118}$$

The absence of external focusing gives rise to the fact that Eq. (5.116) has a double pole, which in turn has the consequence that longitudinal Landau damping of unbunched beams involves the derivative of $\rho(\omega_0)$, as expressed in Eq. (5.118).

Denoting the spectrum width by $\Delta\omega$, the dispersion relation (5.118) can be written as

$$\frac{\xi_2}{n^2\Delta\omega^2} = \frac{1}{f(u) + i\,\text{sgn}(n)g(u)} \equiv \mathscr{D}_2, \tag{5.119}$$

where $u = (n\bar{\omega}_0 - \Omega)/(n\,\Delta\omega)$ and we have introduced

$$\begin{aligned} f(u) &= n\,\Delta\omega^2\,\text{P.V.}\int d\omega_0 \frac{\rho'(\omega_0)}{n\omega_0 - \Omega}, \\ g(u) &= \pi\,\Delta\omega^2\rho'\left(\frac{\Omega}{n}\right). \end{aligned} \tag{5.120}$$

[17]See for example Francis F. Chen, *Introduction to Plasma Physics*, Plenum Press, New York, 1977; Stanley Humphries, Jr., *Charged Particle Beams*, Wiley, New York, 1990.

Note that the functions f and g introduced here are different from those of Eq. (5.27). Equation (5.120) applies to the special case without external focusing.

For a δ-function spectrum (no Landau damping), we have

$$f = \frac{1}{u^2} \quad \text{and} \quad g = 0. \tag{5.121}$$

For a Lorentz spectrum (5.21), we have

$$f = \frac{u^2 - 1}{(u^2 + 1)^2} \quad \text{and} \quad g = \frac{2u}{(u^2 + 1)^2}. \tag{5.122}$$

For a rectangular spectrum Eq. (5.30), we have

$$f(u) = \frac{1}{u^2 - 1} \quad \text{and} \quad g(u) = \frac{\pi}{2}[\delta(u - 1) - \delta(u + 1)]. \tag{5.123}$$

For a tri-elliptical spectrum[18]

$$\rho(v) = \frac{8}{3\pi\,\Delta\omega}(1 - v^2)^{3/2} H(1 - |v|), \qquad v = \frac{\bar{\omega}_0 - \omega_0}{\Delta\omega}, \tag{5.124}$$

with $H(x)$ the step function, we have

$$\begin{aligned} f &= -4\left[1 - 2u^2 + 2|u|\sqrt{u^2 - 1}\, H(|u| - 1)\right], \\ g &= 8u\sqrt{1 - u^2}\, H(1 - |u|). \end{aligned} \tag{5.125}$$

For a parabolic spectrum (5.32), we have

$$\begin{aligned} f &= -3\left[1 - \frac{u}{2} \ln\left|\frac{u + 1}{u - 1}\right|\right], \\ g &= \frac{3\pi}{2} u H(1 - |u|). \end{aligned} \tag{5.126}$$

For a bi-Lorentzian spectrum (5.34), we have

$$f = \frac{u^4 + 6u^2 - 3}{(u^2 + 1)^3} \quad \text{and} \quad g = \frac{8u}{(u^2 + 1)^3}. \tag{5.127}$$

Figure 5.7 exhibits the functions $f(u)$ and $g(u)$ for the various spectra. The function f resembles, but is not identical to, the second derivative ρ''.

[18]The tri-elliptical spectrum was not one of the examples mentioned in Eqs. (5.28–5.35). The reason for introducing it here will become clear when we reach Eq. (5.130).

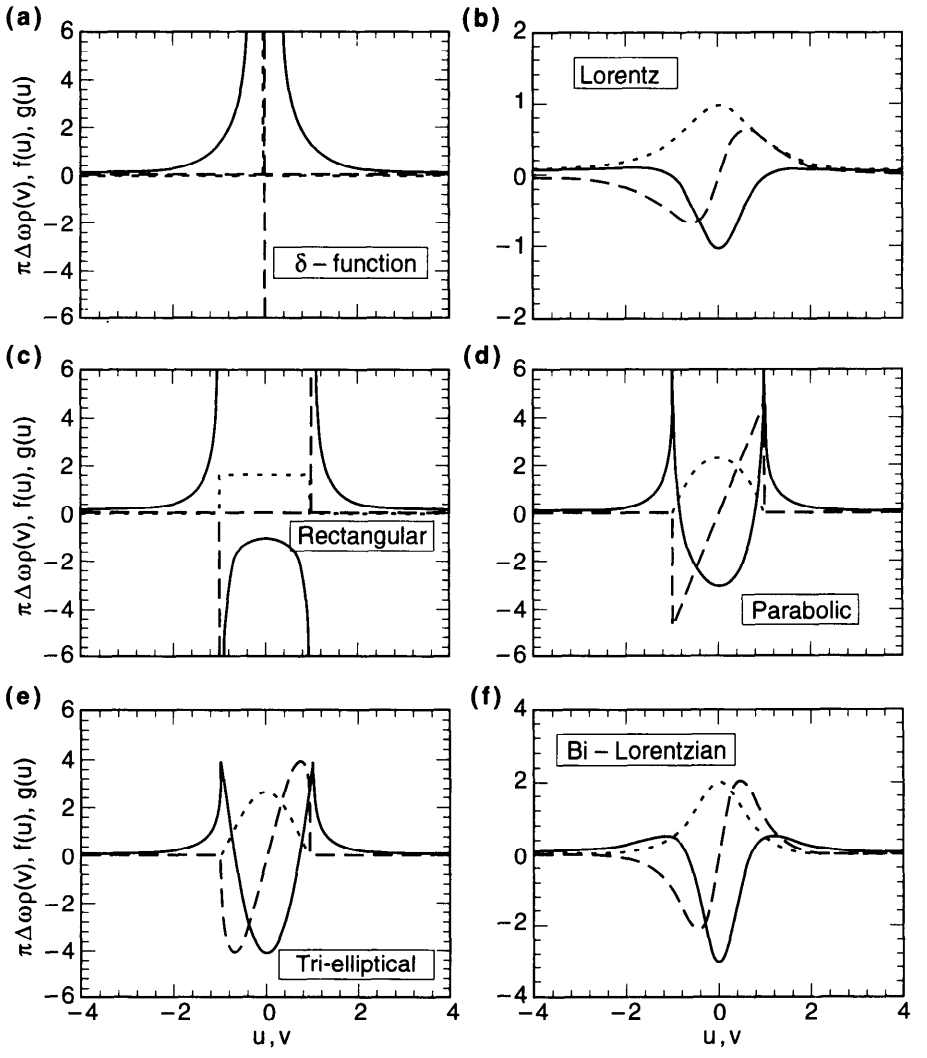

Figure 5.7. Functions $f(u)$ (solid curves) and $g(u)$ (dashed curves) of Eq. (5.120) for various spectra of revolution frequencies. Dotted curves are for $\pi\,\Delta\omega\,\rho(v)$. The function g is proportional to ρ' and the function f resembles $-g' \propto \rho''$.

The case of Lorentz spectrum is particularly simple. The mode frequency shift is the same as the case without Landau damping, Eq. (5.113), except that the impedance is to be evaluated at $n\bar{\omega}_0$. The growth rate is given by

$$\tau^{-1} = \mp\sqrt{\frac{\pi N r_0}{\gamma T_0^3}\left(|n\eta Z_0^{\parallel}| + n\eta\ \mathrm{Im}\ Z_0^{\parallel}\right)} - |n|\,\Delta\omega. \qquad (5.128)$$

Compared with Eq. (5.114), Eq. (5.128) contains an extra term $-|n|\,\Delta\omega$, which is always negative, demonstrating a damping effect. Note that the damping term, unlike its transverse counterpart Eq. (5.87), is proportional to the mode index n. The higher the mode index, therefore, the more strongly the mode is Landau damped. This behavior is expected because the disturbance $\Delta\hat{\lambda}\, e^{-ins/R}$ in beam density distribution disperses faster for higher mode index n due to a spread $\Delta\omega$ of the revolution frequency.

To damp the negative mass instability with a Lorentz spectrum requires a spectral width

$$\frac{\Delta\omega}{\bar{\omega}_0} > \sqrt{\frac{Nr_0\eta}{2\pi\gamma^3 R}\left(2\ln\frac{b}{a}+1\right)} \qquad (\eta > 0). \tag{5.129}$$

Take for example a proton accelerator with $R = 150$ m, $N = 2\times 10^{12}$, $\gamma = 10$, $\eta = 0.01$, $b = 10$ cm, and $a = 5$ mm; the required spread of revolution frequency is $\Delta\omega/\bar{\omega}_0 = 0.5\times 10^{-6}$. If this spread is to come from an energy spread, the required energy spread is $\Delta\delta = \Delta\omega/|\eta|\bar{\omega}_0 = 0.5\times 10^{-4}$.

For a general spectrum, the procedure following Eqs. (5.57–5.58) can also be applied here to obtain the stability boundary diagrams. Figure 5.8 shows the lotus of $\mathscr{D}_2$ of Eq. (5.119) as the parameter u is scanned from $-\infty$ to ∞ in the complex $\mathscr{D}_2$-plane. The beam is unstable if the value of $\xi_2/(n^2\,\Delta\omega^2)$ lies in the shaded region. Case (a) in Figure 5.8 is without Landau damping; the stability region is only along the positive real axis. This is not much improved with the rectangular spectrum in case (c). The stability region is extended to $(-1, 0)$, but stays confined to the real axis. The most stable case is offered by the Lorentz spectrum (b); the stability region is inside a parabolic boundary. Case (d), for a parabolic spectrum, gives a stable region which is cherry-shaped (complete with a stem). Case (e), for the tri-elliptical spectrum, gives a circular stable region (a lollipop). In the unstable region, the unbunched beam is said to have a *longitudinal microwave instability*.

If one does not have detailed spectral information and is interested in a rough estimate whether the beam is stable against the longitudinal microwave instability, a simplified stability criterion can be used,[19]

$$|\xi_2| = \frac{2\pi Nr_0}{\gamma T_0^3}\left|n\eta Z_0^{\parallel}(n\omega_0)\right| < \frac{1}{4}n^2\,\Delta\omega^2, \tag{5.130}$$

where the factor $\frac{1}{4}$ is such that the condition is exact for the tri-elliptical spectrum. An analogous treatment for the transverse microwave instability was given in Eq. (5.91).

[19]E. Keil and W. Schnell, CERN Report TH-RF/69-48 (1969); V. K. Neil and A. M. Sessler, Rev. Sci. Instr. **36**, 429 (1965). This is sometimes referred to as the *Keil-Schnell criterion* in the literature.

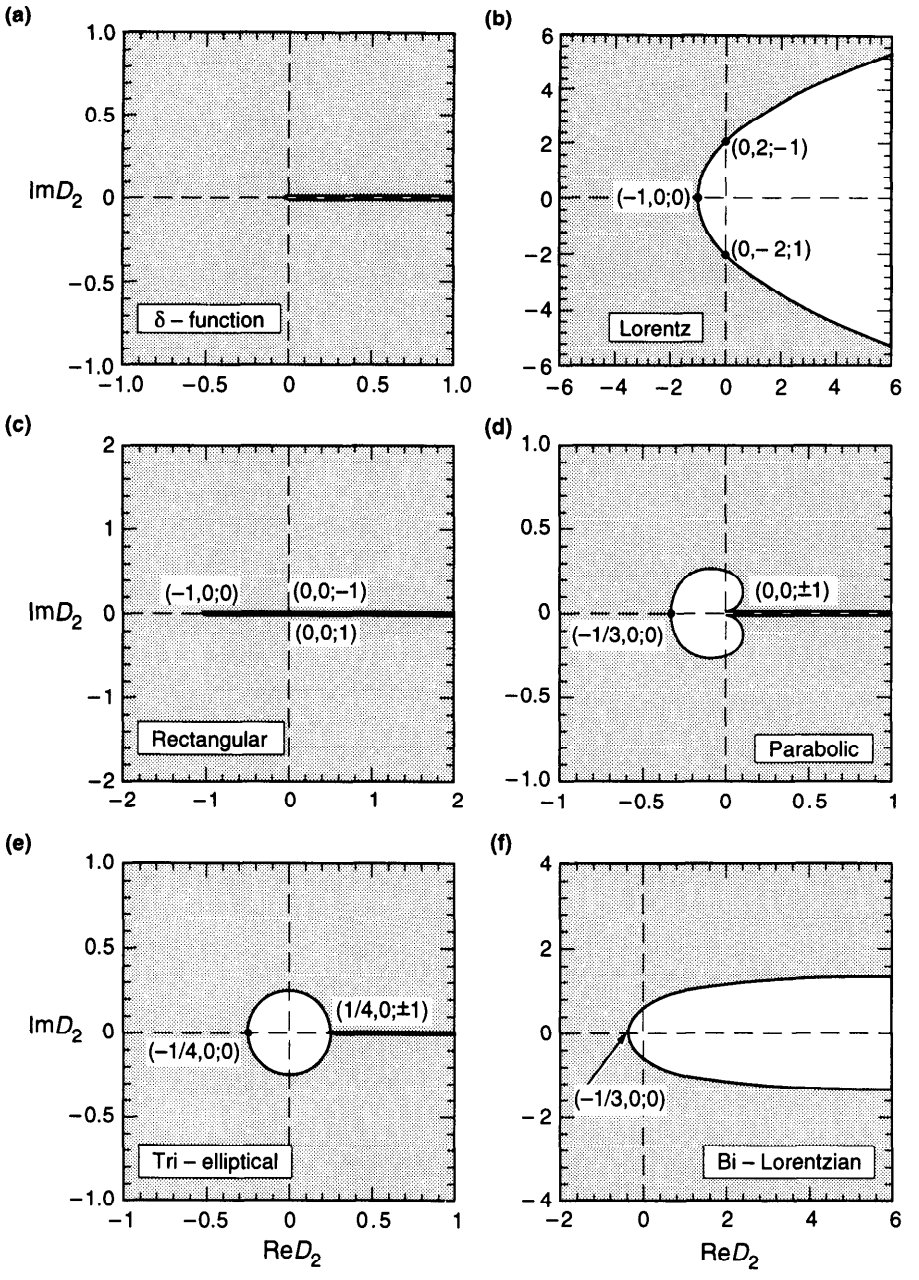

Figure 5.8. Stability boundary diagrams for various spectra in the complex $\mathscr{D}_2$-plane. If the complex quantity $\xi_2 / (n^2 \Delta\omega^2)$ lies in a shaded region, the beam is unstable. The numbers in parentheses are (Re $\mathscr{D}_2$, Im $\mathscr{D}_2$; sgn$(n)u$).

Relating $\Delta\omega$ to the half width at half maximum for the tri-elliptical distribution, we rewrite Eq. (5.130) as

$$|\xi_2| < \frac{1}{4}n^2\frac{\Delta\omega_{1/2}^2}{1-\left(\frac{1}{2}\right)^{2/3}} = 0.68n^2\,\Delta\omega_{1/2}^2. \tag{5.131}$$

If the spread in revolution frequency ω_0 comes from the energy spread of the beam, we must consider, to be consistent, also a tri-elliptical distribution for δ with

$$\Delta\omega_{1/2} = \bar{\omega}_0|\eta|\,\Delta\delta_{1/2}. \tag{5.132}$$

We then obtain from Eq. (5.131) the stability condition

$$\left|\frac{Z_0^{\parallel}(n\bar{\omega}_0)}{n}\right| < 0.68Z_0\frac{\pi|\eta|\gamma R}{Nr_0}\,\Delta\delta_{1/2}^2, \tag{5.133}$$

where $Z_0 = 377\ \Omega$.

Observe that, instead of imposing a condition on the impedance $Z_0^{\parallel}$ directly, Eq. (5.133) imposes a stability condition on $Z_0^{\parallel}/n$. In the present context, the quantity $Z_0^{\parallel}/n$ is a consequence of balancing the instability strength $|\xi_2|$, which is proportional to $nZ_0^{\parallel}$, and the Landau damping effect, which is proportional to $n^2\,\Delta\omega^2$. [See Eq. (5.130).] One may take another viewpoint, that the final stability condition should involve not the impedance but the impedance per unit length. By identifying $N/2\pi R$ on the right hand side of Eq. (5.133) as the line density of the beam, and recognizing that $Z_0^{\parallel}/n$ has the meaning of the impedance per unit length, one may anticipate the form of Eq. (5.133).

For a resistive-wall impedance, the worst mode is the one with the smallest n, i.e., $n = \pm 1$ (the mode $n = 0$ is excluded by charge conservation). The stability condition is given by

$$\Delta\delta_{1/2}^2 > \frac{Nr_0}{0.68|\eta|\gamma T_0 b\sqrt{\pi\sigma\bar{\omega}_0}}. \tag{5.134}$$

Resuming the numerical example following Eq. (5.129), and taking $\sigma = 3 \times 10^{17}\ \text{s}^{-1}$ for aluminum, the required beam energy spread is about 1×10^{-5}, a condition easily fulfilled.

In the case of a bunched beam, if the microwave instability growth rate is much faster than the synchrotron oscillation frequency, one may apply the Boussard criterion and modify Eq. (5.133) as was done in Eq. (5.95) for the transverse microwave instability. This is accomplished by replacing the unperturbed uniform density $N/2\pi R$ by the peak density across the length of the

bunch.[20] For a tri-elliptical distribution, it is replaced by $0.516N_B/\Delta z_{1/2}$, where N_B is the number of particles in the beam bunch. The resulting stability criterion for a bunched beam against longitudinal microwave instability reads

$$\left|\frac{Z_0^{\parallel}(n\bar{\omega}_0)}{n}\right| < 0.66Z_0\frac{|\eta|\gamma}{N_B r_0}\Delta\delta_{1/2}^2\,\Delta z_{1/2}. \tag{5.135}$$

If the impedance comes from a broad-band resonator, we have from Eq. (2.124) that $|Z_0^{\parallel}/n| \approx fZ_0/2$, where f is the effective fraction of the accelerator circumference occupied by deep cavities of size comparable to the vacuum chamber radius. Taking $\eta = 0.01$, $N_B = 10^{10}$, $\gamma = 10$, $\Delta\delta_{1/2} = 10^{-4}$, and $\Delta z_{1/2} = 0.1$ m, we find the stability condition $f < 1\%$.

An application of Eq. (5.96) gives an alternative form of Eq. (5.135),

$$\left|\frac{Z_0^{\parallel}(n\bar{\omega}_0)}{n}\right| < 0.66Z_0\frac{\omega_s^2\gamma}{|\eta|c^2N_B r_0}\Delta z_{1/2}^3. \tag{5.136}$$

Additional discussion of this can be found in connection with Eq. (6.160).

It may be instructive to sketch a more physical picture for the form of Eq. (5.136) as follows. Consider a bunch of length $\Delta z_{1/2}$. It induces a wake voltage $V \approx \hat{I}Z_0^{\parallel}$ where $\hat{I} \approx N_B ec/\Delta z_{1/2}$ is the peak beam current and $Z_0^{\parallel}$ is evaluated at the beam spectral frequency $\omega \approx c/\Delta z_{1/2} = n\omega_0$. Beam stability requires that V be less than the variation of the externally applied rf voltage across the bunch length, i.e.,

$$\left|\frac{1}{2\pi R}\frac{eV}{E}\right| < \left|\frac{1}{\eta}\left(\frac{\omega_s}{c}\right)^2\Delta z_{1/2}\right|. \tag{5.137}$$

Equation (5.136) follows from Eq. (5.137).

As in the transverse case [see discussion following Eq. (5.99)], we have two forms of the simplified stability criterion for the longitudinal instability of bunched beams: Eq. (5.136) when the growth rate $\gg \omega_s$, and Eq. (5.69) when the growth rate $\ll \omega_s$. Also as in the transverse case, these two forms are related to each other if one observes $|\Sigma_p(p\omega_0 + \omega_s)Z_0^{\parallel}(p\omega_0 + \omega_s)| \approx \omega_0(\omega_c/\omega_0)^3(Z_0^{\parallel}/n)$, where $\omega_c \approx c/\Delta z_{1/2}$, and if the synchrotron frequency spread $\Delta\omega_{1/2}$ is replaced by ω_s.

Comparing the microwave stability criteria of bunched beams in the transverse case, Eqs. (5.101–5.102), and the longitudinal case, Eq. (5.135), we

[20] D. Boussard, CERN Lab II/RF/Int 75-2 (1975); J. M. Wang and C. Pelligrini, *Proc. 11th Int. Conf. High Energy Accel.*, Geneva, 1980, p. 554.

conclude that the longitudinal microwave instability demands a more stringent stability condition if

$$\Delta\delta_{1/2} \lesssim 0.8\begin{cases} b/\beta_Z, & \text{short bunch,} \\ b^2/(\beta_Z \Delta z_{1/2}), & \text{long bunch.} \end{cases} \tag{5.138}$$

Since $\Delta\delta_{1/2}$ is proportional to $\Delta z_{1/2}$, it follows from Eq. (5.138) that the longitudinal instability is more stringent for short bunches. This feature should be evident from Figure 2.6.

For high energy applications, as the design energy of the accelerator increases, there is a tendency (for cost saving reasons) to reduce the vacuum chamber size b and increase the β-function. According to Eq. (5.138), this means the transverse microwave instability becomes increasingly more important relative to the longitudinal microwave instability unless the bunch length is reduced. To optimize the accelerator design, one may choose a short bunch with

$$\Delta\delta \approx 0.8b/\beta_Z$$

so that the transverse and the longitudinal instability limits are reached simultaneously.

5.5 BEAM TRANSFER FUNCTIONS

In practical accelerator operations, it is often useful to find out how the beam responds to a sinusoidal driving force. This beam response can be described in terms of a quantity called the *beam transfer function* (BTF), which is the subject of this section. The interest in the BTF is based on the fact that it contains a wealth of detailed information about the beam and the accelerator. The examination of the BTF constitutes a valuable diagnostic technique in operating an accelerator.[21]

When driven by an external sinusoidal force of frequency ω_d, the beam responds according to Eq. (5.36) with Ω replaced by ω_d. The result is conveniently summarized by the quantity $f(u) + ig(u)$, where $u = (\omega_x - \omega_d)/\Delta\omega$ with ω_x the central value of the beam frequency spectrum and $\Delta\omega$ the spectrum width. As we will soon see, the quantity $f + ig$ is the zero-intensity limit of the BTF.

When the driving frequency ω_d is far from ω_x, the BTF $f + ig$ is small and is almost purely real. This means the beam hardly responds, and the weak response $\langle x \rangle$ is either in phase or 180° out of phase relative to the

[21] H. Grunder and G. Lambertson, *Proc. 8th Int. Conf. High Energy Accel.*, CERN 1971, p. 308; A. Faltens, E. C. Hartwig, D. Möhl, and A. M. Sessler, *Proc. 8th Int. Conf. High Energy Accel.*, CERN, 1971, p. 338; A. Hofmann and B. Zotter, IEEE Trans. Nucl. Sci. **NS-24**, 1478 (1977); J. Borer et al., IEEE Trans. Nucl. Sci. **NS-26**, 3405 (1979); A. Hofmann, *Proc. 11th Int. Conf. High Energy Accel.*, Geneva, 1980, p. 540; J. Gareyte, *AIP Proc.* **184**, *Phys. Part. Accel.*, Fermilab 1987 and Cornell 1988, p. 343.

driving force depending on whether ω_x is above or below ω_d, respectively. When ω_d is close to ω_x, the BTF is almost purely imaginary with a large magnitude. This means the beam responds resonantly and $\langle x \rangle$ has a 90° phase relative to the driving force. This behavior can be seen from Figure 5.3, which shows the functions $f(u)$ and $g(u)$ for several spectral distributions. Figure 5.7 shows f and g for the special case when there is no external focusing.

We learned from the previous sections that the reciprocal of the BTF [for example, $\mathscr{D}_1$ in Eq. (5.58), $\mathscr{D}_2$ in Eq. (5.119)] plays a key role in the analysis of Landau damping. Figure 5.5 shows the lotus of $\mathscr{D}_1$ in the complex $\mathscr{D}_1$-plane as ω_d is scanned across the beam spectrum. The resulting diagram is the stability boundary diagram. Figure 5.8 shows similar results for $\mathscr{D}_2$.

The functions f and g, like the real and imaginary parts of an impedance, form Hilbert transforms pairs,[22]

$$f(u) = -\frac{1}{\pi}\text{P.V.}\int_{-\infty}^{\infty} du' \frac{g(u')}{u' - u},$$
$$g(u) = \frac{1}{\pi}\text{P.V.}\int_{-\infty}^{\infty} du' \frac{f(u')}{u' - u}. \tag{5.139}$$

The BTF $f + ig$ does not have singularities in the lower half of the complex u-plane. Its Fourier transform

$$G(t) = -\frac{i}{2\pi}\int_{-\infty}^{\infty} \frac{d\omega}{\Delta\omega}\left[f\left(\frac{\omega_x - \omega}{\Delta\omega}\right) + ig\left(\frac{\omega_x - \omega}{\Delta\omega}\right)\right]e^{-i\omega t} \tag{5.140}$$

satisfies the causality condition that $G(t) = 0$ if $t < 0$. In fact, $G(t)$ describes the beam response to a shock excitation (or to the initial conditions x_0 and $\dot{x}_0$) at time $t = 0$.

Exercise 5.12 With a Lorentz spectrum, (a) show that the BTF has only one pole at $u = i$; (b) verify the Hilbert transform property (5.139); (c) compute the Green's function $G(t)$; and (d) using Eq. (5.25), relate $G(t)$ to $\langle x \rangle / x_0$ when $\dot{x}_0 = 0$, and to $(1/\dot{x}_0)\, d\langle x \rangle / dt$ when $x_0 = 0$.

The BTF, or its reciprocal 1/BTF, can be determined experimentally by measuring the phase and amplitude of the beam response to an externally applied sinusoidal driving force. The information obtained gives detailed data about the beam frequency spectrum. In its simplest form, this is the routine method used to measure the central betatron tunes of circular accelerators.

[22]A. Hofmann, *Proc. CERN Accel. School*, Berlin, 1987, CERN Report 89-01 (1989), p. 40.

In a more sophisticated application, the detailed frequency spectrum can be related to the nonlinearities in the accelerator focusing system.

In addition, the BTF also provides a way to determine the impedance of the accelerator. To illustrate this, consider a one-particle bunched beam under the influence of a transverse impedance. Let the beam intensity be sufficiently low that the beam is stable against collective instabilities. When an external sinusoidal force is applied to the beam, the equation of motion is[23] [cf. Eq. (5.46)]

$$y''(s) + \left(\frac{\omega_\beta}{c}\right)^2 y(s) = -\frac{Nr_0}{\gamma C}\sum_{k=1}^{\infty}\langle y\rangle(s - kC)W_1(-kC) + \frac{A}{c^2}e^{-i\omega_d s/c}. \tag{5.141}$$

As a result of the driving force, the beam responds with the driving frequency. Let the beam response $\langle y\rangle$ be written as

$$\langle y\rangle(s) = Be^{-i\omega_d s/c}. \tag{5.142}$$

The right hand side of Eq. (5.141) then reads

$$\left(-\frac{Nr_0}{\gamma C}B\mathscr{W} + \frac{A}{c^2}\right)e^{-i\omega_d s/c}, \tag{5.143}$$

where $\mathscr{W}$ is given by Eqs. (5.49) or (5.50), but with the substitution $\omega_\beta \to \omega_d$.

Following an analysis similar to that for Landau damping, with Eq. (5.143) assuming the role of a driving force, allows us to write down the self-consistency condition

$$B = \left(-\frac{Nr_0\mathscr{W}c}{\gamma T_0}B + A\right)\frac{1}{2\omega_\beta\,\Delta\omega}[f(u) + ig(u)], \tag{5.144}$$

which can be solved for the beam transfer function, defined as

$$\begin{aligned}\text{BTF} &\equiv 2\omega_\beta\,\Delta\omega\,\frac{B}{A}\\ &= \frac{1}{\mathscr{D}_1(u) + \dfrac{\xi_1}{\Delta\omega}},\end{aligned} \tag{5.145}$$

[23]We have assumed both the impedance and the driving force are uniformly distributed around the accelerator circumference. Localized impedance and driving force complicate the analysis and are beyond the scope of the present treatment.

where $\mathscr{D}_1 = 1/(f + ig)$, and ξ_1 is the complex mode frequency shift (5.56) in the absence of Landau damping. A similar analysis for the longitudinal one-particle model leads to the same Eq. (5.145) with ξ_1 given by Eq. (5.68).

For low intensity beams, Eq. (5.145) gives BTF $= 1/\mathscr{D}_1 = f + ig$, as mentioned at the beginning of this section. Since $f(u)$ and $g(u)$ are intimately related to the beam spectral distribution, measurements of 1/BTF (or BTF) for a weak beam as ω_d scans across the beam spectrum yield detailed information on the spectral distribution. As the beam intensity increases, the measured 1/BTF contains additional information on $\mathscr{W}$, which in turn contains information on the impedance.

When the beam is stable against the collective instability, the BTF remains finite as ω_d is scanned across the beam spectrum. As the beam intensity gets closer to the instability threshold, the beam responds more strongly to the driving force, the BTF becomes larger, the lotus in the complex BTF plane moves away from the origin, and the 1/BTF lotus gets closer to—but does not cross—the origin in the complex 1/BTF plane. At the instability threshold (5.57), the denominator of the BTF (5.145) vanishes and the BTF diverges when ω_d reaches the value Ω of the collective mode frequency.

Exercise 5.13 Instead of driving the beam with a sinusoidal force, one could kick the beam at $t = 0$ and observe its subsequent response. Consider a beam behavior described by Eq. (5.54). Show that the beam response $\langle x \rangle(t)$ after the initial kick $x(0) = x_0$ and $\dot{x}(0) = \dot{x}_0$ satisfies the equation

$$\langle x \rangle(t) = x_0 \dot{G}(t) + \dot{x}_0 G(t) + \int_0^t dt' \, G(t - t') \left[W_1 \langle x \rangle(t') + \frac{W_2}{\omega_x} \frac{d}{dt'} \langle x \rangle(t') \right], \quad (5.146)$$

where

$$G(t > 0) = \int d\omega \, \rho(\omega) \frac{\sin \omega t}{\omega}. \quad (5.147)$$

Show that the solution of $\langle x \rangle$ in terms of the Fourier transformed quantities is

$$\langle \tilde{x} \rangle(\omega) = \frac{\tilde{G}(\omega)(-i\omega x_0 + \dot{x}_0)}{1 - 2\tilde{G}(\omega)\left(W_1 - i\dfrac{\omega}{\omega_x} W_2\right)}. \quad (5.148)$$

Specialize this to a Lorentz spectrum for a more concrete example. Make use of the result obtained in Exercise 5.12. Equation (5.146), the time-domain equivalent of the BTF, can be used as an experimental means to extract information on the wake function and the impedance.

For a bunched beam, the quantity ξ_1 is related to the impedance in a complicated manner according to Eqs. (5.50) and (5.66). For unbunched beams, the relation becomes simpler if we consider a driving force $\propto \exp(-i\omega_d t + ins/R)$ applied to a beam with zero chromaticity, causing it to execute a dipole motion with displacement $\Delta \exp(-i\omega_d t + ins/R)$. For a particle that passes location S at time $t = 0$, the equation of motion is [cf. Eq. (5.74)]

$$\ddot{y} + \omega_\beta^2 y = \left[\frac{Nr_0c^2}{\gamma T_0} i \frac{Z_1^\perp(\omega_d)}{2\pi R}\Delta + A\right] \exp\left[in\frac{S}{R} - i(\omega_d - n\omega_0)t\right]. \quad (5.149)$$

Following the now familiar procedure to solve Eq. (5.149) and demanding self-consistency, we obtain

$$\text{BTF} \equiv 2\omega_\beta \Delta\omega \frac{\Delta}{A} = \frac{1}{\mathscr{D}_1(u) + \xi_1/\Delta\omega}, \quad (5.150)$$

where $u = (\omega_\beta + n\omega_0 - \omega_d)/\Delta\omega$, and ξ_1 is given by Eq. (5.78) with the impedance evaluated at ω_d. For an unbunched beam, ξ_1 is therefore directly related to the impedance at the well-defined frequency ω_d. Having measured the 1/BTF with a weak beam to obtain $\mathscr{D}_1$, a measurement of an unbunched beam at modest intensity therefore yields direct information on the impedance.

Take a resonator impedance for example. We have

$$\frac{1}{\text{BTF}} = \frac{1}{f(u) + ig(u)} - i\frac{Nr_0c^2R_S\omega_R}{2\omega_\beta\gamma T_0^2\,\Delta\omega} \frac{1}{\omega_R\omega_d + iQ(\omega_R^2 - \omega_d^2)}. \quad (5.151)$$

If the resonator impedance is sufficiently broad that its width is larger than the width of $\omega_\beta + n\omega_0$ in the beam spectrum, the 1/BTF lotus is simply shifted by an amount proportional to $Z_1^\perp(\omega_\beta + n\omega_0)$. If the resonator width is smaller than the beam spectrum width, the 1/BTF lotus makes a loop when the driving frequency is scanned through the resonant frequency ω_R.

Figure 5.9 illustrates the behavior. The parameters used[24] are $\omega_R/\omega_0 = 200.1$, $Nr_0c^2R_S\omega_R/(8\pi^2\omega_\beta\gamma\,\Delta\omega) = 2 \times 10^4$, $\omega_\beta/\omega_0 = 6.094$, and a betatron tune spread of $\Delta\omega/\omega_0 = 0.005$. The most prominent mode under these conditions is a fast wave with $n = 194$. The resonance $\omega_d = \omega_R$ occurs slightly above ω_β and is within the spectrum width. Two cases are shown in Figure 5.9: one with $Q = 5 \times 10^5$, corresponding to a resonance whose width is narrower than the beam spectrum; the other with $Q = 2000$, having a resonance wider than the spectrum. Being a fast wave, the mode is necessarily stable. The same conclusion can be drawn by observing the fact that the

[24]These numbers are for illustration purpose only; they are not necessarily realistic.

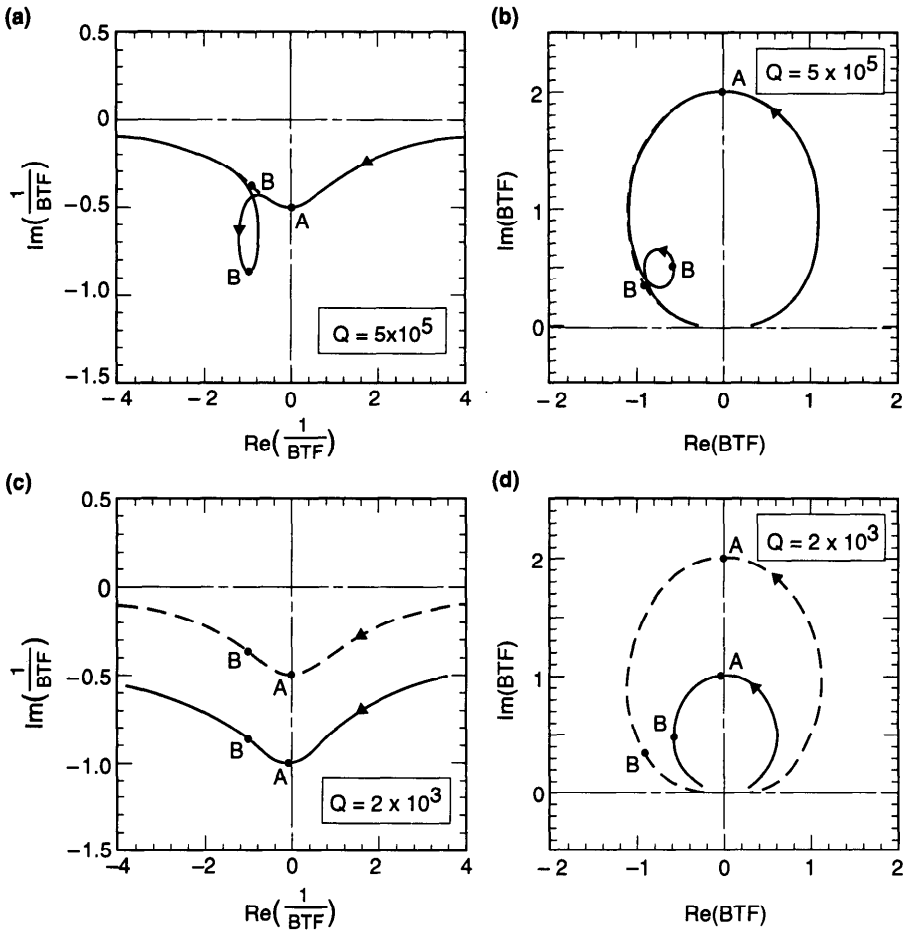

Figure 5.9. The beam transfer functions and their reciprocals trace out lotuses in their respective complex planes as the driving frequency is scanned across the beam spectrum. (a) 1/BTF for a resonator impedance whose width is sharper than the beam spectrum. (b) BTF for the impedance of case (a). (c) 1/BTF for a resonator impedance whose width is broader than the beam spectrum. (d) BTF for the impedance of case (c). A bi-Lorentzian spectrum has been assumed. The dashed curves are for the case of zero beam intensity. The dashed curves in (a) and (c) are reproductions of the stability boundary diagram shown in Figure 5.5(f). Arrows indicate the direction of the trace as ω_d sweeps through the beam spectrum from below. Locations marked by *A* and *B* are where ω_d is equal to $\omega_\beta - 6\omega_0$ and $\omega_R - 200\omega_0$, respectively.

resonant frequency ω_R is slightly above an integer times ω_0 and $\Delta_\beta > 0$, which assures beam stability according to Eq. (4.32). This is also reflected in the fact that the solid curves in Figure 5.9(b) and (d) stay on the inner side of the dashed curves. In case of Figure 5.9(c), the entire 1/BTF curve shifts by approximately a constant amount $\xi_1/\Delta\omega$, which for the case shown is almost purely imaginary.

CHAPTER 6

Perturbation Formalism

In Chapter 4, we studied the various instability mechanisms using highly simplified models in which the particle beam was modeled either as a single point charge without any internal structure, or as two point charges interacting with each other through wake fields. This approach offers intuitive pictures of the physics of several collective instabilities encountered in high intensity circular accelerators. Similar simplified models were applied in Chapter 3 to the case of linear accelerators.

However, these simplified macroparticle models have their limitations. One limitation is that their quantitative predictions can be rather crude. Another is that the instabilities are treated one by one, and it may be desirable to have a more formal treatment that allows them to be cast into one framework. Still another limitation, which is perhaps more serious, is the fact that some instabilities observed in circular accelerators involve higher oscillation modes in the longitudinal structure of the beam that are not properly treated by the simplified models.

Figure 6.1 gives sketches of a few of the collective modes of the beam motion. We use the symbol l to denote the longitudinal mode number. In contrast, we have been using the index m to denote the transverse modes. Two-particle models clearly do not suffice for studying any mode with mode number higher than $l = 2$.

Exercise 6.1 Extend Figure 6.1 to include the $m = 2$ modes.

The mode frequencies depend on the beam intensity. Figure 6.2 is a sketch of what is expected of this dependence. The (m, l) mode has an

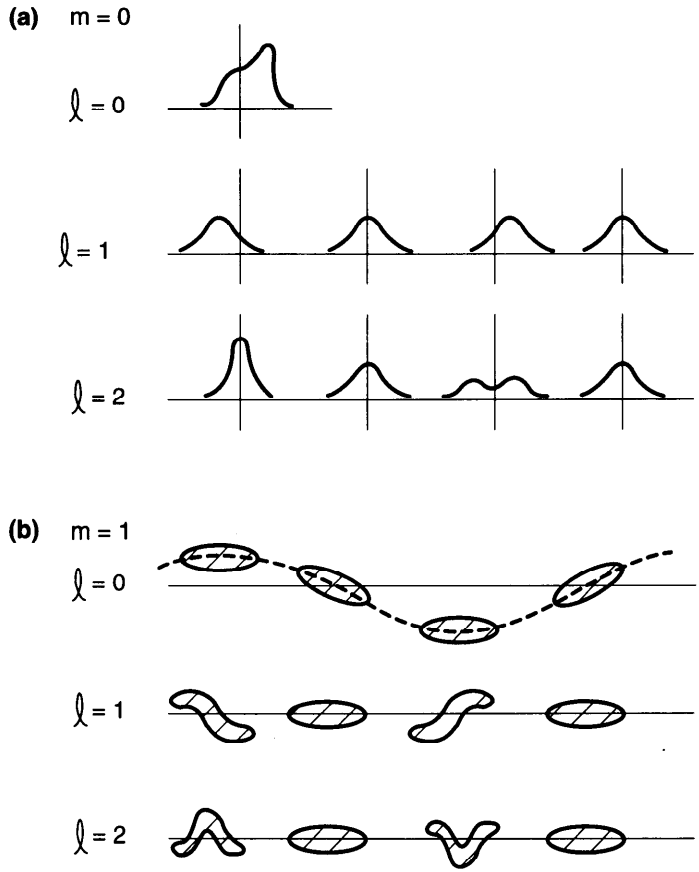

Figure 6.1. Sketches of the lowest few modes in the longitudinal structure of the beam. Successive snapshots are taken for each mode as the beam executes collective (a) longitudinal ($m = 0$) and (b) transverse ($m = 1$) motions. These sketches depict the behavior at low beam intensities. The mode patterns become more complicated as the beam intensity increases. The mode with $m = 0$ and $l = 0$ is a static mode.

unperturbed frequency of $m\omega_\beta + l\omega_s$ at zero beam intensity $N = 0$. As N increases, the mode frequencies shift. There are a few general rules—reflected in Figure 6.2—for how these mode frequencies shift with beam intensity. These are: (i) The ($m = 0$, $l = 0$) mode frequency stays zero for all beam intensities. (ii) For short bunches, the ($m = 1$, $l = 0$) and the ($m = 2$, $l = 0$) modes shift down with increasing beam intensity. (iii) For short bunches, the ($m = 1$, $l \neq 0$) modes tend to shift up with increasing beam intensity. For long bunches, these modes tend to shift down. (iv) The ($m = 0$, $l = \pm 1$) modes do not shift for small to medium beam intensities. These facts will be explained as we proceed.

We assume in general that $\omega_\beta \gg \omega_s$. As a result, when we consider the mode coupling effects in Sections 6.5 and 6.7, we do not consider coupling

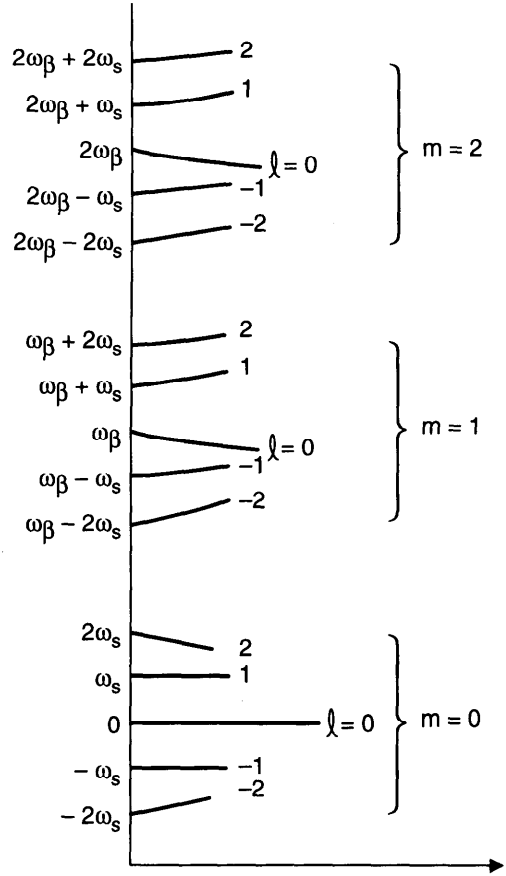

Figure 6.2. Sketch of the dependence of the mode frequencies on the intensity N for a short bunched beam. Ignoring the radial modes, a mode is specified by its transverse mode index m and longitudinal index l. When $N = 0$, the mode frequencies are given by $m\omega_\beta + l\omega_s$. As N increases, the mode frequencies shift, obeying some general rules mentioned in the text.

among modes with different m's. The modes in Figure 6.2 therefore form three disjoint clusters, specified by $m = 0$, 1, and 2, respectively. Figure 6.2 also does not include the radial modes, which are the subject of Section 6.4. The consideration of radial modes would result in a splitting of each mode frequency in Figure 6.2 into a family of frequencies.

One could, of course, increase the number of macroparticles in the simplified model, but when there are more than two macroparticles in the system, the analysis along this line becomes cumbersome. A computer simulation may be used to extend the model to anywhere from three to several thousand macroparticles, but then dealing with 10^{12} particles this way seems hopeless.

The solution to this difficulty is to go to the other extreme, in which ideally one would have an infinite number of particles, and then apply the result to

our 10^{12}-particle system. In this approach, the motion of the beam is described by a superposition of modes, rather than a collection of individual particles.

In principle, the mode representation and the particle representation of the beam motion are identical. To describe fully 10^{12} particles, one needs 10^{12} modes, and vice versa. The detailed methods of analysis in the two approaches are different—the particle representation usually is conveniently treated in the time domain, while in the mode representation the frequency domain is more convenient—but, in principle, they necessarily give the same final results.

In practice, the mode representation offers a formalism that can be used systematically to treat the instability problem and, in many cases, can be used to obtain analytic results for arbitrarily high mode numbers (at least when the mode order is much lower than 10^{12}). The advantage over the particle representation in these respects will become clear as we proceed.

In Section 6.1, the basic mathematical tool, namely the Vlasov equation,[1] used for the mode representation of the beam motion, will be derived. This technique is applied in all following sections. In Section 6.2, we describe a phenomenon in which the longitudinal wake field distorts the parabolic potential well formed by the accelerating rf voltage, and as a result the longitudinal beam distribution is deformed. Such a phenomenon is depicted as the static mode with $m = 0$ and $l = 0$ in Figure 6.1(a).

From Section 6.3 on, a perturbation treatment of the Vlasov equation that leads to the evaluation of the mode frequencies and mode patterns will be presented. The stability of the beam requires that all modes be stable; if any one of the modes shows the potential of growing exponentially, the beam will be unstable. A critical analysis of the modes, therefore, leads to the stability criterion for the beam. The mode analysis that we will follow was largely developed by Sacherer[2] and extended by others.[3] We will also mention work using other approaches when appropriate.[4]

[1]A. A. Vlasov, J. Phys. USSR **9**, 25 (1945). See also, for example, S. Chandrasekhar, *Plasma Physics*, Univ. of Chicago, 1960; Francis F. Chen, *Introduction to Plasma Physics*, Plenum, New York, 1977; J. D. Lawson, *The Physics of Charged-Particle Beams*, Clarendon, Oxford, 1977.

[2]F. Sacherer, CERN Report SI-BR/72-5 (1972); F. Sacherer, IEEE Trans. Nucl. Sci. **NS-20**, 825 (1973); F. J. Sacherer, *9th Int. Conf. High Energy Accel.*, Stanford, 1974, p. 347; F. J. Sacherer, IEEE Trans. Nucl. Sci. **NS-24**, 1393 (1977); B. Zotter and F. Sacherer, *Proc. Int. School Part. Accel.*, Erice, 1977, CERN Report 77-13, p. 175.

[3]See for example G. Besnier, Nucl. Instr. Meth. **164**, 235 (1979); J. L. Laclare, *Proc. 11th Int. Conf. High Energy Accel.*, Geneva, 1980, p. 526; B. Zotter, CERN Reports SPS/81-18, SPS/81-19, SPS/81-20 (1981); Toshio Suzuki and Kaoru Yokoya, Nucl. Instr. Meth. **203**, 45 (1982); Kohtaro Satoh and Yongho Chin, Nucl. Instr. Meth. **207**, 309 (1983); Toshio Suzuki, Yongho Chin, and Kohtaro Satoh, Part. Accel. **13**, 179 (1983); G. Besnier, D. Brandt, and B. Zotter, Part. Accel. **17**, 51 (1985).

[4]In addition to references mentioned elsewhere, see C. Pellegrini and A. M. Sessler, Nuovo Cimento **3A**, 116 (1971); A. N. Lebedev, *Physics with Intersecting Storage Rings*, Academic Press,

Strictly speaking, in a complete treatment of the beam-surroundings system, an oscillation mode λ is specified by the quantities

$$\psi^{(\lambda)}, \vec{E}^{(\lambda)}, \vec{B}^{(\lambda)}, \text{ and } \Omega^{(\lambda)}, \tag{6.1}$$

where $\psi^{(\lambda)}$ is the beam distribution function, $\vec{E}^{(\lambda)}$ and $\vec{B}^{(\lambda)}$ are the electromagnetic wake fields, and $\Omega^{(\lambda)}$ is the mode frequency that describes the time dependence of $\psi^{(\lambda)}$, $\vec{E}^{(\lambda)}$, and $\vec{B}^{(\lambda)}$. To study such a problem would require setting up and solving the "Vlasov-Maxwell" equations in which $\vec{E}^{(\lambda)}$ and $\vec{B}^{(\lambda)}$ appear in the Vlasov equation as the force terms and $\psi^{(\lambda)}$ appears in the Maxwell equation as the source term. This solution scheme is difficult to handle, but fortunately it is also not necessary for our purpose. What we have done previously has allowed us to express $\vec{E}^{(\lambda)}$ and $\vec{B}^{(\lambda)}$ directly in terms of $\psi^{(\lambda)}$ through the wake functions for relativistic beams. By doing so, the number of variables of the problem is greatly reduced, and one needs then only to solve the Vlasov equation for $\psi^{(\lambda)}$ without having to pay attention to $\vec{E}^{(\lambda)}$ and $\vec{B}^{(\lambda)}$.

The Vlasov equation obtained is nonlinear in $\psi^{(\lambda)}$, and we need to linearize it in order to search for the beam oscillation modes. This will be done in Section 6.3. Modes will be found and their stability conditions discussed in Sections 6.4 and 6.5. It turns out that when the beam is unstable, particles will not immediately be lost from the beam, but the bunch length and the energy spread of the beam will increase; we will describe this phenomenon also in Section 6.5.

Sections 6.2 through 6.5 treat the longitudinal motions. The Sacherer formalism also applies to the transverse dipole motion of the beam. This will be treated in Sections 6.6 and 6.7. The remaining two sections of the chapter, Sections 6.8 and 6.9, deal with the special case of beams with multiple bunches and the case of unbunched beams, respectively.

6.1 THE VLASOV EQUATION

The Vlasov equation describes the collective behavior of a multiparticle system under the influence of electromagnetic forces. To construct the Vlasov equation, one starts with the single-particle equations of motion

$$\begin{aligned} \dot{q} &= f(q, p, t), \\ \dot{p} &= g(q, p, t), \end{aligned} \tag{6.2}$$

New York, 1971, p. 184; R. D. Kohaupt, DESY Report 80/22 (1980); R. D. Ruth, Ph.D. Thesis, BNL Report 51425 (1981); C. Pellegrini, *AIP Proc.* **87**, *Phys. High Energy Part. Accel.*, Fermilab, 1981, p. 77; Jiunn-Ming Wang, *AIP Proc.* **153**, *Phys. Part. Accel.*, Fermilab 1984 and SLAC 1985, p. 697; S. Y. Lee and J. M. Wang, IEEE Trans. Nucl. Sci. **NS-32**, 2323 (1985).

where q and p are the coordinate and momentum variables, respectively, and the (q, p) plane is the phase space. The state of a particle at a given time t is represented by a point in the phase space. The motion of a particle is described by the motion of its representative point. For a particle executing a simple harmonic motion, for example, its representative point in phase space traces out an ellipse. We often do not distinguish between the representative point in phase space and the particle itself in real space; although somewhat ambiguous, this should not cause much confusion.

In a conservative deterministic system, the particle trajectory in phase space is completely determined by the initial conditions (q_0, p_0) at time $t = t_0$.[5] Two particles having the same initial conditions must have exactly the same trajectory in phase space. It follows that the only way for two trajectories to meet at a given time is for them to coincide at all times. In other words, trajectories either completely coincide or never intersect.

Consider now a distribution of particles occupying an area in the phase space. Because they cannot intersect with particles on the boundary of the distribution as the distribution evolves in time, particles inside the distribution cannot leak out by crossing the boundary. Similarly, no particles from outside can penetrate into the distribution.

If the system is conservative, i.e., if the system is not influenced by any damping or diffusion effects due to external sources,[6] we have the conditions that

$$f = \frac{\partial H}{\partial p} \quad \text{and} \quad g = -\frac{\partial H}{\partial q}, \tag{6.3}$$

where H is the Hamiltonian. It follows that

$$\frac{\partial f}{\partial q} + \frac{\partial g}{\partial p} = 0. \tag{6.4}$$

As will be seen in Eq. (6.10), the condition (6.4) leads to an area conservation property: as the particle distribution evolves in the phase space, its shape may be distorted but its area remains constant. In fact, in a nonconservative system, the left hand side of Eq. (6.4) has the physical meaning of the rate of area shrinkage.

[5]In particular, one does not need to know $\ddot{q}_0$; this follows from the fact that Newton's equation is a second order differential equation in time.

[6]It is possible that the degrees of freedom of the system are coupled among themselves *internally* so that motions in some degrees of freedom grow exponentially at the expense of having some other motions damped. In fact, this possibility of damping and antidamping through internal couplings is the origin of beam instability we are studying. One way of telling whether the damping and antidamping come from an external source or an internal source is to sum over the growth rates of all modes (provided they can be found); the sum should vanish for an internal source. See Eqs. (4.120) and (6.217).

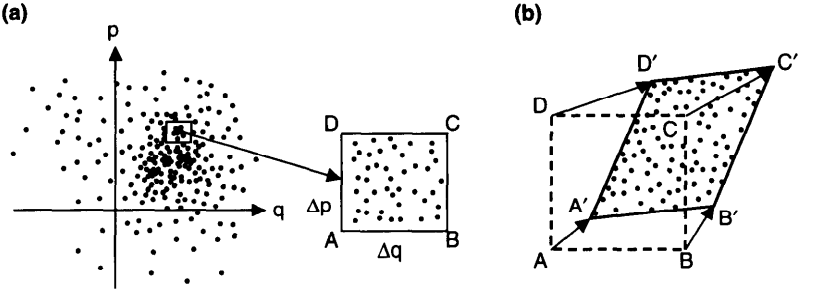

Figure 6.3. (a) Phase space distribution of particles at time t. A rectangular box $ABCD$ with area $\Delta q\,\Delta p$ is drawn and magnified. (b) At a later time, $t + dt$, the box moves and deforms into a parellelogram with the same area as $ABCD$. All particles inside the box move with the box.

In Figure 6.3(a) we have sketched the distribution of a group of particles in the phase space at time t. A rectangular $\Delta q\,\Delta p$ box is then drawn:

$$\begin{aligned} &A(q, p), \\ &B(q + \Delta q, p), \\ &C(q + \Delta q, p + \Delta p), \\ &D(q, p + \Delta p). \end{aligned} \tag{6.5}$$

The box is small enough so that the numbers of particles contained in adjacent boxes of the same size—if drawn—are about equal. The box is also large enough so that it contains at least several particles.

Let the number of particles enclosed by the box be

$$\psi(q, p, t)\,\Delta q\,\Delta p, \tag{6.6}$$

where ψ is the phase space distribution density depending on q, p, and t and is normalized by

$$\int_{-\infty}^{\infty} dq \int_{-\infty}^{\infty} dp\, \psi(q, p, t) = N, \tag{6.7}$$

with N the total number of particles in the system.

At time $t + dt$, the box has moved to $A'B'C'D'$ as shown in Figure 6.3(b). We have used Δq and Δp (rather than dq and dp) to denote the dimensions of the box, but have used dt to denote the time increment. This is because we do not want the box size to be vanishingly small, but dt should be considered truly infinitesimal.

In general, the rectangular box deforms into a parallelogram. (The only case in which the rectangular box remains rigid in shape as time evolves is

simple harmonic motion.) The vertices of the parallelogram are

$$\begin{aligned} &A'[q + f(q,p,t)\,dt,\, p + g(q,p,t)\,dt], \\ &B'[q + \Delta q + f(q+\Delta q,p,t)\,dt,\, p + g(q+\Delta q,p,t)\,dt], \\ &C'[q + \Delta q + f(q+\Delta q,p+\Delta p,t)\,dt, \\ &\quad p + \Delta p + g(q+\Delta q,p+\Delta p,t)\,dt], \\ &D'[q + f(q,p+\Delta p,t)\,dt,\, p + \Delta p + g(q,p+\Delta p,t)\,dt]. \end{aligned} \tag{6.8}$$

The condition that no particles leak into or out of the box gives

$$\psi(q,p,t)\,\text{area}(ABCD) = \psi(q + f\,dt,\, p + g\,dt,\, t + dt)\,\text{area}(A'B'C'D'). \tag{6.9}$$

For a Hamiltonian system, the condition (6.4) implies the area of the box is conserved:

$$\begin{aligned} \text{area}(A'B'C'D') &= \left| \overrightarrow{A'B'} \times \overrightarrow{A'D'} \right| \\ &= \Delta q\,\Delta p\left[1 + \left(\frac{\partial f}{\partial q} + \frac{\partial g}{\partial p}\right) dt\right] \\ &= \Delta q\,\Delta p = \text{area}(ABCD). \end{aligned} \tag{6.10}$$

Equation (6.9) then gives

$$\begin{aligned} \psi(q,p,t) &= \psi(q + f\,dt,\, p + g\,dt,\, t + dt) \\ &= \psi + \frac{\partial \psi}{\partial q} f\,dt + \frac{\partial \psi}{\partial p} g\,dt + \frac{\partial \psi}{\partial t}\,dt, \end{aligned} \tag{6.11}$$

or, after canceling out ψ on both sides,

$$\frac{\partial \psi}{\partial t} + f\frac{\partial \psi}{\partial q} + g\frac{\partial \psi}{\partial p} = 0. \tag{6.12}$$

Equation (6.12) is the *Vlasov equation*—particularly when the forces involved are electromagnetic in origin. It can also be put in the form

$$\frac{d\psi}{dt} = 0, \qquad \text{or} \quad \psi = \text{const in time}. \tag{6.13}$$

Equation (6.13), sometimes loosely referred to as the *Liouville theorem*,[7] states that the local particle density does not change if (an important if) the observer moves with the flow of boxes, but it does not tell how the boxes flow. The Vlasov form (6.12), on the other hand, does not have this ambiguity, since it contains explicitly the single-particle information f and g.

Strictly speaking, f and g are given by external forces. Collisions among discrete particles in the system, for example, are excluded. However, if a particle interacts more strongly with the *collective* fields of the other particles than with its nearest neighbors, the Vlasov equation still applies if one treats the collective fields on the same footing as the external fields. This in fact forms the basis of treating the collective instabilities using the Vlasov technique.

One special case where the Vlasov equation (6.12) can be solved exactly is when the system is described by a Hamiltonian $H(q, p)$ which does not have an explicit time dependence. Using the properties (6.3), a stationary solution to Eq. (6.12) is found to be

$$\psi(q, p) = \text{any function of } H(q, p). \tag{6.14}$$

In this system, individual particles stream along constant-Hamiltonian contours in the phase space in such a way that the overall distribution is stationary.

Exercise 6.2 Solve the Vlasov equation for a system of particles subject to simple harmonic motions with Hamiltonian $H = \omega(q^2 + p^2)/2$. Show that the Vlasov equation can be written as

$$\frac{\partial \psi}{\partial t} + \omega \frac{\partial \psi}{\partial \phi} = 0 \tag{6.15}$$

and its general solution is

$$\psi(q, p, t) = \text{any function of } (r, \phi - \omega t), \tag{6.16}$$

where r and ϕ are the polar coordinates defined by $q = r \cos \phi$ and $p = -r \sin \phi$. Once the initial distribution of the beam is given at $t = 0$, Eq. (6.16) means that the distribution at time t is obtained by rigidly rotating the initial distribution in phase space angle ϕ at a constant angular speed of ω. A stationary distribution is any function of r without dependence on ϕ, or equivalently, any function of the Hamiltonian H.

[7]The Vlasov equation applies to a system of many particles. Strictly, the Liouville theorem applies to an *ensemble* of many systems, each containing many particles. It describes the conservation of density of the ensemble in the $2N$-dimensional Γ-space and applies to situations much more general than that considered here, such as when collisions among discrete particles are included.

Exercise 6.3 Consider a damped simple harmonic motion with $f = \omega p$ and $g = -\omega q - 2\alpha p$, where $\alpha > 0$ is the damping rate. The Vlasov equation needs to be modified here because the conservation of phase space area is violated. Following the derivation from Eq. (6.9) to Eq. (6.12), show that the modified Vlasov equation reads

$$\frac{\partial \psi}{\partial t} + \omega p \frac{\partial \psi}{\partial q} - (\omega q + 2\alpha p)\frac{\partial \psi}{\partial p} = 2\alpha \psi. \tag{6.17}$$

Note that a straightforward substitution of f and g into the form (6.12) would lose the term on the right hand side of Eq. (6.17). Note also that $\partial f/\partial q + \partial g/\partial p = -2\alpha$ is negative, which means the area of phase space boxes shrinks with time according to Eq. (6.10). Show that the general solution of Eq. (6.17) is

$$\psi(q, p, t) = e^{2\alpha t} \times (\text{any function of } A \text{ and } \Phi), \tag{6.18}$$

where

$$\begin{aligned} A^2 &= e^{2\alpha t}\left(q^2 + p^2 + \frac{2\alpha}{\omega} qp\right), \\ \Phi &= \tan^{-1}\left(\frac{\omega p + \alpha q}{q\sqrt{\omega^2 - \alpha^2}}\right) + \sqrt{\omega^2 - \alpha^2}\, t. \end{aligned} \tag{6.19}$$

Equation (6.18) is that of a distribution peaking up while spiraling inward with time.

In the derivation of the Vlasov equation, we have assumed that there are no significant diffusion or external damping effects. This is usually a good approximation for proton beams. For electron beams, synchrotron radiation contributes to both damping and diffusion,[8] and one needs to modify the Vlasov equation accordingly to obtain another equation called the *Fokker-Planck equation*.[9] Strictly speaking, our results obtained using the Vlasov equation apply only to protons and not electrons. However, when the instability occurs in a time shorter than the damping or diffusion times, the Vlasov treatment can apply also to electrons. The treatment of collective instabilities using the Fokker-Planck equation is beyond our scope here.[10]

[8]Matthew Sands, *The Physics of Electron Storage Rings, an Introduction*, SLAC Report 121 (1970).

[9]See for example, S. Chandrasekhar, Rev. Mod. Phys. **15**, 1 (1943).

[10]A. Renieri, Frascati Laboratory Report LNF-76/11(R) (1976); Toshio Suzuki, Part. Accel. **14**, 91 (1983).

6.2 POTENTIAL-WELL DISTORTION

As a first application of the Vlasov technique, we will study the effect of longitudinal wake fields on a distortion of the equilibrium shape of a beam bunch.[11] The mechanism is a static one; no part of the beam bunch is executing collective oscillation. The extent of the bunch shape distortion depends on the beam intensity; higher beam intensities cause larger distortions. The dynamics of the bunch shape oscillations will be treated in later sections of this chapter.

Consider a bunched beam that travels along the axis of the vacuum chamber pipe in a circular accelerator. We assume the beam does not have any transverse dimension, i.e., the beam has the shape of an infinitesimally thin thread. Such a beam does not generate transverse wake fields; only the $m = 0$ wake is excited.

Consider now a particle in the beam executing longitudinal synchrotron oscillation. The physical quantities of interest are the longitudinal displacement z of the particle relative to the bunch center and the relative energy error δ. The phase space coordinates q and p of the previous section are related to these quantities by

$$q = z \quad \text{and} \quad p = -\frac{\eta c}{\omega_s}\delta, \tag{6.20}$$

where η is the slippage factor defined in Eq. (1.10) and ω_s is the synchrotron oscillation frequency.

As mentioned, the Vlasov equation is constructed by first writing down the single-particle equations of motion. In the present case, the equations are

$$z' = -\eta\delta \quad \text{and} \quad \delta' = K(z), \tag{6.21}$$

where a prime means taking derivative with respect to the distance s along the accelerator circumference. In contrast with Eq. (1.9), we have left the δ'-equation open for the time being, except that we do know the function K cannot depend on δ, because the system is conservative. [See Eq. (6.4).]

The Vlasov equation corresponding to Eq. (6.21) is[12]

$$\frac{\partial\psi}{\partial s} - \eta\delta\frac{\partial\psi}{\partial z} + K(z)\frac{\partial\psi}{\partial\delta} = 0, \tag{6.22}$$

[11] C. Pellegrini and A. M. Sessler, Nuovo Cimento **3A**, 116 (1971); B. Zotter, *Proc. 4th Advanced ICFA Beam Dynamics Workshop on Collection Effects in Short Bunches*, Tsukuba, 1990, KEK Report 90-21.

[12] A subtlety arises if one (incorrectly) uses time t, instead of s, as the independent variable here. The point is that the impedance is an object localized in s, not t. The difference, however, is negligibly small. What happens is that the quantity $Z_0^{\parallel}(\omega')/\omega'$ of Eq. (6.74) later will be replaced by $Z_0^{\parallel}(\omega')/p\omega_0$, where $\omega' = p\omega_0 + \omega_s$. See Toshio Suzuki, Part. Accel. **12**, 237 (1982).

where we will set $\partial\psi/\partial s = 0$, since we are looking for a stationary distribution. The general stationary solution can be written as

$$\psi(z,\delta) = \text{any function of the Hamiltonian } H,$$
$$H = \frac{\eta^2 c^2}{\omega_s}\left[\frac{\delta^2}{2} + \frac{1}{\eta}\int_0^z K(z')\,dz'\right]. \tag{6.23}$$

The second integral term in the Hamiltonian is the potential-well term. A simple harmonic system would have a parabolic potential well.

If the potential well is provided by an external rf voltage $V_{\mathrm{rf}}(z)$, we have

$$K(z) = \frac{eV_{\mathrm{rf}}(z)}{CE} = \frac{\omega_s^2}{c^2\eta V'_{\mathrm{rf}}(0)}V_{\mathrm{rf}}(z), \tag{6.24}$$

where E is the particle energy, C is the accelerator circumference, V'_{rf} is the derivative of V_{rf} with respect to z, and we have used the expression

$$\omega_s^2 = \frac{e\eta c^2 V'_{\mathrm{rf}}(0)}{CE}. \tag{6.25}$$

A practical case is given by $V_{\mathrm{rf}} = \hat{V}\sin(\omega_{\mathrm{rf}} z/c)$. The deviation of $V_{\mathrm{rf}}(z)$ from a linear dependence on z is a cause of potential-well distortion. The general stationary distribution (6.23) is given by any function of the Hamiltonian

$$H = \frac{\eta^2 c^2}{2\omega_s}\delta^2 + \frac{\omega_s c^2}{\omega_{\mathrm{rf}}^2}\left[1 - \cos\left(\frac{\omega_{\mathrm{rf}} z}{c}\right)\right]. \tag{6.26}$$

This Hamiltonian also describes the form of the rf bucket. A stationary distribution must conform to the contours of constant Hamiltonian (6.26) inside the bucket. For small oscillation amplitudes, we have $K = \omega_s^2 z/\eta c^2$, the case of simple harmonic motion.

One noteworthy special case of the stationary beam distribution is that given by $\exp(-\text{const} \times H)$. This distribution is always Gaussian in δ. In case the bunch length is much shorter than the rf wavelength ($z \ll c/\omega_{\mathrm{rf}}$), the familiar quadratic form of the Hamiltonian is reestablished, and the distribution is also Gaussian in z. As the bunch length increases, the bunch shape deviates from Gaussian; the potential well is distorted by the rf bucket, although the distribution remains Gaussian in δ.

There is another reason for the Hamiltonian to deviate from the quadratic form, and thus to cause potential-well distortion, namely, the wake fields of high intensity beams. To illustrate this, consider a bunch that is short compared with the rf wavelength. Let the wake fields be characterized by a wake function $W'_0(z)$ (integrated over the accelerator circumference), and

assume that the wake has dissipated before the beam completes one revolution. Then the single-particle motion can be described by Eq. (6.21) with

$$K(z) = \frac{\omega_s^2}{\eta c^2} z - \frac{r_0}{\gamma C} \int_z^\infty dz' \, \rho(z') W_0'(z - z'), \tag{6.27}$$

where the second term is the retarding voltage seen by a particle at longitudinal location z due to the wake force produced by all particles in front of it; $\rho(z')$ is the particle density at location z' and is normalized by

$$\int_{-\infty}^{\infty} dz \, \rho(z) = N. \tag{6.28}$$

The corresponding Hamiltonian is

$$H = \frac{\eta^2 c^2}{2\omega_s} \delta^2 + \frac{\omega_s}{2} z^2 - \frac{\eta c^2 r_0}{\omega_s \gamma C} \int_0^z dz'' \int_{z''}^\infty dz' \, \rho(z') W_0'(z'' - z'). \tag{6.29}$$

The stationary solution to the Vlasov equation must be a function of H. The complication here, compared with the case of rf bucket distortion, is that the complicated z-dependence of H now involves the beam density ρ, which in turn is determined by the stationary distribution itself. Clearly some self-consistency requirement is involved in solving the problem. Below we will give a few explicit examples of this procedure.

Continuing the Gaussian example mentioned above, even though the z-dependence is complicated, the stationary distribution maintains its gaussian distribution in δ,

$$\psi(z, \delta) = \frac{1}{\sqrt{2\pi}\,\sigma_\delta} \exp\left(- \frac{\delta^2}{2\sigma_\delta^2} \right) \rho(z), \tag{6.30}$$

where σ_δ is the rms beam energy spread.

The Gaussian form and the value of σ_δ in Eq. (6.30) are arbitrary as long as the collective beam behavior is governed by the Vlasov equation, as in the case of a proton beam. However, if the beam behavior is governed, as for an electron beam, by the Fokker-Planck equation, then Eq. (6.30) with a specific value for σ_δ will be the unique solution of the stationary beam distribution.

Equation (6.30) matches the stationary solution

$$\psi(z, \delta) \propto \exp\left(- \frac{\omega_s}{\eta^2 c^2 \sigma_\delta^2} H \right). \tag{6.31}$$

Substituting Eq. (6.29) into Eq. (6.31), we obtain a transcendental equation

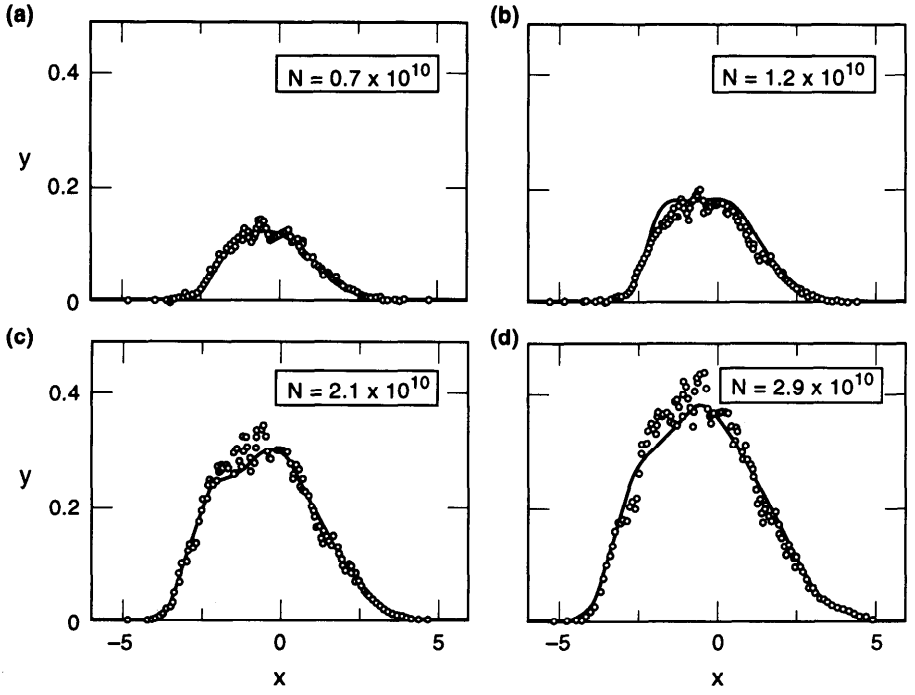

Figure 6.4. Potential-well distortion of bunch shape for various beam intensities for the SLC damping ring. The open circles are the measured results. The horizontal axis is $x = -z/\sigma_{z0}$, where σ_{z0} is the unperturbed rms bunch length. The vertical scale gives $y = 4\pi e\rho(z)/V'_{rf}(0)\sigma_{z0}$. (Courtesy Karl Bane, 1992.)

for the line density $\rho(z)$,[13]

$$\rho(z) = \rho(0)\exp\left[-\frac{1}{2}\left(\frac{\omega_s z}{\eta c\sigma_\delta}\right)^2 + \frac{r_0}{\eta\sigma_\delta^2\gamma C}\int_0^z dz''\int_{z''}^{\infty} dz'\,\rho(z')W_0'(z''-z')\right]. \tag{6.32}$$

In the limit of zero beam intensity, the solution reduces to the bi-Gaussian form, where the rms bunch length is related to σ_δ by $\sigma_z = \eta c\sigma_\delta/\omega_s$.

For high beam intensities, $\rho(z)$ deforms from Gaussian shape. Together with Eq. (6.28), Eq. (6.32) can in principle be solved numerically for $\rho(z)$ once the wake function $W_0'(z)$ is known and σ_δ specified. Figure 6.4 shows the result of one such attempt for the electron damping ring for the SLAC Linear Collider.[14] The bunch shape is Gaussian at low beam intensities, and

[13]J. Haissinski, Nuovo Cimento **18B**, 72 (1973).

[14]Karl L. F. Bane and Ronald D. Ruth, *Proc. IEEE Conf. Part. Accel.*, Chicago, 1989, p. 789.

it distorts as the beam intensity is increased. The calculated bunch shapes agree well with the measured results[15] shown as open circles in Figure 6.4.

One feature of Figure 6.4 is that the distribution leans forward ($z > 0$) as the beam intensity increases. This effect comes from the parasitic loss of the beam bunch, and is a consequence of the real (resistive) part of the impedance. Since the SLC damping ring is operated above transition, the bunch moves forward so that the parasitic energy loss can be compensated by the rf voltage.[16]

Another feature of Figure 6.4 is that the bunch length increases as the beam intensity increases. As we will elaborate later, the bunch shape distortion comes mainly from the imaginary part of the impedance. That the bunch lengthens in Figure 6.4 is a consequence of the fact that the imaginary part of the impedance seen by the beam is mostly inductive.

Another example allowing closed-form solution of Eq. (6.29) occurs when the wake function has the special form

$$W_0'(z) = S\delta'(z), \tag{6.33}$$

where $\delta(z)$ is the δ-function. Under this condition, the retarding wake at location z can be related to the local derivative of the line density,

$$\int_z^\infty dz'\, \rho(z') W_0'(z - z') = S\rho'(z). \tag{6.34}$$

The wake field (6.33) can be produced by a purely imaginary impedance

$$Z_0^\parallel(\omega) = i\frac{S\omega}{c^2}. \tag{6.35}$$

The quantity S can be related to the familiar quantity $Z_0^\parallel/n$ by $S = -i(c^2/\omega_0)(Z_0^\parallel/n)$. Strictly speaking, the frequency dependence of the impedance (6.35) says it is inductive with an inductance $L = -S/c^2$, and one has $S < 0$; but we will extend the meaning of this impedance to capacitive impedances by including $S > 0$. One physical effect that produces such a wake function is that due to the space charge Coulomb repulsion [see Eq. (2.80)] with

$$S = \frac{2C}{\gamma^2}\left(\ln\frac{b}{a} + \frac{1}{2}\right), \tag{6.36}$$

[15] L. Rivkin et al., *Proc. Euro. Part. Accel. Conf.*, Rome, 1988, p. 634.

[16] In fact, one way to measure the parasitic loss is by measuring the position of the bunch center as a function of beam intensity. And a measurement of parasitic loss as a function of the bunch length is a way to measure the real part of the impedance as a function of frequency. See P. B. Wilson et al., IEEE Trans. Nucl. Sci. **NS-24**, 1211 (1977).

where b is the vacuum chamber pipe radius, and a is the transverse beam radius.

In the present example, we will not assume a Gaussian solution, but will write the stationary distribution of the beam bunch in the ansatz form

$$\psi(z,\delta) = \begin{cases} \dfrac{3\eta cN}{2\pi\omega_s \hat{z}_0^3}\sqrt{\hat{z}_0^2 - \dfrac{1}{\kappa}\left(\dfrac{\eta c}{\omega_s}\delta\right)^2 - \kappa z^2} & \text{if } \dfrac{1}{\kappa}\left(\dfrac{\eta c}{\omega_s}\delta\right)^2 + \kappa z^2 < \hat{z}_0^2, \\ 0 & \text{otherwise,} \end{cases} \tag{6.37}$$

where the dimensionless parameter κ, yet to be found as a function of beam intensity, specifies the degree of distortion of the beam distribution due to the wake fields. The unperturbed beam would have $\kappa = 1$. The form (6.37) is such that the unperturbed beam has an elliptical distribution in the phase space; and when perturbed by the wake field, the beam distribution remains elliptical but distorted in such a way that its phase space area (the emittance) is independent of κ, i.e., independent of the beam intensity. The fact that the bunch centroid is located at $z = 0$ assumes there is no net parasitic loss of the bunch, and this is a consequence of the wake (6.33) being considered.

The distribution (6.37) has a parabolic line density

$$\rho(z) = \frac{3N\sqrt{\kappa}}{4\hat{z}_0^3}\left(\hat{z}_0^2 - \kappa z^2\right) \qquad \text{if} \quad z < \frac{\hat{z}_0}{\sqrt{\kappa}}. \tag{6.38}$$

The unperturbed beam has a total length $2\hat{z}_0$; the perturbed beam has a total length $2\hat{z} = 2\hat{z}_0/\sqrt{\kappa}$.

To be self-consistent, the distribution has to be a function of the Hamiltonian (6.29). Using Eqs. (6.34) and (6.38), we have

$$H = \frac{\eta^2 c^2}{2\omega_s}\delta^2 + \frac{\omega_s}{2}(1 + D\kappa^{3/2})z^2, \tag{6.39}$$

where

$$D = \frac{3Nr_0\eta c^2 S}{2\omega_s^2 \gamma C \hat{z}_0^3}. \tag{6.40}$$

Comparing Eq. (6.39) with the ansatz (6.37) indicates that the stationary distribution must have the form

$$\psi = \frac{3\eta cN}{2\pi\omega_s \hat{z}_0^3}\sqrt{\hat{z}_0^2 - \frac{2}{\kappa\omega_s}H} \tag{6.41}$$

and that self-consistency requires

$$\kappa^2 - 1 - D\kappa^{3/2} = 0, \tag{6.42}$$

or, in terms of the beam length $\hat{z}$, a fourth order equation[17]

$$\left(\frac{\hat{z}}{\hat{z}_0}\right)^4 + D\frac{\hat{z}}{\hat{z}_0} - 1 = 0. \tag{6.43}$$

In the limit of weak beam intensity, $D = 0$, we have $\hat{z} = \hat{z}_0$. As the beam intensity increases, the beam shape remains parabolic, but its length changes —either shortens or lengthens according to the sign of D. Figure 6.5(a) illustrates the phase space distributions of the unperturbed ($D = 0$), the shortened ($D > 0$), and the lengthened ($D < 0$) bunches. The solid curve in Figure 6.6 gives the dependence of $\hat{z}/\hat{z}_0$ on the wake strength parameter D. For any given value of D, there is a solution of $\hat{z}$. The bunch lengthens below transition and shortens above transition if the impedance is capacitive. The opposite holds if the impedance is inductive.

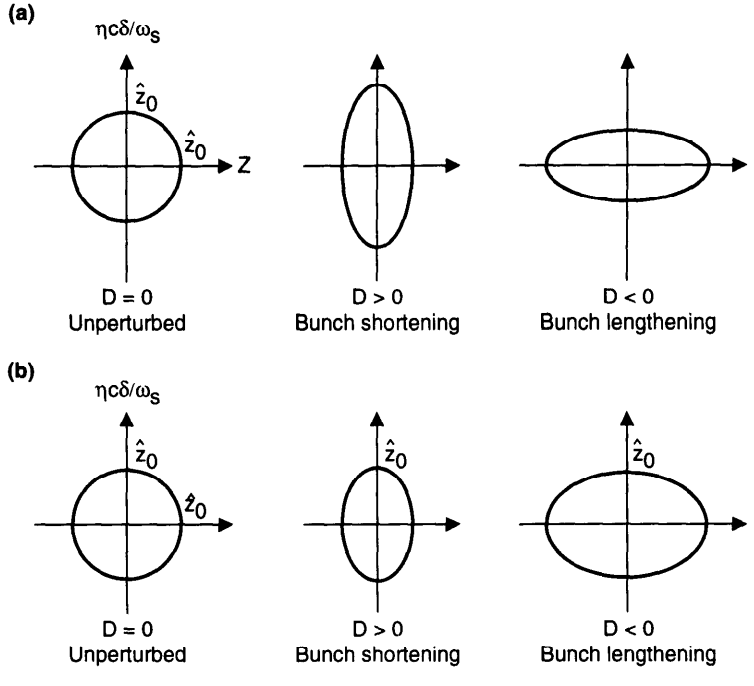

Figure 6.5. (a) The unperturbed and the potential-well distorted beam distributions in phase space for model (6.37) with the wake function (6.33). (b) Same as (a), but for the model (6.44). The phase space area is held fixed in (a). The maximum extent of δ is held fixed in (b).

[17]A. Hoffman, *Frontiers of Particle Beams*, Lecture Notes in Phys., **296**, Springer-Verlag, 1986, p. 99.

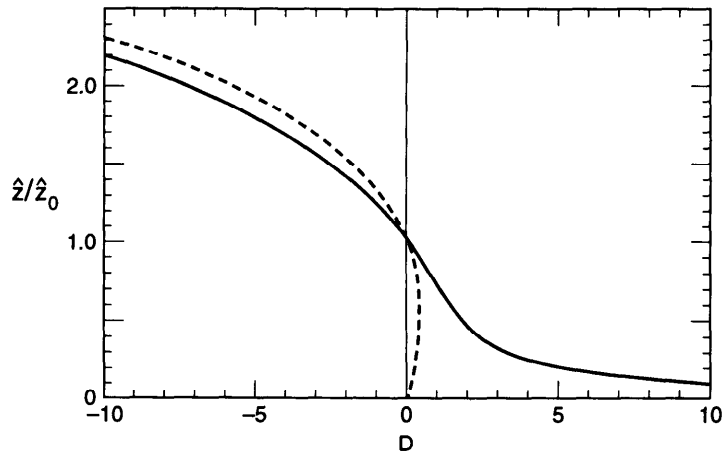

Figure 6.6. Bunch length $\hat{z}/\hat{z}_0$ as a function of wake strength D for two models. The solid curve is the solution to Eq. (6.43). The dashed curve is the solution to Eq. (6.45). There is no physical solution to Eq. (6.45) when $D > 2/3^{3/2}$.

In the previous model, the beam area in phase space is kept constant as the beam intensity is varied. As we have just seen, this leads to a fourth order algebraic equation for the parabolic bunch length. The condition of constant phase space area applies to a proton beam when the accelerator operator carefully matches the injected beam (a different beam intensity requires a different matching) to the distorted potential well so that there is no increase in emittance.

As mentioned, for an electron beam, the stationary distribution has to assume a Gaussian form (6.30–6.32), and its δ-distribution is unperturbed by the potential-well distortion. However, to obtain a qualitative illustration of potential-well distortion of an electron beam, one could compromise the requirement of a Gaussian distribution and modify Eq. (6.37) slightly to obtain

$$\psi(z,\delta) = \begin{cases} \dfrac{3N\eta c\sqrt{\kappa}}{2\pi\omega_s\hat{z}_0^3}\sqrt{\hat{z}_0^2 - \left(\dfrac{\eta c}{\omega_s}\delta\right)^2 - \kappa z^2} & \text{if } \left(\dfrac{\eta c}{\omega_s}\delta\right)^2 + \kappa z^2 < \hat{z}_0^2, \\ 0 & \text{otherwise.} \end{cases} \tag{6.44}$$

The distribution (6.44) maintains a constant spread in δ, while the bunch length varies with the beam intensity.

The line density $\rho(z)$ is still given by Eq. (6.38) with the total bunch length $2\hat{z}_0/\sqrt{\kappa}$. The total spread in δ is equal to $2\hat{z}_0\omega_s/|\eta|c$, independent of the beam intensity. The Hamiltonian, which involves the line density $\rho(z)$, is still

given by Eq. (6.39). Following a procedure like the one in the previous model, we obtain a self-consistency condition that leads to a cubic equation for $\hat{z}/\hat{z}_0$,

$$\left(\frac{\hat{z}}{\hat{z}_0}\right)^3 - \frac{\hat{z}}{\hat{z}_0} + D = 0, \tag{6.45}$$

where D is given in Eq. (6.40).

Again, $\hat{z} = \hat{z}_0$ when $N = 0$, and the bunch lengthens or shortens as $D < 0$ or $D > 0$. The phase space distribution of this beam is illustrated in Figure 6.5(b). Bunch length as a function of wake strength D is shown in Figure 6.6 as the dashed curve. One difference from the model (6.37) is that the model (6.44) does not allow a stationary solution for $D > 2/3^{3/2}$. At $D = 2/3^{3/2}$, the bunch assumes a length of $\hat{z}_0/\sqrt{3}$. In the region $D > 2/3^{3/2}$, the beam cannot maintain an unperturbed δ-spread in its stationary state. A similar observation is made in Exercise 6.4. See also the discussion following Eq. (6.160).

Exercise 6.4

(a) For the wake (6.33), show that the potential-well distorted beam distribution in the Gaussian form (6.31) satisfies

$$f(z) = f(0)e^{-z^2/2\sigma_z^2}, \tag{6.46}$$

where $f(z) = \alpha\rho(z)e^{-\alpha\rho(z)}$ with $\alpha = r_0 S/\eta\sigma_\delta^2\gamma C$.

(b) Given α, find $\rho(z)$ numerically as a function of $N = \int_{-\infty}^{\infty} dz\,\rho(z)$. Is there always a solution for any value of N? Figure 6.7 gives the result. Give an approximate expression for the bunch length when $|\alpha| \ll 1$.

(c) Show that the bunch lengthens if $\alpha < 0$, and shortens if $\alpha > 0$. Give a physical reason why this is so. Show that $\rho(z) < 1/\alpha$ for all z if $\alpha > 0$.

(d) Repeat the study for the wake $W_0'(z) = S\delta(z)$. Observe that in this case there is a shift of the beam centroid, which is absent in the previous case. Explain the physical origin of this shift.

Exercise 6.5 For the wake $W_0'(z) = S\delta(z)$, or equivalently a purely resistive impedance $Z_0^{\parallel} = S/c$, show that a closed form solution for the Gaussian form (6.31) is given by[18]

$$\rho(z) = \frac{\sqrt{2/\pi}\,e^{-z^2/2\sigma_z^2}}{\alpha\sigma_z\left[\coth(\alpha N/2) - \operatorname{erf}\left(z/\sqrt{2}\,\sigma_z\right)\right]}, \tag{6.47}$$

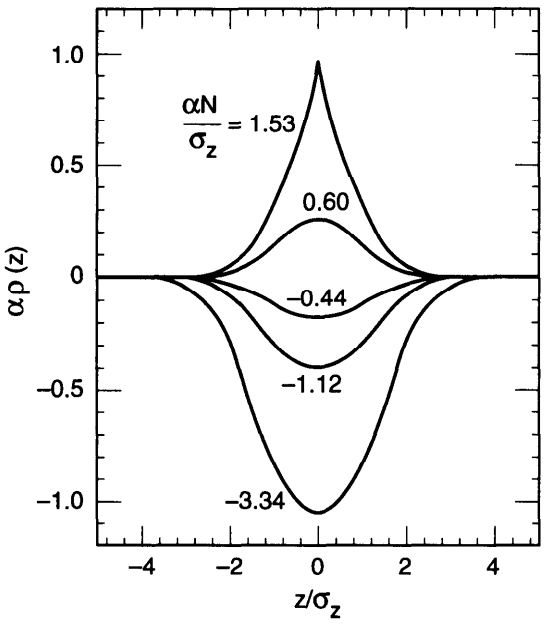

Figure 6.7. A Gaussian beam potential well distorted by the wake (6.33). The graph shows $\alpha\rho(z)$ as a function of z/σ_z for five values of $\alpha N/\sigma_z$, where α is defined after Eq. (6.46). The bunch lengthens if $\alpha < 0$, and shortens if $\alpha > 0$. There is no solution if $\alpha\rho(0) > 1$, corresponding to $\alpha N/\sigma_z > 1.53$.

where $\mathrm{erf}(x) = (2/\sqrt{\pi})\int_0^x e^{-t^2}\,dt$ is the error function, $\sigma_z = |\eta| c\sigma_\delta/\omega_s$, and $\alpha = r_0 S/\eta\sigma_\delta^2\gamma C$. Show that for a weak beam with $|\alpha N| \lesssim 1$, the peak beam density occurs at

$$z \approx \frac{\alpha N}{\sqrt{2\pi}}\sigma_z. \tag{6.48}$$

This peak location moves forward above transition and backward below transition as the beam intensity increases. Figure 6.8 shows the bunch shape for various beam intensities. Does a Gaussian form solution exist for any beam intensity?

Exercise 6.6

(a) Consider the following ansatz distribution for a proton beam:

$$\psi(z,\delta) = \frac{N\eta c}{2\pi\omega_s\hat{z}_0}\frac{1}{\sqrt{\hat{z}_0^2 - \frac{1}{\kappa}\left(\frac{\eta c}{\omega_s}\delta\right)^2 - \kappa(z-\bar{z})^2}}, \tag{6.49}$$

[18]A. G. Ruggiero, IEEE Trans. Nucl. Sci. **NS-24**, 1205 (1977).

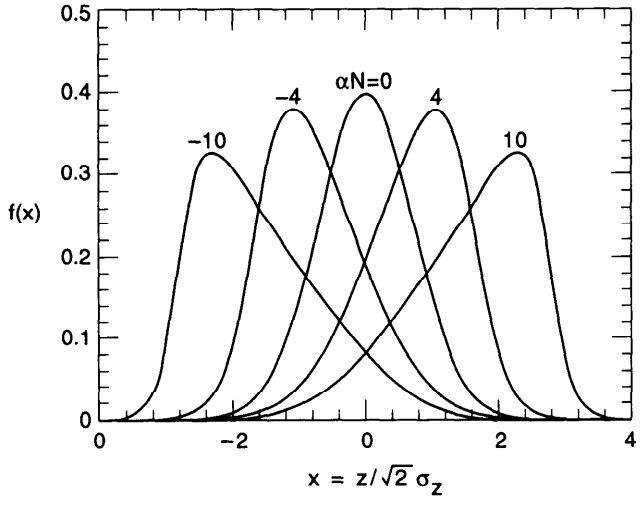

Figure 6.8. Bunch shape for different beam intensities according to Eq. (6.47), where $\rho(z) = Nf(x)/\sigma_z$ and $x = z/\sqrt{2}\sigma_z$. The $\alpha N = 0$ case is Gaussian. The beam peak density is located approximately according to Eq. (6.48). Cases with $\alpha N > 0$ are above transition; those with $\alpha N < 0$ are below transition. The head of the bunch is toward the right.

where κ parametrizes the potential-well distortion and $\bar{z}$ gives the bunch centroid shift due to the parasitic beam loss. This beam has a uniform distribution in z. For a constant wake function $W_0'(z < 0) = -W_0$, show that a self-consistent condition gives,

$$\left(\frac{\hat{z}}{\hat{z}_0}\right)^4 - D\left(\frac{\hat{z}}{\hat{z}_0}\right)^3 - 1 = 0, \tag{6.50}$$

where

$$D = \frac{Nr_0\eta c^2 W_0}{2\omega_s^2 \gamma C \hat{z}_0}. \tag{6.51}$$

The same self-consistency condition also gives the bunch centroid shift

$$\bar{z} = -D\hat{z}_0. \tag{6.52}$$

Above transition, $D > 0$, the bunch centroid shifts forward and the bunch lengthens. Below transition, the opposite occurs.

(b) Repeat (a) for electrons. Show that Eq. (6.52) still holds, but Eq. (6.50) becomes

$$\left(\frac{\hat{z}}{\hat{z}_0}\right)^2 - D\left(\frac{\hat{z}}{\hat{z}_0}\right) - 1 = 0 \quad \text{or} \quad \frac{\hat{z}}{\hat{z}_0} = \sqrt{1 + \frac{D^2}{4}} + \frac{D}{2}. \tag{6.53}$$

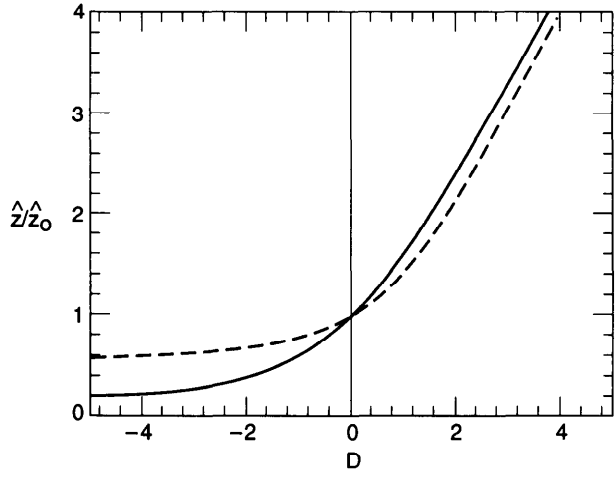

Figure 6.9. Bunch length versus beam intensity for the models (6.50) (dashed curve) and (6.53) (solid curve).

Figure 6.9 gives the bunch length dependence on the strength parameter D for cases (6.50) and (6.53).

(c) Repeat (a) and (b) for the wake function $W_0'(z) = S\delta(z)$ as in Exercise 6.5. Does the bunch shape distort? Explain the result obtained. Show that the bunch centroid shifts to the location

$$\bar{z} = \frac{Nr_0\eta c^2 S}{2\omega_s^2 \gamma C \hat{z}_0}. \tag{6.54}$$

The synchrotron frequency of single-particle motion in the potential well can be derived from the potential-well distorted Hamiltonian (6.39). For both models (6.37) and (6.44), the incoherent synchrotron frequency shift $\Delta\omega_s$ satisfies

$$\left(\frac{\omega_s + \Delta\omega_s}{\omega_s}\right)^2 = 1 + \frac{3Nr_0\eta c^2 S}{2\omega_s^2 \gamma C \hat{z}^3}. \tag{6.55}$$

For small frequency shifts, we have

$$\Delta\omega_s \approx \frac{3Nr_0\eta c^2 S}{4\omega_s \gamma C \hat{z}^3}. \tag{6.56}$$

For the space charge wake, S is given by Eq. (6.36); Eq. (6.56) reproduces Eq. (1.48) obtained in Chapter 1.

Consider the numerical example that followed Eq. (1.48) for a 1 GeV proton synchrotron with $N = 10^{10}$, $C/2\pi = 60$ m, $b = 5$ cm, $a = 0.38$ cm, $\eta = -0.45$, and $\nu_s = 0.04$. We find $S = 1100$ m and $D = -0.83(\hat{z}/\hat{z}_0)^3$. The bunch lengthens because $D < 0$. If we further assume the model (6.37) with unperturbed bunch length $\hat{z}_0 = 0.30$ m,[19] we find a lengthened bunch with $\hat{z} = 0.47$ m. Equation (6.55) then predicts a perturbed synchrotron tune of $\nu_s + \Delta\nu_s = 0.016$.

Equation (6.55) is established by combining Eqs. (6.3), (6.20), and (6.39). Instead of using Eq. (6.39), one may repeat the calculation using the more general Hamiltonian (6.29). By Taylor expanding the Hamiltonian to second order in z, one finds the perturbed synchrotron frequency

$$\Delta\omega_s \approx -\frac{\eta c^2 r_0}{2\omega_s \gamma C}\int_0^\infty dz'\,\rho(z')W_0''(-z'), \tag{6.57}$$

where W_0'' is the second derivative of W_0. In terms of the impedance, we have

$$\Delta\omega_s \approx -i\frac{\eta c^2 r_0}{4\pi\omega_s \gamma C}\int_{-\infty}^\infty d\omega\,\tilde{\rho}(\omega)\frac{\omega}{c}Z_0^{\parallel}(\omega). \tag{6.58}$$

If the process is repeated taking into account the wake fields for multiple turns, the result becomes

$$\Delta\omega_s \approx -i\frac{\eta c^2 r_0}{2\omega_s \gamma C^2}\sum_{p=-\infty}^{\infty}\tilde{\rho}(p\omega_0)p\omega_0 Z_0^{\parallel}(p\omega_0). \tag{6.59}$$

For a point bunch with $\tilde{\rho} = N$, we have reproduced the potential-well distortion term (the first term on the right hand side) of Eq. (4.9) obtained for the one-particle model of Robinson instability.

When $\Delta\omega_s > 0$, the bunch length shortens due to the tighter focusing. Similarly, $\Delta\omega_s < 0$ means the bunch lengthens. From Eq. (6.58), the sign of $\Delta\omega_s$ is determined by the overlap integral of the bunch spectrum $\tilde{\rho}(\omega)$ and the function $\omega\,\mathrm{Im}\,Z_0^{\parallel}(\omega)$. Consider a resonator impedance; $\omega\,\mathrm{Im}\,Z_0^{\parallel}(\omega)$ is negative at low frequencies (inductive) and positive at high frequencies (capacitive). For a long bunch, the spectrum is limited to low frequencies; the overlap integral gives a $\Delta\omega_s$ that has the same sign as $-\eta$, according to Eq. (6.58). Conversely, for a short bunch, $\Delta\omega_s$ tends to have the same sign as η. It follows that, above transition, a long bunch tends to become longer and a short bunch tends to become shorter. Below transition, the tendencies are reversed.

[19] We do not assume model (6.44), because this is for a proton beam.

Exercise 6.7 Find the incoherent synchrotron tune shift due to a resonator impedance (2.82). Substitute the Gaussian bunch spectrum (2.193) to show that

$$\Delta\nu_s = \frac{\Delta\omega_s}{\omega_0} \approx \sqrt{\frac{\pi}{2}} \frac{Nr_0\eta c^2}{4\pi^2\gamma\omega_s\sigma_z^2} \frac{R_S}{Q} \begin{cases} -c/\omega_R\sigma_z, & \text{long bunch,} \\ \omega_R\sigma_z/c, & \text{short bunch,} \end{cases} \tag{6.60}$$

where the long and short bunches are compared with c/ω_R. Above transition, a long bunch lengthens and a short bunch shortens. Perform the integration numerically for various parameter values. Show that the bunch keeps its length when $\sigma_z \approx 1.2c/\omega_R$ if $Q = 1$.

6.3 LINEARIZATION OF THE VLASOV EQUATION

On top of the static potential-well distorted bunch shape, particles in a beam execute accidental collective motions. Although they may have only infinitesimal amplitudes initially, these motions grow exponentially under unfavorable conditions. When this happens, the beam is unstable. Some of these instabilities were examined in Chapter 4, using simplified beam models. In this and the following sections, the Vlasov technique will be applied to treat this subject. The approach basically follows Sacherer's. The result contains all the instabilities of Chapter 4 as special cases.

Consider again a thread beam as we did in the previous section. At first, let us switch off the wake field and let the beam have an initial phase-space distribution ψ_0. Being an equilibrium distribution, ψ_0 is only a function of r, i.e.,

$$\psi_0 = \psi_0(r), \tag{6.61}$$

where we have introduced the polar coordinates

$$\begin{aligned} z &= r\cos\phi, \\ \frac{\eta c}{\omega_s}\delta &= r\sin\phi. \end{aligned} \tag{6.62}$$

Note that r is related to the unperturbed Hamiltonian by $H = \omega_s r^2/2$, and Eq. (6.61) follows from the fact that the stationary distribution must be a function of the Hamiltonian. The coordinate system is indicated in Figure 6.10.

Now we turn on the wake fields and suppose there is a disturbance in the distribution, so that now we have

$$\psi(r, \phi, s) = \psi_0(r) + \psi_1(r, \phi)e^{-i\Omega s/c}. \tag{6.63}$$

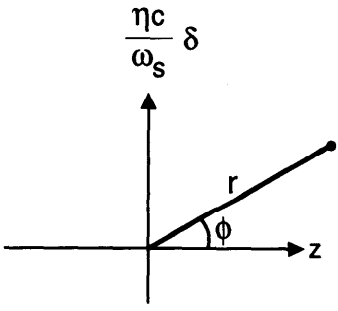

Figure 6.10. Coordinate system in the longitudinal phase space.

We have assumed the disturbance has a single frequency Ω, i.e., it contains only one single mode of oscillation. We will consider the disturbance to be small.

The mode frequency Ω and the mode distribution ψ_1 are not arbitrary. The disturbance ψ_1 first generates a wake field. Being an oscillation mode, the additional disturbance in the beam distribution caused by this wake field must have the same pattern as the original disturbance ψ_1. The beam-wake system, therefore, has to be solved self-consistently. As a result, only a discrete set of values are possible for Ω, and associated with each value of Ω there is a well-defined distribution ψ_1. Below, we will show how to obtain these solutions for Ω and ψ_1 using the Vlasov technique.

If we project ψ_1 onto the z-axis, we obtain the longitudinal distribution

$$\rho_1(z)e^{-i\Omega s/c} = \int_{-\infty}^{\infty} d\delta\, \psi_1(r,\phi)e^{-i\Omega s/c}. \tag{6.64}$$

This $\rho_1(z)$ is the distribution observed at a fixed location in the accelerator; it is the distribution that a localized impedance responds to, and is slightly different from the snapshot beam disturbance observed as a function of z at a given time. See Figure 6.11. The snapshot distribution is given by

$$\rho_1(z)|_{\text{snapshot}} = \rho_1(z)e^{-i\Omega z/c}. \tag{6.65}$$

One revolution before, the beam observed at the same location has a distribution $\rho_1(z)\exp[-i\Omega(s/c - T_0)]$, with T_0 the revolution period.

The wake field excited by ρ_1 produces a retarding voltage. The voltage seen by a particle at z (relative to the bunch center) as it passes by the location s in the accelerator is

$$V(z,s) = e\int_{-\infty}^{\infty} dz' \sum_{k=-\infty}^{\infty} \rho_1(z')e^{-i\Omega[(s/c)-kT_0]}W_0'(z - z' - kcT_0). \tag{6.66}$$

In writing down this expression, we have included the multiturn wake fields and have used the causality property that $W_0'(z) = 0$ if $z > 0$.

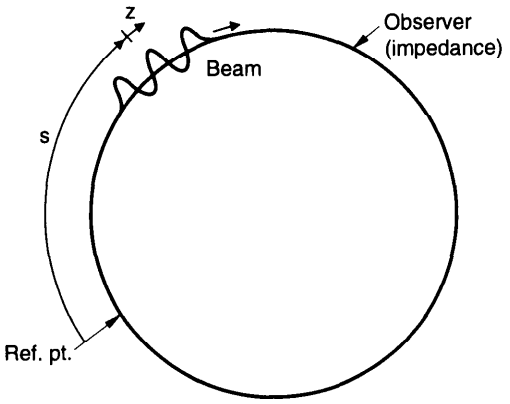

Figure 6.11. Snapshot of a disturbance on the beam in a circular accelerator. The signal seen by a localized impedance is slightly different. The disturbance shown is that of an $l = 4$ mode.

As we anticipate solving the problem in the frequency domain, we will now introduce the Fourier transform of ρ_1 according to Eq. (2.104) and the impedance $Z_0^{\parallel}(\omega)$ according to Eq. (2.72). Equation (6.66) then becomes

$$V(z,s) = \frac{e}{T_0} e^{-i\Omega s/c} \sum_{p=-\infty}^{\infty} \tilde{\rho}_1(p\omega_0 + \Omega) e^{i(p\omega_0+\Omega)z/c} Z_0^{\parallel}(p\omega_0 + \Omega), \tag{6.67}$$

where $\omega_0 = 2\pi/T_0$ and we have made use of the identity (2.210).

Note that the snapshot frequency spectrum is related to $\tilde{\rho}_1(\omega)$ by

$$\tilde{\rho}_1(\omega)|_{\text{snapshot}} = \tilde{\rho}_1(\omega + \Omega). \tag{6.68}$$

Had we used the snapshot spectrum in Eq. (6.67), the frequency offset in the argument of $\tilde{\rho}_1$ would have dropped out.

Having obtained $V(z,s)$, the Vlasov equation reads

$$\frac{\partial \psi}{\partial s} - \eta\delta \frac{\partial \psi}{\partial z} + \frac{\omega_s^2}{\eta c^2} z \frac{\partial \psi}{\partial \delta} - \frac{e}{T_0 Ec} V(z,s) \frac{\partial \psi}{\partial \delta} = 0, \tag{6.69}$$

where E is the design energy of the beam particles. The two middle terms can be simplified if we use polar coordinates (6.62), yielding

$$\frac{\partial \psi}{\partial s} + \frac{\omega_s}{c} \frac{\partial \psi}{\partial \phi} - \frac{e}{T_0 Ec} V(z,s) \frac{\partial \psi}{\partial \delta} = 0. \tag{6.70}$$

We now substitute Eqs. (6.63) and (6.67) into the above equation, and linearize it by keeping only the first order terms in ψ_1. Remembering that V

is already first order and that ψ_0 depends only on r, we obtain the linearized Vlasov equation

$$-i\Omega\psi_1 + \omega_s\frac{\partial\psi_1}{\partial\phi} - \frac{\eta r_0 c}{\gamma T_0^2\omega_s}\sin\phi\,\psi_0'(r) \times \sum_{p=-\infty}^{\infty}\tilde{\rho}_1(p\omega_0+\Omega)e^{i(p\omega_0+\Omega)z/c}Z_0^{\parallel}(p\omega_0+\Omega) = 0. \quad (6.71)$$

Actually, ψ_0 also produces a wake field, which means V contains a zeroth order term, which has been ignored here. Inclusion of such a term is equivalent to imposing a perturbed potential well on the motion of ψ_1; it is dropped because it it not essential to the illustration of the mechanism of collective beam instabilities. However, the potential-well distortion does contribute to a redefinition of ω_s. As a result, all ω_s's from here on should be regarded as potential-well shifted, as given by Eqs. (6.57–6.59). The coordinates (6.62) are redefined accordingly. The "unperturbed" distribution ψ_0 is thus a function of this redefined, perturbed r.

In the procedure leading to Eq. (6.71), we have linearized with respect to the perturbation ψ_1, not with respect to the impedance or the beam intensity. The impedance and the beam intensity do not have to be small in this linearization procedure. On the other hand, the linearization with respect to ψ_1 poses an important limitation in our analysis. For a given unperturbed distribution $\psi_0(r)$, Eq. (6.71) describes the behavior of an infinitesimal deviation from it. If this deviation grows in time, the beam is unstable; otherwise it is stable. The analysis does not give any information on other unperturbed distributions. Showing the beam is unstable with a certain ψ_0 does not prove the beam is necessarily unstable, because it may stabilize with a different ψ_0. This point will be illustrated further by Figure 6.16.

Having linearized the Vlasov equation, we are now ready to discuss the collective modes of beam motion under the influence of beam-impedance interaction. To do so, we first Fourier expand ψ_1 according to

$$\psi_1(r,\phi) = \sum_{l=-\infty}^{\infty}\alpha_l R_l(r)e^{il\phi}. \quad (6.72)$$

This is possible because ψ_1 must be periodic in ϕ with period 2π. We have used l as the summation index in anticipation that it actually is the longitudinal model index used in Figure 6.1 in the limit of weak beam intensities.

Substituting Eq. (6.72) into Eq. (6.71), we obtain

$$-i\sum_{l'}\alpha_{l'}R_{l'}(r)e^{il'\phi}(\Omega - l'\omega_s) - \frac{\eta r_0 c}{\gamma T_0^2\omega_s}\sin\phi\,\psi_0'(r) \times \sum_{p}\tilde{\rho}_1(\omega')Z_0^{\parallel}(\omega')e^{i(\omega' r/c)\cos\phi} = 0, \quad (6.73)$$

where ω' in the summation over p is an abbreviation for $p\omega_0 + \Omega$. Multiply the equation by $\exp(-il\phi)$ and integrate over ϕ from 0 to 2π, and repeat for all values of l. We obtain an infinite set of equations,

$$-i(\Omega - l\omega_s)\alpha_l R_l(r) + \frac{\eta r_0 c^2}{\gamma T_0^2 \omega_s} l i^l \frac{\psi_0'(r)}{r} \sum_p \tilde{\rho}_1(\omega') \frac{Z_0^{\parallel}(\omega')}{\omega'} J_l\left(\frac{\omega' r}{c}\right) = 0,$$

$$l = 0, \pm 1, \pm 2, \ldots, \quad (6.74)$$

where $J_l(x)$ is the Bessel function. Some properties of the Bessel functions that we will use later in the text are given in Table 6.1.[20] Note the appearance of the quantity $Z_0^{\parallel}(\omega')/\omega'$ in Eq. (6.74).

We still need an expression for $\tilde{\rho}_1(\omega')$ in Eq. (6.74). This is found below:

$$\begin{aligned}
\tilde{\rho}_1(\omega') &= \int_{-\infty}^{\infty} dz\, e^{-i\omega' z/c} \rho_1(z) \\
&= \int_{-\infty}^{\infty} dz \int_{-\infty}^{\infty} d\delta\, e^{-i\omega' z/c} \psi_1(r, \phi) \\
&= \frac{\omega_s}{\eta c} \int_0^{\infty} r\, dr \int_0^{2\pi} d\phi \exp\left(-i \frac{\omega' r}{c} \cos\phi\right) \sum_{l'} \alpha_{l'} R_{l'}(r) e^{il'\phi} \\
&= \frac{2\pi\omega_s}{\eta c} \sum_{l'} \int_0^{\infty} r\, dr\, \alpha_{l'} R_{l'}(r) i^{-l'} J_{l'}\left(\frac{\omega' r}{c}\right). \qquad (6.75)
\end{aligned}$$

When Eq. (6.75) is substituted into Eq. (6.74), we obtain the integral equation

$$\begin{aligned}
(\Omega - l\omega_s)\alpha_l R_l(r) = &-i \frac{2\pi r_0 c}{\gamma T_0^2} l \frac{\psi_0'(r)}{r} \sum_{l'=-\infty}^{\infty} \int_0^{\infty} r'\, dr'\, \alpha_{l'} R_{l'}(r') i^{l-l'} \\
&\times \sum_{p=-\infty}^{\infty} \frac{Z_0^{\parallel}(\omega')}{\omega'} J_l\left(\frac{\omega' r}{c}\right) J_{l'}\left(\frac{\omega' r'}{c}\right). \qquad (6.76)
\end{aligned}$$

The fact that Bessel functions appear prominently in Eq. (6.76) has been addressed in Eq. (4.19). Given the impedance $Z_0^{\parallel}$ and the unperturbed distribution ψ_0, we have to find the $R_l(r)$'s and α_l's to satisfy Eq. (6.76). This is obviously not easy to do in general. Below we will first proceed by choosing a simplified model of ψ_0, namely,

$$\psi_0(r) = \begin{cases} 0 & \text{if} \quad r > \hat{z}, \\ \dfrac{N\eta c}{\pi \hat{z}^2 \omega_s} & \text{if} \quad r < \hat{z}. \end{cases} \qquad (6.77)$$

[20] I. S. Gradshteyn and I. M. Ryzhik, *Table of Integrals, Series and Products*, Academic Press, 1980.

Table 6.1. Some properties of Bessel functions.

$$\frac{1}{2\pi}\int_0^{2\pi} d\phi\, e^{il\phi - ix\cos\phi} = i^{-l}J_l(x)$$

$$e^{-ix\cos\phi} = \sum_{l=-\infty}^{\infty} i^{-l}J_l(x)e^{il\phi}$$

$$J_l(-x) = (-1)^l J_l(x) = J_{-l}(x)$$

$$J_l(x) \approx \frac{1}{l!}\left(\frac{x}{2}\right)^l \qquad \text{for} \quad |x| \ll 1$$

$$J_l(0) = \delta_{l0}$$

$$\sum_{l=-\infty}^{\infty} J_l^2(x) = 1$$

$$\frac{1}{2\pi}\int_0^{2\pi} d\phi \sin\phi\, e^{-il\phi + ix\cos\phi} = -i^l\frac{l}{x}J_l(x)$$

$$J_l'(x) = \tfrac{1}{2}[J_{l-1}(x) - J_{l+1}(x)]$$

$$\int_0^{\infty}\frac{dx}{x}J_{\nu+2l}(x)J_{\nu+2l'}(x) = \frac{\delta_{ll'}}{2(\nu+2l)} \qquad (\nu > 0)$$

$$\int_0^{\infty} x\,dx\,J_l(kx)J_l(k'x) = \frac{1}{k}\delta(k-k')$$

$$\int_0^{\infty} x^{-\alpha}\,dx\,J_\mu(x)J_\nu(x) = \frac{\Gamma(\alpha)\Gamma[\frac{1}{2}(\mu+\nu+1-\alpha)]}{2^\alpha\Gamma[\frac{1}{2}(-\mu+\nu+1+\alpha)]\Gamma[\frac{1}{2}(\mu+\nu+1+\alpha)]\Gamma[\frac{1}{2}(\mu-\nu+1+\alpha)]}$$

$$(\mu+\nu+1 > \alpha > 0)$$

$$\int_{-\infty}^{\infty} dx\, e^{iyx}J_l(x) = \frac{2i^l}{\sqrt{1-y^2}}\cos(l\cos^{-1}y)H(1-|y|)$$

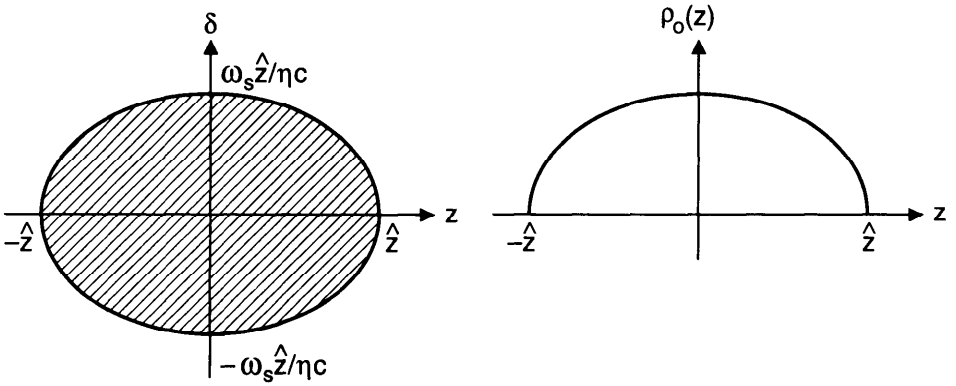

Figure 6.12. Phase space distribution and longitudinal distribution of a water-bag beam. For this distribution, $\rho_0(z) = 2N\sqrt{\hat{z}^2 - z^2}\,/\,\pi\hat{z}^2$ and $\sigma_z = \hat{z}\,/\,2$.

The impedance, on the other hand, is left general. The case of general $\psi_0(r)$ will be treated in the next section.

The distribution (6.77) is called the *water-bag model*. Its phase space distribution and projection onto the z-axis are shown in Figure 6.12. The distribution is normalized so that

$$\int_{-\infty}^{\infty} d\delta \int_{-\infty}^{\infty} dz\, \psi_0 = \frac{\omega_s}{\eta c} \int_0^{\infty} 2\pi r\, dr\, \psi_0 = N. \tag{6.78}$$

Any perturbation on a water-bag beam will have to occur around the edge of the bag, i.e., around $r = \hat{z}$. As a result, all R_l's are δ-functions,

$$R_l(r) \propto \delta(r - \hat{z}). \tag{6.79}$$

The result (6.79) also follows from Eq. (6.76) by inspection if we note that $\psi_0' \propto \delta(r - \hat{z})$. Having obtained Eq. (6.79), the integral equation (6.76) reduces to a set of equations for the coefficients α_l:

$$(\Omega - l'\omega_s)\alpha_{l'} = i\frac{2Nr_0\eta c^2}{\gamma T_0^2 \omega_s \hat{z}^2} l' \sum_{l''} \alpha_{l''} i^{l'-l''} \sum_p \frac{Z_0^{\parallel}(\omega')}{\omega'} J_{l'}\left(\frac{\omega'\hat{z}}{c}\right) J_{l''}\left(\frac{\omega'\hat{z}}{c}\right),$$

$$l' = 0, \pm 1, \pm 2, \ldots . \tag{6.80}$$

We are finally ready to discuss modes. There are infinite number of solutions to Eq. (6.80), each specifying a collective mode. Equation (6.80) is written in terms of running indices l' and l'', reserving l for the mode index. First note that when $N = 0$, i.e., in the zero-intensity limit, the solution to

Eq. (6.80) for the lth mode is

$$\alpha_{l'}^{(l)} = \delta_{ll'}, \qquad l' = 0, \pm 1, \pm 2, \ldots,$$
$$\Omega^{(l)} = l\omega_s, \tag{6.81}$$

where $\delta_{ll'} = 1$ if $l = l'$, and 0 if $l \neq l'$. The lth mode therefore is described by

$$\psi_1^{(l)} e^{-i\Omega s/c} \propto \underbrace{\delta(r - \hat{z}) e^{il\phi}}_{\text{long. dist.}} \underbrace{e^{-il\omega_s s/c}}_{\text{time dep.}}. \tag{6.82}$$

These are the modes illustrated in Figure 6.1(a). The phase space distributions, as well as their projections onto the z-axis, without the time dependences, are drawn in Figure 6.13.

Observing at a fixed location, a pickup electrode (or an impedance) will receive a signal that contains an unperturbed contribution from $\rho_0(z)$, superimposed on a contribution from $\rho_1^{(l)}(z)$ if the beam is executing the lth mode. Figure 6.14 displays the signals as the beam traverses the electrode in several different passages. The signals show l nodes in the z-distribution if the beam is executing the lth mode.

In case the beam intensity is nonzero but still weak, we can find the lth mode frequency by substituting the zeroth order solution (6.81) into the right hand side of Eq. (6.80) to obtain

$$\Omega^{(l)} - l\omega_s = i\frac{2Nr_0\eta c^2}{\gamma T_0^2 \omega_s \hat{z}^2} l \sum_{p=-\infty}^{\infty} \frac{Z_0^{\parallel}(\omega')}{\omega'} J_l^2\left(\frac{\omega'\hat{z}}{c}\right), \tag{6.83}$$

where $\omega' = p\omega_0 + l\omega_s$.

Some results on instabilities at last! Given the impedance, Eq. (6.83) gives the complex mode frequencies for a water-bag beam with weak intensities. In particular, the real part of $\Omega^{(l)}$ gives the mode frequency shift $\Delta\Omega^{(l)}$; the imaginary part gives the instability growth rate $1/\tau^{(l)}$.

One should be careful in obtaining $\Delta\Omega^{(l)}$ from Eq. (6.83), because it does not contain all contributions. A potential-well frequency shift term was dropped when we linearized the Vlasov equation back in Eq. (6.71).

The $l = 0$ mode is a trivial mode with $\Omega^{(0)} = 0$. It describes the potential-well distortion mode addressed in Section 6.2 and is not of much interest here. Take next the $l = 1$ mode for consideration. Let us assume the beam bunch is short enough so that $\omega'\hat{z}/c \ll 1$, i.e., the wake field lasts much longer than the bunch length. Then $J_1(\omega'\hat{z}/c) \approx \omega'\hat{z}/2c$, and we have recovered from the imaginary part of Eq. (6.83) the Robinson growth rate, Eq. (4.10). The real part of Eq. (6.83) reproduces the second term of the

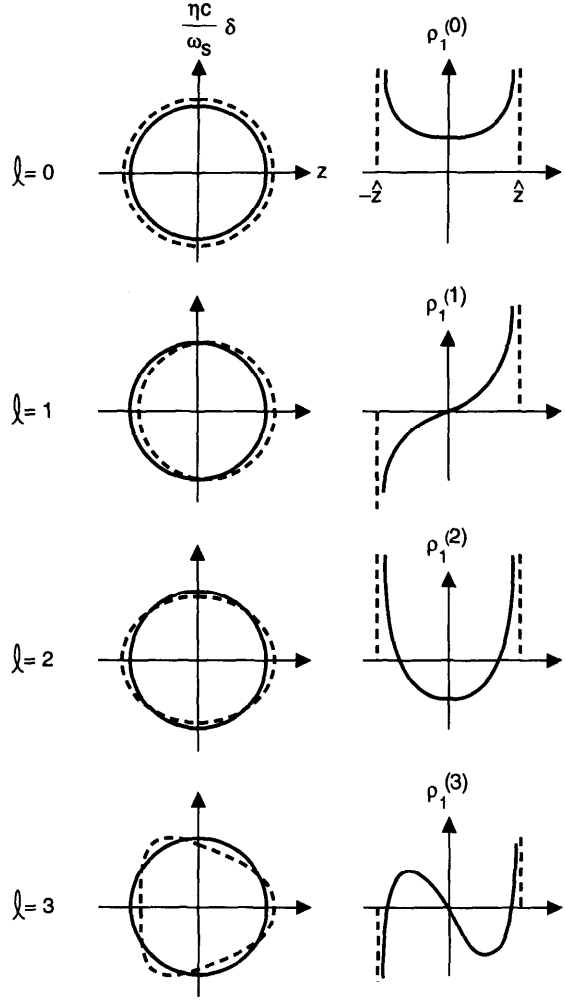

Figure 6.13. The phase space distributions (6.82) and corresponding longitudinal projections $\rho_1^{(l)} \propto \cos(l \cos^{-1} x) / \sqrt{1-x^2}$, where $x = z/\hat{z}$ [see Exercise 6.8(a)], for the modes $l = 0, 1, 2, 3$. A water-bag beam with vanishing intensity is assumed. In the phase space distributions on the left, solid curves (circles) are the unperturbed water bag; dashed curves are the perturbed distributions. The $l = 0$ mode as shown cannot be excited due to charge conservation, although a static mode, corresponding to a potential-well distortion, does exist.

mode frequency shift (4.9). The first term of Eq. (4.9) comes from the potential-well distortion and was addressed in Eq. (6.59).

On the other hand, Eq. (6.83) is much more general than the one-particle results (4.9) and (4.10). It applies to higher order modes $l > 1$ and arbitrary bunch length $\hat{z}$. In particular, when it is applied to the $l > 1$ cases, a sharp resonator impedance yields Robinson stability criteria for the $l > 1$ beam

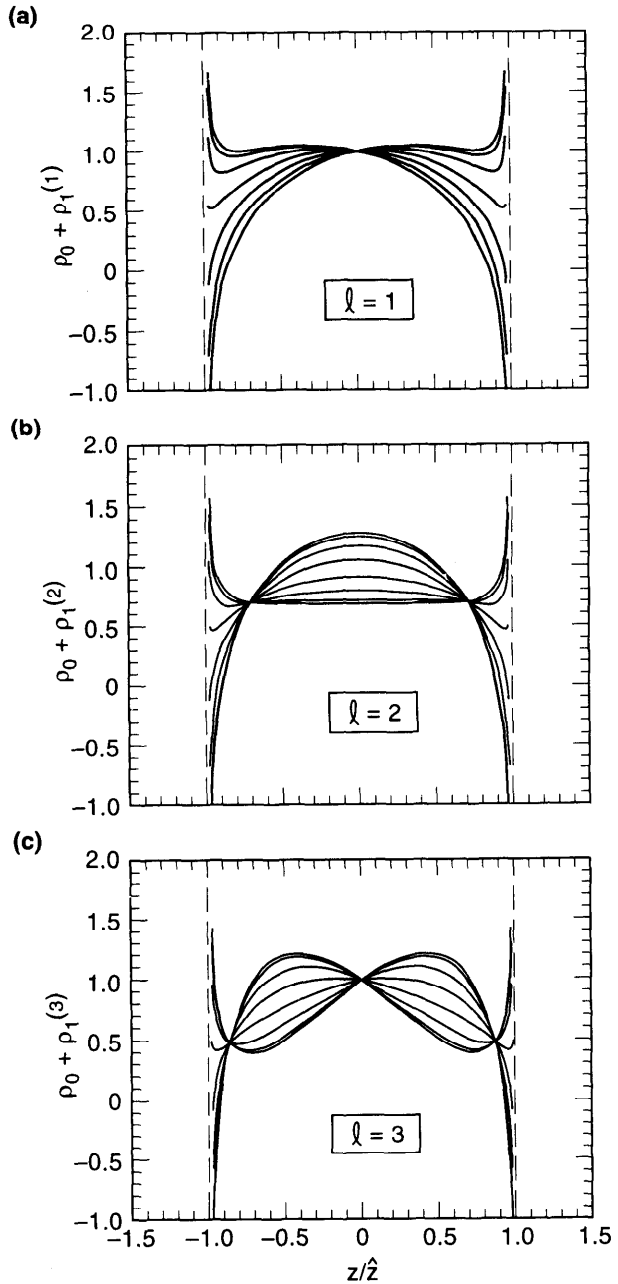

Figure 6.14. Signal received by an electrode when the beam is executing the lth longitudinal mode. Signals of several beam passages are superimposed for modes (a) $l = 1$, (b) $l = 2$, and (c) $l = 3$. The number of nodes is equal to l. The divergences at the bunch edge $z = \pm\hat{z}$ are an artifact of the water-bag model.

oscillation modes. Considering the fundamental rf mode at frequency close to $h\omega_0$, the Robinson growth rate for the lth beam mode is found to be

$$\frac{1}{\tau^{(l)}} = \frac{l}{(l!)^2}\left(\frac{h\omega_0\hat{z}}{2c}\right)^{2l-2}\frac{Nr_0\eta h\omega_0}{2\gamma T_0^2\omega_s} \times\left[\operatorname{Re} Z_0^{\parallel}(h\omega_0 + l\omega_s) - \operatorname{Re} Z_0^{\parallel}(h\omega_0 - l\omega_s)\right]. \tag{6.84}$$

For $l = 1$, this reduces to the familiar result (4.20). It follows from Eq. (6.84) that the Robinson stability requirement for the higher ($l > 1$) modes is the same as for $l = 1$: the rf frequency ω_R must be detuned below (above) $h\omega_0$ when operated above (below) transition. Higher order Robinson growth rates, however, drop off rapidly with increasing mode index l if the bunch length is much less than the rf wavelength, which is typically the case.

Exercise 6.8

(a) Show that for a water-bag beam,

$$\tilde{\rho}_0(\omega) = 2N\frac{c}{\omega\hat{z}}J_1\left(\frac{\omega\hat{z}}{c}\right),$$
$$\tilde{\rho}_1^{(l)}(\omega) \propto J_l\left(\frac{\omega\hat{z}}{c}\right), \tag{6.85}$$
$$\rho_1^{(l)}(z) \propto \frac{1}{\sqrt{\hat{z}^2 - z^2}}\cos\left[l\cos^{-1}\left(\frac{z}{\hat{z}}\right)\right].$$

Figure 6.15 shows the frequency spectra $\tilde{\rho}_0(\omega)$ and $\tilde{\rho}_1^{(l)}(\omega)$ of the various modes. The density $\rho_1^{(l)}(z)$ was shown in Figure 6.13. As shown in Figure 6.15, the spectrum shifts towards higher frequencies as the mode index l increases.

(b) Using Eq. (6.59), show that the synchrotron frequency shift due to the potential well for a water-bag beam is

$$\Delta\omega_s = \frac{Nr_0\eta c}{\gamma T_0^2\omega_s\hat{z}}\sum_{p=-\infty}^{\infty}J_1\left(\frac{p\omega_0\hat{z}}{c}\right)\operatorname{Im} Z_0^{\parallel}(p\omega_0). \tag{6.86}$$

(c) Show that in case the wake field is much longer than the bunch length but much shorter than the accelerator circumference, the potential-well term, Eq. (6.86), and the dynamics term, the real part of Eq. (6.83), cancel each other for the $l = 1$ mode. The dipole mode frequency $\Omega^{(l=1)}$ therefore does not shift. This property was reflected in Figure 6.2. Physically, this is because as the bunch executes a rigid longitudinal

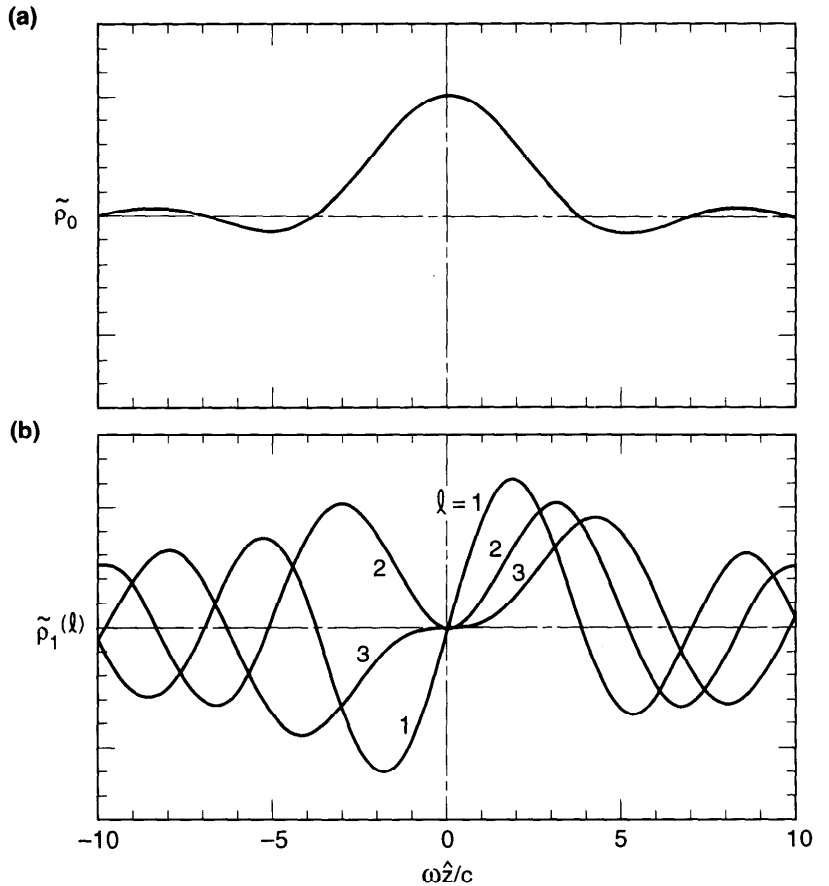

Figure 6.15. (a) Fourier spectrum $\tilde{\rho}_0(\omega)$ of the unperturbed bunch shape for a water-bag beam. (b) Fourier spectra $\tilde{\rho}_1^{(l)}(\omega)$ of the lowest three collective modes $l = 1, 2, 3$.

dipole motion, the wake field, and therefore the potential well, moves with it. The motion of the beam as a whole is not affected by the wake field. The net result is that the collective dipole mode oscillates at the unperturbed synchrotron frequency up to moderate beam intensities.

Exercise 6.9 Apply Eq. (6.83) to calculate the complex mode frequencies of a water-bag beam of weak intensity in the presence of a broad-band resonator impedance. Ignore the multiturn and the potential-well distortion effects. Obtain limits for $\omega_R \hat{z}/c \gg 1$ and $\ll 1$. Use the result to estimate the synchrotron mode frequency shifts for mode l in the accelerator of Figure 2.19. Note that the incoherent synchrotron frequency shift (for a Gaussian beam) was found in Exercise 6.7. What happens if Eq. (6.83) is applied to the space charge impedance?

Exercise 6.10 Equation (6.76) has a frequency-domain counterpart. Define

$$\tilde{\rho}_1^{(l)}(p) = \frac{2\pi\omega_s}{\eta c} i^{-l} \int_0^\infty r\,dr\, R_l(r) J_l\left(\frac{p\omega_0 + \Omega}{c} r\right) \tag{6.87}$$

so that Eq. (6.75) reads $\tilde{\rho}_1(\omega') = \sum_l \alpha_l \tilde{\rho}_1^{(l)}(p)$.

(a) Use Eq. (6.76) to show that

$$(\Omega - l\omega_s)\alpha_l \tilde{\rho}_1^{(l)}(q) = -i \frac{2\pi r_0 c}{\gamma T_0^2} l \sum_{l'} \alpha_{l'} \times \sum_p \frac{Z_0^{\parallel}(p\omega_0 + \Omega)}{p\omega_0 + \Omega} \tilde{\rho}_1^{(l')}(p) F_l(p, q), \tag{6.88}$$

where

$$F_l(p, q) = \int_0^\infty r\,dr\, \frac{\psi_0'(r)}{r} J_l\left(\frac{p\omega_0 + \Omega}{c} r\right) J_l\left(\frac{q\omega_0 + \Omega}{c} r\right). \tag{6.89}$$

(b) The problem is analytically soluble for an arbitrary impedance if $F_l(p, q)$ factorizes so that

$$F_l(p, q) = -T_l(p\omega_0 + \Omega) T_l(q\omega_0 + \Omega). \tag{6.90}$$

Show that the solution to Eq. (6.88) is given by

$$\tilde{\rho}_1^{(l)}(p) \propto i^{-l} T_l(p\omega_0 + \Omega), \tag{6.91}$$

with

$$(\Omega - l\omega_s)\alpha_l = i \frac{2\pi r_0 c}{\gamma T_0^2} l \sum_{l'} \alpha_{l'} i^{l-l'} \times \sum_p \frac{Z_0^{\parallel}(p\omega_0 + \Omega)}{p\omega_0 + \Omega} T_{l'}(p\omega_0 + \Omega) T_l(p\omega_0 + \Omega). \tag{6.92}$$

(c) One factorizable example is that of the water-bag model. Apply the result to the water-bag model to obtain Eqs. (6.79–6.80). Another factorizable example will be given in Eqs. (6.151–6.154).

The Robinson instability described by Eq. (6.84) is an application of Eq. (6.83) to a sharply peaked impedance. It was pointed out in Section 4.1 that a broad-band impedance does not cause instabilities of a one-particle beam.

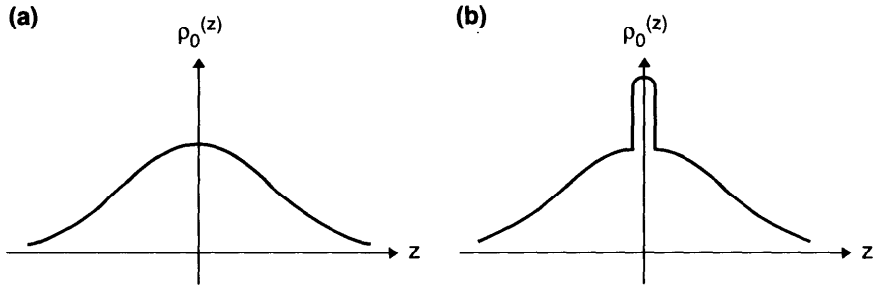

Figure 6.16. Two possible unperturbed beam distributions: (a) is a smooth distribution; (b) has a δ-function spike at the origin. Depending on the impedance, they may have very different stability criteria, but the significance of the difference is rather limited.

This same conclusion can be reached with the more general Eq. (6.83). For a broad-band impedance, the summation over p can be approximated by an integral; the real part of the integral vanishes because $\mathrm{Re}\, Z_0^{\parallel}(\omega')/\omega'$ is an odd function of ω'.

It should be mentioned that the water-bag beam is particularly simple in that one can readily solve for $R_l(r)$ in Eq. (6.79). The price we pay here is that all radial structures are degenerate and some information has been lost. This will be remedied in the next section. However, one must remember another weakness of the present analysis, namely, the stability obtained here depends on the choice of the unperturbed distribution ψ_0. Sketched in Figure 6.16 are two possible unperturbed beam distributions. For an impedance that has a significant high frequency tail, one can imagine a situation in which a beam with distribution (a) is stable, while one with distribution (b) is unstable due to the larger overlap between its spectrum and the impedance. But the significance of the instability of distribution (b) is rather limited, because after losing the particles in the spike, the beam stabilizes.

Another important limitation of the linearized Vlasov equation is that it is applicable only at the onset of the instability. Once the instability starts to grow, it no longer applies. In particular, some instabilities may saturate instead of growing indefinitely. Studies of such saturation and of overshoot effects are excluded by the linearized Vlasov treatment and are beyond our present scope.

6.4 RADIAL MODES

So far we have solved the linearized Vlasov equation using a highly idealized water-bag model as the unperturbed distribution ψ_0. For a more realistic distribution, the analysis becomes more involved. In a water-bag model, a

collective mode is described by two mode indices m and l. The index m specifies the transverse behavior of the beam; in the present analysis of longitudinal collective modes, we have $m = 0$. The other index l specifies the *azimuthal* structure of the mode in the longitudinal phase space. In the water-bag model, all perturbation on the beam distribution occurs at the edge of the water bag, $r = \hat{z}$; the azimuthal index l thus completely specifies the longitudinal structure of the mode. For a general distribution, however, the mode has to be specified by two longitudinal indices l and n, where n is an index describing the *radial* structure of the mode in the longitudinal phase space. This complication will be addressed in this section.

In the limit of zero beam intensity, all radial modes with the same azimuthal index l but different radial indices n have the same mode frequency $\Omega = l\omega_s$. As the beam intensity is increased slightly, their frequencies shift away from this unperturbed value and modes with different n's shift differently, thus breaking the degeneracy. For weak beams, these frequency shifts are much smaller than ω_s. In that case, the radial modes will couple if they belong to the same azimuthal family with a given l, but coupling among radial modes that belong to different azimuthal families can be ignored. For a given l, Eq. (6.76) for a weak beam then becomes

$$\left(\frac{\Omega}{\omega_s} - l\right) R_l(r) = W(r) \int_0^\infty r'\, dr'\, R_l(r') G_l(r, r'), \tag{6.93}$$

where we have introduced a weight function

$$W(r) = -\frac{\omega_s}{N\eta c} \frac{\psi_0'(r)}{r}, \tag{6.94}$$

and a kernel function

$$G_l(r, r') = i \frac{2\pi N r_0 \eta c^2}{\gamma T_0^2 \omega_s^2} l \sum_{p=-\infty}^{\infty} \frac{Z_0^{\parallel}(\omega')}{\omega'} J_l\left(\frac{\omega' r}{c}\right) J_l\left(\frac{\omega' r'}{c}\right), \tag{6.95}$$

where $\omega' = p\omega_0 + l\omega_s$.

Equation (6.93), together with Eqs. (6.94–95), is called the *Sacherer integral equation* for the longitudinal ($m = 0$) instabilities. Information on $\psi_0(r)$ is contained in the weight function; information on $Z_0^{\parallel}(\omega)$ is contained in the kernel function. Since $\psi_0'(r)$ tends to be negative, a minus sign is introduced in the definition of $W(r)$ to make it positive, at least for $\eta > 0$.

The Sacherer equation describes an eigensystem. There are an infinite number of solutions of the system, specified by the index $n = 0, 1, 2, \ldots$. Each solution consists of an eigenvalue $(\Omega/\omega_s) - l$ and a corresponding eigenfunction $R_l(r)$. Note that $G_l(r, r') = G_l(r', r)$ and that $G_0(r, r') = 0$.

To proceed, let us introduce a complete set of orthonormal functions $\{f_k(r),\ k = 0, 1, 2, \ldots\}$ that satisfies the condition

$$\int_0^\infty r\,dr\,W(r)f_k(r)f_{k'}(r) = \delta_{kk'}. \tag{6.96}$$

We then decompose the eigenfunction $R_l(r)$ according to

$$R_l(r) = W(r)\sum_{k=0}^{\infty} a_k f_k(r). \tag{6.97}$$

Substituting Eq. (6.97) into Eq. (6.93) and using the orthonormality condition (6.96), we obtain an infinite set of equations

$$\left(\frac{\Omega}{\omega_s} - l\right)a_k = \sum_{k'=0}^{\infty} M_{kk'}a_{k'}, \qquad k = 0, 1, 2, \ldots, \tag{6.98}$$

where

$$M_{kk'} = \int_0^\infty r\,dr\,W(r)f_k(r)\int_0^\infty r'\,dr'\,W(r')f_{k'}(r')G_l(r, r'). \tag{6.99}$$

For a nontrivial solution to exist, the eigenvalues $(\Omega/\omega_s) - l$ must satisfy

$$\det\left[\left(\frac{\Omega}{\omega_s} - l\right)I - M\right] = 0, \tag{6.100}$$

where I is the identity matrix and M is the *interaction matrix* with elements given by Eq. (6.99). The infinite number of solutions for the eigenvalue is specified by the radial mode index n for the given azimuthal index l.

Substituting Eq. (6.95) into Eq. (6.99) and introducing the quantity

$$g_{lk}(\omega) = \int_0^\infty r\,dr\,W(r)f_k(r)J_l\left(\frac{\omega r}{c}\right), \tag{6.101}$$

we obtain the expression

$$M_{kk'} = i\frac{2\pi N r_0 \eta c^2}{\gamma T_0^2 \omega_s^2} l \sum_{p=-\infty}^{\infty} \frac{Z_0^{\parallel}(\omega')}{\omega'} g_{lk}(\omega')g_{lk'}(\omega'). \tag{6.102}$$

The functions $W(r)$, $f_k(r)$, and $g_{lk}(\omega)$ have the dimensionalities L^{-4}, L, and L^{-1}, respectively. Elements of the interaction matrix M are dimensionless.

The quantity $g_{lk}(\omega)$ is related to the Fourier spectrum of the distribution perturbation. This can be seen by following steps similar to Eq. (6.75),

$$\tilde{\rho}_1^{(l)}(\omega) = \int_{-\infty}^{\infty} dz\, e^{-i\omega z/c} \int_{-\infty}^{\infty} d\delta\, \psi_1^{(l)}$$
$$= \frac{2\pi\omega_s}{\eta c} i^{-l} \alpha_l \sum_{k=0}^{\infty} a_k g_{lk}(\omega), \tag{6.103}$$

where use has been made of Eqs. (6.72), (6.97), and (6.101).

We have now a well-defined procedure of finding the radial modes for a given unperturbed distribution $\psi_0(r)$. To do so, we first obtain the weight function (6.94); a set of orthonormal functions $\{f_k(r)\}$ is then introduced satisfying Eq. (6.96). The eigenmodes are obtained using Eq. (6.100), where the interaction matrix M is obtained from Eq. (6.102) with $g_{lk}(\omega)$ given by Eq. (6.101). This procedure is repeated for each given azimuthal index l. Coupling among different azimuthal families, which occurs at higher beam intensities than considered here, will be considered in the next section.

First let us consider the highly degenerate water-bag model. In this case we have

$$W(r) = \frac{1}{\pi \hat{z}^3} \delta(r - \hat{z}). \tag{6.104}$$

The orthonormal condition (6.96) allows one and only one value of the radial index: $k = 0$, with $f_0(r) = \sqrt{\pi}\,\hat{z}$. This leads to

$$g_{l0}(\omega) = \frac{1}{\sqrt{\pi}\,\hat{z}} J_l\left(\frac{\omega \hat{z}}{c}\right). \tag{6.105}$$

The distribution perturbation is proportional to the Fourier transform of Eq. (6.105) and is related to the Chebyshev polynomials $T_l(x) = \cos(l \cos^{-1} x)$ by

$$\tilde{\rho}_1^{(l)} \propto \frac{T_l(x)}{\sqrt{1 - x^2}}. \tag{6.106}$$

where $x = z/\hat{z}$. [See Eq. (6.85).] These modes are referred to as the *Chebyshev modes*.

Substituting Eq. (6.105) into Eq. (6.102) gives the element of the 1×1 matrix

$$M_{00} = i \frac{2Nr_0\eta c^2}{\gamma T_0^2 \omega_s^2 \hat{z}^2} l \sum_{p=-\infty}^{\infty} \frac{Z_0^{\parallel}(\omega')}{\omega'} J_l^2\left(\frac{\omega' \hat{z}}{c}\right). \tag{6.107}$$

This gives an eigenvalue that coincides with Eq. (6.83).

Parabolic Model

As a model more realistic than the water bag, consider the distribution

$$\psi_0(r) = \frac{3N\eta c}{2\pi\omega_s \hat{z}^3}\sqrt{\hat{z}^2 - r^2}, \qquad r < \hat{z}. \tag{6.108}$$

The coefficient on the right hand side is the result of the normalization (6.78). The corresponding unperturbed longitudinal distribution is parabolic,

$$\rho_0(z) = \frac{3N}{4\hat{z}^3}(\hat{z}^2 - z^2), \qquad |z| < \hat{z}, \tag{6.109}$$

and the rms bunch length is $\sigma_z = \hat{z}/\sqrt{5}$. This model is called the *parabolic model*.[21] The weight function is

$$W(r) = \frac{3}{2\pi\hat{z}^3}\frac{1}{\sqrt{\hat{z}^2 - r^2}}, \qquad r < \hat{z}. \tag{6.110}$$

The orthonormal functions with weight function (6.110) are given by the Jacobi polynomials $P_k^{(\alpha,\beta)}(x)$ evaluated at $x = 1 - (2r^2/\hat{z}^2)$. The closed form expressions are

$$f_k(r) = \hat{z}\sqrt{\frac{4\pi}{3}\frac{(l + 2k + \frac{1}{2})k!\Gamma(l + k + \frac{1}{2})}{(l + k)!\Gamma(k + \frac{1}{2})}}\left(\frac{r}{\hat{z}}\right)^l P_k^{(l,-1/2)}\left(1 - \frac{2r^2}{\hat{z}^2}\right), \tag{6.111}$$

where $\Gamma(x)$ is the gamma function. Some properties of the Jacobi polynomials are given in Table 6.2.[20]

Substituting Eq. (6.111) into Eq. (6.101) and making use of the properties listed in Table 6.2 give

$$g_{lk}(\omega) = \frac{1}{\hat{z}}\sqrt{\frac{3}{2\pi}\frac{(l + 2k + \frac{1}{2})\Gamma(k + \frac{1}{2})\Gamma(l + k + \frac{1}{2})}{k!(l + k)!}}\frac{J_{l+2k+1/2}(\omega\hat{z}/c)}{\sqrt{\omega\hat{z}/c}}. \tag{6.112}$$

The longitudinal distribution of the disturbance $\rho_1(z)$ of this mode is related to the Fourier transform of $g_{lk}(\omega)$ according to Eq. (6.103). Again

[21] Note that what is parabolic is $\rho_0(z)$. This is in contrast to the water-bag model, for which what resembles a "water bag" is $\psi_0(r)$, not $\rho_0(z)$.

Table 6.2. Some properties of Jacobi polynomials

$$P_k^{(\alpha,\beta)}(x) = \frac{(-1)^k}{2^k k!}(1-x)^{-\alpha}(1+x)^{-\beta}\frac{d^k}{dx^k}[(1-x)^{\alpha+k}(1+x)^{\beta+k}]$$

$$P_k^{(0,0)}(x) = P_k(x) = \text{Legendre polynomial}$$

$$\int_{-1}^{1} dx\,(1-x)^{\alpha}(1+x)^{\beta}P_k^{(\alpha,\beta)}(x)P_{k'}^{(\alpha,\beta)}(x) = \frac{2^{\alpha+\beta+1}\Gamma(\alpha+k+1)\Gamma(\beta+k+1)}{k!(\alpha+\beta+2k+1)\Gamma(\alpha+\beta+k+1)}\delta_{kk'}$$

$$\int_0^{\infty}\sqrt{x}\,dx J_{l+2k+1/2}(x)J_l(xy) = \frac{\sqrt{2}\,k!}{\Gamma\left(k+\frac{1}{2}\right)}\frac{y^l}{\sqrt{1-y^2}}P_k^{(l,-1/2)}(1-2y^2)H(1-|y|)$$

$$\int_{-\infty}^{\infty} dx\,e^{ixy}\frac{J_{k+1/2}(x)}{\sqrt{x}} = i^k\sqrt{2\pi}P_k(y)$$

$$P_0^{(0,-1/2)} = 1, \qquad P_1^{(0,-1/2)} = \tfrac{1}{4}(3x+1)$$

$$P_2^{(0,-1/2)} = \tfrac{1}{32}(35x^2+10x-13)$$

$$P_0^{(1,-1/2)} = 1, \qquad P_1^{(1,-1/2)} = \tfrac{1}{4}(5x+3)$$

$$P_2^{(1,-1/2)} = \tfrac{1}{32}(63x^2+42x-9)$$

$$P_0^{(2,-1/2)} = 1, \qquad P_1^{(2,-1/2)} = \tfrac{1}{4}(7x+5)$$

$$P_2^{(2,-1/2)} = \tfrac{1}{32}(99x^2+90x+3)$$

$$P_0 = 1, \qquad P_1 = x$$

$$P_2 = \tfrac{1}{2}(3x^2-1)$$

$$P_3 = \tfrac{1}{2}(5x^3-3x)$$

using Table 6.2, we find

$$\rho_1^{(l,k)} \propto \int_{-\infty}^{\infty} d\omega\, e^{i\omega z/c}g_{lk}(\omega) \propto P_{l+2k}\left(\frac{z}{\hat{z}}\right), \tag{6.113}$$

where $P_{l+2k}(x)$ is the Legendre polynomial of order $l+2k$.

Substituting Eq. (6.112) into Eq. (6.102) gives the elements of the interaction matrix M. In case the impedance is sharply peaked around the frequency $\omega \approx \pm h\omega_0$, we may keep only the terms $p = \pm h$ in the summation of Eq. (6.102). If we further assume that the bunch length is much shorter than the range of the wake fields, i.e., $h\omega_0\hat{z}/c \ll 1$, the most prominent radial mode is that given by the matrix element M_{00} (because it is the largest matrix element), for which the mode frequency is

$$\Omega - l\omega_s \approx M_{00}\omega_s. \tag{6.114}$$

In particular, the instability growth rate, provided by the imaginary part of Ω,

is given by

$$\frac{1}{\tau^{(l)}} = \frac{3\sqrt{\pi}}{4(l-1)!\Gamma\left(l+\frac{3}{2}\right)}\left(\frac{h\omega_0\hat{z}}{2c}\right)^{2l-2}\frac{Nr_0\eta h\omega_0}{2\gamma T_0^2\omega_s} \times\left[\operatorname{Re} Z_0^{\parallel}(h\omega_0 + l\omega_s) - \operatorname{Re} Z_0^{\parallel}(h\omega_0 - l\omega_s)\right]. \quad (6.115)$$

The Robinson growth rate (6.115) for the parabolic model is slightly different from Eq. (6.84) for the water-bag model. For the dipole $l = 1$ mode, however, it does give the same result, and both reduce to Eq. (4.20). This is expected, because a short bunch executing dipole motion behaves as a point bunch and the details of ψ_0 cannot matter. Furthermore, the Robinson stability criterion of the positioning of the impedance peak relative to $h\omega_0$ remains the same for all l.

An interesting case occurs when the impedance is purely inductive with inductance $iZ_0^{\parallel}/\omega = \text{const}$, independent of ω. If we further assume $\omega_0\hat{z}/c \ll 1$, i.e., the bunch is much shorter than the accelerator circumference and the impedance is broad-band, we may approximate the summation over p by an integral,

$$\sum_{p=-\infty}^{\infty} \to \int_{-\infty}^{\infty}\frac{d\omega'}{\omega_0}. \quad (6.116)$$

Table 6.2 and Eq. (6.102) then give

$$M_{kk'} = \Upsilon_1\frac{3}{2\pi}\frac{l\Gamma\left(k+\frac{1}{2}\right)\Gamma\left(l+k+\frac{1}{2}\right)}{k!(l+k)!}\delta_{kk'}, \quad (6.117)$$

where we have introduced a dimensionless parameter that consists essentially of the beam current multiplied by the impedance, divided by the beam rigidity,

$$\Upsilon_1 = \frac{Nr_0\eta c^3}{\gamma T_0\omega_s^2\hat{z}^3}\left(i\frac{Z_0^{\parallel}}{\omega}\right). \quad (6.118)$$

The matrix M is *diagonal*. For a purely inductive impedance, the eigenmodes are readily solved by our choice of Jacobi polynomials as the base polynomials. The eigenmodes are the *Legendre modes*,

$$\begin{aligned}\Omega^{(l,n)} &= (l + M_{nn})\omega_s,\\ \rho_1^{(l,n)}(z) &\propto P_{l+2n}\left(\frac{z}{\hat{z}}\right),\\ \tilde{\rho}_1^{(l,n)}(\omega) &\propto \frac{J_{l+2n+1/2}(\omega\hat{z}/c)}{\sqrt{\omega\hat{z}/c}},\end{aligned} \quad (6.119)$$

where l and n are the azimuthal and radial mode indices, respectively. The

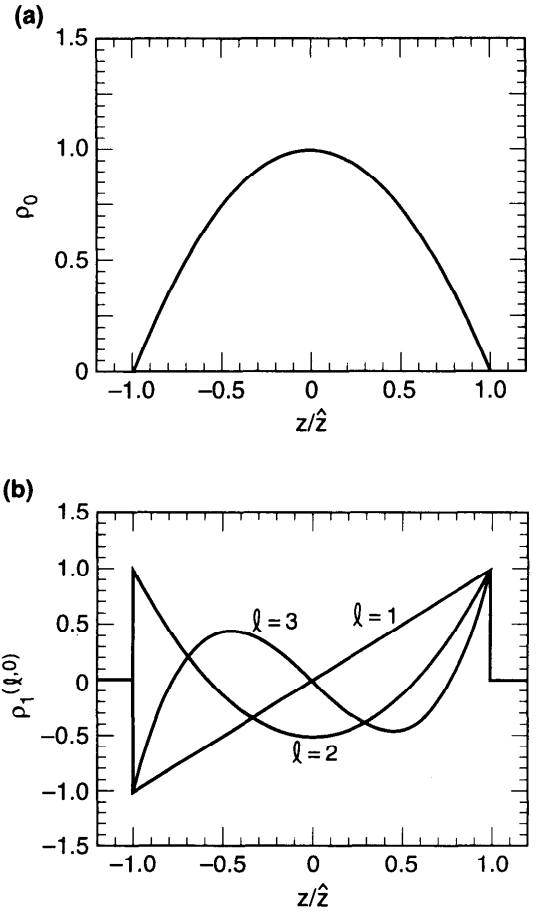

Figure 6.17. (a) Parabolic bunch distribution; (b) eigenmodes of a parabolic bunch when the impedance is purely inductive and broad-band. The modes shown have indices $l = 1, 2, 3$ and $n = 0$. These figures are to be compared with Figures 6.12 and 6.13 for the water-bag model.

Legendre modes are associated with a parabolic model for ψ_0. Some of the lower modes are shown in Figure 6.17, and their frequency spectra are shown in Figure 6.18. Modes with the same value of $l + 2n$ [for example, the mode $(l = 0,\ n = 1)$ and the mode $(l = 2,\ n = 0)$] have the same projection onto the longitudinal z-axis, although they have very different mode frequencies. In the longitudinal phase space, the Legendre modes can be constructed by combining the above information,

$$\psi_1^{(l,n)}(r,\phi)e^{-i\Omega s/c} \propto \underbrace{\frac{(r/\hat{z})^l}{\sqrt{1-(r/\hat{z})^2}} P_n^{(l,-1/2)}\left(1-\frac{2r^2}{\hat{z}^2}\right)}_{\text{radial dist.}} \underbrace{e^{il\phi}}_{\substack{\text{azim.}\\ \text{dist.}}} \underbrace{e^{-i\Omega^{(l,n)}s/c}}_{\text{time dep.}}. \tag{6.120}$$

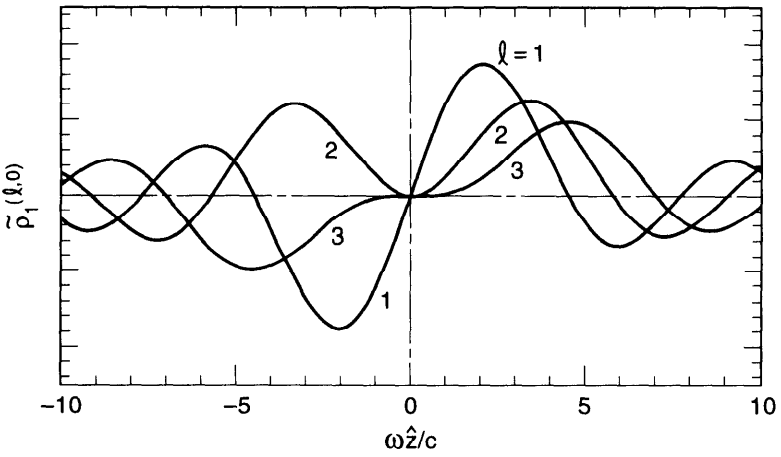

Figure 6.18. Fourier spectra of the modes shown in Figure 6.17(b). This figure can be compared with Figure 6.15(b) for the water-bag model.

Note that the matrix elements M_{nn}, and therefore the mode frequencies, are real. It follows that in the present case there are no collective instabilities, only mode frequency shifts. This is in contrast to the case of a sharp impedance for which the Robinson mechanism is a source of instability as seen in Eq. (6.115). The only collective instability so far is the Robinson type which involves long range wake fields. This conclusion has been reached already in the previous section; what is new here is that it continues to hold when coupling among the radial modes within one azimuthal family is included.

Given l, the most prominent radial mode—the one that has the largest complex frequency shift—is that with $n = 0$. It has

$$\Omega^{(l,0)} - l\omega_s \approx M_{00}\omega_s = \frac{3}{2\sqrt{\pi}} \frac{\Gamma\left(l + \frac{1}{2}\right)}{(l-1)!} \Upsilon_1 \omega_s. \tag{6.121}$$

Note that this frequency shift increases with the mode index l; for large l, it grows indefinitely as $\sqrt{l}$. This means the higher azimuthal modes are important in this model; the most prominent mode would have a radial mode index $n = 0$, but its azimuthal mode index l diverges and is undefined. This importance of high frequency modes is an unsatisfactory consequence of the assumption that the impedance is proportional to ω indefinitely.

Figure 6.19 shows the mode frequencies as functions of the parameter Υ_1. One observes three sets of frequencies clustered around $\Omega = \omega_s$, $2\omega_s$, and $3\omega_s$, corresponding to the azimuthal mode indices $l = 1$, 2, and 3, respectively. The five leading radial modes ($n = 0$ to 4) are shown for each azimuthal family. In the analysis we have assumed that the mode frequency shifts are much smaller than ω_s so that coupling among azimuthal modes

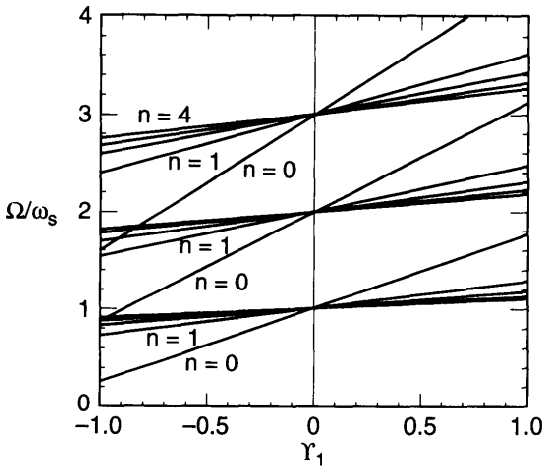

Figure 6.19. Mode frequencies versus the beam intensity parameter Υ_1. A parabolic bunch and a purely inductive impedance have been assumed. Although the figure exhibits the range up to $|\Upsilon_1| = 1$, the range of applicability of the analysis is restricted to $|\Upsilon_1| \ll 1$ so that the mode frequency shifts are much less than ω_s. The mode frequency shifts increase with the mode index l.

can be ignored. This assumption gives rise to the fact that all mode frequencies in Figure 6.19 depends linearly on Υ_1. As we will see in the next section, inclusion of coupling (at higher beam intensities) among the azimuthal modes causes these dependences to deviate from linearity.

As mentioned before, one has to be careful when applying the frequency shift results (6.119) and (6.121) because a potential-well distortion term has been dropped. To demonstrate this in the present model, consider the mode with $l = 1$ and $n = 0$. The mode frequency shift, according to Eq. (6.121), is

$$\Omega^{(1,0)} - \omega_s = \frac{3}{4}\Upsilon_1 = \frac{3Nr_0\eta c^3}{4\gamma T_0 \omega_s \hat{z}^3}\left(i\frac{Z_0^{\parallel}}{\omega}\right). \tag{6.122}$$

This shift is exactly equal and opposite to the shift in ω_s due to the potential-well distortion, Eq. (6.56), if one identifies $S = -(iZ_0^{\parallel}/\omega)c^2$. When the potential-well effect is included, therefore, the mode frequency $\Omega^{(1,0)}$ does not shift with beam intensity for weak beam intensities. The physical reason for this phenomenon was given in Exercise 6.8(c).

Exercise 6.11 Although the interplay between potential-well distortion and the dynamics of collective modes[22] is ignored in the analysis, one could

[22] K. Oide, *AIP Proc.* **230**, *Nonlinear Dynamics and Particle Acceleration*, Tsukuba, 1990, p. 266; K. Oide, *Proc. 4th Advanced ICFA Workshop on Collective Effects in Short Bunches*, 1990, KEK Report 90-21, p. 64.

consider an approximate description, valid to first order in beam intensity, by simply adding the two contributions algebraically. Show that, with a space charge impedance (2.80), the frequency of the lth mode, including the contribution from the potential-well distortion, is approximately

$$\Delta\nu^{(l,0)} \equiv \frac{\Omega^{(l,0)} - l\omega_s}{\omega_0}$$

$$\approx l\frac{3Nr_0\eta R^2}{2\beta^2\gamma^3\hat{z}^3\nu_s}\left(\ln\frac{b}{a} + \frac{1}{2}\right)\left[1 - \frac{2}{\sqrt{\pi}}\frac{\Gamma\left(l + \frac{1}{2}\right)}{l!}\right], \quad (6.123)$$

where the first term in the square brackets gives the contribution from the potential-well distortion $l\,\Delta\nu_s$, where $\Delta\nu_s$ is the incoherent synchrotron tune shift calculated in Eq. (6.56). More explicitly, show that

$$\Delta\nu^{(1,0)} \approx 0, \qquad \Delta\nu^{(2,0)} \approx \tfrac{1}{2}\Delta\nu_s, \qquad \Delta\nu^{(3,0)} \approx \tfrac{9}{8}\Delta\nu_s. \quad (6.124)$$

Gaussian Model

The same procedure for the parabolic model can also be followed for a Gaussian model,

$$\psi_0(r) = \frac{N\eta c}{2\pi\sigma^2\omega_s}e^{-r^2/2\sigma^2},$$
$$\rho_0(z) = \frac{N}{\sqrt{2\pi}\sigma}e^{-z^2/2\sigma^2}, \quad (6.125)$$

where σ is the rms bunch length. The corresponding weight function is

$$W(r) = \frac{1}{2\pi\sigma^4}e^{-r^2/2\sigma^2}. \quad (6.126)$$

The orthonormal polynomials are found in terms of generalized Laguerre polynomials $L_k^{(l)}(x)$ as

$$f_k(r) = \sigma\sqrt{\frac{2\pi k!}{(l+k)!}}\left(\frac{r}{\sqrt{2}\sigma}\right)^l L_k^{(l)}\left(\frac{r^2}{2\sigma^2}\right). \quad (6.127)$$

Some properties of generalized Laguerre polynomials are listed in Table 6.3.

Table 6.3. Some properties of generalized Laguerre polynomials

$$L_k^{(l)}(x) = \sum_{m=0}^{k} (-1)^m \frac{(l+k)!}{(k-m)!(l+m)!} \frac{x^m}{m!}$$

$$\int_0^\infty dx\, e^{-x} x^l L_k^{(l)}(x) L_{k'}^{(l)}(x) = \frac{(l+k)!}{k!} \delta_{kk'}$$

$$\int_0^\infty dx\, x^{l+1} e^{-\beta x^2} J_l(xy) L_k^{(l)}(\alpha x^2) = \frac{(\beta-\alpha)^k}{2^{l+1}\beta^{l+k+1}} y^l e^{-y^2/4\beta} L_k^{(l)}\left[\frac{\alpha y^2}{4\beta(\alpha-\beta)}\right]$$

$$L_0^{(0)} = 1, \qquad L_1^{(0)} = 1 - x$$
$$L_2^{(0)} = 1 - 2x + \tfrac{1}{2}x^2$$
$$L_3^{(0)} = 1 - 3x + \tfrac{3}{2}x^2 - \tfrac{1}{6}x^3$$
$$L_0^{(1)} = 1, \qquad L_1^{(1)} = 2 - x$$
$$L_2^{(1)} = 3 - 3x + \tfrac{1}{2}x^2$$
$$L_3^{(1)} = 4 - 6x + 2x^2 - \tfrac{1}{6}x^3$$
$$L_0^{(2)} = 1, \qquad L_1^{(2)} = 3 - x$$
$$L_2^{(2)} = 6 - 4x + \tfrac{1}{2}x^2$$

It follows that

$$g_{lk}(\omega) = \frac{1}{\sigma\sqrt{2\pi k!(l+k)!}} \left(\frac{\omega\sigma}{\sqrt{2}\,c}\right)^{l+2k} e^{-\omega^2\sigma^2/2c^2} \tag{6.128}$$

and

$$M_{kk'} = i \frac{Nr_0\eta c^2}{\gamma T_0^2 \omega_s^2 \sigma^2} \frac{l}{\sqrt{k!k'!(l+k)!(l+k')!}} \times \sum_{p=-\infty}^{\infty} \frac{Z_0^{\parallel}(\omega')}{\omega'} e^{-\omega'^2\sigma^2/c^2} \left(\frac{\omega'^2\sigma^2}{2c^2}\right)^{l+k+k'}, \tag{6.129}$$

where $\omega' = p\omega_0 + l\omega_s$. The longitudinal distribution of the mode is related through Eq. (6.103) to the Fourier transform of $g_{lk}(\omega)$,

$$\int \frac{d\omega}{2\pi} e^{i\omega z/c} g_{lk}(\omega) \propto e^{-z^2/2\sigma^2} H_{l+2k}\left(\frac{z}{\sqrt{2}\,\sigma}\right), \tag{6.130}$$

where $H_{l+2k}(x)$ is the Hermite polynomial of order $l + 2k$. The indices l and k appear as the combination $l + 2k$, just as in the Legendre modes (6.119).

For an impedance sharply peaked around $\omega \approx \pm h\omega_0$ and a short bunch with $h\omega_0\sigma/c \ll 1$, the Robinson growth rate for the most prominent radial

mode can be estimated by M_{00} as

$$\frac{1}{\tau^{(l)}} = \mathrm{Im}(\Omega - l\omega_s) \approx \mathrm{Im}(M_{00}\omega_s)$$

$$= \frac{1}{(l-1)!}\left(\frac{h\omega_0\sigma}{\sqrt{2}\,c}\right)^{2l-2}\frac{Nr_0\eta h\omega_0}{2\gamma T_0^2\omega_s}$$

$$\times\left[\mathrm{Re}\,Z_0^{\parallel}(h\omega_0 + l\omega_s) - \mathrm{Re}\,Z_0^{\parallel}(h\omega_0 - l\omega_s)\right]. \quad (6.131)$$

Just as in the water-bag and parabolic models, this reduces to the familiar result when $l = 1$, and the same Robinson stability criterion applies for all l.

In the case of a purely inductive impedance, we have

$$M_{kk'} = \Upsilon_2 \frac{l(2l + 2k + 2k' - 1)!!}{4^{l+k+k'}\sqrt{k!k'!(l+k)!(l+k')!}}, \quad (6.132)$$

where

$$\Upsilon_2 = \frac{Nr_0\eta c^3}{2\sqrt{\pi}\,\gamma T_0\omega_s^2\sigma^3}\left(i\frac{Z_0^{\parallel}}{\omega}\right). \quad (6.133)$$

This time the matrix M is no longer diagonal, although the elements $M_{kk'}$ remain real. The generalized Laguerre polynomials do not happen to be the eigenmodes for the Gaussian model for the purely inductive impedance. For a given azimuthal mode l, the eigenmode frequencies are obtained numerically by truncating the matrix to an appropriate dimension. The results are exhibited in Figure 6.20. One observes again that mode frequencies depart from their unperturbed values $l\omega_s$ linearly in Υ_2, and that all radial modes are stable. The only instability at this point is still of the Robinson type.

Exercise 6.12 Consider a resistive-wall impedance (2.76), make the broad-band approximation[23] (6.116), and ignore the potential-well distortion.

(a) Show that for the water-bag model,

$$\Omega - l\omega_s = \frac{Nr_0\eta c^2}{\pi\gamma\omega_s b\hat{z}^2}\sqrt{\frac{c}{\hat{z}\sigma}}\,\frac{l\Gamma(l+\frac{1}{4})}{\left[\Gamma(\frac{3}{4})\right]^2\Gamma(l+\frac{3}{4})}, \quad (6.134)$$

which increases as $\sqrt{l}$ for large l.

(b) Use Table 6.1 to obtain a closed form expression for $M_{kk'}$ for a parabolic beam. Calculate numerically the eigenmode frequencies as

[23]The broad-band approximation is justified here even for the resistive-wall impedance, because there is no singularity at $\omega \to 0$ in these applications.

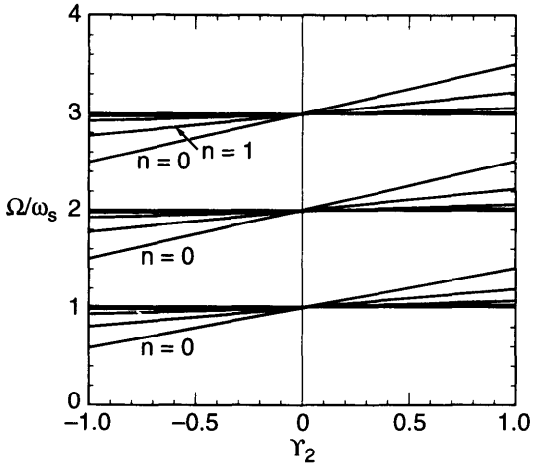

Figure 6.20. Mode frequencies versus the beam intensity parameter Υ_2, for a Gaussian bunch and a purely inductive impedance.

functions of

$$\Upsilon_3 = \frac{3}{16\pi} \frac{Nr_0\eta c^2}{\gamma\omega_s^2 b\hat{z}^2} \sqrt{\frac{c}{\sigma\hat{z}}} \,. \tag{6.135}$$

The result is shown in Figure 6.21. How does the frequency shift $\Omega - l\omega_s$ depend on the mode index l as l increases? For a given l, is the frequency of the leading radial mode well approximated by $\Omega - l\omega_s \approx M_{00}\omega_s$? In Eqs. (6.134–6.135), σ is the conductivity of the resistive wall.

Ignoring coupling among different azimuthal modes, we have now dealt with three bunch distribution models: the water-bag, the parabolic, and the Gaussian models. The eigenmodes for the water-bag model were found to be Chebyshev modes (6.106) regardless of the impedance. For the parabolic model, we do not have a closed form expression of the eigenmodes in general, but for a broad-band, purely inductive impedance, the eigenmodes are given by the Legendre modes (6.119). For the Gaussian model, we did not find closed form expression of the eigenmodes even for a purely inductive impedance. However, a convenient choice of the base functions had led to the Hermite modes (6.130).

Effective Impedance

Given the impedance $Z_0^{\parallel}$ and the unperturbed beam distribution ψ_0, the beam stability problem is solved by analyzing the eigensystem as described so

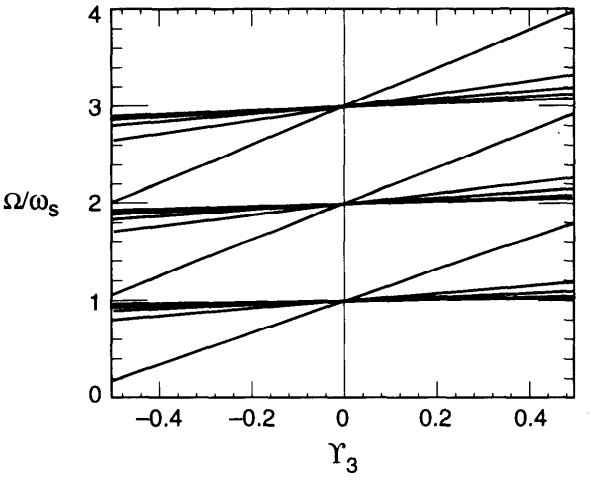

Figure 6.21. Mode frequencies of a parabolic beam in the presence of a resistive-wall impedance.

far. This, however, is a tedious procedure, particularly because $Z_0^{\parallel}$ may have a frequency dependence much more complicated than a purely inductive impedance, and ψ_0 may not be as simple as the parabolic model. In practice, therefore, one often compromises and, instead of results of detailed eigenanalysis, asks only for a rough idea of the instability picture. Questions raised are typically of immediate relevance to the accelerator at hand, such as which modes are most likely to be affected by the given impedance, and what are the orders of magnitude of the growth rates and frequency shifts of these modes. These questions can be addressed, in a short-cut manner, using a quantity called the *effective impedance*.[24]

The procedure followed in this section resembles closely the perturbation technique used in quantum mechanics. Indeed, the interaction matrix element $M_{kk'}$ in Eq. (6.102) can be expressed in a quantum mechanical notation as

$$\left\langle l, k \left| \frac{Z_0^{\parallel}}{\omega} \right| l, k' \right\rangle \equiv \sum_p \frac{Z_0^{\parallel}(\omega')}{\omega'} g_{lk}(\omega') g_{lk'}(\omega'), \tag{6.136}$$

where one recalls the notation $\omega' = p\omega_0 + l\omega_s$. The reason that the impedance samples the frequency at ω' was given in Eq. (4.19).

If the problem has been diagonalized so that the eigenmodes have been found and $\tilde{\rho}_1^{(l,n)}(\omega) \propto i^{-l} g_{ln}(\omega)$ are known, then by Eq. (6.102) we can write

[24] F. Sacherer, IEEE Tran. Nucl. Sci. **NS-24**, 1393 (1977); B. Zotter, CERN Report ISR-TH/78-16 (1978); B. Zotter, CERN Report ISR-TH/80-03 (1980); K. Balewski and R. D. Kohaupt, DESY Report 90-152 (1990).

the mode frequency as

$$\Omega^{(l,n)} - l\omega_s = M_{nn}\omega_s$$
$$= \frac{2\pi N r_0 \eta c^2}{\gamma T_0^2 \omega_s} li\left(\frac{Z_0^{\parallel}}{\omega}\right)_{\text{eff}} \sum_{p=-\infty}^{\infty} |g_{ln}(\omega')|^2, \qquad (6.137)$$

where we have introduced an effective impedance

$$\left(\frac{Z_0^{\parallel}}{\omega}\right)_{\text{eff}} = \frac{\sum_{p=-\infty}^{\infty} \frac{Z_0^{\parallel}(\omega')}{\omega'} |\tilde{\rho}_1^{(l,n)}(\omega')|^2}{\sum_{p=-\infty}^{\infty} |\tilde{\rho}_1^{(l,n)}(\omega')|^2}, \qquad (6.138)$$

which depends on the mode indices l and n.[25] The quantity $(Z_0^{\parallel}/\omega)_{\text{eff}}$ is essentially the weighted average of the impedance over the bunch mode spectral power $|\tilde{\rho}_1^{(l,n)}|^2$. Whether a particular mode is driven significantly by the impedance is determined by the degree to which the impedance overlaps the mode spectrum.

If the problem has not been diagonalized, but one has the situation where the most prominent radial mode has the frequency $\Omega^{(l)} \approx (l + M_{00})\omega_s$, or if one is interested only in an order-of-magnitude estimate of the complex mode frequency shifts, one may still apply Eqs. (6.137–6.138), even without explicitly finding the eigenmodes. Although not rigorous, Eqs. (6.139–6.143) below are often used in practical applications.

Take the parabolic bunch for example. We have diagonalized the problem for the special case of a purely inductive impedance. For a general impedance, Eq. (6.137) gives, for the most prominent radial mode,

$$\Omega^{(l)} - l\omega_s \approx \frac{3}{2\sqrt{\pi}} \frac{\Gamma\left(l + \frac{1}{2}\right)}{(l-1)!} \frac{N r_0 \eta c^3}{\gamma T_0 \omega_s \hat{z}^3} i\left(\frac{Z_0^{\parallel}}{\omega}\right)_{\text{eff}}, \qquad (6.139)$$

where

$$\left(\frac{Z_0^{\parallel}}{\omega}\right)_{\text{eff}} = \frac{\sum_{p=-\infty}^{\infty} \frac{Z_0^{\parallel}(\omega')}{\omega'} h_l(\omega')}{\sum_{p=-\infty}^{\infty} h_l(\omega')}, \qquad (6.140)$$

[25] Expressions (6.137–6.138) are not very useful for the water-bag model because the summation in Eq. (6.137)—and, equivalently, the denominator in Eq. (6.138)—diverges. The sharp cutoff in the water-bag distribution has introduced a large high frequency contribution. This divergence does not occur for the more realistic parabolic or the Gaussian distribution.

and, from Eq. (6.112),

$$h_l(\omega) = \frac{\left[J_{l+1/2}(\omega\hat{z}/c)\right]^2}{|\omega\hat{z}/c|}. \tag{6.141}$$

Because we are addressing the most prominent radial mode, the effective impedance of Eq. (6.140) depends on the mode index l but not the radial mode index n. Also, the effective impedance describes the effect of impedance on beam dynamics. It is not the same as the raw impedance we have been used to up to now. In particular, the effective impedance depends on the beam properties, while the raw impedance does not.

As mentioned, Eq. (6.112) is the mode spectrum only for a purely inductive impedance. In obtaining Eq. (6.139), however, we have insisted that the same eigenmode spectra apply even for the arbitrary impedance under consideration, and we have made the broad-band approximation (6.116) when we performed the summation over p in Eq. (6.137). For a purely inductive impedance, Eq. (6.139) becomes (6.121), as it should.

The real and the imaginary parts of $(Z_0^{\parallel}/\omega)_{\text{eff}}$ give the growth rate and the frequency shift of the mode under consideration. For a broad-band impedance, $(Z_0^{\parallel}/\omega)_{\text{eff}}$ is purely imaginary because $\text{Re}\, Z_0^{\parallel}(\omega)$ is an even function of ω; the growth rate vanishes and there is no instability.

A similar procedure can be followed for a Gaussian beam. We obtain

$$\Omega^{(l)} - l\omega_s \approx \frac{1}{2\pi} \frac{\Gamma\left(l + \frac{1}{2}\right)}{2^l(l-1)!} \frac{Nr_0\eta c^3}{\gamma T_0 \omega_s \sigma^3} i \left(\frac{Z_0^{\parallel}}{\omega}\right)_{\text{eff}}, \tag{6.142}$$

where the effective impedance is given by Eq. (6.140) with

$$h_l(\omega) = \left(\frac{\omega\sigma}{c}\right)^{2l} e^{-\omega^2\sigma^2/c^2}. \tag{6.143}$$

More justification of Eqs. (6.142–6.143), at least for short Gaussian bunches, can be found in Exercise 6.14.

Exercise 6.13 Perform one of the following two calculations numerically: (a) $(Z_0^{\parallel}/\omega)_{\text{eff}}$ for a parabolic bunch and a broad-band resonator impedance; (b) the same for a Gaussian bunch. The real part of $(Z_0^{\parallel}/\omega)_{\text{eff}}$ vanishes. Which azimuthal mode is driven most strongly? How does the sign of $(Z_0^{\parallel}/\omega)_{\text{eff}}$ depend on the azimuthal mode index l? Relate the answers to the overlap between the impedance and the mode spectra. The result for a Gaussian bunch is shown in Figure 6.22. The overlap consideration is illustrated in Figure 6.23. Compare result with that obtained for a water-bag model in Exercise 6.9.

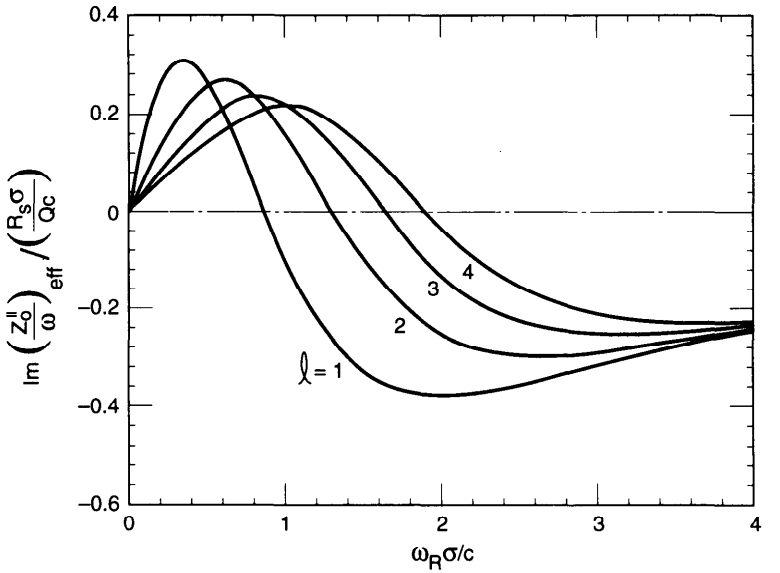

Figure 6.22. The effective impedance seen by a Gaussian bunch when the impedance is that of a broad-band resonator. The graph shows $\mathrm{Im}(Z_0^{\parallel}/\omega)_{\mathrm{eff}}/(R_S\sigma/Qc)$ as a function of $\omega_R\sigma/c$ for $l = 1, 2, 3$, and 4 and $Q = 1$. The behavior can be understood by relating it to the overlapping between the impedance $Z_0^{\parallel}(\omega)/\omega$ and the mode spectra $h_l(\omega)$ as illustrated in Figure 6.23.

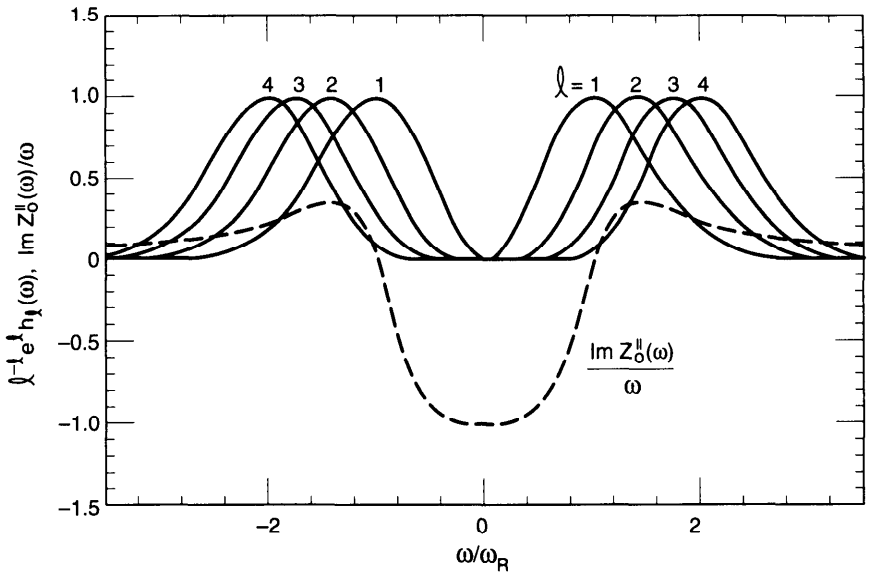

Figure 6.23. The effective impedance $\mathrm{Im}(Z_0^{\parallel}/\omega)_{\mathrm{eff}}$ is obtained from the overlap integral between $Z_0^{\parallel}(\omega)/\omega$ and $h_l(\omega)$. The solid curves are $h_l(\omega)$ for a Gaussian beam and $l = 1, 2, 3, 4$ (normalized so that they have the same value at their respective maxima). The dashed curve is $\mathrm{Im}\,Z_0^{\parallel}(\omega)/\omega$ for a broad-band resonator. The frequency extent of the impedance is ω_R. The frequency extent of the mode spectra is related to σ, with the spectral peak of the lth mode located at $\omega = \sqrt{l}\,c/\sigma$. For the parameters chosen, with $c/\sigma = \omega_R$ and $Q = 1$, the $l = 1$ and 2

The ideas of the effective impedance and the broad-band resonator model, Eqs. (2.121) and (2.128), can be combined into a useful package for practical applications. Take for example an electron accelerator with $N = 10^{11}$, $\eta = 0.02$, $b = \sigma = 5$ cm, $\omega_s = 1.9 \times 10^5$ s^{-1}, $E = 7$ GeV and a broad-band resonator impedance with $Q = 1$ and $R_S = 720\ \Omega$ (one deep cavity every 25 m, $Z_0^{\parallel}/n = R_S b/R = 0.75\ \Omega$). Figure 6.22 gives $(Z_0^{\parallel}/n)_{\text{eff}} = 0.10 Z_0^{\parallel}/n$ for $l = 1$ and $-0.15 Z_0^{\parallel}/n$ for $l = 2$, according to which one obtains the mode tune shifts of $\Delta\nu_s^{(l)} = 0.7 \times 10^{-5}$ for $l = 1$ and -0.8×10^{-5} for $l = 2$.

6.5 AZIMUTHAL MODES

In Section 6.3 we derived for the water-bag model the collective mode frequency (6.83) for a weak beam. We then obtained the Robinson instability growth rate (6.84) and pointed out that the only instability that the weak beam allows is of the Robinson type. In other words, instability occurs only when the impedance consists of sharp peaks like those sketched in Figure 2.27 below cutoff, or equivalently, when the wake field lasts longer than the revolution period. In case the impedance is broad-band, we concluded at the time that all modes are necessarily stable.

This conclusion was not changed when we included the radial modes in Section 6.4.[26] The beam intensity considered is weak, so that the mode frequency shifts are small compared with ω_s and we could ignore the coupling among modes of different azimuthal families. The only instability found there is still of the Robinson type. If we further increase the beam intensity, however, the frequency shifts become comparable to ω_s so that coupling among azimuthal modes must be considered. Such a phenomenon, referred to as "mode coupling,"[27] "mode mixing," or "turbulence" in the literature, can lead to instabilities other than the Robinson type.

To demonstrate this *mode coupling instability*, consider first a water-bag beam (ignoring the radial modes) and a broad-band impedance for which the approximation (6.116) holds—the Robinson instability is therefore excluded. From Eq. (6.80), the eigenvalue Ω/ω_s is determined by the condition

$$\det\left(\frac{\Omega}{\omega_s} I - M\right) = 0, \tag{6.144}$$

[26]Recall that the water-bag model does not allow the study of the radial modes. What we demonstrated in Section 6.4 says that the lack of radial structure of the modes is not the cause of this conclusion.

[27]The "mode" here refers to the azimuthal modes. Coupling of radial modes was already considered in Section 6.4.

where I is a unit matrix and M is a matrix with elements

$$M_{ll'} = l\delta_{ll'} + i\frac{Nr_0\eta c^2}{\pi\gamma T_0\omega_s^2\hat{z}^2}li^{l-l'}\int_{-\infty}^{\infty} d\omega\,\frac{Z_0^{\parallel}(\omega)}{\omega}J_l\left(\frac{\omega\hat{z}}{c}\right)J_{l'}\left(\frac{\omega\hat{z}}{c}\right). \quad (6.145)$$

By applying Eq. (6.116), we have, in effect, ignored the multiturn effects. Written out explicitly, M is a real matrix; it has the form

$$M = \begin{bmatrix} \cdots & & & & & & \\ \cdots & & & & & & \\ & 2+I & R & I & R & I & \\ & R & 1+I & R & I & R & \\ & 0 & 0 & 0 & 0 & 0 & \\ & R & I & R & -1+I & R & \\ & I & R & I & R & -2+I & \\ & & & & & & \cdots \\ & & & & & & \cdots \end{bmatrix}, \quad (6.146)$$

where the $l = 0$ elements all vanish; the I's and R's are real quantities, all different from one another, with I coming only from Im $Z_0^{\parallel}$ and R coming only from Re $Z_0^{\parallel}$. All R's and I's are proportional to the beam intensity N. If we drop all the off-diagonal mode coupling terms, we will obtain the weak beam result (6.83). The off-diagonal elements are antisymmetric, i.e., $M_{-l,-l'} = -M_{l,l'}$.

It follows from the structure of the interaction matrix M that the mode coupling instability results from an interplay between the real and the imaginary parts of the impedance, with the leading contribution in the product form RI and quadratic in N. Note also that $\Omega = 0$ is always a solution; this is the mode that describes the static potential-well distortion.

Equation (6.145) assumes a broad-band impedance. Mode coupling also has an effect for sharp impedances.[28] Consider the case when the beam is happily Robinson damped by proper tuning of a sharp impedance whose resonant frequency is close to $h\omega_0$. Instability can still occur at higher beam intensities due to the mode coupling mechanism, thus spoiling the Robinson damping. However, we will not pursue this possibility.

Let us proceed again with an illustrative example. Consider the broad-band impedance

$$Z_0^{\parallel}(\omega) = R_0\left|\frac{\omega_0}{\omega}\right|^{1/2}[1 + \mathrm{sgn}(\omega)i], \quad (6.147)$$

where R_0 is a real positive constant. This impedance corresponds to the

[28] Tai-sen F. Wang, Part. Accel. **34**, 105 (1990).

diffraction model (2.145) and has the associated wake function $W_0'(z) \propto |z|^{-1/2}$. The matrix elements of M are

$$M_{ll'} = l\delta_{ll'} - lC_{ll'}\Upsilon, \tag{6.148}$$

with

$$C_{ll'} = \frac{\frac{1}{2}\Gamma\left(\frac{l+l'-\frac{1}{2}}{2}\right)}{\Gamma\left(\frac{l'-l+\frac{5}{2}}{2}\right)\Gamma\left(\frac{l+l'+\frac{5}{2}}{2}\right)\Gamma\left(\frac{l-l'+\frac{5}{2}}{2}\right)} \times \begin{cases} (-1)^{(l-l')/2} & \text{if } l-l' \text{ is even,} \\ (-1)^{(l-l'-1)/2} & \text{if } l-l' \text{ is odd,} \end{cases} \tag{6.149}$$

where we have defined a dimensionless parameter

$$\Upsilon = \frac{Nr_0\eta R_0}{\gamma\omega_s^2}\left(\frac{c}{T_0\hat{z}}\right)^{3/2} \tag{6.150}$$

and use has been made of Table 6.1.

We have evaluated the eigenvalues Ω/ω_s numerically as functions of Υ; the results for the lowest few modes are shown in Figure 6.24. Unlike Figures 6.19–6.21, each azimuthal family in Figure 6.24 has only one radial mode because of the radial degeneracy of the water-bag model. At $\Upsilon = 0$, the mode frequencies are simply multiples of ω_s. As Υ increases, the mode frequencies shift. Also unlike Figures 6.19–6.21, the frequency shifts here are not linear in Υ. As Υ reaches the critical value $\Upsilon_{\text{th}} \approx 1.45$, two of the mode frequencies become equal, and when $\Upsilon > \Upsilon_{\text{th}}$, they become imaginary and the beam is unstable. The parameter Υ_{th} thus defines the instability threshold of the beam. Note that the instability growth rate increases sharply as soon as Υ exceeds Υ_{th}, in the sense that a slight increase in beam intensity beyond the threshold leads to a growth rate comparable to ω_s. This is a general property of the mode coupling instabilities.

The matrix (6.148) has infinite dimensions. The eigenvalues in Figure 6.24 are evaluated numerically with the matrix truncated. For the truncation procedure to converge, the beam spectrum, as well as the impedance, must not have long tails at high frequencies. For a water-bag model, the impedance at high frequencies must decrease sufficiently rapidly with increasing frequency. The impedance (6.147) [and also (6.215) and (6.224) in later illustrations] is chosen with these considerations in mind.

The purely inductive, the space charge, and the resistive-wall impedances thus cannot be treated by this approach for the water-bag model. The lack of

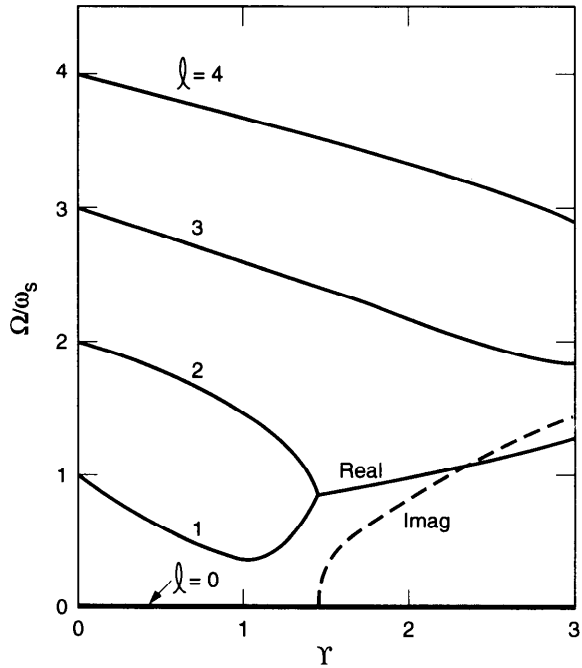

Figure 6.24. Longitudinal mode frequencies Ω / ω_s versus the parameter Υ for a water-bag beam with the impedance (6.147). Instability occurs when $\Upsilon > \Upsilon_{th} \approx 1.45$ and the $l = 1$ and $l = 2$ mode-frequency lines merge. The solid curves give the real part of the mode frequencies; the dashed curve gives the imaginary part (magnitude only) of the $l = 1$ and $l = 2$ mode frequencies above threshold. There is always a static mode with $\Omega = 0$. The spectra for $l < 0$ are mirror images with respect to the $\Omega = 0$ line. Effects of potential-well distortion have been ignored; otherwise the $l = 1$ mode frequency would not shift, at least for small Υ.

convergence is also reflected by the fact that the mode frequency shift increases with the azimuthal index l as discussed in the previous section. [See Eqs. (6.121) and (6.134).] In case the truncation procedure does not converge, the formalism based on the expansion (6.72) breaks down. Better convergence may be obtained by expanding ψ_1 in the Cartesian coordinates z and δ instead of the present polar coordinates r and ϕ. The beam behaves more like an unbunched beam. The mode coupling instability treated here for bunched beams then makes a transition to become the microwave instability treated in Section 5.4 for unbunched beams.

We already know that the $l = 0$ mode is always static; its frequency $\Omega = 0$ does not move as the beam intensity is varied. We also know that for moderate beam intensities, the dipole $l = 1$ mode frequency does not move either, as it should when the bunch executes a rigid longitudinal motion and the wake field pattern moves with the bunch—mathematically, this is due to a cancellation between the potential-well and the dynamical contributions, as

discussed in Exercises 6.8 and 6.11. In Figure 6.24, the instability occurs as the $l = 1$ and the $l = 2$ modes merge when $\Upsilon = 1.45$, but that is when the potential-well contribution has been ignored. If included, the $l = 1$ mode frequency would not move as shown. This means the longitudinal mode coupling instability is forced to involve high order modes of order $|l| \geq 2$, making the convergence issue more pronounced. This situation, as we will see in Section 6.7, is quite different from the transverse situation when the main effects are carried out by the $l = 0$ and the $l = -1$ modes in a clean manner. Longitudinal mode coupling is intrinsically more complex than its transverse counterpart.

Gaussian and Parabolic Models

So far we have been considering the water-bag model. Similar treatment can be applied to the Gaussian model (6.125) except that analytic expressions are available only for short bunches. To proceed, consider the function $F_l(p, q)$ of Eq. (6.89). For a Gaussian beam, we have

$$F_l(p,q) = -\frac{N\eta c}{2\pi\sigma^2\omega_s}\exp\left[-\frac{\sigma^2}{2c^2}(p\omega_0+\Omega)^2-\frac{\sigma^2}{2c^2}(q\omega_0+\Omega)^2\right] \times I_l\left[\frac{\sigma^2}{c^2}(p\omega_0+\Omega)(q\omega_0+\Omega)\right], \tag{6.151}$$

where $I_l(x)$ is the Bessel function. For short bunches, the argument in the Bessel function is $\ll 1$, $F_l(p, q)$ factorizes as prescribed in Eq. (6.90), with

$$T_l(\omega) = \sqrt{\frac{N\eta c}{2\pi l!\sigma^2\omega_s}}\left(\frac{\omega\sigma}{\sqrt{2}c}\right)^l e^{-\sigma^2\omega^2/2c^2}. \tag{6.152}$$

This $T_l(\omega)$ is related to the $k = 0$ component of the spectrum $g_{lk}(\omega)$ of Eq. (6.128) by $T_l(\omega) = g_{l0}(\omega)\sqrt{N\eta c/\omega_s}$. This indicates that for short bunches, the $k = 0$ component describes the most prominent radial mode.

As worked out in Exercise 6.10, a factorizable $F_l(p, q)$ means the problem is soluble (a condition which is sufficient but not necessary); the solution is given by Eqs. (6.91–6.92). Equation (6.91), when Fourier transformed, gives the distribution perturbation [see Eq. (6.130)],

$$\rho_1^{(l)}(z) \propto e^{-z^2/2\sigma^2}H_l\left(\frac{z}{\sqrt{2}\sigma}\right), \tag{6.153}$$

where $H_l(x)$ is the Hermite polynomial. Equation (6.92) can be written in the

matrix form (6.144) to give the mode frequency Ω, where

$$M_{ll'} = l\delta_{ll'} + i\frac{Nr_0\eta c^2}{2\pi\gamma T_0\omega_s^2\sigma^2}\frac{li^{l-l'}}{\sqrt{l!l'!}} \times \int_{-\infty}^{\infty} d\omega\, \frac{Z_0^{\parallel}(\omega)}{\omega} e^{-\sigma^2\omega^2/\sigma^2}\left(\frac{\sigma\omega}{\sqrt{2}c}\right)^{l+l'}. \tag{6.154}$$

Equation (6.154) is the Gaussian model counterpart of Eq. (6.145). Radial modes are ignored in this treatment.

Exercise 6.14 If mode coupling can be ignored, we may keep only the diagonal terms of the matrix M. Show that for a short Gaussian beam, this procedure reproduces the expression (6.142) in terms of the effective impedance.

Exercise 6.15 Specialize the result (6.154) to the space charge impedance. Perform a numerical calculation to construct the mode frequency diagram like Figure 6.24. Do the higher order modes converge in this model?

Exercise 6.16 In analogy to the result (6.154) for a Gaussian beam, show that the mode frequency Ω for a parabolic beam satisfies Eq. (6.144) with

$$M_{ll'} = l\delta_{ll'} + i\frac{3Nr_0\eta c^2}{2\gamma T_0\omega_s^2\hat{z}^2} li^{l-l'}\sqrt{\frac{\Gamma(l+\frac{3}{2})\Gamma(l'+\frac{3}{2})}{\pi l!l'!}} \times \int_{-\infty}^{\infty} d\omega\, \frac{Z_0^{\parallel}(\omega)}{\omega} \frac{J_{l+1/2}(\omega\hat{z}/c)J_{l'+1/2}(\omega\hat{z}/c)}{\omega\hat{z}/c}. \tag{6.155}$$

Show that for a purely inductive impedance, the matrix M is diagonal and the eigenmode frequencies are given by Eq. (6.121). The beam is stable in this case even in the presence of mode coupling.

We have now obtained results for three bunch distributions—the water-bag, parabolic, and Gaussian models—under the following two circumstances: (a) when the beam intensity is weak so that coupling among the azimuthal modes can be ignored; (b) when the azimuthal modes are coupled, but only one radial mode (the most prominent mode) is considered per azimuthal family. The full problem, of simultaneous consideration of all azimuthal and radial modes, is considered to be beyond our scope. It is interesting to note that the special case of a parabolic bunch and a purely inductive impedance has been diagonalized in both circumstances mentioned above [see Eqs. (6.117) and (6.155)], but the same analysis does not diagonalize the full problem.

Bunch Lengthening

One consequence of mode coupling instability is the *bunch lengthening* effect, often observed in circular accelerators for electrons.[29] The exact mechanism of the bunch lengthening phenomenon is a research topic.[30] One possible explanation is offered by the mode coupling instability.[31] As mentioned before, a proper explanation will invoke the higher order modes $|l| \geq 2$ and to assure their proper convergence, but as an illustration of this idea, let us consider Figure 6.24. Suppose a beam of "natural" bunch length $\hat{z}_0$ and intensity N is stored in the accelerator. If the intensity is $\Upsilon < \Upsilon_{\text{th}}$, the beam will keep its length $\hat{z}_0$ and little will happen. But if $\Upsilon > \Upsilon_{\text{th}}$, the instability takes over and the bunch starts to lengthen. An inspection of Eq. (6.150) indicates that as the beam lengthens, Υ drops and when Υ drops below Υ_{th}, the beam becomes stable again. In equilibrium, one might presume that the beam will be lengthened just enough so that Υ stays at the instability threshold. When this happens, we have

$$\hat{z} = \frac{c}{T_0}\left(\frac{Nr_0\eta R_0}{\gamma\omega_s^2\Upsilon_{\text{th}}}\right)^{2/3}. \tag{6.156}$$

The behavior of bunch length as a function of beam intensity therefore looks like Figure 6.25(a). For the impedance (6.147), the curve above the bunch lengthening threshold has $\hat{z} \propto N^{2/3}$. Below the threshold, we have shown a slight potential-well bunch shortening.

The change of bunch distribution due to potential-well distortion and that due to mode coupling instability are distinctly different. In the former case, the energy distribution of the beam (we consider an electron beam) is unaffected. In the latter case, the synchrotron oscillation brings the changes in $\hat{z}$ rapidly into proportional changes in $\hat{\delta}$. As a result, the energy spread of the beam behaves like that shown in Figure 6.25(b). Below the bunch lengthening threshold, $\hat{\delta}$ is constant; above the threshold, $\hat{\delta} \propto N^{2/3}$.

We have been using the impedance (6.147) as an illustration. It turns out that, in general, for a given accelerator with an arbitrary impedance, the

[29]F. Amman, IEEE Trans. Nucl. Sci. **NS-16**, No. 3, 1073 (1969); ADONE Group, IEEE Trans. Nucl. Sci. **NS-18**, 217 (1971); B. Richter, IEEE Trans. Nucl. Sci. **NS-20**, 752 (1973).

[30]For more references, see P. Channell and A. M. Sessler, Nucl. Instr. Meth. **136**, 473 (1976); A. Renieri, Frascati Report LNF-76/11R (1976); P. B. Wilson, K. Bane, and K. Satoh, IEEE Trans. Nucl. Sci. **NS-28**, 2525 (1981); T. Weiland, DESY Report 81/088 (1981); R. Siemann, Nucl. Instr. Meth. **203**, 57 (1982); Toshio Suzuki, Yongho Chin, and Kohtaro Satoh, Part. Accel. **13**, 179 (1983); T. Suzuki, Part. Accel. **14**, 91 (1983); Kohji Hirata, Part. Accel. **22**, 57 (1987); R. Meller, *Proc. IEEE Part. Accel. Conf.*, Washington, 1987, p. 1155; K. Hirata, S. Petracca, and F. Ruggiero, Phys. Rev. Lett. **66**, 1693 (1991); Toshio Suzuki, *AIP Proc.* **249**, *Phys. Part. Accel.*, 1992, Vol. 1, p. 491.

[31]F. Sacherer, IEEE Trans. Nucl. Science **NS-24**, No. 3, 1393 (1977); A. W. Chao and J. Gareyte, SLAC Report SPEAR-197/PEP-224 (1976) and Part. Accel. **25**, 229 (1990).

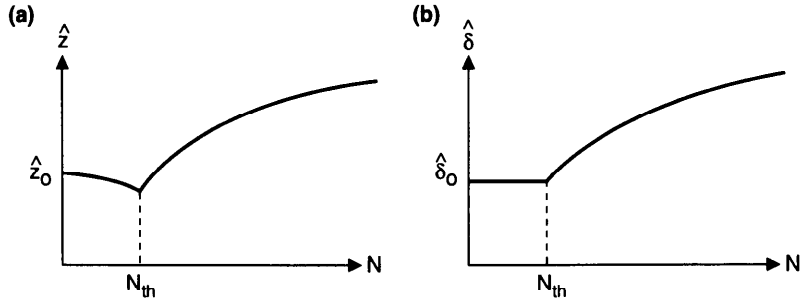

Figure 6.25. Bunch length $\hat{z}$ and energy spread $\hat{\delta}$ as functions of beam intensity N for circular electron accelerators, assuming the mode coupling instability is the underlying mechanism of bunch lengthening. Below a certain bunch lengthening threshold N_{th}, $\hat{z}$ changes (shortens in the case shown) due to potential-well distortion, while $\hat{\delta}$ stays constant. Above N_{th}, both $\hat{z}$ and $\hat{\delta}$ increase with N. If the impedance is given by Eq. (6.147), $\hat{z}$ and $\hat{\delta}$ are proportional to $N^{2/3}$ in the region $N > N_{th}$.

bunch length $\hat{z}$ above threshold depends only on the single parameter

$$\xi = \frac{\eta I_{av}}{\nu_s^2 E}. \tag{6.157}$$

In other words, the accelerator may be operated with various possible values of the average beam current $I_{av} = Ne/T_0$, slippage factor η (which is about equal to the momentum compaction factor α for most electron accelerators), synchrotron tune $\nu_s = \omega_s/\omega_0$, and beam energy E, but the bunch length above the lengthening threshold depends only on these factors combined as specified by Eq. (6.157). This behavior is called the *scaling law*, and ξ is the *scaling parameter*.[32] Equation (6.156), of course, obeys the scaling. Figure 6.26 shows some experimental data for the storage ring SPEAR.[33] The scaling property of these data is apparent.

There is more. An inspection of Eq. (6.145) shows that if the impedance behaves like

$$Z_0^{\parallel}(\omega) \propto \omega^a, \tag{6.158}$$

then the bunch length above the lengthening threshold will behave like

$$\hat{z} \propto \xi^{1/(2+a)}. \tag{6.159}$$

For example, the impedance (6.147) has $a = -\frac{1}{2}$, and thus $\hat{z} \propto \xi^{2/3}$ in Eq.

[32]A. W. Chao and J. Gareyte, Part. Accel. **25**, 229 (1990); M. Month and E. Messerschmidt, IEEE Trans. Nucl. Sci. **NS-24**, 1208 (1977).
[33]P. B. Wilson et al., IEEE Trans. Nucl. Sci. **HS-24**, 1211 (1977).

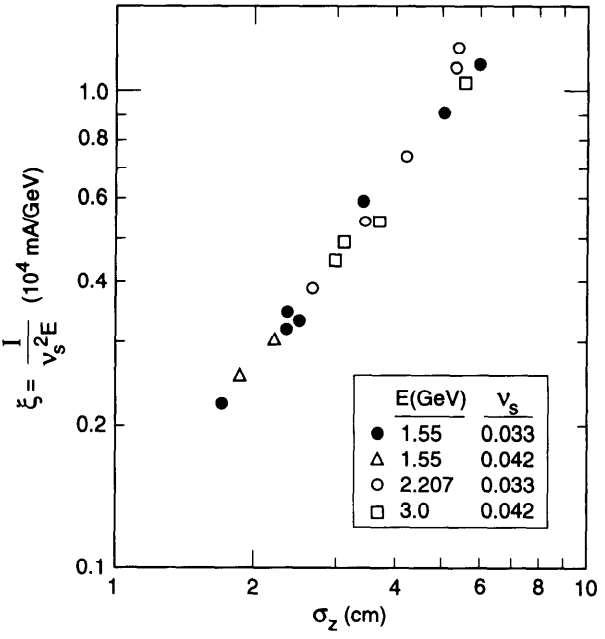

Figure 6.26. Bunch length versus the scaling parameter for the electron storage ring SPEAR. Data are taken above the lengthening threshold. The momentum compaction factor α was kept constant in these experiments, and σ_z is the rms bunch length.

(6.156). Figure 6.26 indicates that for SPEAR, $\sigma_z \propto \xi^{0.76}$, from which we deduce that $a = -0.68$ in the frequency range of interest, which covers from c/σ_z to a few times c/σ_z. With σ_z ranging from 1 to 6 cm, the corresponding frequency $f = \omega/2\pi$ ranges from approximately 1 to several GHz. The impedance is therefore a moderately decreasing function of ω in this frequency range for SPEAR.

Consider an accelerator whose integrated impedance over its circumference resembles that of a resonator impedance with $\omega_R \sim c/b$, where b is the vacuum chamber pipe radius. A long bunch with $\sigma_z \gg b$ samples the impedance at low frequencies where the parameter is approximately proportional to ω and $a \approx 1$. The bunch length above threshold, according to Eq. (6.159), scales with the beam intensity as $\sigma_z \propto N^{1/3}$. For short bunches with $\sigma_z \ll b$, the impedance $\sim \omega^{-1}$ and $a \approx -1$, and we find $\sigma_z \propto N$. For the SPEAR case, σ_z is slightly shorter than b, and we have $a \approx -0.68$ and $\sigma_z \propto N^{0.76}$. Figure 6.27 gives a qualitative sketch of this behavior.

The same scaling behavior is displayed by the microwave instabilities of unbunched beams. To see this, consider the stability criterion (5.136) derived by imposing Landau damping on the longitudinal microwave instability of unbunched beams, but extrapolated to bunched beams. Assuming the bunch length, in the unstable regime, is such that it maintains equality of the two

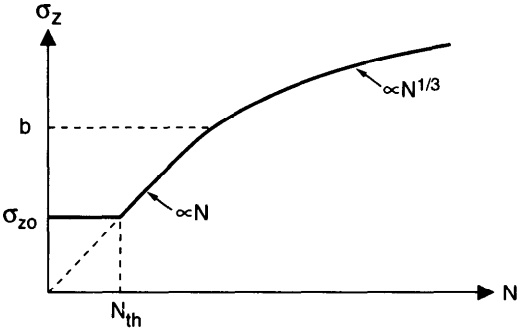

Figure 6.27. The solid curve is a sketch of how the bunch length is expected to behave for a broad-band resonator impedance. Below the threshold, $N < N_{th}$, $\sigma_z = \sigma_{z0}$ is unperturbed by the wake fields. Above the threshold, $\sigma_z \propto N$ if $\sigma \ll b$ and $\sigma_z \propto N^{1/3}$ if $\sigma_z \gg b$, where b is the vacuum chamber pipe radius.

sides of Eq. (5.136), we obtain the bunch length above threshold

$$\Delta z_{1/2} = 0.91\left(\frac{Nr_0\eta c^3}{\gamma T_0 \omega_s^2}\left|\frac{Z_0^{\parallel}}{\omega}\right|\right)^{1/3}. \tag{6.160}$$

Since this holds for $|Z_0^{\parallel}/\omega| = \text{const}$, we have $a = 1$, and therefore the bunch length scales as $\xi^{1/3}$.

As a further illustration, consider the example of potential-well distortion we worked out for the impedance (6.35). One result obtained in that example —the one based on Eq. (6.44), applicable for electrons—was that when the wake strength parameter $D > 2/3^{3/2}$, the beam cannot stay in a state that maintains an unperturbed energy spread. This consideration also yields Eq. (6.160), except that the numerical factor 0.91 now becomes $3^{5/6}/2^{2/3} = 1.57$. Yet another similar situation occurs in Exercise 6.4.

6.6 TRANSVERSE MODES

By the transverse modes here, we mean those modes with $m = 1$, i.e., the beam has a dipole moment (pointing, say, in the vertical y-direction) in the transverse plane. This dipole moment is not necessarily constant longitudinally from the bunch head to the bunch tail. Instead, it may go positive and negative and, depending on the longitudinal mode number l, its longitudinal structure may be simple or complicated as sketched in Figure 6.1(b).

What we will do in this section is to study these transverse modes. Note that, although they are called the *transverse* modes, the transverse structure of these modes is simple (after all, how complicated can a dipole be?), and our main task is, in fact, to find their *longitudinal* structure. This section is

the transverse $m = 1$ counterpart of Sections 6.3 and 6.4 for the longitudinal $m = 0$ case.

It may seem that the problem is going to be much more complicated than the longitudinal case; the Vlasov equation, for example, now needs to take into account both the transverse and the longitudinal phase spaces. Fortunately, however, the transverse structure of the beam is simple and can be found with ease. The strategy is that, after factoring out the transverse dimension from the Vlasov equation, we are left with an equation very similar to the $m = 0$ case; the analysis developed for the longitudinal case can then be followed straightforwardly for the transverse case as well.

The phase space distribution $\psi(y, p_y, z, \delta, s)$ satisfies the Vlasov equation

$$\frac{\partial \psi}{\partial s} + y' \frac{\partial \psi}{\partial y} + p_y' \frac{\partial \psi}{\partial p_y} + z' \frac{\partial \psi}{\partial z} + \delta' \frac{\partial \psi}{\partial \delta} = 0, \tag{6.161}$$

where a prime means taking the derivative with respect to s. The dynamics of the beam is contained in the single-particle equations of motion

$$\begin{aligned} y' &= p_y, \\ p_y' &= -\left(\frac{\omega_\beta}{c}\right)^2 y + \frac{1}{E} F_y(z, s), \\ z' &= -\eta \delta, \\ \delta' &= \frac{1}{\eta}\left(\frac{\omega_s}{c}\right)^2 z + \frac{y}{E} \frac{\partial F_y(z, s)}{\partial z}. \end{aligned} \tag{6.162}$$

The quantity F_y is the transverse wake force generated by the dipole moment of the beam, E is the particle energy, and ω_β and ω_s are the unperturbed betatron and synchrotron frequencies.

In Eq. (6.162), we have included a wake field term in the δ'-equation. It comes from the fact that a dipole moment generates not only a transverse deflecting force, but also a longitudinal retarding force. It also follows from the requirement that the system be Hamiltonian. Equation (6.162), in fact, is a consequence of the Hamiltonian

$$H = \frac{1}{2}\left(\frac{\omega_\beta}{c}\right)^2 y^2 + \frac{1}{2} p_y^2 - \frac{1}{2\eta}\left(\frac{\omega_s}{c}\right)^2 z^2 - \frac{\eta}{2}\delta^2 - \frac{y}{E} F_y(z, s). \tag{6.163}$$

In what follows, however, the term in question will be dropped; the system is therefore, strictly speaking, non-Hamiltonian. Thus, the betatron motion is affected by the wake, but the synchrotron motion is treated as unperturbed.

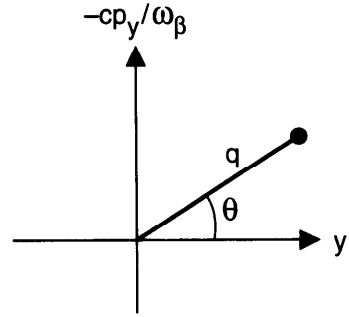

Figure 6.28. Coordinates in the betatron phase space.

This is a good approximation provided the synchro-betatron resonance conditions $\omega_\beta \pm l\omega_s = n\omega_0$ are avoided and the transverse beam size has not grown too large.[34]

We now transform the longitudinal and the transverse coordinates into their polar forms defined by Eq. (6.62) and

$$\begin{aligned} y &= q\cos\theta, \\ p_y &= -\frac{\omega_\beta}{c} q\sin\theta. \end{aligned} \tag{6.164}$$

The transverse phase space coordinates are shown in Figure 6.28. Equation (6.161) then becomes

$$\frac{\partial\psi}{\partial s} + \frac{\omega_\beta}{c}\frac{\partial\psi}{\partial\theta} + \frac{1}{E}F_y(z,s)\frac{\partial\psi}{\partial p_y} + \frac{\omega_s}{c}\frac{\partial\psi}{\partial\phi} = 0. \tag{6.165}$$

The unperturbed stationary distribution of the beam is a function only of r and q. On top of the unperturbed distribution, we will consider a small perturbation that describes a transverse dipole oscillation mode. The distribution is therefore written as

$$\psi = f_0(q)g_0(r) + f_1(q,\theta)g_1(r,\phi)e^{-i\Omega s/c}, \tag{6.166}$$

where Ω is the mode frequency, the unperturbed distributions f_0 and g_0 are considered to be given, and f_1 and g_1 describe the transverse and longitudi-

[34]The synchro-betatron coupling was discussed in the context of a two-particle model in Section 4.3. For more references, see Ronald M. Sundelin, IEEE Trans. Nucl. Sci. **NS-26**, 3604 (1979); T. Suzuki, Nucl. Instr. Meth. **A241**, 89 (1985); F. Ruggiero, Part. Accel. **20**, 45 (1986); Y. H. Chin, CERN Report SPS/85-33 (DI-MST) (1985); T. Suzuki, CERN Report LEP-TH/87-55 (1987). See also Exercise 6.18 below.

nal beam structures of the mode. As we did for the longitudinal instabilities, our job now is to look for self-consistent solutions for Ω, f_1, and g_1.

In writing down Eq. (6.166), we have implicitly assumed that the center of the unperturbed beam coincides with the accelerator pipe axis. Effects associated with a distorted beam trajectory (i.e., a distorted closed orbit) are excluded from our study.

We next introduce an important complication that comes from the head-tail effect discussed in Section 4.5. What happens is that the betatron frequency is not a constant; it depends on δ through the chromaticity ξ. The quantity ω_β in Eq. (6.165) is therefore replaced by $\omega_\beta(1 + \xi\delta)$. Substituting Eq. (6.166) into Eq. (6.165) and linearizing with respect to the perturbation, keeping in mind that F_y is already first order, we find the linearized equation

$$\left[-i\frac{\Omega}{c}f_1 g_1 + \frac{\omega_\beta}{c}(1 + \xi\delta)\frac{\partial f_1}{\partial\theta}g_1 + \frac{\omega_s}{c}f_1\frac{\partial g_1}{\partial\phi}\right]e^{-i\Omega s/c}$$

$$-\frac{c}{E\omega_\beta}\sin\theta F_y f_0' g_0 = 0. \tag{6.167}$$

As mentioned before, the transverse structure f_1 is easy to find. Indeed, since it describes a dipole motion, we anticipate a solution

$$f_1(q,\theta) = -Df_0'(q)e^{i\theta}, \tag{6.168}$$

where D is the dipole displacement of this distribution:

$$\frac{\int q\,dq\int d\theta\; yf_1}{\int q\,dq\int d\theta\, f_0} = -D\frac{\pi\int q^2\,dq f_0'(q)}{2\pi\int q\,dq f_0(q)} = D. \tag{6.169}$$

This dipole motion is sketched in Figure 6.29.

Substituting Eq. (6.168) into Eq. (6.167), one obtains a reduced Vlasov equation that involves only longitudinal coordinates:

$$\left[i(\Omega - \omega_\beta - \xi\omega_\beta\delta)g_1 - \omega_s\frac{\partial g_1}{\partial\phi}\right]De^{-i\Omega s/c} + i\frac{c^2}{2E\omega_\beta}F_y g_0 = 0. \tag{6.170}$$

In obtaining Eq. (6.170), the factor $\sin\theta$ in Eq. (6.167) has been replaced by $e^{i\theta}/2i$. Rigorously, one needs both $e^{i\theta}$ and $e^{-i\theta}$ components, but the $e^{-i\theta}$ component can be ignored if the frequency shift due to the wake field is small compared with the betatron frequency ω_β.

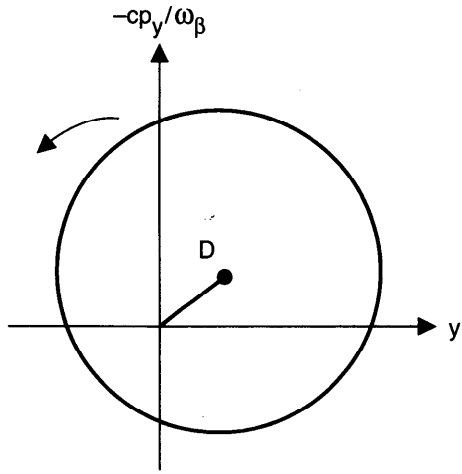

Figure 6.29. Dipole motion in the transverse phase space. The unperturbed distribution $f_0(q)$ is displaced by a distance D. The displaced distribution then rotates around the origin.

We need to find F_y. The dipole moment of the beam, observed as location s as a function of z, is

$$De^{-i\Omega s/c}\int_{-\infty}^{\infty} d\delta\, g_1(r,\phi) = De^{-i\Omega s/c}\rho_1(z). \tag{6.171}$$

The deflecting force is then obtained by summing the wake field over all previous revolutions:

$$F_y(z,s) = -\frac{De^2}{cT_0}\int_{-\infty}^{\infty} dz' \sum_{k=-\infty}^{\infty} \rho_1(z')e^{-i\Omega[(s/c)-kT_0]}W_1(z - z' - kcT_0), \tag{6.172}$$

where W_1 is the transverse wake function integrated over the accelerator circumference cT_0. The longitudinal counterpart of this expression is Eq. (6.66). As before, the distribution $\rho_1(z)$ is what is observed at the fixed location of the impedance and is not the snapshot distribution.

Going to the frequency domain, Eq. (6.172) reads

$$F_y(z,s) = i\frac{De^2}{cT_0^2}e^{-i\Omega s/c} \sum_{p=-\infty}^{\infty} \tilde{\rho}_1(\omega')Z_1^{\perp}(\omega')e^{i\omega' z/c}, \tag{6.173}$$

where $\omega' = p\omega_0 + \Omega$, and $Z_1^{\perp}(\omega)$ is the total transverse impedance in the accelerator.

Substituting Eq. (6.173) into Eq. (6.170), the factor $De^{-i\Omega s/c}$ drops out; we get

$$i(\Omega - \omega_\beta - \omega_\beta \xi\delta)g_1 - \omega_s \frac{\partial g_1}{\partial \phi} - \frac{cr_0}{2\gamma\omega_\beta T_0^2} g_0 \sum_p \tilde{\rho}_1(\omega') Z_1^\perp(\omega') e^{i\omega' z/c} = 0. \tag{6.174}$$

We next Fourier expand g_1 as

$$g_1(r,\phi) = \sum_{l=-\infty}^{\infty} \alpha_l R_l(r) e^{il\phi} e^{i\xi\omega_\beta z/c\eta}. \tag{6.175}$$

This expansion is in analogy to Eq. (6.72) except for the difference that, due to the chromaticity, we now have an additional head-tail phase factor. The same factor appeared in our two-particle treatment in Section 4.5. As mentioned there, it has the remarkable property that it depends only on z, and not on δ. From here on, the treatment is very similar to what we did for the longitudinal case.

Substituting Eq. (6.175) into Eq. (6.174), we find the chromaticity term is canceled nicely except for the phase factor, and we have

$$i\sum_{l'} (\Omega - \omega_\beta - l'\omega_s)\alpha_{l'} R_{l'}(r) e^{il'\phi} - \frac{r_0 c}{2\gamma\omega_\beta T_0^2} g_0(r) e^{-i\xi\omega_\beta z/c\eta} \sum_p \tilde{\rho}_1(\omega') Z_1^\perp(\omega') e^{i\omega' z/c} = 0. \tag{6.176}$$

Multiplying the result by $e^{-il\phi}$ and integrating over ϕ from 0 to 2π, we get an infinite set of equations,

$$i(\Omega - \omega_\beta - l\omega_s)\alpha_l R_l(r) = \frac{r_0 c}{2\gamma\omega_\beta T_0^2} i^l g_0(r) \times \sum_{p=-\infty}^{\infty} \tilde{\rho}_1(\omega') Z_1^\perp(\omega') J_l\left(\frac{\omega'}{c} r - \frac{\xi\omega_\beta}{c\eta} r\right), \quad l = 0, \pm 1, \pm 2, \ldots. \tag{6.177}$$

Furthermore, similarly to Eq. (6.75), we have

$$\tilde{\rho}_1(\omega') = 2\pi \frac{\omega_s}{c\eta} \sum_{l=-\infty}^{\infty} \int_0^\infty r\,dr\, \alpha_l R_l(r) i^{-l} J_l\left(\frac{\omega'}{c} r - \frac{\xi\omega_\beta}{c\eta} r\right). \tag{6.178}$$

Combining Eqs. (6.177–6.178) gives

$$(\Omega - \omega_\beta - l\omega_s)\alpha_l R_l(r) = -i\frac{\pi r_0 \omega_s}{\gamma \omega_\beta T_0^2 \eta} g_0(r) \sum_{l'=-\infty}^{\infty} \int_0^\infty r'\, dr'\, \alpha_{l'} R_{l'}(r') i^{l-l'} \times \sum_{p=-\infty}^{\infty} Z_1^\perp(\omega') J_l\left(\frac{\omega' - \omega_\xi}{c} r\right) J_{l'}\left(\frac{\omega' - \omega_\xi}{c} r'\right), \tag{6.179}$$

where

$$\omega' \equiv p\omega_0 + \omega_\beta + l\omega_s. \tag{6.180}$$

Note that in spite of the head-tail phase, the beam signal observed at a fixed location (at the impedance) is ω', independent of the chromaticity. The effect of the chromaticity is only to cause a shift in the Bessel function spectrum,

$$\omega' \to \omega' - \omega_\xi, \qquad \text{where} \quad \omega_\xi \equiv \frac{\xi \omega_\beta}{\eta}. \tag{6.181}$$

To proceed further, we will assume a simple model of the unperturbed longitudinal distribution, namely,

$$\begin{aligned} g_0(r) &= \frac{N\eta c}{2\pi\omega_s \hat{z}} \delta(r - \hat{z}), \\ \rho_0(z) &= \frac{N}{\pi\sqrt{\hat{z}^2 - z^2}}, \qquad z < |\hat{z}|. \end{aligned} \tag{6.182}$$

In this distribution, shown in Figure 6.30, particles populate an elliptical shell in the phase space. This is called a hollow beam model, or an *air-bag* model.

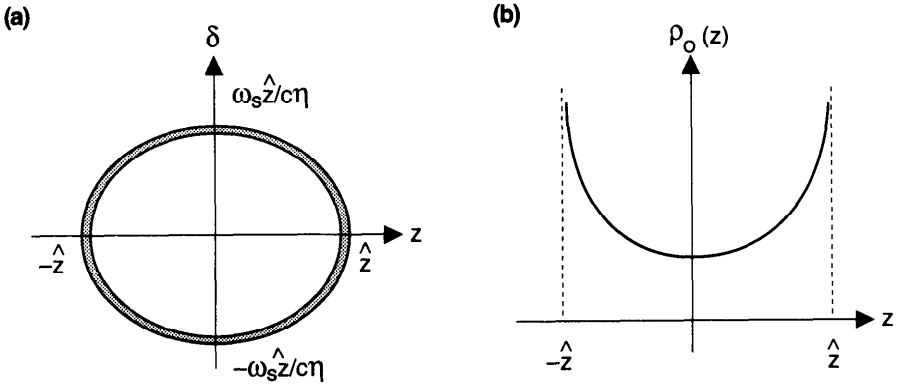

Figure 6.30. (a) Phase space distribution and (b) longitudinal distribution of an air-bag beam. For this distribution, $\sigma_{rms} = \hat{z} / \sqrt{2}$.

The advantage of using the air-bag model is obvious: all R_l's degenerate into $\delta(r - \hat{z})$, i.e., we have $R_l(r) \propto \delta(r - \hat{z})$, and consequently Eq. (6.179) reduces to

$$(\Omega - \omega_\beta - l'\omega_s)\alpha_{l'} = -i\frac{Nr_0c}{2\gamma T_0^2\omega_\beta}\sum_{l''}\alpha_{l''}i^{l'-l''} \times \sum_p Z_1^\perp(\omega')J_{l'}\left(\frac{\omega' - \omega_\xi}{c}\hat{z}\right)J_{l''}\left(\frac{\omega' - \omega_\xi}{c}\hat{z}\right), \quad l' = 0, \pm 1, \pm 2, \ldots . \tag{6.183}$$

A mode is now specified by the frequency $\Omega^{(l)}$ and the set of coefficients $\alpha_{l'}^{(l)}$, where l is the mode index. In the absence of the wake field, the right hand side of Eq. (6.183) vanishes; the lth mode is described by

$$\begin{aligned} \alpha_{l'}^{(l)} &= \delta_{ll'}, \\ \Omega^{(l)} &= \omega_\beta + l\omega_s. \end{aligned} \tag{6.184}$$

The distribution of this mode is given by

$$\underbrace{f_0'(q)e^{i\theta}}_{\text{trans. dist.}}\ \underbrace{\delta(r - \hat{z})e^{il\phi}}_{\text{long. dist.}}\ \underbrace{e^{i\xi\omega_\beta z/c\eta}}_{\text{head-tail phase factor}}\ \underbrace{e^{-i(\omega_\beta + l\omega_s)s/c}}_{\text{time dep.}}. \tag{6.185}$$

These modes, without the head-tail phase factor, are those sketched in Figure 6.1(b).

The mode (6.185) gives rise to a dipole moment. Observed at a fixed location such as a pickup electrode or an impedance, we have

$$\text{dipole moment} \propto \frac{1}{\sqrt{\hat{z}^2 - z^2}}\cos\left[l\cos^{-1}\left(\frac{z}{\hat{z}}\right)\right]\cos\left(\Omega^{(l)}\frac{s}{c} - \chi\frac{z}{\hat{z}}\right), \tag{6.186}$$

where we have defined a *head-tail phase*[35]

$$\chi = \frac{\omega_\xi\hat{z}}{c} = \frac{\xi\omega_\beta\hat{z}}{c\eta}. \tag{6.187}$$

As we will see, χ plays a crucial role in the mechanism of transverse collective instabilities. As a result, the chromaticity ξ often needs to be controlled carefully. The fact that $\chi \propto 1/\eta$ is another indication of the fact that transition crossing (when $\eta \approx 0$) when accelerating an intense beam in a synchrotron is an involved process.

A superposition of the signal (6.186) at several beam passages is shown in Figure 6.31 for different modes and different values of χ. For mode l, there

[35]Remember that $\hat{z}$ is half the total bunch length.

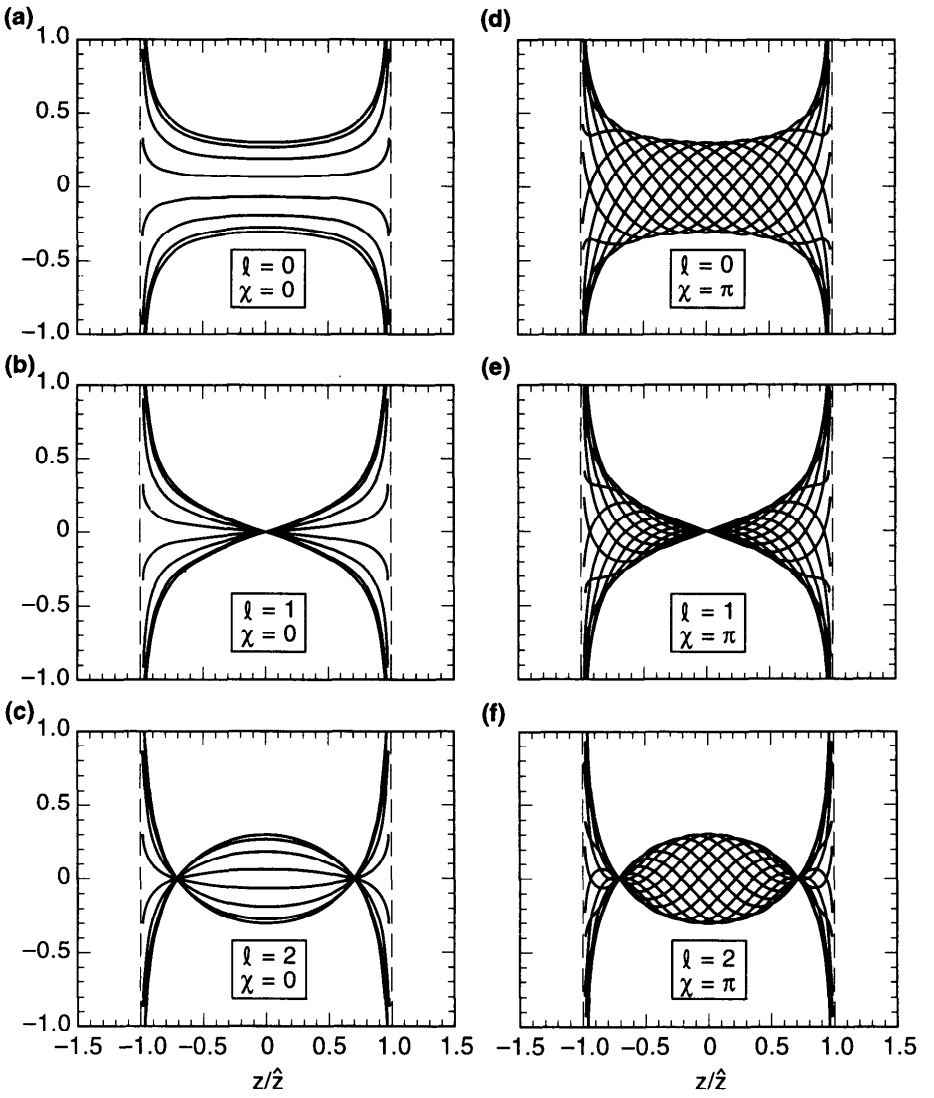

Figure 6.31. Dipole moment observed by a pickup electrode as an air-bag beam executes a collective mode l. Several signals observed at different beam passages are superimposed. In (a) to (c), the head-tail phase $\chi = 0$; in (d) to (f), $\chi = \pi$. The beam is assumed to have a vanishing intensity.

are l nodes in the signal pattern. The locations of these nodes are not affected by a nonzero χ, although the signal away from the nodes becomes more complex.

The signal (6.186) diverges at the bunch edges $z = \pm\hat{z}$ because of the air-bag distribution assumed. The real beam is not likely to have an air-bag distribution. Figure 6.32 shows the beautiful mode patterns observed at the

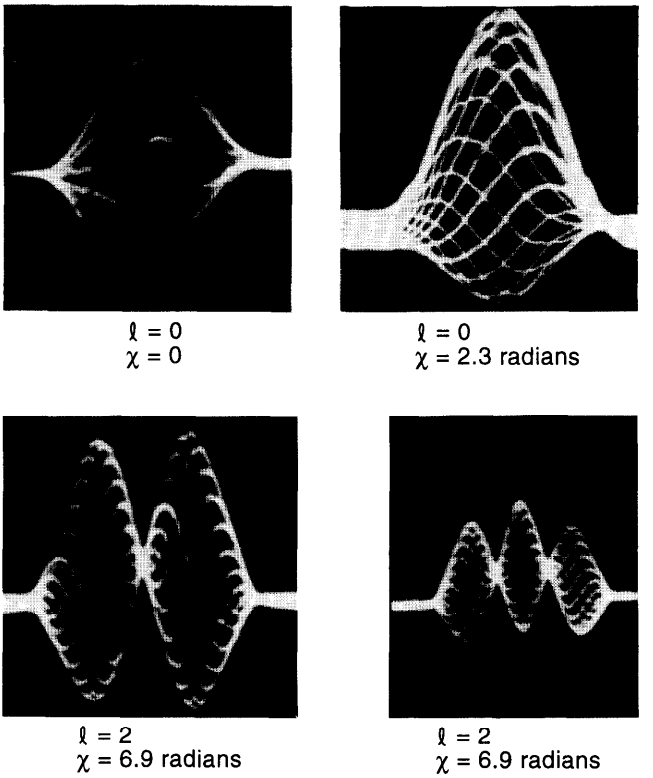

Figure 6.32. Transverse beam oscillation modes observed at the CERN PS Booster. The head-tail phase χ is properly defined for the observed bunch shape. (Courtesy Jacques Gareyte, 1992).

CERN Proton Synchrotron Booster.[36] These patterns are to be compared with those of Figure 6.31.

For a weak beam, the mode frequency shifts are small compared with ω_s; one can obtain the first order perturbation by substituting the unperturbed solution Eq. (6.184) into the right hand side of Eq. (6.183) to obtain

$$\Omega^{(l)} - \omega_\beta - l\omega_s = -i\frac{Nr_0c}{2\gamma T_0^2\omega_\beta}\sum_{p=-\infty}^{\infty} Z_1^\perp(\omega')J_l^2\left(\frac{\omega'\hat{z}}{c} - \chi\right). \quad (6.188)$$

Again, the real part of this expression gives the mode frequency shift, and the imaginary part gives the instability growth rate.

Exercise 6.17 Consider an air-bag beam executing the mode (6.185). Show that the center of charge of the beam as a whole has an oscillation

[36]J. Gareyte and F. Sacherer, *Proc. 9th Int. Conf. on High Energy Accel.*, Stanford, 1974, p. 341.

amplitude proportional to $J_l(\chi)$. Therefore, if $\chi = 0$, a pickup electrode will see only the $l = 0$ mode, but all modes show up if $\chi \neq 0$.

Exercise 6.18

(a) The wake term in the δ'-equation of Eq. (6.162) was dropped. To see the significance of this term, let us keep it but drop the wake term in the p_y'-equation instead. Follow closely the development of this section, assuming f_0 Gaussian and g_0 water bag. Show that

$$f_1 = \frac{D}{\sigma_y^2} f_0(q) q e^{i\theta} \tag{6.189}$$

and that $(\Omega - \omega_\beta - l'\omega_s)\alpha_{l'}$ equals

$$i\frac{Nr_0\eta\hat{z}}{\gamma T_0^2\omega_s}\left(\frac{\sigma_y}{\hat{z}}\right)^2 l' \sum_{l''} \alpha_{l''} i^{l'-l''} \sum_p \omega' Z_1^\perp(\omega') \left[\frac{J_{l'}(x)J_{l''}(x)}{x}\right]_{x=(\omega'\hat{z}/c)-\chi}. \tag{6.190}$$

Compare with (6.183). Show that this wake effect can be ignored if σ_y is small compared with $\sqrt{\omega_s/\eta\omega_\beta}$ times the bunch length $\hat{z}$.

(b) If there is a longitudinal impedance $Z_0^\parallel$ present, one can also compare the above result with Eq. (6.80). Show that the effect can be ignored if $Z_1^\perp(\omega)$ is much less than $cZ_0^\parallel(\omega)/\omega\sigma_y^2$. If $Z_0^\parallel(\omega)$ is related to $Z_1^\perp(\omega)$ through Eq. (2.107), then the criterion becomes $\sigma_y \ll b$. Both the conditions $\sigma_y \ll \hat{z}\sqrt{\omega_s/\eta\omega_\beta}$ and $\sigma_y \ll b$ are fulfilled in most accelerators.

Exercise 6.19 There is a frequency-domain version of Eq. (6.179). Follow similar steps as in Exercise 6.10 to establish

$$(\Omega - \omega_\beta - l\omega_s)\alpha_l \tilde{\rho}_1^{(l)}(q) = -i\frac{\pi r_0 \omega_s}{\gamma\omega_\beta T_0^2 \eta} \sum_{l'} \alpha_{l'} \sum_p Z_1^\perp(p\omega_0 + \Omega)\tilde{\rho}_1^{(l')}(p) F_l(p,q), \tag{6.191}$$

where

$$F_l(p,q) = \int_0^\infty r\,dr\, g_0(r) J_l\left(\frac{q\omega_0 + \Omega - \omega_\xi}{c} r\right) J_l\left(\frac{p\omega_0 + \Omega - \omega_\xi}{c} r\right). \tag{6.192}$$

If $F_l(p, q)$ factorizes like Eq. (6.90), show that the solution to Eq. (6.191) is given by Eq. (6.91) and

$$(\Omega - \omega_\beta - l\omega_s)\alpha_l = -i\frac{\pi r_0 \omega_s}{\gamma \omega_\beta T_0^2 \eta} \sum_{l'} \alpha_{l'} i^{l-l'} \times \sum_p Z_1^\perp(p\omega_0 + \Omega) T_{l'}(p\omega_0 + \Omega) T_l(p\omega_0 + \Omega). \tag{6.193}$$

Apply these results to the air-bag model to obtain Eq. (6.183).

We will return to Eq. (6.188) and continue the discussion of transverse collective instabilities in the next section. In the rest of this section, we will discuss the radial modes by following steps very similar to those of Section 6.4. Consider a weak beam, whose mode frequency shift from the unperturbed values $\omega_\beta + l\omega_s$ is small compared with ω_s, so that modes with different azimuthal indices l do not couple.

For a given l, introduce a weight function

$$W(r) = \frac{\omega_s}{N\eta c} g_0(r) \tag{6.194}$$

and a kernel function

$$G_l(r, r') = -i\frac{\pi N r_0 c}{\gamma T_0^2 \omega_\beta \omega_s} \sum_{p=-\infty}^{\infty} Z_1^\perp(\omega') J_l\left(\frac{\omega' - \omega_\xi}{c} r\right) J_l\left(\frac{\omega' - \omega_\xi}{c} r'\right). \tag{6.195}$$

We obtain the *Sacherer's integral equation* for $m = 1$,

$$\left(\frac{\Omega - \omega_\beta}{\omega_s} - l\right) R_l(r) = W(r) \int_0^\infty r'\, dr'\, R_l(r') G_l(r, r'). \tag{6.196}$$

We next form a set of functions $\{f_k(r),\ k = 0, 1, 2, \ldots\}$ that satisfy the orthonormality condition (6.96) with the present choice of weight function. The frequencies of the radial modes are determined by the eigenvalue condition

$$\det\left[\left(\frac{\Omega - \omega_\beta}{\omega_s} - l\right) I - M\right] = 0. \tag{6.197}$$

The interaction matrix M is given by

$$M_{kk'} = -i\frac{\pi N r_0 c}{\gamma T_0^2 \omega_\beta \omega_s} \sum_{p=-\infty}^{\infty} Z_1^\perp(\omega') g_{lk}(\omega' - \omega_\xi) g_{lk'}(\omega' - \omega_\xi), \quad (6.198)$$

where $\omega' = p\omega_0 + \omega_\beta + l\omega_s$ and $\omega_\xi = \xi\omega_\beta/\eta$. The function $g_{lk}(\omega)$ has the expression (6.101). In contrast to the longitudinal case, the weight function has the dimension L^{-2}, and f_k, g_{lk}, and $M_{kk'}$ are dimensionless.

Consider a bunch with a uniform longitudinal distribution $\rho_0(z)$,

$$\begin{aligned} g_0(r) &= \frac{N\eta c}{2\pi\omega_s \hat{z}} \frac{1}{\sqrt{\hat{z}^2 - r^2}}, \qquad r < \hat{z}, \\ \rho_0(z) &= \frac{N}{2\hat{z}}, \qquad |z| < \hat{z}, \\ \sigma_z &= \frac{\hat{z}}{\sqrt{3}}. \end{aligned} \quad (6.199)$$

The weight function

$$W(r) = \frac{1}{2\pi\hat{z}\sqrt{\hat{z}^2 - r^2}} \quad (6.200)$$

is very close to that of the parabolic model solved in Section 6.4. It follows that, for the present case,

$$\begin{aligned} f_k(r) &= \sqrt{4\pi \frac{(l + 2k + \frac{1}{2})k!\Gamma(l + k + \frac{1}{2})}{(l + k)!\Gamma(k + \frac{1}{2})}} \\ &\quad \times \left(\frac{r}{\hat{z}}\right)^l P_k^{(l, -1/2)}\left(1 - \frac{2r^2}{\hat{z}^2}\right), \\ g_{lk}(\omega) &= \sqrt{\frac{1}{2\pi} \frac{(l + 2k + \frac{1}{2})\Gamma(k + \frac{1}{2})\Gamma(l + k + \frac{1}{2})}{k!(l + k)!}} \\ &\quad \times \frac{J_{l+2k+1/2}(\omega\hat{z}/c)}{\sqrt{\omega\hat{z}/c}}. \end{aligned} \quad (6.201)$$

If we further assume the impedance $Z_1^\perp(\omega) = \text{const}$, independent of ω, and make the broad-band approximation (6.116), the problem is readily

diagonalized. The matrix elements are

$$M_{kk'} = -\frac{Nr_0c^2}{4\pi\gamma T_0\omega_\beta\omega_s\hat{z}} iZ_1^\perp \frac{\Gamma\left(k+\frac{1}{2}\right)\Gamma\left(l+k+\frac{1}{2}\right)}{k!(l+k)!}\delta_{kk'}. \quad (6.202)$$

Note that the chromaticity does not play a role here. This is because the constant impedance does not respond to a shift of spectrum dictated by the chromaticity. The eigenmodes are the Legendre modes

$$\begin{aligned}
\Omega^{(l,n)} &= \omega_\beta + l\omega_s + M_{nn}\omega_s, \\
\rho_1^{(l,n)} &\propto P_{l+2n}\left(\frac{z}{\hat{z}}\right), \\
\psi_1^{(l,n)}e^{-i\Omega s/c} &\propto f'(q)e^{i\theta}\frac{(r/\hat{z})^l}{\sqrt{1-(r/\hat{z})^2}} P_n^{(l,\ 1/2)}\left(1-\frac{2r^2}{\hat{z}^2}\right) \\
&\quad \times e^{il\phi}e^{i\omega_\xi z/c}e^{-i\Omega^{(l,n)}s/c}.
\end{aligned} \quad (6.203)$$

One can also study the Hermite modes of a Gaussian model. The relevant quantities are

$$\begin{aligned}
g_0(r) &= \frac{N\eta c}{2\pi\sigma^2\omega_s}e^{-r^2/2\sigma^2}, \\
W(r) &= \frac{1}{2\pi\sigma^2}e^{-r^2/2\sigma^2}, \\
f_k(r) &= \sqrt{\frac{2\pi k!}{(l+k)!}}\left(\frac{r}{\sqrt{2}\,\sigma}\right)^l L_k^{(l)}\left(\frac{r^2}{2\sigma^2}\right), \\
g_{lk}(\omega) &= \frac{1}{\sqrt{2\pi k!(l+k)!}}\left(\frac{\omega\sigma}{\sqrt{2}\,c}\right)^{l+2k} e^{-\omega^2\sigma^2/2c^2}, \\
\tilde{g}_{lk}(z) &\propto e^{-z^2/2\sigma^2}H_{l+2k}\left(\frac{z}{\sqrt{2}\,\sigma}\right).
\end{aligned} \quad (6.204)$$

Given l and $Z_1^\perp(\omega)$, the radial modes are in general obtained by solving the eigenvalue problem (6.197) with the interaction matrix (6.198).

In the same spirit as Eqs. (6.139–6.143), one can also define an effective impedance even if the problem has not been diagonalized, i.e.,

$$\left(Z_1^\perp\right)_{\text{eff}} = \frac{\sum_{p=-\infty}^{\infty} Z_1^\perp(\omega')h_l(\omega'-\omega_\xi)}{\sum_{p=-\infty}^{\infty} h_l(\omega'-\omega_\xi)}. \quad (6.205)$$

One notable difference from Eq. (6.140) is of course the beam spectral shift (6.181) due to the chromaticity.

For a uniform beam model (6.199), $h_l(\omega)$ is given by Eq. (6.141), and the complex mode frequency shift is given by

$$\Omega^{(l)} - \omega_\beta - l\omega_s \approx -\frac{1}{4\sqrt{\pi}} \frac{\Gamma(l+\frac{1}{2})}{l!} \frac{Nr_0c^2}{\gamma T_0 \omega_\beta \hat{z}} i(Z_1^\perp)_{\text{eff}}. \quad (6.206)$$

For a Gaussian beam, we have $h_l(\omega)$ given by Eq. (6.143) and

$$\Omega^{(l)} - \omega_\beta - l\omega_s \approx -\frac{1}{4\pi} \frac{\Gamma(l+\frac{1}{2})}{2^l l!} \frac{Nr_0c^2}{\gamma T_0 \omega_\beta \sigma} i(Z_1^\perp)_{\text{eff}}. \quad (6.207)$$

Equations (6.205–6.207) are handy expressions for order-of-magnitude estimates. Take for example a Gaussian beam with $N = 10^{11}$, $\gamma = 10$, $T_0 = 3$ μs, $\nu_\beta = \omega_\beta/\omega_0 \approx 12$, and $\sigma = 10$ cm. If there is reason to believe that $i(Z_1^\perp)_{\text{eff}} = 1$ MΩ/m,[37] Eq. (6.207) gives mode tune shifts of -0.0013 for $l = 0$ and -0.00033 for $l = 1$. The $l = 0$ mode frequency shift can be compared with $\omega_s/2$. When the shift becomes comparable to $\omega_s/2$, the strong head-tail instability is likely to set in.

Exercise 6.20 The most prominent transverse mode is likely to be the one with $l = 0$. Consider the $l = 0$ mode of a point bunch. Let the chromaticity $\xi = 0$. Use Eq. (6.206) to show that the mode frequency shift is given by

$$\Omega^{(0)} - \omega_\beta \approx -\frac{Nr_0c}{2\gamma T_0^2 \omega_\beta} i \sum_{p=-\infty}^{\infty} Z_1^\perp(\omega'). \quad (6.208)$$

The same result is obtained for a Gaussian bunch using Eq. (6.207) as should be obtained for a point bunch. The expression (6.208) was obtained before in Eqs. (4.27–4.28) using a one-particle model.

Like its longitudinal counterpart, the effective impedance (6.205) involves the overlap integral between the impedance $Z_1^\perp(\omega)$ and the beam spectra $h_l(\omega)$—except that $l = 0$ is now an allowed mode and that there is the spectral shift (6.181)—as illustrated in Figure 6.33. One consequence of the spectral shift (6.181) is that the real part of $(Z_1^\perp)_{\text{eff}}$ no longer vanishes even for broad-band impedances. The mode frequency therefore acquires an imaginary part, and if $\text{Re}(Z_1^\perp)_{\text{eff}} < 0$, the beam can become unstable. Inspection of the $l = 0$ member of Figure 6.33(b) indicates that this mode becomes

[37] For example, one may have the information from elsewhere that the longitudinal impedance has $(Z_0^\parallel/n)_{\text{eff}} = 8.8$ Ω. By applying Eq. (2.108) to the effective impedances and knowing $b = 5$ cm, one obtains $(Z_1^\perp)_{\text{eff}} = 1$ MΩ/m, provided $\xi = 0$.

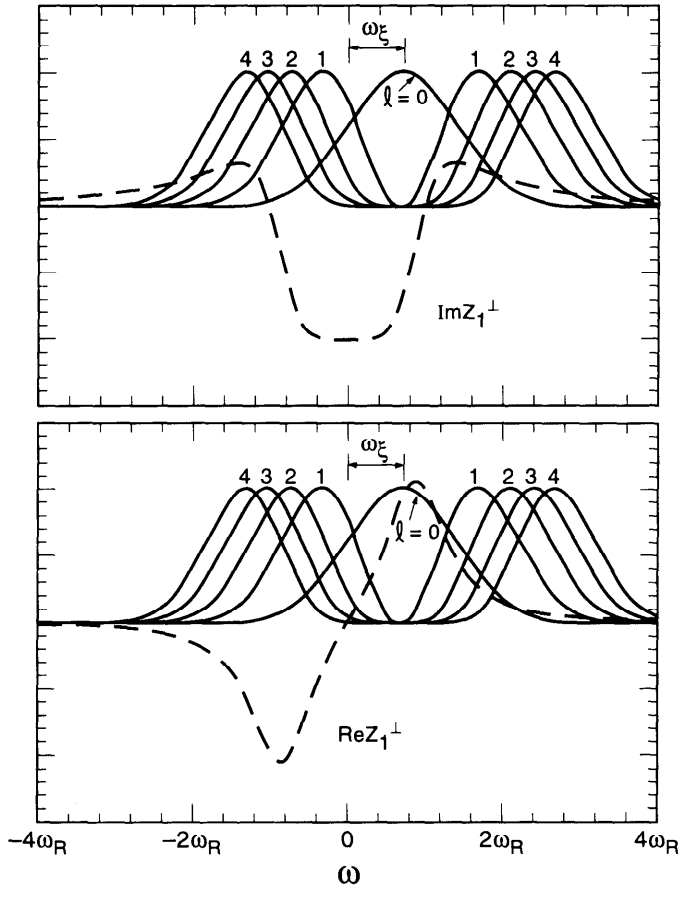

Figure 6.33. Solid curves are the spectra $h_l(\omega - \omega_\xi)$ of a Gaussian beam (normalized so that they have the same value at their respective maxima). Dashed curves are the broad-band impedance $Z_1^\perp(\omega)$: (a) imaginary part; (b) real part. The parameters are such that $c/\sigma = \omega_R$, $\omega_\xi = 0.7\omega_R$, and $Q = 1$. The real part of $(Z_1^\perp)_{\text{eff}}$ vanishes if $\xi = 0$ due to symmetry. When $\xi \neq 0$, however, $\text{Re}(Z_1^\perp)_{\text{eff}} \neq 0$ and there can be instability growth.

unstable if $\omega_\xi = \xi\omega_\beta/\eta$ is negative. This confirms again the head-tail stability criterion that for the $l = 0$ mode to be stable, one needs to have $\xi > 0$ above transition and $\xi < 0$ below transition.

Exercise 6.21 With a broad-band resonator impedance and a Gaussian beam, show that for a short bunch, $\sigma \ll c/\omega_R$,

$$\frac{1}{\tau^{(0)}} \approx -\frac{Nr_0\sigma^2\omega_R\omega_\xi}{\gamma T_0\omega_\beta b^2}\frac{R_S}{Q}. \tag{6.209}$$

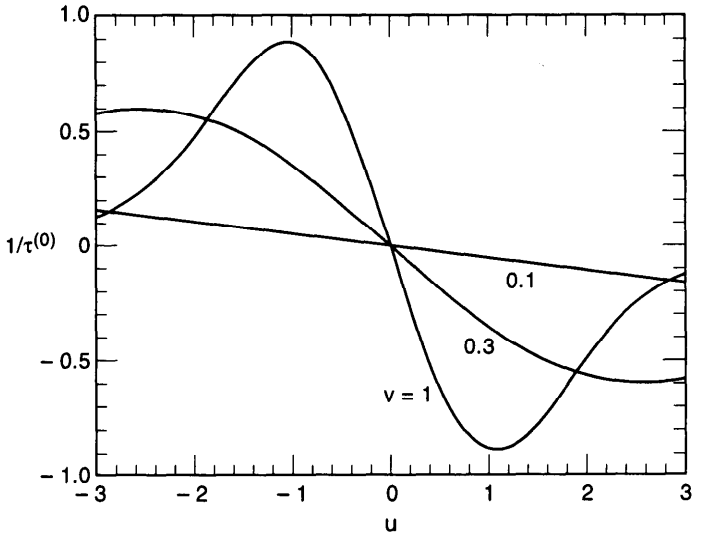

Figure 6.34. Growth rate $1/\tau^{(0)}$ (normalized by $Nr_0c^2R_S/2\pi\gamma T_0\omega_\beta b^2$) for the $l=0$ mode versus $u=\omega_\xi/\omega_R$. A $Q=1$ resonator impedance and a Gaussian bunch are assumed. Results are given for three values of $v=\omega_R\sigma/c$. Equation (6.209) gives an approximate expression when $v \ll 1$.

Compare the result with that for the water-bag model. Compute $1/\tau^{(0)}$ numerically as a function of ω_ξ/ω_R. Show that the worst growth rate occurs when $\omega_\xi \approx -\omega_R$. Some results can be found in Figure 6.34.

The dependence of $(Z_1^\perp)_{\text{eff}}$ on the chromaticity provides a way to measure $Z_1^\perp$ as a function of ω, particularly for proton synchrotrons that go through transition during acceleration with long bunches. Consider the $l=0$ mode, whose spectrum centers around $\omega=\omega_\xi=\xi\omega_\beta/\eta$. The effective impedance is approximately given by $Z_1^\perp(\omega_\xi)$ if the bunch length is longer than the range of the wake field. It follows from Eqs. (6.206–6.207) that

$$\Omega^{(0)}-\omega_\beta \approx -\frac{Nr_0c^2}{4\gamma T_0\omega_\beta} iZ_1^\perp(\omega_\xi)\begin{cases}\dfrac{1}{\hat{z}}, & \text{uniform beam,}\\[2ex] \dfrac{1}{\sqrt{\pi}\,\sigma}, & \text{Gaussian beam.}\end{cases} \tag{6.210}$$

Measuring the frequency shift and the growth rate of the $l=0$ mode of a long bunch therefore provides information on the imaginary and the real parts of the transverse impedance $Z_1^\perp$. This impedance measuring technique was used at the CERN Proton Synchrotron.[36] By varying the chromaticity ξ

and the slippage factor η, $Z_1^\perp$ as a function of frequency can be measured. The reachable frequency range can be expanded by choosing to operate the accelerator close to transition when η is small. The resolution of the technique requires $\xi\omega_\beta/\eta \gtrsim c/\sigma_z$.

6.7 TRANSVERSE INSTABILITIES

In this section, we will study the transverse collective instabilities, ignoring the radial modes. Our starting point is Eq. (6.188), developed in the previous section for a weak air-bag beam using the Vlasov technique. Equation (6.188) gives the complex mode frequency for mode l. For example, the $l = 0$ mode describes a rigid beam mode in which the entire beam bunch, from head to tail, has the same dipole moment. Consider a point bunch, $\hat{z} = 0$; the only mode that this bunch can have is the $l = 0$ mode, and its mode frequency is

$$\Omega^{(0)} - \omega_\beta = -i\frac{Nr_0c}{2\gamma T_0^2\omega_\beta}\sum_{p=-\infty}^{\infty} Z_1^\perp(p\omega_0 + \omega_\beta). \tag{6.211}$$

This result has been obtained before in Eq. (4.25) using a one-particle model. As pointed out there, Eq. (6.211) leads to the transverse Robinson instability if the impedance has sharp peaks with widths $\Delta\omega \lesssim [\omega_\beta]$, where $[\omega_\beta]$ is the betatron frequency modulo the revolution frequency ω_0. It also leads to the resistive-wall instability summarized by Eqs. (4.34–4.35).

Exercise 6.22 Consider an impedance sharply peaked at $\omega \approx \pm h\omega_0$. Use Eq. (6.188) to show that the transverse Robinson growth rate for the lth mode is

$$\frac{1}{\tau^{(l)}} \approx -\frac{Nr_0c}{2\gamma T_0^2\omega_\beta}\left[\mathrm{Re}\, Z_1^\perp(h\omega_0 + \Delta)\, J_l^2\left(h\omega_0\frac{\hat{z}}{c} - \chi\right)\right.$$
$$\left. - \mathrm{Re}\, Z_1^\perp(h\omega_0 - \Delta)\, J_l^2\left(h\omega_0\frac{\hat{z}}{c} + \chi\right)\right], \tag{6.212}$$

where $\Delta = [\omega_\beta] + l\omega_s$. The two terms in the square brackets are weighted differently according to the head-tail phase χ defined by Eq. (6.187). When $\hat{z} = 0$, Eq. (4.31) is recovered.

Head-Tail Instability

Equation (6.188) is more general than Eq. (6.211) in two ways. First, it can be applied to the $l \neq 0$ modes as well, and second, it contains the chromaticity information that leads to the head-tail instability. As demonstrated in Eq.

(6.212), a sharply peaked impedance would introduce transverse Robinson instabilities in the $l \neq 0$ modes. What is more interesting, however, is the head-tail instability. To study that, let us consider a broad-band impedance (single-turn wake field), so that the summation in Eq. (6.188) can be approximated by an integral over p. The growth rate then reads

$$\frac{1}{\tau^{(l)}} = -\frac{Nr_0 c}{4\pi\gamma T_0 \omega_\beta} \int_{-\infty}^{\infty} d\omega' \, \mathrm{Re}\, Z_1^{\perp}(\omega') \, J_l^2\left(\omega' \frac{\hat{z}}{c} - \chi\right). \tag{6.213}$$

The quantity $\mathrm{Re}\, Z_1^{\perp}(\omega')$ is odd in ω'. If $\chi = 0$, the integral (6.213) vanishes and there will be no instability. One then obtains the familiar situation when the chromaticity $\xi = 0$ (and therefore $\chi = 0$), namely, the only instability of weak beams is of the Robinson type. This, however, is no longer true if $\xi \neq 0$. For finite but small χ, Eq. (6.213) becomes, to first order in χ,

$$\frac{1}{\tau^{(l)}} \approx \frac{Nr_0 c}{\pi\gamma T_0 \omega_\beta} \chi \int_0^{\infty} d\omega \, \mathrm{Re}\, Z_1^{\perp}(\omega) \, J_l\left(\frac{\omega\hat{z}}{c}\right) J_l'\left(\frac{\omega\hat{z}}{c}\right), \tag{6.214}$$

where J_l' is the derivative of the Bessel function J_l.

The physical reason there is no instability for short range wakes when $\chi = 0$ can be related to the mode patterns, shown in Figure 6.31(a)–(c). In this case, the beam displacement at any point along the bunch is either in phase or out of phase with the displacement at any other point along the bunch. The wake force a particle experiences can therefore only be in phase or out of phase with its displacement, thus lacking the 90° phase component required for instability. Such a 90° phase can be provided by the head-tail phase when $\chi \neq 0$, as Figure 6.31(d)–(f) shows.

As an illustration, let us consider an impedance that gives rise to a constant wake (4.37), namely,

$$Z_1^{\perp}(\omega) = W_0\left[\frac{1}{\omega} - i\pi\delta(\omega)\right]. \tag{6.215}$$

The integration in Eq. (6.214) can be performed using Table 6.1, yielding the head-tail instability growth rate[38]

$$\frac{1}{\tau^{(l)}} = \frac{Nr_0 c W_0}{\gamma T_0 \omega_\beta} \chi \frac{2}{\pi^2(4l^2 - 1)}. \tag{6.216}$$

One can compare Eq. (6.216) with the result (4.99) obtained using the two-particle model. The present expression is clearly superior in that it gives

[38]The same result was obtained in M. Sands, SLAC Report TN-69-8 (1969).

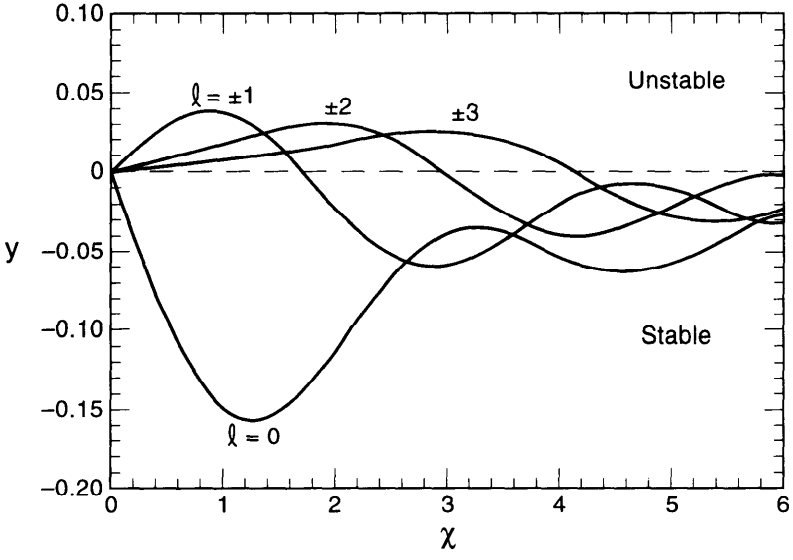

Figure 6.35. The growth rate $1/\tau^{(l)}$ versus the head-tail phase χ for the impedance (6.215), for $|l| = 0, 1, 2, 3$. The vertical axis y is $1/\tau^{(l)}$, normalized by $Nr_0cW_0/\gamma T_0\omega_\beta$. For $\chi < 0$, τ^{-1} can be obtained using the fact that it is an odd function of χ.

the growth rate for all modes. By associating the + and the − modes with the $l = 0$ and the $l = 1$ modes, respectively, the two-particle model predicts that the growth and damping rates of the two modes are equal in magnitude, with $1/\tau^{(0)} = -1/\tau^{(1)}$. In the present, more accurate, treatment, we find $1/\tau^{(1)}$ is suppressed by a factor of 3 relative to the $l = 0$ mode. The two-particle model thus overestimates the effect on the $l = 1$ mode—the air-bag model is obviously more realistic than the two-particle model. Nevertheless, because of its sharp edges, even the air-bag model is likely to have overestimated the effect of the higher order modes.

According to Eq. (6.216), the $l = 0$ mode is unstable if $\chi < 0$, and the higher order modes are unstable if $\chi > 0$.[39] Strictly speaking, the beam is stable only when $\chi = 0$ exactly. In practice, however, since the $l = 0$ mode has the largest growth rate, χ is often chosen to be small but slightly positive if the head-tail instability is a problem. This means the chromaticity ξ is typically chosen to be small but slightly positive above transition and slightly negative below transition. One should keep in mind, however, that this behavior is model dependent. If the impedance is different from Eq. (6.215) or if χ is not small compared with unity, this conclusion may change. Figure 6.35 shows the growth rates $1/\tau^{(l)}$ versus χ for $l = 0, \pm 1, \pm 2$, and ± 3, assuming an air-bag beam and that the impedance is given by Eq. (6.215). Equation (6.216) gives only the linear portion of these curves for small χ.

[39]Remember that W_0 must be positive by the property of wake functions.

Exercise 6.23 From Eq. (6.213), show that

$$\sum_{l=-\infty}^{\infty} \frac{1}{\tau^{(l)}} = 0. \tag{6.217}$$

This result is valid for arbitrary impedance and arbitrary chromaticity. See footnote 6 of this chapter for the significance of Eq. (6.217).

Exercise 6.24 The imaginary part of the impedance (6.215) gives rise to a mode frequency shift. Show that

$$\Delta\Omega^{(l)} = -\frac{Nr_0cW_0}{4\gamma T_0\omega_\beta} J_l^2(\chi). \tag{6.218}$$

All shifts are negative. If $\chi = 0$, the only mode that suffers a frequency shift is $l = 0$. Compare this $\chi = 0$ result with the two-particle strong head-tail result shown in Figure 4.8. The beam becomes unstable when the $l = 0$ mode frequency shifts by ω_s and becomes equal to that of the $l = -1$ mode. Estimate the strong head-tail instability threshold this way. Compare the result with that of the two-particle model, Eq. (4.46), and that of Exercise 6.25 below.

It may be instructive to examine the structure of Eqs. (6.216) and (6.218) for the $l = 0$ mode, at least when $\chi = 0$. From Table 2.2, the wake force integrated over the accelerator circumference is $\sim Ne^2W_0\langle x\rangle$. For $l = 0$, the beam bunch acts as a rigid charge distribution, and this wake force can be interpreted as an equivalent quadrupole magnet of gradient

$$\frac{1}{B\rho}\frac{\partial B_y}{\partial x} \sim -\frac{Nr_0W_0}{\gamma C}. \tag{6.219}$$

The corresponding mode tune shift is given by Eq. (1.15):

$$\frac{\Delta\Omega^{(0)}}{\omega_0} \sim \frac{1}{4\pi}\int_0^C ds\,\beta_Z \frac{1}{B\rho}\frac{\partial B_y}{\partial x}, \tag{6.220}$$

where β_Z is the β-function at the location of the impedance; it is taken to be $\omega_0 R/\omega_\beta$ in a smooth accelerator model. Equation (6.220) readily reproduces Eq. (6.218) for $l = 0$. Having established $\Delta\Omega^{(0)}$, the instability growth rate $1/\tau^{(0)}$ in Eq. (6.216) is basically just a factor χ times $\Delta\Omega^{(0)}$. This is because the instability comes from the phase lag between the bunch head and tail, and for small χ, the phase factor $e^{i\chi}$ gives an imaginary part of $i\chi$.

Mode Coupling

As the beam intensity increases, the expression (6.188) breaks down. One has to consider the general case described by Eq. (6.183) and take into consideration the coupling among azimuthal modes. A mode is no longer approximately given by Eqs. (6.184–6.185). Instead, it has to be described as a linear mixture of all the unperturbed modes. This phenomenon has been referred to as "mode coupling," "mode mixing," "transverse turbulence," and "strong head-tail" in the literature.[40] The associated instability mechanism has been illustrated by a two-particle model in Section 4.3.

Let us consider a broad-band impedance and $\chi = 0$. We mentioned before that there is no collective instability under these conditions for weak beams. At high intensities, however, the mode coupling effect can cause instability of the air-bag beam. To demonstrate this, Eq. (6.183) is written as

$$\det\left(\frac{\Omega - \omega_\beta}{\omega_s} I - M\right) = 0, \tag{6.221}$$

which has the same form as Eq. (6.144) except for a shift in Ω by ω_β. The matrix elements of M are

$$M_{ll'} = l\delta_{ll'} - i\frac{Nr_0 c}{4\pi\gamma T_0 \omega_\beta \omega_s} i^{l-l'} \int_{-\infty}^{\infty} d\omega\, Z_1^{\perp}(\omega) J_l\left(\frac{\omega\hat{z}}{c}\right) J_{l'}\left(\frac{\omega\hat{z}}{c}\right). \tag{6.222}$$

The matrix M has the following form:

$$M = \begin{bmatrix} \cdots & & & & & & \\ \cdots & & & & & & \\ & 2+I & R & I & R & I & \\ & R & 1+I & R & I & R & \\ & I & R & I & R & I & \\ & R & I & R & -1+I & R & \\ & I & R & I & R & -2+I & \\ & & & & & & \cdots \\ & & & & & & \cdots \end{bmatrix}. \tag{6.223}$$

The symbols are the same as those used in Eq. (6.146). The elements of M are all real. Unlike Eq. (6.146), the $l = 0$ row does not vanish.

A mode coupling instability was already hinted at in Exercise 6.24, although we ignored the off-diagonal matrix elements there. This exercise will be continued in Exercise 6.25. Here we will introduce another example.

[40] R. D. Kohaupt, *Proc. 11th Int. Conf. High Energy Accelerators*, Geneva, 1980, p. 562; K. Satoh and Y. Chin, Nucl. Instr. Meth. **207**, 309 (1983).

Take the impedance

$$Z_1^{\perp}(\omega) = \frac{2c}{b^2\omega_0} R_0 \left| \frac{\omega_0}{\omega} \right|^{3/2} [\mathrm{sgn}(\omega) + i]. \tag{6.224}$$

This impedance is related to the longitudinal impedance (6.147) through Eq. (2.107) and gives the diffraction model (2.145) if R_0 is properly chosen. The corresponding transverse wake function is

$$W_1(z) = -\frac{8R_0}{b^2} \sqrt{\omega_0 c} \, |z|^{1/2}. \tag{6.225}$$

Substituting Eq. (6.224) into Eq. (6.222), we find

$$M_{ll'} = l\delta_{ll'} + \frac{\Upsilon'}{2} C_{ll'}, \tag{6.226}$$

where $C_{ll'}$ are the coefficients given by Eq. (6.149) and Υ' is a dimensionless parameter defined by

$$\Upsilon' = \frac{N r_0 c^2 R_0}{\gamma T_0 \omega_\beta \omega_s b^2} \sqrt{\frac{\hat{z}}{cT_0}}. \tag{6.227}$$

Figure 6.36 shows the results of a numerical calculation using Eq. (6.221) and the matrix (6.226). The eigenvalues $(\Omega - \omega_\beta)/\omega_s$ are plotted versus the transverse strength parameter Υ' for several modes. At $\Upsilon' = 0$, the mode frequencies are located at $\omega_\beta, \omega_\beta \pm \omega_s, \omega_\beta \pm 2\omega_s, \ldots$. As Υ' increases, the mode frequencies shift, and at $\Upsilon' \approx 0.28$, the two modes $l = 0$ and $l = -1$ become degenerate. At this value of Υ', the other modes have shifted only slightly. Further increase of Υ' renders the beam unstable.

The parameter Υ' can be related to the longitudinal strength parameter Υ, Eq. (6.150), by

$$\Upsilon' = \Upsilon \left(\frac{\hat{z}}{b} \right)^2 \frac{\omega_s}{\eta \omega_\beta}. \tag{6.228}$$

As a rough estimate of whether the longitudinal or the transverse instabilities dominate the beam behavior, we can compare Υ and Υ' relative to their respective threshold values $\Upsilon_{\mathrm{th}} = 1.45$ and $\Upsilon'_{\mathrm{th}} = 0.28$. If $\Upsilon'/\Upsilon \gtrsim 0.28/1.45 \approx 0.2$, the limiting beam instability is probably transverse, while if $\Upsilon'/\Upsilon \lesssim 0.2$, the longitudinal instability may have a lower threshold.

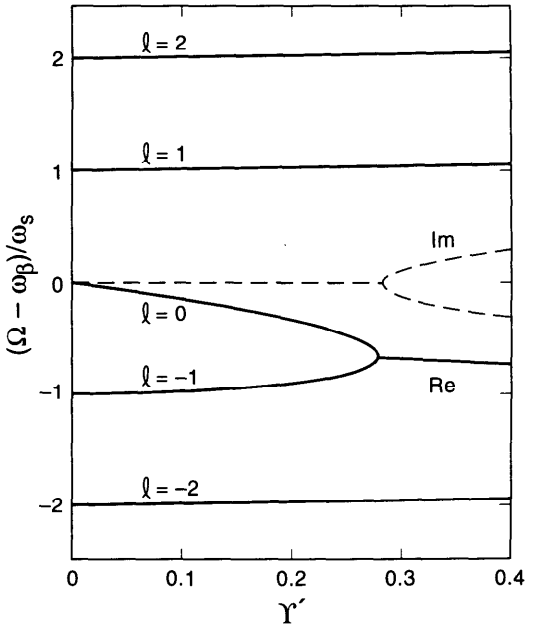

Figure 6.36. Transverse mode frequencies $(\Omega - \omega_\beta)/\omega_s$ versus the parameter Υ' for an air-bag beam with the impedance (6.224). The instability threshold is located at $\Upsilon'_{th} \approx 0.28$, where the modes $l = 0$ and -1 become degenerate. The dashed curves give the imaginary part of the mode frequencies for $l = 0$ and $l = -1$.

As an alternative expression to Eq. (6.228), one can write

$$\frac{\Upsilon'}{\Upsilon} = \frac{2\sigma_z \sigma_\delta \beta_Z}{b^2}, \tag{6.229}$$

where σ_z is the rms bunch length, $\sigma_\delta = \omega_s \sigma_z / \eta c$ is the rms relative energy spread, and β_Z is the β-function at the location of the transverse impedance. Equation (6.229) is to be compared with Eq. (5.138) derived using unbunched beams. Note that short bunches tend to be more unstable longitudinally, and long bunches transversely. Given the design of an electron storage ring, σ_z and σ_δ are proportional to the operating beam energy. It follows that the transverse instability tends to be more important at high operating energies, and the longitudinal instability at low energies.

In the present example, the beam is found to be more stable transversely for shorter bunches, since $\Upsilon' \propto \hat{z}^{1/2}$. Although this tendency is generally true, its functional dependence is model dependent. For a different impedance, Υ' would depend on $\hat{z}$ differently. The scaling with respect to the other parameters, on the other hand, is more robust. For example, for a given accelerator and given bunch length $\hat{z}$, the threshold beam intensity

obeys the scaling property

$$N_{\text{th}} \propto \omega_s \omega_\beta E, \tag{6.230}$$

or alternatively,

$$I_{\text{th}} \propto \frac{\nu_s E}{\beta_Z}, \tag{6.231}$$

where I_{th} is the threshold beam current, and $\nu_s = \omega_s/\omega_0$ is the synchrotron tune.

Exercise 6.25 Show that for an air-bag beam and an impedance (6.215), the matrix M has the elements

$$M_{ll'} = l\delta_{ll'} + \frac{\Upsilon}{\pi^2} \begin{cases} \dfrac{4}{\pi(l^2 - l'^2)} & \text{if } l - l' \text{ is odd,} \\ -\pi\delta_{l0}\delta_{l'0} & \text{if } l - l' \text{ is even,} \end{cases} \tag{6.232}$$

where Υ is the same parameter defined by Eq. (4.42) when we studied the two-particle model using the same impedance. Using the two-particle model, we obtained Figure 4.8. Using the matrix M above, we obtain Figure 6.37. Note that the two-particle model greatly exaggerates the effect of wake field on the higher order modes.

In Figures 6.36–6.37, the $l = 0$ mode frequency shifts downward as the beam intensity increases from zero. This is a general behavior for short bunches. The transverse wake force produced by an off-axis beam has the polarity that deflects the beam further away from the pipe axis. This force acts as a defocusing force for the rigid beam mode ($l = 0$), and as a result, its mode frequency shifts downward. Such a downshift of the betatron frequency is routinely observed in electron accelerators.[41] As discussed following Eq. (4.52), the measurement of the betatron frequency shift with beam intensity provides one of the most available handles on the impedance.

In general, the mode frequency shift is determined by the overlap integral between the mode spectrum and Im $Z_1^\perp$. For a resonator impedance and $\omega_\xi = 0$, the $l = 0$ mode samples mainly the low frequency region where Im $Z_1^\perp < 0$. [See Figure 6.33(a).] For a short bunch, the $l = \pm 1$ mode spectra extend to high frequencies and sample mainly the region where Im $Z_1^\perp > 0$, and their mode frequencies shift up. Instability results when the frequencies

[41] R. D. Kohaupt, IEEE Trans. Nucl. Sci. **NS-26**, 3480 (1979); J. Le Duff et al., *Proc. 11th Int. Conf. High Energy Accel.*, Geneva, 1980, p. 566; D. Rice et al., IEEE Trans. Nucl. Sci. **NS-28**, 2446 (1981); M. P. Level et al., IEEE Trans. Nucl. Sci. **NS-32**, 2215 (1985); M. P. Level, *Proc. 4th Advanced ICFA Beam Dynamics Workshop*, KEK, 1990, KEK Report 90-21, p. 101.

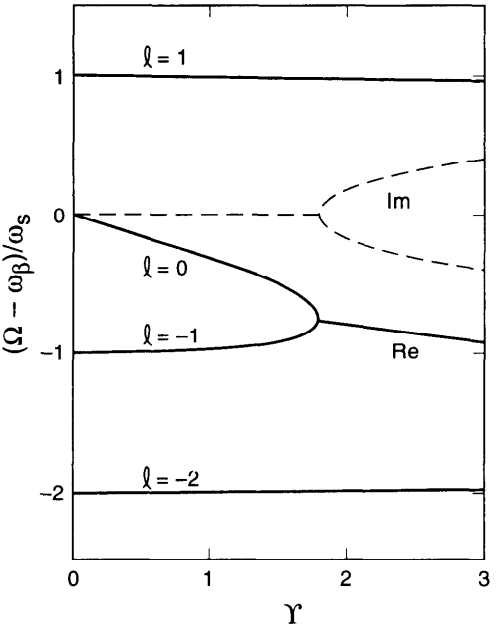

Figure 6.37. Transverse mode frequencies $(\Omega - \omega_\beta)/\omega_s$ versus the parameter Υ for an air-bag beam and an impedance (6.215). The instability threshold is located at $\Upsilon_{th} \approx 1.8$. At the threshold, the $l = 0$ mode frequency has shifted down from ω_β by $\sim 0.8\omega_s$. The dashed curves are the imaginary part of the mode frequencies for $l = 0$ and $l = -1$. This graph can be compared with Figure 4.8 for the two-particle model.

of the $l = 0$ mode (which shifts down) and the $l = -1$ mode (which shifts up) meet. These tendencies were reflected in Figure 6.2, which assumed a short bunch. For a long bunch, the $l = \pm 1$ modes sample the low frequency region and their mode frequencies shift down just like that of the $l = 0$ mode.

Recall that in the longitudinal case, as the beam becomes unstable, the bunch lengthens essentially without losing beam particles. The same does not happen in the transverse case. As soon as the threshold is crossed, beam particles will be lost, at least according to the linearized theory.

Aside from this apparent difference, however, the transverse and longitudinal instabilities are remarkably parallel. For each longitudinal effect, there is most likely a transverse analogy, and vice versa. For example, we have mentioned that the Robinson instability, originally introduced as a longitudinal effect, has its transverse analog, and that at high beam intensities, both the longitudinal and the transverse cases have the mode coupling instabilities.

One may ask then whether there is a head-tail instability in the longitudinal case and whether there is a transverse counterpart of the potential-well

distortion. The answer to both questions is yes. The *longitudinal head-tail instability*, first suggested by Hereward[42] and possibly observed at the CERN SPS,[43] results from the fact that the phase slippage factor η is not strictly a constant; it depends on the instantaneous energy error δ just as the betatron frequency ω_β does. The longitudinal beam distribution then acquires a head-tail phase, and instability may arise as a result.

One transverse analog of the potential-well distortion has been introduced in Chapter 1, namely, the space charge effect that led to the Laslett tune shifts. Another, perhaps less obvious, effect occurs when the trajectory of the unperturbed beam is off the accelerator pipe axis. Such a displacement of the unperturbed beam may result from a closed orbit error caused by imperfections of the accelerator magnets. The transverse wake field associated with the closed orbit error deflects the bunch tail by a fixed amount every time the beam passes by the impedance. The result is that the beam is distorted into a banana shape and this distortion is static in time when observed at a fixed location.[44]

Exercise 6.26 Consider a beam bunch stored in a circular accelerator with a closed orbit distortion so that it passes by a broad-band impedance $Z_1^\perp$ with a transverse displacement y_0. The head of the bunch follows the distorted closed orbit. The bunch tail, on the other hand, acquires an additional static wake induced kick $\Delta y'(z)$, given by Eq. (3.49), every time the bunch passes by the impedance. The bunch tail therefore follows a closed orbit that differs from that of the bunch head by an amount of the order of $\sqrt{\beta_Z \beta(s)}\ \Delta y'(z)$, where β_Z and $\beta(s)$ are respectively the β-functions at the locations of the impedance and the observation point. The beam becomes banana-shaped in the y-z plane. Give an approximate expression of the tilt angle between bunch head and bunch tail in terms of the quantity $Z_0^\parallel/n$.

In the most general description, Eq. (6.76) for $m = 0$ and (6.179) for $m = 1$ are part of a grand scheme in which modes with different m's and l's are all coupled together. To study the beam instability, one then has to solve the eigenvalue problem of a doubly infinite matrix (ignoring radial modes)—if the vacuum pipe were not axially symmetric, this matrix would have been triply infinite—of which we have separately studied only the $m = 0$ and the $m = 1$ components. In reality, as long as the mode frequency shifts are small compared with ω_β (modulo ω_0), the matrix degenerates into blocks, each with a distinct value of m. If the mode frequency shifts are small even

[42]H. Hereward, Rutherford Lab. Reports RL-74-062, EPIC/MC/48 (1974), and RL-75-021, EPIC/MC/70 (1975). See also B. Chen and A. W. Chao, SSCL Report 606 (1992).
[43]D. Boussard and T. Linnecar, *Proc. 2nd Euro. Part. Accel. Conf.*, Nice, 1990, p. 1560.
[44]A. W. Chao and S. Kheifets, IEEE Trans. Nucl. Sci. **NS-30**, 2571 (1983).

compared with ω_s, further degeneracy occurs and indeed we obtain results like Eqs. (6.83) and (6.188).

6.8 MULTIPLE BUNCHES

In the previous sections, we have assumed that there is only one bunch of particles in the accelerator. We will now show that with a slight modification, the analysis can be extended to a beam of M bunches, provided the bunches are equally spaced and equally populated. The macroparticle treatment of multiple bunches was given in Section 4.6.

Consider first the longitudinal instabilities. A mode of the multibunch beam is described by

$$\psi_n(r,\phi,s) = \psi_0(r) + \psi_1(r,\phi)\exp\left[-i\Omega\left(\frac{s}{c} - \frac{nT_0}{M}\right)\right]\exp\left(2\pi i\frac{\mu n}{M}\right),$$
$$n = 0,1,\ldots,M-1, \quad (6.233)$$

where ψ_n is the distribution of the nth bunch observed at a fixed location s,[45] ψ_0 is the unperturbed distribution normalized by Eq. (6.78), N is the number of particles per bunch, ψ_1 is the perturbation distribution (the same for all bunches), and μ is the multibunch mode index, which assumes the values $0,1,\ldots,M-1$. Successive bunches oscillate with a phase difference of $2\pi\mu/M$ if the phases are compared at a given time. The mode number μ and the phase factor $\exp(2\pi i\mu n/M)$ have been introduced in Section 4.6.

We will concentrate on the reference bunch, for which $n = 0$. The retarding wake voltage seen by particles in this bunch is

$$V(z,s) = e\int_{-\infty}^{\infty} dz' \sum_{k=-\infty}^{\infty} \rho_1(z') \sum_{n=0}^{M-1} W_0'\left(z - z' - kC - \frac{nC}{M}\right)$$
$$\times \exp\left[-i\Omega\left(\frac{s}{c} - \frac{nT_0}{M} - kT_0\right) + 2\pi i\frac{\mu n}{M}\right]. \quad (6.234)$$

Compared with Eq. (6.66), this expression contains an additional summation over the M bunches. The quantity ρ_1 is the projection of ψ_1 onto the z-axis defined in Eq. (6.64). In the frequency domain, Eq. (6.234) reads

$$V(z,s) = \frac{Me}{T_0}e^{-i\Omega s/c}\sum_{p=-\infty}^{\infty}\tilde{\rho}_1(\omega')e^{i\omega' z/c}Z_0^{\parallel}(\omega'), \quad (6.235)$$

[45] ψ_n is not the snapshot distribution. This explains the extra time-of-flight factor $\exp(i\Omega nT_0/M)$ in Eq. (6.233).

where

$$\omega' = pM\omega_0 + \mu\omega_0 + \Omega. \tag{6.236}$$

Compared with Eq. (6.67), Eq. (6.235) has an additional factor of M in front, but the summation over p is M times more sparse.

We then follow the procedures of Sections 6.3 to 6.5 to linearize and analyze the Vlasov equation for the $n = 0$ bunch. For a water-bag beam, for example, we obtain again Eq. (6.83) for weak beams, with the modifications

$$\sum_{p=-\infty}^{\infty} (\ )_{\omega'=p\omega_0+\Omega} \to M \sum_{p=-\infty}^{\infty} (\ )_{\omega'=pM\omega_0+\mu\omega_0+\Omega}. \tag{6.237}$$

This modification is a general rule for obtaining multibunch results. The same observation was made in Section 4.6.

As discussed following Eq. (4.128), the multibunch Robinson instability occurs mainly for the $\mu = 0$ mode, and the corresponding growth rate is proportional to the total beam current, not the single-bunch beam current.

For a broad-band impedance (wake range shorter than bunch spacing), the summation over p is replaced by an integral. The replacement removes the factor of M in front, and one obtains results identical to the single-bunch results. This is expected, because having a broad-band impedance means the wake force is short ranged and instability is a result of a local interaction among particles in a single bunch.

Treatment of the transverse motion of a multibunch beam is again very similar. The nth bunch executes the motion

$$\psi_n = f_0(q)g_0(r) + f_1(q,\theta)g_1(r,\phi)\exp\left[-i\Omega\left(\frac{s}{c} - \frac{nT_0}{M}\right)\right]\exp\left(i2\pi\frac{\mu n}{M}\right), \tag{6.238}$$

where f_1 is given by Eq. (6.168). The dipole deflecting force is

$$F_y(z,s) = -\frac{e^2D}{cT_0}\sum_{k=-\infty}^{\infty}\int_{-\infty}^{\infty} dz'\,\rho_1(z')\sum_{n=0}^{M-1}\exp\left[-i\frac{\Omega}{c}\left(s - kC - \frac{nC}{M}\right)\right]$$
$$\times \exp\left(i2\pi\frac{\mu n}{M}\right) W_1\left(z - z' - kC - \frac{nC}{M}\right). \tag{6.239}$$

In terms of impedance, we have

$$F_y(z,s) = i\frac{Me^2D}{cT_0^2}e^{-i\Omega s/c}\sum_{p=-\infty}^{\infty}\tilde{\rho}_1(\omega')e^{i\omega' z/c}Z_1^{\perp}(\omega'), \tag{6.240}$$

where ω' is given by (6.236). The deflecting force therefore observes the rule (6.237). It follows that the mode frequency shifts and growth rates of the μth transverse multibunch mode can all be obtained from the single-bunch results by simply applying the substitution rule (6.237).

6.9 UNBUNCHED BEAMS

The discussion so far in this chapter has been for bunched beams. The Vlasov technique can also be applied to unbunched beams. The analysis for unbunched beams, including Landau damping, was given in Sections 5.3 and 5.4. In this section, we will content ourselves with a rederivation, using the Vlasov technique, the main results of Sections 5.3 and 5.4.

First consider the longitudinal case. For an unbunched beam, the single-particle equations of motion are

$$\dot{z} = -\eta c\delta \quad \text{and} \quad \dot{\delta} = -\frac{eV(z,t)}{ET_0}, \tag{6.241}$$

where the retarding voltage $V(z,t)$ contains only the wake field contributions because there is no rf focusing. The Vlasov equation is

$$\frac{\partial \psi}{\partial t} - \eta c\delta \frac{\partial \psi}{\partial z} - \frac{eV(z,t)}{ET_0}\frac{\partial \psi}{\partial \delta} = 0. \tag{6.242}$$

Let us write the distribution $\psi(z,\delta,t)$ as an unperturbed term plus an infinitesimal perturbation term,

$$\psi = g_0(\delta) + g_1(\delta)e^{in\Theta}e^{-i\Omega t}, \tag{6.243}$$

where n is the mode index, and

$$\Theta = \bar{\omega}_0 t + \frac{z}{R}. \tag{6.244}$$

Equations (6.243–6.244) follow from the fact that the quantity z is defined relative to a reference particle that circulates around the accelerator with the ideal revolution frequency $\bar{\omega}_0 \equiv c/R$. The distribution must then be periodic in Θ with period 2π.

For an unbunched beam, the unperturbed distribution g_0 is a function only of δ, normalized by

$$\int_{-\infty}^{\infty} d\delta\, g_0(\delta) = \frac{N}{2\pi R}. \tag{6.245}$$

The unperturbed uniform beam does not generate longitudinal wake forces. The wake retarding voltage is given by

$$V(z,t) = e\int_{\Theta}^{\infty} R\,d\Theta'\,\rho_1\left(\Theta, t - \frac{R\Theta' - R\Theta}{c}\right) W_0'(R\Theta - R\Theta')$$

$$= e\int_{-\infty}^{\infty} d\delta\, g_1(\delta) \times \int_{\Theta}^{\infty} R\,d\Theta'\, e^{in\Theta} e^{-i\Omega[t-(R\Theta'-R\Theta)/c]} W_0'(R\Theta - R\Theta'). \tag{6.246}$$

In terms of impedance, we have

$$V(z,t) = ece^{in\Theta} e^{-i\Omega t} Z_0^{\parallel}(\Omega) \int_{-\infty}^{\infty} d\delta\, g_1(\delta). \tag{6.247}$$

Substitute Eqs. (6.243) and (6.247) into Eq. (6.242) and linearize the result with respect to g_1. We find

$$g_1(\delta) = i\frac{r_0 c}{\gamma T_0} \frac{g_0'(\delta)}{\Omega - n\bar{\omega}_0(1-\eta\delta)} Z_0^{\parallel}(\Omega) \int_{-\infty}^{\infty} d\delta'\, g_1(\delta'). \tag{6.248}$$

Integrate Eq. (6.248) over δ on both sides. The factor $\int d\delta'\, g_1(\delta')$ drops out. We obtain a dispersion relation

$$1 = i\frac{r_0 c}{\gamma T_0} Z_0^{\parallel}(\Omega) \int d\delta\, \frac{g_0'(\delta)}{\Omega - n\bar{\omega}_0(1-\eta\delta)}. \tag{6.249}$$

We learned from the discussions of Landau damping in Chapter 5 that, given the impedance $Z_0^{\parallel}$ and the unperturbed energy spectrum $g_0(\delta)$ of the beam, Eq. (6.249) can be used to predict the instability threshold boundary by attaching an infinitesimal positive imaginary part to Ω, i.e., $\Omega \to \Omega + i\epsilon$.

Equation (6.249) is our main result. We can also cast it in a different form as follows. The revolution frequency of a particle with energy error δ is

$$\omega_0 = \bar{\omega}_0(1 - \eta\delta). \tag{6.250}$$

Let the ω_0 spectrum of the beam be $\rho(\omega_0)$, normalized by $\int d\omega_0\, \rho(\omega_0) = 1$. Then we have

$$g_0(\delta) = \frac{N|\eta|\bar{\omega}_0}{2\pi R} \rho(\omega_0). \tag{6.251}$$

Changing variable from δ to ω_0 yields another form of the dispersion

relation,

$$1 = -i\frac{2\pi N r_0 \eta}{\gamma T_0^3} Z_0^{\parallel}(\Omega) \int d\omega_0 \frac{\rho'(\omega_0)}{\Omega - n\omega_0}, \tag{6.252}$$

which is just the result obtained in Eq. (5.118). All results subsequent to Eq. (5.118) then follow. We have thus rederived the longitudinal instability conditions discussed in Section 5.4.

The transverse $m = 1$ case is similar, except for the complication due to the head-tail phase. If we ignore the longitudinal component of the $m = 1$ wake force, the Vlasov equation reads

$$\frac{\partial \psi}{\partial t} + \omega_\beta(1 + \xi\delta)\frac{\partial \psi}{\partial \theta} + \frac{c}{E}F_y(z,t)\frac{\partial \psi}{\partial p_y} - c\eta\delta\frac{\partial \psi}{\partial z} = 0. \tag{6.253}$$

The beam distribution $\psi(q, \theta, z, \delta, t)$ is written as

$$\psi = f_0(q)g_0(\delta) + f_1(q,\theta)g_1(\delta)e^{in\Theta}e^{i\omega_\xi(z+\eta\delta ct)/c}e^{-i\Omega t}, \tag{6.254}$$

where $\omega_\xi = \xi\omega_\beta/\eta$ is the head-tail frequency. In Eq. (6.254) we have adopted the polar coordinates (q, θ) for the transverse phase space and the Cartesian coordinates (z, δ) for the longitudinal phase space. Since the distribution is the one observed at a fixed location, the head-tail phase depends on the longitudinal position at a previous time $z - \dot{z}t = z + \eta\delta ct$ for a particle with energy error δ.

The solution for f_1 is given by Eq. (6.168). The transverse deflecting wake force is

$$F_y = -\frac{De^2}{cT_0}\int_{-\infty}^{\infty} d\delta\, g_1(\delta)\int_{\Theta}^{\infty} R\, d\Theta'\, e^{in\Theta + i\omega_\xi(z+\eta\delta ct)} \times e^{-i\Omega[t-(R\Theta'-R\Theta)/c]}W_1(R\Theta - R\Theta'), \tag{6.255}$$

or in terms of impedance,

$$F_y = i\frac{De^2}{T_0}e^{in\Theta + i\omega_\xi(z+\eta\delta ct)}e^{-i\Omega t}Z_1^{\perp}(\Omega)\int_{-\infty}^{\infty} d\delta\, g_1(\delta). \tag{6.256}$$

Substituting Eqs. (6.168), (6.254), and (6.256) into Eq. (6.253) gives

$$g_1(\delta) = -i\frac{r_0 c^2}{2\gamma T_0 \omega_\beta}Z_1^{\perp}(\Omega)\frac{g_0(\delta)}{\Omega - n\bar{\omega}_0(1 - \eta\delta) - \omega_\beta(1 + \xi\delta)}\int_{-\infty}^{\infty} d\delta'\, g_1(\delta'). \tag{6.257}$$

An integration over δ then yields the dispersion relation

$$1 = -i\frac{r_0 c^2}{2\gamma T_0 \omega_\beta} Z_1^\perp(\Omega) \int d\delta \, \frac{g_0(\delta)}{\Omega - n\bar{\omega}_0(1 - \eta\delta) - \omega_\beta(1 + \xi\delta)}. \quad (6.258)$$

The only effect of the chromaticity ξ is to introduce an extra term in the denominator of the integrand on the right hand side. With a δ-function energy distribution, $g_0(\delta) = N\delta(\delta)/2\pi R$, Eq. (6.258) reduces to Eqs. (5.77–5.78). Otherwise, it describes the Landau damping effect due to an energy spread of the beam.

Changing variable from δ to $\omega \equiv \omega_\beta - (n\bar{\omega}_0\eta - \xi\omega_\beta)\delta$, and defining $\rho(\omega)$ to be the spectrum in ω, normalized by $\int d\omega \, \rho(\omega) = 1$, we have

$$g_0(\delta) = \frac{N|-n\eta\bar{\omega}_0 + \xi\omega_\beta|}{2\pi R}\rho(\omega) \quad (6.259)$$

and a new dispersion relation

$$1 = -i\frac{Nr_0 c}{2\gamma T_0^2 \omega_\beta} Z_1^\perp(\Omega) \int d\omega \, \frac{\rho(\omega)}{\Omega - n\bar{\omega}_0 - \omega}, \quad (6.260)$$

which is the same result obtained in Eq. (5.84). We have thus reproduced Section 5.3.

In passing, we have also explicitly shown that the transverse Landau damping is provided by the spread in the combined quantity $n\omega_0 + \omega_\beta$, as asserted in Eq. (5.92). Equation (6.260) is more general than Eq. (6.258) in that the spread in ω does not have to come from chromatic sources. A spread in ω_β, for instance, can also be incorporated.

As an application of Eq. (6.258), consider a beam with a Lorentz spectrum in δ,

$$g_0(\delta) = \frac{N\Delta\delta}{2\pi^2 R}\frac{1}{\delta^2 + \Delta\delta^2}. \quad (6.261)$$

The dispersion relation can be solved to give the complex mode frequency shift

$$\Omega - n\bar{\omega}_0 - \omega_\beta = -i\frac{Nr_0 c}{2\gamma T_0^2 \omega_\beta} Z_1^\perp(n\bar{\omega}_0 + \omega_\beta) - i\,\Delta\delta\,|-n\bar{\omega}_0\eta + \xi\omega_\beta|, \quad (6.262)$$

where we have assumed the perturbation is weak, so that the impedance is evaluated at the unperturbed frequency $\Omega = n\bar{\omega}_0 + \omega_\beta$.

The beam is stable if the imaginary part of Ω is negative, or

$$-\frac{Nr_0c}{2\gamma T_0^2\omega_\beta}\,\mathrm{Re}\,Z_1^\perp(n\bar{\omega}_0+\omega_\beta) < \Delta\delta\,|-n\bar{\omega}_0\eta+\xi\omega_\beta|. \qquad (6.263)$$

This result is consistent with Eq. (5.88). A sufficient (but not necessary) condition for beam stability is $\mathrm{Re}\,Z_1^\perp(n\bar{\omega}_0+\omega_\beta)>0$, which in turn is satisfied if $n\bar{\omega}_0+\omega_\beta>0$ according to Eq. (2.106). The general fact that the collective mode frequency, $\mathrm{Re}\,\Omega$, is unaffected by Landau damping for a Lorentz spectrum is also evident from Eq. (6.262).

The potentially most dangerous situation occurs when Landau damping is least effective, i.e., when $-n\bar{\omega}_0\eta+\xi\omega_\beta\approx 0$. This occurs for the mode with index

$$n\approx\frac{\xi\omega_\beta}{\eta\bar{\omega}_0}. \qquad (6.264)$$

It would be desirable to arrange the parameters in such a way that this mode is naturally damped without Landau damping. As just mentioned, this can be accomplished by having $n\bar{\omega}_0+\omega_\beta>0$, where n is given by Eq. (6.264). This requires

$$\frac{\xi}{\eta}+1>0. \qquad (6.265)$$

The condition (6.265) can be satisfied by arranging the chromaticity ξ to have the same sign as the slippage factor η, i.e., $\xi>0$ above transition and <0 below transition. This feature has been mentioned in connection with Eq. (5.93).

Equation (6.263) can be rewritten as

$$-\mathrm{Re}\,Z_1^\perp(n\bar{\omega}_0+\omega_\beta) < Z_0\frac{2\pi R\gamma|-n\eta+\xi\nu_\beta|}{Nr_0\beta_Z}\,\Delta\delta, \qquad (6.266)$$

where $Z_0=4\pi/c=377\ \Omega$, $\nu_\beta=\omega_\beta/\omega_0$, and β_Z is the β-function at the location of the impedance. Equation (6.266) is the equivalent of the expression (5.93) for a Lorentz spectrum.

The beam is stable if the imaginary part of Ω is negative, or

$$-\frac{Nr_0c}{2\gamma T_0^2\omega_\beta}\,\mathrm{Re}\,Z_1^\perp(n\bar{\omega}_0+\omega_\beta) < \Delta\delta\,|-n\bar{\omega}_0\eta+\xi\omega_\beta|. \qquad (6.263)$$

This result is consistent with Eq. (5.88). A sufficient (but not necessary) condition for beam stability is $\mathrm{Re}\,Z_1^\perp(n\bar{\omega}_0+\omega_\beta)>0$, which in turn is satisfied if $n\bar{\omega}_0+\omega_\beta>0$ according to Eq. (2.106). The general fact that the collective mode frequency, $\mathrm{Re}\,\Omega$, is unaffected by Landau damping for a Lorentz spectrum is also evident from Eq. (6.262).

The potentially most dangerous situation occurs when Landau damping is least effective, i.e., when $-n\bar{\omega}_0\eta+\xi\omega_\beta\approx 0$. This occurs for the mode with index

$$n\approx\frac{\xi\omega_\beta}{\eta\bar{\omega}_0}. \qquad (6.264)$$

It would be desirable to arrange the parameters in such a way that this mode is naturally damped without Landau damping. As just mentioned, this can be accomplished by having $n\bar{\omega}_0+\omega_\beta>0$, where n is given by Eq. (6.264). This requires

$$\frac{\xi}{\eta}+1>0. \qquad (6.265)$$

The condition (6.265) can be satisfied by arranging the chromaticity ξ to have the same sign as the slippage factor η, i.e., $\xi>0$ above transition and <0 below transition. This feature has been mentioned in connection with Eq. (5.93).

Equation (6.263) can be rewritten as

$$-\mathrm{Re}\,Z_1^\perp(n\bar{\omega}_0+\omega_\beta) < Z_0\frac{2\pi R\gamma|-n\eta+\xi\nu_\beta|}{Nr_0\beta_Z}\Delta\delta, \qquad (6.266)$$

where $Z_0=4\pi/c=377\ \Omega$, $\nu_\beta=\omega_\beta/\omega_0$, and β_Z is the β-function at the location of the impedance. Equation (6.266) is the equivalent of the expression (5.93) for a Lorentz spectrum.

Index

Errata

Physics of Collective Beam Instabilities in High Energy Accelerators

January 2, 2026

p.vii, Table of Contents, last line

Original text Heat-Tail

New text Head-Tail

p.29, Eq.(1.65)

Original text $\xi = \frac{4Q^2 r_0 \lambda}{A\beta^2\gamma^2}$

New text $\xi = \frac{4Q^2 r_0 \lambda}{A\beta^2\gamma^3}$

p.30, last line

Original text second number of Eq.(1.70).

New text second member of Eq.(1.70).

p.43, one line above Eq.(2.12)

Original text continuity of $\tilde{E}_z$.

New text continuity of $\tilde{E}_s$.

p.44, 9th line

Original text $\tilde{E}_z$

New text $\tilde{E}_s$

p.45, Eq. (2.17)

Original text $\frac{Z_0^{\parallel}}{L} = \frac{Z_0}{2\pi b}\frac{\tilde{E}_s}{\tilde{B}_\theta}\Big|_{r=b^-}$

New text $\frac{Z_0^{\parallel}}{L} = -\frac{Z_0}{2\pi b}\frac{\tilde{E}_s}{\tilde{B}_\theta}\Big|_{r=b^-}$

p.74, the horizontal scale of Fig.2.12(d)

Original text 4, 2, 0, 2, 4

New text -4, -2, 0, 2, 4

p.92, 4th line
Original text 25 m.
New text 20 m.

p.100, 1st line in Eq.(2.160)
Original text $E_S(0,0,ct)$
New text $E_s(0,0,ct)$

p.103, 1st line after Eq.(2.169)
Original text It follows from Eqs.(2.155) and (2.157) that
New text It follows from Eq.(2.159) that

p.112, Ref.52
Original text **SP**-14, 302 (1966).
New text **AP**-14, 302 (1966).

p.120, 6th line from bottom
Original text $P_{\text{parasitic}} = 8$ W.
New text $P_{\text{parasitic}} = 6.5$ W.

p.125, Eq.(2.213)
Original text $\Delta\mathcal{E} \approx -\frac{\omega_0 q^2 R_S}{2\pi} \ldots$
New text $\Delta\mathcal{E} \approx -\frac{\omega_0 q^2 R_S}{\pi} \ldots$

p.140, 5th line
Original text Eq.(3.28) becomes
New text Eq.(3.27) becomes

p.148, 5th and 6th lines
Original text $(n-1)$th order ... $(n-1)$th order ...
New text nth order ... nth order ...

p.183, Fig.4.9

Original text (vertical scale is missing marks for $0.5 \times 10^{-2}, 0.5 \times 10^{-1}, 0.5 \times 10^{0}, 0.5 \times 10^{1}$)

p.184, one line above Eq.(4.51)
Original text amplitude
New text power amplitude

p.201, 12th line
Original text growth rate
New text growth time

p.210, Eq.(4.124)
Original text $W_0''(-kC - \frac{M-n}{M}C)$
New text $W_0''(-kC - \frac{m-n}{M}C)$

p.213, Eq.(4.133)
Original text The (2,1)-element $-\eta$
New text The (2,1)-element $-\eta C$

p.214, Eq.(4.137)
Original text $e^{-(i\bar{\omega}+\alpha)(C+z_j^{(1)}-z_j)}$
New text $e^{-(i\bar{\omega}+\alpha)(C+z_j^{(1)}-z_j)/c}$

p.218, reference 2
Original text Rev. Sci. Instr. **6**, 429 (1965).
New text Rev. Sci. Instr. **36**, 429 (1965).

p.240, 11th line
Original text is rater small
New text is rather small

p.240, one line above Eq.(5.64)
Original text In pace of
New text In place of

p.242, 2 lines above Fig. 5.6
Original text a reduction of an enhancement
New text a reduction or an enhancement

p.249, Eq.(5.98)
Original text $\frac{\pi\gamma\omega_s}{3N_\beta r_0\beta Z\omega_0}$
New text $\frac{\pi\gamma\omega_s}{3N_B r_0\beta_Z\omega_0}$

p.251, 3rd line from bottom
Original text as it passes by
New text as it passed by

p.252, Eq.(5.108)
Original text $\frac{nr_0c^2}{\gamma T_0}$
New text $\frac{\eta r_0c^2}{\gamma T_0}$

p.266, 3rd line from bottom
Original text Equation (5.146),
New text Equation (5.148),

On the following pages/lines, "lotus" should be replaced by "locus", as follows:

- p.236, 1st, 3rd, 5th, 7th, and 10th line from bottom
- p.259, 17th line
- p.264, 10th line
- p.266, 14th and 15th line
- p.267, 12th and 14th line from bottom
- p.268, Fig. 5.9, "lotuses" should be replaced by "loci"

p.285, Ref.17
Original text A. Hoffman,

New text A. Hofmann,

p.309, 2nd line from bottom
Original text this mode
New text this model

p.311, 1st line after Eq.(6.116)
Original text Table 6.2 and
New text Table 6.1 and

p.314, Eq.(6.122)
Original text $\frac{3}{4}\Upsilon_1$
New text $\frac{3}{4}\Upsilon_1\omega_s$

p.328, Eq.(6.154)
Original text $e^{-\sigma^2\omega^2/\sigma^2}$
New text $e^{-\sigma^2\omega^2/c^2}$

p.336, 1st line
Original text observed as location
New text observed at location

p.338, Eq.(6.180)
Original text $\omega' \equiv p\omega_0 + \omega_\beta + \ell\omega_s.$
New text $\omega' = p\omega_0 + \Omega.$

p.341, caption of the lower-left figure
Original text $\ell = 2$
New text $\ell = 1$

p.341, Eq.(6.188)
Original text (add after equation)
New text where $\omega' = p\omega_0 + \omega_\beta + \ell\omega_s.$

p.347, Fig.6.33
Original text (add figure labels)
New text (a) for the upper figure, (b) for the lower figure

p.358, Ref.42
Original text SSCL Report 606 (1992).
New text Part. Accel. **43**, 77 (1993).

p.368, right column
Original text Impedance, resonator, broad-band, $m = 1$ 90
New text Impedance, resonator, broad-band, $m = 1$ 89